Hydrodynamic Evaluation of the Effects of Fluid Physical Properties and Sieve Tray Geometry on Entrainment and Weeping

by

Royston Kyle Moses

Thesis presented in partial fulfilment of the requirements for the Degree

of

MASTER OF ENGINEERING (CHEMICAL ENGINEERING)

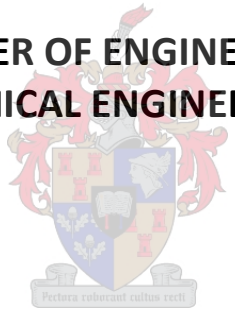

in the Faculty of Engineering at Stellenbosch University

Supervisor
Prof A.J. Burger

Co-Supervisor
Prof. J.H. Knoetze

December 2014

Declaration

By submitting this thesis electronically, I declare that the entirety of the work contained therein is my own, original work, that I am the sole author thereof (save to the extent explicitly otherwise stated), that reproduction and publication thereof by Stellenbosch University will not infringe any third party rights and that I have not previously in its entirety or in part submitted it for obtaining any qualification.

Date: 14 November 2014

Abstract

Distillation is one of the most widely used processes for the separation of fluids with different volatilities. Due to the popularity of this process it is often assumed that the hydrodynamic behaviour inside distillation columns is well-defined. However, this is not always the case and this study therefore endeavoured to provide additional insight into the topic through a systematic investigation into the hydrodynamics and the capacity limitations of a sieve tray distillation column.

The objective of the study was to measure and evaluate the effects of the following variables on entrainment and weeping:

- Fluid flow rate (gas and liquid).
- Plate geometry (*i.e.* hole diameter and fractional hole area).
- Liquid properties (*i.e*. surface tension, viscosity and density).
- Gas properties (*i.e*. viscosity and density).

The hydrodynamic effects were evaluated at zero mass transfer in a pilot-scale tray column, by passing pure liquids and gases in counter current configuration. The pilot column was rectangular in shape with internal dimensions of 175 mm by 635 mm. A chimney tray was used to capture the weeping liquid, while a de-entrainment tray was used in combination with a mist eliminator pad to capture the entrained liquid. The fractional hole areas for the sieve trays under investigation were 7%, 11% and 15% and the hole diameters were 3.2 mm (⅛ in.), 6.4 mm (¼ in.) and 12.7 mm (½ in.). The experimental liquids were ethylene glycol, butanol, water and silicone oil, while the gases were air and carbon dioxide (CO_2).

These experimental measurements produced over 10 000 data points for entrainment and over 7 000 data points of weeping. The results were repeatable and the entrainment values compared reasonably well with previous data produced by Nutter (1971) and Uys (2012).

The differences between entrainment for the different liquids were more significant in the spray regime than in the froth regime, and butanol was entrained more readily than silicone oil, ethylene glycol and water. Fluids that caused a larger spray layer in the dispersion zone produced more entrainment. Entrainment increased with decreasing liquid density, decreasing liquid surface tension and decreasing liquid viscosity. The more unstable the dispersion layer, the higher the entrainment.

The liquid density strongly influenced weeping, *i.e.* weeping increased with increasing liquid density. On the other hand, gases with higher densities – and thus with a higher mass flow rates at similar volumetric flow rates through the sieve tray – displayed less weeping and more entrainment than less dense gases, because of an increased upward drag force on the fluids.

When considering tray geometry and when operating in the spray regime, the magnitude of entrainment increased with decreasing fractional hole area, while the dependency of entrainment on fractional hole area was more prominent at lower fractional hole areas. When operating in the froth regime – typically above 23 $m^3/(h.m)$ – the fractional hole area had a relatively small influence on the magnitude of entrainment, while the cross-flowing liquid rate dominated related effects.

In the spray regime, *i.e.* typically below 23 m^3/(h.m), the entrainment increased with increasing sieve tray hole diameter, while hole diameter had a relatively small influence on entrainment at higher liquid flow rates between 23 and 60 m^3/(h.m). However, at even higher liquid flow rates in the froth regime, *i.e.* above 60 m^3/(h.m), the effect of hole diameter on the entrainment became more prominent again, with increased entrainment for smaller hole diameters.

The effect of hole diameter on weeping differed with changing fluid combinations and the 12.7 mm hole size caused notably less weeping than the 3.2 mm and 6.4 mm trays at higher liquid flow rates. It is believed that weeping occurred preferentially at so-called localised high pressure zones on the sieve tray. At high gas and liquid flow rates, the resultant extended dispersion layer allows minimal intimate contact between the plate and the liquid (minimising such localized high-pressure zones). In effect, the liquid 'jumps' over the entire flow path length in the test rig, thus resulting in low weeping rates at high gas and liquid rates.

The effects of fractional hole area and hole diameter on entrainment and weeping can be correlated with combinations of well-known hydrodynamic dimensionless numbers, such as the *Weber number* (We), *Froude number* (Fr) and *Reynolds number* (Re). Within the limitations of this study, the *flow-Froude number* was shown to be the most useful dimensionless number, since it displayed a monotonic relationship with magnitude of entrainment for different combinations of fluid systems and tray configurations. Furthermore, both the *construction number* and *fluid density ratio* could be used in a sensible manner to correlate some of the effects of tray geometry on entrainment.

Samevatting

Distillasie word wêreldwyd op groot en klein skaal toegepas as 'n metode om chemiese komponente van mekaar te skei, gebasseer op hul verskil in vlugtigheid. Die hidrodinamiese gedrag van vloeistowwe en hul damp binne 'n distillasiekolom beïnvloed die effektiwiteit van die skeidingsproses. Hierdie studie beoog dus om bykomende insig te verskaf tot die hidrodinamika en kapasiteitsbeperkings van 'n plaat-distilleerkolom.

Die doelwit van die studie was om die invloed van die volgende veranderlikes op die meesleuring en deurdripping van vloeistowwe te ondersoek:

- Gas- en vloeistof vloeitempo.
- Plaatgeometrie (i.e. gatdeursnit en fraksionele deurvloei-area).
- Vloeistofeienskappe (i.e. oppervlakspanning, viskositeit en digtheid).
- Gaseienskappe (i.e. viskositeit en digtheid).

Die hidrodinamiese studie is uitgevoer in 'n reghoekige plaatkolom met interne afmetings van 175 mm x 635 mm. Die vloeistof en gasfases is in kontak gebring op 'n teenstroom basis, met geen massa-oordrag wat plaasvind nie. 'n Skoorsteenplaat het die vloeistof opgevang wat deurdrip terwyl 'n ekstra plaat aan die bokant van die kolom die meegesleurde vloeistof opgevang het. Hierdie ekstra plaat is gebruik tesame met 'n mis-elimineerder om al die meegesleurde vloeistof op te vang. Plate met verskillende deurvloei-areas (7%, 11% en 15%) en gat deursnitte (3.2 mm, 6.4 mm en 12.7 mm) is gebruik in die ondersoek. Die vloeistowwe wat gebruik is, sluit in etileen glikol, butanol, water en silikon olie. Lug en koolstofdioksied is as gasse gebruik.

Die eksperimentele data het goeie herhaalbaarheid getoon en is vergelykbaar met die gepubliseerde data van Nutter (1971) en Uys (2012). Meer as 10 000 data punte is gemeet vir vloeistofmeesleuring en meer as 7 000 vir deurdripping.

Die verskil in hoeveelheid meesleuring tussen die vloeistowwe, soos ondersoek in hierdie studie, was mees beduidend in die spoei-regime. Butanol is die meeste meegesleur, gevolg deur silikon olie en dan etileen glikol. Water is die minste meegesleur is. Vloeistowwe wat 'n groter sproeivolume in die dispersielaag bo die plaat gevorm het, is die meeste meegesleur. Meesleuring het toegeneem met 'n afname in digtheid, oppervlakspanning en viskositeit van die vloeistof. 'n Onstabiele dispersielaag bo die plaat het meer meesleuring tot gevolg gehad.

Vloeistofdeurdripping is sterk beïnvloed deur vloeistofdigtheid, i.e. deurdripping het sterk toegeneem met digtheid. Gasse met 'n hoër digtheid veroorsaak weer 'n afname in deurdripping a.g.v. die hoër opwaartse sleurkragte wat 'n gas met hoë digtheid op die vloeistof uitoefen.

In die sproei-regime (tipies by vloeistofvloeitempos laer as 23 m^3/(h.m) is gevind dat meesleuring toeneem met 'n afname in fraksionele deurvloei-area. Meesleuring se afhanklikheid van fraksionele deurvloei-area was meer beduidend by laer fraksionele deurvloei-areas. In die skuim-regime (tipies by vloeistofvloeitempos hoër as 23 m^3/(h.m)) was die afhanklikheid van meesleuring op fraksionele deurvloei-area relatief klein.

In die sproei-regime is gevind dat meesleuring toeneem met 'n toename in gat deursnit, terwyl dieselfde veranderlike 'n minder beduidende invloed op meesleuring getoon het by hoër vloeistofvloeitempos (tussen 23 en 60 $m^3/(h.m)$). By vloeitempos hoër as 60 $m^3/(h.m)$ het meesleuring weer begin toeneem met 'n afname in gat deursnit.

By hoë vloeistofvloeitempos het die plaat met 12.7 mm gat deursnit aansienlik minder deurdripping getoon as plate met 3.2 mm en 6.4 mm deursnitte. Daar word vermoed dat deurdripping hoofsaaklik plaasvind by lokale hoëdruk gebiede op die plaat. By hoër vloeistof- en gasvloeitempos beslaan die dispersielaag 'n groter volume en is daar dus minder gebiede van digte vloeistofkontak met die plaat, wat 'n afname in die lokale drukgebiede veroorsaak. Dit lei tot 'n afname in deurdripping by hoër gas- en vloeistofvloeitempos.

Die invloed van fraksionele deurvloei-area en gatdeursnit op meesleuring en deurdripping korreleer goed met kombinasies van welbekende hidrodinamiese dimensielose getalle, i.e. die *Webergetal* (We), die *Froudegetal* (Fr) en die *Reynoldsgetal* (Re). Die *vloei-Froudegetal* is mees bruikbaar om die invloed van vloeistof-en-gas kombinasies en kolomuitleg op meesleuring te korreleer. Die *konstruksiegetal* asook die *digtheidsverhoudings tussen vloeistof en gas* kan op 'n sinvolle manier aangewend word om van die invloede van plaatgeometrie op meesleuring te beskryf.

Acknowledgements

Firstly I would like to thank GOD for creating me and giving me a purpose which I am discovering every day.

I would like to thank my mother (Alice Meyer), who constantly motivates me and reminds me what my goals are and that no problems are too big overcome. Thank you for all the phone calls late at night when I was busy performing my experiments motivating me to keep on going, and for all the meals you prepared throughout my masters.

I would like to thank my stepfather (Ricardo Meyer) for your constant support throughout my life and for being a father figure to me whenever I needed one although I was stubborn at times.

Thank you Prof. A.J. Burger and Prof. J.H. Knoetze for your guidance as supervisors and constant support. I would like to thank you for the long hours you spent guiding me to be a better engineer and for being good role models in the field of chemical engineering.

A special thank you has to be given to Vincent Carolissen without whom the project would not be completed in the given timeline. Thank you for continually helping me change the trays in the distillation column and for your help with fixing whatever problems I had with my pilot plant. Thank you for always being a person I could talk to when times were hard. Without you my project would be bleak and unenjoyable.

I would like to thank Sarel Lamprecht for your continued support in teaching me what I needed to know in order to operate the distillation pilot plant and for sacrificing your time so that I could complete my project in the given timeline.

I would like to thank Eben Uys for building the distillation pilot plant and without whom the world of sieve tray distillation would possibly not be opened up to me. Thank you for your work in sieve tray distillation.

Thank you to Jannie Barnard, Anton Cordier, Oliver Jooste, Alvin Petersen and Jos Weerdenberg for your help in fixing and maintenance of any process equipment I needed throughout my project. Thank you guys for the constant support and stories that helped to make my project a more joyful experience. Thank you Hanlie Botha and Levine Simmers for your help with the usage of the analytical equipment.

Thank you to everyone in the Separation Technology group for your constant support and time and for making me a better engineer by opening the world up to new projects and for help in improving my engineering skills.

A special thanks needs to be given to NRF, Sasol and Stellenbosch University Process Engineering department for financial assistance and making this project possible.

To name everyone that helped me along the way is a difficult task in itself. So I would like to thank all my family, friends and colleagues that helped me along the way and I promise to everyone I will become the best engineer and role model that I can be.

Table of Contents

Abstract iii
Samevatting iv
Acknowledgements vii
Table of Contents viii
Table of Tables xi
Table of Figures xii
Key Words, Definitions and Symbols xxi
Glossary xxi
Abbreviations xxii
Nomenclature xxiii
Nomenclature (Greek symbols) xxvi
Chapter 1 - Introduction 1
1.1 Background 1
1.2 Distillation Column Configuration 2
1.2.1 Packed Distillation Columns 2
1.2.2 Tray Distillation Columns 2
1.3 Project Rationale 6
1.4 Objectives 7
Chapter 2 – Literature Review 8
2.1 Flow Regimes 8
2.2 Dispersion Layer and Clear Liquid 11
2.3 Pressure Drop 16
2.4 Flow Regime Transition 19
2.5 Sieve Tray Distillation Capacity 23
2.5.1 Entrainment 24
2.5.2 Weeping 34
2.5.3 Sieve tray capacity 37
2.6 Critical Evaluation 39
2.7 Literature Summary 52
Chapter 3 – Objectives and Outcomes 56
3.1 Objectives of Study 56
3.2 Expected Outcomes of Study 56

Chapter 4 - Experimental Equipment Design 57
4.1 Experimental Design and Materials 57
4.2 Entrainment Data Validation 65
4.3 Weeping Data Validation 67
Chapter 5 - Entrainment Results and Discussion 69
5.1 Effect of Fluid Physical Properties and Fluid Flow 69
5.1.1 Effect of Liquid Physical Properties and Flow on Entrainment 69
5.1.2 Effect of Gas Properties and Flow on Entrainment 75
5.2 Effect of Plate Characteristics 80
5.2.1 Effect of Fractional Hole Area on Entrainment 80
5.2.2 Effect of Hole Diameter on Entrainment 83
5.3 Evaluation of Correlations and Predictive Models 87
5.3.1 Literature Correlations Entrainment Model Comparison 87
5.3.2 Dimensionless Number Predictive Model Trends for Entrainment 93
5.4 Entrainment Results Summary 106
Chapter 6 - Weeping Results and Discussion 107
6.1 Effect of Fluid Physical Properties and Fluid Flow 107
6.1.1 Effect of Liquid Properties and Flow on Weeping 107
6.1.2 Effect of Gas Properties and Flow on Weeping 112
6.2 Effect of Plate Characteristics 116
6.2.1 Effect of Fractional Hole Area on Weeping 116
6.2.2 Effect of Hole Diameter on Weeping 121
6.3 Evaluation of Dimensionless Number Trends for Weeping 127
6.4 Hydrodynamic Hold-Up Result Evaluation 136
6.5 Weeping Results Summary 140
Chapter 7 - Conclusions 141
Chapter 8 - Recommendations 144
Chapter 9 – References 146
Appendix A – Extended Literature Analysis 151
A.1 Dispersion Liquid and Clear Liquid 151
A.2 Pressure Drop 152
A.3 Flow Regime Transition 152
A.4 Additional Entrainment Literature 153
A.5 Additional Weeping Literature 155

A.6 Distillation Capacity 155
Appendix B – Correlation Graphs 157
Appendix C – Experimental Sieve Tray Designs 162
Appendix D – Equipment Design Specification 172
Appendix E – Experimental Methodology 181
E.1 Start up Procedure 181
E.2 Experimental Operating Procedure 181
E.3 Shutdown Procedure 183
E.4 Gas Loading Procedure 183
E.5 Sampling Techniques 184
Appendix F – Experimental Result Graphs 185
Appendix G - Raw Experimental Results 207

Table of Tables

Table 1 – Entrainment model validity range (adapted from Kister and Haas, 1988) 29
Table 2 – Model validity ranges (redrawn from Bennett *et al.*, 1995) 31
Table 3 – Experimental variables of Uys (2012) 33
Table 4 – Entrainment models range of application 40
Table 5 – Investigations into fractional hole area and hole diameter reported in literature 53
Table 6 – Literature parameters investigated and differences 54
Table 7 – Experimental liquid flow settings 58
Table 8 – Tray design specifications 59
Table 9 – Column internals dimensions 59
Table 10 – Fluids and physical properties typically used industrial distillation applications [modified with permission from Uys *et al.* (2009)] 63
Table 11 – Physical properties of gases investigated 64
Table 12 – Physical properties of liquids investigated 64
Table 13 – Experimental system properties and measuring limits 69
Table 14 – Experimental system capacity factors (C_s) and flow factors (F_s) 70
Table 15 – Blower gas specification [obtained with permission from (Uys *et al.*, 2009)] 174
Table 16 – Blower (E-102) design specifications [obtained with permission from (Uys *et al.*, 2009)] 177
Table 17 – Pump liquid specification [obtained with permission from (Uys *et al.*, 2009)] 177
Table 18 – Pump (E-204) design specifications [obtained with permission from (Uys *et al.*, 2009)]. 177
Table 19 – Surge tank (E-101) geometrical specification [obtained with permission from (Uys *et al.*, 2009)] 178
Table 20 – Heat exchanger (E-205) fluid specification [obtained with permission of (Uys *et al.*, 2009)] 178
Table 21 – Heat exchanger (E-205) design conditions [obtained with permission from (Uys *et al.*, 2009)] 178
Table 22 – Differential pressure transmitter specifications [obtained with permission from (Uys *et al.*, 2009)] 179
Table 23 – Absolute pressure transmitter specifications [obtained with permission from (Uys *et al.*, 2009)] 179
Table 24 – Liquid flow meter specifications [obtained with permission by (Uys *et al.*, 2009)] 180
Table 25 – Gas flow meter specifications [obtained with permission of (Uys *et al.*, 2009)] 180
Table 26 – Silicone oil/air tray 1 (15.8%, 6.4 mm) entrainment 207
Table 27 – Silicone oil/CO_2 tray 1 (15.8%, 6.4 mm) entrainment 210
Table 28 – Silicone oil/air tray 1 (15.8%, 6.4 mm) weeping 212
Table 29 – Silicone oil/CO_2 tray 1 (15.8%, 6.4 mm) weeping 215

Table of Figures

Figure 1 – Tray types [adapted with permission from Lockett (1986)]. 3
Figure 2 – Sieve tray distillation column configuration. 4
Figure 3 – Flow regimes in sieve tray distillation [obtained with permission from Lockett (1986)]. 9
Figure 4 – Flow regime limits [redrawn from Hofhuis and Zuiderweg (1979)]. 10
Figure 5 – Dispersion changes in a sieve tray column (a) with increasing liquid rate 1 to 5 (b) with increasing gas flow rates [obtained with permission from Uys *et al.* (2012)]. 16
Figure 6 – Region pressure diagram as used by Lockett (1986). 17
Figure 7 – Froth-to-spray transition. 20
Figure 8 – Modelling the effect of liquid flow rate on entrainment for u_s = 1.5 m/s. 41
Figure 9 – Modelling the effect of liquid flow rate on entrainment for u_s = 2.5 m/s. 41
Figure 10 – Modelling the effect of superficial gas velocity rate on entrainment for Q_L = 5.7 m^3/(h.m). 42
Figure 11 – Modelling the effect of superficial gas velocity on entrainment for Q_L = 68.6 m^3/(h.m). 43
Figure 12 – Modelling the effect of hole diameter on entrainment for Q_L = 5.7 m^3/(h.m) and u_s = 2 m/s. 43
Figure 13 – Modelling the effect of hole diameter on entrainment for Q_L = 34.3 m^3/(h.m) and u_s = 2.5 m/s. 44
Figure 14 – Modelling the effect of fractional hole area on entrainment for Q_L = 5.7 m^3/(h.m) and u_s = 2 m/s. 45
Figure 15 – Modelling the effect of fractional hole area on entrainment for Q_L = 34.3 m^3/(h.m) and u_s = 2.5 m/s. 45
Figure 16 – Modelling the effect of tray spacing on entrainment for Q_L = 5.7 m^3/(h.m) and u_s = 2 m/s. 46
Figure 17 – Modelling the effect of weir height on entrainment for Q_L = 5.7 m^3/(h.m) and u_s = 2 m/s. 47
Figure 18 – Modelling the effect of liquid density on entrainment for Q_L = 5.7 m^3/(h.m) and u_s = 2 m/s. 47
Figure 19 – Modelling the effect of liquid density on entrainment for Q_L = 34.3 m^3/(h.m) and u_s = 2.5 m/s. 48
Figure 20 – Modelling the effect of surface tension on entrainment for Q_L = 5.7 m^3/(h.m) and u_s = 2 m/s. 49
Figure 21 – Modelling the effect of surface tension on entrainment for Q_L = 34.3 m^3/(h.m) and u_s = 2.5 m/s. 49
Figure 22 – Modelling the effect of liquid viscosity on entrainment for Q_L = 5.7 m^3/(h.m) and u_s = 2 m/s. 50
Figure 23 – Modelling the effect of gas density on entrainment for Q_L = 5.7 m^3/(h.m) and u_s = 2 m/s. 51
Figure 24 – Modelling the effect of gas density on entrainment for Q_L = 34.3 m^3/(h.m) and u_s = 2.5 m/s. 51
Figure 25 – Sieve tray design for the distillation column [altered with permission from Uys *et al.* (2009)]. 58

Figure 26 – Mesh grid [obtained with permission from Uys *et al.* (2009)]..... 60
Figure 27 – Sieve tray distillation column PFD [Adapted with permission from Uys *et al.* (2009)]. 61
Figure 28 – L'/G entrainment repeatability and 'Uys' data comparison for Tray 10 (15.6%, 6.3 mm) and u_s = 2.6 m/s. 65
Figure 29 – Liquid hold-up repeatability and 'Uys' data comparison for Tray 10 (15.6%, 6.3 mm) and u_s = 2.6 m/s. 66
Figure 30 – L'/L experimental data comparison (Nutter, 1971) for Tray 6 (7%, 12.7 mm) and Q_L = 13.1 m^3/(h.m)..... 67
Figure 31 – W'/L weeping repeatability for Tray 10 (15.6%, 6.3 mm) and u_s = 2.6 m/s. 68
Figure 32 – W'/G weeping repeatability for Tray 10 (15.6%, 6.3 mm) and u_s = 2.6 m/s. 68
Figure 33 – Entrainment (L'/L) of different liquids with air for Tray 1 (15.8% fractional hole area, 6.4 mm hole diameter) at a superficial gas velocity of 1.7 m/s..... 71
Figure 34 – Entrainment (L'/G) of different liquids with air for Tray 1 (15.8% fractional hole area, 6.4 mm hole diameter) at a superficial gas velocity of 1.7 m/s..... 72
Figure 35 – Entrainment (L'/L) of different liquids with CO_2 for Tray 1 (15.8% fractional hole area, 6.4 mm hole diameter) at a superficial gas velocity of 1.7 m/s..... 73
Figure 36 – Entrainment (L'/G) of different liquids with CO_2 for Tray 1 (15.8% fractional hole area, 6.4 mm hole diameter) at a superficial gas velocity of 1.7 m/s..... 74
Figure 37 – Entrainment (L'/G) of different liquids with CO_2 for Tray 1 (15.8% fractional hole area, 6.4 mm hole diameter) at a superficial gas velocity of 2.3 m/s..... 75
Figure 38 – Entrainment of water (L'/L) with different gases for Tray 1 (15.8% fractional hole area, 6.4 mm hole diameter) at a superficial gas velocity of 1.7 m/s..... 76
Figure 39 – Entrainment of water (L'/G) with different gases for Tray 1 (15.8% fractional hole area, 6.4 mm hole diameter) at a superficial gas velocity of 1.7 m/s..... 76
Figure 40 – Entrainment of water (L'/G) with different gases for Tray 1 (15.8% fractional hole area, 6.4 mm hole diameter) at a superficial gas velocity of 2.6 m/s..... 77
Figure 41 – Entrainment of silicone oil (L'/L) with different gases for Tray 1 (15.8% fractional hole area, 6.4 mm hole diameter) at a superficial gas velocity of 1.7 m/s..... 78
Figure 42 – Entrainment of silicone oil (L'/G) with different gases for Tray 1 (15.8% fractional hole area, 6.4 mm hole diameter) at a superficial gas velocity of 1.7 m/s..... 78
Figure 43 – Effect of superficial gas velocities on entrainment (L'/L) at different liquid flow rates for Tray 1 (15.8% fractional hole area, 6.4 mm hole diameter) and silicone-oil/air. 79
Figure 44 – Effect of fractional hole area on entrainment (L'/L) for water/air with a 6.4 mm hole diameter and a superficial gas velocity of 2.3 m/s. 80
Figure 45 – Effect of fractional hole area on entrainment (L'/G) for water/air with a 6.4 mm hole diameter and a superficial gas velocity of 2.3 m/s. 81
Figure 46 – Effect of fractional hole area on entrainment (L'/G) for silicone-oil/CO_2 with a 6.4 mm hole diameter and a superficial gas velocity of 2.3 m/s. 82
Figure 47 – Effect of hole diameter on entrainment (L'/L) for water/air with a 15% fractional hole area and a superficial gas velocity of 2.3 m/s..... 83
Figure 48 – Effect of hole diameter on entrainment (L'/G) for water/air with a 15% fractional hole area and a superficial gas velocity of 2.3 m/s..... 84
Figure 49 – Effect of hole diameter on entrainment (L'/G) for silicone-oil/CO_2 with a 11% fractional hole area and a superficial gas velocity of 2.3 m/s..... 85

Figure 50 – Effect of tray geometry on entrainment (L'/G) for ethylene-glycol/air with changing superficial gas velocity and a liquid flow rate of 8.6 m^3/(h.m). 86
Figure 51 – Effect of tray geometry on entrainment (L'/G) for ethylene-glycol/air with changing superficial gas velocity and a liquid flow rate of 34.3 m^3/(h.m). 86
Figure 52 – Experimental entrainment comparison to entrainment models for Tray 1 (15.8% fractional hole area, 6.4 mm hole diameter) with water/air at a superficial gas velocity of 1.7 m/s. . 87
Figure 53 – Experimental entrainment comparison to entrainment models for Tray 1 (15.8% fractional hole area, 6.4 mm hole diameter) with water/air at a superficial gas velocity of 2.6 m/s. . 88
Figure 54 – Experimental entrainment comparison to entrainment models for Tray 2 (15.8% fractional hole area, 3.2 mm hole diameter) with water/air at a superficial gas velocity of 2 m/s. 89
Figure 55 – Experimental entrainment comparison to entrainment models for Tray 3 (15.6% fractional hole area, 12.7 mm hole diameter) with water/air at a superficial gas velocity of 2 m/s. .. 89
Figure 56 – Experimental entrainment comparison to entrainment models for Tray 4 (7% fractional hole area, 6.4 mm hole diameter) with water/air at a superficial gas velocity of 2.3 m/s. 90
Figure 57 – Experimental entrainment comparison to entrainment models for Tray 7 (11.5% fractional hole area, 6.4 mm hole diameter) with water/air at a superficial gas velocity of 2.3 m/s. . 91
Figure 58 – Experimental entrainment comparison to entrainment models for Tray 1 (15.8% fractional hole area, 6.4 mm hole diameter) with water/CO_2 at a superficial gas velocity of 2 m/s. .. 92
Figure 59 – Experimental entrainment comparison to entrainment models for Tray 1 (15.8% fractional hole area, 6.4 mm hole diameter) with ethylene-glycol/air at a superficial gas velocity of 2.3 m/s. 92
Figure 60 – Entrainment (L'/G) changing with the liquid hold-up Froude number (Fr_h^+) for ethylene-glycol/air with Tray 1 (15.8% fractional hole area, 6.4 mm hole diameter) in the spray regime. 93
Figure 61 – Entrainment (L'/L) changing with the liquid hold-up Froude number (Fr_h^+) for water/air with Tray 1 (15.8% fractional hole area, 6.4 mm hole diameter) at different gas superficial velocities. 94
Figure 62 – Entrainment (L'/G) changing with the Weber number (We) for silicone-oil/air with Tray 1 (15.8% fractional hole area, 6.4 mm hole diameter) in the spray regime. 95
Figure 63 – Entrainment (L'/G) changing with the liquid Reynolds number (Re) for ethylene-glycol/air with Tray 1 (15.8% fractional hole area, 6.4 mm hole diameter) in the spray regime. 96
Figure 64 – Entrainment (L'/L) changing with the flow Froude number (Fr^+) for water/air with Tray 1 (15.8% fractional hole area, 6.4 mm hole diameter) at different gas superficial velocities. 97
Figure 65 – Entrainment (L'/L) changing with the gas Reynolds number (Re_g) divided by the flow Froude number (Fr^+) for butanol/CO_2 with Tray 1 (15.8% fractional hole area, 6.4 mm hole diameter) at different liquid flow rates. 98
Figure 66 – Entrainment (L'/L) changing with the gas Reynolds number (Reg) divided by the flow Froude number (Fr+) for different fluids systems with Tray 1 (15.8% fractional hole area, 6.4 mm hole diameter). 99
Figure 67 – Entrainment (L'/G) changing with the tray hole lip length divided by the weir height (h_{wo}) for water/air with different sieve trays. 99
Figure 68 – Entrainment (L'/G) changing with the construction number (Co) for water/air at a liquid flow rate of 8.6 m^3/(h.m) with different sieve trays. 100
Figure 69 – Entrainment (L'/L) changing with the flow Froude number (Fr^+) for water/air at a fractional hole area of 15% and different hole diameters. 101

Figure 70 – Entrainment (L'/L) changing with the flow Froude number (Fr^+) for water/air at a hole diameter of 6.4 mm and different fractional hole areas. 102
Figure 71 – Entrainment (L'/L) changing with the flow Froude number (Fr^+) to construction number (Co) ratio for ethylene-glycol/air at a fractional hole area of 15% and different hole diameters. 103
Figure 72 – Entrainment (L'/L) changing with the flow Froude number (Fr^+) to construction number (Co) ratio for ethylene-glycol/air at a hole diameter of 6.4 mm and different fractional hole areas. 103
Figure 73 – Entrainment (L'/L) changing with the flow Froude number (Fr^+) to fluid density ratio for water with Tray 1 (15.8% fractional hole area, 6.4 mm hole diameter). 104
Figure 74 – Entrainment (L'/L) changing with the flow Froude number (Fr^+) for different liquids with air and Tray 1 (15.8% fractional hole area, 6.4 mm hole diameter). 105
Figure 75 – Entrainment (L'/L) changing with the flow Froude number (Fr+) to fluid density ratio for different liquids with air and Tray 1 (15.8% fractional hole area, 6.4 mm hole diameter). 105
Figure 76 – Weeping (W'/L) of different liquids with air for Tray 1 (15.8% fractional hole area, 6.4 mm hole diameter) at a superficial gas velocity of 1.7 m/s. 108
Figure 77 – Weeping (W'/G) of different liquids with air for Tray 1 (15.8% fractional hole area, 6.4 mm hole diameter) at a superficial gas velocity of 1.7 m/s. 109
Figure 78 – Weeping (W'/L) of different liquids with CO_2 for Tray 1 (15.8% fractional hole area, 6.4 mm hole diameter) at a superficial gas velocity of 1.7 m/s. 110
Figure 79 – Weeping (W'/G) of different liquids with CO_2 for Tray 1 (15.8% fractional hole area, 6.4 mm hole diameter) at a superficial gas velocity of 1.7 m/s. 111
Figure 80 – Weeping (W'/L) of different liquids with CO_2 for Tray 1 (15.8% fractional hole area, 6.4 mm hole diameter) at a superficial gas velocity of 2.3 m/s. 112
Figure 81 – Weeping of water (W'/L) with different gases for Tray 1 (15.8% fractional hole area, 6.4 mm hole diameter) at a superficial gas velocity of 1.7 m/s. 113
Figure 82 – Weeping of water (W'/G) with different gases for Tray 1 (15.8% fractional hole area, 6.4 mm hole diameter) at a superficial gas velocity of 1.7 m/s. 113
Figure 83 – Weeping of water (W'/L) with different gases for Tray 1 (15.8% fractional hole area, 6.4 mm hole diameter) at a superficial gas velocity of 2.6 m/s. 114
Figure 84 – Weeping of silicone oil (W'/L) with different gases for Tray 1 (15.8% fractional hole area, 6.4 mm hole diameter) at a superficial gas velocity of 1.7 m/s. 115
Figure 85 – Weeping of silicone oil (W'/G) with different gases for Tray 1 (15.8% fractional hole area, 6.4 mm hole diameter) at a superficial gas velocity of 1.7 m/s. 115
Figure 86 – Effect of superficial gas velocities on weeping (W'/L) at different liquid flow rates for Tray 1 (15.8% fractional hole area, 6.4 mm hole diameter) and silicone-oil/air. 116
Figure 87 – Effect of fractional hole area on weeping (W'/L) for water/air with a 3.2 mm hole diameter and a superficial gas velocity of 1.7 m/s. 117
Figure 88 – Effect of fractional hole area on weeping (W'/G) for water/air with a 3.2 mm hole diameter and a superficial gas velocity of 1.7 m/s. 118
Figure 89 – Effect of fractional hole area on weeping (W'/L) for water/air with a 3.2 mm hole diameter and a superficial gas velocity of 2.6 m/s. 119
Figure 90 – Effect of fractional hole area on weeping (W'/L) for silicone-oil/CO_2 with a 3.2 mm hole diameter and a superficial gas velocity of 1.7 m/s. 120
Figure 91 – Effect of fractional hole area on weeping (W'/L) for water/air with a 6.4 mm hole diameter and a superficial gas velocity of 1.7 m/s. 120

Figure 92 – Effect of hole diameter on weeping (W'/L) for silicone-oil/air with a 15% fractional hole area and a superficial gas velocity of 1.7 m/s. 122
Figure 93 – Effect of hole diameter on weeping (W'/G) for silicone-oil/air with a 15% fractional hole area and a superficial gas velocity of 1.7 m/s. 122
Figure 94 – Effect of hole diameter on weeping (W'/L) for silicone-oil/air with a 15% fractional hole area and a superficial gas velocity of 2.6 m/s. 123
Figure 95 – Effect of hole diameter on weeping (W'/L) for water/air with a 15% fractional hole area and a superficial gas velocity of 2.6 m/s. 124
Figure 96 – Effect of hole diameter on weeping (W'/L) for silicone-oil/CO_2 with a 15% fractional hole area and a superficial gas velocity of 1.7 m/s. 124
Figure 97 – Effect of hole diameter on weeping (W'/L) for silicone-oil/CO_2 with a 15% fractional hole area and a superficial gas velocity of 2.6 m/s. 126
Figure 98 – Effect of tray geometry on weeping (W'/L) for ethylene-glycol/air with changing superficial gas velocity and a liquid flow rate of 8.6 m^3/(h.m). 126
Figure 99 – Effect of tray geometry on weeping (W'/L) for ethylene-glycol/air with changing superficial gas velocity and a liquid flow rate of 34.3 m^3/(h.m). 127
Figure 100 – Weeping (W'/L) changing with the inverse of the liquid hold-up Froude number (Fr_h^+) for ethylene-glycol/air with Tray 1 (15.8% fractional hole area, 6.4 mm hole diameter) in the spray regime. 128
Figure 101 – Weeping (W'/G) changing with the inverse of the liquid hold-up Froude number (Fr_h^+) for ethylene-glycol/air with Tray 1 (15.8% fractional hole area, 6.4 mm hole diameter) in the spray regime. 129
Figure 102 – Weeping (W'/L) changing with the Weber number (We) for silicone-oil/air with Tray 1 (15.8% fractional hole area, 6.4 mm hole diameter) in the spray regime. 130
Figure 103 – Weeping (W'/G) changing with the Weber number (We) for silicone-oil/air with Tray 1 (15.8% fractional hole area, 6.4 mm hole diameter) in the spray regime. 131
Figure 104 – Weeping (W'/L) changing with the liquid Reynolds number (Re) for ethylene-glycol/air with Tray 1 (15.8% fractional hole area, 6.4 mm hole diameter) in the spray regime. 132
Figure 105 – Weeping (W'/G) changing with the liquid Reynolds number (Re) for ethylene-glycol/air with Tray 1 (15.8% fractional hole area, 6.4 mm hole diameter) in the spray regime. 132
Figure 106 – Weeping (W'/L) changing with the gas Reynolds number (Re_g) for water/air with Tray 1 (15.8% fractional hole area, 6.4 mm hole diameter) at different liquid rates. 133
Figure 107 – Weeping (W'/L) changing with the flow Froude number (Fr) for water/air with Tray 1 (15.8% fractional hole area, 6.4 mm hole diameter) at different gas superficial velocities. 134
Figure 108 – Weeping (W'/L), changing with the tray hole total lip length divided by the weir height (h_{wo}) for water/air with different sieve trays at a liquid flow rate of 8.6 m^3/(h.m). 135
Figure 109 – Weeping (W'/L), changing with the construction number (Co) for water/air with different sieve trays at a liquid flow rate of 8.6 m^3/(h.m). 136
Figure 110 – Liquid hold-up of different liquids with CO_2 for Tray 1 (15.8% fractional hole area, 6.4 mm hole diameter) at a superficial gas velocity of 1.7 m/s. 137
Figure 111 – Effect of gases in water systems on the liquid hold-up for Tray 1 (15.8% fractional hole area, 6.4 mm hole diameter) at a superficial gas velocity of 1.7 m/s. 137
Figure 112 – Effect of hole diameter on the liquid hold-up for 15.8% fractional hole area trays in water/air at a superficial gas velocity of 1.7 m/s. 138

Figure 113 – Effect of fractional hole area on the liquid hold-up for 6.4 mm hole diameter trays in water/air at a superficial gas velocity of 1.7 m/s.....139
Figure 114 – Modelling the effect of liquid flow rate on entrainment for u_s = 2 m/s.....157
Figure 115 – Modelling the effect of gas superficial velocity on entrainment for Q_L = 23 [m^3/(h.m)].....157
Figure 116 – Modelling the effect of hole diameter on entrainment for Q_L = 34.3 [m^3/(h.m)] and u_s = 2 m/s.....158
Figure 117 – Modelling the effect of fractional hole area on entrainment for QL = 34.3 [m^3/(h.m)] and us = 2 m/s.....158
Figure 118 – Modelling the effect of tray spacing on entrainment for Q_L = 34.3 [m^3/(h.m)] and u_s = 2 m/s.....159
Figure 119 – Modelling the effect of tray spacing on entrainment for Q_L = 34.3 [m^3/(h.m)] and u_s = 2.5 m/s.....159
Figure 120 – Modelling the effect of liquid density on entrainment for Q_L = 34.3 [m^3/(h.m)] and u_s = 2 m/s.....160
Figure 121 – Modelling the effect of surface tension on entrainment for Q_L = 34.3 [m^3/(h.m)] and u_s = 2 m/s.....160
Figure 122 – Modelling the effect of gas density on entrainment for Q_L = 34.3 [m^3/(h.m)] and u_s = 2 m/s.....161
Figure 123 – Tray 1 with ¼ in. (6.4 mm) hole diameter and a fractional hole area of 15.8%.....162
Figure 124 – Tray 2 with ⅛ in. (3.2 mm) hole diameter and a fractional hole area of 15.8%.....163
Figure 125 – Tray 3 with ½ in. (12.7 mm) hole diameter and a fractional hole area of 15.6%.....164
Figure 126 – Tray 4 with ¼ in. (6.4 mm) hole diameter and a fractional hole area of 7%.....165
Figure 127 – Tray 5 with ⅛ in. (3.2 mm) hole diameter and a fractional hole area of 7%.....166
Figure 128 – Tray 6 with ½ in. (12.7 mm) hole diameter and a fractional hole area of 7.3%.....167
Figure 129 – Tray 7 with ¼ in. (6.4 mm) hole diameter and a fractional hole area of 11. 5%.....168
Figure 130 – Tray 8 with ⅛ in. (3.2 mm) hole diameter and a fractional hole area of 11.5%.....169
Figure 131 – Tray 9 with ½ in. (12.7 mm) hole diameter and a fractional hole area of 11.5%.....170
Figure 132 – Tray 11 with 6.3 mm holes and a fractional hole area of 15.6%.....171
Figure 133 – Front view of distillation column [obtained with permission from (Uys *et al.*, 2009)].....172
Figure 134 – Side view of distillation column [obtain with permission from (Uys *et al.*, 2009)].....173
Figure 135 – Small entrainment measuring tank [obtained from (Uys *et al.*, 2009)].....174
Figure 136 – Distillation pilot plant [Adapted with permission from (Uys *et al.*, 2009)].....175
Figure 137 – Large entrainment measuring tank [obtained from (Uys *et al.*, 2009)].....176
Figure 138 – Temperature control system [obtained with permission from (Uys *et al.*, 2009)].....176
Figure 139 – L'/L entrainment repeatability and 'Uys' data comparison for Tray 10 (15.6%, 6.3 mm) and u_s = 2.6 m/s.....185
Figure 140 – Dry tray pressure drop repeatability and 'Uys' data comparison for Tray 10 (15.6%, 6.3 mm).....185
Figure 141 – L'/G experimental data comparison (Nutter, 1971) for Tray 6 (7%, 12.7 mm) and Q_L = 13.1 m^3/(h.m).....185
Figure 142 – Entrainment (L'/L) of different liquids with air for tray 1 (15.8% fractional hole area, 6.4 mm hole diameter) at a superficial gas velocity of 2.3 m/s.....186
Figure 143 – Entrainment (L'/G) of different liquids with air for tray 1 (15.8% fractional hole area, 6.4 mm hole diameter) at a superficial gas velocity of 2.3 m/s.....186

Figure 144 – Entrainment (L'/L) of different liquids with CO_2 for tray 1 (15.8% fractional hole area, 6.4 mm hole diameter) at a superficial gas velocity of 2.3 m/s.....186
Figure 145 – Entrainment of water (L'/L) with different gasses for tray 1 (15.8% fractional hole area, 6.4 mm hole diameter) at a superficial gas velocity of 2.6 m/s.....187
Figure 146 – Entrainment of silicone oil (L'/L) with different gasses for tray 1 (15.8% fractional hole area, 6.4 mm hole diameter) at a superficial gas velocity of 2.6 m/s.....187
Figure 147 – Entrainment of silicone oil (L'/G) with different gasses for tray 1 (15.8% fractional hole area, 6.4 mm hole diameter) at a superficial gas velocity of 2.6 m/s.....187
Figure 148 – Effect of fractional hole area on entrainment (L'/L) for silicone-oil/CO_2 with a 12.7 mm hole diameter and a superficial gas velocity of 2.3 m/s. 188
Figure 149 – Effect of hole diameter on entrainment (L'/L) for silicone-oil/CO_2 with a 11% fractional hole area and a superficial gas velocity of 2.3 m/s.....188
Figure 150 – Effect of tray geometry on entrainment (L'/L) for ethylene-glycol/air with changing superficial gas velocity and a liquid flow rate of 8.6 [m^3/(h.m)].....189
Figure 151 – Effect of tray geometry on weeping (L'/L) for ethylene-glycol/air with changing superficial gas velocity and a liquid flow rate of 34.3 [m^3/(h.m)].....189
Figure 152 – Experimental entrainment comparison to entrainment models for tray 2 (15.8% fractional hole area, 3.2 mm hole diameter) with water/air at a superficial gas velocity of 2.3 m/s.190
Figure 153 – Experimental entrainment comparison to entrainment models for tray 3 (15.6% fractional hole area, 12.7 mm hole diameter) with water/air at a superficial gas velocity of 2.3 m/s. 190
Figure 154 – Experimental entrainment comparison to entrainment models for tray 4 (7% fractional hole area, 6.4 mm hole diameter) with water/air at a superficial gas velocity of 2.6 m/s. 191
Figure 155 – Experimental entrainment comparison to entrainment models for tray 7 (11.5% fractional hole area, 6.4 mm hole diameter) with water/air at a superficial gas velocity of 2.6 m/s.191
Figure 156 – Experimental entrainment comparison to entrainment models for tray 1 (15.8% fractional hole area, 6.4 mm hole diameter) with water/CO_2 at a superficial gas velocity of 2.3 m/s. 192
Figure 157 – Experimental entrainment comparison to entrainment models for tray 1 (15.8% fractional hole area, 6.4 mm hole diameter) with silicone-oil/air at a superficial gas velocity of 2.6 m/s. 192
Figure 158 – Entrainment (L'/G) changing with the liquid holdup Froude number (Fr_h^+) for ethylene-glycol/air with tray 1 (15.8% fractional hole area, 6.4 mm hole diameter) in the froth regime. 193
Figure 159 – Entrainment (L'/L) changing with the Weber number (We) for silicone-oil/air with tray 1 (15.8% fractional hole area, 6.4 mm hole diameter) in the spray regime.....193
Figure 160 – Entrainment (L'/G) changing with the Reynolds number (Re) for ethylene-glycol/air with tray 1 (15.8% fractional hole area, 6.4 mm hole diameter) in the froth regime. 194
Figure 161 – Entrainment (L'/L) changing with the flow Froude number (Fr^+) to construction number (Co) ratio for water/air at a fractional hole area of 15% and different hole diameters.....194
Figure 162 – Entrainment (L'/L) changing with the flow Froude number (Fr^+) to construction number (Co) ratio for water/air at a hole diameter of 6.4 mm and different fractional hole areas. 195
Figure 163 – Entrainment (L'/L) changing with the flow Froude number (Fr^+) to construction number (Co) ratio for silicone-oil/air at a fractional hole area of 15% and different hole diameters.....195
Figure 164 – Entrainment (L'/L) changing with the flow Froude number (Fr^+) to construction number (Co) ratio for silicone-oil/air at a hole diameter of 6.4 mm and different fractional hole areas. 196

Figure 165 – Entrainment (L'/L) changing with the flow Froude number (Fr^+) and fluid density ratio for different gasses in silicone oil with tray 1 (15.8% fractional hole area, 6.4 mm hole diameter).. 196
Figure 166 – Entrainment (L'/L) changing with the flow Froude number (Fr^+) and fluid density ratio for different gasses in ethylene glycol with tray 1 (15.8% fractional hole area, 6.4 mm hole diameter). 197
Figure 167 – Entrainment (L'/L) changing with the flow Froude number (Fr^+) for different liquid in CO_2 with tray 1 (15.8% fractional hole area, 6.4 mm hole diameter) in the spray regime. 197
Figure 168 – Weeping (W'/G) of different liquids with air for tray 1 (15.8% fractional hole area, 6.4 mm hole diameter) at a superficial gas velocity of 2.3 m/s..... 198
Figure 169 – Weeping (W'/L) of different liquids with air for tray 1 (15.8% fractional hole area, 6.4 mm hole diameter) at a superficial gas velocity of 2.3 m/s..... 198
Figure 170 – Weeping (W'/G) of different liquids with CO_2 for tray 1 (15.8% fractional hole area, 6.4 mm hole diameter) at a superficial gas velocity of 2.3 m/s..... 198
Figure 171 – Weeping of water (W'/G) with different gasses for tray 1 (15.8% fractional hole area, 6.4 mm hole diameter) at a superficial gas velocity of 2.6 m/s..... 199
Figure 172 – Weeping of silicone oil (W'/L) with different gasses for tray 1 (15.8% fractional hole area, 6.4 mm hole diameter) at a superficial gas velocity of 2.6 m/s..... 199
Figure 173 – Weeping of silicone oil (L'/G) with different gasses for tray 1 (15.8% fractional hole area, 6.4 mm hole diameter) at a superficial gas velocity of 2.6 m/s..... 199
Figure 174 – Effect of fractional hole area on weeping (W'/G) for water/air with a 3.2 mm hole diameter and a superficial gas velocity of 2.6 m/s. 200
Figure 175 – Effect of fractional hole area on weeping (W'/G) for silicone-oil/CO_2 with a 3.2 mm hole diameter and a superficial gas velocity of 1.7 m/s. 200
Figure 176 – Effect of fractional hole area on weeping (W'/G) for silicone-oil/CO_2 with a 6.4 mm hole diameter and a superficial gas velocity of 1.7 m/s. 200
Figure 177 – Effect of hole diameter on weeping (W'/G) for silicone-oil/air with a 15% fractional hole area and a superficial gas velocity of 2.6 m/s. 201
Figure 178 – Effect of hole diameter on weeping (W'/G) for water/air with a 15% fractional hole area and a superficial gas velocity of 2.6 m/s. 201
Figure 179 – Effect of hole diameter on weeping (W'/G) for silicone-oil/CO_2 with a 15% fractional hole area and a superficial gas velocity of 1.7 m/s. 202
Figure 180 – Effect of hole diameter on weeping (W'/G) for silicone-oil/CO_2 with a 15% fractional hole area and a superficial gas velocity of 2.6 m/s. 202
Figure 181 – Effect of tray geometry on weeping (W'/G) for ethylene-glycol/air with changing superficial gas velocity and a liquid flow rate of 8.6 m^3/(h.m). 203
Figure 182 – Effect of tray geometry on weeping (W'/G) for ethylene-glycol/air with changing superficial gas velocity and a liquid flow rate of 34.3 m^3/(h.m). 203
Figure 183 – Weeping (W'/L) changing with the inverse liquid holdup Froude number (Fr_h^+) for ethylene-glycol/air with tray 1 (15.8% fractional hole area, 6.4 mm hole diameter) in the froth regime. 204
Figure 184 – Weeping (W'/L) changing with the Weber number (We) for silicone-oil/air with tray 1 (15.8% fractional hole area, 6.4 mm hole diameter) in the froth regime. 204
Figure 185 – Weeping (W'/G) changing with the Weber number (We) for silicone-oil/air with tray 1 (15.8% fractional hole area, 6.4 mm hole diameter) in the froth regime. 205

Figure 186 – Weeping (W'/L) changing with the liquid Reynolds number (Re) for ethylene-glycol/air with tray 1 (15.8% fractional hole area, 6.4 mm hole diameter) in the froth regime. 205
Figure 187 – Weeping (W'/G) changing with the liquid Reynolds number (Re) for ethylene-glycol/air with tray 1 (15.8% fractional hole area, 6.4 mm hole diameter) in the froth regime. 206

Key Words, Definitions and Symbols

Glossary

Bubbling area	:	Column cross sectional area minus the inlet and outlet downcomer area.
Clear liquid height	:	The height of liquid hold-up on the tray that is unaffected by the gas/vapour mixture (no froth characteristics). It also represents the pressure drop of the un-aerated liquid above the tray.
Downcomer escape area	:	The area of escape through which the liquid phase exits the downcomer.
Dry tray pressure drop	:	The pressure drop across a tray, in which no liquid is present (pressure drop caused by friction losses on the gas flowing upward through the column).
Dispersion layer	:	Volume above the sieve tray controlled (filled) with liquid.
Entrainment	:	The loss of liquid upward though the distillation column by the gas.
Entrainment (L'/L)	:	Entrainment as a column efficiency indicator (Flow rate of entrained liquid divided by flow rate of liquid into distillation column).
Entrainment (L'/G)	:	Entrainment as a column capacity indicator (Flow rate of entrained liquid divided by flow rate of gas into distillation column).
Flooding	:	The build-up of liquid on trays (caused by entrainment) to the point that more liquid flows into the column than out of it.
Fluid system	:	Fluid combination used during experimentation (example air and water as Water/Air system).
Fractional hole area	:	The area that the sieve tray holes consume on the sieve tray divided by the perforation area.
Froth height	:	The height of the froth dispersion above the tray.
Froth layer	:	Lower dispersion layer characteristic of bubbling and slug like (coalesced liquid) fluid movement.
Froth regime	:	The froth (mixed bubbling) regime the gas passes through the liquid as ill-defined gas bubbles of rapidly changing shape.

Hole lip length	:	Sum of sieve tray hole circumference lengths
Liquid flow path length	:	The length between the downcomer escape and the outlet weir.
Liquid holdup	:	The total wet pressure drop minus the dry tray pressure drop head.
Perforated area	:	The area of the tray covered by holes.
Residual pressure drop	:	The total wet pressure drop minus the clear liquid head pressure drop and the dry tray pressure drop head.
Spray layer	:	Upper dispersion layer characteristic of gas jetting and spray droplet behaviour
Spray regime	:	In the spray regime the gas phase is continuous and is characterized by gas jetting through the flowing liquid.
Superficial gas velocity	:	The velocity of the gas based on the column cross sectional area minus the downcomer area.
Turndown ratio	:	The range of vapour load between which the column can operate without substantially affecting its separation efficiency.
Weeping	:	The seeping of liquid through the sieve tray holes.
Weeping (W'/L)	:	Weeping as a column efficiency indicator (Flow rate of weeping liquid divided by flow rate of liquid into distillation column).
Weeping (W'/G)	:	Weeping as a column capacity indicator (Flow rate of weeping liquid divided by flow rate of gas into distillation column).

Abbreviations

AW	: Air/Water
EG	: Ethylene glycol
NAW	: Non-Air/Water
Si	: Silicone oil

Nomenclature

Symbols	Definition	Units
A_{ad}	Area between the splash baffle and tray deck	m^2
A_b	Bubbling area (A_c-$2A_d$)	m^2
A_c	Column cross sectional area	m^2
A_d	Downcomer area	m^2
A_p	Active perforation area (Including blank area)	m^2
A_{ap}	Downcomer escape area	m^2
A_h	Total hole area	m^2
A_h*	Total hole area	ft^2
A_n	Net available area for vapour/liquid disengagement	m^2
A_f	Fractional hole area (tray free area)	
B	Weir length per unit bubbling area	m^{-1}
C_b	Capacity factor based on A_b	m/s
C_D	Venturi discharge coefficient	
C_d	Weir coefficient	
$C_{b(max)}$	Maximum capacity factor based on A_p	m/s
$C_{b(inc)}$	Capacity factor based on A_b at incipient flooding	m/s
C_{bw}	Capacity factor based on A_b at weeping point	m/s
C_p	Capacity factor based on A_p	m/s
C_s	Capacity factor based on A_n	m/s
C_f	Flooding factor (Souders and Brown flooding constant (1934))	m/s
D_{32}	Sauter mean drop diameter	µm
D_H	Hole diameter	m
d_H	Hole diameter	mm
d_H*	Hole diameter	in.
d_p	Differential pressure	Pa
E	Entrainment rate	(kg liquid/kg vapour)
e	Entrainment rate	(lb liquid/lb vapour)
E_f	Entrainment in the froth regime	(kg liquid/kg vapour)
E_S	Entrainment in the spray regime	(kg liquid/kg vapour)
E_W	Entrainment during weeping conditions	(kg liquid/kg vapour)
F_S	F-factor based on u_s	$(kg/m)^{1/2}/s$
F_{lg}	Two phase kinetic F-factor	$(kg/m)^{1/2}/s$
F*	F-factor based on u_b	$(lb/ft)^{1/2}/s$
F_P	F-factor based on u_P	$(kg/m)^{1/2}/s$

F_P*	F-factor based on u_P	$(lb/ft)^{1/2}/s$
G	Gas/liquid mass flow rate	kg/s
G’	Gas/liquid mass flow rate	lb./(hr.sq. ft)
g	Gravitational acceleration (9.81)	m/s^2
g^*	Gravitational acceleration (32.2)	ft/s^2
g_c	Gravitational acceleration	$lbm/(lbf.s^2)$
$H_{2\phi}$	Two phase dispersion height	m
H_b	Bed height	m
h_b	Bed height	mm
H_{ct}	Clear liquid height at froth-to-spray transition (constant liquid flow rate)	mm
H_d	Dynamic dry head pressure drop	m, water
h_d	Dynamic dry head pressure drop	mm, water
h_d*	Dynamic dry head pressure drop	in., water
H_{DP}*	Dry tray pressure drop head	ft, water
H_F	Froth height	m
H_{fe}	Effective froth height	m
h_F	Froth height	mm
h_f*	Froth height	in.
$H_{f,t}$	Dispersion height at the froth-to-spray transition	m
H_L	Clear liquid height	m
$H_{L,tr}$	Clear liquid height at low-to-high liquid layer transition	m
h_L	Clear liquid height	mm
h_L^*	Clear liquid height	in.
$h_{L,f}$	Clear liquid height in the froth regime	mm
$h_{L,t}$	Clear liquid height at the froth-to-spray transition	mm
$h_{L,t}$*	Clear liquid height at the froth-to-spray transition	in.
h_M	Momentum heads	mm, water
H_{ow}	Height of froth flowing over weir	m
H_R	Residual pressure drop head	m, water
H_t	Total tray pressure drop head	m, water
h_t*	Total tray pressure drop head	in., water
H_{wo}	Weir height	m
h_{wo}	Weir height	mm
L	Liquid mass flow rate	kg/s
L’’	Liquid mass flow rate per weir length	lb/(hr.ft)
L’	Entrained liquid mass flow	kg/s
l	Weir length	m

N_T	Number of tray holes	
P	Hole pitch	m
p	Hole pitch	mm
ΔP_d	Dry tray pressure drop	in. liquid
ΔP_t	Total pressure drop	in. liquid
P_t	Hole pitch	mm
q_L	Liquid volumetric flow rate per weir length	$m^3/(m.s)$
Q_L	Liquid volumetric flow rate per weir length	$m^3/(m.s)$
Q_L*	Liquid volumetric flow rate per weir length	(US)gpm/ft
Q_L+	Liquid volumetric flow rate per weir length	(Imp)gpm/ft
Q_V	Gas volumetric flow rate	m^3/s
R	Universal gas constant	J/(kg.K)
S	Tray spacing	m
s	Tray spacing	mm
S*	Tray spacing	in.
S'	Effective tray spacing	in.
t	Tray thickness	mm
u	Fluid velocity	m/s
u_C	Gas velocity based on column area	m/s
u_{DO}	Droplet ejection velocity	m/s
u_b	Gas/vapour velocity based on A_b	m/s
u_h	Gas/vapour hole velocity based on A_h	m/s
u_h*	Gas/vapour velocity based on A_h*	ft/s
u_l	Liquid escape velocity based on A_{ap}	m/s
u_p	Gas/vapour velocity based on A_p	m/s
u_p*	Gas/vapour velocity based on A_p	ft/s
u_S	Superficial vapour velocity based on A_n	m/s
u_s^*	Superficial vapour velocity	ft/s
u_t	Droplet terminal velocity	m/s
u_t*	Droplet terminal velocity	ft/s
W'	Weeping rate	kg/s
W^*	Weeping rate	gpm
V_g	Gas volumetric flow rate	m^3/s
V_l	Liquid volumetric flow rate	m^3/s
V_L	Liquid volumetric flow rate	m^3/h

Nomenclature (Greek symbols)

Symbols	Definition	Units
α	Average liquid hold-up fraction	
ε	Bubbling area (A_c-$2A_d$)	m^2
ε_w	Gas hold-up in froth	
ξ	Orifice coefficient	
ξ_o	Orifice coefficient (as $A_f \rightarrow 0$)	
ρ_g	Gas density	kg/m^3
ρ_g^*	Gas density	lb/ft^3
ρ_l	Liquid density	kg/m^3
ρ_l^*	Gas density	lb/ft^3
σ	Liquid surface tension	mN/m
σ_l	Liquid surface tension	Dynes/cm
μ_g	Gas viscosity	mPa.s
μ_l	Liquid viscosity	mPa.s
ζ	Correction term	
η	Dispersion density	
η_e	Effective froth density	

Chapter 1 - Introduction

1.1 Background

Distillation is the most widely used separation method for the separation of liquid mixtures, by taking into account the differences in the volatilities of the various liquid to achieve separation. Distillation was first used in the Chou Dynasty (1040 to 256 BC) for the production of distilled liquors (Lockett, 1986). The distillation process was then further developed over time, where before 500 AD it was used for the production of mead in Britain and only in 1500 AD was used for the production of liquors such as whiskey in Scotland.

Even though distillation is still used for the production of alcoholic beverages, it has a great importance in other processes where liquid mixture separation is vital. Distillation is used in the pharmaceutical and petroleum industry, for the production of fuels such as petrol (or gasoline) and kerosene. The distillation process is the most dominant separation process in the chemical technology industry despite its inefficient use of energy (Olujić *et al.*, 2009).

In the distillation process the liquid mixtures are fed into the distillation column, where the component with the higher volatility separates from the liquid phase mixture into the vapour phase. The vapour flows out of the top of the distillation column and the liquid with the lower volatility remains in the liquid phase and escapes out of the distillation column through the column bottoms. There are alternative separation processes to the distillation process such as absorption, solvent extraction and membranes separation that are much more energy efficient than the distillation process but require a higher capital investment.

An adaptation of the distillation process is the absorption and stripping process, where the processes are used to purify a vapour mixture stream. The vapour mixture is fed to the absorption column and absorbed into absorbent liquid that selectively removes certain vapours from the vapour mixture stream. The stripping process is the inverse of the absorption process where a dissolved substance is selectively stripped from a liquid mixture by a vapour stream.

In order to understand the performance of the distillation process the hydrodynamics, thermodynamics and the mass of the transfer effects inside the column needs to be understood (Lockett, 1986). In this study, the hydrodynamic effects inside a sieve tray column were investigated at zero mass transfer, *i.e.* passing pure liquids and gases with different physical properties in counter-current manner to characterise phenomena such as entrainment and weeping with different sieve tray configurations. In the process industry it is generally believed that the hydrodynamics of the distillation process is well understood because of the popularity of the distillation process. This is false as can be seen by the following literature analysis which shows that the techniques used in the past to define the hydrodynamics were based on rudimentary equipment and experimental methods.

Hydrodynamics is the study of fluids in motion under the influence of internal and external forces. The hydrodynamics of a distillation column is investigated as to better define and understand the capacity limits and optimization limitations of a distillation column.

1.2 Distillation Column Configuration

In the distillation process there are generally two different configurations used for distilling liquid mixtures in industry. The first is packed column distillation and the other is tray distillation separation. The following two sections give a brief explanation of the two methods.

1.2.1 Packed Distillation Columns

Packed distillation columns are divided into two column configurations, namely as randomly packed columns and structured packed columns. In randomly packed columns, packing materials of specific geometric shapes are randomly packed into the distillation column. The purpose of the packing materials in the distillation column is to increase the surface area between the vapour and the liquid flowing inside the distillation column. Randomly packed columns are generally used for smaller diameter columns where corrosive materials are separated. In this instance the column is packed with plastic packing instead of metallic packing (Seader and Henley 1998).

In structured packing columns, the ordered packing increases the surface area between the vapour and the liquid mixtures. The column is packed with material to defined heights simulating stages in a tray distillation column. Structured packing was first developed between the 1950's and 1960's (Lamprecht *et al.*, 2010), where Panapak structured packing was first developed. Packed distillation is preferred over tray distillation when distillation is needed to be conducted with minimal pressure drop and a high liquid throughput (high capacity limits) is needed. In the use of liquid mixtures where foaming may occur, packed distillation is preferred over tray distillation columns (Uys *et al.*, 2009).

In the following discussion packed distillation columns will not be discussed any further and only the tray distillation process will be discussed.

1.2.2 Tray Distillation Columns

In tray distillation processes liquids are separated by the use of plates arranged to a possible height of over 90 m. Tray distillation columns are typically preferred over packed columns because of the ease in design and accurate prediction of the overall separation efficiency. Tray distillation columns are also significantly less expensive than packed distillation columns. In tray distillation the liquid mixture flows across the tray and is contacted by the vapour flowing upward through perforations of different tray types such as sieve, bubble-cap and valve trays, which are the most common tray types used in the separation process industry. Figure 1 shows the different tray types generally found in the industry.

In Figure 1 the sieve trays possess circular perforations, typically punched or laser cut where the liquid is contacted by the vapour flowing upward through the perforation either in the form of bubbles or as vapour jets. The sieve tray configurations has a lower capital cost and the hydrodynamics are much easier to define than the other tray perforation configurations. The typical sizes of the perforation in sieve tray distillation columns in the industry are between 3.2 and 25.4 mm. Sieve trays are also used over other forms of distillation tray types when the fluid contains a high amount of solid content (Shen Li, Song, Wu, Liu and Qian, 2008). In valve tray types the vapour flows upward and forces the valve open when the force below the valve is greater than that holding

it down by the liquid layer flowing above the valve tray surface. The valve tray design is typically used for columns with a lower turndown ratio and has a 5 to 10% higher capital cost than the sieve tray hole configuration (Lockett, 1986). The typical sizes of valve perforation diameters in the industry range from 38 to 51 mm (Uys *et al.*, 2009).

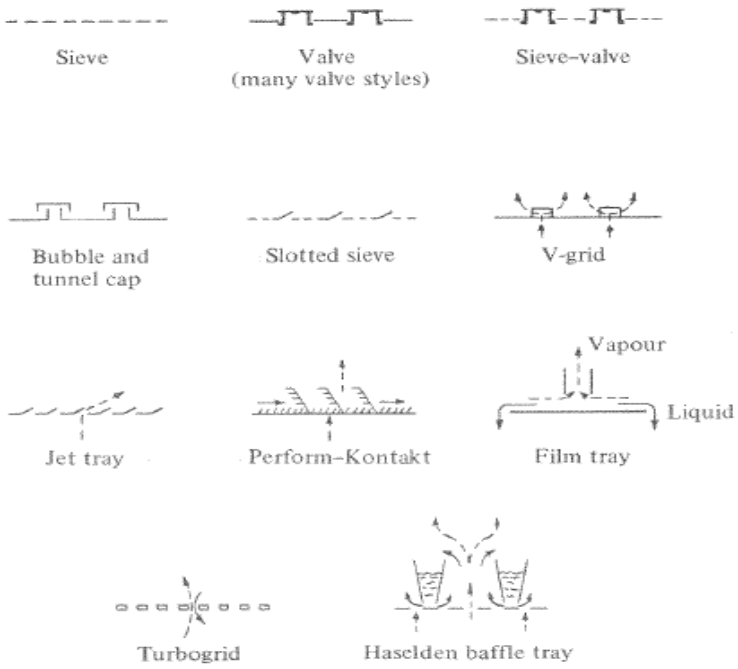

Figure 1 – Tray types [adapted with permission from Lockett (1986)].

The bubble-cap tray is the oldest distillation tray type used in tray distillation columns, where the gas flows upward through a cap, with fixed openings as shown in Figure 1. The typical diameter of the caps on the trays range from 76 to 152 mm, where the slots in the caps are typically rectangular or triangular shaped (Uys *et al.*, 2009). A bubble-cap tray is used in distillation columns for operations with extremely low turndown ratios and is of a comparatively higher cost than that of sieve and valve tray configurations. Sieve trays have low pressure drops across the tray, with valve trays having an intermediate pressure drop and bubble cap trays having the highest pressure drop (Seader and Henley, 2006). In comparing the separation efficiency between the three most significant tray types, sieve trays possess the lowest efficiency, with bubble-cap and valve trays having higher tray efficiencies (Seader and Henley, 2006). The other tray types shown in Figure 1 are adapted from the sieve, valve and bubble-cap trays and are only used in industry under special operating conditions.

Figure 2 shows a typical configuration of a sieve tray distillation column. The liquid then flows across the tray, makes contact with the vapour flowing through the sieve holes in the tray and reaches a certain height on the tray by the use of a weir which increases the liquid layer height on the tray. The liquid with the higher volatility is changed into a vapour phase and is separated from the liquid mixture of low volatility. It then flows upward through the distillation column. Once the liquid layer reaches a sufficient height, it flows off the weir and down the downcomer to the tray below.

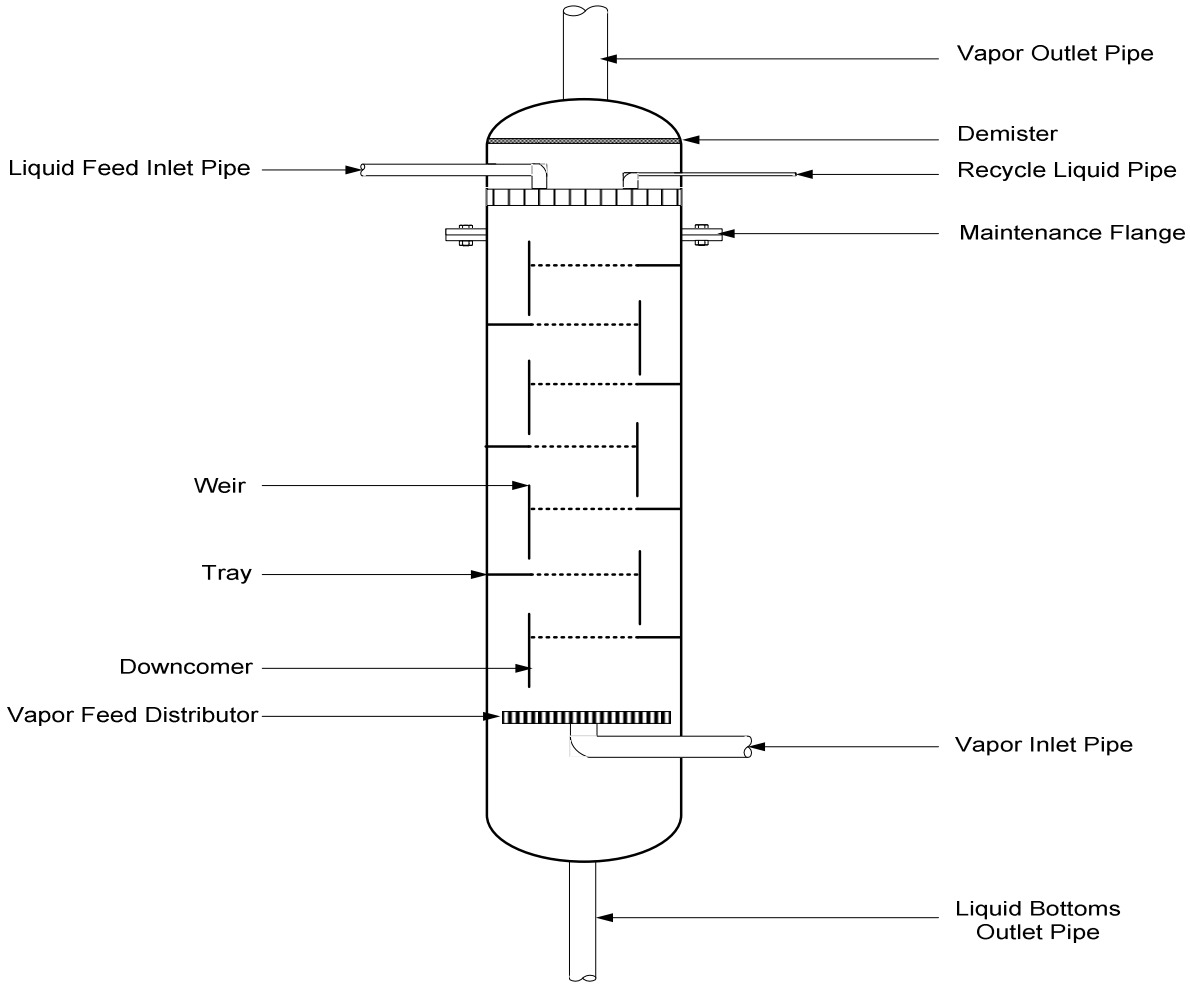

Figure 2 – Sieve tray distillation column configuration.

The entrainment of liquid occurs when the gas velocity upward through the tray in the column is sufficient to transport the liquid to the tray above. In the distillation process entrainment increases the fraction of low volatility components in the tops of the distillation columns, which reduces the overall separation efficiency of the distillation column. The entrainment process and entrainment models are further discussed in Section 2.5.1. In the distillation process weeping occurs when the liquid hold-up above the tray is high, so that liquid starts to seep (weep) through the pores of the tray. Weeping increases the fractional concentration of the high volatility component in the column bottoms. This decreases the overall efficiency of the distillation process. The weeping process and the column configuration that promotes weeping in a distillation column are further discussed in Section 2.5.2.

In sieve tray distillation columns, Keskinen, Ahlfors and Aittamaa (2006) state that the variables that can be adjusted on the distillation column are the downcomer clearance area, the sieve tray hole diameter, the fractional hole area, the gas flow rate, the liquid flow rate, the plate thickness, the number of holes, the outlet weir height and tray spacing. The responses that can be identified in a tray distillation column are entrainment, weeping, pressure drop across the trays, the vapour/liquid dispersions, the flow patterns, clear liquid height and froth height (Keskinen *et al.*, 2006). The overall

efficiency of the distillation column depends on the point efficiency, velocity profile, stripping factor, location and amount of weeping and entrainment and the random mixing of the vapour and liquid as defined by Bennett, Watson and Wiescinski (1997). By altering the parameters of a distillation process such as the distillation tray configuration (fractional hole area and hole diameter) and mixture properties, the separation efficiency inside a distillation column can be influenced significantly.

In an investigation performed by Bennett and Ludwig (1994), the validity of the use of air/water data in defining the responses for sieve tray distillation column systems is investigated. It is shown that air/water systems can accurately predict the dry tray pressure drop (h_d) and the clear liquid height (H_L) if the tray and column geometry is identical to the air/water test at the same liquid volumetric flow rate per weir length (Q_L) and density corrected superficial velocity (K_s) or capacity factor (C_s) as represented by Equation 1.2.2.1.

$$K_s = C_S = u_s\sqrt{\left(\frac{\rho_g}{\rho_l - \rho_g}\right)} \qquad [1.2.2.1]$$

The following is a guide to air/water testing on trays as obtained from Bennett and Ludwig (1994):

- Conduct a full scale test in which the tray geometry is kept constant.
- Ensure that the air flow rate yields the same corrected superficial velocity throughout.
- Maintain the same inlet vapour distribution and liquid volumetric flow rate.

In an investigation done by Bennett and Ludwig (1994), the air/water test is of high value for determining the froth height, pressure drop, tray flow patterns and liquid inventory. Air/water tests are of moderate value in the prediction of the froth-to-spray regime transition, modelling density corrected entrainment, predicting the onset of weeping and establishing an understanding of the hydraulic gradient over the tray. The air/water test is of little value in the study of mass transfer, studying the downcomer capacity, evaluating the quantity of weeping and modelling the hydraulic behaviour in the distillation column.

In defining the hydrodynamics behaviour in a distillation column, the most commonly used dimensionless numbers are the Bond (Bo), Froude (Fr) and the Weber (We) (Uys *et al.*, 2009). Models used to calculate responses such as column capacity, entrainment and weeping, typically incorporate dimensionless numbers.

The Bond number is defined by Equation 1.2.2.2, where it can be seen that the Bond number is the ratio of the gravitational forces acting on the fluid to the surface tension forces of the fluid flowing in the distillation column.

$$Bo = \frac{(\rho_l - \rho_g){D_H}^2 g}{\sigma} \qquad [1.2.2.2]$$

The Froude number is defined by Equation 1.2.2.3, where it can be seen that the Froude number is the ratio of the inertial forces to the gravitational forces acting on the fluid (speed over length ratio) (Uys *et al.*, 2009).

$$Fr = \frac{u_{D0}^2}{gH_F} \; or \; Fr = \frac{u_b}{\sqrt{gH_L}} \qquad [1.2.2.3]$$

The Weber number is defined by Equation 1.2.2.4, where it can be seen that the Weber number is the ratio between the inertial forces to surface tension forces of the fluid. The Weber number is used in multiphase flow to describe the behaviour of thin films and the tendency for the formation of bubbles and droplets.

$$We = \frac{\rho_g u_s Q_L}{3.6\sigma} \qquad [1.2.2.4]$$

The hydrodynamics of sieve distillation columns will be further investigated in the following sections and other tray types will not be discussed further.

Bennett, Watson and Wiescinski (1997) identifies the following important dimensionless numbers used to characterize the hydrodynamics of the sieve tray distillation column:

- Reynolds number based on the hole velocity in the sieve plate.
- Effective froth density.
- Fractional hole area.
- Ratio of clear liquid height to the hole diameter.

[It should be noted that the distillation separation technique is not generally used when liquids have to be separated that contain similar volatilities, the compounds that need to be separated are thermally unstable, the liquid mixtures are corrosive or produce fouling and the mixture contains components of lower volatility (Lamprecht *et al.*, 2010).]

1.3 Project Rationale

In the process industry it is generally believed that the hydrodynamics of the distillation process is well defined because of the popularity of the distillation process. However, this is false, based on the following literature analysis (Chapter 2) which shows that the sieve tray distillation hydrodynamics (entrainment and weeping) trends and models are based on imperfect experimental methods, equipment and simplified distillation parameter limits.

The current project acts as a continuation in the understanding and experimental investigation performed by (Uys, 2012), where the effect of sieve tray geometry was not investigated. In this study the effect of the fractional hole area, sieve tray hole diameter and fluid physical properties on entrainment and weeping was investigated. The chimney tray was used to capture the weeping liquid and a de-entrainment tray and a mist eliminator pad was used to capture the entrained liquid. The (Uys, 2012) investigation did not evaluate the effect of tray geometry on the weeping, thus a clear undestanding of the hydrodynamics inside the distillation column has to be produced. The fractional hole areas that will be investigated are 7, 11 and 15% and the hole diameters are ⅛, ¼ and ½ in. size holes. The liquids that are used in the experimental investigation are ethylene glycol, water, silicone-oil and butanol and the gases are air and carbon dioxide (CO_2). In the investigation thermally stable fluids are used to ensure that the hydrodynamics can be tested under zero mass transfer.

This study presents entrainment, weeping and pressure drop data over a wide range of fluid properties, tray geometries and fluid flow rates. This aids in the understanding of not just the effect of a single parameter, but also the impact of the interactions between the different parameters on entrainment and weeping. It expands on the knowledge of the effect of weeping and the causes of

weeping. The investigation also aids in the development of a clear understanding of future experimental investigations that have to be performed to define and model the sieve tray entrainment and weeping completely.

1.4 Objectives

The aim of this project is to evaluate the effect of liquid and gas physical properties and tray geometry on entrainment and weeping. The objectives are:

- Conduct a literature investigation into sieve tray distillation.
- Manufacture sieve tray distillation trays, that will allow the experimental investigation into changing hole diameter and fractional hole area.
- Evaluate the effect of fluid flow rate on entrainment and weeping.
- Evaluate the effect of dispersion regime state (shape, size and dynamics) on entrainment and weeping.
- Evaluate the effect of liquid properties on entrainment and weeping, by changing the liquid surface tension, liquid viscosity and liquid density.
- Evaluate the effect of gas properties on entrainment and weeping, by changing the gas viscosity and gas density.

Chapter 2 – Literature Review

2.1 Flow Regimes

In sieve tray distillation, the flow of fluid above the tray is defined by different flow regimes, which depend on the vapour flow rates, fluid physical properties and the configuration geometry of the column. The column configuration aspects that affect the flow dynamics on the tray are the shape of the column (circular or rectangular), column size, hole diameter, fractional hole area, downcomer area, weir height, weir design, calming zone length, tray spacing, sieve tray hole pitch and tray thickness. The fluid properties that affect the hydrodynamics in the sieve tray distillation column are the gas/vapour and liquid density, surface tension and viscosity. The degree of influence of the column configuration and fluid physical properties are diverse in the different flow regimes.

The different flow regimes that occur in the sieve distillation columns are the spray regime, froth (mixed bubbling) regime, emulsion regime, bubble (free bubbling) regime and the foam regime. Figure 3 shows the different flow regime dispersions as defined by Lockett (1986). In the spray regime, the gas phase is continuous and is characterized by gas jetting through the flowing liquid. The jetting of gas produces a high amount of liquid drops being projected upward by the gas/vapour. The liquid is projected to the tray above if the upward drop velocity is positive, which produces entrainment or falls back onto the tray when the upward drop velocity is less than the upward gas/vapour superficial velocity. The spray regime is favoured by high gas momentum and low liquid depths, and perceived as an inverted rainstorm (Lockett, 1986). In the spray regime, if the gas upward velocity is high and the liquid flow rate is low, flooding could occur in the distillation column, as more liquid can accumulate on the tray above due to the liquid entrainment during these conditions.

In the froth, emulsion, bubble and foam regime the liquid phase is continuous across the sieve tray. In the froth (mixed bubbling) regime, the gas passes through the liquid as ill-defined gas bubbles of rapidly changing shape (Lockett, 1986). Bubble sizes vary over a wide range in the froth regime. The froth regime is bounded by the spray regime at high gas velocities and the bubble (free bubbling) regime which occurs at low gas velocities (Lockett, 1986). To completely define the froth structure in the froth regime, Lockett (1986) describes that the bubble size distribution, bubble rise velocity distribution, height and diameter of the jet protruding out of the liquid layer and proportion of gas passing through froth as jets should be known.

In the emulsion regime, gas bubbles rising through the sieve tray are coalesced by the horizontal flow of the liquid on the tray. The emulsion regime is typically produced during high liquid momentum across the tray. The emulsion regime has adverse effects on the tray behaviour in the distillation column. The emulsion regime produces choking at the mouth of the downcomer, high sensitivity to foaming, premature downcomer flooding, vapour entrainment and a reduction in separation efficiency (Lockett, 1986).

The bubble (free bubbling) regime is defined as a regime in which gas/vapour passes through a motionless liquid phase as well defined gas/vapour bubbles, with a nearly constant bubble size distribution. The bubble regime only occurs at low gas velocities, since high gas velocity produce ill-

defined bubbles (froth regime). In the foam regime, bubble coalescence is hindered by the surface tension forces of the bubbles. In the foam regime, cellular foam is produced that is composed of dodecahedral bubbles. The foam regime occurs at low gas and liquid momentums in aqueous systems with columns that possess small diameters (Lockett, 1986).

Fluid systems are defined as surface tension positive systems, when the liquid surface tension increases as the liquid proceeds down the distillation column. Fluid systems are surface tension negative, when the surface tension decreases as the liquid proceeds down the distillation column and surface tension neutral, when the surface tension remains relatively constant as the liquid proceeds down the distillation column. Surface tension positive always produce foam, whereas surface tension negative and neutral never produce foaming systems (Lockett, 1986). Antifoaming agents are often used in the industry to prevent foaming, but the use of it leads to the contamination of the liquid mixture (increasing production cost).

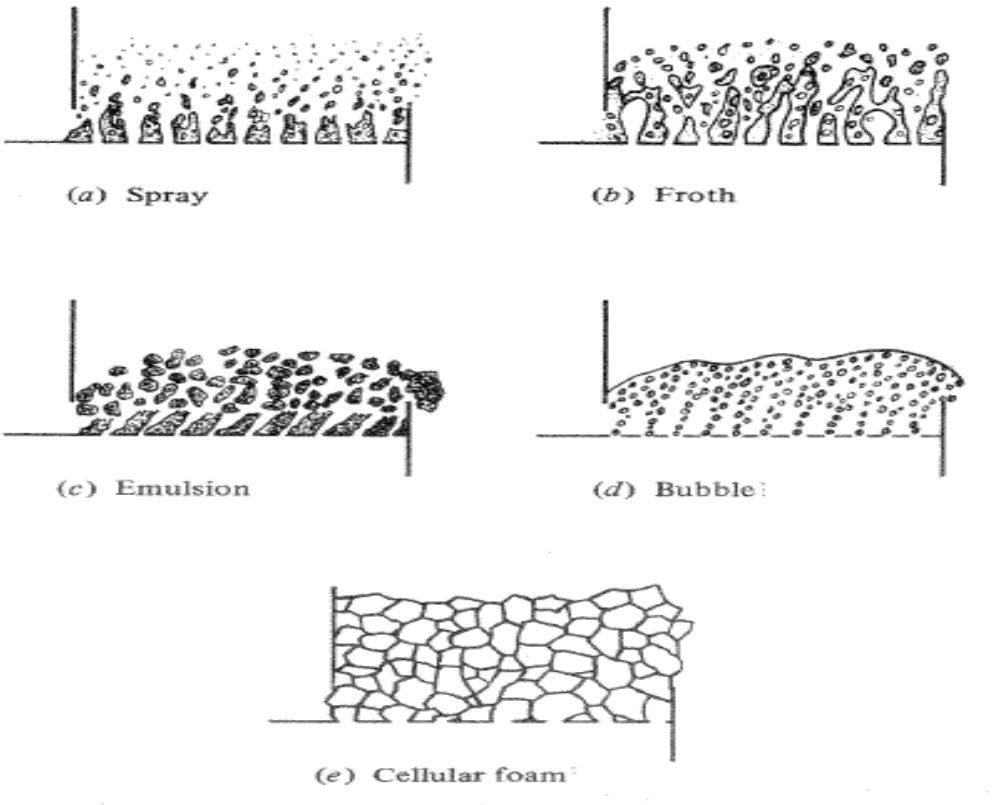

Figure 3 – Flow regimes in sieve tray distillation [obtained with permission from Lockett (1986)].

The flow regime boundary limits are shown in Figure 4, as obtained from Hofhuis and Zuiderweg (1979). The figure shows the upper flooding and lower weeping limits in tray distillation columns. It can be seen from the figure that liquids with high density have larger capacity limits than that of lower densities.

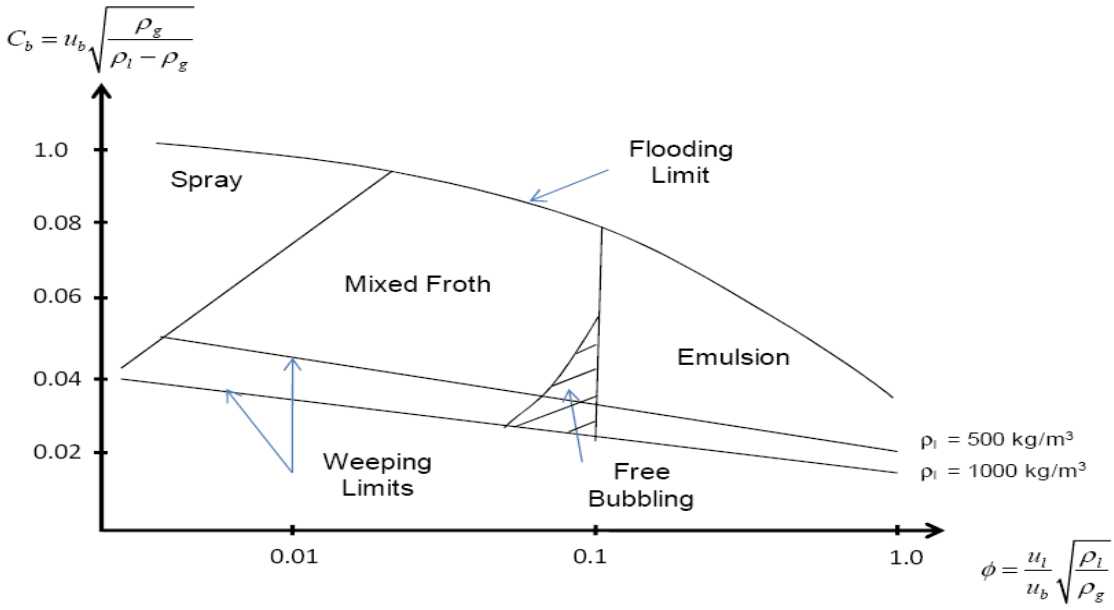

Figure 4 – Flow regime limits [redrawn from Hofhuis and Zuiderweg (1979)].

Raper, Kearney, Burgess and Fell (1981) investigated the structure of froth dispersion in a sieve tray distillation column by using a bubble size velocity measurement probe and gamma-ray densitometry. The experimental investigation showed that with low fractional hole area and large hole diameter trays, the liquid fraction in the dispersion is large for a certain height, then rapidly decreases. The mean bubble diameter and the bubble interfacial area increases with increasing hole diameter and tray fractional hole area. The investigation showed that in the froth regime gas flows through the sieve tray holes as intermittent jets, since the predicted hole gas velocity is substantially lower than actual measured gas velocity.

In an investigation performed by Van Sinderen, Wijn and Zanting (2003), the hydrodynamics of the dispersion above the tray is described by two models, a low liquid height regime and a high liquid height regime. In the low liquid height regime, the configuration is defined in terms of a two phase model and in the high liquid height regime the configuration is described in terms of a three phase model. In the two phase model, the bottom layer consists of a liquid continuous dispersion layer, a bubbling regime and the top layer a gas continuous regime (spray-like). In the low liquid height regime, entrainment is described as decreasing with increasing liquid height and entrainment depends strongly on the column configuration (tray and column characteristics).

In the regime transition described by Van Sinderen *et al.* (2003), a third layer forms in between the spray-like and bubbling layers. The high liquid height regime consist of three phase layers, where entrainment increases with increasing liquid height above the tray and is less dependent on the column configuration than in the two phase regime.

A computational fluid dynamic (CFD) investigation were performed by Rahimi, Sotoodeh and Bahramifar (2012) to determine the effect of tray geometry on tray efficiency, where it was found that the flow pattern on a sieve tray for small sieve tray holes were close to plug flow, leading to an increase in the mass transfer efficiency.

2.2 Dispersion Layer and Clear Liquid

In the current section, the dispersion in the froth and spray regime in terms of dispersion height, dispersion density and clear liquid height will be investigated. The clear liquid height is one of the most important variables in hydraulic calculations as it appears in nearly every hydraulic equation. The clear liquid height is the height of clear liquid continuous phase below the dispersion. The height of clear liquid is determined by the use of vertical hold-up profiles [height above tray floor versus volume fraction of liquid in the dispersion (α)], which is tedious, thus models have been developed in order to predict the clear liquid height.

Lockett (1986) defined the clear liquid height as being related to the readings on the manometer that is placed across a tray. In another study, Uys (2012) defined the clear liquid height as the height of the liquid that remains above the tray under zero gas flow through the tray assuming no dumping (100% of liquid weeping) occurs. The equation used by Lockett (1986) developed from a vertical momentum balance between the dispersion and the liquid on the surface of the tray is shown by Equation 2.2.1. In Equation 2.2.1, 'H_M' represents the head reading on the manometer and 'r_m' is the radius of the manometer tube.

$$H_L = H_M + \frac{u_s \rho_g (u_h - u_s)}{\rho_l g} - \frac{2\sigma}{\rho_l g r_m} \qquad [2.2.1]$$

The clear liquid height when measured at the centre of a sieve tray is generally smaller than the average clear liquid height measured over the tray. It was shown by Lockett (1986) that care has to be taken when clear liquid heights are measured in small columns, because of the wall effects which produce circulation flow on the tray.

The Francis weir equation was used to predict the flow of the froth over the weir and is represented by Equation 2.2.2 (Lockett, 1986). The Francis weir equation is used in many models to predict the clear liquid height, which is presented later in the text.

$$H_{ow} = \frac{1.04}{C_D^{0.67} g^{0.33}} \left(\frac{Q_L}{(1-\varepsilon_w) l} \right)^{0.67} \qquad [2.2.2]$$

The assumptions made in the Francis weir equation are (Colwell, 1981):

- The liquid flows uniformly across the weir length.
- The froth layer exists as a uniform and continuous layer above the tray.
- There is no obstruction to the free flow of the froth over the weir.
- Retention time is characteristic of the fluid flow over the weir.

In an investigation done by Wijn (1999), it was stated that the weir height contributes to the height of the liquid on the tray and is an important parameter in distillation columns. Liquid height on the tray has an influence on the tray efficiency, pressure drop flow regime and the upper and lower capacity limit of a distillation column. In the spray regime, Wijn (1999) considered droplets to be projected in a random fashion with a wide range of droplet sizes and velocities. In the froth regime, it was thought that there are two regions, a lower region containing heterogeneous bubbling and an upper region containing spray regime-like behaviour.

The velocity of the liquid over the weir was considered to be influenced by three mechanisms, the flow of the liquid over the weir as a uniform flow (using the Francis weir equation), the stochastic splashing in the spray regime of the liquid over the weir and the stochastic displacement packets of liquid over the weir in the froth regime. If the liquid flow over the weir is as a clear liquid, Equation 2.2.3 is used to determine the velocity of the liquid flowing over the weir.

$$u_{lw} = \frac{\left[\frac{g\left(\frac{Q_L}{l}\right)}{\varepsilon_W}\right]^{\frac{1}{3}}}{1.43} \qquad [2.2.3]$$

If the liquid is considered to be flowing over the weir as splashing droplets (spray regime), then the velocity of the liquid flow over the weir is equal to the variance in the horizontal velocity distribution. In splashing droplets flow, the height of the liquid flowing over the weir is half the height of the liquid at the centre of the tray (Wijn, 1999). If the liquid is considered to flow over the weir as packets splashing (froth regime), the bubbles displace liquid of equal volume in all directions and the velocity of the liquid flowing over the weir is between 0.5 and 1 m/s (Wijn, 1999).

The first model presented to predict the clear liquid height is that by Colwell (1981). It was stated that the clear liquid height is useful in the prediction of pressure drop, efficiency and residence time of fluid in a sieve tray column. In the determination of the model validity, experiments were performed on a rectangular tray so that there is uniform flow over the weir as defined in the Francis weir equation. The Francis weir equation was adapted by Colwell (1981) and used to relate the froth height to the flow of the froth over the tray.

The relationship between the clear liquid height and the froth height is shown by Equation 2.2.4 (Colwell, 1981). Equation 2.2.5 predicts the clear liquid height when the Francis weir equation is assumed to apply. In Equation 2.2.5, 'C_d' represents the weir coefficient.

$$\alpha = \frac{H_L}{H_F} \qquad [2.2.4]$$

$$H_L = \alpha H_{ow} + 7.3\left(\frac{\alpha^{\frac{1}{2}} Q_L}{C_d l}\right)^{\frac{2}{3}} \qquad [2.2.5]$$

$$\alpha = \frac{1}{\eta+1} \qquad [2.2.6]$$

$$\eta = 12.6 F_r^{0.4}\left(\frac{A_c}{A_b}\right)^{-0.25} \qquad [2.2.7]$$

If Equation 2.2.5 is used for circular columns, the equation has to be corrected for the contraction of the liquid occurring at the weir, especially in smaller columns. In the investigation presented by Colwell (1981), it was defined that it is more correct to consider the liquid flowing over the weir as froth rather than clear liquid, when the weir is high.

In the development of the froth density and the clear liquid height by Colwell (1981), the Froude number was adapted to include the vapour and liquid density and is shown by Equation 2.2.8. The clear liquid height in a large commercial column bottom tray is lower than those at the top trays, because of the decreasing liquid flow rates which may be caused by entrainment (Faesan, 1987).

$$Fr^* = \frac{\rho_g u_b^2}{g\left(\frac{H_L}{1000}\right)(\rho_l - \rho_g)} \quad [2.2.8]$$

In the development of equations for the clear liquid height and froth density (Colwell, 1981), it was assumed that when calming zones are used, the liquid flows over the weir as an un-aerated clear liquid. The pressure drop across the sieve tray also increases with increasing calming zone length. The clear liquid height can be determined when a calming zone is used by Equation 2.2.9 (Colwell, 1981). Wijn (1999) showed that when a distillation column contains a large calming zone, the pressure drop, weeping, clear liquid height and the dispersion height increases.

$$\left(\frac{H_L}{H_{Lcz}}\right)^2 = \alpha - \frac{2Q_L^2\alpha}{l^2 H_{Lcz}^2 g}\left(\frac{1}{H_L} - \frac{1}{H_{Lcz}}\right) x\ 10^3 \quad [2.2.9]$$

In the event that splash baffles are used in the sieve tray distillation column, Equation 2.2.10 is used, where 'H_{da}' is the head loss under the baffle (Colwell, 1981). In Equation 2.2.10, 'k' is equal to 1, when the area between the splash baffle and the outlet weir is greater than the area between the splash baffle and the tray deck. Otherwise it is equal to 2.

$$H_L = H_{wo} + \left(\frac{Q_L}{C_d l}\right)^{\frac{2}{3}} + kH_{da} \quad [2.2.10]$$

$$H_{da} = 0.000165\left(\frac{Q_L}{A_{da}}\right)^2 \quad [2.2.11]$$

The model for the clear liquid height presented by Colwell (1981) applies only to the froth regime but does not account for the droplet projection in this regime, which is addressed by Stichlmair (1978) in Equation 2.2.12. In Equation 2.2.12, the weir coefficient (C_d) has a value of 0.61.

$$H_L = (1 - \varepsilon_w)\left(H_{wo} + \frac{0.49}{C_d^{0.67}}\left(\frac{Q_L}{(1-\varepsilon_w)l}\right)^{0.67} + \frac{125(u_s - u_b)^2\rho_g}{g(\rho_l - \rho_g)\varepsilon_w^2}\right) \quad [2.2.12]$$

A clear liquid height model developed by Jacimovic and Genic (2000) is presented by Equation 2.2.13. In Equation 2.2.13 and 2.2.14, 'F_{lg}' represents the two phase kinetic F-factor.

$$H_L = (0.04 + 0.9\ H_{wo})\sqrt{F_{lg}} \quad [2.2.13]$$

$$F_{lg} = \frac{L}{G}\sqrt{\frac{\rho_l}{\rho_g}} \quad [2.2.14]$$

In the evaluation of the effects of the drop projection in both the froth and the spray regime, Hofhuis and Zuiderweg (1979) has proposed the following model for the clear liquid flow over the weir, represented by Equation 2.2.15.

$$H_L = 0.26\psi^{-0.37}\left(\frac{Q_L}{l}\right)^{0.67} \quad [2.2.15]$$

$$\psi = \frac{Q_L}{l u_s}\left(\frac{\rho_L}{\rho_g}\right)^{\frac{1}{2}} \quad [2.2.16]$$

In an investigation performed by Zuiderweg (1982) into the hydrodynamics of sieve trays, Equations 2.2.17 and 2.2.18 were used in order to describe the clear liquid height above the sieve tray.

$$H_L = 0.6 H_{wo}^{0.5} P_t^{0.25} \left(\frac{FPA_b}{l}\right)^{0.25} \quad (25\ \text{mm} < h_{wo} < 100\ \text{mm}) \qquad [2.2.17]$$

$$FP = \frac{L}{G}\sqrt{\frac{\rho_g}{\rho_l}} \qquad [2.2.18]$$

Kister, Pinczewski and Fell (1981) showed that the liquid-hold-up on the tray is constant with increasing gas rate, but depends strongly on the hole diameter and fractional hole area. In the determination of which clear liquid height equation to use, Lockett (1986) showed that the clear liquid height equation by (Colwell, 1981) represents typical fluid systems the best, especially when the column contains a long calming zone and splash baffles.

In the vapour/liquid dispersion layer above the tray in the spray and froth regime, the dispersion layer density changes with increasing height above the tray due to the change in the fraction of liquid above the tray. Hunt, Hanson and Wilke (1955) showed that when the liquid head is varied while keeping the tray spacing constant, the dispersion density changes between ⅓ to ½ of the clear liquid density. Many models have been developed in order to predict the change in the dispersion layer density (η) such as that produced by Colwell (1981) in Equation 2.2.7.

Pinczewski and Fell (1974) investigated the nature of the dispersion layer and showed that:

- The higher the gas velocity, the greater the amount of liquid is held in the upper portion of the dispersion layer, when keeping the liquid flow rate constant.
- The dispersion layer density is shown to increase at all levels except close to the tray floor, when keeping the gas rate constant and increasing the liquid load.
- In large hole diameter sieve trays, the dispersion layer density is lower at the holes than it is in between them. In the level close to the tray floor the dispersion layer density is mainly impacted by the orifice action.
- At high tray heights, the dispersion density is homogeneous across the tray.
- At constant gas velocities, large sieve tray hole diameters produces a higher liquid hold-up on the tray.
- A small decrease in the liquid hold-up is observed when the gas velocity is increased at constant liquid flow rate.

In a study done on the droplet size distribution in the spray regime by Pinczewski and Fell (1977), the size distribution of the droplets was determined by the use of a photographic (visual) and an electronic technique. The photographic technique gives an indication of the spatial distribution of the droplets and the electronic technique gives an indication of temporal distribution of the liquid drops.

It was shown that the droplet size distribution depends strongly on the hole gas velocity and weakly on the fractional hole area, hole diameter and liquid flow rate. In industrial size columns, droplet atomization takes place as high as 20 to 60 mm above the tray. Droplet capturing techniques were ineffective in determining the droplet size distribution because of droplet splatter (Pinczewski and Fell, 1977). The equation used to determine the effect of the hole gas velocity on the mean droplet size (D_{32}) is 2.2.19.

$$D_{32} = \frac{31500}{u_h^{0.94}} \qquad [2.2.19]$$

Chen, Chuang, Chien and Ye (1992) showed that bubble diameter increases and distillation column separation efficiency decreases with increasing liquid surface tension. If calming zones are used in distillation columns, distance is allowed for the droplets that are sprayed to be returned to the tray. In a study by Wijn (1999) it was found that the height of the liquid increases as the weir height, liquid flow and gas flow rate all increase.

The number of droplets formed in a distillation column was shown to decrease with increasing liquid viscosity, which also leads to a decrease in the separation efficiency of the distillation column as described by Mahiout and Vogelpohl (1984). In an investigation performed by Decent *et al.* (2009) into the stability of spiralling jets using viscous systems, it was found that viscosity has a non-monotonic relationship with the break up length of the spiralling gas jet. The break-up length is the distance between the onset of the jet and the point at which droplets develop. In the study there was also a non-monotonic relationship between the droplet size and viscosity, showing that viscosity plays a significant role in the spray regime at least.

The factors affecting bubble size distribution was investigated by Hu, Yang and Hewitt (2007), where it was shown that gas flow rate, weir height and sieve tray hole size has a significant effect on the bubble size distribution in the dispersion whereas the liquid flow rate has an insignificant effect. In the experimental measurement performed it was proven that bubble coalescence occurs in the dispersion, since the bubble size increase with increasing height above the tray.

Pan and Hung (2010) investigated the impact of a liquid droplet with a wet surface and showed that droplets with a high viscosity are less susceptible to droplet break-up upon impact and are generally more stable, whereas surface tension has the opposite effect. In another study performed by Fakhari and Rahimian (2010) it was shown that liquid viscosity is the principle factor in droplet disintegration, whereas gas viscosity has a trivial effect on the droplet disintegration.

In an experimental investigation performed by Uys *et al.* (2012), Figure 5 was produced, which showed the change in the dispersion profiles inside a rectangular sieve tray, where the profiles were determined by visual observations. In Figure 5(a), the liquid rate is increased at a constant superficial gas velocity from Profiles 1 to 5. It is first observed that the liquid dispersion height increases with increasing liquid rate (Profiles 1 to 2). At Profile 2, a high pressure area is produced at the outlet weir which produces weeping near the weir, increasing the velocity through the sieve tray hole and ultimately increasing the dispersion height. The liquid flow rate is increased (Profiles 2 to 3), where the high pressure area moves to the downcomer, reducing the dispersion height [Fig. 5(a)]. The liquid rate is increased further (Profiles 3 to 4) at which a choking effect is produced in the downcomer, limiting the flow of liquid into the downcomer. The liquid rate increases from Profiles 4 to 5, where the dispersion height increases due to the choke flow in the downcomer. In Figure 5(b), the gas rate is increased at a constant liquid flow rate (Profiles a to b). The dispersion height increases with increasing gas rate. Uys *et al.* (2012) stated that entrainment is at a maximum when the froth dispersion has a parabolic shape.

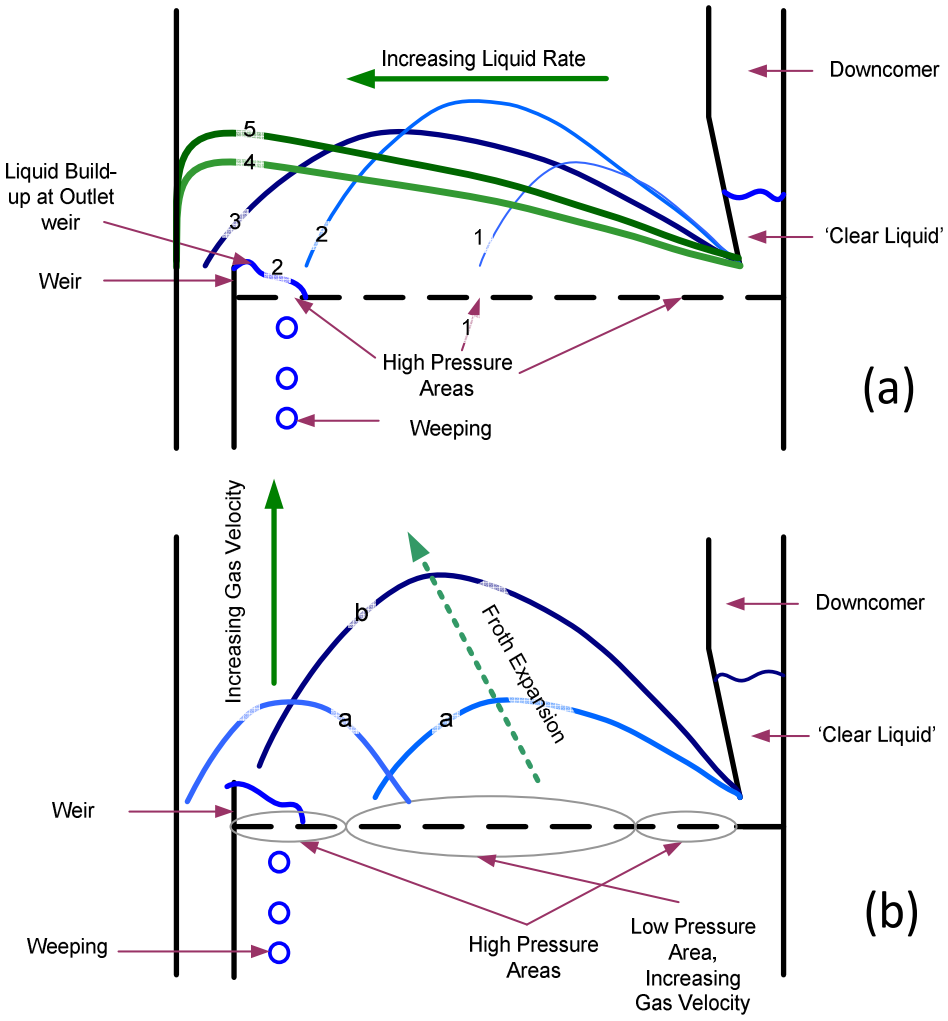

Figure 5 – Dispersion changes in a sieve tray column (a) with increasing liquid rate 1 to 5 (b) with increasing gas flow rates [obtained with permission from Uys *et al.* (2012)].

2.3 Pressure Drop

In the operation of the sieve tray distillation column, there is a drop in the pressure as the gas/vapour flows upward through the column. The pressure change in the liquid mixture as it flows down the column is of little concern as the liquid is transported by gravity. However, the drop in pressure by the gas/vapour across the tray is of great concern in the construction of a distillation column, as can be expected when considering that the operating cost of the tray distillation column increases with the increase in the pressure drop across the column.

The pressure drop in the sieve tray is significantly less than in valve and bubble-cap trays. It can be realized that when the hole diameter decreases on a sieve tray, with a constant fractional hole area, that the pressure drop across the tray increases, because of the greater contraction at the holes (Thomas and Ogboja, 1978). In the determination of the pressure drop across the plate, the pressure on dry plates is lower than when the column is wet, because of the increased resistance of the liquid phase. In Figure 6, the tray is wet and the pressure drop across the tray is represented by Equation 2.3.1 (Lockett, 1986). In the equation, 'ΔP_{13}^{w}' represents the pressure drop from region 1 to 3 when the tray is wet, where it is shown that the total pressure is the sum of the pressure drop from

regions 1 to 2 and 2 to 3. The dry tray pressure drop relation is shown by Equation 2.3.2 (Lockett, 1986).

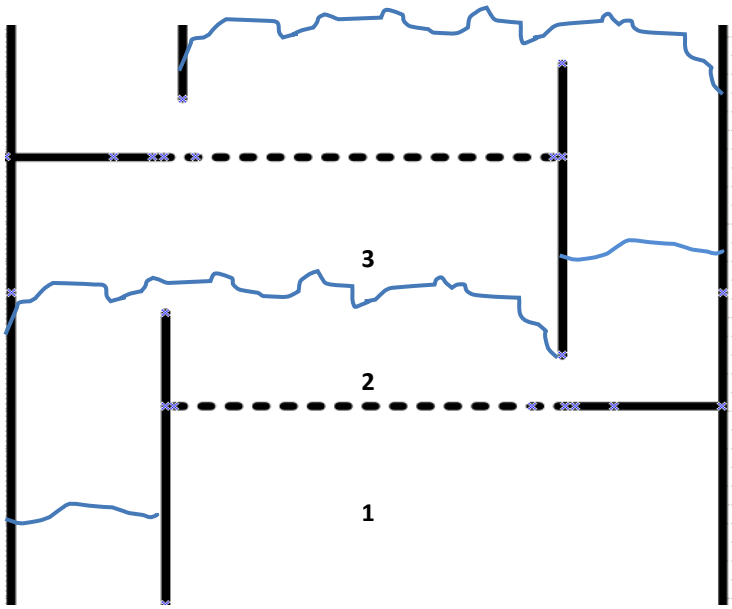

Figure 6 – Region pressure diagram as used by Lockett (1986).

$$\Delta P_{13}^{w} = \Delta P_{12}^{w} + \Delta P_{23}^{w} \quad [2.3.1]$$

$$\Delta P_{13}^{d} = \Delta P_{12}^{d} + \Delta P_{23}^{d} \quad [2.3.2]$$

The determination of the wet tray pressure drop for region 1 to 2 is represented by Equation 2.3.3. In the equation 'ΔP_{R1}' represent the pressure drop that occurs due to the surface tension forces that affect the flow of gas/vapour through the sieve tray holes (Lockett, 1986).

$$\Delta P_{12}^{w} = \Delta P_{12}^{d} + \Delta P_{R1} \quad [2.3.3]$$

The determination of the wet tray pressure drop for the regions 2 to 3 is represented by Equation 2.3.4 (Lockett, 1986). In the equation, the first term accounts for the static pressure drop and the second accounts for the dynamic pressure drop, where 'ΔP_{R2}' represent the pressure drop that is accounted for by pressure variations near the tray floor.

$$\Delta P_{23}^{w} = H_L \rho_l g - u_s \rho_g (u_h - u_s) + \Delta P_{R2} \quad [2.3.4]$$

The dry plate pressure drop for the regions 2 to 3 is represented by Equation 2.3.5 (Lockett, 1986), where 'ΔP_{R3}' is the pressure drop accounted for by liquid dispersion resistance.

$$-\Delta P_{23}^{d} = u_s \rho_g (u_h - u_s) + \Delta P_{R3} \quad [2.3.5]$$

The total pressure drop (wet) across the trays in the distillation column is represented by Equation 2.3.6, where 'ΔP_R' is the sum of 'ΔP_{R1}', 'ΔP_{R2}' and 'ΔP_{R3}' and is termed the residual pressure drop.

$$\Delta P_{13}^{w} = \Delta P_{13}^{d} + H_L \rho_l g + \Delta P_R \quad [2.3.6]$$

If Equation 2.3.6 is written in terms of the liquid head pressure drop, then Equation 2.3.7 is produced which is the basic form used in many literature sources (Lockett, 1986).

$$H_t = H_d + H_L + H_R \qquad [2.3.7]$$

In an investigation performed by Lemieux and Scotti (1969), it was found that the pressure drop affects the tray capacity and that the total tray pressure drop is independent of the spacing of the holes. It was also shown that at high hole diameters, the pressure drop is nearly independent of the liquid rate at high gas rates, since the dry plate pressure drop has a great effect on the total pressure drop. In the investigation done by Lemieux and Scotti (1969), the fractional hole area was changed by blanketing coordinated holes on the tray (sealing holes on the tray), which questions the validity of the findings.

In most literature it is usual practice to represent the dry tray pressure drop (H_d) in terms of an orifice type equation. Therefore, the orifice coefficient is a very important variable that has to be calculated. The orifice coefficient is a relative measure of the efficiency by which an orifice can let fluid through. The dry orifice coefficient is independent of the plate thickness, drilling pattern and the hole size (Mayfield, Church, Green, Lee and Rasmussen, 1952). The dry tray pressure drop decreases as the hole size decreases for a constant fractional hole area tray, which is opposite to the effect that would occur if total tray pressure drop is measured (Lockett, 1986). The dry tray pressure drop equation in the form of the orifice coefficient is presented by Lockett in Equation 2.3.8 (1986).

$$H_d = \frac{\xi \rho_g u_h^2}{2g\rho_l} \qquad [2.3.8]$$

In a hydraulic investigation performed by Faesan (1987), pressure drop equations were developed for a 0.63 m inner diameter column, where the dry tray pressure drop was used in the development of other pressure drop equations in this study is presented by Equation 2.3.9.

$$\Delta P_d = 0.187 \frac{u_h^2 \rho_g}{\xi^2 \rho_l} \qquad [2.3.9]$$

In a study by Hunt *et al.* (1955), the pressure drop through a single hole is determined for a 6 in. diameter column. The dry pressure drop equation is correlated in terms of an orifice equation, since the plate thickness to perforation diameter was greater than 0.9 and represented by Equation 2.3.10.

$$H_{d(single\ hole)} = \frac{U_h}{2g_o}\left[0.4\left(1.25 + \frac{A_h}{A_c}\right) + \left(1 - \frac{A_h}{A_c}\right)^2\right] \qquad [2.3.10]$$

The total pressure drop used by Faesan (1987) is shown by Equation 2.3.11. It was found that the total pressure drop increases with increasing gas velocity.

$$\Delta P_t = 0.187 \frac{u_h^2 \rho_g}{\xi^2 \rho_l} + H_L + \frac{32.1}{\rho_l} \qquad [2.3.11]$$

The total head loss (pressure drop) equation as determined by Thomas and Ogboja (1978) is shown by Equations 2.3.12 and 2.3.13.

$$H_T = 0.024L'' + 0.2F^{*2} + 3.66 \qquad \text{for rectangular columns} \qquad [2.3.12]$$

$$H_T = 0.038L'' + 0.533F^{*2} + 2 \qquad \text{for round columns} \qquad [2.3.13]$$

Lockett (1986) presented Equation 2.3.14, to determine the effect that entrainment has on the dry tray pressure drop. In the equation, entrainment (E or L'/G) is written in terms of the amount of liquid entrained divided by the vapour flow rate.

$$H_d = (H_d)_{E=0}\left(1 + \frac{E\rho_g}{\rho_l}\right)(1 + E) \qquad [2.3.14]$$

The residual pressure (H_R) is determined by Equation 2.3.7, by subtracting the clear liquid height (H_L) and the dry tray pressure drop from the total wet tray pressure drop (H_T). The residual pressure drop is a useful parameter that aids in identifying the froth-to-spray transition point. A model has been developed by Bennett, Agawal and Cook (1983) to describe the residual pressure drop by Equation 2.3.15, where 'b' was determined experimentally (air/water system b equals 1.27).

$$H_R = \frac{6}{b\rho_l}\left(\frac{\sigma}{g}\right)^{0.67}\left(\frac{\rho_l - \rho_g}{D_h}\right)^{0.33} \qquad [2.3.15]$$

Hunt *et al.* (1955) showed that residual pressure drop in a sieve tray increases with increasing gas velocity through the column and with decreasing sieve tray hole diameter. Thomas and Ogboja (1978) stated that the residual pressure drop for round columns is much greater than that for rectangular columns with the same cross-sectional area.

2.4 Flow Regime Transition

In industry distillation columns are typically run in the spray and the froth regimes, because of the high fluid flow rates that need to be separated. Understanding the regime in which the distillation column is operated is vitally important in understanding the hydrodynamics, overall efficiency and capacity limits of the distillation column. The models and techniques used to define the point at which the flow regime transitions from the froth to spray regime takes place are discussed.

Lockett (1986) summarized the different techniques during experimentation used to predict the point at which the transition from the froth-to-spray regime occurs. The first technique is the light beam technique, where the attenuation of the light beam is measured when the transition from froth to spray regime occurs. The froth regime is considered to be a liquid continuous regime and the spray regime to consist of a gas continuous regime above the tray. The froth regime is considered mainly to be focused with bubbling and the spray regime with jetting. Therefore, there would be a considerable difference in the light beam attenuation in the two regimes. The light beam is placed at the top of the liquid layer where the beam is attenuated by drops intercepting the horizontal beam. The transition from the spray to the froth regime is accompanied by an increase in the amount of light transmitted, providing the beam is placed above the froth surface (Lockett, 1986).

The second technique is the measurement of the change in the entrainment magnitude, where entrainment in the spray regime is significantly higher than that of the froth regime. The transition point is measured as the rapid increase in the amount of entrainment when the regimes are changed from the froth-to-spray regime, which will be challenged by other literature investigation findings shown later in the text.

In the third technique, the change in the hole pulse frequency at the transition is used. In this method an electrical resistant probe is placed at the opening of the tray and measures the pulsation frequency at the hole (Lockett, 1986). The pulsation frequency for the froth regime is around 20 pulses per second which drops to about 5 pulses per second at the transition to the spray regime, which corresponds to the change from bubbling to jetting at the tray hole.

The final technique identified by Lockett (1986) is the determination of the residual pressure drop (H_R). The equation for the residual pressure drop is shown by Equation 2.3.7 in Section 2.3. Residual pressure drop is measured as the total pressure drop (H_t) minus the clear liquid height (H_L) and the dry plate pressure drop (H_d). Payne and Prince (1975) describe the residual pressure drop as going through a maximum as the momentum transfers from gas to liquid (spray to froth regime). Payne and Prince (1975) suggest that the residual pressure drop only be used for sieve trays with fractional hole areas below 4%, as the validity of what the maximum actually predicts is by no means clear (Lockett, 1986).

In an investigation performed by Porter and Wong (1969) on the transition from the spray regime to the bubbling regime, experiments were performed on a static sieve plate with no cross flow. In the investigation it was defined that the nature of the dispersion layer above the tray depends on the amount (height) of liquid on the tray. In determining the dispersion layers' transition points, a light transmission technique was used. The effect of fluid physical properties was tested by adding sodium chloride to liquid to change its density and the use of aqueous glycerol to test the effect of liquid viscosity on the transition data. The transition from the spray-to-froth regime is identified by a minimum in entrainment as in Figure 7.

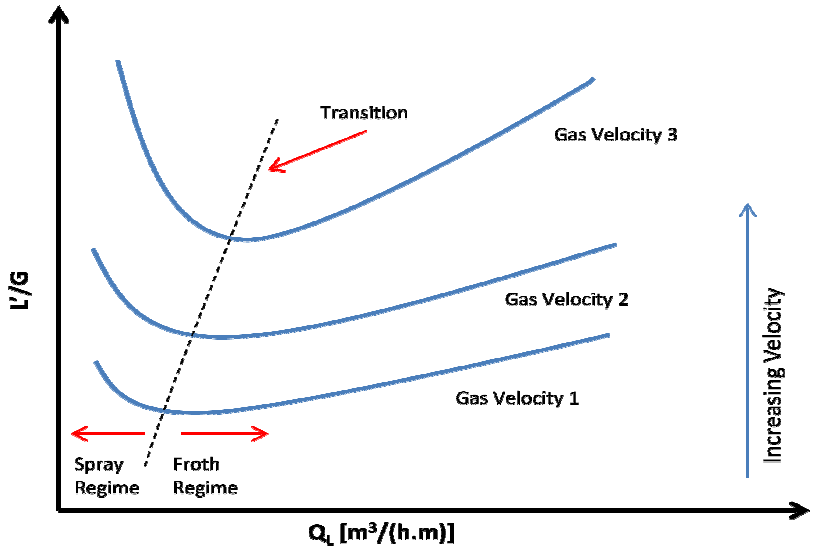

Figure 7 – Froth-to-spray transition.

The determination of the transition from bubbling to spray flow by eye (visually) is unreliable. It was shown that the liquid hold-up at the transition increases with decreasing fractional hole area, when using column gas velocity, but is brought together by the use of hole gas velocity (Porter and Wong, 1969). The liquid hold-up on the tray is greater for larger sieve tray hole diameters. It was shown that the liquid hold-up at the transition decreases with increasing liquid density, but the liquid

viscosity does not have any effect on the liquid hold-up at the transition (Porter and Wong, 1969). In an investigation by De Goederen (1965), the spray regime efficiency depends on the surface tension. Surface tension negative systems produce spray type dispersions and surface tension positive systems produce minimal spray liquid because of the bubble coalescence effect.

Porter and Wong (1969) believed that the transition from spray to bubbling takes place when a sufficient amount of liquid is added to the tray to increase the liquid drop density to a point when multiple drop coalescence takes place (producing large drops). Bubble dispersion differs from spray dispersion in that bubble dispersion has a definite dispersion surface, in which the light transmission technique may be taken advantage of.

The terminal velocity (u_t) for a drop diameter greater than 0.2 in. is presented by Equation 2.4.1 (Porter and Wong, 1969). The equation developed by Porter and Wong (1969) for the transition between spray and bubbling regime is presented by Equation 2.4.2, for plates with a pitch to hole diameter ratio of 0.4 ($\frac{p_t}{D_H} > 0.4$.).

$$u_t = 0.04\left(\frac{g\rho_l}{\rho_g}\right)^{\frac{1}{2}} \qquad [2.4.1]$$

$$\frac{H_{ft}}{D_H\eta} = 4 + 9\left[\frac{1-1.04A_f\left(\frac{\rho_l}{\rho_g}\right)^{\frac{1}{2}}\left(\frac{1}{u_S}\right)}{1-A_f}\right] \qquad [2.4.2]$$

In an investigation for the froth-to-spray transition performed by Pinczewski and Fell (1972), the point at which the froth-to-spray transition was determined with the use of an electric resister probe. Large hole diameter sieve trays and low tray free areas were shown to favour the spray regime. Across the tray in the distillation column, the gas flow rate at the froth-to-spray transition increases with increasing liquid cross flow. In the investigation of the effect of the hole diameter, the free fractional hole area on the tray was kept nearly constant with changing hole diameter. Weir height had a minimal effect on the transition at low liquid flow rates and has no effect on the transition at high liquid flow rates. Pinczewski and Fell (1972) also showed that the transition equation presented by Porter and Wong (1969) (Equation 2.4.2), does not take the fractional hole area into account, which makes it unreliable when using it on another column and tray configuration. It should be noted that Pinczewski and Fell (1972) used a single plate (tray) in their distillation column for their investigations.

In an investigation performed by Jeronimo and Sawistowski (1973) a correlation was developed for the gas hole velocity and the height of the dispersion at the transition. The hole velocity at the transition (u_{ht}) is shown by Equation 2.4.3. The dispersion height at the transition is shown by Equation 2.4.4.

$$u_{ht} = \frac{0.655\left(\frac{g\Delta\rho_g\sigma^2}{D_H\rho_g^3}\right)^{\frac{1}{6}}}{A_f\left(1+0.000104V_g^{-0.59}A_f^{-1.79}\right)} \qquad [2.4.3]$$

$$H_{ft} = \frac{0.694\left(\frac{gD_H^5}{\sigma\Delta\rho g}\right)^{\frac{1}{6}} A_f^{-0.791}}{1+0.000104V_g^{-0.59}A_f^{-1.79}} \quad [2.4.4]$$

The effect of the hole velocity on the clear liquid height at the transition is presented by Equation 2.4.5 (Loon, Pincewski and Fell, 1973). In Equation 2.4.5, 'K' is a dimensionless constant determined experimentally for different sieve tray hole diameters.

$$H_{Lt} = \frac{KD_H^{\frac{3}{2}}\rho_l^{\frac{1}{2}}u_h}{\sigma^{\frac{1}{2}}} \quad [2.4.5]$$

Pinczewski, Benke and Fell (1975) showed the effects of the phase transition from the froth-to-spray regime, where it was shown that the dry tray pressure drop increases steadily beyond the point of the phase inversion. It was shown that the difference between the wet and dry pressure drop decreases beyond the phase inversion.

The transition from jetting to bubbling in a single orifice plate was investigated by Payne and Prince (1975). In the investigation, the transition was determined by the change in the residual pressure drop across the submerged orifice. It was described that the transition from jetting to bubbling has similar characteristics to the transition from the spray-to-froth regime. The froth and the spray regime are the most important regimes in industrial distillation columns, since the columns were operated at high fluid flow rates in order to increase production capacity.

In the jetting regime, the jetting is divided into two characteristics, pulsating jetting (mist-like) and steady jetting (spray-like). At high gas velocities, the reduction of liquid hold-up produces jetting above the tray surface. At low gas velocities, a reduction in the liquid hold-up on the tray produces bubbling (Payne and Prince, 1975). In the investigation the residual pressure drop reaches a maximum at the phase transition.

The residual pressure drop is a result of the gas and liquid interaction across the tray (Payne and Prince, 1975). In the distillation column as the liquid depth above the orifice increases, the residual pressure drop increases, because of the increased interaction between the gas liquid above the tray to the point of the transition from jetting to bubbling after which the residual pressure drop decreases with increasing liquid hold-up. The proposed mechanism by which the transition begins is when the momentum transfer is insufficient to prevent the flow of liquid into the jet, so that the liquid bridges over the orifice (Payne and Prince, 1975).

The surface tension stabilizes the jet, since it opposes the flow of the liquid into the jet. Therefore it is believed that increasing the liquid surface tension increases transition liquid hold-up on the tray at low gas velocities, but the effect of the liquid surface tension at high gas velocities is insignificant (Payne and Prince, 1975). The liquid viscosity has no effect on the jetting to bubbling transition (Payne and Prince, 1975). The transition depth is shown to increase with increasing liquid and gas density. At low gas velocities in the bubbling regime, the projection drop size increases with increasing gas velocity, whereas at high gas velocities in the jetting regime the projected drop size decreases with increasing gas velocity.

In the study by Payne and Prince (1977), the conditions that affect the froth-to-spray transition was unaffected by the liquid cross flow and the plate position in the column. The transition was modelled

by Equation 2.4.6 and 2.4.7, which makes use of the modified Froude number. Payne and Prince measured the dispersion height by using a light transmission technique (1977). It was found that decreasing the fractional hole area increases the liquid hold-up at the transition slightly and increases the dispersion density. The volume of the chamber below the sieve tray is also shown to have no effect on the transition at large chamber volumes.

$$\frac{H_{ft}}{D_H} = 1.5Fr' \qquad [2.4.6]$$

$$Fr' = \left(\frac{\rho_g u_h^2}{\alpha \rho_l g D_H}\right)^{\frac{1}{2}} \qquad [2.4.7]$$

A correlation developed empirically by Lockett (1981), for the prediction of the froth-to-spray transition is shown by Equation 2.4.8. The clear liquid height decreases with increasing gas velocity, at high gas velocities and it is not dependent on the weir height.

$$\frac{H_L}{D_H} = 2.78\left(\frac{\rho_g}{\rho_l}\right)^{0.5} u_h \qquad [2.4.8]$$

Bennett, Kao and Wong (1995) showed the criterion for the froth to spray transition by:

- $\frac{H_L}{D_H} < 1$ spray-like regime
- $1 < \frac{H_L}{D_H} < 2$ transitional
- $\frac{H_L}{D_H} > 2$ froth-like regime

The transition from spray into the emulsion regime was investigated by Zuiderweg, Hofhuis and Kuzniar (1984), where it has a major influence on the two phase density above the tray, liquid mixing, mass transfer and the vapour/liquid separation. The regime transition occurs when the horizontal momentum flux of the liquid exceeds the vertical momentum flux of the vapour.

Zuiderweg *et al.* (1984) showed that the emulsion regime is influenced by the ratio of the gas/vapour density to the liquid density and therefore the pressure of the column. The transition studies are performed using air/water systems; therefore fluid physical properties are not adjusted to identify the transition to the emulsion regime. In the emulsion regime gas jets are bent over, where the angle of the jet out of the holes depends strongly on the vapour velocity and the hole diameter. The transition from the spray regime into the emulsion regime is large where the first regime observed is the froth regime (Zuiderweg, 1982), as in Figure 4.

2.5 Sieve Tray Distillation Capacity

In this section a literature analysis will be done into entrainment and weeping, as well as its effect on the capacity limits of the sieve tray distillation column. The investigation into entrainment will be done from the oldest published articles to the present studies on entrainment. The sieve tray column stability will be investigated to show how it effects the operation of the distillation column.

2.5.1 Entrainment

In distillation columns entrainment of liquid occurs when the gas velocity upward through the tray in the column is sufficient to transport the liquid to the tray above. In the distillation process entrainment increases the fraction of the low volatility components in the tops of the distillation column which reduces the overall separation efficiency, possibly contaminating products or damaging rotating machinery of the distillation column.

The different techniques used to identify the entrainment magnitude have been determined by Lockett (1986). The free entrainment is measured by sampling drops at the top of the dispersion layer and on the tray above. The dry tray entrainment is measured by placing a dry tray above and measuring the accumulation of liquid on the tray. Wet tray entrainment is measured by the use of a non-volatile tracer which is introduced into the tray below and measuring the amount of tracer in the tray above. Finally efficiency entrainment is measured by the reduction in the efficiency caused by entrainment effects. Lockett (1986) stated that the tracer technique is the most reliable technique, but this contaminates the products produced by distillation. It was stated by Lockett (1986) that if entrainment is above 5% of the amount of liquid entering the distillation column, that the column diameter should be increased, the tray spacing should increase and the tray geometry should be judiciously varied.

In an investigation performed by Hunt *et al.* (1955), it was shown that the magnitude of entrainment is strongly dependent on the velocity of the gas/vapour flow in the distillation column. A predictive model for entrainment was produced by Hunt *et al.* (1955), which showed that entrainment is proportional to the gas density, inversely proportional to the liquid surface tension and independent of the liquid density. The model shows that entrainment is proportional to the third power of gas velocity divided by the distance between the liquid dispersion surface and the plate floor.

The entrainment model developed by Hunt *et al.* (1955) is shown by Equation 2.5.1.1, where it was shown that the amount of liquid entrained is independent of the gas density. It is stated that the entrainment is primarily caused by the splashing or the rupture of the bubbles in the foam regime at the top of the dispersion. The entrainment magnitude as defined by Equation 2.5.1.1 is unreliable since a 6 in. distillation column is used, where the liquid height above the tray is maintained at a constant height with no liquid flow across the tray.

$$\frac{L'}{G} = 0.22 \left(\frac{73}{\sigma_l}\right)\left(\frac{u_s^*}{S^* - 2.5h_L^*}\right)^{3.2} \qquad [2.5.1.1]$$

Hunt *et al.* (1955) stated that the magnitude of entrainment does not change with hole gas velocity, but with the column gas velocity. The entrainment was shown to increase exponentially with decreasing plate spacing, where entrainment is inversely proportional to a power of 3.2 to the effective tray spacing (S') and increasing column gas velocity. The effective tray spacing is the distance between the top tray and the liquid dispersion layer surface on the tray below. Hunt *et al.* (1955) stated that the entrainment magnitude is not a capacity limiting factor in the distillation column as much as the pressure drop is, since flooding occurs long before the entrainment becomes seriously significant in the distillation column.

In the study of the entrainment performed by Bain and Van Winkle (1961), an air/water system was tested in a 6 in. by 28.75 in. (152 mm by 730 mm) rectangular column. The entrainment was thought

to increase with increasing gas rate, increasing hole diameter, decreasing plate spacing and decreasing weir height. The entrainment was shown to reduce the separation efficiency in the distillation column by as much as 25%, where a 10% fractional hole area plate was used in the experimental investigations. The entrainment increases as much as six to twelve times as the gas mass flow rate doubles. An empirical equation developed by Bain and Van Winkle (1961) for the entrainment for an air/water system is shown by Equation 2.5.1.2, where 'a', 'b', 'c', 'd', 'e', 'f' and 'g' are empirically determined constants.

$$e\frac{\rho_g}{\rho_l} = a\left(\frac{L''}{\mu_l}\right)^b\left(\frac{G'D_H}{\mu_l}\right)^c\left(\frac{H_{wo}}{D_H}\right)^d\left(\frac{S}{D}\right)^e\left(\frac{\sigma D_H \rho_g}{\mu_g \mu_l}\right)^f\left(\frac{\rho_l \mu_g}{\rho_g \mu_l}\right)^g \qquad [2.5.1.2]$$

Calcaterra, Nicholls and Weber (1968) defined two forms of entrainment measurement techniques, namely free and captured entrainment measurement. The free entrainment is the amount of liquid that reaches a certain level in the distillation column and the captured entrainment is the amount of liquid entrained in the tray above. The free entrainment technique described by Calcaterra *et al.* (1968) is the dry tray entrainment technique described by Lockett (1986). An 8% fractional hole area tray was used in a 13 in. (330 mm) diameter column. The free entrainment in the investigation was captured by sponge chips and it was found that the entrainment increases with decreasing tray spacing, decreasing liquid rate when the gas flow rate is above 4.15 ft/s (1.27 m/s) and increases with increasing gas rate. Calcaterra *et al.* (1968) stated that the entrainment occurs when the liquid droplets are projected upward by the gas stream reaching a height at which the gas velocity increases, which is close to the top tray (superficial gas velocity to hole gas velocity). This is comprehensible since the gas flow rate is constant through the column, but the gas velocity through the holes in the sieve tray is greater than that between the trays, increasing the upward force of the gas on the liquid droplet close to the tray.

The effect of entrainment has been investigated by Lemieux and Scotti (1969), where it was shown that entrainment increases with increasing hole diameter. The entrainment was also shown to increase with decreasing fractional hole areas at low liquid flow rates, but is independent of fractional hole area at high liquid flow rates. The phase transition from the froth-to-spray regime was investigated by Pinczewski *et al.* (1975), where it is shown that the entrainment increases with increasing gas flow rate beyond the point of the dispersion transition, but the dependence of the entrainment in the regime transition changes. Pinczewski *et al.* (1975) considered entrainment to occur inside the distillation column, when the superficial gas velocity exceeds the terminal velocity of the liquid droplets.

The effect of operating regime on the entrainment was investigated by Lockett, Spiller and Porter (1976). The magnitude of entrainment changed for the different regimes, since it occurs by means of different mechanisms. It was shown by Lockett (1986) that entrainment plays an important role in identifying the regime transition from the froth-to-spray regime, where entrainment in the spray regime is significantly higher than that of the froth regime.

In the entrainment investigation done by Lockett *et al.* (1976), a 0.46 m diameter column was used, where the magnitude of entrainment was measured using a tracer capturing technique. In the experiment it is observed that at low liquid rates there is a considerable amount of entrainment (spray regime), with a sudden reduction in the entrainment at the transition (froth regime) when the liquid rate is increased at constant gas rate.

Entrainment measurements were performed by Thomas and Ogboja (1978), where it was shown that models used to predict entrainment by Hunt *et al.* (1955) and Bain and Van Winkle (1961) do not fit the experiment results well. The method in which Thomas and Ogboja (1978) measured the entrainment was by the use of a catch-pot, where the accuracy is not justified by the measurement of the entrainment using this technique. The catch pot contains silica gel which absorbs liquid drops caught in the pot. Equation 2.5.1.3 shows the entrainment model developed by Thomas and Ogboja (1978).

$$\frac{L'}{G} = 0.88\left(\frac{u_p^*}{S^* - h_f^*}\right)^{0.77} \qquad [2.5.1.3]$$

The magnitude of entrainment produced by sieve trays was investigated by Kister *et al.* (1981) for the spray regime. The entrainment in the froth regime is stated to occur by the break-up of bubbles at the froth surface, producing projected droplets. The spray regime entrainment is stated as to occur due to the atomization of liquid droplets at the tray floor (development of droplets). Kister *et al.* (1981) stated that in the industry, columns operating at vacuum conditions operate mostly in the spray regime because of the gas flow rate used. It was shown that at constant superficial gas velocity, the entrainment magnitude is highly dependent on the fractional hole area, where entrainment increases with decreasing fractional hole area. In the distillation column, a hole diameter of ½ in. was used and three fractional hole areas were investigated (5.9%, 10.7% and 16.1%).

Kister *et al.* (1981) showed that the outlet weir height has no effect on the magnitude of the entrainment, when the weir height is between 25 and 75 mm. It was also shown that the entrainment increases with decreasing tray spacing and decreases with increasing liquid flow rate as also shown by Hunt *et al.* (1955). The entrainments dependency on column configuration and fluid physical properties as defined by the spray regime is shown by Equation 2.5.1.4 (Kister *et al.*, 1981), where 'a', 'b', 'c' and 'd' are constants that are determined experimentally. Kister *et al.* (1981) suggest the form of the equation represented by Equation 2.5.1.5, which represents air/water systems.

$$E \propto \left(\frac{\rho_g u_s^3}{\rho_l L g}\right)^a \left(\frac{u_s \rho_l \mu_g}{\rho_g \sigma}\right)^b \left(\frac{D_H}{H_L}\right)^c \left(\frac{S}{H_L}\right)^d \qquad [2.5.1.4]$$

$$E \propto \frac{u_s^{3a+b} D_H^c S^d}{L^a H_L^{c+d}} \qquad [2.5.1.5]$$

The constants determined by Kister *et al.* (1981) are determined to be 1.17 for both constants 'a' and 'b' and 2.34 for both constants 'c' and 'd'. In the investigation of the effect of fluid physical properties on entrainment, it was stated that the liquid surface tension effects the entrainment significantly in the spray regime, but does not define how it affects the entrainment.

Yanagi and Sakata (1982) investigated the performance of a commercial scale sieve tray with a fractional hole of 14%. The distillation column investigated was 1.2 m in diameter and a ½ in. (12.7 mm) hole diameter tray was used. Two non-air/water systems were investigated, namely cyclohexane/n-heptane at 165 kPa and isobutene/n-butane at 138 kPa. In the investigation it was found that the entrainment when using larger fractional hole area sieve trays is larger than that at the 14% fractional hole area, when the experimental data are compared with data obtained from

the Fractionation Research Incorporated (FRI, 2011). It was shown that the gas flow at low liquid flow rates produced a high amount of entrainment, since the momentum of the vapour is significantly less impeded by the liquid hold-up on the tray. At high liquid flow rates, entrainment is significantly lower because of the increase in the damping effect on the vapour momentum. Thus more vapour is required to produce the same amount of entrainment as that at lower liquid flow rates until a maximum point is reached, after which the vapour rate is decreased with increasing liquid rate to maintain the same amount of entrainment.

The entrainment model developed by Zuiderweg (1982) is shown by Equation 2.5.1.6, where the ratio of the bed height to tray spacing was considered to be the most important variable because of the high magnitude of entrainment in the spray regime. Equation 2.5.1.6 shows the amount of entrainment in terms of the amount of liquid entrained (L'), divided by the liquid flow rate to the distillation column (L). Lockett (1986) showed a model developed by Zuiderweg (1982) for the entrainment in the spray regime represented by Equation 2.5.1.7, based on hydrocarbon data obtained from the Fractional Research Incorporation (FRI, 2009).

$$\frac{L'}{L} = 1x10^{-8}\left(\frac{H_b}{S}\right)^3\left(\frac{u_h}{u_l}\right)^2 \qquad \text{for } 0.3 < \frac{H_b}{S} < 0.9 \qquad [2.5.1.6]$$

$$\left(\frac{L'}{G}\right)_s = 1x10^{-8}A_f^{-2}\left(\frac{H_L}{S}\right)^3\left(\frac{G}{L}\right)\left(\frac{\rho_l}{\rho_g}\right)^2\left\{1 + 265\left[\left(\frac{u_s}{(gH_L)^{0.5}}\right)\left(\frac{\rho_g}{\rho_l}\right)^{0.5}\right]^{1.7}\right\}^3 \qquad [2.5.1.7]$$

Zuiderweg (1982) also discussed another form of entrainment (vapour entrainment) in which vapour is entrained with liquid into the downcomer and flows to the bottom of the distillation column. Vapour entrainment occurs at high liquid rates, typically in the emulsion regime, when a large amount of gas can be entrained in the liquid, which can lead to flooding in the distillation column. In the determination of the entrainment magnitude, liquid is collected on the top tray and measured (dry tray entrainment) as defined by Lockett (1986), then recycled back to the column.

The effect of tray geometry and operating parameters on entrainment was investigated by Kister and Haas (1988) for the froth regime for air/water systems and tray spacing above 300 mm. It was shown that entrainment adversely affects the efficiency and capacity of the tray. The froth regime was stated to occur when the liquid flow rate is moderate to high, the pressures are moderate to high and the gas velocity is low to moderate. Pinczewski and Fell (1982) suggested that entrainment in the froth regime occurred due to the breakup of gas bubbles at the froth surface, which produces low velocity droplets. In the froth regime, an increase in the liquid flow rate increases the height at which the bubbles emerge from the froth, increasing entrainment.

In the investigation of the effect of hole diameter on entrainment, it was found that the entrainment rises steadily where this trend is favoured by high gas rates, large hole diameters and low liquid rates. Entrainment increased by a small degree when the hole diameters are small at high liquid flow rates. A large jump in the magnitude of entrainment occurs when large hole diameters (greater than 13 mm) combined with low liquid and gas rates are used (Kister and Haas, 1988). The study of the effect of the tray spacing on the entrainment showed that entrainment decreases as the tray spacing increases and entrainment is inversely proportional to the tray spacing to a power 2 to 3 (same trend observed for the spray regime) (Kister and Haas, 1988).

The investigation performed by Kister and Haas (1988) on the effect of the fractional hole area on the amount of entrainment showed that entrainment increases readily with decreasing fractional hole area which is favoured by high gas rates, low fractional hole areas and low liquid rates. The entrainment was shown to be only slightly dependent on the fractional hole area, when the gas velocity is low, fractional hole area is large and the liquid flow rate is high. The effect of the outlet weir height on the entrainment showed that entrainment decreases with increasing weir height, which is favoured by low outlet weir heights and low liquid flow rates. The entrainment is unaffected by the weir height, which is favoured by high weir heights, high gas velocities. When low liquid flow rates are used, entrainment increases with increasing weir height, which is favoured by low gas velocities and high liquid flow rates (Kister and Haas, 1988).

In the study of the influence of the entrainment by the liquid flow rate it was found that entrainment increases with increasing liquid flow rate. It reaches a maximum and then decreases. A narrow drop in the amount of entrainment occurs over a narrow range of liquid flow rates. Regions are observed where the entrainment is weakly dependent on the liquid flow rate, which is favoured by the use of large hole diameters greater than 19 mm (Kister and Haas, 1988). In the study of the effect of the gas flow rate on the amount of entrainment, it was found that the entrainment always increases with increasing gas rate and entrainment is proportional to the gas velocity to a power of 4 to 5 in the spray regime (Kister and Haas, 1988).

Kister and Haas (1988) compared their experimental data to that of Hunt *et al.* (1955) and Bain and Van Winkle (1961), and found that there were large deviations at low liquid flow rates [<10 $m^3/(h.m)$], large hole diameters (>12.7 mm), small fractional hole areas (< 7%) and when no weir is used. It was found that uniform froths are formed on the tray when small hole diameters, large fractional hole areas, large liquid flow rates and high weir heights were used.

A model used to predict the magnitude of entrainment in the froth regime (E_f) (developed by Kister and Haas, 1988) is shown by Equation 2.5.1.8. The term 'ζ', is a correction term for non-uniform froth dispersions, where the froth is non-uniform at low gas velocities, low liquid flow rates, large hole diameters and zero weir heights. In the investigation into the amount of entrainment performed by Kister and Haas (1988) it was assumed that liquid surface tension has a negligible effect on entrainment and the liquid density is insignificant in the froth regime. It was also suggested that the viscosity has no effect on the entrainment.

$$\left(\frac{L'}{G}\right)_f = 111\left(\frac{u_s}{S-H_F}\right)^2 D_H^{0.5}(1+\zeta) \qquad [2.5.1.8]$$

The correction term is obtained from Colwell (1981) and is represented as follows in Equations 2.5.1.9 and 2.5.1.10:

$$\zeta = \frac{0.00225}{A_f^3}\left(\frac{h_{L,t}}{H_L} - 1\right) \quad \text{for } h_{L,t} > H_L \qquad [2.5.1.9]$$

$$\zeta = 0 \quad \text{for } h_{L,t} \leq H_L \qquad [2.5.1.10]$$

A model developed by Kister and Haas (1988) to predict entrainment when weeping is significant, is shown by Equation 2.5.1.11, where '$h_{l,f}$' is the clear liquid height in the froth regime.

$$\left(\frac{L'}{G}\right)_w = \frac{0.3 D_H p_t^2}{h_{l,f}(S - H_F)} \quad [2.5.1.11]$$

A model developed by Kister *et al.* (1981) for the entrainment magnitude in the spray regime is defined by Equation 2.5.1.12 and the clear liquid height in the spray regime by Equation 2.5.1.14. The clear liquid height at the froth-to-spray regime transition is shown by Equation 2.5.1.15, for a constant liquid flow rate. Kister and Haas (1988) defined the entrainment by being equal to the spray regime entrainment $\left(\frac{L'}{G}\right)_s$, weeping entrainment $\left(\frac{L'}{G}\right)_w$ or the froth regime entrainment $\left(\frac{L'}{G}\right)_f$, which ever one is the largest (the controlling regime is the largest).

$$\left(\frac{L'}{G}\right)_s = 4.742^{\left(\frac{10}{\sigma^{\frac{1}{2}}}\right)^{1.64}} x^{\left(\frac{10}{\sigma^{\frac{1}{2}}}\right)} \quad [2.5.1.12]$$

$$x = 872 \left(\frac{u_s H_{L,t}}{(d_H S)^{\frac{1}{2}}}\right)^4 \left(\frac{\rho_g}{L \rho_l}\right) \left(\frac{\rho_l - \rho_g}{\sigma}\right)^{0.25} \quad [2.5.1.13]$$

$$H_{L,t} = \frac{h_{ct}}{1 + 0.00262 H_{wo}} \left(\frac{996}{\rho_l}\right)^{0.5(1-n)} \quad [2.5.1.14]$$

$$h_{ct} = \frac{0.497 A_f^{-0.791} d_H^{0.833}}{1 + 0.013 L^{-0.59} A_f^{-1.79}} \quad [2.5.1.15]$$

$$n = \frac{0.00091 d_H}{A_f} \quad [2.5.1.16]$$

The recommended range for the application for the entrainment Equations 2.5.1.8, 2.5.1.11 and 2.5.1.12 is shown by Table 1 (Kister and Haas, 1988).

Table 1 – Entrainment model validity range (adapted from Kister and Haas, 1988)

Variable	Range
System	Air/water only at atmospheric pressure
Gas Velocity	0.3 to 3.5 m/s
Liquid Flow Rate	2 to 130 m^3/(h.m)
Tray Spacing	300 to 1000 mm
Hole Diameter	15 to 25 mm
Fractional Hole Area	4 to 20%
Weir Height	0 to 80 mm

An investigation was done by Kister and Haas (1990) into entrainment, where entrainment has been found to occur at an identified rare occasion when the combined effect of the ratio of path length to

tray spacing is above 2.5, the liquid flow rate is above 50 $m^3/(h.m)$ and the fractional hole area is greater than 11%.

A model used to predict the magnitude of entrainment was developed by Kozoil and Mackowaik (1990) and is defined by Equation 2.5.1.17. Kozoil and Mackowaik (1990) obtained a mean weighted error of 1.84% when comparing the model Equation 2.5.1.17 to experimental data.

$$\frac{L'}{G} = 0.37 Fr_g^{\frac{2}{3}} Fr_l^{-\frac{1}{5}} Fl^{-\frac{1}{3}} \left(\frac{We}{Co}\right)^{n_4} \left(\frac{\rho_g}{\rho_l}\right) \quad [2.5.1.17]$$

$$n_4 = 133.7 Fl^{-\frac{1}{6}} \quad [2.5.1.18]$$

In Equation 2.5.1.17, 'Co' is the construction number and relates the F-factor dependence on the construction parameters of the tray. This is represented by Equation 2.5.1.19 (Kozoil and Mackowaik, 1990).

$$Co = \left(\frac{A_f S}{(D_c D_H)^{\frac{1}{2}}}\right) \quad [2.5.1.19]$$

In Equation 2.5.1.17, 'We' is the Weber number which relates the entrainment to the droplet size distribution (Kozoil and Mackowaik, 1990) and is represented by Equation 1.2.2.4.

$$We = \frac{\rho_g u^2 l}{\sigma} \quad [1.2.2.4]$$

The extended Froude number (Fr_g) shows the dependence of entrainment on the gas velocity and the extended Froude number (Fr_l) defines the dependence of entrainment on the liquid load. These are shown by Equations 2.5.1.20 and 2.5.1.21.

$$Fr_g = \frac{u_h^2 \rho_g}{Sg(\rho_l - \rho_g)} \quad [2.5.1.20]$$

$$Fr_l = \frac{\left(\frac{V_l(1+e_L)}{SD_c}\right)^2}{D_c g} \quad [2.5.1.21]$$

The fluid number (Fl) is shown by Equation 2.5.1.22, where the fluid number relates the droplet terminal velocity to the entrainment (Kozoil and Mackowaik, 1990).

$$Fl = \frac{\sigma^3 \rho_g^2}{g\mu_g^4(\rho_l - \rho_g)} \quad [2.5.1.22]$$

$$e_L = \frac{V_g}{V_l}\left(\frac{L'}{G}\right)\left(\frac{\rho_g}{\rho_l}\right) \quad [2.5.1.23]$$

An investigation was done by Bennett *et al.* (1995) into the development of entrainment in sieve tray distillation columns, where an entrainment model was developed. The model developed showed that entrainment is a function of the ratio of tray spacing to the froth height ($\frac{S}{H_F}$) and average froth density (η). A two zone model was used to describe the relationship between froth density and the entrainment by Bennett *et al.* (1995). In the description of the dispersion layer on top of the tray, the froth is broken down into a bottom liquid continuous region, a middle vapour

continuous region (where gravitational and momentum forces dominate the liquid droplets' behaviour) and a mist region (where the force acting on the liquid droplets influence the froth height).

Data were gathered from multiple sources in the development of the entrainment model by Bennett *et al.* (1995), where the model's applicability is defined by Table 2 for both air/water (AW) and non-air/water (NAW) systems.

Table 2 – Model validity ranges (redrawn from Bennett *et al.*, 1995)

Parameter	Min. Value (AW)	Max. Value (AW)	Min. Value (NAW)	Max. Value (NAW)
(A_H/A_T)	0.06	0.12	0.08	0.12
d_H, mm	1.59	25.4	12.7	25.4
l, m (x10^3)	0	76.2	38.1	63.5
s, mm	152	914	610	610
ρ_l, kg/m^3	1000	1000	493	770
ρ_g, kg/m^3	1.224	1.224	1.13	28
σ, kg/s^2 (x10^3)	74	74	5	24
Q_L, m^3/(h.m)	4.2	134	0.3	0.3
u_s, m/s	0.45	2.3	0.07	2.4

The entrainment model for the froth regime (using froth-to-spray transition data from Pinczewski and Fell, 1982) is shown by Equation 2.5.1.24 for non-air/water systems.

$$\left(\frac{L'}{G}\right)_{NAW,f} = 0.00405\eta^{0.00095}\left(\frac{S}{H_F}\right)^{-1.967}\left(\frac{\rho_l}{\rho_g}\right)^{0.5} \qquad [2.5.1.24]$$

The model developed by Bennett *et al.* (1995) for the froth regime using a compound database of entrainment data is shown by Equation 2.5.1.25 for air/water and 2.5.1.26 for non-air/water systems. In the equations Bennett *et al.* (1995) assumes that the surface tension is negligible in the froth regime and liquid viscosity has an insignificant effect on entrainment.

$$\left(\frac{L'}{G}\right)_{AW,f} = 0.00164\left(\frac{K_s^2}{g\eta_e S}\right)^{1.86}\left(\frac{gH_L}{K_s^2} + \frac{9\sqrt{3}}{2(A_f)}\left[1 + 6.9\left(\frac{D_H}{H_L}\right)^{1.85}\right]\right)^{1.86}\left(\frac{\rho_l}{\rho_g}\right)^{0.5} \qquad [2.5.1.25]$$

$$\left(\frac{L'}{G}\right)_{NAW,f} = 0.742\left(\frac{K_s^2}{g\eta_e S}\right)^{2.77}\left(\frac{gH_L}{K_s^2}\right)^{1.81}\left(\frac{\rho_l}{\rho_g}\right)^{1.19} \qquad [2.5.1.26]$$

In the study on entrainment in the froth regime by Bennett *et al.* (1995), it was found that when the effect of tray spacing on entrainment is determined, the entrainment is proportioned to tray spacing to a power of 2 instead of between 2 to 3, as reported by Kister and Haas (1988). At high values of $\frac{K_S}{gH_L}$, the entrainment increases rapidly with decreasing fractional hole area, especially at high gas

velocities. Fractional hole area becomes less important at high liquid flow rates and low gas velocities.

It was shown by Bennett *et al.* (1995), that the outlet weir height is only important because of its impact on the clear liquid height, which increases with increasing weir height. At high vapour velocities and low liquid flow rates, entrainment depends on corrected superficial velocity (K_s) to a power of 5. At typical values of $\frac{gH_L}{K_S^2}$ equal to 100, entrainment depends on K_s to a power of 3 (Bennett *et al.*, 1995).

The model developed by Bennett *et al.* (1995) for the spray regime, using a compound database of entrainment data is represented by Equation 2.5.1.27 for air/water and Equation 2.5.1.28 for non-air/water systems. In the spray regimes, Bennett *et al.* (1995) assumes that the surface tension is negligible.

$$\left(\frac{L'}{G}\right)_{AW,S} = 0.005\left(\frac{K_S^2}{g\eta_e S}\right)^{1.26}\left(\frac{gH_L}{K_S^S} + \frac{9\sqrt{3}}{2A_f}\left[1 + 4.77\left(\frac{D_H}{H_L}\right)^{3.29}\right]\right)^{1.26}\alpha^{\beta}\left(\frac{\rho_l}{\rho_g}\right)^{0.5} \quad [2.5.1.27]$$

$$\left(\frac{L'}{G}\right)_{NAW,S} = 8x10^{-18}\left(\frac{K_S^2}{g\eta_e S}\right)^{1.56}\left(\frac{gH_L}{K_S^S} + \frac{2.48}{\frac{A_H}{A_T}}\left[1 + 8.27\left(\frac{D_H}{H_L}\right)^{-0.614}\right]\right)^{7.4}\alpha^{\beta}\left(\frac{\rho_l}{\rho_g}\right)^{1.08} \quad [2.5.1.28]$$

In the spray regime, it was found that the entrainment is proportional to the average liquid hold-up fraction (α), where the froth regime shows no dependency of the entrainment on the average liquid hold-up fraction (Bennett *et al.*, 1995). In the spray regime, entrainment is strongly dependent on the hole diameter when the ratio of clear liquid height to hole diameter is greater than 10, whereas in the froth regime the entrainment is independent of the hole diameter. In the spray regime, entrainment is proportional to K_s to a power of 5 to 6 and the magnitude of entrainment is less dependent on the tray spacing in the spray regime than in the froth regime.

An investigation into entrainment characteristics was performed by Ohe and Yanagi (2001), where it was found that entrainment increases with liquid load and at a constant vapour rate. The entrainment has a minimum which is due to the transition from the spray-to-froth regime transition.

In an investigation performed by Van Sinderen *et al.* (2003), free entrainment was measured in a 0.2 by 0.2 m column. The results were determined in terms of a two phase or three phase model as defined in Section 2.2. The entrainment model developed is shown by Equation 2.5.1.29 (Van Sinderen *et al.*, 2003).

$$\frac{L'}{\rho_l A_p} = 0.029(\pm 0.01)\exp\left[-4.38\left(\sqrt{2g\left(S - 0.7H_{wo} + \frac{130C_p^2}{g}\right)} - 17C_p\right)\right] \quad [2.5.1.29]$$

The method used by Van Sinderen *et al.* (2003) to capture the entrained liquid used a slanted mesh pad to capture entrained liquid and a collection gutter to collect the entrained liquid flowing down the slanted mesh pad. This method does not simulate actual industrial entrainment mechanisms, since most trays in industrial columns are parallel to one another. The capturing method does not produce the same amount of entrainment in the centre of the tray as that on the side of the tray. Tilting the sieve distillation trays has been shown to increase the amount of liquid entrained, because of the increase in liquid height on the tray (Mayfield *et al.*, 1952).

The hydrodynamics effects inside a sieve tray distillation column were investigated by Uys *et al.* (2009) and Uys (2012) in a distillation pilot plant. The effects of the liquid flow rate, gas flow rate, gas properties, liquid properties and tray spacing on the entrainment and liquid dispersion properties were investigated. The test were composed with a single sieve tray, with a hole diameter of 6.3 mm and a fractional hole area of 15.61%.

It should be noted that the pilot plant investigated by Uys *et al.* (2009) and Uys (2012) is used in the current experimental investigation and is discussed in chapter 4. In pilot plant validation, performed by Uys *et al.* (2009), it was shown that the downcomer escape area has an insignificant effect on the magnitude of entrainment when the liquid cross flow velocity is between 0.23 m/s and 0.6 m/s. The variables investigated by Uys (2012) are shown in Table 3.

Table 3 – Experimental variables of Uys (2012)

Variable	Specification
Gas Flow Rates	1.4 to 2.9 m/s
Liquid Flow Rates	0.5 to 93.2 m^3/(h.m)
Tray Spacing	315, 415, 515 and 615 mm
Liquids	Water, n-Butanol, Isopar G, Ethylene Glycol and Silicone Oil
Gas	Air, CO_2 and SF_6

In the study of the entrainment magnitude performed by Uys (2012), the entrainment is defined using the following terms:

- $\frac{L'}{G} \rightarrow$ When the tray capacity is of importance.
- $\frac{L'}{L} \rightarrow$ When the column efficiency is of importance.

In the study performed by Uys (2012), $\frac{L'}{L}$ was shown to decrease exponentially with an increase in the liquid flow rate, and it was suggested that the column efficiency increases with increasing liquid flow rate. High values of $\frac{L'}{G}$ lead to entrainment flooding (spray or froth flooding) and high values of $\frac{L'}{L}$ indicate a reduction in the column efficiency.

Uys (2012) showed that an increase in gas density leads to an increase in the amount of entrainment at a constant superficial gas velocity. This allows distillation columns to be operated at a higher gas flow factor with increasing gas density. Dimensionless numbers were developed to describe the fluid physical properties and fluid flow rate effects inside a distillation column using the Buckingham-π theorem.

In Equation 2.5.1.30, the modified Reynolds number was developed in order to describe the effect of gas physical properties (Uys, 2012). In the experimental investigation done by Uys (2012), it was shown that a decrease in the entrainment ($\frac{L'}{G}$) leads to an increase in the Reynolds number.

Therefore an increase in gas viscosity, decrease in the liquid flow rate and a decrease in the gas viscosity leads to an increase in entrainment. The ratio between the gas density and the difference between the liquid density and gas density in Equation 2.5.1.30 shows that an increase in the liquid density leads to a decrease in the modified Reynolds number and an increase in entrainment.

$$Re^{+} = \frac{\rho_g\left(\frac{Q_L}{3600}\right)}{\mu_g}\left(\frac{\rho_g}{\rho_l - \rho_g}\right)^{n} \quad \rightarrow \quad \text{Modified Reynolds number} \qquad [2.5.1.30]$$

The entrainment ($\frac{L'}{L}$) can be described with the dimensionless modified Froude number (Uys *et al.*, 2012) in Equation 2.5.1.31. The use of the modified Froude number makes the equation independent of the flow regime, where an increase in the Froude number increases the magnitude of entrainment.

$$Fr^{+} = \frac{3600u_s^3}{gQ_L}\left(\frac{\rho_g}{\rho_l - \rho_g}\right)^{n} \quad \rightarrow \quad \text{Modified Froude number} \qquad [2.5.1.31]$$

Different correlations were developed for the spray (Equation 2.5.1.32) and the froth regime (Equation 2.5.1.33), where the spray regime was defined using the method developed by Porter and Jenkins (1979), by the minimum in the $\frac{L'}{G}$ graph.

$$\left(\frac{L'}{G}\right)_s = 817\left(\left(\frac{\rho_l}{945\rho_g}\right)^{-1.89} + 4.27\right)^{1.33}\left(\frac{\sigma}{9.7\rho_g u_s Q_L}\right)^{-0.673}\left(\left(\frac{\mu_L}{15.9\rho_g Q_L}\right)^{0.9} + 6\right)^{-6} \ldots.$$

$$\left(\frac{u_s^3}{1.86gQ_L}\right)^{-0.171}\left(\frac{\mu_g}{6x10^{-3}\rho_g Q_L}\right)^{1.347}\left(\frac{u_s^2}{3.44x10^{-3}gs}\right)^{1.53} \qquad [2.5.1.32]$$

$$\left(\frac{L'}{G}\right)_f = 547\left(\left(\frac{\rho_l}{949\rho_g}\right)^{0.08} + 2.19\right)^{-3.72}\left(\left(\frac{\sigma}{9.55\rho_g u_s Q_L}\right)^{0.39} + 0.94\right)^{-5.12}\left(\left(\frac{\mu_L}{9.35\rho_g Q_L}\right)^{2.69} + 2.18\right)^{-4.81}\left(\left(\frac{u_s^3}{0.433Q_L g}\right)^{0.41} + 0.28\right)^{5.81}\left(\left(\frac{\mu_g}{2.96x10^{-3}\rho_g Q_L}\right)^{-3.38} + 1.47\right)^{-0.27}\left(\left(\frac{u_s s}{223Q_L}\right)^{-1.68} + 0.97\right)^{1.63}\left(\left(\frac{Q_L}{162u_s FPL}\right) + 1.41\right)^{-3.44} \qquad [2.5.1.33]$$

The model developed by Uys (2012) does not take into account the changes in the sieve tray geometry, therefore the effect of the contribution of geometry changes to entrainment from Kister and Haas (1988) was added to the correlation developed by Uys (2012) and is represented by Equation 2.5.1.34.

$$\left(\frac{L'}{G}\right)_{Application\ in\ question} = \left(\frac{L'}{G}\right)_{Uys} + \left[\left(\frac{L'}{G}\right)_{\substack{K\ and\ H \\ (Geometry\ in\ question)}} - \left(\frac{L'}{G}\right)_{\substack{K\ and\ H \\ Uys\ geometry}}\right] \qquad [2.5.1.34]$$

2.5.2 Weeping

This section addresses the effect of weeping in sieve tray distillation columns. In the distillation process, weeping occurs when the liquid dispersion is significantly high that liquid would start to seep (weep) through the pores of the tray. Weeping increases the fractional concentration of the

high volatility component in the column bottoms. This decreases the overall separation efficiency of the distillation process.

Mayfield *et al.* (1952) showed that magnitude of weeping in a distillation column can be reduced when an inlet weir is used, but the perforation holes have to be spaced at least 4 to 8 in. (101.6 to 203.2 mm) from the inlet weir. The weeping magnitude investigated by Hunt *et al.* (1955) increases slowly, then rapidly increases with decreasing gas velocity. Weeping was also shown to slowly increases when the hole pitch is below $2D_H$ with decreasing gas velocity. Lemieux and Scotti (1969) showed that weeping decreases with increasing gas velocity and increases with increasing liquid rate. In the investigation done by Lemieux and Scotti (1969), weeping for larger hole diameters (1 in.) is lower at high liquid rates (667 to 905 gal/hr) than they are for smaller hole diameter plates, but is higher at the lowest liquid rate of 100 gal/hr investigated. The lowest gas velocity in the column is defined as the velocity at which weeping is just negligible through the plate, where it was found by Lemieux and Scotti (1969) that the minimum velocity is the same for the ½ in. (12.7 mm) and 1 in. (25.4 mm) hole diameter plates in the distillation column.

Thomas and Ogboja (1978) investigated weeping in sieve tray columns, where it was found that weeping occurs when the gas flow rate is reduced to a point at which the gas can no longer support the liquid on the tray. The weeping point as defined by Thomas and Ogboja (1978) was found by plotting the vapour pressure drop versus the vapour velocity. To prevent weeping, it was defined that the head loss through the holes plus the head loss due to the liquid surface tension should be greater than the head loss caused by the froth (H_f).

Yanagi and Sakata (1982) showed that weeping is evident when there is large reduction in the total pressure drop across the tray, when reducing the gas vapour velocity. It was shown that significant tray weeping occurs at high weir heights, low gas velocities, large hole diameters and large fractional hole areas (Kister and Haas, 1988). Mohan, Rao and Rao (1983) showed that the efficiency increases with the flow path length until a point of weeping, which showed that the magnitude of weeping increases with increasing flow path length.

The effect of weeping on the hydrodynamics of a sieve tray distillation column has been investigated by Lockett and Banik (1986), where the experimental investigation was performed with a rectangular column (1.22 m x 0.63 m) for both an air/water and an air/isopar M system. Lockett and Banik (1986) showed that an increase in the clear liquid height leads to an increase in weeping. In the experimental investigation, it was noted that weeping had low values at high liquid rates and low weir heights, which is stated to be attributed to the high horizontal liquid velocity. It was shown that a sieve tray distillation column can operate well below the weeping point without a substantial loss in efficiency.

Lockett and Banik (1986) investigated three different hole diameters (3.2 mm, 6.4 mm and 12.7 mm) and three different fractional hole areas (10.2%, 15% and 20%) in the experimental investigation. It was found in the investigation that the sieve tray with a 6.4 mm hole diameter had the highest amount of weeping and that the 3.2 mm and 12.7 mm holes exhibited a lower weeping magnitude. Weeping is shown to increase with increasing fractional hole area. Through visual observations it was shown that the three different hole diameter trays at a constant fractional hole area exhibited different mechanisms of droplet disengagement through the holes.

The weeping liquid disengagement process as defined by Lockett and Banik (1986) is defined as follows:

- In the 3.2 mm hole trays it is observed that severe bridging occurs under the tray, where the weeping liquid disengages as streams from the bridging layer.
- In the 6.4 mm hole trays weeping liquid disengages from the tray as jets at all the weeping magnitudes.
- For the 12.7 mm hole trays:
    - Weeping takes place directly from the sieve tray holes at high weeping magnitudes.
    - The jet diameter of the liquid through the sieve tray holes is smaller than the hole diameter, whereas at the highest weeping magnitudes the jets filled the hole.
    - At the low weeping magnitudes it was observed that weeping occurred from a layer covering the underside of the sieve tray.

In the experimental investigation, it was observed that weeping increased with the percentage of free fractional hole area and there was little difference in the weeping magnitude between the air/water and the air/isopar M system. Lockett and Banik (1986) collected the weeping liquid onto the chimney tray, where the chimney tray had a baffle placed in the centre in order to split the tray into two sections. In the investigation, it was found that weeping occurred mainly in the inlet half of the tray for a liquid flow rate of 30 m^3/(h.m). Weeping occurred at the exit half of the tray at a liquid flow rate of 60 m^3/(h.m). It was described that the reason for the difference is that a hydraulic jump may be present at the inlet of the tray at high liquid loads.

The effect of different parameters on weeping was determined using a correlation developed by Lockett and Banik (1986) represented by Equations 2.5.2.1 and 2.5.2.2 as described by Kister (1992).

$$\frac{W^*}{A_h^*} = \frac{29.45}{\sqrt{Fr_h}} - 44.18 \qquad [2.5.2.1]$$

$$Fr_h = 0.373 \frac{u_h^{*2}}{h_L^*} \left(\frac{\rho_g^*}{\rho_l^* - \rho_g^*} \right) \qquad [2.5.2.2]$$

In an investigation done by Lockett (1986), it was shown that the clear liquid height increases with the outlet weir height which increases the magnitude of weeping by the sieve tray. The graphical weeping point is identified as the point at which there is a change in the slope of pressure drop versus gas velocity graph at constant liquid flow rate. The graphical weeping point is often different from the measured weeping point, especially when the fractional hole area is greater than 15%. It was shown by Lockett (1986) that just as the bubble has left the hole on the sieve tray and before the next bubble starts to form, weeping is possible when the pressure of the liquid above the tray surface is greater than the chamber pressure below the tray hole. During weeping, oscillating and sloshing above a tray causes the liquid height to change in different areas of the tray, causing weeping to occur in the high liquid hold-up region (Kister, 1992).

Uys *et al.* (2012) showed that weeping increases with the liquid rate in the spray regime to the point of the spray-to-froth transition point, due to the increase in the liquid hold-up on the sieve tray. The magnitude of weeping continues to increase with the increasing liquid rate to the point at which the high pressure region range changes from the tray to the downcomer, at which point weeping

decreases. The weeping magnitude decreases further to the point at which the dispersion height (liquid hold-up) increases.

2.5.3 Sieve tray capacity

The current section addresses the capacity of a distillation column and what factors limit the capacity of the sieve tray distillation column. It was described by Zuiderweg (1982) that the operating limits of the distillation column are traditionally described by an upper boundary (flooding limit) and a lower boundary limit (weeping limit). In an investigation performed by Hofhuis and Zuiderweg (1979) the flooding point is stated to occur when the bed height is equal to the tray spacing.

The percentage of flooding can be determined using Equation 2.5.3.1 (Thomas and Ogboja, 1978). '$u_{s(design)}$' is chosen to be less than '$u_{s(flooding)}$' for the series of constant L/G values, which produces a curve.

$$\%\, flooding = \frac{u_{s(flooding)}}{u_{s(design)}}\, x\, 100 \qquad [2.5.3.1]$$

In an investigation performed by Yanagi and Sakata (1982) on commercial scale sieve distillation columns, it was stated that the column capacity is limited by two mechanisms, tray flooding by exceeding the downcomer capacity, or by extremely large amount of entrainment (jet) flooding. The downcomer capacity limitation is a result of the high liquid flow rates (loads) in high pressure columns. In an investigation done by Lockett (1986), it was stated that flooding occurs when liquid flow rate exceeds the capacity of the distillation column.

In an investigation performed by Puppich and Geodecke (1987) on tray columns, the F-factor (F_x) was used to compare different responses of different tray designs with one another. The F-factor is shown by Equation 2.5.3.2, where the subscript is defined by the area used in determining the F-factor.

$$F_x = u_x\sqrt{\rho_g} \qquad [2.5.3.2]$$

The F-factor is an expression of the vapour load through the distillation column. The maximum F-factor (F_{max}) is determined using Equation 2.5.3.3 (Puppich and Geodecke, 1987).

$$F_{max} = 2.5\left(A_f\sigma(\rho_l - \rho_g)\right)^{\frac{1}{4}} \qquad [2.5.3.3]$$

An investigation by Hunt *et al.* (1955) showed that the stability of the sieve tray distillation column is independent of the liquid density and viscosity. The stability was also shown to increase with increasing liquid wetting power, increasing liquid surface tension and increasing gas density. In the experimental investigation performed by Hunt *et al.* (1955), it was also found that the distillation column became unstable when a sieve tray with a fractional hole area of greater than 20% is used, since weeping increased significantly. The sieve tray stability also increases when the hole pitch is greater than $2D_H$.

The mechanisms of flooding as defined by Kister (1992) are defined as follows:

- Spray entrainment flooding.
- Froth entrainment flooding.
- Downcomer choke flooding.
- Downcomer back-up flooding.

In the distillation column spray flooding (jet flooding) occurs at high gas superficial velocities and typical low liquid flow rates, when most of the liquid on the tray is blown to the tray above, where the liquid accumulates in the column. Froth entrainment flooding typically occurs at high liquid flow rates, where the superficial gas velocity is increased, increasing the height of the dispersion to the point at which the dispersion reaches the tray above and typically occurs at low tray spacing below 457 mm (Kister, 1992). Downcomer choke flooding occurs when the liquid flow rate is raised, also increasing the velocity of the aerated liquid into the downcomer, choking the flow of liquid into the downcomer. In downcomer back-up flooding the liquid flow rate into the downcomer is greater than the rate at which it leaves the downcomer, which is influenced by the liquid dispersion height, tray pressure drop and frictional losses through the downcomer apron.

Resetarits and Ogundeji (2009) investigated the effect of weir loading rates on the hydrodynamic interactions in a distillation column and showed the possible effect of high weir loadings to be:

- High pressure drops caused by high froth dispersion heights.
- Large dispersion crest and high froth heights that lead to jet flooding.
- Large crest that choke the downcomer flow causing downcomer flooding.

Resetarits and Ogundeji (2009) showed that increasing the tray spacing accommodates for large weir loadings inside the distillation column. It was also shown that increasing the column diameter decreases the weir loadings. Therefore, the maximum weir loading in a distillation column depends on the column diameter, tray spacing, column internal geometry and the vapour rate.

2.6 Critical Evaluation

This section takes an in-depth look into the different entrainment models highlighted in the previous sections. The models are plotted in figures to evaluate the effect (trends) that superficial gas velocity, liquid flow rate, tray spacing, hole diameter, fractional hole area, weir height, liquid density, gas density, liquid surface tension and liquid viscosity has on entrainment. The ranges of applicability of the different models are shown in Table 4. The range of applicability of the non-air/water systems (Bennett *et al.*, 1995) and (Van Sinderen *et al.*, 2003) entrainment model is shown, but will not be addressed because of its entrainment predictions deviating by an order of magnitude compared to the other models addressed.

In the model comparison figures that follow, the gas velocities, liquid flow rates, fluid properties, tray and column geometries are chosen based on the average value (most tested magnitudes) of tested ranges, when viewing the literature model testing limits in Table 4. The purpose of the current entrainment model investigation is to show the agreement and the difference in entrainment prediction magnitude and trends of the entrainment models. The investigation will show the need for further entrainment model improvement, by highlighting parameter ranges that need to be further investigated. The entrainment models which do not incorporate distillation parameters into their model are shown in grey and left clear when the entrainment models incorporates the distillation parameter in table 4. Models which do not incorporate distillation parameters into their entrainment model are not shown in the following figures.

The fluid properties values when evaluating the effect of gas velocities, liquid flow rates, sieve tray and column geometries on entrainment are those of an air/water system. The models are plotted beyond their range of applicability, in order to compare them with other systems and to show to what extent they may be extrapolated to produce a logical entrainment prediction. Models that are plotted beyond their defined recommended parameter ranges are shown with dashed lines (with O in the legends) and within their recommended range as solid lines (with I in the legends).

The discussion will make reference to the following model references as 'Kister & H' for Kister *et al.* (1981), 'Bennett *et al.*' for the Bennett *et al.* (1995) air/water model, 'Uys' for Uys (2012), 'Zuiderweg' for Zuiderweg (1982), 'Kozoil & M' for Kozoil and Mackowaik (1990), 'Hunt *et al.*' for Hunt *et al.* (1955) and 'Thomas & O' for Thomas and Ogboja (1978). The model plots are shown partly in the current section and in Appendix B, where the parameters used in the models are shown in the figures. The entrainment estimations are only defined as $\frac{L'}{G}$ (capacity factor), in order to show the changes in the magnitude of the entrainment. The models are determined with fluid properties close to that of water for the fluid flow rate, tray geometry and column geometry evaluations. Entrainment models by 'Bennett *et al.*', 'Kister & H' and 'Uys' are plotted for both the froth and spray regime in a single model line, where only the controlling regime mechanism model is shown. The 'Zuiderweg' and 'Kozoil & M' models are only valid in the spray regime. The model comparison is performed at a fractional hole area of 11% making the 'Uys' model invalid, however the model is still shown so that the model trends and magnitude can be evaluated so that the largest areas (parameter ranges) of uncertainty can be highlighted. Models are shown for both a spray regime liquid flow range [Q_L = 5.7 m^3/(h.m) or V_L = 1 m^3/h] and a froth regime liquid flow range[Q_L = 34.3 m^3/(h.m) or V_L = 4 m^3/h].

Table 4 – Entrainment models range of application

Author	Hunt *et al.* (1955)	Thomas & Ogboja (1978)	Zuiderweg (1982)	Kister & Haas (1988)	Kozoil & Mackowaik (1990)	Bennett *et al.* (Air/Water) (1995)	Bennett *et al.* (Non-Air/Water) (1995)	Van Sinderen *et al.* (2003)	Uys (2012)
Liquid Flow Rate [m^3/(h.m)]	0	4.5 to 40.3	9.3 to 88.9	2 to 130	1 to 14	4.2 to 134	0.3 to 100	2	2.9 to 92
Superficial Gas Velocity (m/s)	1 to 4.3	1.9 to 3.2	0.1 to 2	0.3 to 3.5	0.9 to 3.2	0.5 to 2.3	0.7 to 2.4	1.1 to 2.1	1.2 to 3.7
Tray Spacing (mm)	200 to 710	300 to 457	500	300 to 1000	400 to 600	152 to 914	610	610	315 to 615
Hole Diameter (mm)	3.2 to 12.7	25.4	12.7	1.5 to 25	6 to 15	1.6 to 25.4	12.7 to 25.4	6 to 12	6.3
Fractional Hole Area	5% to 21.5%	12.4% and 11.8%	7% to 14%	4 % to 20 %	2.7% to 34.3%	6% to 12.4%	6% to 12.4%	6% to 7%	15.6%
Liquid Density (kg/m^3)	673 to 1602	≅1000	493 to 700	≅1000	640 to 1000	1000	493 to 770	≅1000	806 to 1102
Liquid Surface Tension (mN/m)	18 to 73	≅60	5 to 18.5	≅60	13.5 to 72.4	73.5	5 to 24	≅60	23 to 60
Liquid Viscosity (Pa.s)	0.3 to 0.9	≅1	0.1 to 0.4	≅1	0.3 to 1	unknown	unknown	≅1	0.9 to 50
Gas Density (kg/m^3)	0.6 to 5	≅1.2	4.8 to 28	≅1.2	0.4 to 4.8	1.224	1.1 to 28	≅1.2	1.2 to 5.9
Weir Height (mm)	0	76.2	25.4	0 to 80	20 to 80	0 to 76.2	38.1 to 63.5	0 to 50	51

The effect of the liquid flow rate on entrainment is evaluated using the literature models in Figure 8 for a superficial gas velocity of 1.5 m/s, Figure 114 in Appendix B for a superficial gas velocity of 2 m/s and in Figure 9 for a superficial gas velocity of 2.5 m/s. In Figure 8, entrainment decreases with increasing liquid flow rate for the 'Uys', the 'Zuiderweg' and the 'Kozoil & M', whereas the other models increase in entrainment in the low liquid flow rate region [$Q_L < 20$ m^3/(h.m)]. However, it can be seen that the 'Uys', the 'Zuiderweg' and the 'Kozoil & M' models are plotted beyond their recommended ranges. The Change in slope of the 'Uys' model [approximately 12 m^3/(h.m)] represents a change in the model regime controlling mechanisms (spray to froth) as the liquid flow rate increases.

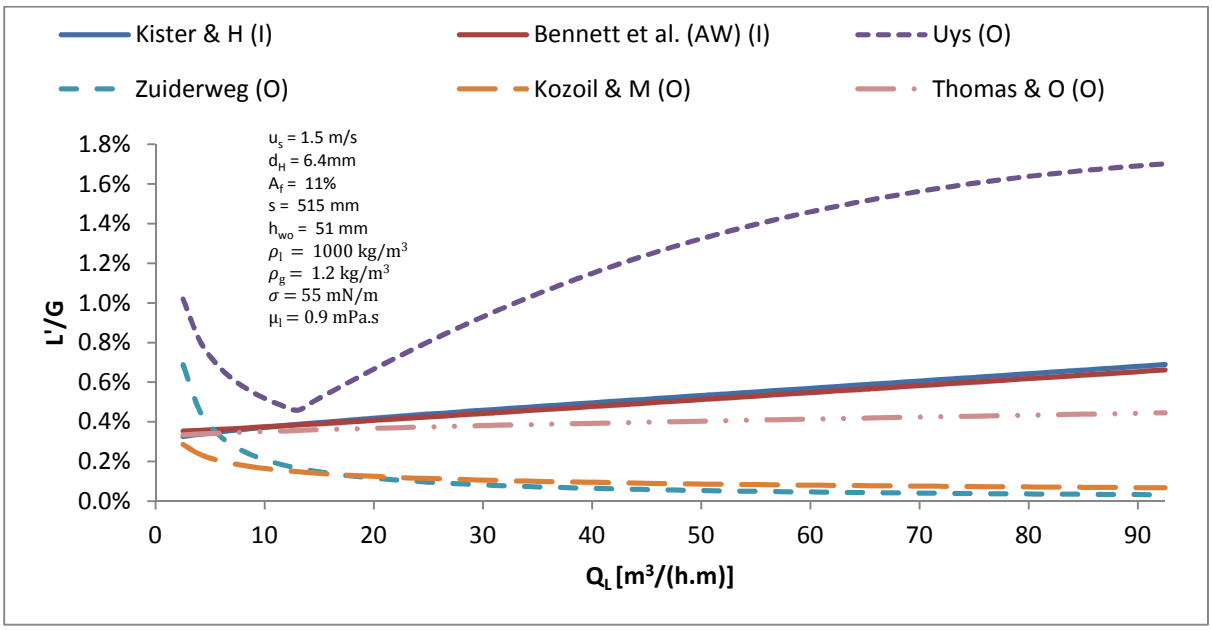

Figure 8 – Modelling the effect of liquid flow rate on entrainment for u_s = 1.5 m/s.

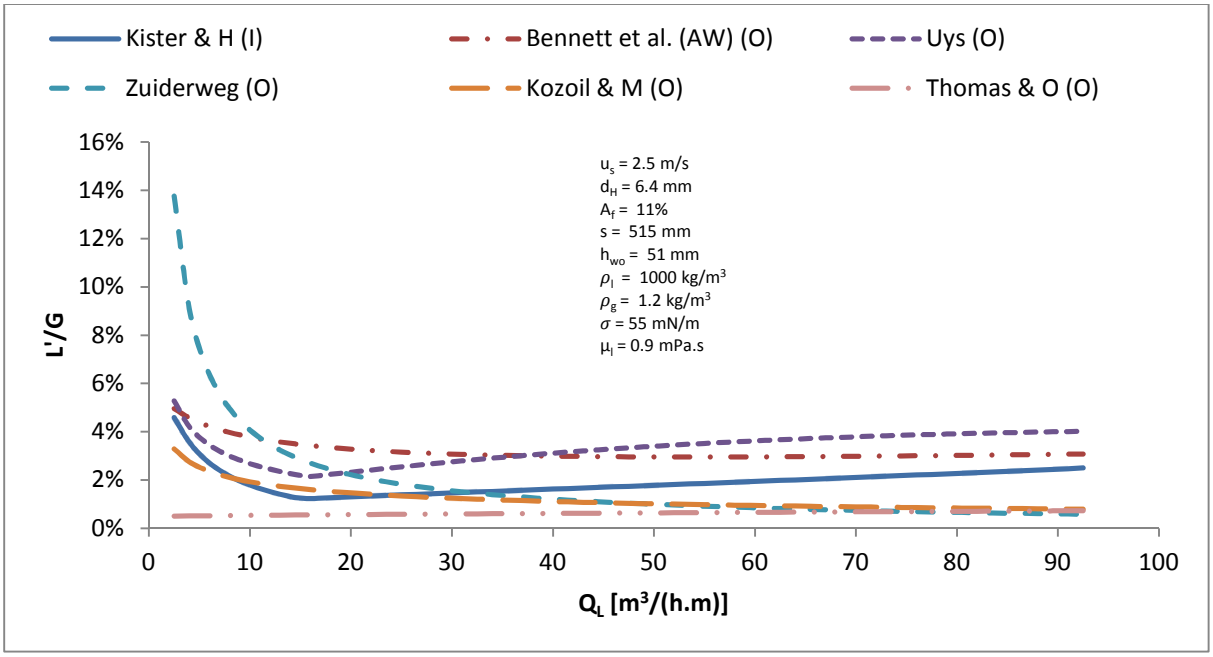

Figure 9 – Modelling the effect of liquid flow rate on entrainment for u_s = 2.5 m/s.

It is also noted that in the high liquid flow rate region [Q_L > 20 m^3/(h.m)], all the models evaluated show an increase in entrainment, except for the 'Zuiderweg' and the 'Kozoil & M' models which define entrainment in the spray regime only. The liquid load has a similar effect on entrainment at the different gas velocities investigated, where the entrainment magnitude increases in all the regions with increasing superficial gas velocity for the different models investigated (Fig. 8, 9 and 114). Only the 'Kister & H' and 'Bennett *et al.*' models are used within their recommended ranges in the liquid flow rate graphs.

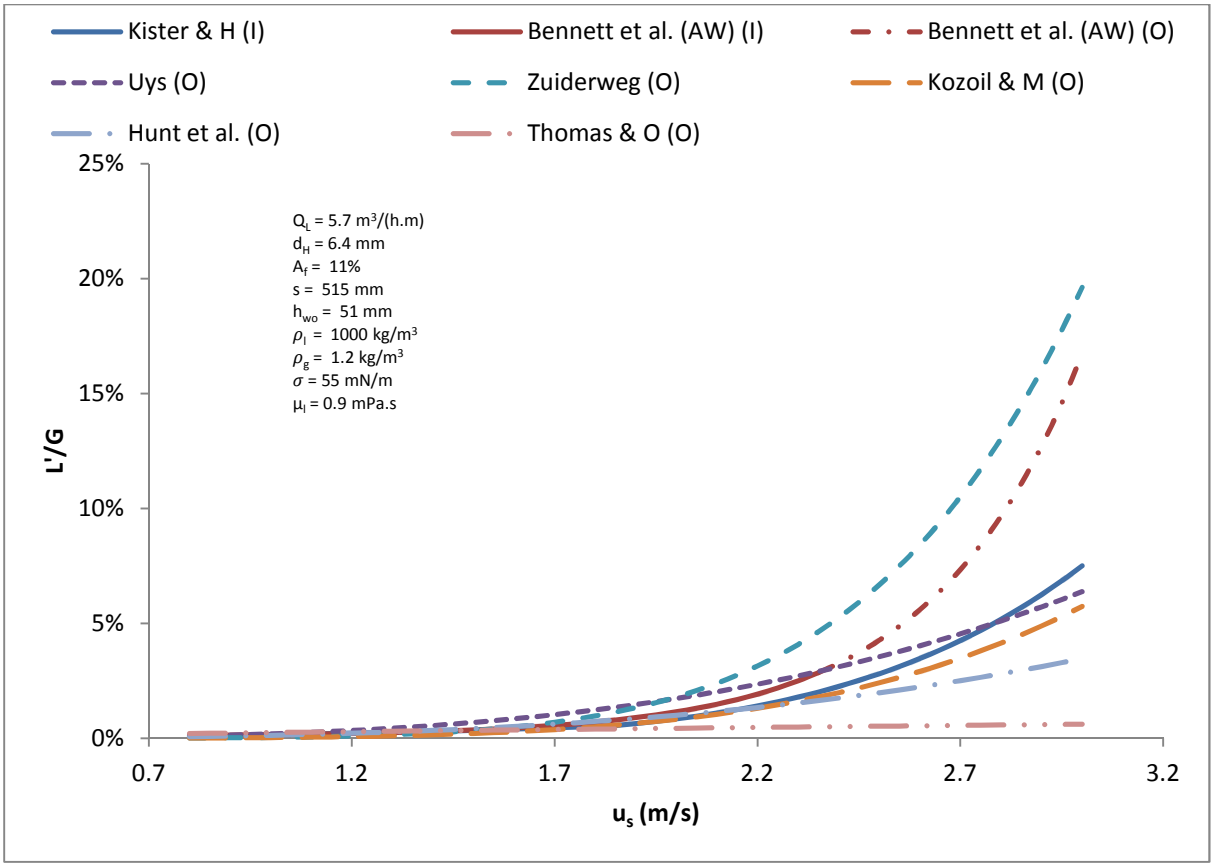

Figure 10 – Modelling the effect of superficial gas velocity rate on entrainment for Q_L = 5.7 m^3/(h.m).

The effect of the superficial gas velocity on entrainment is evaluated in Figure 10 for a liquid flow rate of 5.7 m^3/(h.m) (V_L = 1 m^3/h), Figure 115 in Appendix B for a liquid flow rate of 22.9 m^3/(h.m) (V_L = 4 m^3/h) and in Figure 11 for a liquid flow rate of 68.6 m^3/(h.m) (V_L = 12 m^3/h). The liquid flow rates are chosen over the wide range in order to simulate spray regime 5.7 m^3/(h.m) to froth regime 68.6 m^3/(h.m) conditions. All the models show an increase in entrainment with increasing superficial gas velocity. The 'Thomas & O' model shows a more linear increase in the entrainment and predicts a low magnitude in the entrainment with increasing superficial gas velocity, when compared to the other models addressed. At low to moderate [Q_L = 5.7 – 22.9 m^3/(h.m)] liquid flow rates the differences in entrainment magnitudes are more significant (higher at low liquid rates), possibly due to the spray regime (jetting) activity in this region. The difference between the entrainment magnitude at moderate [Q_L = 68.6 m^3/(h.m)] to high liquid rates [Q_L = 68.6 m^3/(h.m)] is less significant, possible due to froth regime activity. Only the 'Kister & H' and 'Bennett *et al.*' (to 2.3 m/s) models are used within their recommended ranges in the superficial gas velocity effect graphs.

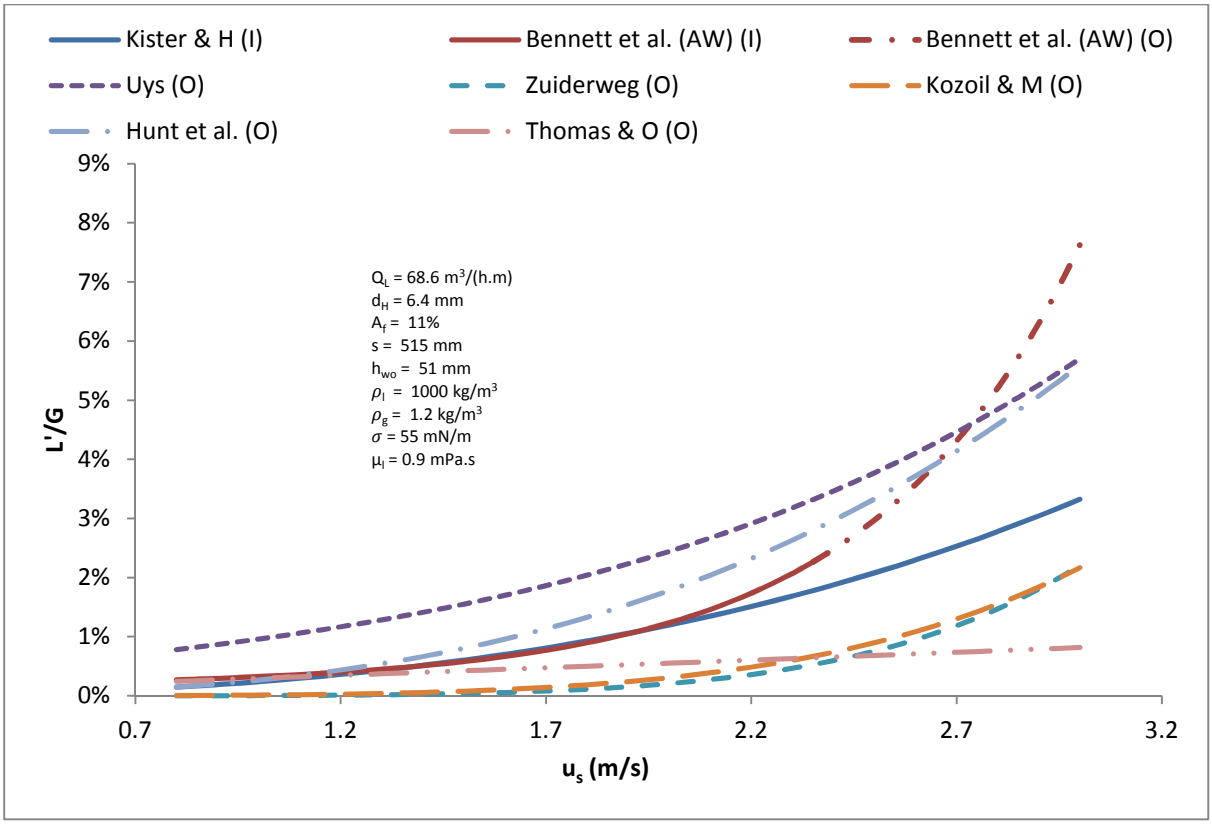

Figure 11 – Modelling the effect of superficial gas velocity on entrainment for Q_L = 68.6 m³/(h.m).

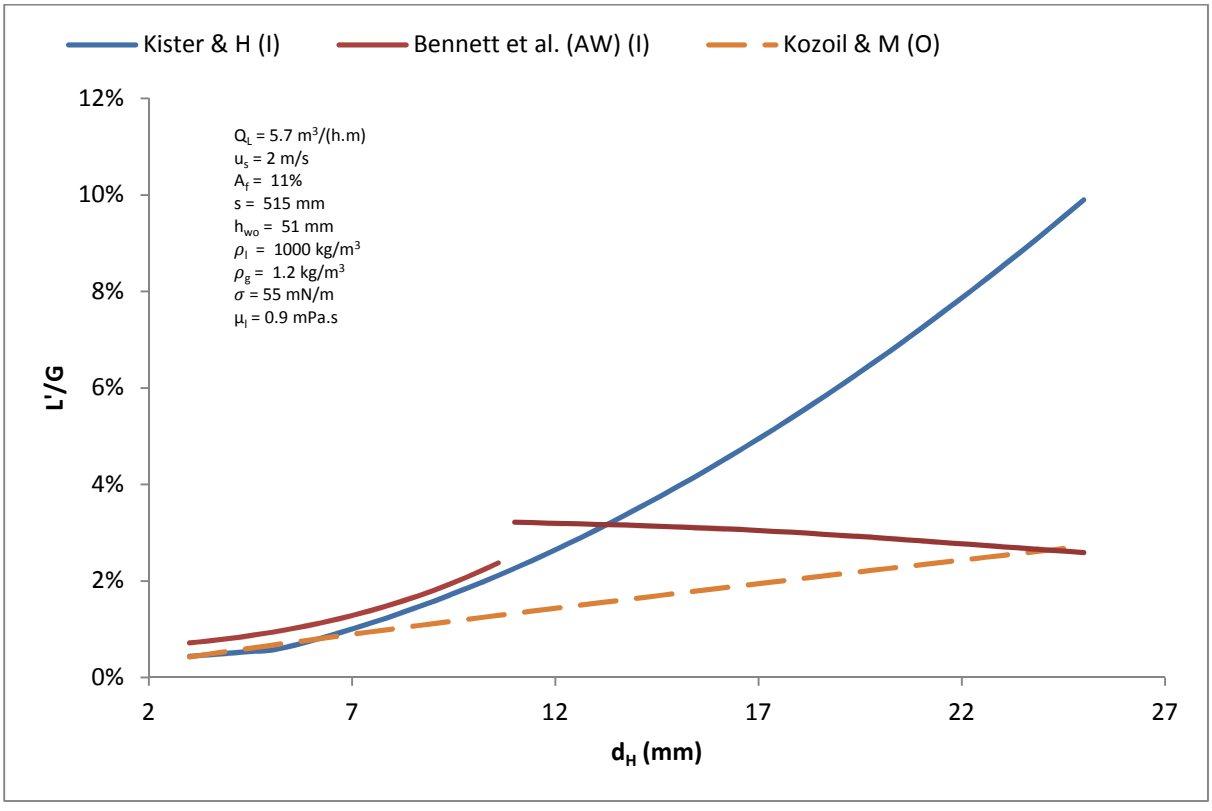

Figure 12 – Modelling the effect of hole diameter on entrainment for Q_L = 5.7 m³/(h.m) and u_s = 2 m/s.

The effect of sieve tray hole diameter is evaluated by the models in Figure 12 for Q_L = 5.7 m^3/(h.m) and u_s = 2 m/s, Figure 13 for Q_L = 34.3 m^3/(h.m) and u_s = 2.5 m/s, and Figure 116 in Appendix B for Q_L = 34.3 m^3/(h.m) and u_s = 2 m/s. The 'Uys', 'Hunt *et al.*', 'Thomas & O' and 'Zuiderweg' models do not take into account the effect of the sieve tray hole diameter on entrainment since it was not investigated. The 'Kister & H', 'Bennett *et al.*' and 'Kozoil & M' shows that entrainment is highly dependent on the tray hole diameter, especially at low liquid flow rates.

The entrainment magnitude predicted by 'Kister & H', 'Bennett *et al.*' and 'Kozoil & M' models show that entrainment increases with hole diameter at low hole diameters. However, the 'Bennett *et al.*' model shows a decrease in the entrainment magnitude at high hole diameters as the model shifts from a froth regime prediction to spray regime prediction. When the 'Kister & H' model shifts from a froth regime to a spray regime model-prediction with increasing hole diameter, the slope of the entrainment prediction increases with increasing hole diameter. Only the 'Kister & H' and 'Bennett *et al.*' (to 2.3 m/s) models are used within their recommended ranges in the graphs displaying the effect of hole diameter.

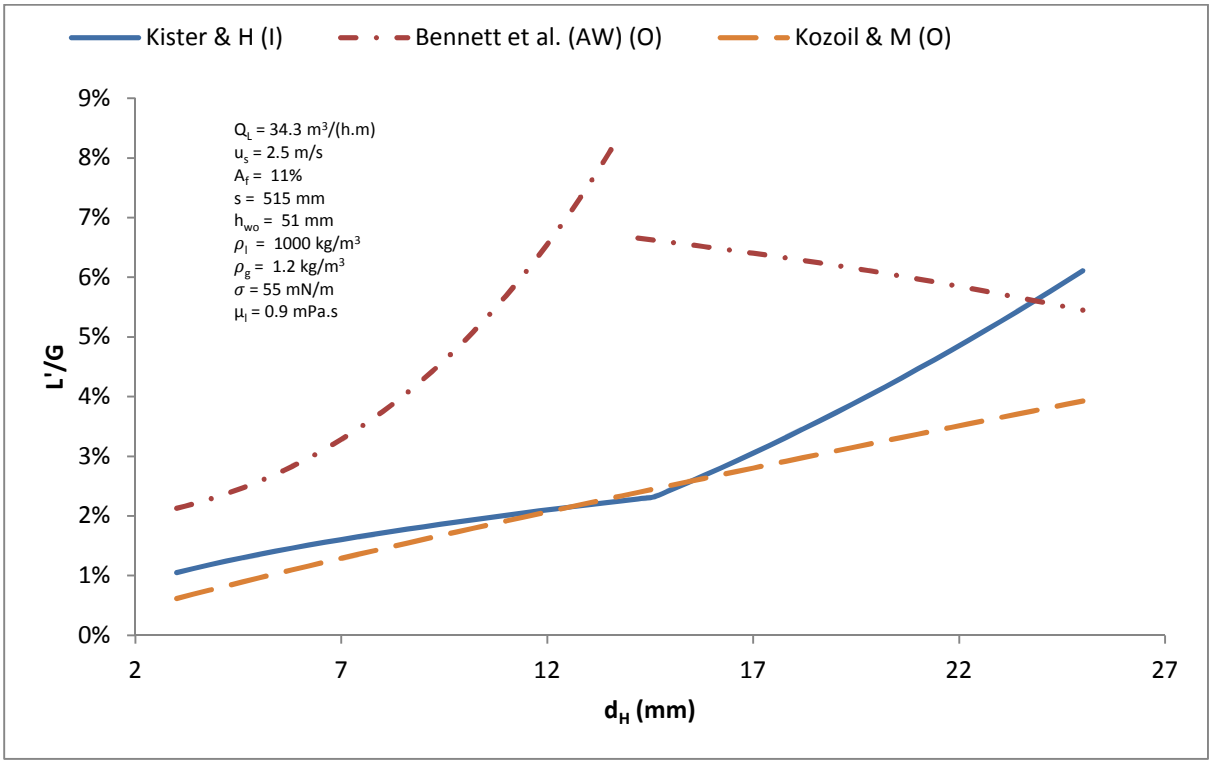

Figure 13 – Modelling the effect of hole diameter on entrainment for Q_L = 34.3 m^3/(h.m) and u_s = 2.5 m/s.

The effect of the sieve tray fractional hole area on entrainment is modelled in Figure 14 for Q_L = 5.7 m^3/(h.m) and u_s = 2 m/s, Figure 117 in Appendix B for Q_L = 34.3 m^3/(h.m) and u_s = 2 m/s and in Figure 15 for Q_L = 34.3 m^3/(h.m) and u_s = 2.5 m/s. The 'Uys' and 'Thomas & O' models do not take into account the effect of the sieve tray hole fractional hole area on entrainment, since it was not investigated. The 'Zuiderweg', 'Kozoil & M' and 'Bennett *et al.*' models show that entrainment always decreases with increasing fractional hole area. The 'Hunt *et al.*' entrainment model has a low dependency on the fractional hole area.

The 'Kister & H' model shows a more complex dependency on the fractional hole area, where at low liquid flow rates entrainment increases with increasing fractional hole area at low fractional hole areas, then decreases with increasing fractional hole area. At higher liquid rates, entrainment decreases with increasing fractional hole area at all the tray fractional hole areas investigated. The rate entrainments magnitude changes with fractional hole area is shown by the model calculations to increase with decreasing liquid flow rate and increasing superficial gas velocity.

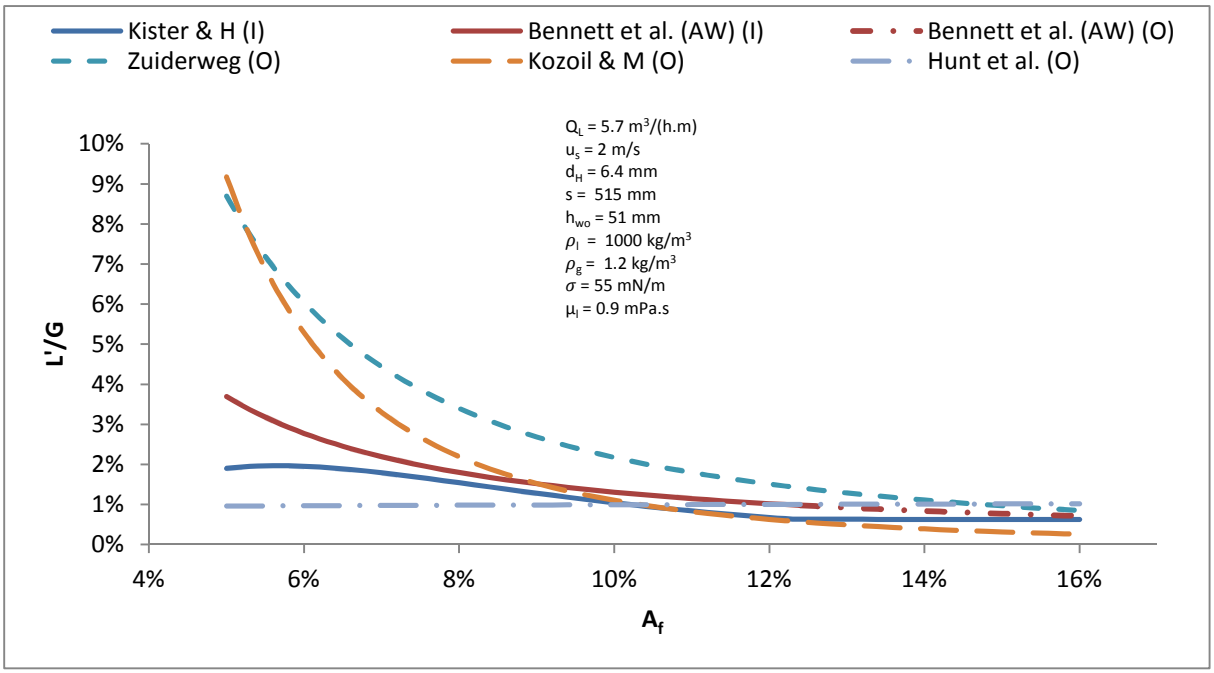

Figure 14 – Modelling the effect of fractional hole area on entrainment for Q_L = 5.7 m³/(h.m) and u_s = 2 m/s.

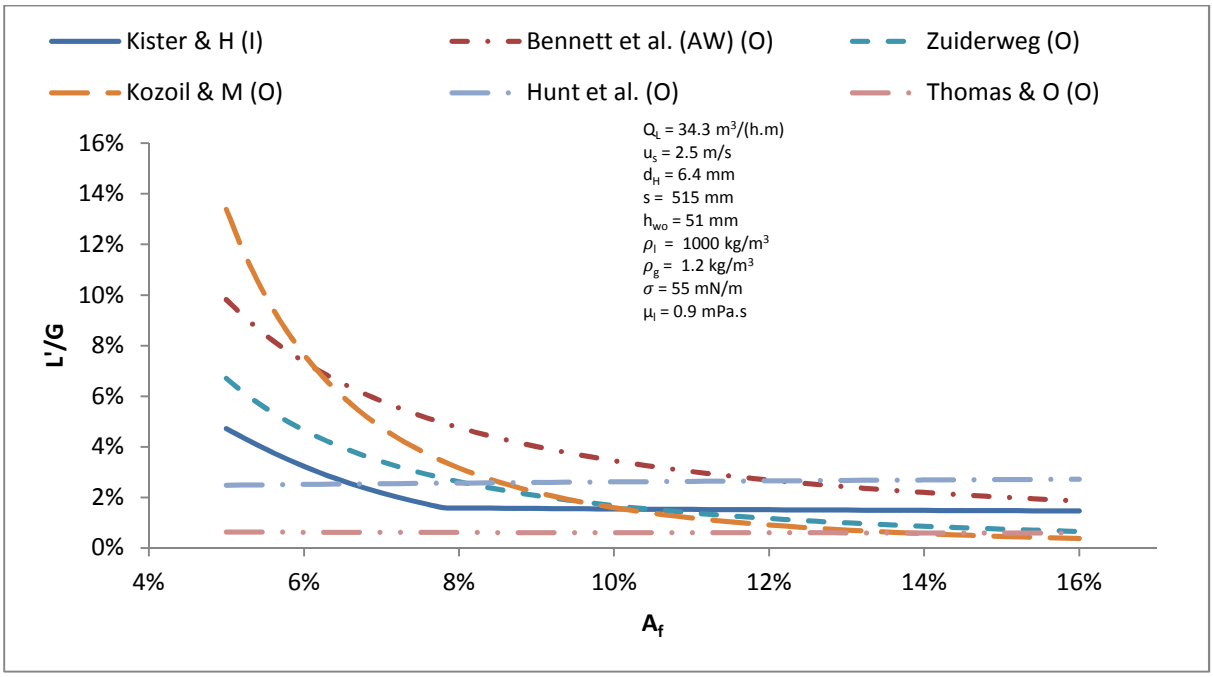

Figure 15 – Modelling the effect of fractional hole area on entrainment for Q_L = 34.3 m³/(h.m) and u_s = 2.5 m/s.

The effect of the sieve tray spacing on entrainment is modelled in Figure 16 for Q_L = 5.7 m^3/(h.m) and u_s = 2 m/s, Figure 118 in Appendix B for Q_L = 34.3 m^3/(h.m) and u_s = 2 m/s and in Figure 119 in Appendix B for Q_L = 34.3 m^3/(h.m) and u_s = 2.5 m/s. All the models predict that entrainment decreases with increasing tray spacing. The models all show a monotonic relationship between entrainment and tray spacing. The entrainments magnitude changes with tray spacing as shown by the model calculations to increase with increasing liquid flow rate and increasing superficial gas velocity. Only the 'Kister & H' and 'Bennett *et al.*' (to 2.3 m/s) models are used within their recommended ranges in the graphs displaying the effect of tray spacing.

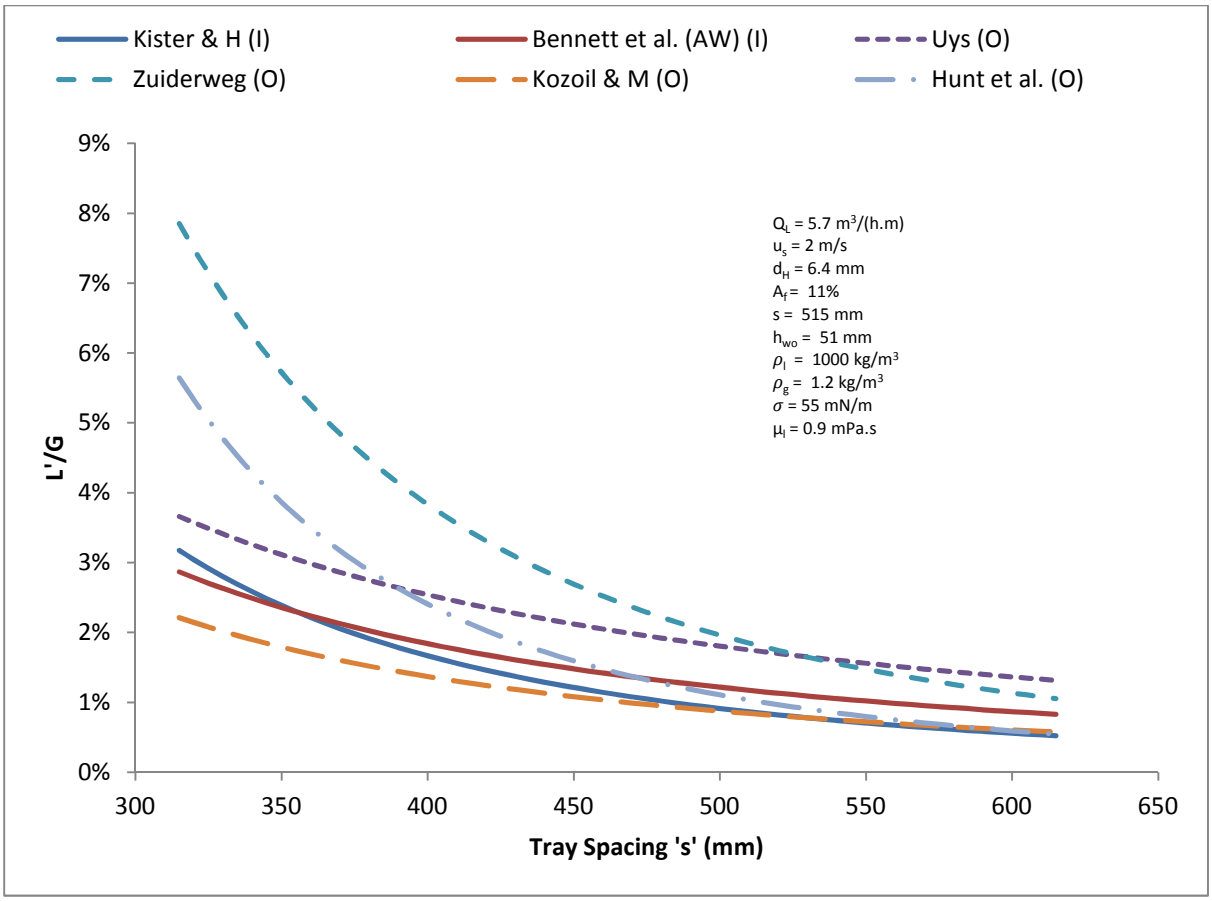

Figure 16 – Modelling the effect of tray spacing on entrainment for Q_L = 5.7 m^3/(h.m) and u_s = 2 m/s.

The effect of the tray weir height on entrainment is modelled in Figure 17 for Q_L = 5.7 m^3/(h.m) and u_s = 2 m/s. The 'Uys' and 'Kozoil & M' models do not take into account the effect of the sieve tray weir height on entrainment since it was not investigated. The 'Thomas & O' entrainment model has a low dependency on the tray weir height, thus it is not shown.

The 'Hunt *et al.*' and 'Zuiderweg' models show an increase in entrainment with increasing weir height over the entire range of the investigation. The 'Kister & H' and 'Bennett *et al.*' entrainment models show a more complex dependency on the weir height, where it is observed that at low liquid flow rates [Q_L = 5.7 m^3/(h.m) in Figure 22] the 'Kister & H' model decreases with weir height. In the 'Bennett *et al.*' model at low weir heights and low liquid flow rates (Transition from spray to froth regime), the entrainment decreases and increases as weir height increases and then decreases with increasing weir height at higher liquid rates (froth regime).

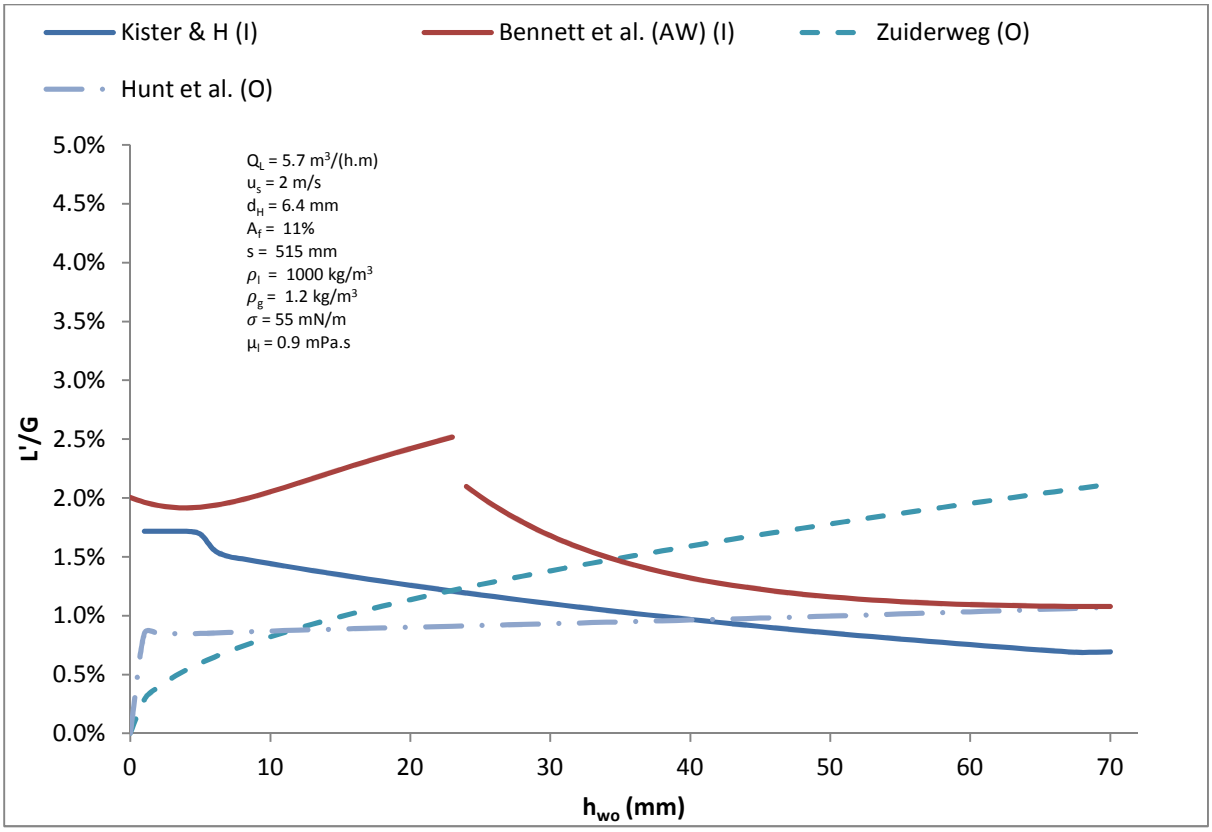

Figure 17 – Modelling the effect of weir height on entrainment for Q_L = 5.7 m³/(h.m) and u_s = 2 m/s.

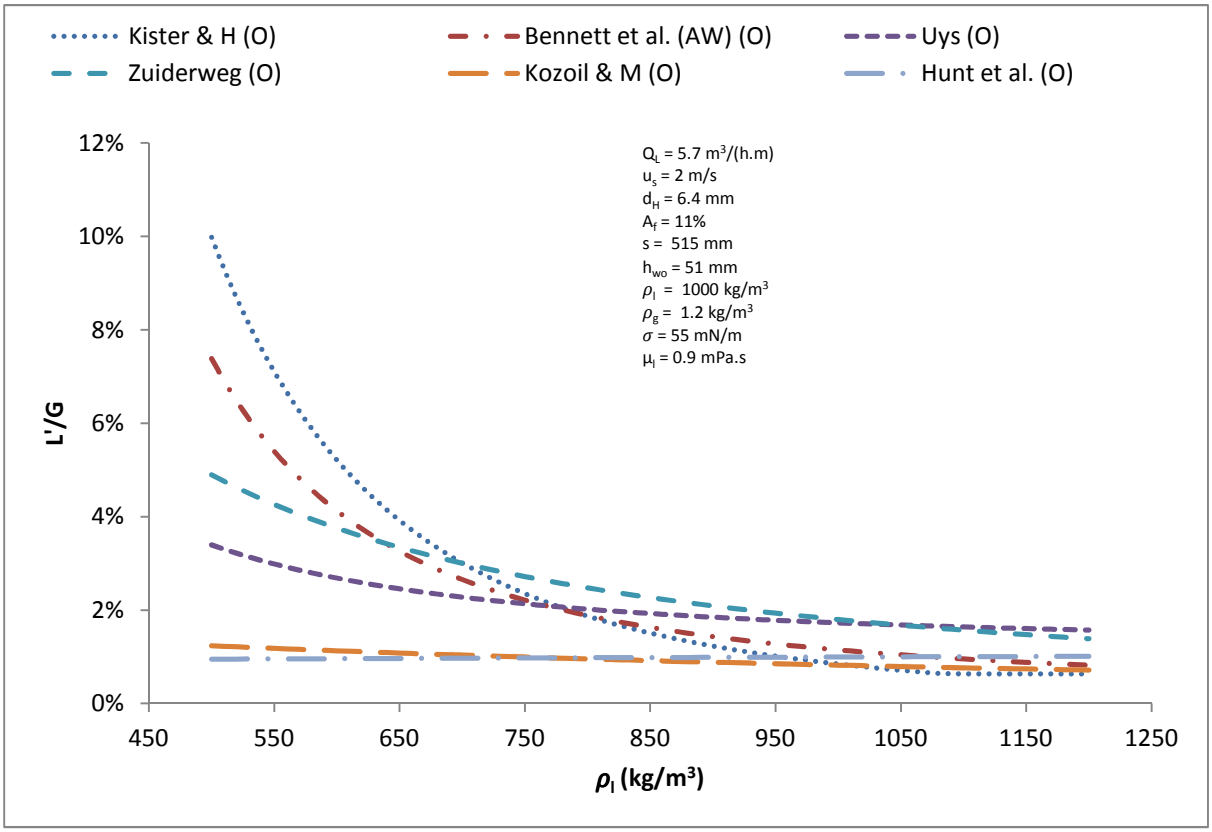

Figure 18 – Modelling the effect of liquid density on entrainment for Q_L = 5.7 m³/(h.m) and u_s = 2 m/s.

The following figures addresses the fluid properties effects on the entrainment, where the liquid density, gas density, liquid surface tension and the liquid viscosities are varied individually while keeping the other fluid properties constant. The effect of liquid density on entrainment is modelled in Figure 18 for Q_L = 5.7 m^3/(h.m) and u_s = 2 m/s, Figure 120 in Appendix B for Q_L = 34.3 m^3/(h.m) and u_s = 2 m/s and in Figure 19 for Q_L = 34.3 m^3/(h.m) and u_s = 2.5 m/s. The 'Thomas & O' model does not take into account the effect of the liquid density on the entrainment since it was not investigated. All the models are used outside their recommended ranges in the graphs displaying the effect of liquid density.

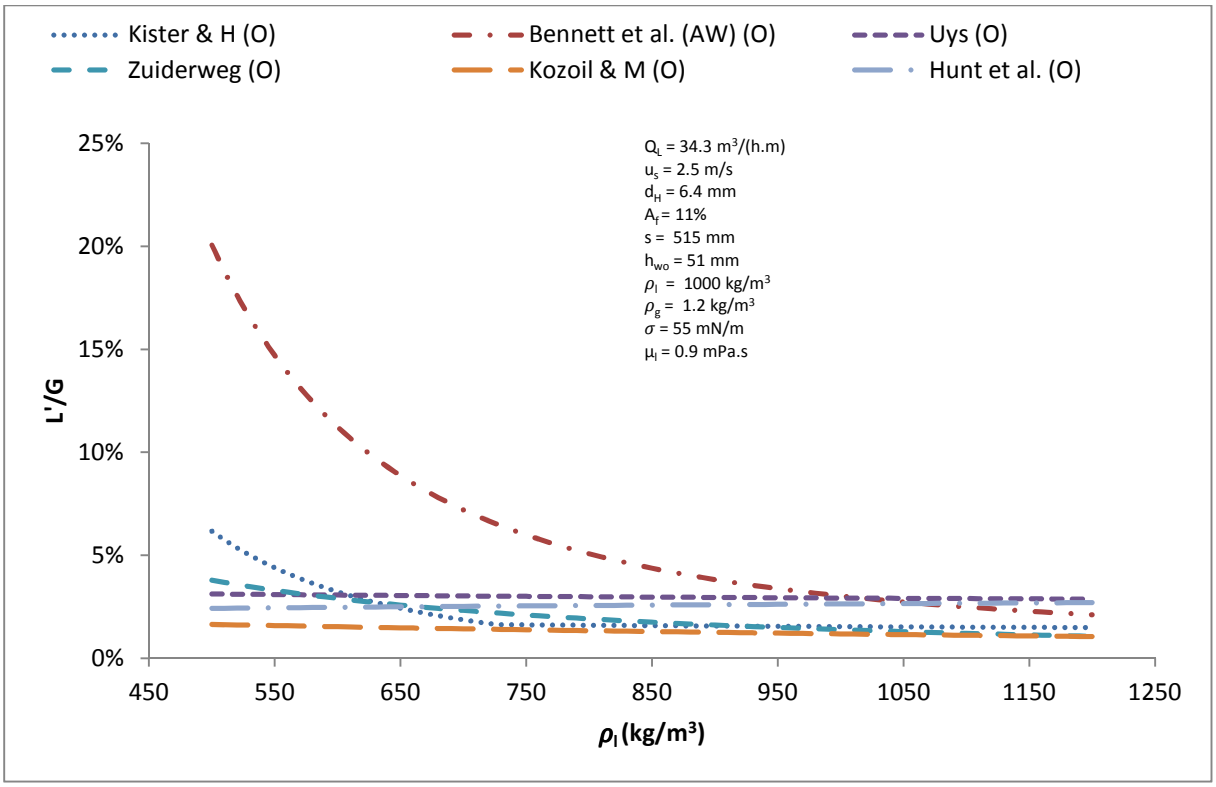

Figure 19 – Modelling the effect of liquid density on entrainment for Q_L = 34.3 m^3/(h.m) and u_s = 2.5 m/s.

In Figures (18, 120 and 19), the 'Uys', 'Kozoil & M' and 'Hunt *et al.*' models show that the entrainment has a low dependency on liquid density. The 'Bennett *et al.*', 'Kister & H' and 'Zuiderweg' models show that entrainment has a high dependency on liquid density. The liquid density dependent models show that entrainment decreases with increasing liquid density, except the 'Hunt *et al.*' model which shows that entrainment increases with increasing liquid density. The figures show that entrainments dependency on the liquid density increases as the superficial gas velocity increases and liquid flow rate decreases.

The effect of the liquid surface tension on entrainment is modelled in Figure 20 for Q_L = 5.7 m^3/(h.m) and u_s = 2 m/s, Figure 121 in Appendix B for Q_L = 34.3 m^3/(h.m) and u_s = 2 m/s and in Figure 21 for Q_L = 34.3 m^3/(h.m) and u_s = 2.5 m/s. The 'Thomas & O', 'Bennett *et al.*' and 'Zuiderweg' models do not take into account the effect of the liquid surface tension on entrainment since it was not investigated. In the 'Kister & H' and 'Bennett *et al.*' entrainment investigations, it was assumed that liquid surface tension has a negligible effect on entrainment. The 'Hunt *et al.*', 'Kozoil & M' and 'Uys'

models show that entrainment decreases with increasing liquid surface tension. The entrainment is shown to be more dependent on the liquid surface tension when the superficial gas velocity and liquid flow rate increases (high magnitudes). All the models are used outside their recommended ranges in the graphs displaying the effect of liquid surface tension.

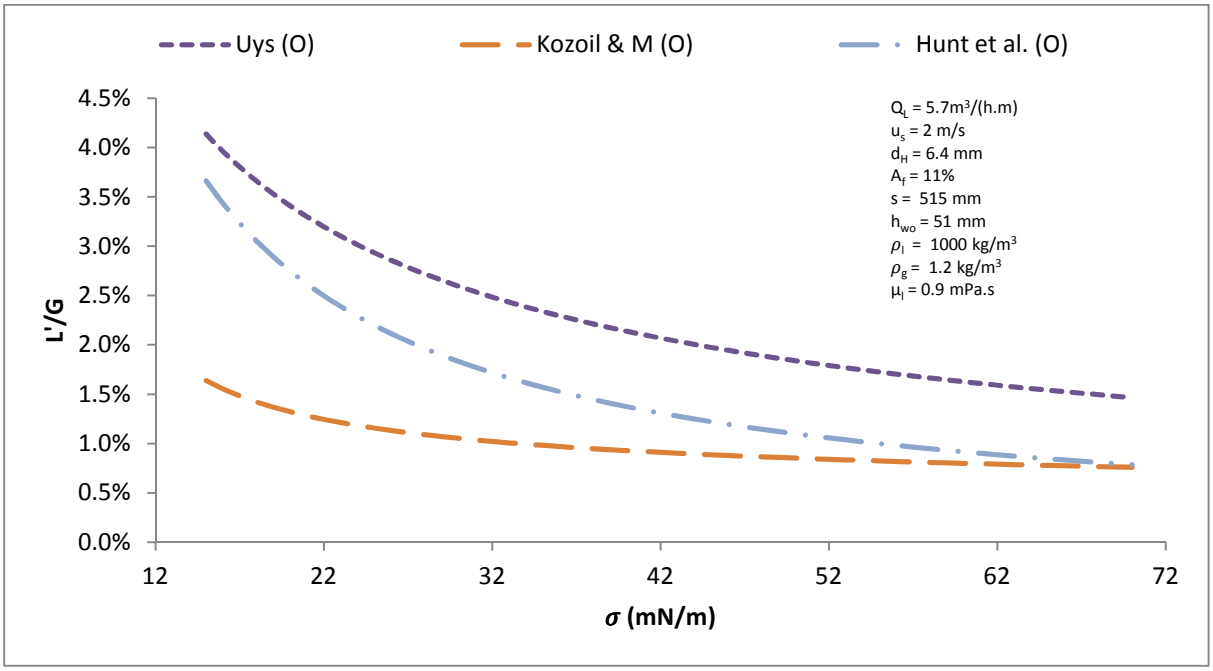

Figure 20 – Modelling the effect of surface tension on entrainment for Q_L = 5.7 m³/(h.m) and u_s = 2 m/s.

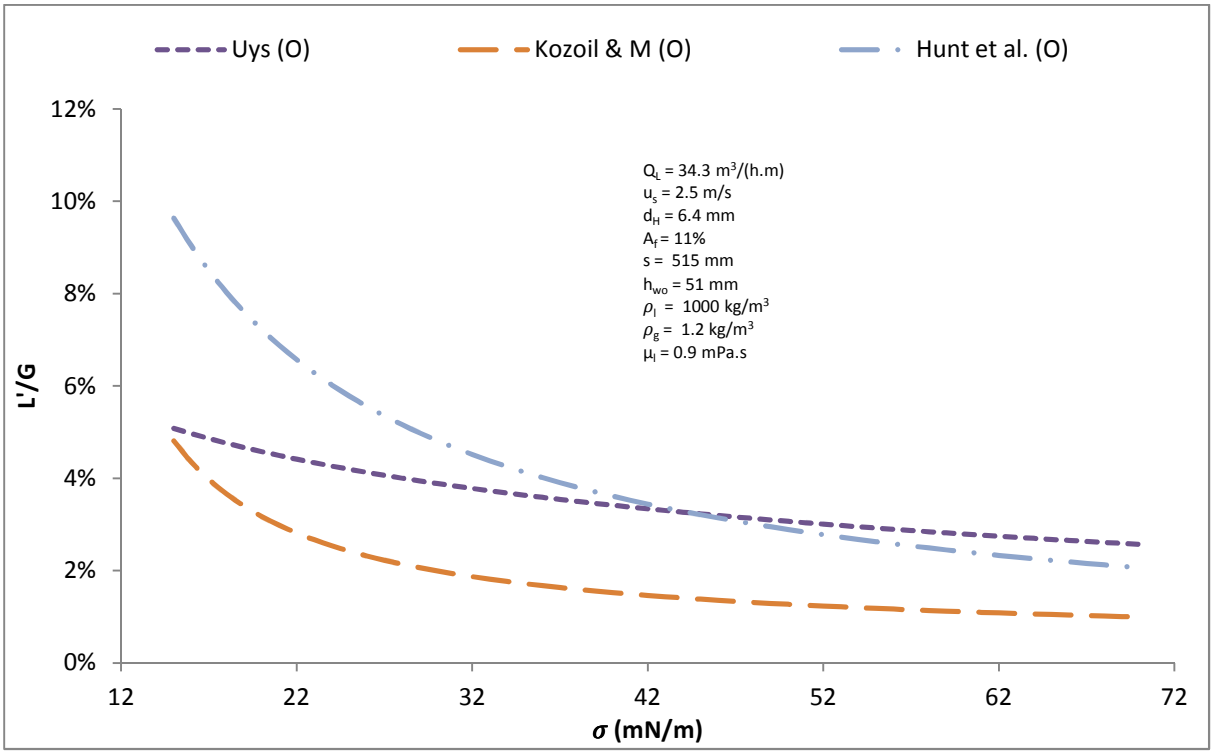

Figure 21 – Modelling the effect of surface tension on entrainment for Q_L = 34.3 m³/(h.m) and u_s = 2.5 m/s.

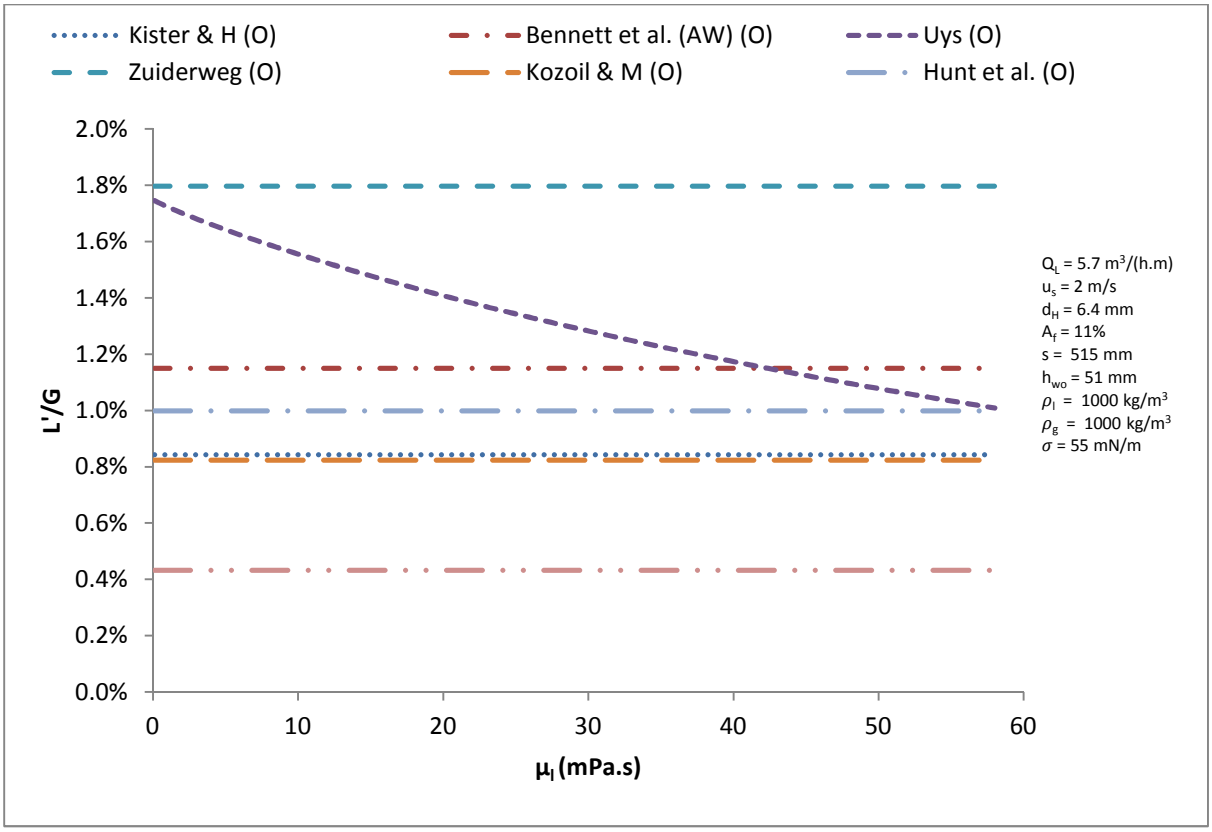

Figure 22 – Modelling the effect of liquid viscosity on entrainment for Q_L = 5.7 m^3/(h.m) and u_s = 2 m/s.

The effect of the liquid viscosity on entrainment is modelled in Figure 22 for Q_L = 5.7 m^3/(h.m) and u_s = 2 m/s. The 'Uys' model is the only model to show that the liquid viscosity has a significant impact on the entrainment magnitude. The other models do not take into account the effect of the liquid viscosity on entrainment since it was not investigated, however the models are still shown to determine the entrainments magnitude prediction discrepancies. The 'Uys' model shows that entrainment decreases with increasing liquid viscosity, but the impact of the liquid viscosity is small although still significant for the liquid viscosity range investigated. All the models are used outside their recommended ranges in the liquid viscosity graphs.

The effect of the gas density on entrainment is modelled in Figure 23 for Q_L = 5.7 m^3/(h.m) and u_s = 2 m/s, Figure 122 in Appendix B for Q_L = 34.3 m^3/(h.m) and u_s = 2 m/s and in Figure 24 for Q_L = 34.3 m^3/(h.m) and u_s = 2.5 m/s. The 'Thomas & O' model does take into account the effect of the gas density on entrainment since it was not investigated. The entrainment magnitudes are shown to increase with increasing gas density with all the gas density dependent entrainment models except the 'Hunt *et al.*' model (over the entire range) and the 'Uys' model (at low gas densities). The jump in the 'Bennett *et al.*' model entrainment magnitude is due to a change in the controlling model regime mechanism (froth to spray regime). All the models are used outside their recommended ranges in the gas density graphs.

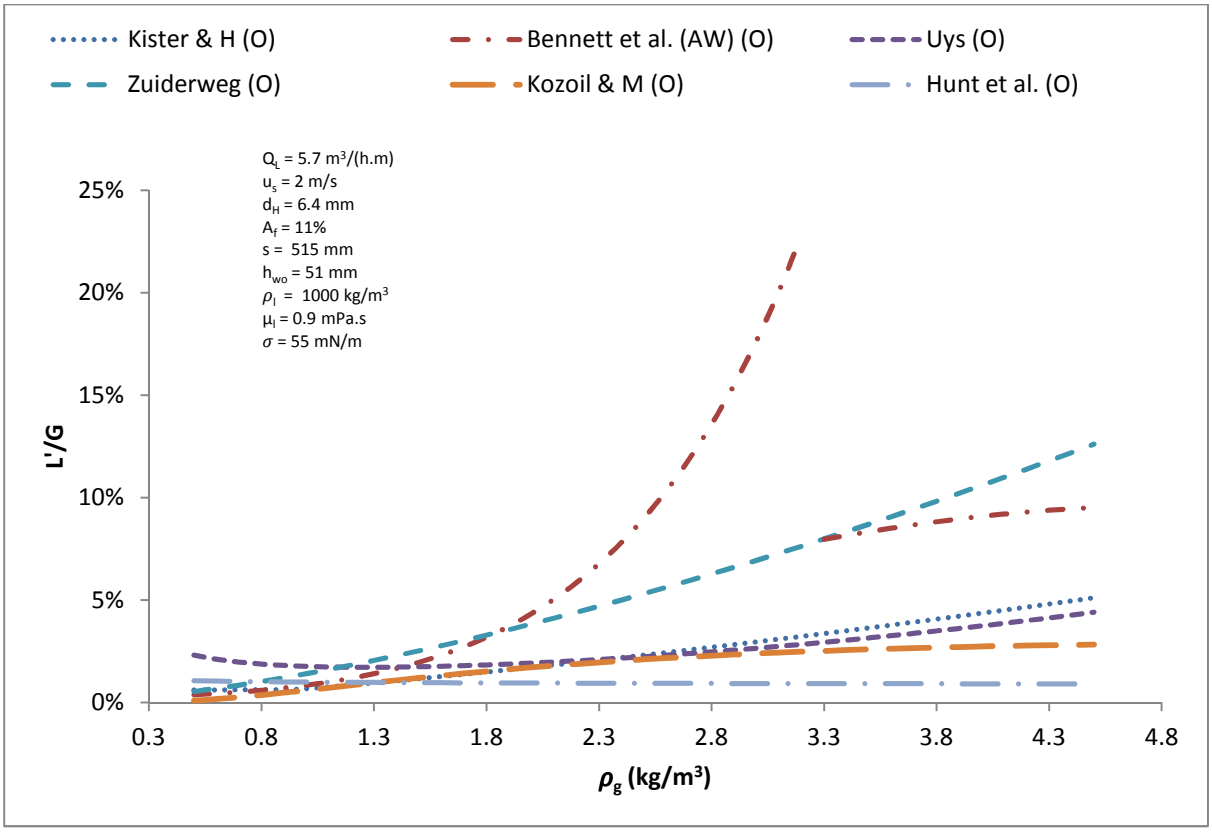

Figure 23 – Modelling the effect of gas density on entrainment for Q_L = 5.7 m^3/(h.m) and u_s = 2 m/s.

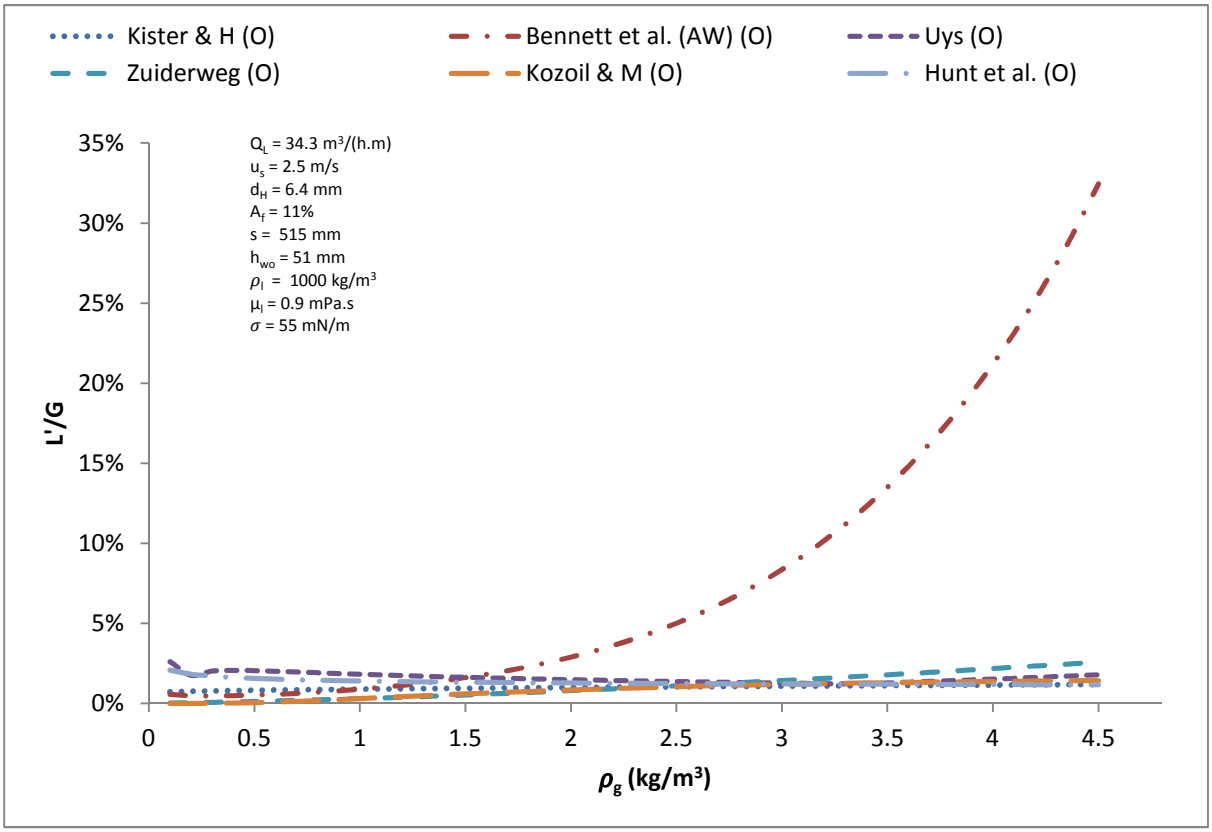

Figure 24 – Modelling the effect of gas density on entrainment for Q_L = 34.3 m^3/(h.m) and u_s = 2.5 m/s.

2.7 Literature Summary

This section highlights the main findings in the sieve tray distillation literature review, where the section focuses on entrainment and weeping effects inside the distillation column. Table 5 and 6 shows the experimental investigations of the literature sources and the main objectives and scopes of their studies into sieve tray hydrodynamics.

It was shown that the dispersion layer above the sieve tray behaves differently in different regimes, spray regime (gas jetting), bubble regime, froth regime (bubbling and jetting through holes), emulsion regime and foam regime. Porter and Jenkins (1979) described the transition from the froth to spray regime as the minimum in the entrainment (L'/G) magnitude. This technique was used by authors such as Bennett *et al.* (1995) and Kister (1992) in the development of entrainment models for a particular regime. The column configuration aspects that affect the flow dynamics on the tray are the shape of the column (circular or rectangular), column size, hole diameter, fractional hole area, downcomer area, weir height, weir design, calming zone length, tray spacing, sieve hole pitch and tray thickness. The fluid properties that affect the hydrodynamics in the sieve tray distillation column are the gas/vapour and liquid density, surface tension and liquid viscosity.

The first model presented to predict the clear liquid height is that by Colwell (1981), in which it is described that the clear liquid height is useful in the prediction of pressure drop, weeping, entrainment, efficiency and residence time of a sieve tray column. The clear liquid height model presented by Colwell (1981) is the most recommended clear liquid height and used in the entrainment models such as Kister (1992) and weeping models presented by Lockett and Banik (1986).

In the process industry it is generally believed that the hydrodynamics of the distillation process is well defined because of the popularity of the distillation process. However this is false based on the literature analysis, which showed that the sieve tray distillation hydrodynamics (entrainment and weeping) trends and models are based on basic experimental methods, equipment and simplified distillation parameters limits. Most of the entrainment models developed are developed using air/water systems. Very little reliable non-air/water data exists that describe entrainment over a wide range of gas flow rates, liquid flow rates, hole diameters, fractional hole areas, tray spacing, weir heights and column geometries.

The entrainment model developed by Hunt *et al.* (1955) is unreliable since a 6 in. distillation column is used, where the liquid height above the tray is maintained at a constant height with no liquid flow across the tray. Thomas and Ogboja (1978) measured the entrainment magnitude with the use of a catch-pot, where the accuracy is not justified in the measurement of the entrainment using this technique. The Kister (1992) and Bennett *et al.* (1995) models described entrainment with the use of data by Yanagi and Sakata (1982). It was shown by Yanagi and Sakata (1982) that the entrainment capturing technique experienced difficulties, making it unclear how accurate the models developed by Kister (1992) and Bennett *et al.* (1995) are and shows that the entrainment models possess limitations. The entrainment model developed by Kozoil and Mackowaik (1990) is based on data produced by the Kister (1992) model.

Table 5 – Investigations into fractional hole area and hole diameter reported in literature

Reference	Hole Diameter (in.)	Fractional Hole Area
Mayfield *et al.* (1952)	1/3, 3/16 and 1/4	Pitch given (1/4 to 3/4 in.)
	1/8, 3/16 and 1/4	4.1% and 6.9%
Hunt *et al.* (1955)	1/8, 1/4, 3/8 and 1/2	4.9% to 21.5% (no full factorial)
Bain and Van Winkle (1961)	1/4, 3/16, 1/8 and 1/16	Pitch given (3/16 to 3/4 in.)
Calcaterra *et al.* (1968)	3/8	Pitch given (1 to 1/8 in.)
Porter and Wong (1969)	1/8, 3/16, 1/4 and 1/2	3.2% to 4.78%
Lemieux and Scotti (1969)	1/2 and 1	7.4%, 9.6% and 10%
Pinczewski and Fell (1972)	1/4, 1/2 and 3/4	5.9%, 10.7%, 11% and 16.1%
Jeronimo and Sawistowski (1973)	1/4, 1/2 and 3/4	5.9% to 16.1%
Loon *et al.* (1973)	1/4, 3/4	5% and 15.1%
Pinczewski and Fell (1974)	1/4, 1/2 and 3/4	5.9%, 10.7%, 11% and 16.1%
Pinczewski and Fell (1975)	1/8, 1/4, 3/8 and 1/2	5% to 13%
Pinczewski *et al.* (1975)	1/2	5.9%, 10.4% and 16.1%
Payne and Prince (1975)	1/8, 3/16, 1/4 and 3/8	Single hole
Lockett *et al.* (1976)	1/8, 3/16, 1/4, 1/2	3.3% to 17.3%
Pinczewski and Fell (1977)	1/4 to 3/4	5% to 16%
Payne and Prince (1977)	3/16 and 1/4	4% and 9%
Thomas and Ogboja (1978)	1	12.4%
Lockett (1981)	1/8, 3/16, 1/4, 1/2	3.2% to 9.4%
Kister *et al.* (1981)	1/4, 1/2 and 3/4	5.9%, 10.7% and 16.1%
Yanagi and Sakata (1982)	1/2	14%
Zuiderweg (1982)	Mixed sources	8% and 14%
Faesan (1987)	1/4	14.2%
Puppich and Geodecke (1987)	1/4 and 1/2	17%
Kozoil and Mackowaik (1990)	1/4 in. and 15 mm	2.7% to 34.3%
Keskinen *et al.* (2006)	3 mm and 5 mm	10.1% and 10.6%
Van Sinderen *et al.* (2003)	1/4 and 1/2	6% and 7.6%
Uys *et al.* (2009)	1/4	15.8%

Table 6 – Literature parameters investigated and differences

Reference	Parameters Investigated	Column Configuration Differences
Mayfield *et al.* (1952)	Fluid physical properties effect on orifice coefficient (AW and NAW)	6 in. diameter plate
	Orifice coefficient (AW and NAW)	6.5 ft. diameter column
Hunt *et al.* (1955)	Capacity factors (pressure drop and entrainment) (AW)	6 in. diameter plate
Bain and Van Winkle (1961)	Entrainment for air/water systems	6 In. wide, 28-3/4 in. rectangular column
Calcaterra *et al.* (1968)	Free and captured entrainment for air/water system	13 in. diameter column
Porter and Wong (1969)	Froth to spray transition data (AW/NAW)	Rectangular column, dimensions unknown
Lemieux and Scotti (1969)	Pressure drop and entrainment	
Pinczewski and Fell (1972)	Froth-to-spray transition (AW)	30.5 cm by 61 cm rectangular plate
Jeronimo and Sawistowski (1973)	Froth-to-spray transition (AW)	Geometry not given
Loon *et al.* (1973)	Froth-to-spray transition (AW)	30.5 cm by 61 cm rectangular plate
Pinczewski and Fell (1974)	Two phase dispersion	30.5 cm by 61 cm rectangular plate
Pinczewski and Fell (1975)	Sieve tray oscillations	Geometry not given
Pinczewski *et al.* (1975)	Phase inversion on sieve trays	30.5 cm by 61 cm rectangular plate
Payne and Prince (1975)	Froth to spray transition data (AW/NAW)	20 cm by 28 cm rectangular column
Lockett *et al.* (1976)	Regime effects on entrainment and pressure drop	0.46 m diameter column
Pinczewski and Fell (1977)	Droplet size in the spray regime (AW)	30.5 cm by 61 cm rectangular plate
Payne and Prince (1977)	Froth-to-spray transition (AW)	431 mm by 452 cm rectangular column
Thomas and Ogboja (1978)	Hydraulic behaviour of sieve trays	3 ft. by 1 ft. rectangular column
Lockett (1981)	Froth-to-spray transition (AW)	1217 mm by 630 mm plate
Kister *et al.* (1981)	Entrainment in the spray regime	Geometry not given (Data obtained from multiple sources)
Yanagi and Sakata (1982)	Commercial scale performance (efficiency and entrainment)	1.2 diameter column
Zuiderweg (1982)	Pressure drop, entrainment and efficiency	Mixed sources of data
Faesan (1987)	Hydraulic behaviour of sieve and valve trays	0.63 m diameter column
Puppich and Geodecke (1987)	Entrainment in tray columns	0.4 m by 0.4 m column
Kozoil and Mackowaik (1990)	Entrainment in tray columns	0.38 m diameter and 1 m diameter column
Keskinen *et al.* (2006)	Hydraulic behaviour of sieve trays	0.5 m by 0.164 m rectangular column
Van Sinderen *et al.* (2003)	Hydraulic behaviour of sieve trays	0.2 m by 0.2 m diameter column
Uys *et al.*(2009)	Entrainment in sieve trays	175 mm by 635 mm internal rectangular column

The investigation performed by Uys (2012) considered the effect of fluid properties on entrainment and expanded on the range of gas and liquid property effects on entrainment, but does not take the effect of tray geometry and column geometry into account. In the model critical evaluation section 2.6, the model comparison is performed at a fractional hole area of 11% making the 'Uys' model invalid, however the model is still shown so that the largest areas (parameter ranges) of uncertainty can be highlighted. The model critical evaluation section 2.6 showed the importance for a detailed sieve tray geometry investigation, based on the differences in the entrainment model magnitude prediction of the Uys (2012) compared to the other entrainment models.

The critical evaluations of existing entrainment models show that the different experimental investigations do not produce a comprehensive description of the effects of the different distillation parameters over a wide range of parameters. The investigation showed that there is a little agreement between the different model entrainment model magnitude predictions, where most models were plotted beyond their recommended ranges. This shows that an experimental investigation should be done within the ranges of parameters not investigated (different fluids, tray and column geometries).

The literature investigations showed that the different authors do not produce a detailed description of the effect of sieve tray hole diameters and fractional hole area on entrainment over multiple systems. This in turn shows that a detailed description of the possible effects of tray geometry on entrainment over a wider range of fluid systems has to be investigated. This will show the combined effect of fluid properties and tray geometry on the entrainment rate. The literature investigation shows that a fundamental model or means of describing the effect of different parameters on entrainment has to be developed.

In the investigation into weeping inside a sieve tray distillation column, the model developed by Lockett and Banik (1986) described the change in weeping using a linear model, making it unreliable. The investigation shows experimental effects of sieve tray geometry on weeping, but does not show an extensive investigation into the effect of liquid and gas physical properties on weeping. The literature investigation shows that the weeping is not investigated over a wide range of distillation parameters (different fluids, tray and column geometries).

Chapter 3 – Objectives and Outcomes

The current chapter highlights the objectives for the distillation hydrodynamic study, the possible outcomes from the objectives of the experimental investigation based on the literature review.

3.1 Objectives of Study

The objectives of the experimental investigation into sieve tray hydrodynamics are as follows:

1. To evaluate the effect of hole diameter on the hydrodynamics of a sieve tray distillation column.
2. To identify the effect of the fractional hole area on the hydrodynamics of a sieve tray distillation column in terms of pressure drop, entrainment and weeping.
3. To identify the effect of fluid physical properties (gas/liquid density, liquid surface tension and gas/liquid viscosity) on the dispersion characteristics, sieve tray pressure drop, entrainment and weeping.
4. To identify how the change in the gas and liquid flow rate affects the hydrodynamics of the sieve tray distillation column.
5. To evaluate the dependency of entrainment on the fluid physical properties and tray geometry during the different defined dispersion phases (spray and froth).

3.2 Expected Outcomes of Study

The expected outcomes of the experimental investigation into sieve tray hydrodynamics were as follows:

1. To produce a wide range of sieve tray distillation entrainment data. This can aid in identifying the fluid phase regime transition points in the dispersions above the trays.
2. To produce sieve tray distillation data that can aid in identifying the capacity limits in a sieve tray distillation column.
3. An increase in understanding of the effects of fractional hole area, hole diameter and fluid physical properties on entrainment of a sieve tray distillation column.
4. The development of basic dimensionless number combinations that will help predict the effects of column configuration and fluid physical properties on entrainment.
5. An increased understanding of the effects of fractional hole area, hole diameter and fluid physical properties on weeping of a sieve tray distillation column.
6. Development of basic dimensionless number combinations that can predict the effects of column configuration and fluid physical properties on weeping of the sieve tray distillation column.
7. Increase in understanding of the effects of the column configuration on phase regime changes and dispersion characteristics.

Chapter 4 - Experimental Equipment Design

The subsequent section addresses the sieve tray distillation pilot plant used (equipment and fluids used) in the experimental investigation. The experimental data validation is shown for both the entrainment results and the weeping experimental results later in this chapter. The sieve tray designs are shown in Appendix C, additional equipment specifications are shown in Appendix D and the procedure for the operation of the distillation column pilot plant is shown in Appendix E.

4.1 Experimental Design and Materials

In the experimental investigation the pilot plant consists of the following units:

- Sieve tray distillation column used for hydrodynamic characterization.
- A pump to circulate the liquid through the column and piping in the place of a condenser, since only hydrodynamics studies are done on the column and the thermodynamics or mass transfer effects are not evaluated.
- A blower to circulate the gas through the column since a re-boiler is not used, for reasons stated above.
- Heat exchanger to control the temperature of the gas and liquid in the column at a constant value of 25℃.
- Hold tank vessel that can be used to measure entrainment and weeping in the distillation column.
- A surge tank to dampen the possible pressure fluctuations caused by the gas expansion and contraction in the distillation column. The vessel should act as a gas loading tank for the distillation pilot plant.
- Sensors to measure the flow rates of the gases and liquids, absolute pressure, differential pressure (pressure drop) and the temperature.
- Control system to control the temperature, pressure and flow rate by manipulating the valves of the pilot plant.

The distillation column is rectangular in shape with a width of 175 mm and breadth of 635 mm, where the section between the trays can be manipulated to heights of 315, 415, 515 and 615 mm. Figures 133 and 134 in Appendix D show the side and front view of the distillation column used in the pilot plant. The column is chosen to be rectangular as to eliminate the wall effects and eliminate the expansion effects at the downcomer escape and contraction effects at the outlet weir (producing a uniform liquid flow).

Perspex windows are placed on the front of the column to monitor the flow patterns of the liquid on the tray (to identify visually the possible regimes in the column). Windows are placed on the side of the column at the downcomer as to monitor the downcomer capacity (to prevent flooding and to ensure the downcomer has an adequate seal at its exit). The gas feed is placed above the sump section to blow the gases upward through the column and the liquid is fed into the downcomer of the top tray. The sump holds the liquid in the bottom of the column and feeds it to the pump so that it can be fed to the top of the column.

The distillation column shown in Figures 133 and 134 consist of removable sections so that the tray spacing can be adjusted, where only the 515 mm tray spacing section was used in the experimental investigation. The distillation column is fitted with an adjustable downcomer that can change the downcomer escape area. The downcomer escape height is manipulated to a particular height so that the liquid velocity through the downcomer escape is within the range of 0.15 to 0.6 m/s. The escape area settings for the experimental investigation are shown in Table 7.

Table 7 – Experimental liquid flow settings

Flow setting	1	2	3	4	5	6	7	8	9	10	11	12	13
V_L (m^3/h)	0.5	1	1.5	2	2.5	3	4	6	8	10	12	14	16
Q_L [m^3/(h.m)]	2.9	5.7	8.6	11.4	14.3	17.1	22.9	34.3	45.7	57.1	68.6	80.0	91.4
Escape opening (mm)	5	5	5	7	9	11	14	21	28	35	42	45	45
u_l (m/s)	0.16	0.32	0.48	0.45	0.44	0.43	0.45	0.45	0.45	0.45	0.45	0.49	0.56

Figure 25 shows the shape and layout of the sieve trays that were used in the experimental investigation, where all the sieve tray holes are laser cut.

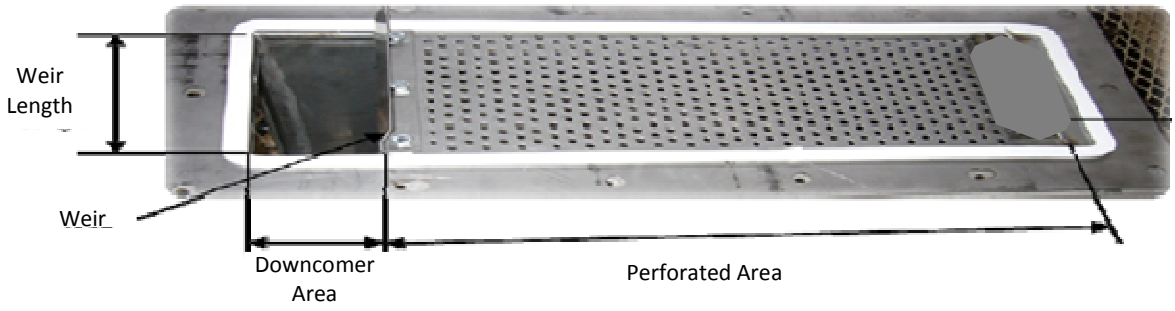

Figure 25 – Sieve tray design for the distillation column [altered with permission from Uys *et al.* (2009)].

In the experimental investigation into hydrodynamics of the distillation column, the sieve trays that were investigated are shown by Table 8. The table shows that three fractional hole areas (7%, 11% and 15%) were tested to see what effect the fractional hole area has on the hydrodynamics and capacity of the distillation column. The rather high fractional hole area of 15% was evaluated to test the experimental limits of sieve distillation hydrodynamics. Three hole diameters (⅛, ¼ and ½ in.) were tested to determine the effect of sieve tray hole diameter sizes on the responses of the distillation process (entrainment, weeping and pressure drop), producing nine different trays for the experimental investigation.

Table 8 – Tray design specifications

Tray No.	Hole diameters (mm)	Hole diameters (in.)	Pitch (mm)	(p_t/d_h)	No. of holes	Fractional hole area
Tray 1	6.4	¼	14.5	2.3	414	15.8%
Tray 2	3.2	⅛	7.3	2.2	1656	15.8%
Tray 3	12.7	½	29	2.3	102	15.6%
Tray 4	6.4	¼	21.6	3.4	184	7%
Tray 5	3.2	⅛	10.8	3.4	736	7%
Tray 6	12.7	½	43.2	3.4	48	7.3%
Tray 7	6.4	¼	16.5	2.6	300	11.5%
Tray 8	3.2	⅛	8.3	2.6	1200	11.5%
Tray 9	12.7	½	33	2.6	75	11.5%
Tray 10	6.3	¼	14.5	2.3	414	15.6%
Tray 11 (L)	6.3	¼	14.5	2.3	414	15.6%

Table 9 – Column internals dimensions

Variable	Description	Magnitude
h_{wo} (mm)	Weir height	51
l (m) ($x10^3$)	Weir length	175
A_b (m^2)	Bubbling area	≅0.8
A_d (m^2)	Downcomer area	≅0.015
Ac (m^2)	Column cross sectional area	≅0.111
FPL (mm)	Flow path length	475
S (mm)	Tray spacing	515

The hole pitch to hole diameter (p_t/d_H) ratio is kept constant for each tray fraction hole area investigated, where the sieve tray holes are triangularly pitched (Table 8). The trays designed for the experimental investigation are shown Figures 123 to 132 in Appendix C. The trays are made so that

weirs of different sizes can be added with little machining in future experimental investigations. In Table 8, Tray 10 was the tray used by Uys (2012) and was used to test the repeatability and validate the experimental results, where the sieve tray holes are punched. Tray 11 is a tray designed to the specifications of Tray 10 where its holes are laser cut. The specification of the distillation column internals is shown in Table 9.

The distillation column contains a chimney tray below the two sieve trays in the distillation column in order to distribute the gas evenly below the bottom sieve tray. The chimney tray also acts as a liquid capturing tray, to detain the liquid that weeps through the bottom sieve tray in order to measure weeping by transferring the liquid to the weeping hold-up tank (MV-203). The wept (weeping magnitude) liquid is determined by measuring the change in the liquid hold-up pressure over time inside the hold-up tank. In the de-entrainment section, a de-entrainment tray was used for separating most of the liquid from the gas and a mesh grid (shown in Figure 26) to remove the liquid trapped in the vapour mist (the remaining droplets).

Figure 26 – Mesh grid [obtained with permission from Uys *et al.* (2009)].

The de-entrainment tray has cylindrical columns with angle louvers cut into the cylindrical columns, to capture liquid droplets where the liquid is separated by centripetal forces. The liquid settles onto the tray and passes to the entrainment tank (MV-204) to measure the mass flow rate of the entrained liquid. The liquid from the mesh grid also falls onto the de-entrainment tray to be measured. The louvers are angled at 32° to 35° to allow the centrifugal force inside the de-entrainment tray cylinders. The specifications of the other equipment and sensory devices in the tray distillation column pilot plant are shown in Appendix D.

Figure 27 shows a process flow diagram of the tray distillation column pilot plant, where a CAD assembly drawing on the pilot plant is shown in Figure 136 in Appendix D. In the process flow diagram (Fig. 27), gas is fed to the surge tank from the gas tanks. The gas blower sucks in the gas and force the gas from the surge tank into the distillation column above the sump, which is filled with liquid to just below the gas inlet pipe. The gas is then redistributed by the chimney tray and flows through the sieve tray holes in Tray 2 and then Tray 1. The downcomer escape has a sufficient seal as to prevent the gas from flowing into the downcomer and only flows through the tray holes in the sieve tray. The gas then flows through the de-entrainment tray and mesh grid which removes any liquid entrained by the gas. The gas flows out through the top of the column and back into the surge tank which absorbs pressure fluctuation of the gas that is caused in the column. The gas is drained out of the column by a purge stream, which vents the gas to the atmosphere (outside of the laboratory).

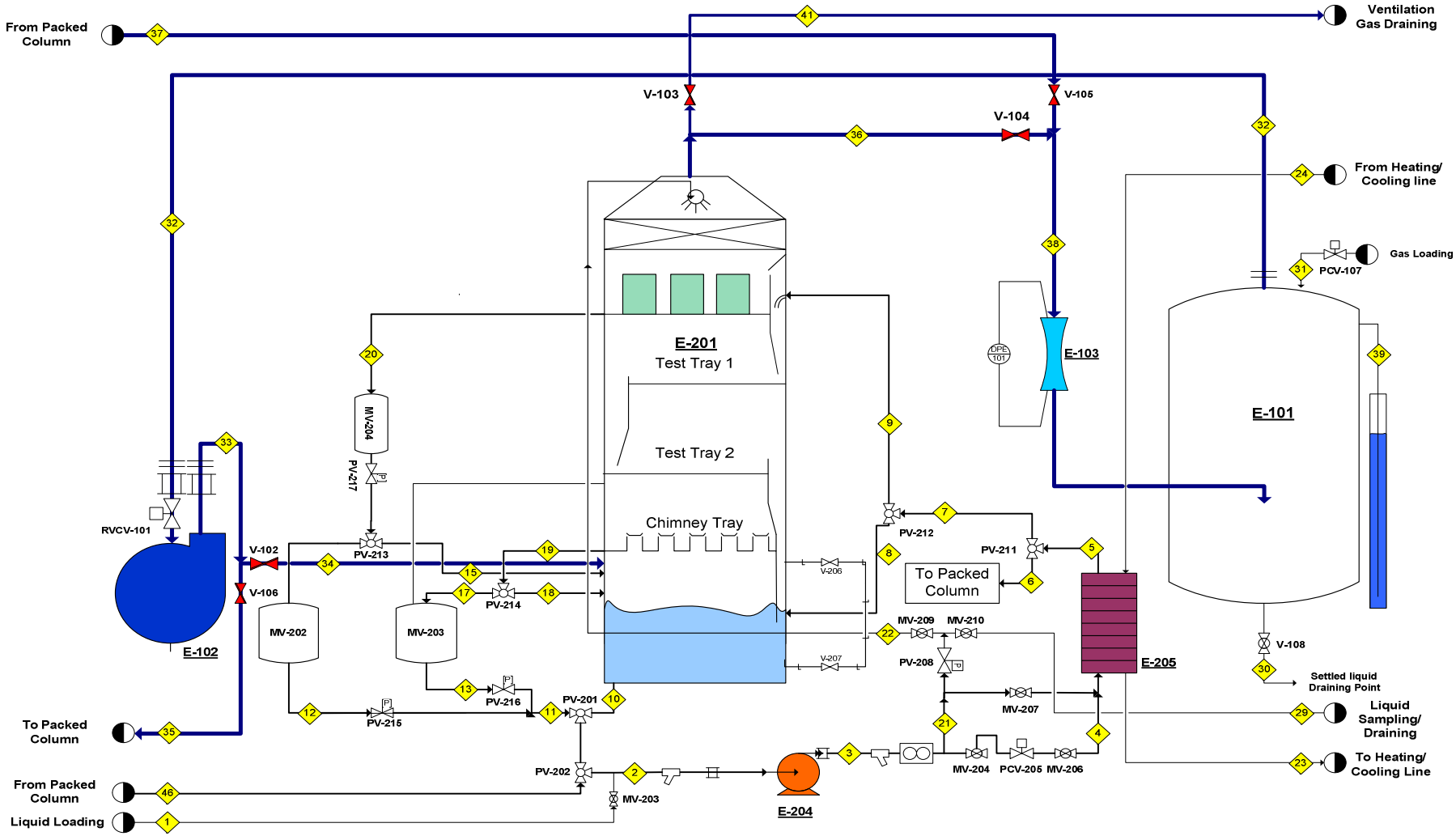

Figure 27 – Sieve tray distillation column PFD [Adapted with permission from Uys *et al.* (2009)].

The liquid is inserted into the pilot plant by filling the sump with liquid. The liquid is transported through to the top of the distillation column by a centrifugal pump which sucks the liquid from the sump and forces it through a heat exchanger. The heat exchanger is used to control the internal temperature of the distillation column at a constant temperature of 25℃, by the use of cooling/heating water. The liquid is pumped through a flow meter and then a flow control valve before the heat exchanger, which could be used to manipulate the flow rate of the liquid. The flow control valve has a bypass so that the flow rate could also be controlled manually by manipulating the inverter frequency of the pump. The liquid then flows into the top downcomer attached to the de-entertainment tray, where the liquid is transported across the top sieve tray (Tray 1) into the downcomer and to the bottom sieve tray and downward through the column back into the sump.

The P&ID for the pilot plant is shown by Uys *et al.* (2009), which shows the control instruments, where the details of the sensor and control equipment are given in Appendix D. In the de-entrainment section, liquid is captured onto the de-entrainment tray and then transported to the hold-up tank (MV-204) shown in Figure 135 in Appendix D. The small hold-up tank measures the liquid mass change over time producing the entrainment magnitude.

The large entrainment hold-up tank (MV-202) is shown in Figure 137 in Appendix D, where it could be used when the entrainment magnitudes are large (close to flooding point). In the current experimental investigation only the small entrainment hold-up tank (MV-204) was used. When the entrainment mass is obtained the hold-up tanks are emptied into the sump of the distillation column, using the pump (E-204).

The weeping magnitude was measured by the liquid that falls onto the chimney tray, which is transported to the hold-up tank (MV-203) as shown in Figure 27. The weeping magnitude was measured as the change in the mass of the tank with time, using the differential pressure meter in the tank. When weeping is measured completely, the hold-up tank is emptied by the use of the pump (E-204) and fed to the top of the distillation column.

The temperature control system of the tray distillation pilot plant is shown in Figure 138 in Appendix D. Liquid is pumped to a water bath (E-13), where the temperature of the tank (E-13) is controlled using a heating element temperature control system. The liquid is sucked from the bath and pumped to the heat exchanger (E-205) in order to control the temperature of the liquid in the tray distillation column at the defined temperature of 25℃. Cooling water is supplied when the temperature of 25℃ in the column is exceeded by the manipulation of the three way valves (V-47 and V-48). A pneumatic control valve is used for the cooling water line and a solenoid valve is used to control the flow of the hot water in the heating line.

The absolute pressure is measured at Tray 1 (PE-206) and the venturi (PE-102) in order to measure the gas physical properties and maintain the distillation column at atmospheric pressure (≅101.15 kPa). In the tray distillation column, digital differential transmitters are placed in the column to measure the pressure drop through the column.

The differential pressure transmitters are placed in the following locations in the column:

- Across the chimney tray (DPE-201), to measure pressure drop.
- Across sieve Trays 1 and 2 (DPE-202 and DPE-203) to measure the dry tray and wet tray pressure drop.
- Across the de-entrainment tray (DPE-204), to measure the pressure drop.
- Across the mesh grid (DPE-205), to measure its pressure drop.
- Across the venture pressure tapping (DPE-201) to determine the gas flow rate.
- Below the entrainment and weeping hold-up tanks (DPE-207 and DPE-208) to measure the mass of liquid in the tanks.

In the distillation column temperature sensors are used in order to monitor and control the temperature in the streams and are found in the following locations:

- The exit stream of the heat exchanger (TE-201).
- The inlet to the distillation column (TE-202).
- Above Tray 1 (TE-203) in the liquid cross flow path.
- Between Tray 1 and 2 (TE-204), in the gas flow path.
- Above Tray 2 (TE-205), in the liquid cross flow path.
- Between Tray 2 and the chimney tray (TE-206), in the gas flow path.
- In the sump (TE-207).
- In the weeping and entrainment hold-up tanks (TE-208 and TE-209).
- At the liquid flow meter exit (TE-210) to determine the mass flow rate from the volumetric flow rate.
- At the gas inlet stream into the distillation column (TE-101).
- At the inlet to the venture (TE-101), to know the gas physical properties.

Table 10 – Fluids and physical properties typically used industrial distillation applications [modified with permission from Uys *et al.* (2009)]

Compound	Formula	Boiling Point Temp [°C]	Absolute Pressure [kPa]	Liquid Density [kg/m^3]	Vapour Density [kg/m^3]	Liquid Viscosity [mPa·s]	Surface Tension [mN/m]
Methane	CH_4	-162	100	422	1.8	0.12	13
Butane	C_4H_{10}	-0.8	100	602	2.7	0.2	15
Pentane	C_5H_{12}	36	100	610	2.9	0.2	14
Octane	C_8H_{18}	125	100	612	3.7	0.2	12
Decane	$C_{10}H_{22}$	174	100	604	4.1	0.2	11
Dodecane	$C_{12}H_{26}$	216	100	595	4.5	0.2	9
Oxygen	O_2	-183	100	1142	4.4	0.2	13
Oxygen	O_2	-153	1000	976	38.5	0.1	6
Cyclohexane	C_6H_{12}	80	100	720	2.97	N/A	18
Water	H_2O	100	100	958	0.59	0.28	59
Water	H_2O	20	2.3	998	0.017	1	73
Water	H_2O	25	3.2	997	0.023	0.89	72
Silicone Oil	(C_2H_6OSi)	140	<1	965	>1	50	19

The fluid ranges typically used in industry can be described in part in table 10. The physical properties of the gases used in the experimental investigation are shown in Table 11. Only air and CO_2 are to be tested, since there is reasonable difference in the physical properties of the two gases.

Table 11 – Physical properties of gases investigated

Gas	Mw (kg/kmol)	Density (kg/m^3)	Dynamic viscosity (mPa.s)	Kinematic viscosity (mPa.s)
Air	29	1.18	1.82×10^{-2}	1.54E-05
CO_2	44	1.78	1.49×10^{-2}	8.37E-06

The physical properties of the liquids tested in the tray distillation experiment are shown in Table 12. Reasonable differences in the liquid physical properties are shown so that the effects of the liquid density, surface tension and viscosity on the hydrodynamics of the distillation process can be easily separated. The liquids and gases are chosen based on the physical properties of differences, availability, flammability, stability and cost. The fluids are chosen as to cover a wide range of industrial distillation processes.

Table 12 – Physical properties of liquids investigated

Liquids	Mw (kg/kmol)	Density (kg/m^3)	Dynamic viscosity (mPa.s)	Surface Tension (mN/m)	Boiling Point @ 1 atm °C
Water	18	999	0.9	57.8	100
Silicone Oil	74	959	51	20.9	130
n-Butanol	74	835	3.2	22.1	118
Ethylene Glycol	62	1110	13.5	36	198

In the experimental investigation the gas velocities were varied between 1.4 and 3.2 m/s in the dry tray pressure test, where the possible superficial gas velocities that are investigated are 1.7, 2, 2.3, 2.6 and 2.9 m/s in the hydrodynamic experimental test. The liquid flow rates were varied between 2.8 and 91.4 $m^3/(h.m)$, as shown in Table 7. The liquid flow rates were evaluated in terms of volumetric flow rate per weir length, so that the flow rate can be scaled according to other distillation columns in the industry. The current project produces over 10 000 data points for entrainment and 7 000 data points weeping. The data points for tray 1 using silicone oil are shown as example in Appendix G, where the rest of the data points if required should be requested with permission from the University of Stellenbosch.

4.2 Entrainment Data Validation

The current section shows entrainment repeatability in the sieve tray test distillation column and compares the experimental data to literature data, where the experiments were performed in a similar nature to the current investigation.

In Figure 28, five repeated experiments (Test 1 to 5) are compared with data from Uys (2012), where the experiments were performed on a similar tray (Tray 10). The experiments were performed with a 15.6% fractional hole area and the 6.3 mm hole diameter tray, for an air/water system at a superficial gas velocity of 2.6 m/s. In Figure 28, entrainment magnitudes are represented as L'/G and in Figure 139 in Appendix F entrainment is represented as L'/L.

Figure 28 (L'/G graph) shows that the repeated experiments vary in a similar way with increasing liquid flow rate, with a standard deviation as high as 0.1% at high entrainment magnitudes and a percentage deviation as high as 9% at low entrainment magnitudes. The deviation is attributed to the noise, the delay and error in the process equipment. In Figure 139 (L'/L graph), the repeated experiments vary similarly with increasing liquid flow rate, with a standard deviation as high as 0.21% at high entrainment magnitudes and a percentage deviation as high as 9.93% at low entrainment magnitudes, where the deviation is attributed to the noise, the delay and the error in the process equipment.

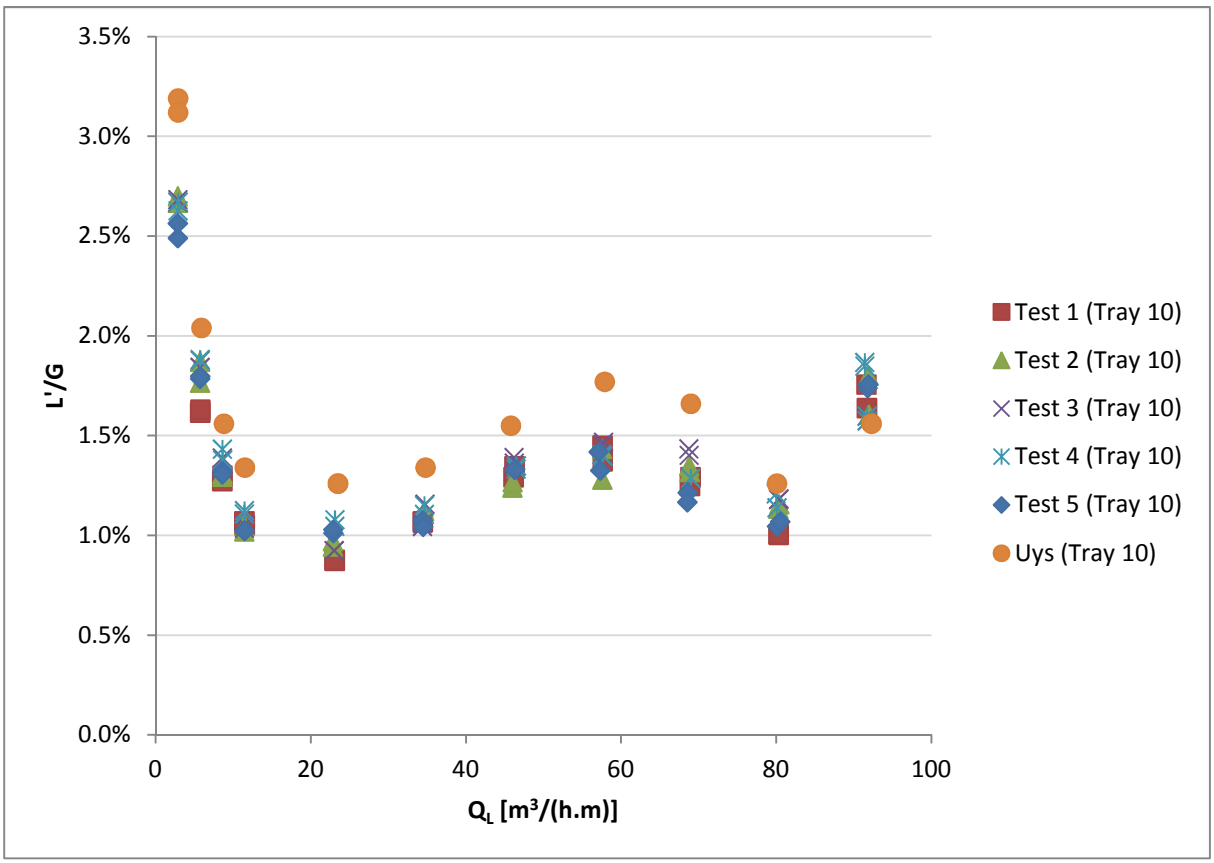

Figure 28 – L'/G entrainment repeatability and 'Uys' data comparison for Tray 10 (15.6%, 6.3 mm) and u_s = 2.6 m/s.

The entrainment magnitudes of the experimental data and that of Uys (2012) deviates significantly, where the experimental data under predicts the entrainment magnitude observed by Uys (2012) (Fig. 28 and 139). The deviations fall within error bounds typical of these hydrodynamics studies. The reason for the deviation is yet unknown, where a possible reason could be that there is a deviation in the experimental procedure, high process equipment error, possible errors in the calibration of process equipment or a possible calculation error.

The liquid hold-up pressure drop for the entrainment experiment is shown in Figure 29 for both the experimental data and the experiment performed by Uys (2012). The repeated experiments vary in a similar manner with increasing liquid flow rate (Fig. 29). A standard deviation as high as 8.5 Pa at a high liquid hold-up and a percentage deviation as high as 4.6% at low liquid hold-up, where the deviation is attributed to the noise, as well as the delay and the error in the process equipment. The experimental liquid hold-up data compares well to the data from Uys (2012), showing that the experiments were performed at a similar gas flow rate and liquid flow rate. The dry tray pressure drop for Uys (2012) and the current experiment data are compared to one another in Figure 140 in Appendix F. The experimental dry tray pressure drop for the current experiment (Test 1 and 2) compares well to that of Uys (2012) for the same tray (Tray 10), reiterating the accuracy in the gas flow rate (Fig. 140). The hold-up tanks were recalibrated to measure entrainment accurately and all the equipment was checked for leaks or possible deformations that might lead to inaccuracies.

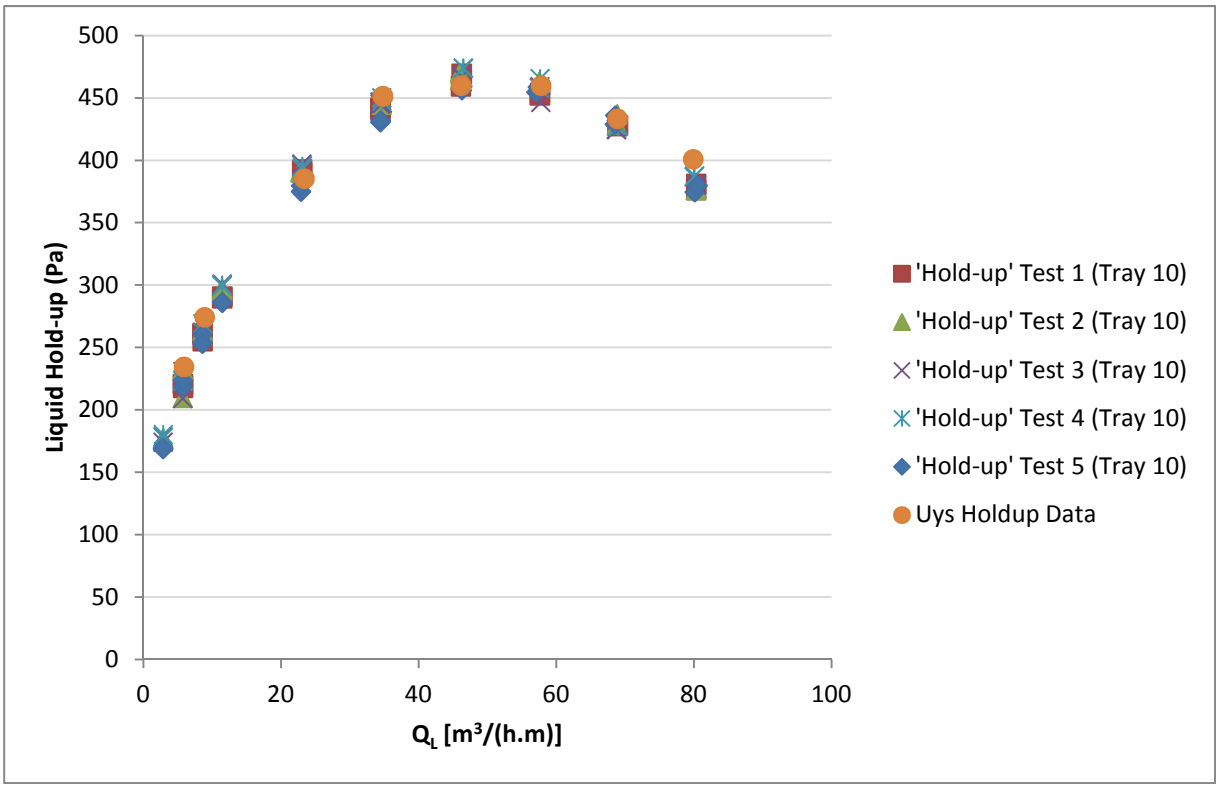

Figure 29 – Liquid hold-up repeatability and 'Uys' data comparison for Tray 10 (15.6%, 6.3 mm) and u_s = 2.6 m/s.

The experiment entrainment magnitudes for the current sieve tray distillation column are compared to that of Nutter (1971) for an air/water system in Figure 30 (L'/L entrainment) and in Figure 141 (L'/G entrainment) in Appendix F at a liquid flow rate of 13.1 m^3/(h.m). The Nutter (1971)

entrainment experiments are performed using a 12.7 mm (½ in.) hole diameter and a 7.9% fractional hole area tray and a round distillation column (1.27 m ID). The current experiment is performed using Tray 6 (7%, 12.7 mm), where the holes in Tray 6 are laser cut. The experimental L'/L entrainment compares reasonably well with the data produced by Nutter (1971). However when comparing the entrainment in Figure 141 as L'/G, the entrainment magnitude deviates significantly, possible due to the differences in the column geometry and slight difference in the fluid physical properties and tray geometry.

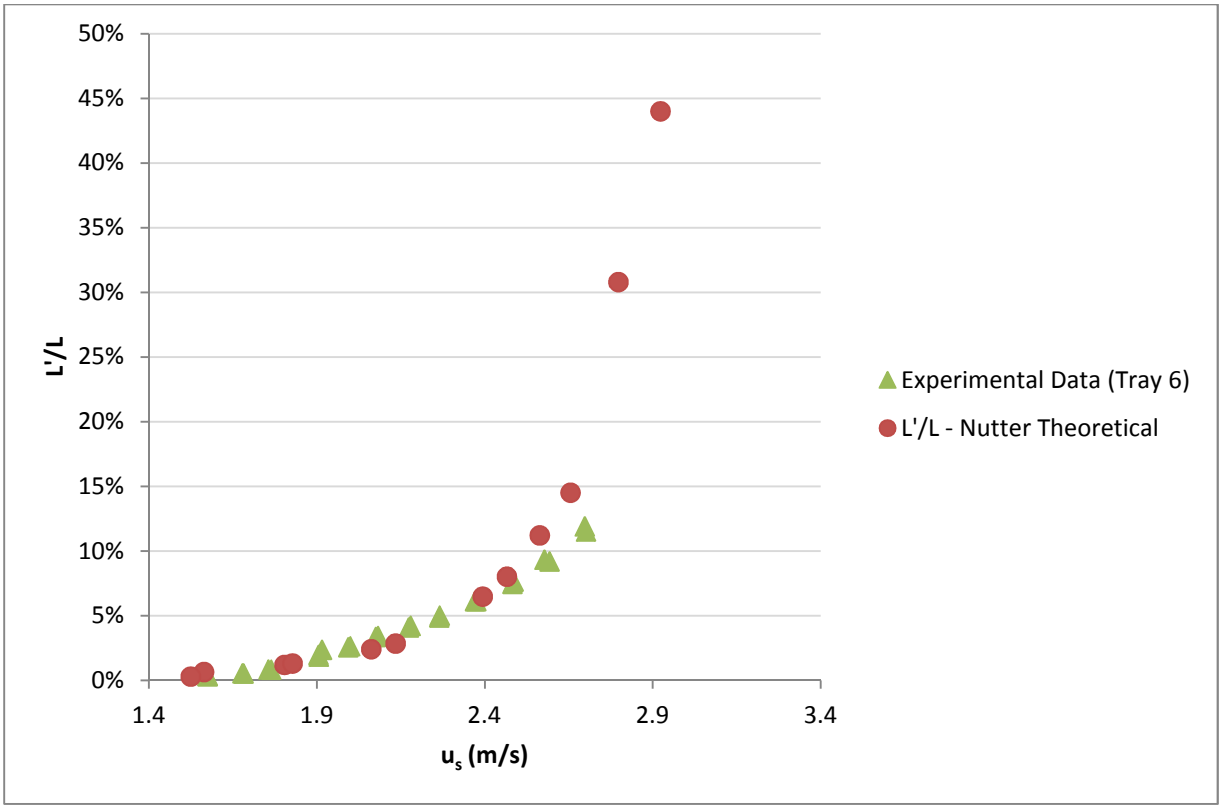

Figure 30 – L'/L experimental data comparison (Nutter, 1971) for Tray 6 (7%, 12.7 mm) and Q_L = 13.1 $m^3/(h.m)$.

4.3 Weeping Data Validation

The following section shows weeping repeatability in the sieve tray test distillation column. Four repeated experiments were performed (Test 1 to 4) with Tray 10 as shown in Figure 31. The experiments were performed with a 15.6% fractional hole area and the 6.3 mm hole diameter tray, for an air/water system at a superficial gas velocity of 2.6 m/s. In Figure 31, weeping is represented as W'/L and in Figure 32 weeping is represented as W'/G.

In Figure 31 (W'/L graph), the repeated experiments vary in a similar manner with increasing liquid flow rate, with a standard deviation as high as 0.9% at high weeping magnitudes and a percentage deviation as high as 7.6% at low weeping magnitudes, where the deviation is attributed to both the noise, delay and the error in the process equipment. The repeated experiments vary in a similar manner with increasing liquid flow rate, with a standard deviation as high as 1.5% at high weeping magnitudes and a percentage deviation as high as 6.9% at low weeping magnitudes (Fig. 32) (W'/G

graph). The reason for the high variability in the repeatability of the weeping and results is due to the nature of weeping, where weeping and entrainment occur as infrequent droplets and not steady stream of fluid.

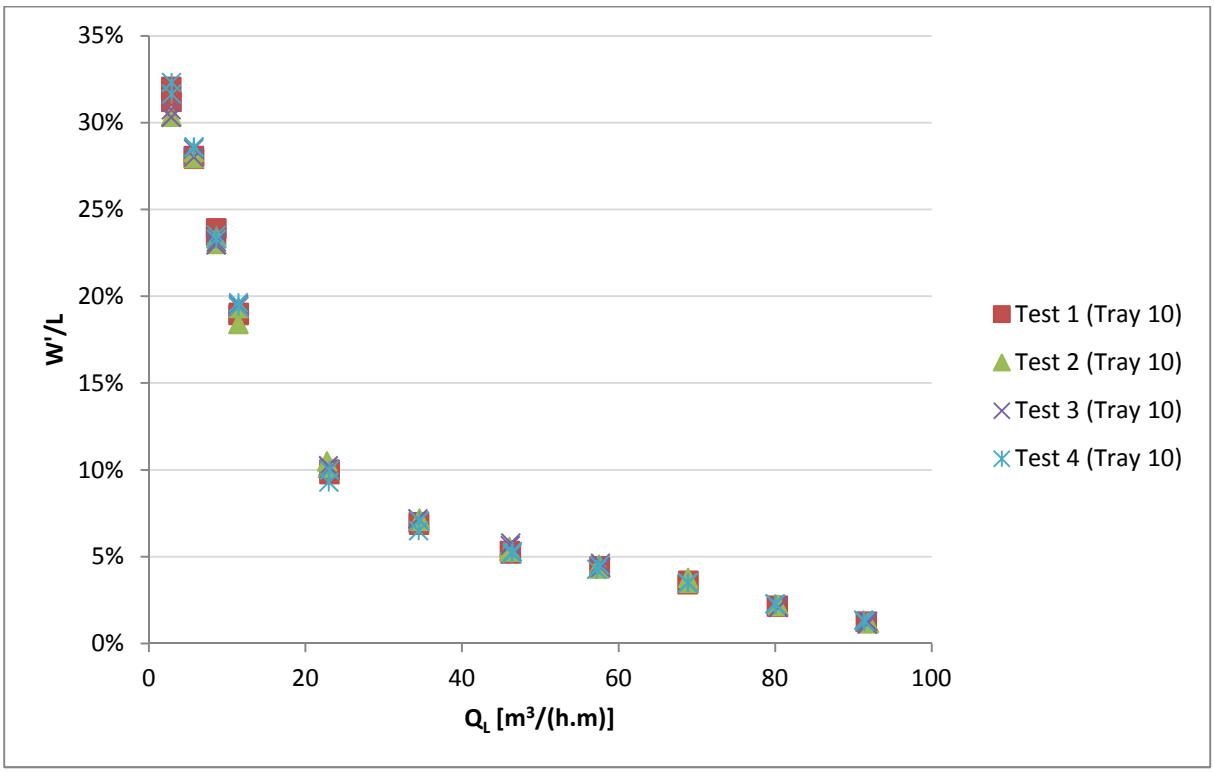

Figure 31 – W'/L weeping repeatability for Tray 10 (15.6%, 6.3 mm) and u_s = 2.6 m/s.

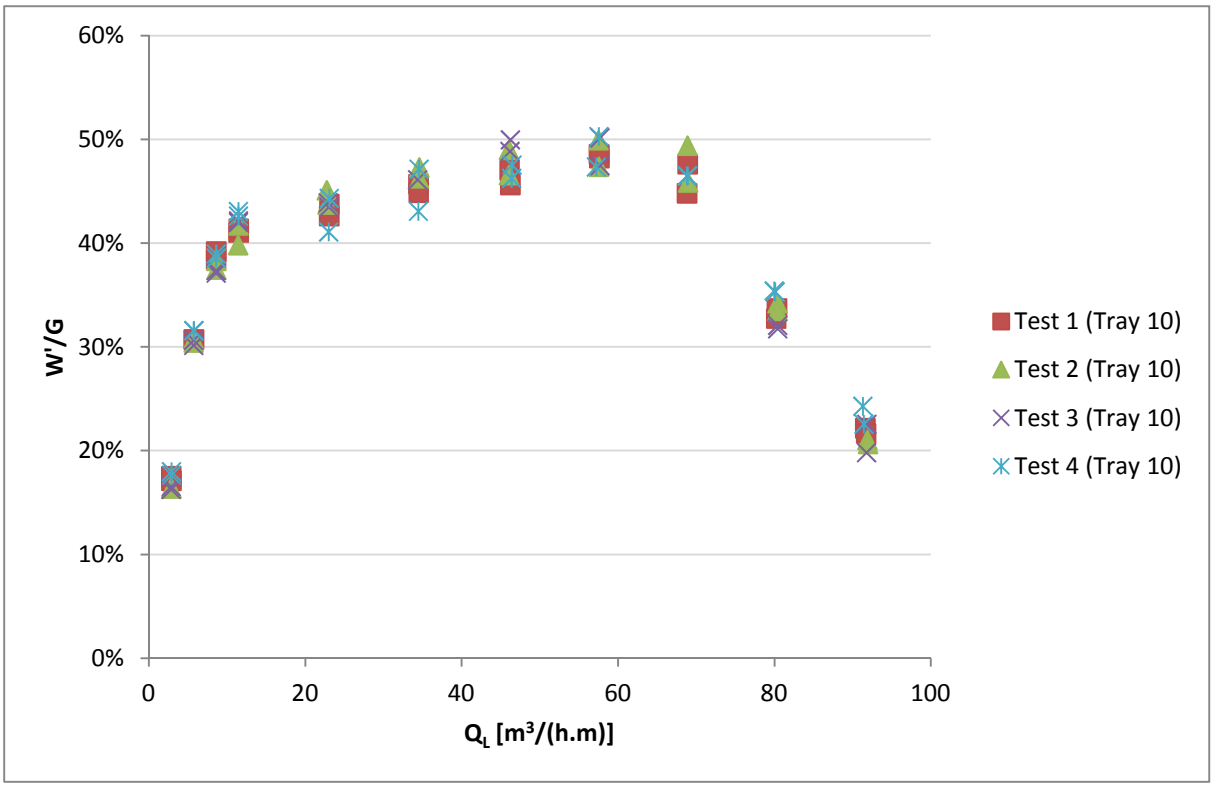

Figure 32 – W'/G weeping repeatability for Tray 10 (15.6%, 6.3 mm) and u_s = 2.6 m/s.

Chapter 5 - Entrainment Results and Discussion

This chapter highlights the results for the entrainment investigation in a sieve tray distillation column and discusses the trends observed with respect to the findings in the open literature. The effects of the different parameters and their impact on entrainment are compared with the models developed in literature. The dimensionless numbers that help describe entrainment trends are shown.

5.1 Effect of Fluid Physical Properties and Fluid Flow

The section highlights the effects of the liquid density, liquid surface tension, liquid viscosity, gas density and gas viscosity, where the effects of these parameters on entrainment are explained as far as they can be separated from one another. The property ranges of the different fluid systems are represented in Table 13, where typical fluids used in the petroleum industry are shown in Table 10. The systems with carbon dioxide (CO_2), are only measured to a superficial gas velocity of 2.6 m/s as the de-entrainment section began to flood at high superficial velocities. Flooding occurred for the butanol system at an even lower superficial gas velocity. The table shows both the capacity factor (C_s) and flow factor (F_s) limits of the different systems, where the effect of the fluid properties are shown with respect to these factors.

Table 13 – Experimental system properties and measuring limits

System	u_S (m/s)	C_S (m/s)	F_S [(m/s)(kg/m^3)$^{0.5}$]	Q_L [m^3/(h.m)]	ρ_l (kg/m^3)	ρ_g (kg/m^3)	μ_l (mPa.s)	μ_g (mPa.s)	σ (mN/m)
Water/Air	1.7-2.9	0.058-0.1	1.84-3.15	2.9 – 92	999	1.16-1.18	0.9	0.0186	57.8
Water/CO_2	1.7-2.6	0.07-0.11	2.28-3.5	2.9 – 80	999	1.7-1.9	0.9	0.0149	57.8
Si/Air	1.7-2.9	0.059-0.1	1.84-3.15	2.9 – 69	959	1.16-1.18	51	0.0186	20.9
Si/CO_2	1.7-2.6	0.073-0.12	2.28-3.5	2.9 – 69	959	1.7-1.9	51	0.0149	20.9
EG/Air	1.7-2.9	0.055-0.095	1.84-3.15	2.9 – 80	1100	1.16-1.18	13.5	0.0186	36
EG/CO_2	1.7-2.6	0.06-0.11	2.28-3.5	2.9 – 69	1100	1.7-1.9	13.5	0.0149	36
Butanol/CO_2	1.7-2.3	0.079-0.107	2.28-3.1	2.9 – 58	835	1.7-1.9	3.2	0.0149	22.1

5.1.1 Effect of Liquid Physical Properties and Flow on Entrainment

The capacity factors (C_s) and the flow factors (F_s) at different gas superficial velocities for the different systems are shown in Table 14, where Equation 1.2.2.1 shows the capacity factor and Equation 2.5.3.2 shows the flow factor (F-Factor). The flow factor only takes the gas physical properties (gas density) into account, while the capacity factor takes both the liquid physical properties (liquid density) and the gas physical properties (gas densities) into account.

$$C_S = u_s\sqrt{\left(\frac{\rho_g}{\rho_l - \rho_g}\right)} \qquad [1.2.2.1]$$

$$F_s = u_s\sqrt{\rho_g} \qquad [2.5.3.2]$$

Table 14 – Experimental system capacity factors (C_s) and flow factors (F_s)

System	u_s (m/s)	ρ_l (kg/m^3)	ρ_g (kg/m^3)	C_S (m/s)	F_S [m/s (kg/m^3)$^{0.5}$]
Water/Air	1.7	999	1.18	0.058	1.85
	2	999	1.18	0.069	2.17
	2.3	999	1.18	0.079	2.5
	2.6	999	1.18	0.089	2.82
	2.9	999	1.18	0.1	3.15
Water/CO_2	1.7	999	1.8	0.072	2.28
	2	999	1.8	0.085	2.68
	2.3	999	1.8	0.098	3.09
	2.6	999	1.8	0.11	3.49
Silicone-Oil/Air	1.7	959	1.18	0.06	1.85
	2	959	1.18	0.07	2.17
	2.3	959	1.18	0.081	2.5
	2.6	959	1.18	0.091	2.82
	2.9	959	1.18	0.102	3.15
Silicone-oil/CO_2	1.7	959	1.8	0.074	2.28
	2	959	1.8	0.087	2.68
	2.3	959	1.8	0.1	3.09
	2.6	959	1.8	0.113	3.49
Ethylene-glycol/Air	1.7	1100	1.18	0.056	1.85
	2	1100	1.18	0.066	2.17
	2.3	1100	1.18	0.075	2.5
	2.6	1100	1.18	0.085	2.82
	2.9	1100	1.18	0.095	3.15
Ethylene-glycol/CO_2	1.7	1100	1.8	0.069	2.28
	2	1100	1.8	0.081	2.68
	2.3	1100	1.8	0.093	3.09
	2.6	1100	1.8	0.105	3.49
Butanol/CO_2	1.7	835	1.8	0.079	2.28
	2	835	1.8	0.093	2.68
	2.3	835	1.8	0.107	3.09

The capacity factors differ considerably from system to system and the liquid densities change from a minimum of 835 kg/m^3 for butanol to as high as 1 100 kg/m^3 for ethylene glycol. In the experimental investigation the surface tension for the different liquids changes from as low as 20.9 mN/m for silicone oil to as high as 57.8 mN/m for water. The surface tensions for silicone oil (20.9 mN/m) and butanol (22.1 mN/m) are similar, making it easier to separate the effects of the liquid surface tension from the liquid density and viscosity. The liquid viscosities of the different liquids changes from 0.9 mPa.s for water to as high as 51 mPa.s for silicone oil, where in the industry, liquid viscosities can exceed 50 000 mPa.s for polymer mixtures.

In the experimental investigation it was clear from observation of the liquid dispersion layer above the sieve tray that the characteristics of the dispersion layers deviate considerably from system to system. In the ethylene glycol (EG) system experiments, it was observed that the dispersion layer above the sieve tray was projected to a lower height than the other liquid systems. The ethylene glycol froth layer (lower dispersion layer) appears to be bubbling at low heights and the spray layer (upper droplet breakup dispersion layer) consists of large liquid droplets projecting to low heights above the froth layer.

The froth dispersion layer of water systems was projected to a greater height than that of ethylene glycol (EG) during the experimental testing. The droplets in the spray layer were projected to a lesser height and the droplets projected in this layer are larger than in the ethylene glycol system. The silicone oil (Si) fluid system produced a higher (larger) froth layer than the water system. The silicone oil droplets in the spray regime were smaller and projected to even greater heights than that of the ethylene glycol and water systems. The key characteristics noted during the butanol investigation was that smaller (very fine) droplets are produced, which were projected to a greater height than with the silicone oil. A clear distinction could be seen between the fine droplets formed and the large liquid droplets (liquid slugs), which were also identified in the investigation by Uys (2012) on the effect of fluid properties on entrainment. It was clear that the fluid systems that produced larger dispersion layers above the sieve tray lead to faster entrainment flooding at high gas superficial velocities in the column. These systems also caused downcomer choke flooding at lower liquid flow rates and increasing superficial gas velocities.

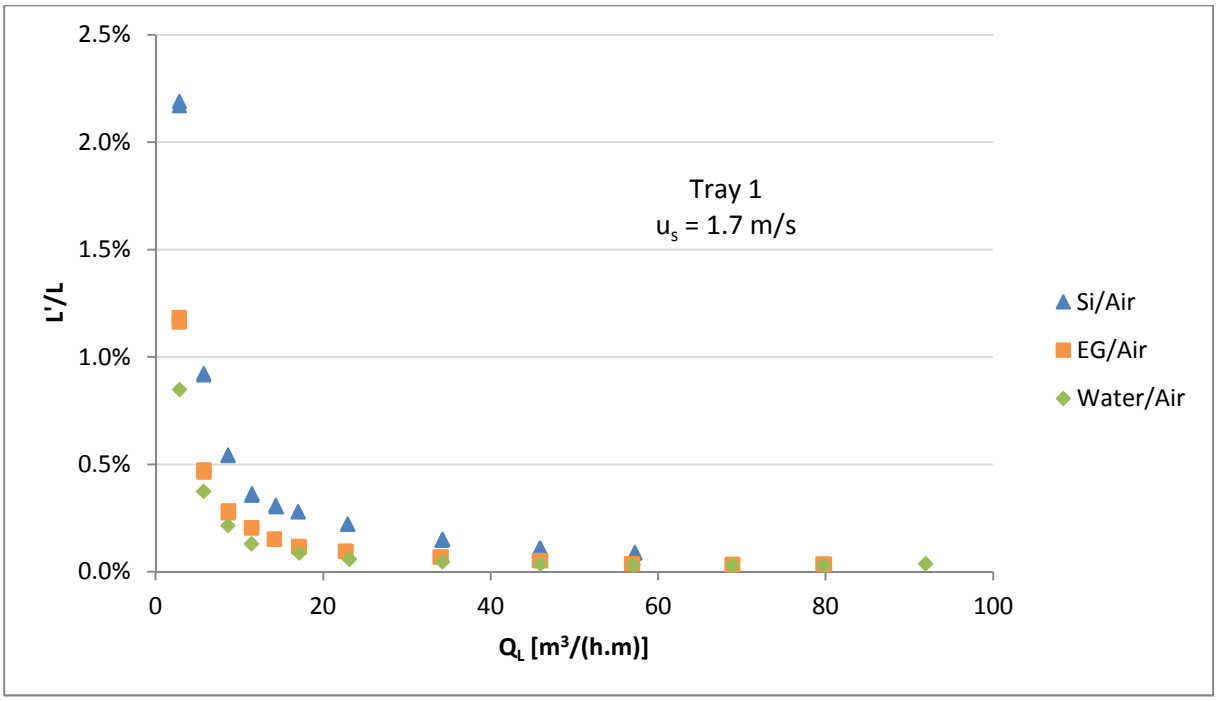

Figure 33 – Entrainment (L'/L) of different liquids with air for Tray 1 (15.8% fractional hole area, 6.4 mm hole diameter) at a superficial gas velocity of 1.7 m/s.

Entrainment can be represented in both an entrainment distillation column efficiency form (L'/L), as in Figure 33, and as an entrainment distillation column capacity form (L'/G), as in Figure 34. In literature, it is typically noted that the spray regime is associated with low liquid flow rates and the

froth regime associated with high liquid flow rates. A clear distinction between dispersion layers at low liquid flow rates [typically below 23 m^3/(h.m)] and at high liquid flow rates [typically above 23 m^3/(h.m)] is seen in the experimental investigation. At low liquid flow rates the dispersion sloshes in different directions, where the gas jetting associated with the spray regime could be seen, whereas at high liquid flow rates the dispersion appears to be more uniform and stable across the tray.

Figure 33 shows the entrainment (L'/L) for different liquids in air at a superficial gas velocity of 1.7 m/s, where the current section identifies the effects of fluid physical properties with only Tray 1 (15.8% fractional hole area, 6.4 mm hole diameter). Section 5.2 identifies the contributing effect of tray configuration (geometry) and fluid physical properties. The figure shows that entrainment (L'/L) decreases with increasing liquid flow rate, where the effect of the liquid flow rate on entrainment is more significant at low liquid flow rates [spray regime typically below 23 m^3/(h.m)] than at higher liquid flow rates [froth regime typically above 23 m^3/(h.m)].

The percentage difference between the entrainment (L'/L) for the different liquids is larger in the spray regime than in the froth regime, since a large dispersion is seen in the spray regime leading to higher entrainment magnitudes (Fig. 33). Silicone oil exhibits as a higher entrainment than ethylene glycol (intermediate entrainment magnitude) and water (lowest entrainment magnitude). The spray layer for silicone oil is larger than that of the other liquids observed in air (noted visually during experimentation). The butanol system was not analyzed in air because of its high flammability. It is clearly shown that entrainment depends highly on the breakup of liquid droplets, that is, the finer the droplets produced in the spray layer, the greater the magnitude of entrainment.

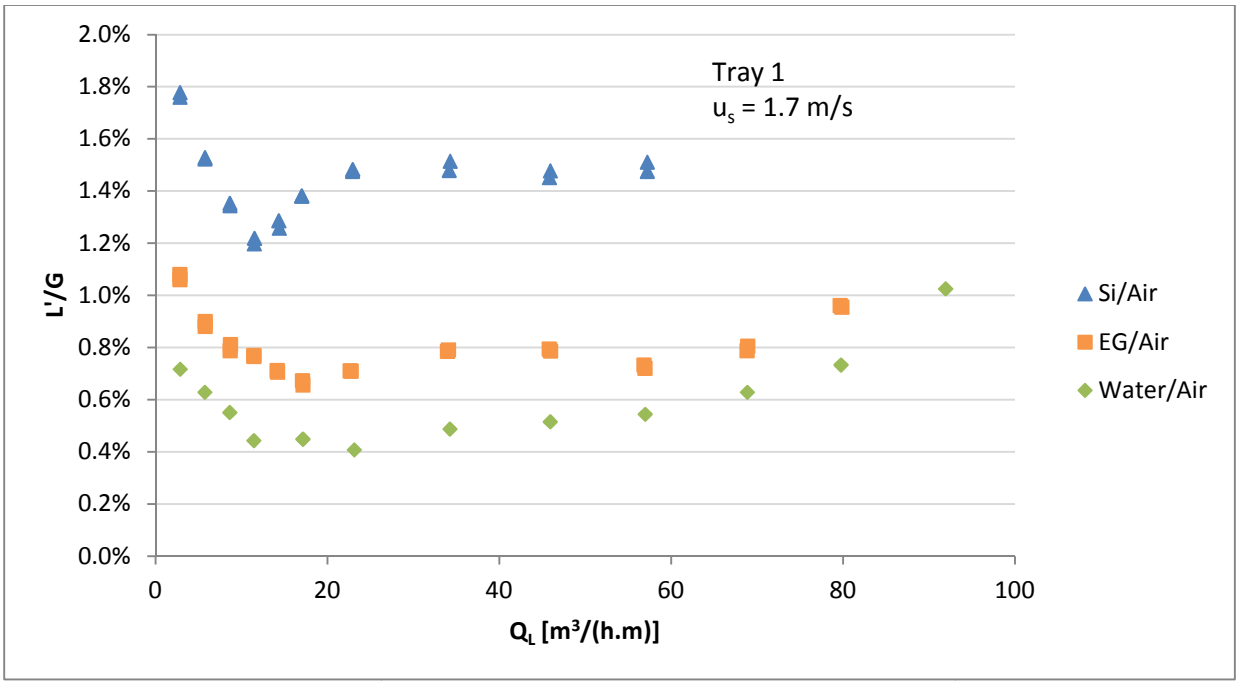

Figure 34 – Entrainment (L'/G) of different liquids with air for Tray 1 (15.8% fractional hole area, 6.4 mm hole diameter) at a superficial gas velocity of 1.7 m/s.

The entrainment (L'/G) is shown in Figure 34 for different liquids in air at a superficial gas velocity of 1.7 m/s, where entrainment is represented as a distillation column capacity parameter. The minimum in the entrainment magnitude on the L'/G graph does not indicate that the dispersion is in

a particular regime (spray or froth), since the ethylene glycol and water entrainment minima occur at much higher liquid flow rates than that of silicone oil. In the discussion that follows, the spray regime will be defined at liquid flow rates typically below 23 m^3/(h.m) (V_L = 4 m^3/h), with the froth regime will defined at liquid flow rates typically above 23 m^3/(h.m) (V_L = 4 m^3/h) as the controlling mechanism. There is no clear distinctive trend between the entrainment (L'/G) and fluid flow rate of different liquids, since the interaction of the gas and liquid in the dispersion is more complex and highly dependent on the different liquid physical properties. The dispersion layer above the sieve tray consists of a froth layer (bottom layer) and spray layer (top layer). The froth layer is associated with both bubbling (stable dispersion layer) and liquid slugs at high liquid flow rates and low gas velocities. The spray layer is associated with both liquid jetting (unstable dispersion layer) and droplets spraying at low liquid flow rates and high gas velocities.

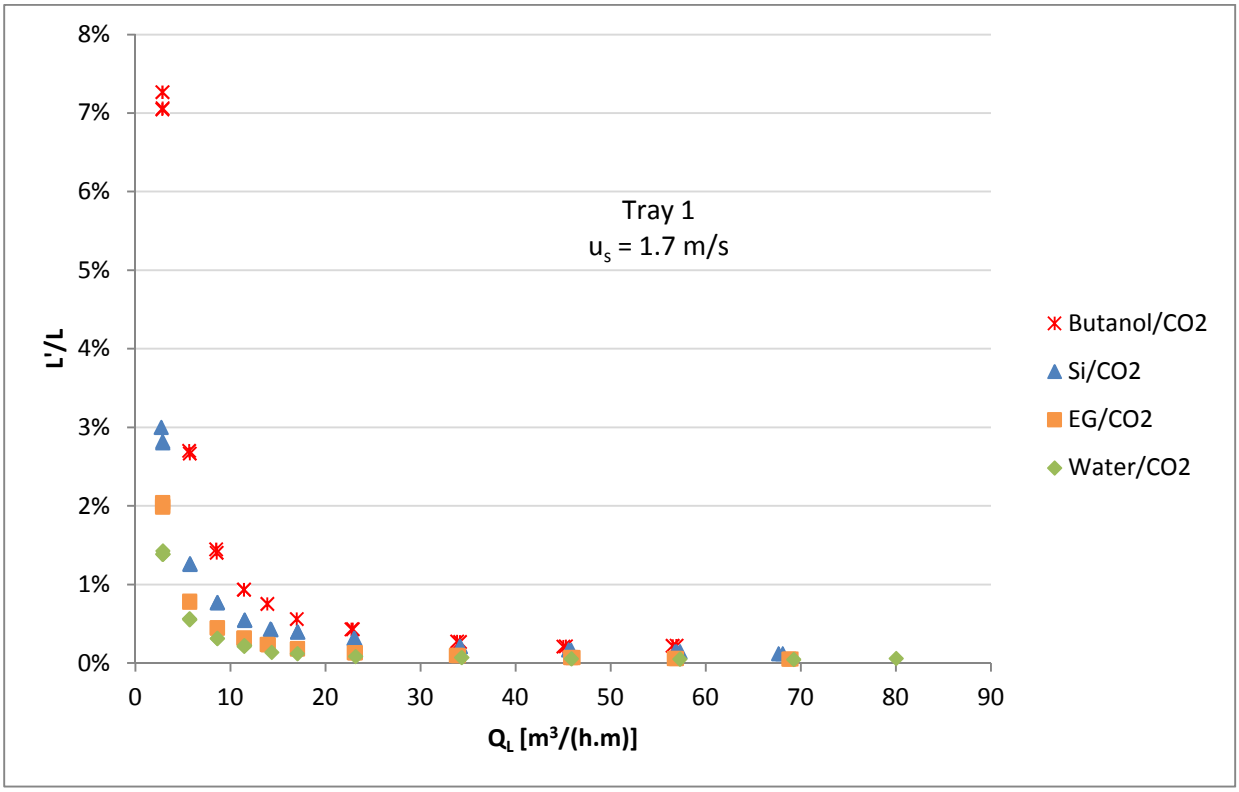

Figure 35 – Entrainment (L'/L) of different liquids with CO_2 for Tray 1 (15.8% fractional hole area, 6.4 mm hole diameter) at a superficial gas velocity of 1.7 m/s.

The entrainment of the different liquids investigated in carbon dioxide is shown in Figure 35 for L'/L entrainment and by Figure 36 for L'/G entrainment. Butanol produces a higher amount of entrainment than silicone oil, where the entrainment magnitude supports the visual observation that butanol produced the largest spray layer (very fine droplets) leading to a higher entrainment. The larger spray layer in the dispersion layer of the butanol system allows the liquid to be closer to the top tray, increasing the entrainment. The differences in magnitude of the entrainment between butanol and the other liquids are larger in the spray regime than in the froth regime. The figures show that liquid density is not the only defining liquid physical property, since ethylene glycol has a higher liquid density (1 100 kg/m^3) than that of water (1 000 kg/m^3) (no distinctive density trend). This shows that entrainment depends on the interaction between the liquid density, liquid surface tension and the liquid viscosity.

Mahiout and Vogelpohl (1984) showed that an increase in liquid viscosity leads to a decrease in the number of droplets formed, supporting the distinction between the entrainment magnitudes observed for butanol and silicone oil. Decent *et al.* (2009) showed that viscosity plays a significant role in the spray regime which is supported by Figures 35 and 36. Silicone oil (highest viscosity) reaches stability faster than liquids with lower viscosities, as can be seen by the minimum in the L'/G graph appearing at a much lower liquid flow rate. This supports the investigation by Decent *et al.* (2009) who showed that an increase in the viscosity leads to an increase in dispersion stability. Liquid viscosity has a high impact on entrainment in the spray regime, although the significance decreases as the dispersion tends to the froth regime.

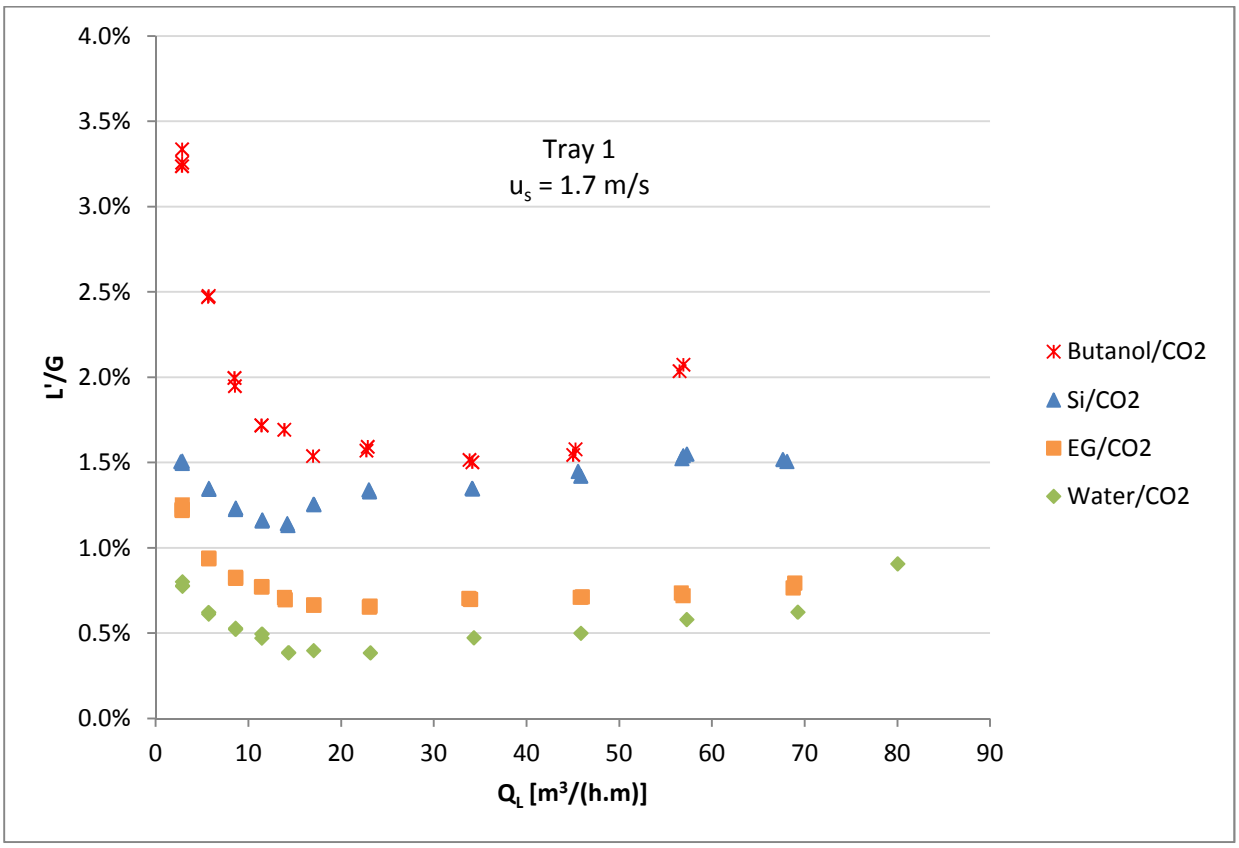

Figure 36 – Entrainment (L'/G) of different liquids with CO_2 for Tray 1 (15.8% fractional hole area, 6.4 mm hole diameter) at a superficial gas velocity of 1.7 m/s.

Figures 33 to 36 show that the surface tension has a significant impact on entrainment, not just in the spray regime as shown by Kister (1992), but also in the froth regime. It is suspected that a reduction in the surface tension, decrease in the liquid density and a decrease in the liquid viscosity leads to an increase in entrainment, although the individual effects cannot truly be separated from one another based on the scope of the liquid systems investigated. An intricate interaction exists between the different liquid physical properties in each regime, where entrainment is not just controlled by liquid density and that the dominating physical property mechanisms changes with gas and liquid flow rate.

The effect of different liquid systems in air at a superficial gas velocity of 2.3 m/s is shown by Figure 142 for L'/L and Figure 143 for L'/G in Appendix F. The effect of different liquids system in carbon dioxide at a superficial gas velocity of 2.3 m/s is shown by Figure 144 for L'/L in Appendix F and

Figure 37 for L'/G. An increase in the superficial gas velocity leads to an increase in the influence of the liquid physical properties in the froth regime, but leads to a decrease in the influence of the liquid properties in the spray regime. As the superficial gas velocity increases, the spray layer (upper dispersion layer) increases in size, leading to an increase in entrainment.

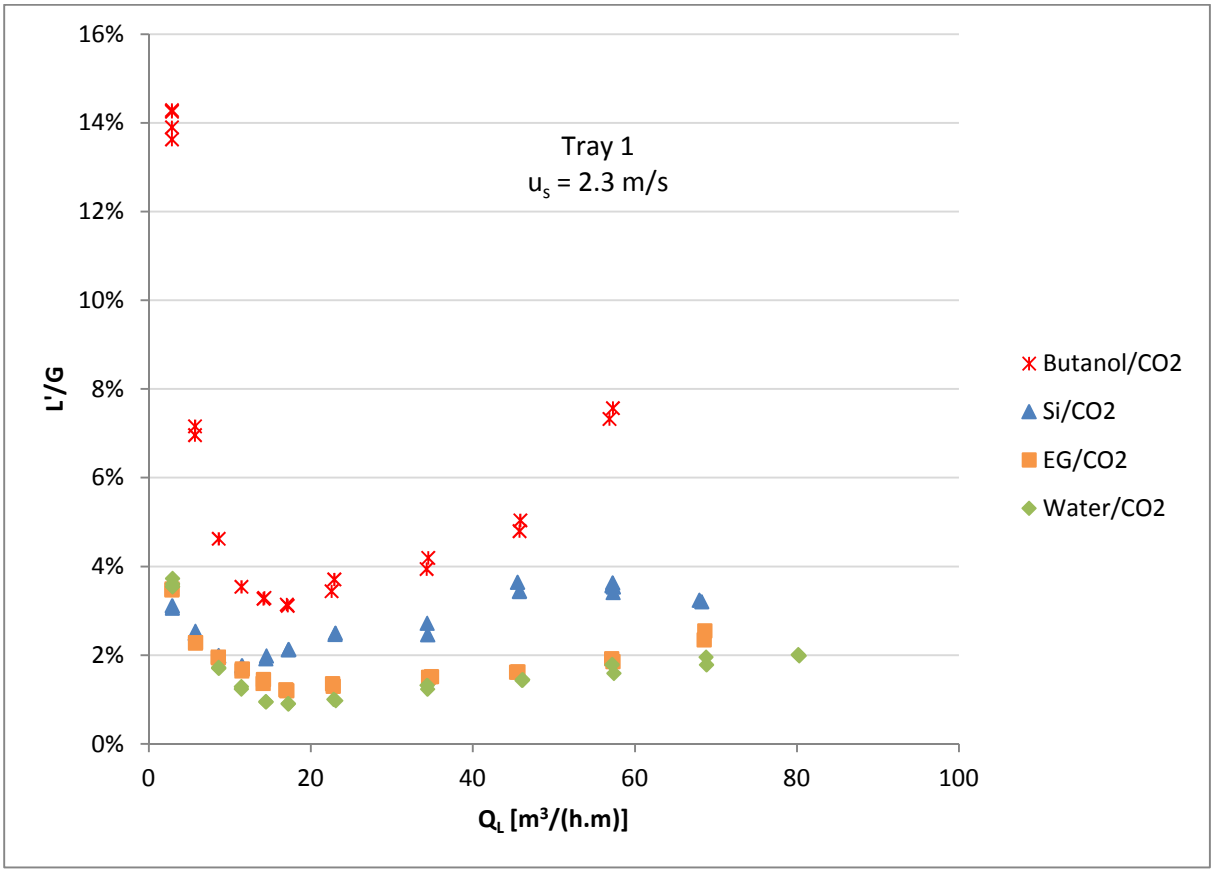

Figure 37 – Entrainment (L'/G) of different liquids with CO_2 for Tray 1 (15.8% fractional hole area, 6.4 mm hole diameter) at a superficial gas velocity of 2.3 m/s.

5.1.2 Effect of Gas Properties and Flow on Entrainment

The experimental investigation only considered the impact of air and carbon dioxide (CO_2) on entrainment. The gas density and gas viscosity for air are 1.18 kg/m^3 and 18.6x10^{-3} mPa.s, respectively, and the gas density and gas viscosity for carbon dioxide are 1.8 kg/m^3 and 14.9x10^{-3} mPa.s, respectively. The L'/L entrainment trends are similar for air and for carbon dioxide, where carbon dioxide is observed to have a higher L'/L entrainment than air over the entire range of liquid flow rates at a superficial gas velocity of 1.7 m/s (Fig. 38). At a constant superficial gas velocity, gases with a high density have a higher mass flow rate through the sieve tray, consequently leading to an increase in the interaction between the liquid and the gas and an increase in entrainment. As the mass flow rate increases, a larger spray layer is produced (greater spray regime characteristics) leading to an increase in the entrainment.

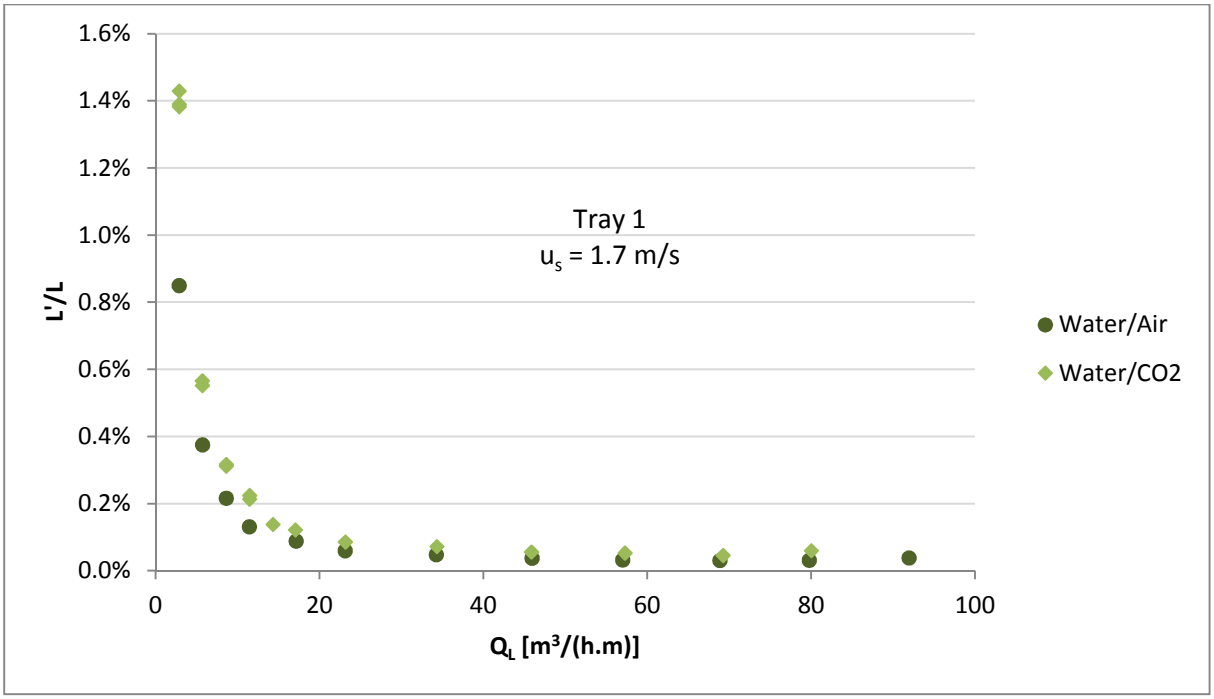

Figure 38 – Entrainment of water (L'/L) with different gases for Tray 1 (15.8% fractional hole area, 6.4 mm hole diameter) at a superficial gas velocity of 1.7 m/s.

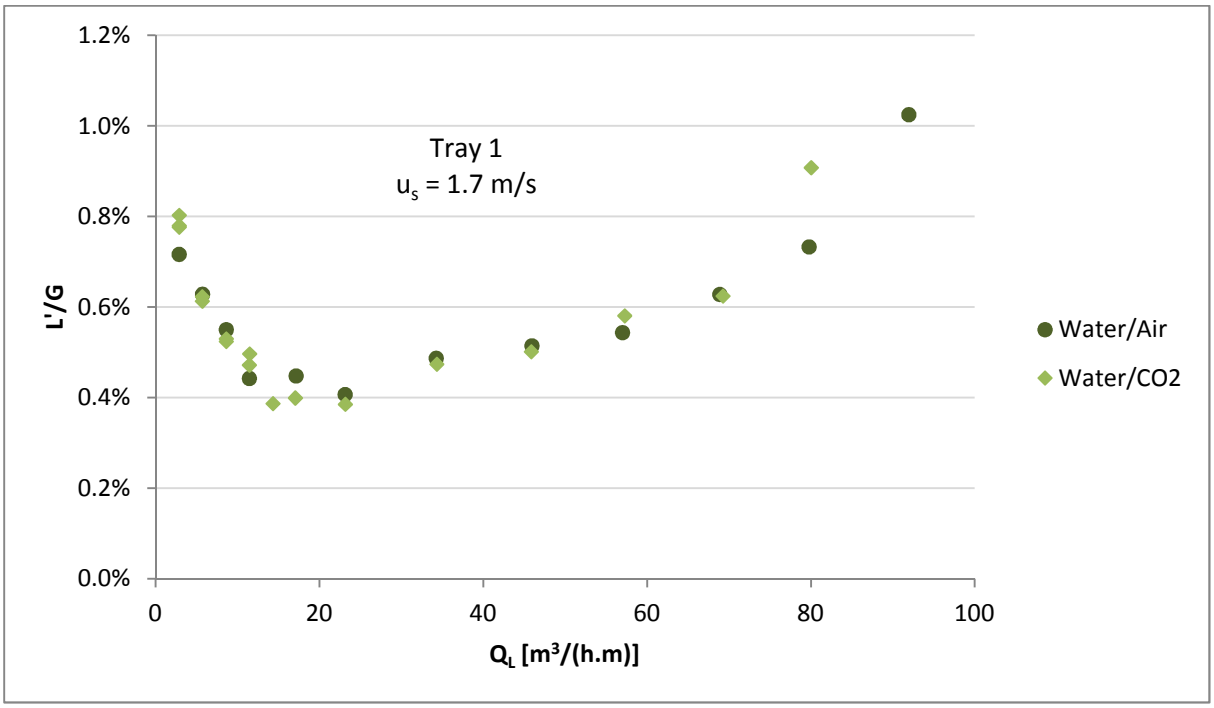

Figure 39 – Entrainment of water (L'/G) with different gases for Tray 1 (15.8% fractional hole area, 6.4 mm hole diameter) at a superficial gas velocity of 1.7 m/s.

The entrainment magnitudes (L'/G) of air and carbon dioxide systems are similar at a superficial gas velocity of 1.7 m/s (Fig. 39). At a superficial gas velocity of 1.7 m/s the capacity factor and flow factor for water/air systems are 0.058 m/s and 1.85 $[(m/s).(kg/m^3)^{0.5}]$, respectively. The capacity factor and flow factor for water/CO_2 systems are 0.072 m/s and 2.28 $[(m/s).(kg/m^3)^{0.5}]$, respectively. Air systems

have lower gas capacity factors and flow factors than carbon dioxide systems at the same superficial gas velocity, where Uys (2012) showed that at constant gas flow factors air produces a higher L'/G entrainment than carbon dioxide. For air and carbon dioxide to have the same capacity and flow factors, the air (lower gas density) system has to be operated at a higher gas velocity than carbon dioxide (higher gas density).

Figure 40 shows the entrainment (L'/G) and Figure 145 in Appendix F shows the entrainment (L'/L) for air and carbon dioxide with water at a superficial gas velocity of 2.6 m/s. At a superficial gas velocity of 2.6 m/s the capacity factor and flow factor for water/air systems are 0.089 m/s and 2.82 [(m/s).(kg/m^3)$^{0.5}$], respectively. The capacity factor and flow factor for the water/CO_2 system are 0.098 m/s and 3.09 [(m/s).(kg/m^3)$^{0.5}$], respectively. The difference in the entrainment between air and carbon dioxide systems expands with increasing superficial gas velocity (Fig. 40 and 145). The differences in the entrainment at higher gas superficial velocities are larger in the spray regime than in the froth regime for water systems.

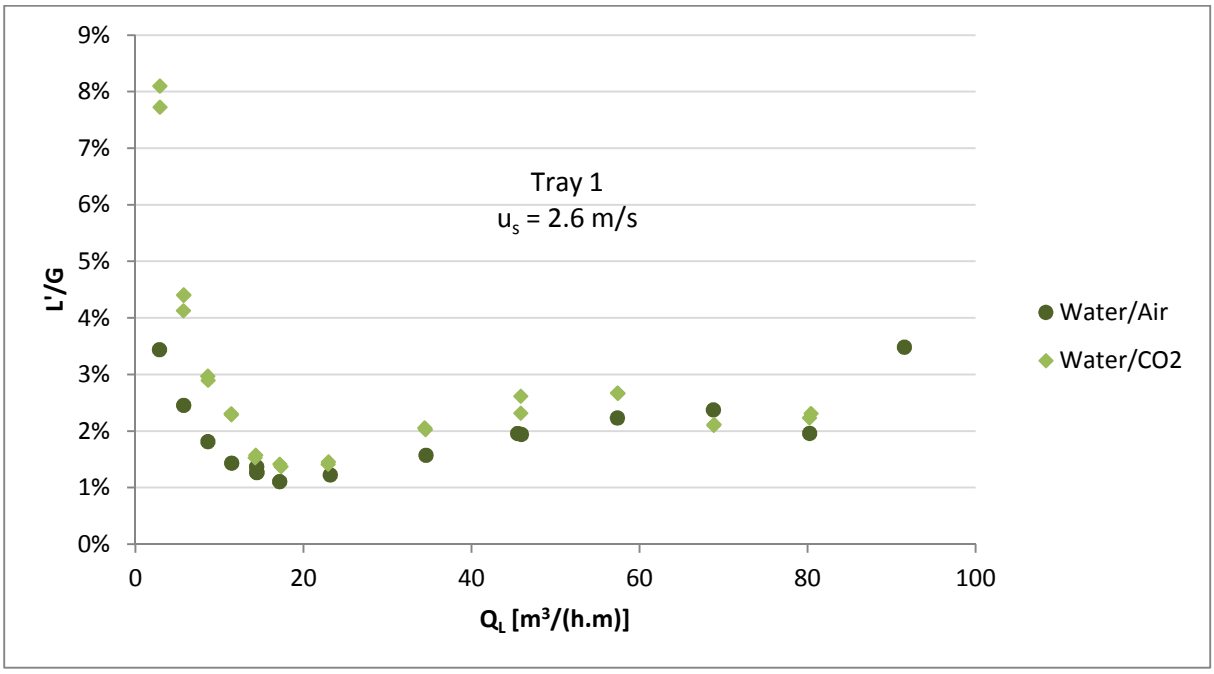

Figure 40 – Entrainment of water (L'/G) with different gases for Tray 1 (15.8% fractional hole area, 6.4 mm hole diameter) at a superficial gas velocity of 2.6 m/s.

The entrainment for silicone oil/air (Si/air) and silicone oil/carbon dioxide (Si/CO_2) systems are shown in Figure 41 for L'/L entrainment and in Figure 42 for L'/G entrainment at a superficial gas velocity of 1.7 m/s. At a superficial gas velocity of 1.7 m/s, the capacity factor and flow factor for silicone-oil/air system are 0.060 m/s and 1.85 [(m/s).(kg/m^3)$^{0.5}$], respectively, and the capacity factor and flow factor for silicone oil/CO_2 system is 0.074 m/s and 2.28 [(m/s).(kg/m^3)$^{0.5}$], respectively. The interactions between silicone oil and the gases are different from that of the water systems. The magnitude difference between the CO_2 and air systems L'/L entrainment decreases when silicone is used as a liquid instead of water (Fig. 41). The entrainment (L'/G) for silicone oil/air is greater than that of silicone oil/CO_2, where the entrainment differences are greater in the spray regime than in the froth regime (Fig. 42). A possible reason for the trend could be that as the liquid viscosity

increases, the gas density becomes less important. Decent (2009) reported that liquid viscosity influences the breakup length of liquid jets into droplets, where an increase in the gas mass flow rate means an increase in the interaction between the gas and the liquid. This will increase the effect the liquid viscous forces have on entrainment.

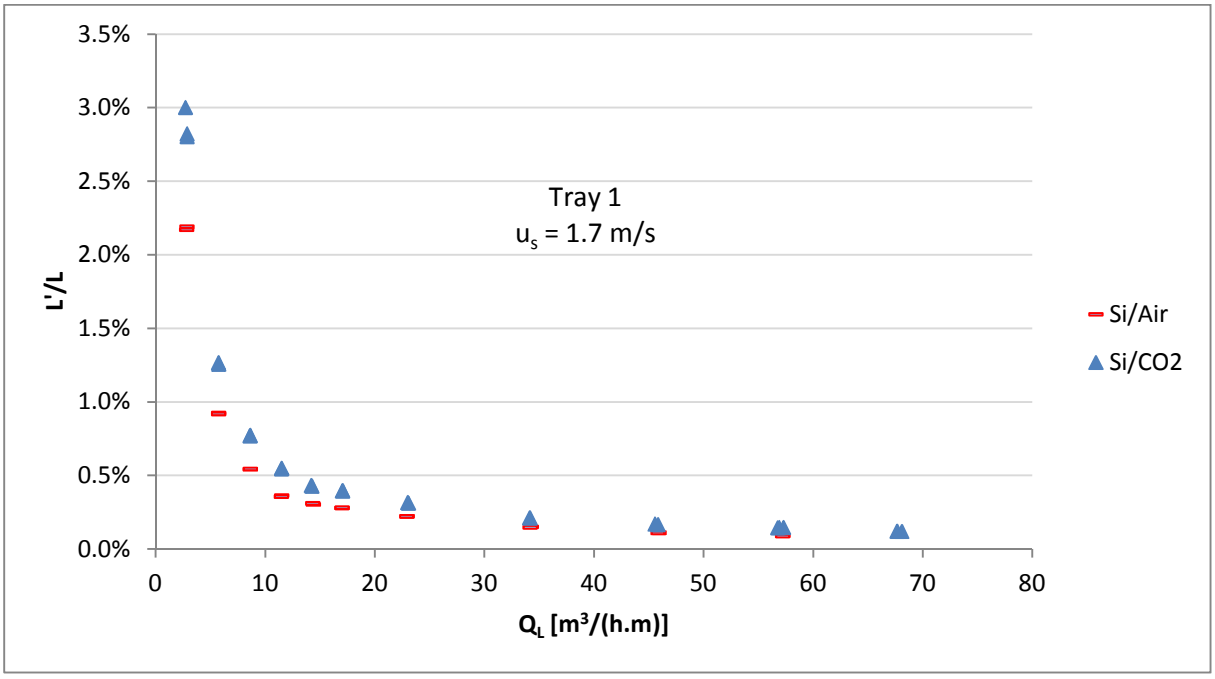

Figure 41 – Entrainment of silicone oil (L'/L) with different gases for Tray 1 (15.8% fractional hole area, 6.4 mm hole diameter) at a superficial gas velocity of 1.7 m/s.

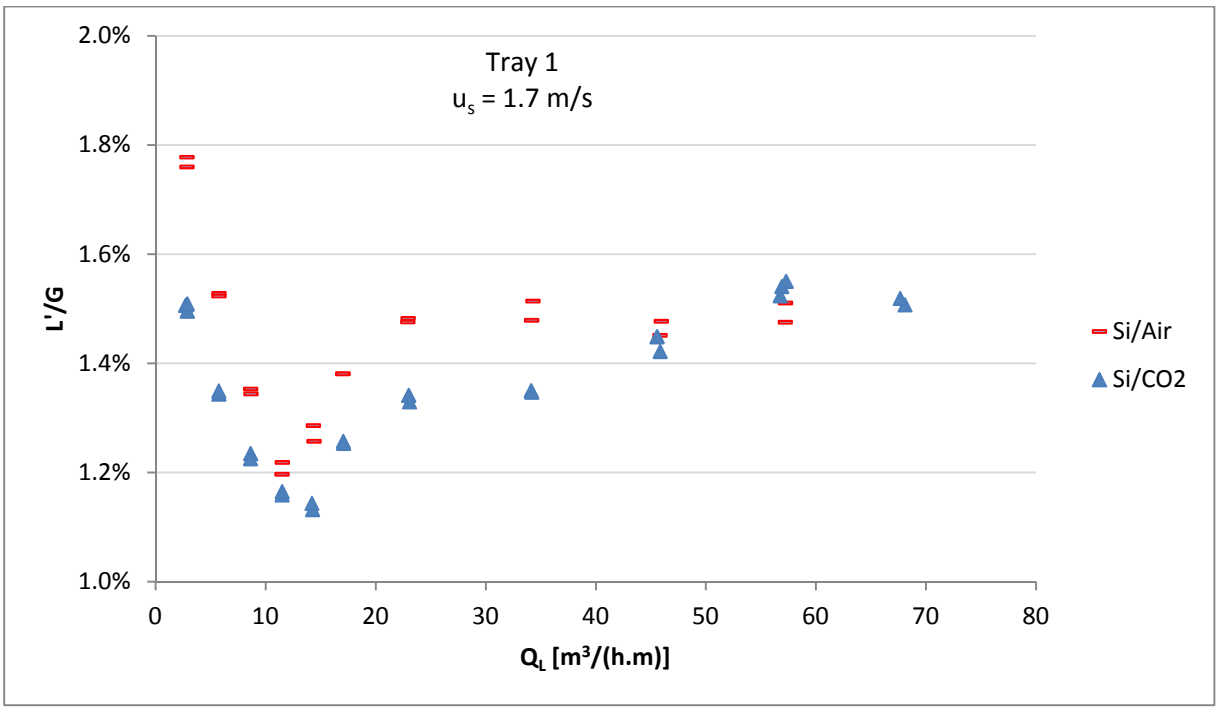

Figure 42 – Entrainment of silicone oil (L'/G) with different gases for Tray 1 (15.8% fractional hole area, 6.4 mm hole diameter) at a superficial gas velocity of 1.7 m/s.

Figure 146 shows that the entrainment (L'/L) for a silicone oil system follows the same trend as with the water system in Figure 145 in Appendix F, where Si/CO_2 systems have higher entrainment magnitudes than the Si/air systems at higher gas superficial velocities. Figure 147 shows that the entrainment (L'/G) for Si/air has a higher magnitude than Si/CO_2 at a superficial gas velocity of 2.6 m/s, opposite to the water system in Figure 40 showing that the interaction between the gas and liquid flow properties are of a complex nature. The percentage differences between the entrainment (L'/G) for silicone oil systems are greater in the froth regime than in the spray regime, a trend opposite to that of water systems (Fig. 147). This supports the idea that an increase in liquid viscosity (high viscous forces), leads to a decrease in the effect that gas density has on entrainment.

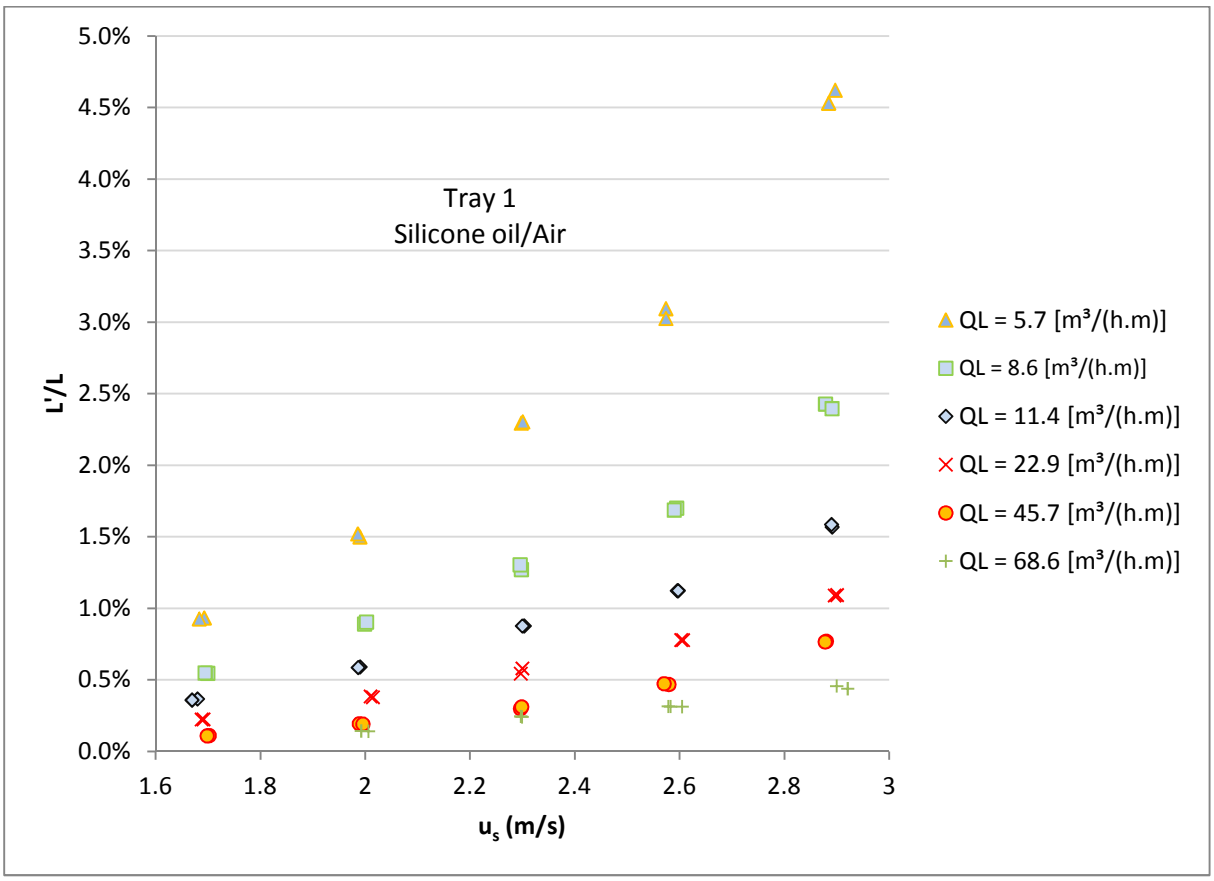

Figure 43 – Effect of superficial gas velocities on entrainment (L'/L) at different liquid flow rates for Tray 1 (15.8% fractional hole area, 6.4 mm hole diameter) and silicone-oil/air.

The entrainment (L'/L) for silicone oil/air at changing gas superficial velocities for different liquid flow rates is shown in Figure 43. The entrainment (L'/L) always increases with increasing superficial gas velocity, to the point of distillation column flooding. As L'/L increases with superficial gas velocity and decreasing liquid flow rate, the separation efficiency decreases inside the distillation column. The experimental entrainment trends observed are compared with the literature models in Section 5.3.1, where fluid property trends are explained in more detail.

5.2 Effect of Plate Characteristics

This section highlights the effects of the sieve tray hole diameter and fractional hole area, where the effects of fluid physical properties and fluid flow rates interacting with tray geometry are evaluated.

5.2.1 Effect of Fractional Hole Area on Entrainment

Three different fractional hole areas were investigated, namely 7%, 11% and 15% at three different hole diameters 3.2 mm (⅛ in.), 6.4 mm (¼ in.) and 12.7 mm (½ in.). In the investigation into tray geometry, the pitch (P_t – distance between the sieve tray holes) to hole diameter (d_H) ratio is kept constant for a particular sieve tray fractional hole area. The hole pitch to hole diameter ratio for 7% fractional hole area is 3.4, 11% fractional hole area is 2.6 and 15% fractional hole area is 2.28.

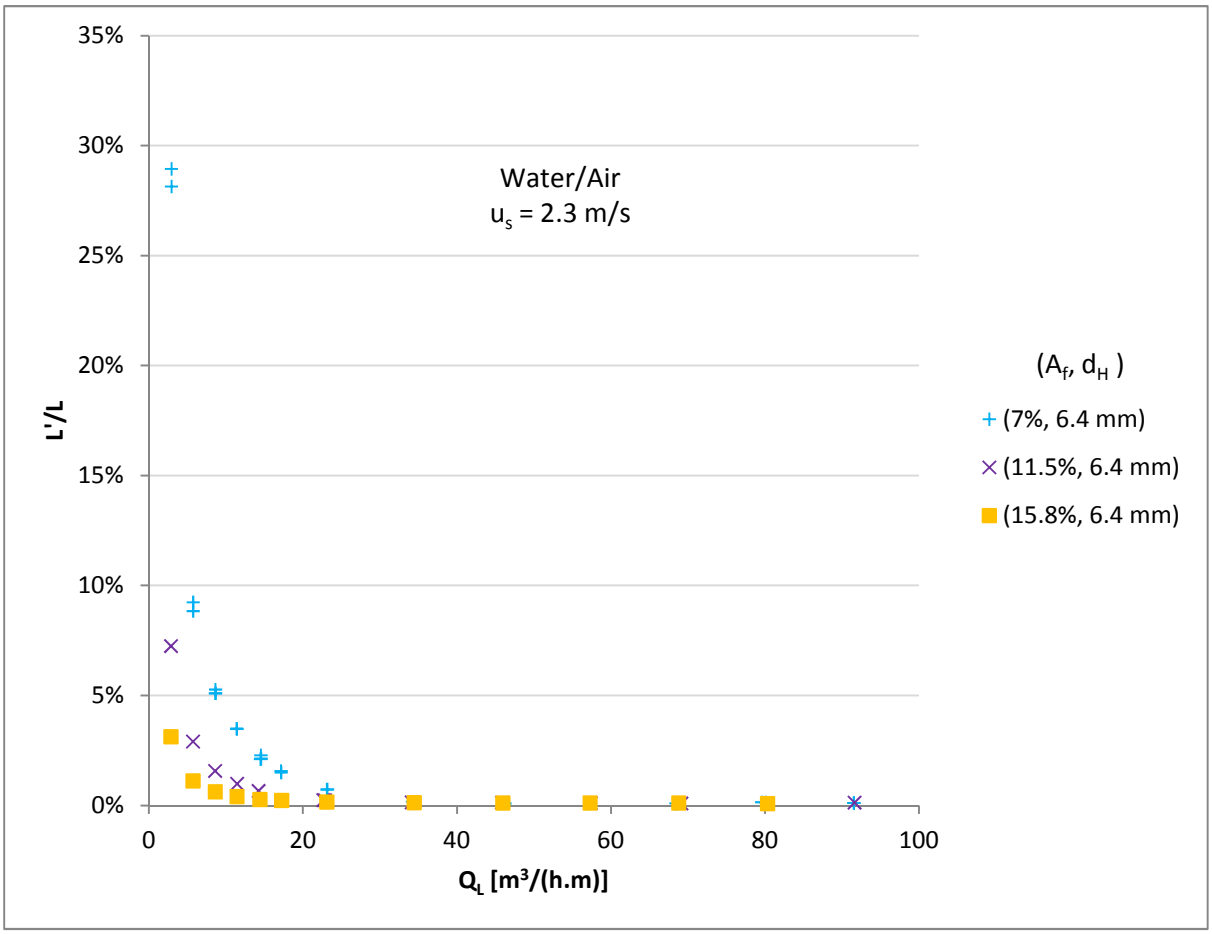

Figure 44 – Effect of fractional hole area on entrainment (L'/L) for water/air with a 6.4 mm hole diameter and a superficial gas velocity of 2.3 m/s.

Figure 44 (L'/L entrainment) and Figure 45 (L'/G entrainment), given for a superficial gas velocity of 2.3 m/s, show that the magnitude of entrainment is influenced by fractional hole area considerably more in the spray regime [typically below 23 m^3/(h.m)] than in the froth regime [typically above 23 m^3/(h.m)]. In the spray regime, entrainment increases with decreasing fractional hole area, where the difference between 7 and 11% fractional hole area entrainment is considerably greater than in the case of the 11% and the 15%. Thus the dependency of entrainment on fractional hole area increases as the fractional hole area decreases in the spray regime.

The entrainment reaches a minimum at high liquid flow rates as the fractional hole area decreases, possibly due to the increase in gas hole velocity (Fig. 44 and 45). At a superficial gas velocity of 2.3 m/s, the hole gas velocity is approximately 32 m/s for a 7% fractional hole area, 20 m/s for a fractional hole area of 11% and 14 m/s for a fractional hole area of 15 %. The entrainment becomes less important in the froth regime [typically above 23 m^3/(h.m)]. The increase in entrainment in the spray regime is due to the increase in the hole velocity of the gas through the sieve tray holes, which increases the dominance of the gas flow force through the spray dispersion layer. In the froth regime, the dominance of the cross flowing liquid is larger in the froth regime as the liquid flow rate increases [23 m^3/(h.m) to 60 m^3/(h.m) intermediate flow rates], which produces a similar entrainment for the changing tray fractional hole areas in the froth regime.

In the froth regime, the magnitude of entrainment is mainly influenced by the height of the dispersion layer, thus the fractional hole area has a small impact on entrainment at intermediate flow rates. The fractional hole area becomes significant at high liquid flow rates as the resulting increase in the hole velocity by changing fractional hole area increases the height of the froth layer in the dispersion to the top tray; this increases entrainment as fractional hole area decreases.

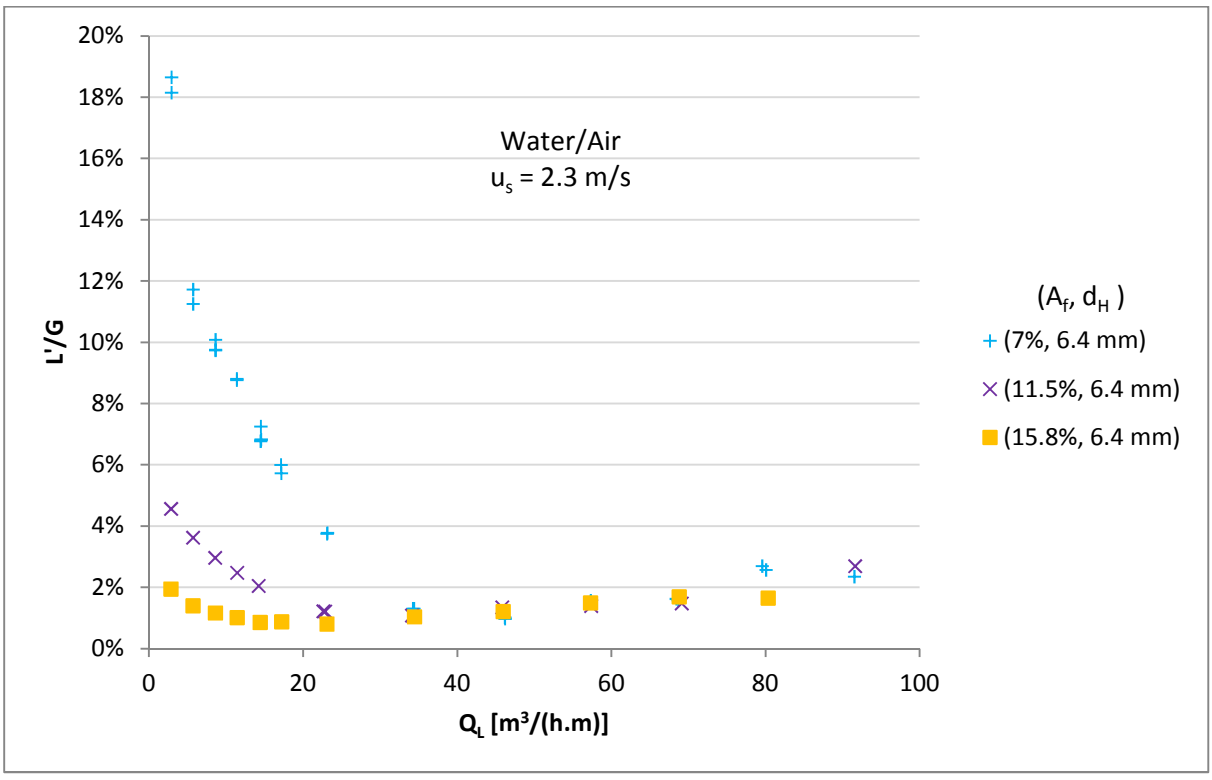

Figure 45 – Effect of fractional hole area on entrainment (L'/G) for water/air with a 6.4 mm hole diameter and a superficial gas velocity of 2.3 m/s.

The entrainment for silicone oil/carbon dioxide (Si/CO_2) at different fractional hole areas is shown in Figure 46 for L'/G entrainment and in Figure 148 in Appendix F for L'/L entrainment for a hole diameter of 12.7 mm and a superficial gas velocity of 2.3 m/s. The entrainment follows a similar trend to that of water/air. The fractional hole area has a large influence on entrainment in the spray regime (low liquid rates), small impact at intermediate liquid flow rates (low froth heights) and a significant impact on entrainment at high liquid rates (high froth heights).

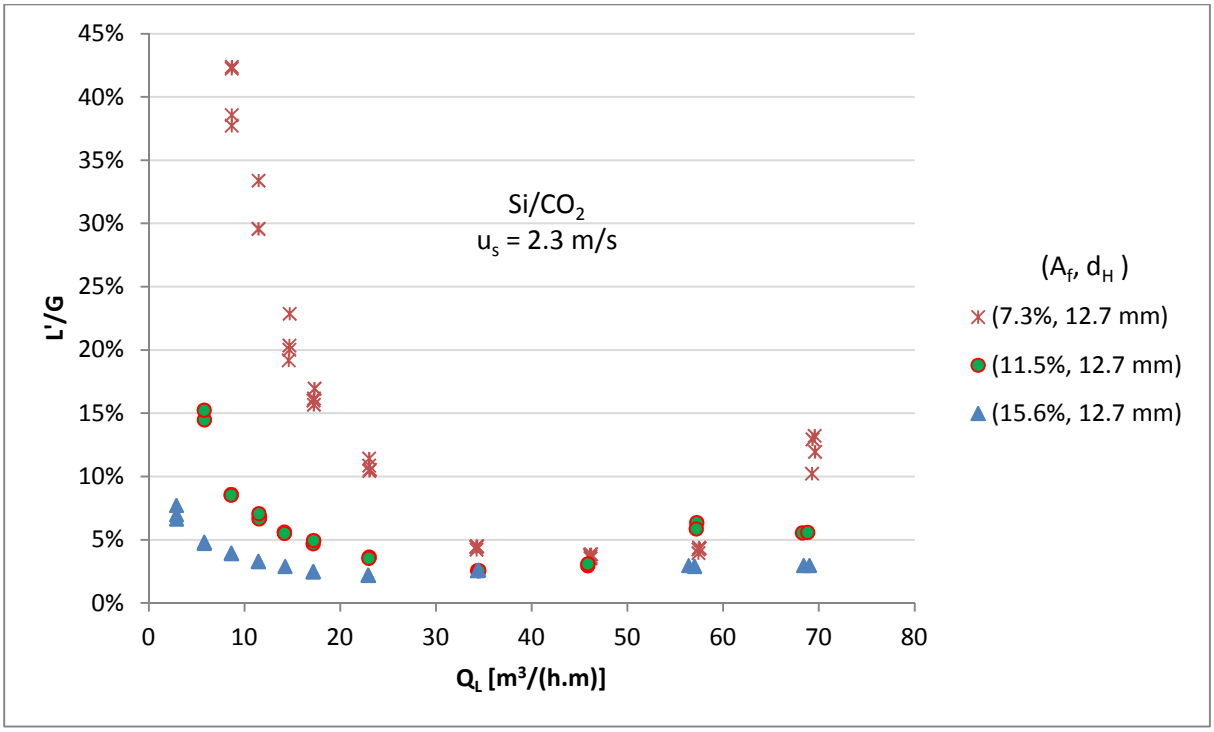

Figure 46 – Effect of fractional hole area on entrainment (L'/G) for silicone-oil/CO_2 with a 6.4 mm hole diameter and a superficial gas velocity of 2.3 m/s.

At intermediate liquid flow rates [approximately 23 to 60 m^3/(h.m)], the impact that fractional hole area has on entrainment increases (liquid flow rate range of constant entrainment magnitude changes when tray hole diameter is changed). Liquids that produce larger dispersion layers produce more entrainment inside a distillation column, this increases the effect that fractional hole area has on the entrainment at higher liquid flow rates. Therefore a decrease in liquid density and a decrease in liquid surface tension increases the effect that fractional hole area has on the amount of entrainment. The trend of the fractional hole area supports the visual trend observed by Uys (2012) for the liquid dispersion layer as shown in Figure 5.

The shape of the dispersion layer during experimentation was similar to that observed by Uys *et al.* (2012). The liquid dispersion trends are shown in Figure 5(a), where Profiles 1 to 5 represent the systematic change in dispersion layer patterns observed above the sieve tray as the liquid flow rate is increased. Profile 1 represents the dispersion in the spray regime, where the dispersion peak occurs at a low flow path length which allows two peaks to form in the dispersion layer. This makes the dispersion layer unstable, increasing the dependence of entrainment on the fractional hole area. As the liquid flow rate increases the dispersion shape changes from Profiles 1 to 2, and then to 3. Profiles 2 and 3 show typical dispersion trends for intermediate liquid flow rates, where the dispersion becomes stable and less dependent on the upward gas force and more dependent on the horizontal liquid force above the sieve tray. As the liquid flow rate increases the dispersion shape changes from Profiles 3 to 4, which causes liquid dispersion to change the force dependency from horizontal liquid flow rate force to upward gas force (at high liquid rates in the froth regime). At high liquid flow rates, entrainment increases as the dispersion height increases (Profiles 4 to 5), because of the increase in the hole gas velocity as the tray fractional hole area decreases. The entrainment follows a similar trend as that observed by Lemieux and Scotti (1969).

5.2.2 Effect of Hole Diameter on Entrainment

The sieve tray hole diameters investigated were 3.2 mm (⅛ in.), 6.4 mm (¼ in.) and 12.7 mm (½ in.), which are multiples of one another. The effect of sieve tray hole diameter is initially shown in Figure 47 for L'/L entrainment and in Figure 48 for L'/G entrainment, where entrainment is represented with a water/air system at a fractional hole area of 15% and a superficial gas velocity of 2.3 m/s.

A clear distinction between the effect that hole diameter has on the amount of entrainment in the spray regime [typically below 23 m^3/(h.m)] and in the froth regime [typically above 23 m^3/(h.m)] can be seen in Figures 47 and 48. In the spray regime, entrainment increases with increasing sieve tray hole diameter. The impact that tray hole diameter has on entrainment increases with increasing hole diameter (larger difference in the entrainment magnitude between the 12.7 mm and the 6.4 mm diameter trays than between the 6.4 mm and 3.2 mm diameter trays). At a similar tray fractional hole area, the trays have a similar gas hole velocity through the sieve tray. Therefore it is believed that in the spray regime, the stability of the gas jet through the sieve tray hole increases with increasing hole diameter at a constant fractional hole area, leading to an increase in entrainment in the spray regime. The increased stability in the gas jets through the sieve tray promotes the formation of liquid droplets and increases the dominance of the spray layer in the liquid dispersion.

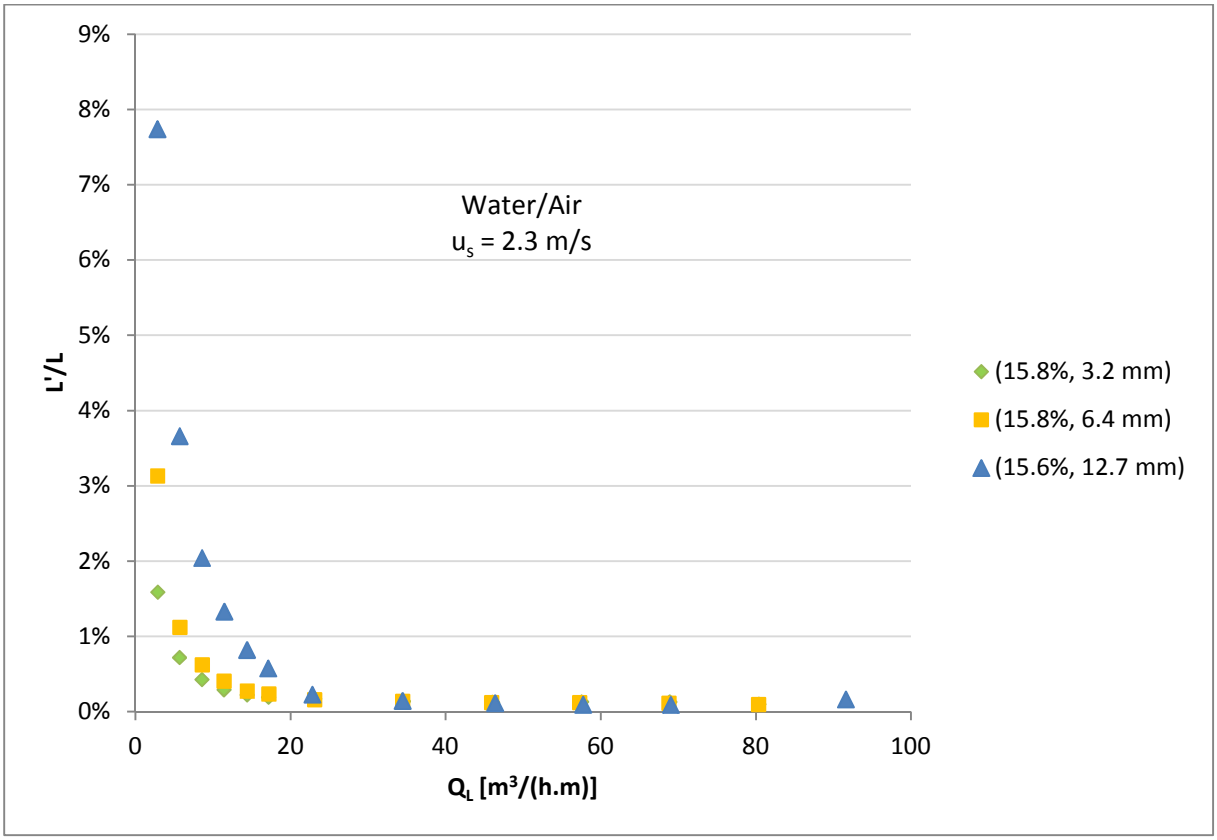

Figure 47 – Effect of hole diameter on entrainment (L'/L) for water/air with a 15% fractional hole area and a superficial gas velocity of 2.3 m/s.

The sieve tray hole diameter has a small influence on entrainment at intermediate liquid flow rates [approximately 23 to 60 m^3/(h.m)] in the froth regime as the horizontal liquid force is larger than the upward gas force through the sieve tray (Fig. 47 and 48). The minimum in the entrainment occurs at

a much higher liquid flow rate with increasing tray hole diameter, this is due to a larger spray regime. At intermediate liquid flow rates the gas flow through the sieve tray changes from jetting at low liquid flow rates (spray regime) to a mixture of jetting and bubbling at moderate liquid flow rates.

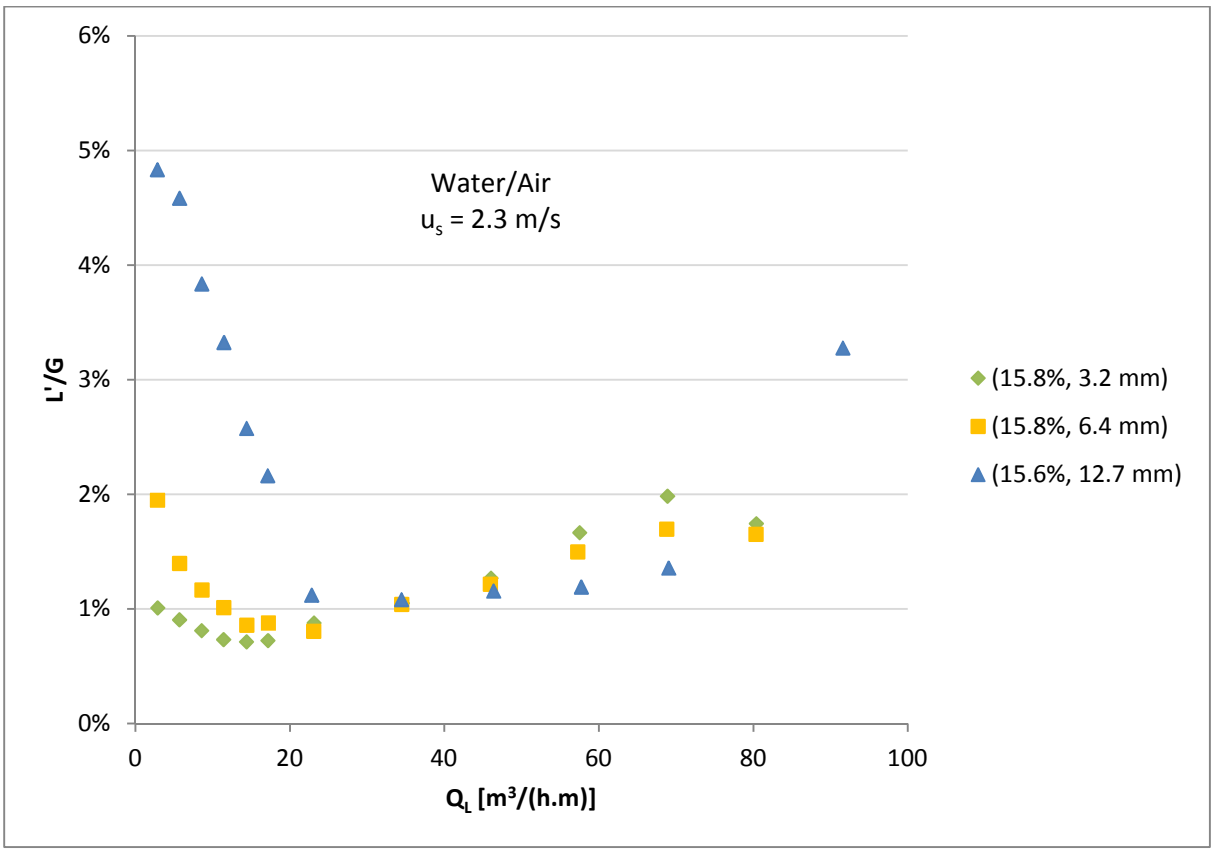

Figure 48 – Effect of hole diameter on entrainment (L'/G) for water/air with a 15% fractional hole area and a superficial gas velocity of 2.3 m/s.

At high liquid flow rates [typically above 60 m^3/(h.m)] the hole diameter's influence on entrainment increases. Entrainment is shown to increase with decreasing hole diameter at high liquid rates in the froth regime. As the hole diameter decreases, the dispersion is observed to become more stable (uniform) across the tray, decreasing the influence of the spray layer in the dispersion and promoting the influence of the froth layer in the dispersion layer. At high liquid flow rates, decreasing the hole diameter increases the height of the froth layer dispersion because of the uniform force of the gas across the tray, moving the dispersion closer to the top tray (increasing entrainment), as in Figure 5 (Profiles 4 to 5).

The effect of sieve tray hole diameter on entrainment for silicone oil/carbon dioxide (Si/CO_2) is shown in Figure 49 for L'/G entrainment and by Figure 149 in Appendix F for L'/L at a superficial gas velocity of 2.3 m/s and a fractional hole area of 11%. The tray hole diameter follows a similar trend to that observed at a fractional hole area of 15% in Figure 48. The trends of the sieve tray hole diameters effect on entrainment follows a similar tendency in the spray regime to that of Lemieux and Scotti (1969), Kister (1992) and Bennett *et al.* (1995). The effect hole diameter has on entrainment at high liquid flow rates changes as the liquid properties change. The liquid viscosity increases the stability of the gas jet and liquid bubbles in the dispersion layer. As the liquid density

decreases and the liquid viscosity increases the influence that hole diameter has on entrainment increases. The trends of the experimental results are compared with literature models in Section 5.3.1.

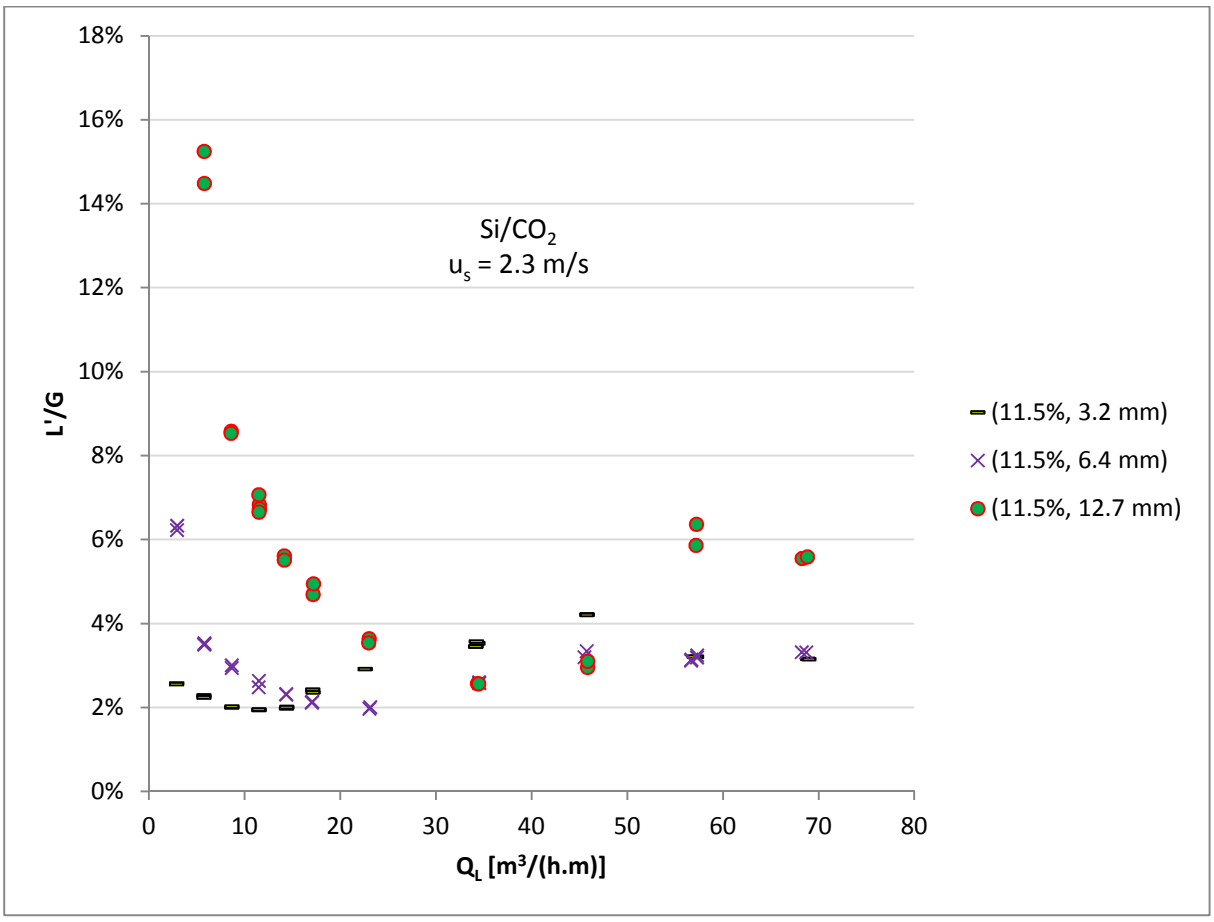

Figure 49 – Effect of hole diameter on entrainment (L'/G) for silicone-oil/CO_2 with a 11% fractional hole area and a superficial gas velocity of 2.3 m/s.

The entrainment for the different sieve trays are shown in Figure 50 for L'/G entrainment and Figure 150 in Appendix F for L'/L entrainment for an ethylene glycol/air (EG/air) system and a liquid flow rate of 8.6 m^3/(h.m) (spray regime) at changing gas superficial velocities. The influence of the tray geometry increases with increasing superficial gas velocity, due to an increase in the dominance of the spray regime characteristics.

The different sieve trays investigated entrainment are shown in Figure 51 for L'/G entrainment and Figure 151 in Appendix F for L'/L entrainment for a liquid flow rate of 34.3 m^3/(h.m) (froth regime moderate liquid flow rates) and changing gas superficial velocities. At a moderate liquid flow rate, the influence of tray does not change with increasing superficial gas velocity. The high entrainment observed for the 12.7 mm diameter and 7.3% fractional hole area tray is due to the high stability of the gas jets through the tray hole. At possible lower fractional hole areas (below 7%) and a hole diameter above 12.7 mm, tray hole diameter influences entrainment over the entire range of liquid flow rates leading to easier column entrainment flooding.

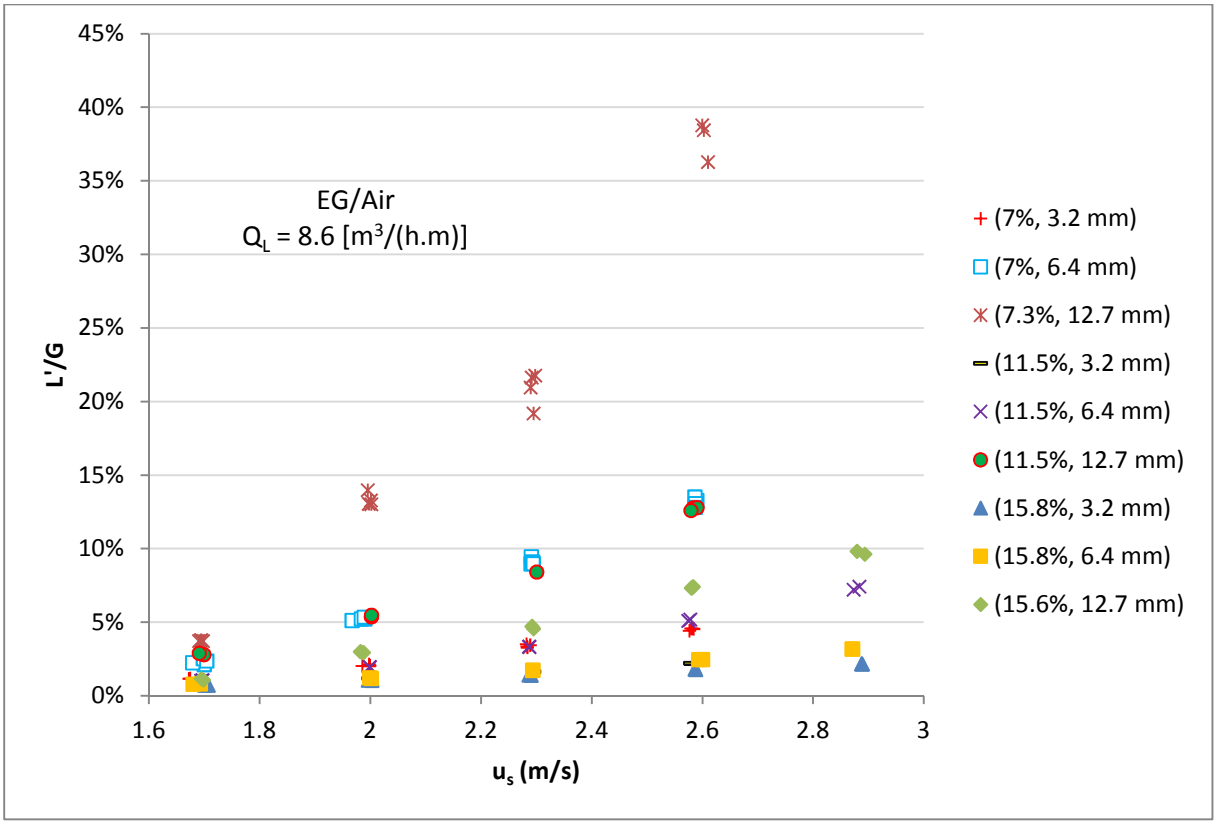

Figure 50 – Effect of tray geometry on entrainment (L'/G) for ethylene-glycol/air with changing superficial gas velocity and a liquid flow rate of 8.6 m^3/(h.m).

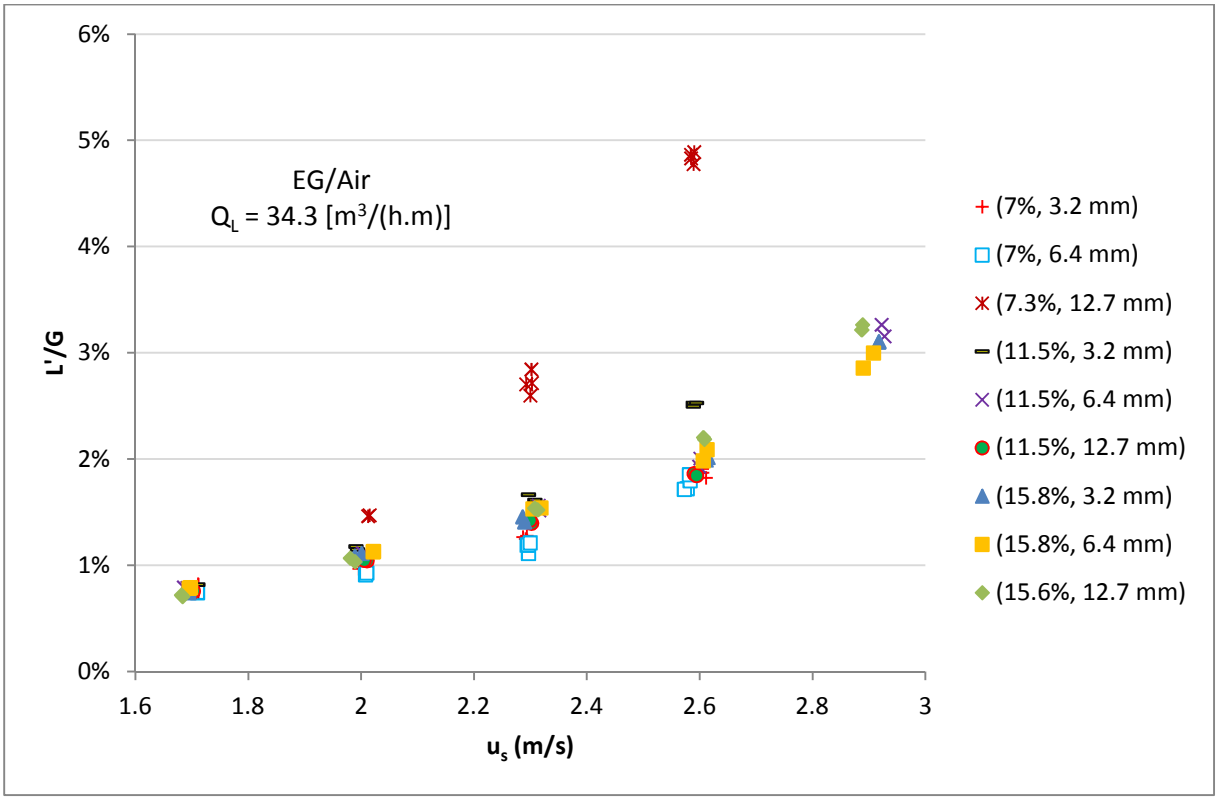

Figure 51 – Effect of tray geometry on entrainment (L'/G) for ethylene-glycol/air with changing superficial gas velocity and a liquid flow rate of 34.3 m^3/(h.m).

5.3 Evaluation of Correlations and Predictive Models

This section compares the experimental entrainment results obtained in the current distillation pilot plant study to existing entrainment models observed in literature. The experimental results are also compared to dimensionless numbers in order to describe entrainment on a fundamental basis.

5.3.1 Literature Correlations Entrainment Model Comparison

In the current section, entrainment results are compared with entrainment models by literature sources. The discussion will make reference to the following model references as 'Kister & H' for Kister *et al.* (1981), 'Bennett *et al.*' for the Bennett *et al.* (1995) air/water model, 'Uys' for Uys (2012), 'Zuiderweg' for Zuiderweg (1982), 'Kozoil & M' for Kozoil and Mackowaik (1990), 'Hunt *et al.*' for Hunt *et al.* (1955) and 'Thomas & O' for Thomas and Ogboja (1978). The recommended ranges for the entrainment models are shown in Table 4. The models are initially compared with water/air system entrainment experimental results to evaluate the effect of tray geometry, since most of the models are applicable with water/air systems. Models that are plotted beyond their defined recommended parameter ranges are shown with dashed lines (with O in the legends) and those that are within their recommended parameter range are shown as solid lines (with I in the legends). Most models are plotted outside their recommended ranges, but the trend predictions are still of importance.

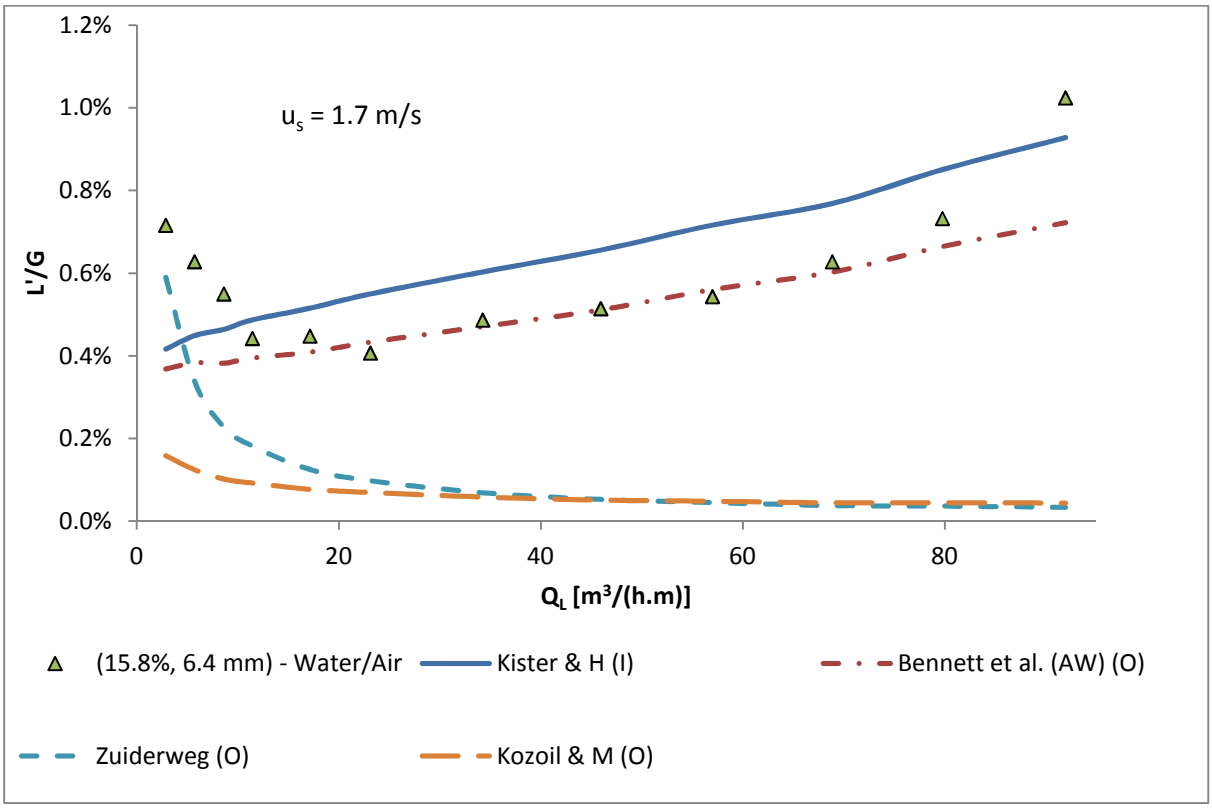

Figure 52 – Experimental entrainment comparison to entrainment models for Tray 1 (15.8% fractional hole area, 6.4 mm hole diameter) with water/air at a superficial gas velocity of 1.7 m/s.

The purpose of the current entrainment model investigation is to show the extent of agreement between the entrainment prediction magnitude and trends of the entrainment correlations. The

investigation will show the need for further entrainment model improvement, by highlighting parameter ranges that need to be further investigated. Other existing models which do not incorporate distillation parameters into their entrainment model are not shown.

The entrainment experimental results for Tray 1 with a superficial gas velocity of 1.7 m/s are compared with entrainment models in Figure 52. The 'Kister & H' model is plotted within its recommended range, where the rest of the models are plotted outside their recommended ranges (Fig. 52). The entrainment results compare well with the model by 'Bennett *et al.*' and the trend observed by 'Kister & H' in the froth regime. The 'Zuiderweg' entrainment trend is similar to the experimental trend in the spray regime, although it under predicts the entrainment at higher liquid flow rates.

The entrainment experimental results for Tray 1 with a superficial gas velocity of 2.6 m/s are compared with entrainment models in Figure 53. The 'Bennett *et al.*' model deviates from the experimental results as the superficial gas velocity increases (Fig. 52 to 53). The 'Kister & H' model is shown to fit the entrainment results much better as the superficial gas velocity increases. The 'Zuiderweg' model over predicts the entrainment in the spray regime, but follows a similar trend to the experimental data. The 'Hunt *et al.*' model over predicts the entrainment and that the 'Kozoil & M' under predicts the entrainment while deviating from the trends in the experimental results (Fig. 52 and 53). The 'Kister & H' model is plotted within its recommended range, where the rest of the models are plotted outside their recommended ranges (Fig. 53).

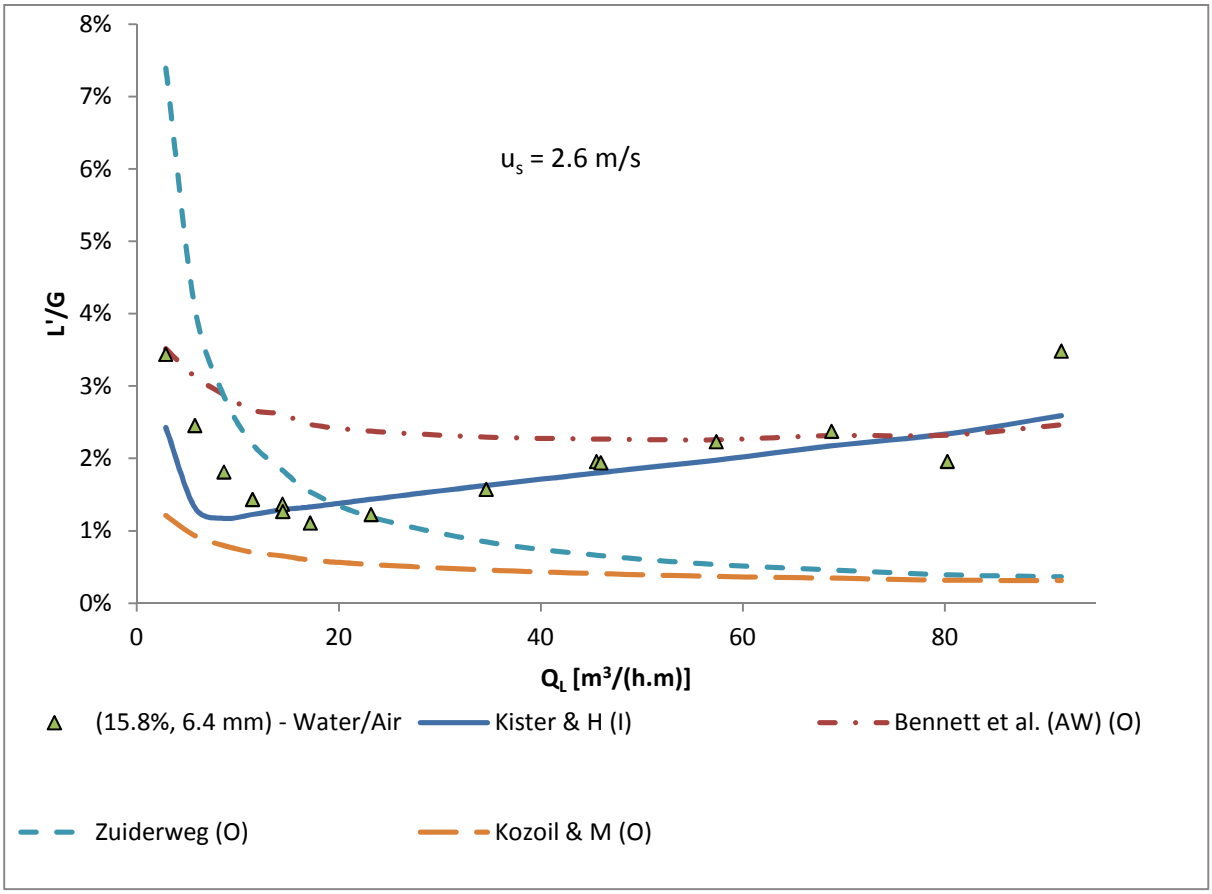

Figure 53 – Experimental entrainment comparison to entrainment models for Tray 1 (15.8% fractional hole area, 6.4 mm hole diameter) with water/air at a superficial gas velocity of 2.6 m/s.

Figure 54 shows the entrainment at a superficial gas velocity of 2 m/s and Figure 152 in Appendix F shows the entrainment of superficial gas velocity of 2.3 m/s with Tray 2. The 'Bennett *et al.*' and 'Kister & H' model compares well with the entrainment results at moderate liquid flow rates, but deviates considerably at high liquid flow rates (Fig. 54 and 152). The 'Kister & H' is plotted within its recommended range, where the rest of the models are plotted outside their recommended ranges.

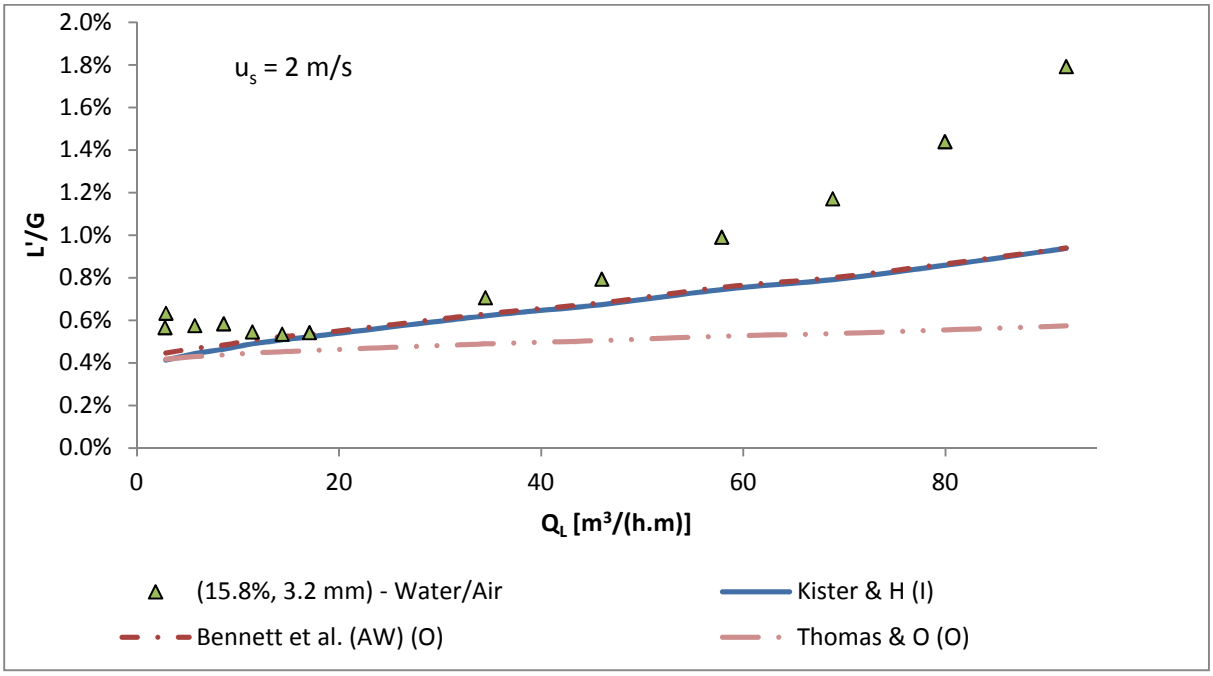

Figure 54 – Experimental entrainment comparison to entrainment models for Tray 2 (15.8% fractional hole area, 3.2 mm hole diameter) with water/air at a superficial gas velocity of 2 m/s.

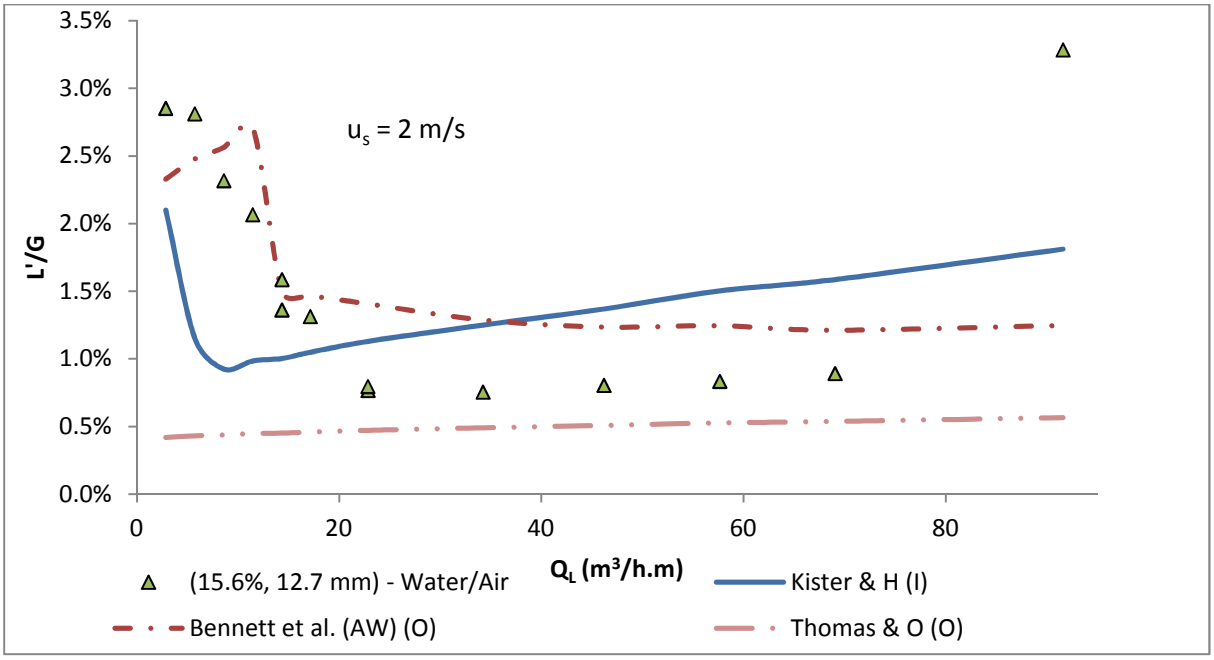

Figure 55 – Experimental entrainment comparison to entrainment models for Tray 3 (15.6% fractional hole area, 12.7 mm hole diameter) with water/air at a superficial gas velocity of 2 m/s.

The entrainment experimental results are compared to entrainment models for Tray 3 at a superficial gas velocity of 2 m/s in Figure 55 and a superficial gas velocity of 2.3 m/s in Figure 153 in Appendix F for water/air systems. The experimental results do not compare well with the entrainment models in the froth regime. The 'Bennett *et al.*' has a good agreement with the experimental results in the spray regime at a superficial gas velocity of 2 m/s (lower velocities) but does not compare well with the experimental results at a higher superficial gas velocity of 2.3 m/s. The 'Kister & H' model follows a similar trend to the experimental results in the spray regime, but under-predicts the experimental results. The 'Kister & H' is plotted within its recommended range, where the rest of the models are plotted outside their recommended ranges (Fig. 55).

The effects of fractional hole area changes are evaluated by comparing experimental results for Tray 4 to entrainment models in Figure 56 for a superficial gas velocity of 2.3 m/s and Figure 154 in Appendix F for a superficial gas velocity of 2.6 m/s. The 'Zuiderweg' entrainment model compares well to experimental results over the entire range of liquid flow rates, where at a fractional hole area of 7%, the distillation column exhibits spray like behaviour. The 'Kister & H' model compares well with the experimental results at high liquid flow rates (froth regime). The 'Bennett *et al.*' over predicts the entrainment at high liquid rates and follows an opposite trend to the experimental results. The 'Kister & H' and 'Bennett *et al.*' models are plotted within their recommended ranges, where the rest of the models are plotted outside their recommended ranges (Fig. 56).

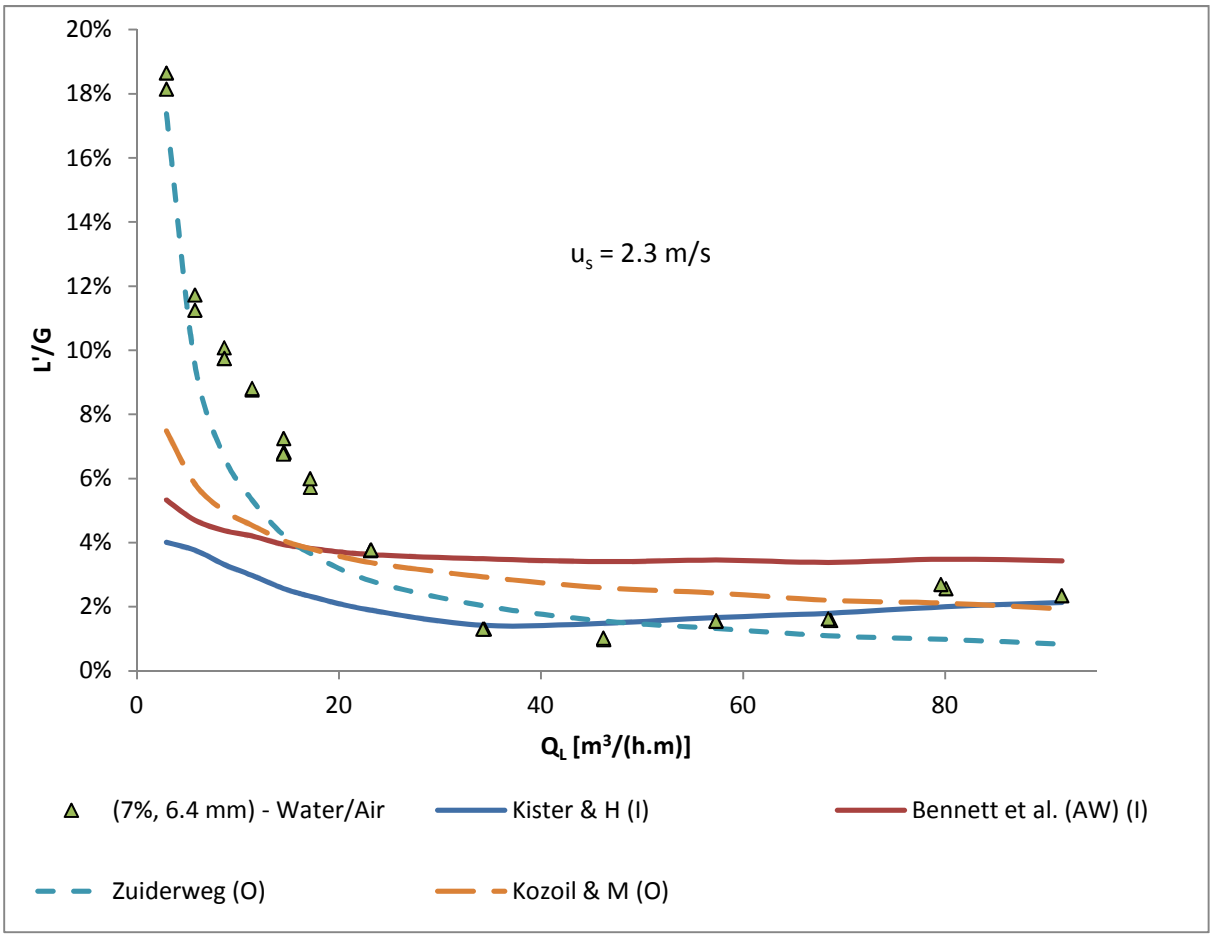

Figure 56 – Experimental entrainment comparison to entrainment models for Tray 4 (7% fractional hole area, 6.4 mm hole diameter) with water/air at a superficial gas velocity of 2.3 m/s.

The entrainment experimental results for Tray 7 are compared with entrainment models at a superficial gas velocity of 2.3 m/s in Figure 57 and a superficial gas velocity of 2.6 m/s in Figure 155 in Appendix F. The 'Zuiderweg' model compares well with the trend shown by the experimental entrainment results in the spray regime, but does not compare well to the trend observed in the froth regime. The 'Kister & H' model compares well with the experimental data in the froth regime, showing that the 'Kister & H' model can be used to predict the effect of fractional hole area at a hole diameter of 6.4 mm for a water/air system in the froth regime. The 'Bennett *et al.*' over predicts the entrainment at high liquid rates and follows an opposite trend to the experimental results. The 'Kister & H' and 'Bennett *et al.*' models are plotted within their recommended ranges, where the rest of the models are plotted outside their recommended ranges (Fig. 57).

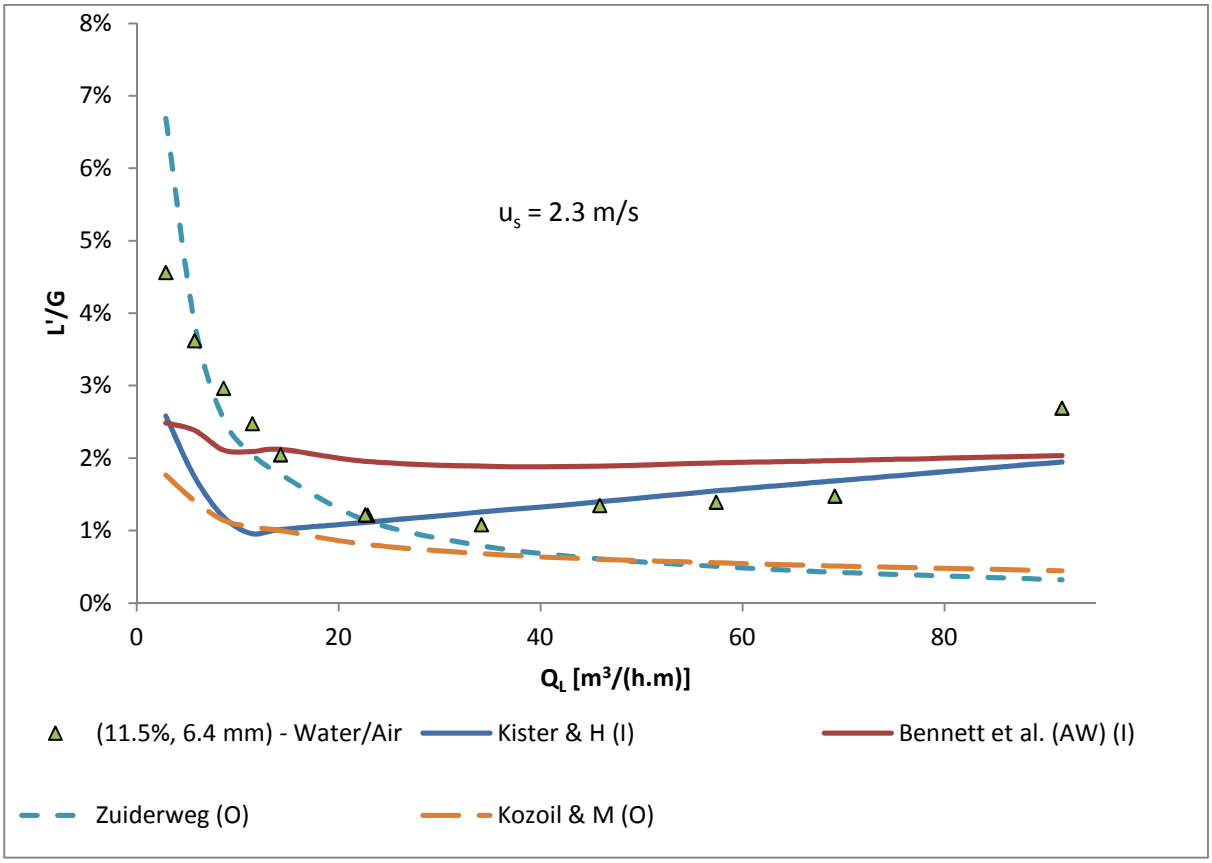

Figure 57 – Experimental entrainment comparison to entrainment models for Tray 7 (11.5% fractional hole area, 6.4 mm hole diameter) with water/air at a superficial gas velocity of 2.3 m/s.

The effect of carbon dioxide physical properties are evaluated by comparing experimental results for Tray 1 to entrainment models in Figure 58 for a superficial gas velocity of 2 m/s and Figure 156 in Appendix F for a superficial gas velocity of 2.3 m/s for a water/CO_2 system. The model comparison is performed at a different tray geometry than that used by 'Uys', 'Zuiderweg', 'Hunt *et al.*' and 'Thomas and O' making them invalid. However, the models are still shown so that the model trends and magnitude can be evaluated so that the largest areas (parameter ranges) of uncertainty can be highlighted when evaluating the effect of fluid physical properties. The 'Uys' model follows a similar trend to experimental data, but over predicts the entrainment model due to the difference in tray geometry. The 'Zuiderweg' model explains the trend of the experimental results in the spray regime well but over predicts the entrainment, whereas the 'Kister & H' model explains the trend of

experimental results well in the froth regime, but still over predicts the magnitude of entrainment. All the models are plotted outside their recommended ranges (Fig. 58 and 156).

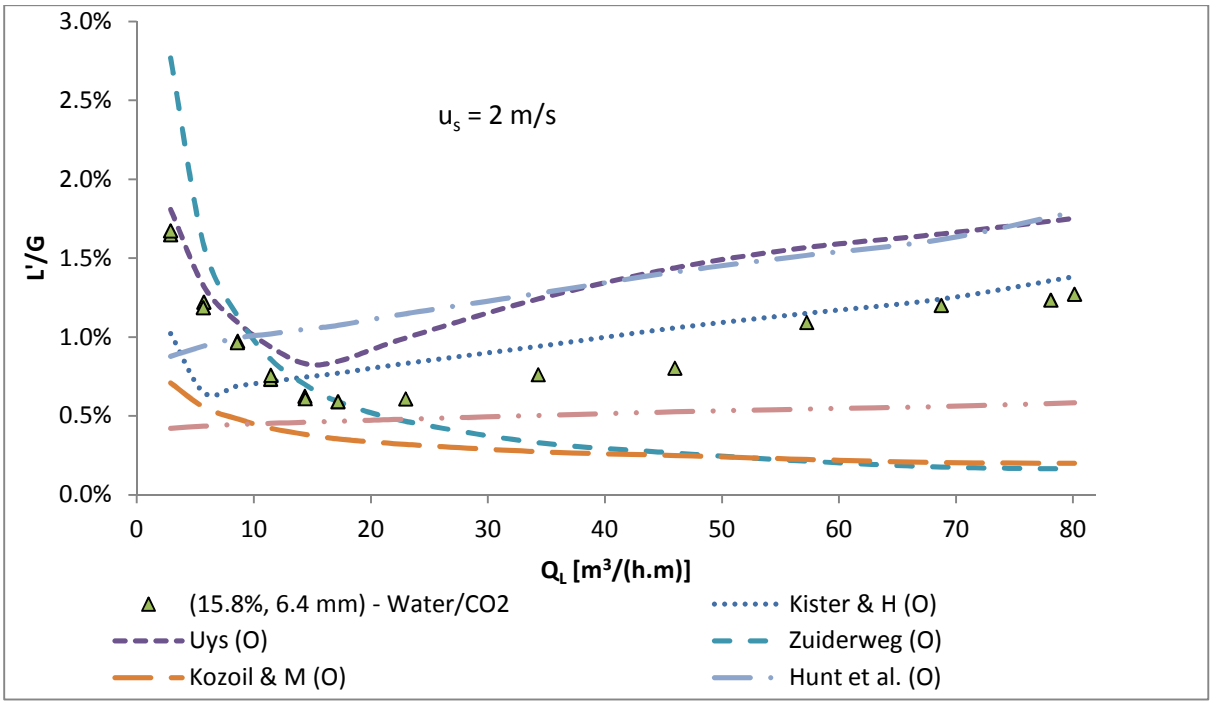

Figure 58 – Experimental entrainment comparison to entrainment models for Tray 1 (15.8% fractional hole area, 6.4 mm hole diameter) with water/CO_2 at a superficial gas velocity of 2 m/s.

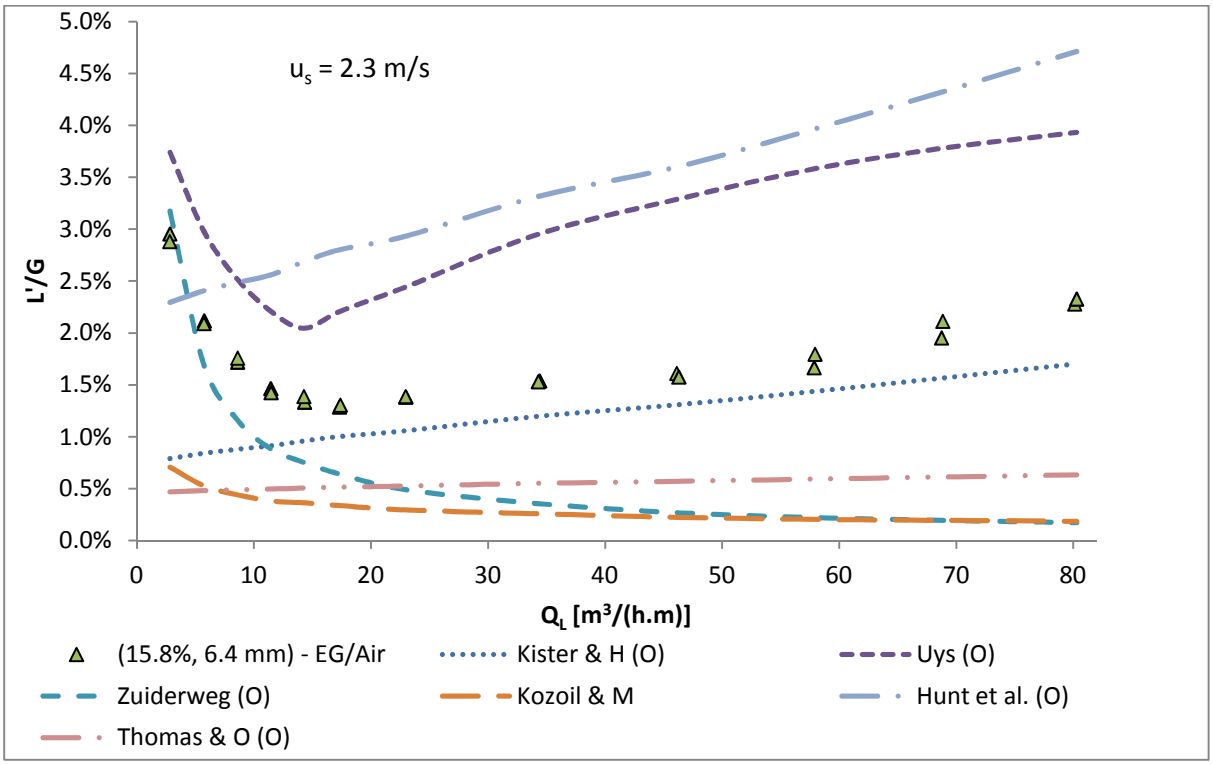

Figure 59 – Experimental entrainment comparison to entrainment models for Tray 1 (15.8% fractional hole area, 6.4 mm hole diameter) with ethylene-glycol/air at a superficial gas velocity of 2.3 m/s.

The effect of liquid physical properties are evaluated by comparing experimental results for Tray 1 to entrainment models in Figure 59 for an ethylene glycol/air (EG/air) system and Figure 157 in Appendix F for a silicone oil/air (Si/air) system at a superficial gas velocity of 2.3 m/s. The 'Uys' model explains the entrainment trends well when different fluids are used, but over predicts the entrainment over the entire range of liquid flow rates and gas superficial velocities due to the difference in tray geometry. The entrainment models do not compare well with experimental results and thus a model has to be developed to predict entrainment for the different liquid properties. All the models are plotted outside their recommended ranges (Fig. 59 and 157).

5.3.2 Dimensionless Number Predictive Model Trends for Entrainment

The experimental entrainment data (L'/L and L'/G) are compared with dimensionless fluid dynamic numbers in order to help explain the trends observed in the previous section. The dimensionless numbers are taken from different literature sources and adjusted to fit the current sieve tray distillation column study. The entrainment is mostly compared with Tray 1 (15.8% fractional hole area and a hole diameter of 6.4 mm), where the effect of fluid physical properties and tray geometry are addressed later in the section.

$$Fr_h^+ = u_h \left(\frac{\rho_g}{h_c \rho_l}\right)^{0.5} \quad \rightarrow \quad \text{Liquid Hold-up Froude Number} \quad [5.3.2.1]$$

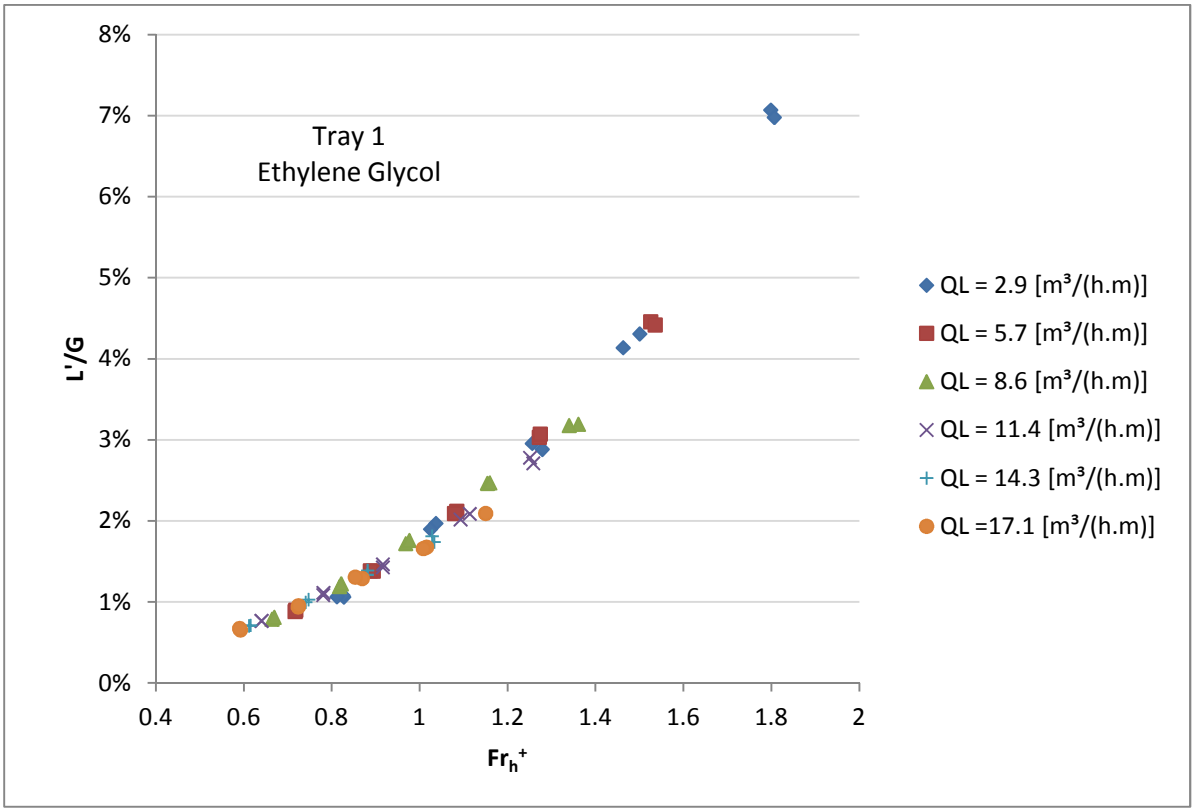

Figure 60 – Entrainment (L'/G) changing with the liquid hold-up Froude number (Fr_h^+) for ethylene-glycol/air with Tray 1 (15.8% fractional hole area, 6.4 mm hole diameter) in the spray regime.

The entrainment (L'/G) experimental data are plotted against the liquid hold-up Froude number (Fr_h^+) in Figure 60 in the spray regime, where the liquid hold-up Froude number is represented by Equation 5.3.2.1 (Lockett and Banik, 1986). The Froude number defines the ratio of the inertial

forces to the gravitational forces acting on the fluid (speed over length ratio). Entrainment changes in a similar fashion at different liquid rates in the spray regime, where entrainment is a strong function of the parameters used to define the liquid hold-up Froude number. Entrainment decreases with increasing liquid flow rate in the spray regime. The entrainment (L'/G) increases with increasing liquid hold-up Froude number in the spray regime. The entrainment (L'/G) increases with increasing hole gas velocity (u_h), increasing gas density (ρ_g), decreasing clear liquid hold-up (h_c) and decreasing liquid density (ρ_l) in the spray regime (Fig. 60).

Figure 158 in Appendix F shows that entrainment (L'/G) has a different dependency on the liquid hold-up Froude number in the froth regime. The change in the liquid hold-up Froude number in the froth regime with the entrainment (L'/G) follows the same liquid dispersion trend identified in Figure 5. Entrainment increases with decreasing liquid hold-up Froude number at low to moderate liquid hold-up Froude numbers in the froth regime [approximately 23 m^3/(h.m) to 69 m^3/(h.m)] (Fig. 158). Therefore entrainment increases with decreasing hole gas velocity (u_h), decreasing gas density (ρ_g), increasing clear liquid hold-up (h_c) and increasing liquid density (ρ_l). The entrainment increases with increasing liquid hold-up Froude number at high liquid flow rates [typically above 69 m^3/(h.m)]. The dispersion layer becomes unstable as the liquid flow rate tends towards sieve tray distillation column flooding.

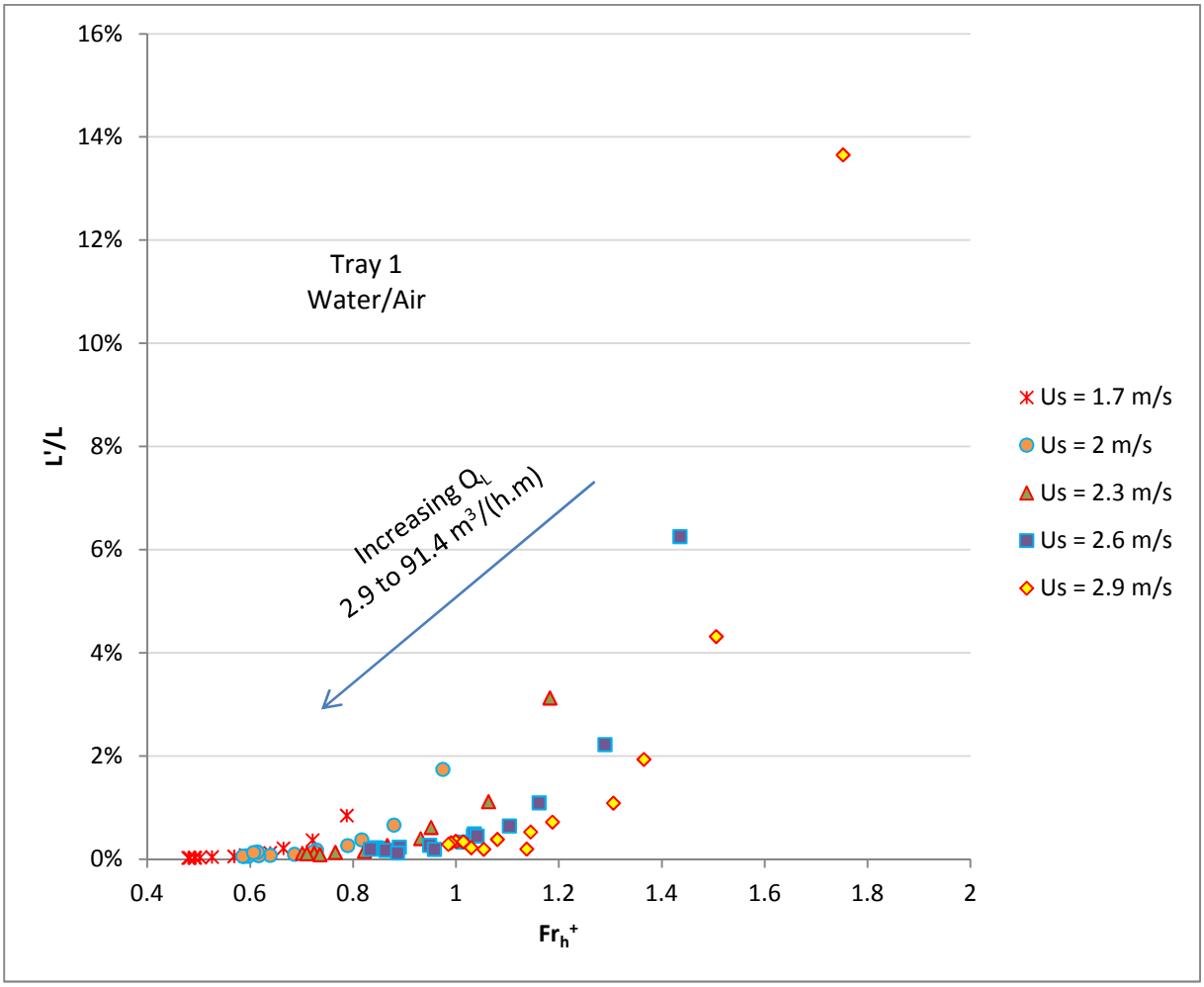

Figure 61 – Entrainment (L'/L) changing with the liquid hold-up Froude number (Fr_h^+) for water/air with Tray 1 (15.8% fractional hole area, 6.4 mm hole diameter) at different gas superficial velocities.

The liquid hold-up Froude number and entrainment increases with increasing superficial gas velocity, which is expected as the hole gas velocity is used in the liquid hold-up Froude number (Fig. 61). The L'/L vs. Fr_h^+ figure follows a similar trend at each superficial gas velocity.

The Weber number is defined by Equation 1.2.2.4, where the Weber number defines the ratio between the inertial forces to surface tension forces of the fluid (Fig. 62). The Weber number is used in multiphase flow to describe the behaviour of thin films and the tendency for the formation of bubbles and droplets (Uys, 2012).

$$We = \frac{\rho_g u_s Q_L}{3.6\sigma} \quad \rightarrow \quad \text{Weber Number} \quad [1.2.2.4]$$

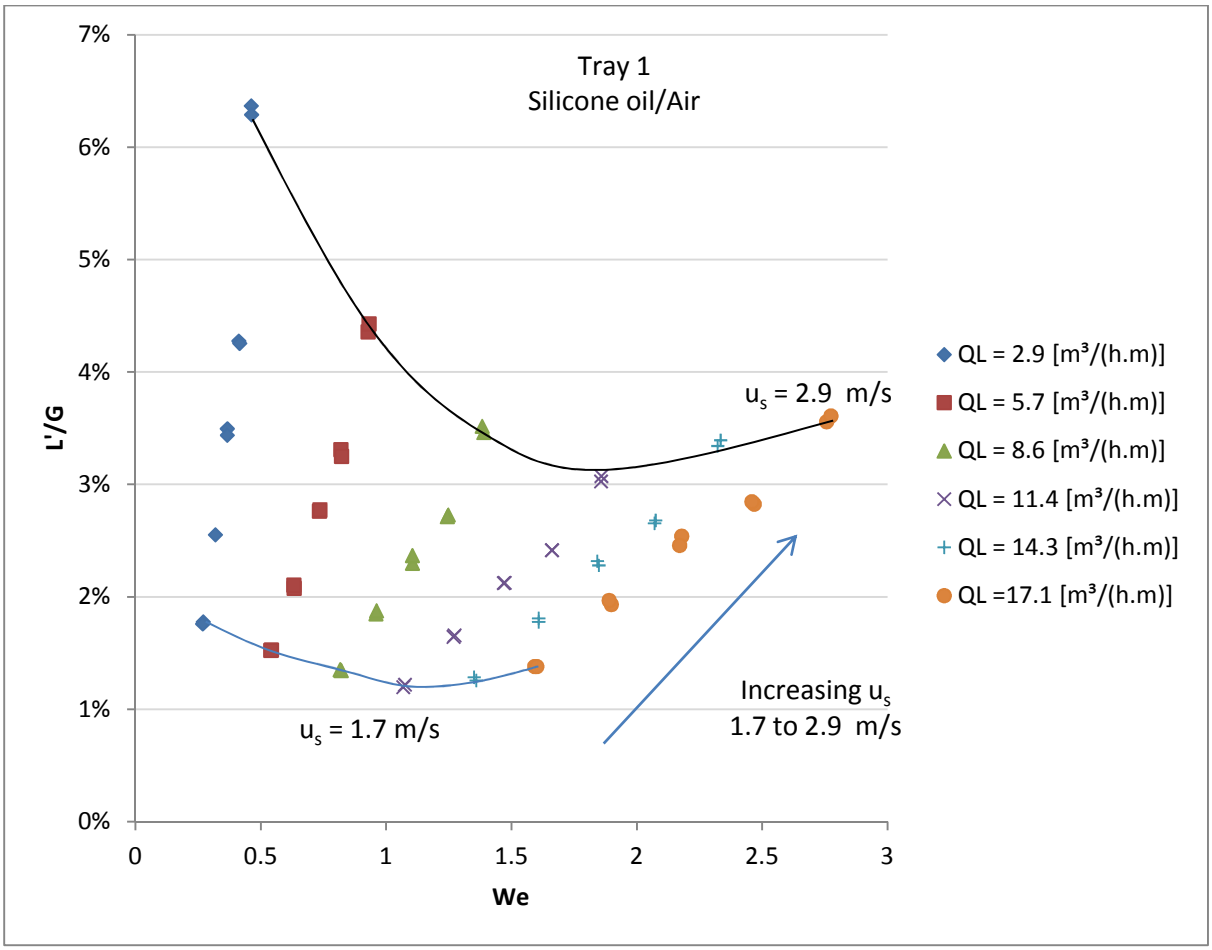

Figure 62 – Entrainment (L'/G) changing with the Weber number (We) for silicone-oil/air with Tray 1 (15.8% fractional hole area, 6.4 mm hole diameter) in the spray regime.

The entrainment increases with increasing Weber number for a particular liquid flow rate in the spray regime (Fig. 62). Entrainment increases with increasing gas density (ρ_g), increasing superficial gas velocity (u_s) and decreasing liquid surface tension (σ). As the liquid flow rate increases, the dependency of the entrainment (L'/G) on the Weber number decreases, supporting the trend observed in earlier sections. The gas velocity increases from 1.7 to 2.9 m/s at increments of 0.3 m/s, where the trend lines in Figure 62 represents a constant superficial gas velocity. Entrainment decreases, reaches a minimum at approximately 11 m^3/(h.m) then increases with increasing Weber number for silicone oil/air. Figure 159 in Appendix F shows that L'/L entrainment follows the same

trend observed in the spray regime, where the entrainment has a lower dependency on the Weber number in the froth regime. The L'/G entrainment follows an opposite trend in the froth regime to that in the spray regime with increasing liquid flow rate. The entrainment (L'/G) increases with increasing liquid flow rate (showing the high dependency of the froth layer in the dispersion on the liquid flow rate) in the froth regime.

The entrainment (L'/G) is plotted versus the liquid Reynolds number (Re) in Figure 63 for the spray regime. The liquid Reynolds number is defined by Equation 2.5.1.30, where it is altered to fit the current entrainment investigation. The liquid Reynolds number defines the ratio between the inertial forces to viscous forces of the fluid (Uys, 2012).

$$Re = \frac{\rho_g\left(\frac{Q_L}{3600}\right)}{\mu_g} \quad \rightarrow \quad \text{Liquid Reynolds number} \qquad [2.5.1.30]$$

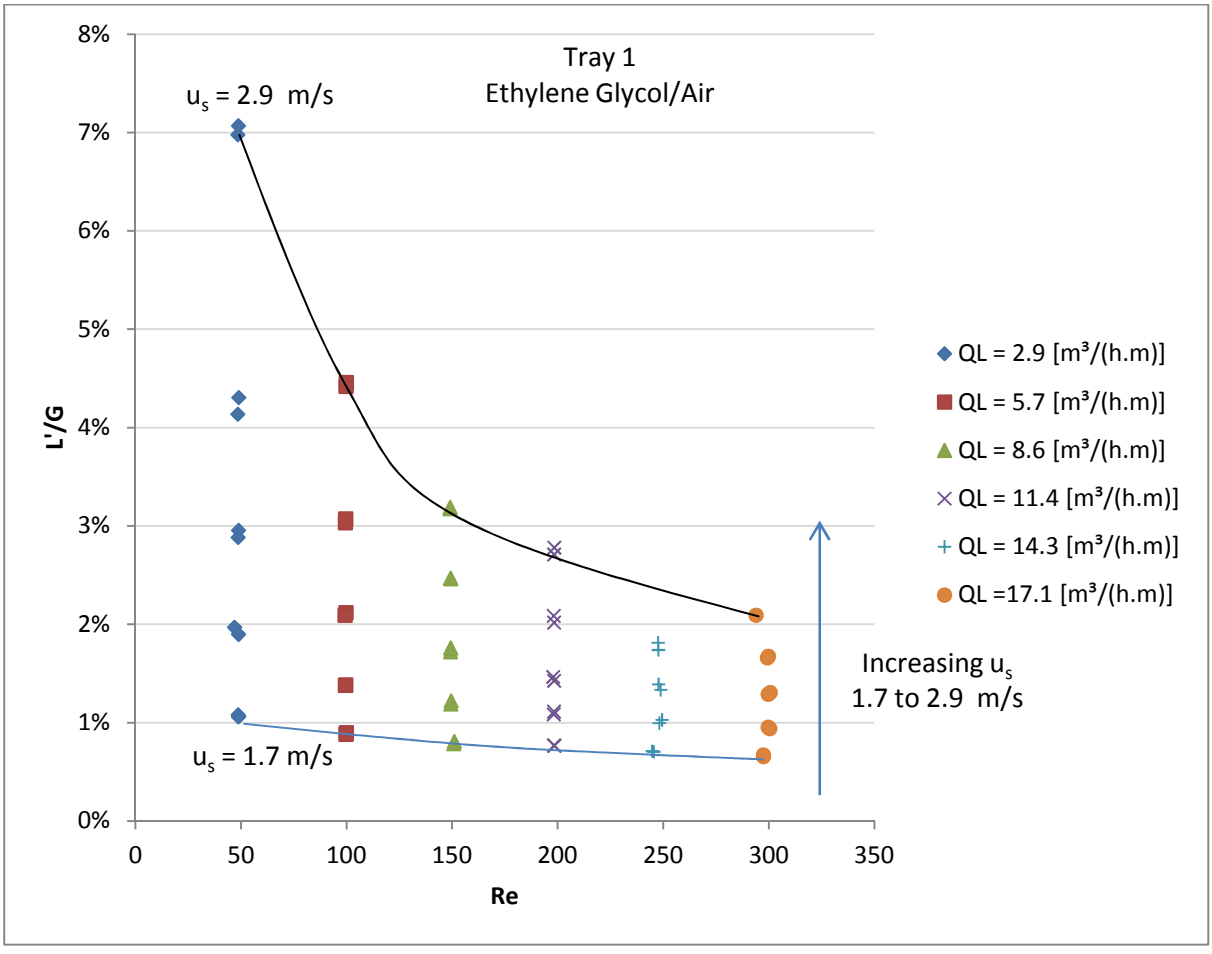

Figure 63 – Entrainment (L'/G) changing with the liquid Reynolds number (Re) for ethylene-glycol/air with Tray 1 (15.8% fractional hole area, 6.4 mm hole diameter) in the spray regime.

The entrainment (L'/G) decreases with increasing liquid Reynolds numbers in the spray regime (Fig. 63). The trends for the liquid Reynolds number shows that entrainment (L'/G) increases with increasing gas viscosity (μ_g), decreasing gas density and decreasing liquid flow rate, supporting the entrainment trends observed in earlier sections. Entrainment increases with increasing liquid Reynolds number at low to moderate liquid flow rate in the froth regime (Fig. 160 in Appendix F). It

can be deduced that the entrainment (L'/G) increases with increasing liquid flow rates, increasing gas density and decreasing gas viscosity at moderate liquid flow rates. At high liquid flow rates, entrainment increases with an increasing liquid Reynolds number, but becomes less dependent on the superficial gas velocity (possible close to the point of entrainment flooding). The gas velocity increases from 1.7 to 2.9 m/s in increments of 0.3 m/s, where the trend lines in Figure 63 represents a constant superficial gas velocity.

The entrainment (L'/L) is plotted against the flow Froude number (Fr^+) in Figure 64 with Tray 1 for a water/air system. The flow Froude number is represented by Equation 2.5.1.31, where the flow Froude number has only fluid flow terms, unlike the liquid hold-up Froude number (Fr_h^+) in Equation 5.3.2.1. The form of the flow Froude number in Equation 2.5.1.31 is taken from Uys (2012) and altered to fit the current entrainment investigation.

$$Fr^+ = \frac{3600 u_s^3}{g Q_L} \qquad \rightarrow \qquad \text{Flow Froude number} \qquad [2.5.1.31]$$

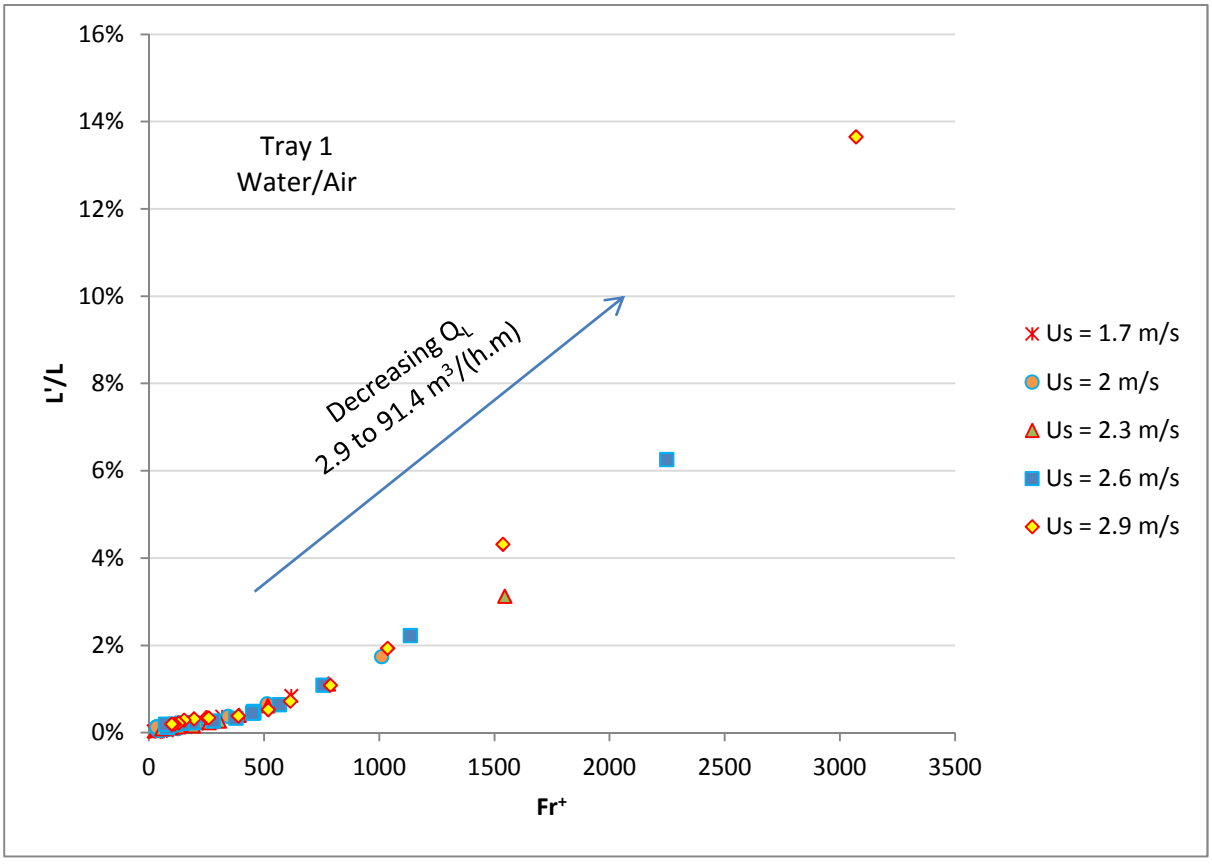

Figure 64 – Entrainment (L'/L) changing with the flow Froude number (Fr^+) for water/air with Tray 1 (15.8% fractional hole area, 6.4 mm hole diameter) at different gas superficial velocities.

The entrainment (L'/L) changes on the same monotonic curve for all the gas superficial velocities, liquid flow rates investigated for a particular sieve tray and fluid system (Fig. 64). The curve produced when plotting L'/L entrainment against the flow Froude number, shows that the flow Froude number is an ideal dimensionless number which can be used in the development of an entrainment model. The L'/L vs. Fr^+ curve shows that different curves for different systems and tray geometries can be compared, an investigation that will be performed later in the section. The

entrainment (L'/L) increases with increasing flow Froude number, showing that the entrainment (L'/L) increases with increasing superficial gas velocity and decreases with increasing liquid flow rate.

The entrainment (L'/L) is plotted against the gas Reynolds number (Re_g) divided by the flow Froude number in Figure 65 for a butanol/CO_2 system and Tray 1. The gas Reynolds number is shown by Equation 5.3.2.2, where the gas Reynolds number replaces the liquid flow rate (Q_L) term in the liquid Reynolds number (Equation 2.5.1.30) with the hole gas velocity (u_h) and the hole diameter (d_H).

$$Re_g = \frac{\rho_g u_h D_H}{\mu_g} \quad \rightarrow \quad \text{Gas Reynolds number} \qquad [5.3.2.2]$$

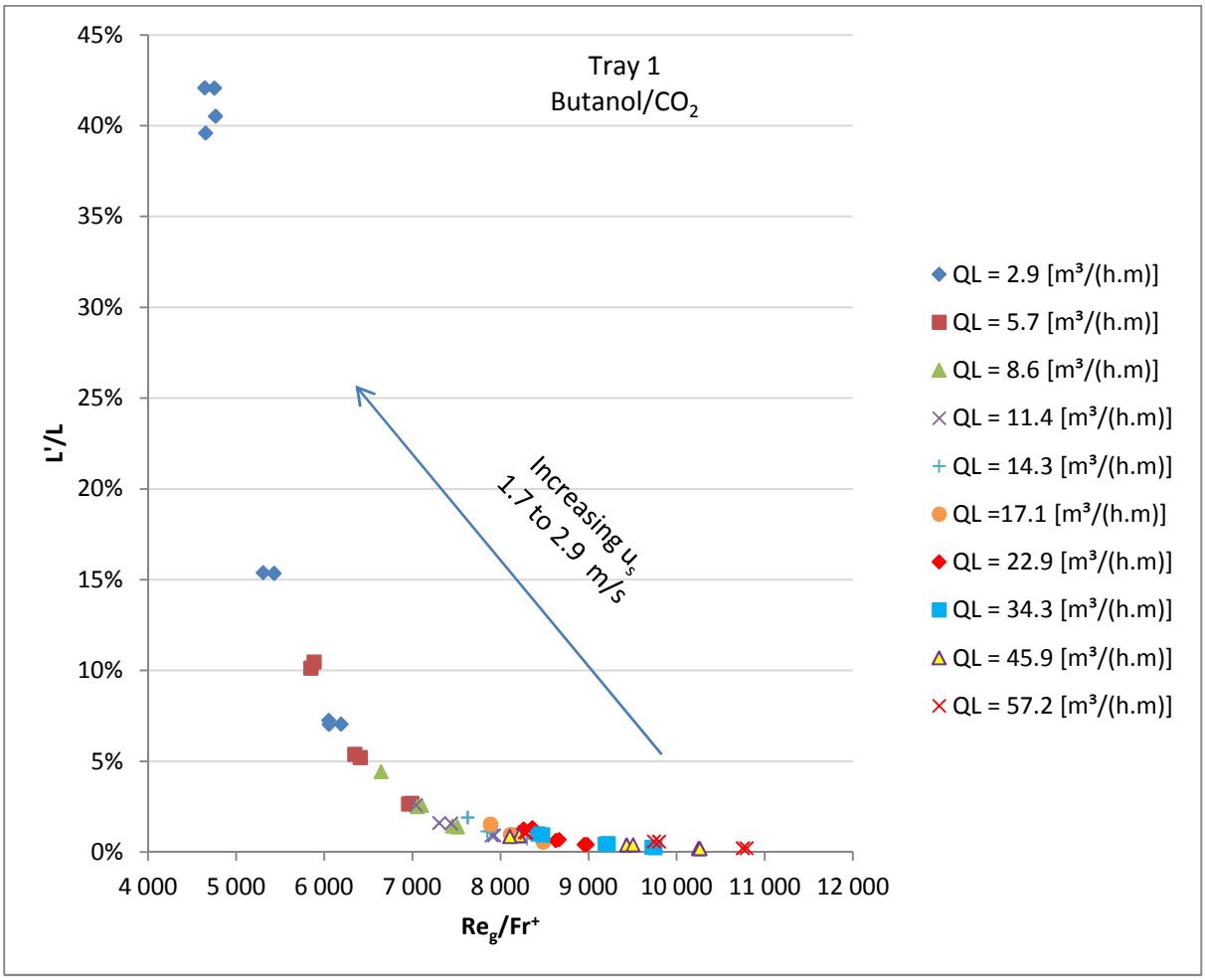

Figure 65 – Entrainment (L'/L) changing with the gas Reynolds number (Re_g) divided by the flow Froude number (Fr^+) for butanol/CO_2 with Tray 1 (15.8% fractional hole area, 6.4 mm hole diameter) at different liquid flow rates.

The L'/L entrainment decreases with increasing Re_g/Fr^+, which follows the typical trend for an L'/L graph when plotted against the liquid flow rate (Q_L) shown in earlier sections (Fig. 65). The L'/L vs. Re_g/Fr^+ graph shows that the gas Reynolds number term can be used to model entrainment. The entrainment (L'/L) decreases with increasing liquid flow rate. The effect of Re_g/Fr^+ on entrainment with different fluid systems is shown in figure 66. The gas Reynolds and flow Froude number ratio entrainment curve allows the prediction of a wide range of sieve tray hole diameters and gas physical properties.

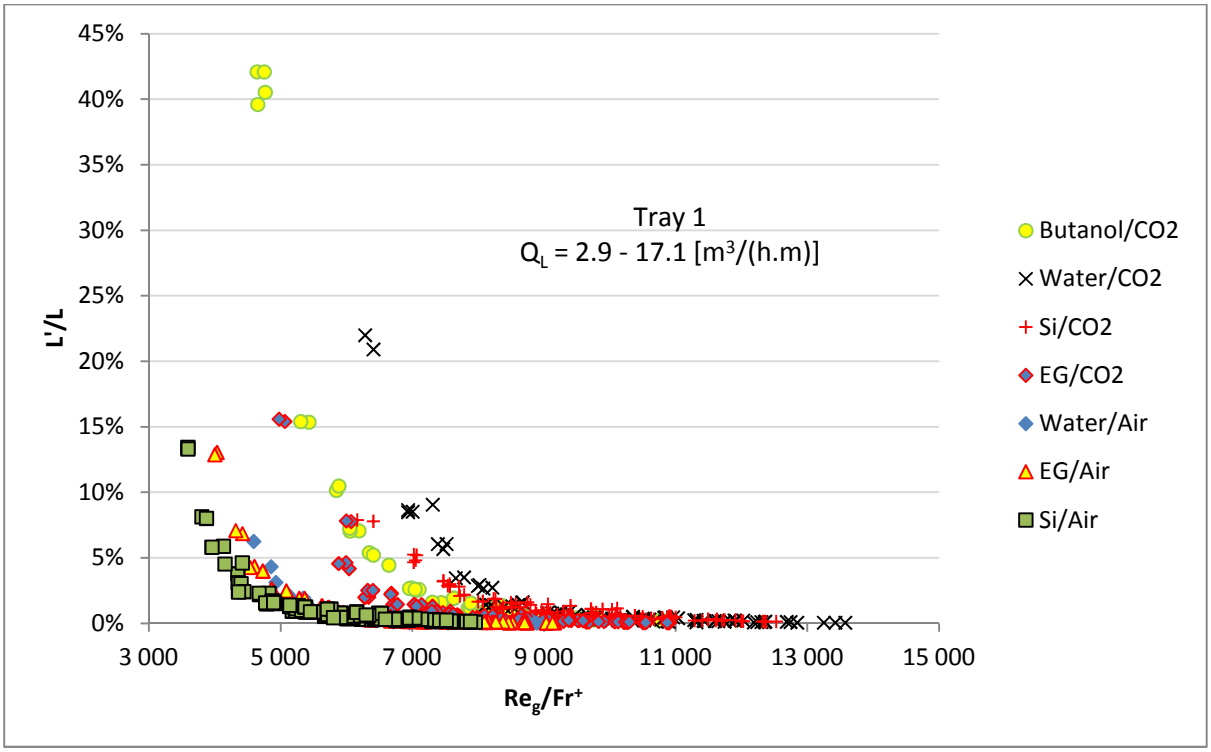

Figure 66 – Entrainment (L'/L) changing with the gas Reynolds number (Reg) divided by the flow Froude number (Fr+) for different fluids systems with Tray 1 (15.8% fractional hole area, 6.4 mm hole diameter).

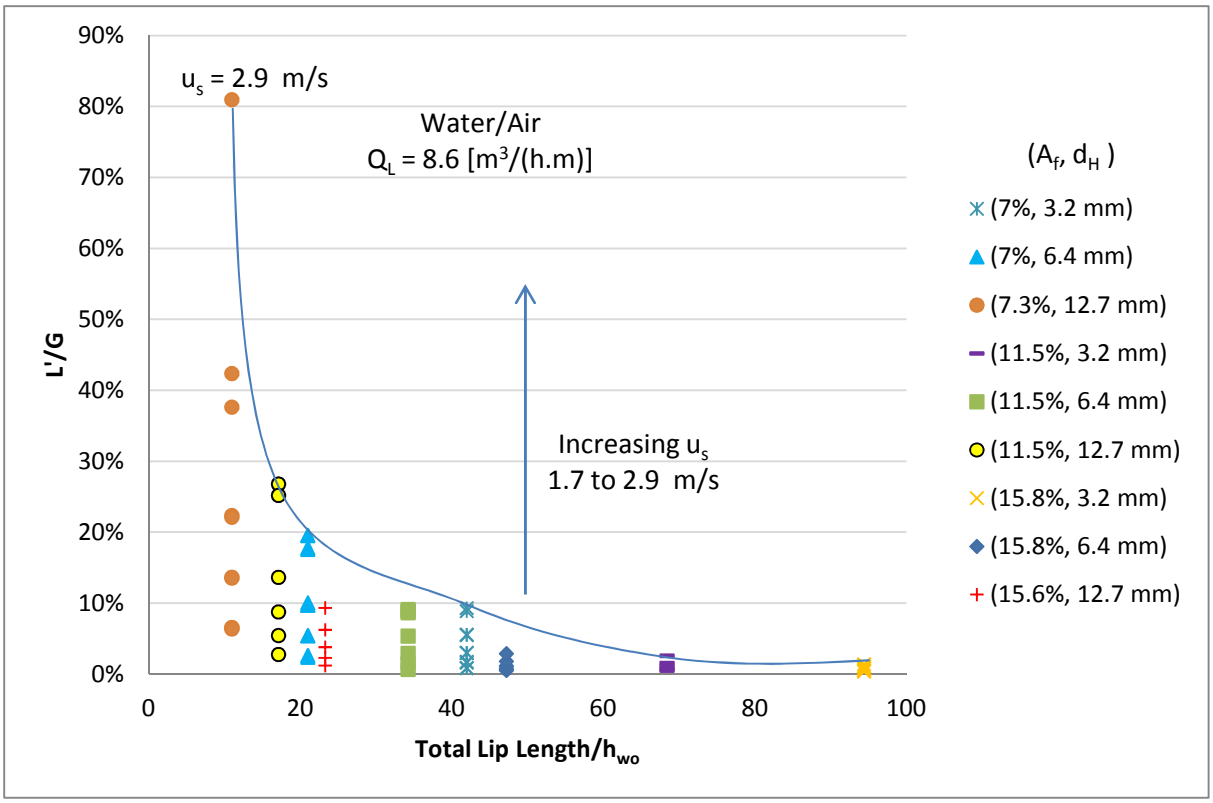

Figure 67 – Entrainment (L'/G) changing with the tray hole lip length divided by the weir height (h_{wo}) for water/air with different sieve trays.

The effect of sieve tray geometry is evaluated in Figure 67, where entrainment (L'/G) is plotted against the total lip length to weir height (h_{wo}) ratio for a water/air system. The total lip length is defined by Equation 5.3.2.3, where the total lip length is defined as the number of holes on a sieve tray multiplied by the circumference of the sieve tray holes. The aim of Figure 67 is to evaluate the impact of lip length in the spray regime during gas jetting through the sieve tray holes, where the weir height is kept constant for the current experimental investigation.

$$Total\ Lip\ Length = (\pi d_H N_T) \qquad [5.3.2.3]$$

The entrainment (L'/G) decreases with increasing total lip length to weir height ratio, which shows that entrainment (L'/G) increases with the increasing amount of holes (increasing fractional hole area) and increasing tray hole diameter (Fig. 67). The entrainment (L'/G) is a stronger function of the number of holes (fractional hole area) than it is of the sieve tray hole diameter in the spray regime. By decreasing the number of sieve tray holes, the gas hole velocity increases, promoting gas jetting through the sieve tray holes (producing a larger spray layer in the liquid dispersion above the sieve tray). The superficial gas velocity increases from 1.7 to 2.9 m/s at increments of 0.3 m/s, where the trend line in Figure 67 represents a constant superficial gas velocity.

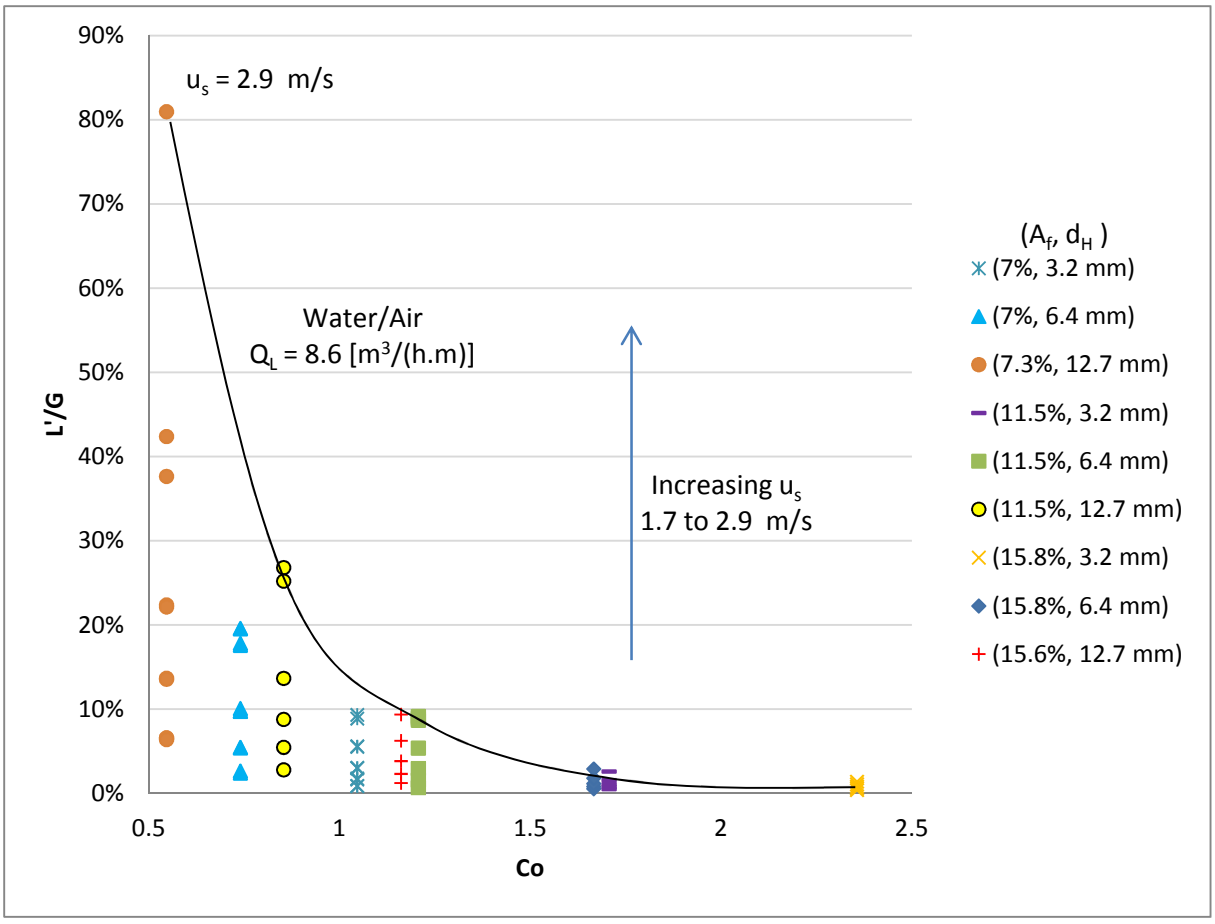

Figure 68 – Entrainment (L'/G) changing with the construction number (Co) for water/air at a liquid flow rate of 8.6 m^3/(h.m) with different sieve trays.

The effect of tray geometry on entrainment (L'/G) is evaluated using the construction number (Co) in Figure 68 for the spray regime, which is shown by Equation 3.5.1.20 (Kozoil and Mackowaik, 1990).

The construction number relates the fractional hole area (A_f), tray spacing (S), column diameter (D_c) and hole diameter (D_H) to one another. In the current entrainment investigation the tray spacing is kept constant at 515 mm and the column diameter for the current rectangular column is determined by making the area of the rectangular column equal to that of a round column.

$$Co = \left(\frac{A_f S}{(D_c D_H)^{\frac{1}{2}}}\right) \quad \rightarrow \quad \text{Construction number} \qquad [3.5.1.20]$$

The entrainment (L'/G) decreases with increasing construction number, showing that entrainment increases with decreasing fraction hole area, decreasing tray spacing and increasing sieve tray hole diameter (similar to the trends observed in literature) (Fig. 68). The trend of the construction number with entrainment (L'/G) shows that the construction number can be used to develop an entrainment model. The gas velocity increases from 1.7 to 2.9 m/s at increments of 0.3 m/s, where the trend line in Figure 68 represents a constant superficial gas velocity.

Entrainment (L'/L) is plotted against the flow Froude number for trays with a fractional hole area of 15% in Figure 69 for a water/air system. The magnitude of entrainment follows a similar trend with the flow Froude number for different hole diameter trays, where entrainment (L'/L) increases with increasing hole diameter. The entrainment for each tray hole diameter is plotted with a different polynomial (order of 2) trend line with a R^2 at above 0.98.

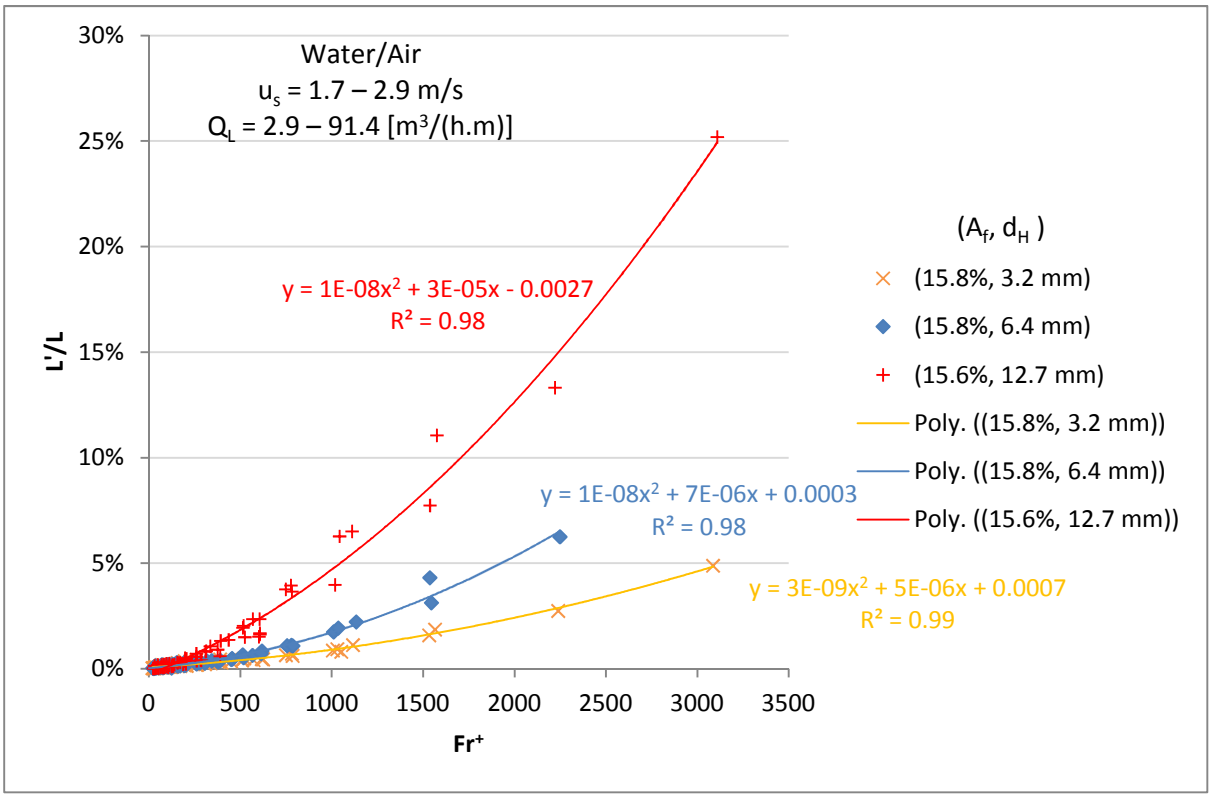

Figure 69 – Entrainment (L'/L) changing with the flow Froude number (Fr^+) for water/air at a fractional hole area of 15% and different hole diameters.

Figure 70 plots the entrainment (L'/L) against the flow Froude number for trays with a sieve tray hole diameter of 6.4 mm in a water/air system. The entrainment follows a similar trend with flow Froude number for different fractional hole area trays, where entrainment (L'/L) increases with decreasing

fractional hole area. The entrainment for each tray hole diameter is plotted with a different polynomial (of second order) trend line with a R^2 value above 0.95.

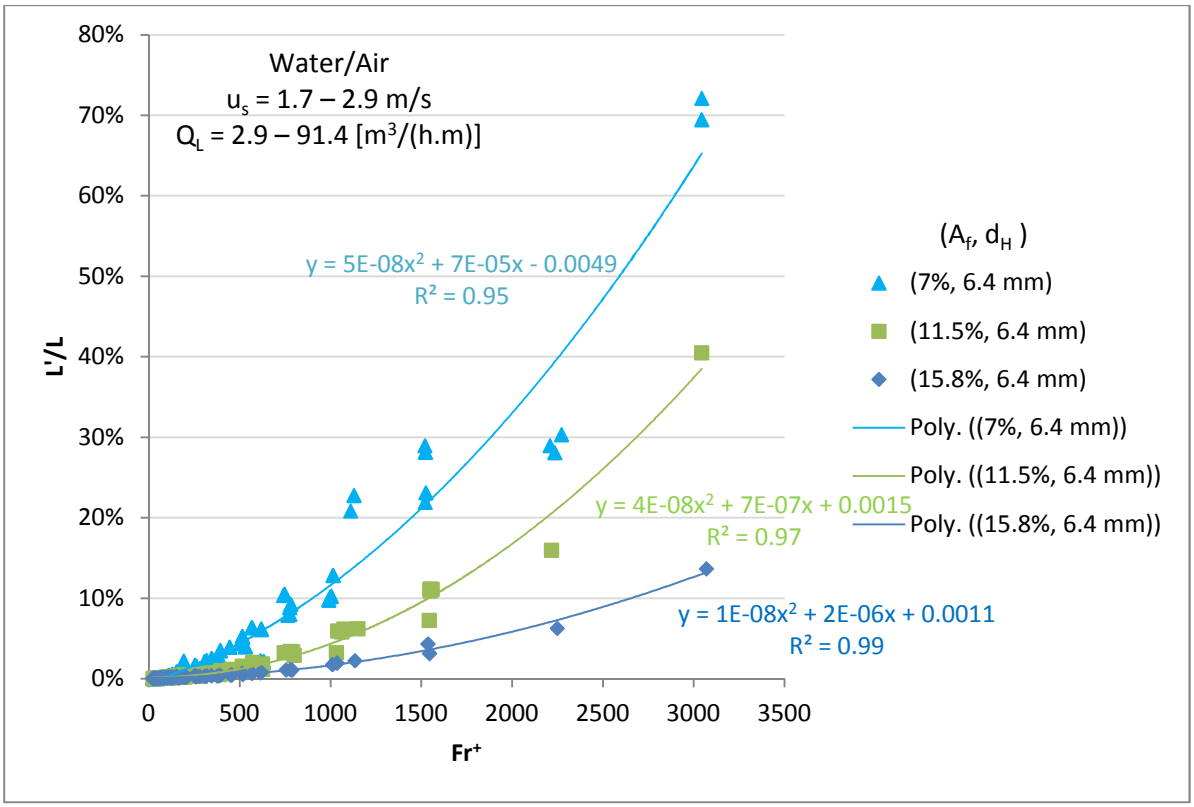

Figure 70 – Entrainment (L'/L) changing with the flow Froude number (Fr^+) for water/air at a hole diameter of 6.4 mm and different fractional hole areas.

The entrainment (L'/L) is plotted against the flow Froude number (Fr^+) and construction number (Co) ratio for trays with a sieve tray fractional hole area of 15% in Figure 71 for an ethylene-glycol/air system. The construction number in Figure 71 is plotted to the power of 1.5, which draws the hole diameter curves as in Figure 69 closer together for the ethylene-glycol/air system. In Figure 161, the construction number is plotted to the power of 1.65 for water/air and to the power of 1.2 for the silicone-oil/air system in Figure 163 in Appendix F. Therefore the construction number can be successfully used to describe the effect that the sieve tray hole diameter has on entrainment (L'/L). There is not a high degree of scatter in the data at high entrainment magnitudes, since a high tray fractional hole area sieve trays are used.

In Figure 72, the entrainment (L'/L) is plotted against the flow Froude number (Fr^+) and construction number (Co) ratio for trays with a sieve tray hole diameter of 6.4 mm for an ethylene-glycol system. The construction number in Figure 72 is plotted to the power of 1.3, which draws the fractional hole areas curves as shown in Figure 70 closer together. In Figure 162, the construction number is plotted to the power of 1.6 for water/air and to the power of 1.15 for a silicone-oil/air system in Figure 164 in Appendix F. As a result the construction number can be successfully used to describe the effect that the sieve tray fractional hole area has on entrainment (L'/L). There is a high degree of scatter at high magnitudes of entrainment, which is expected since entrainment flooding occurs at high superficial gas velocities.

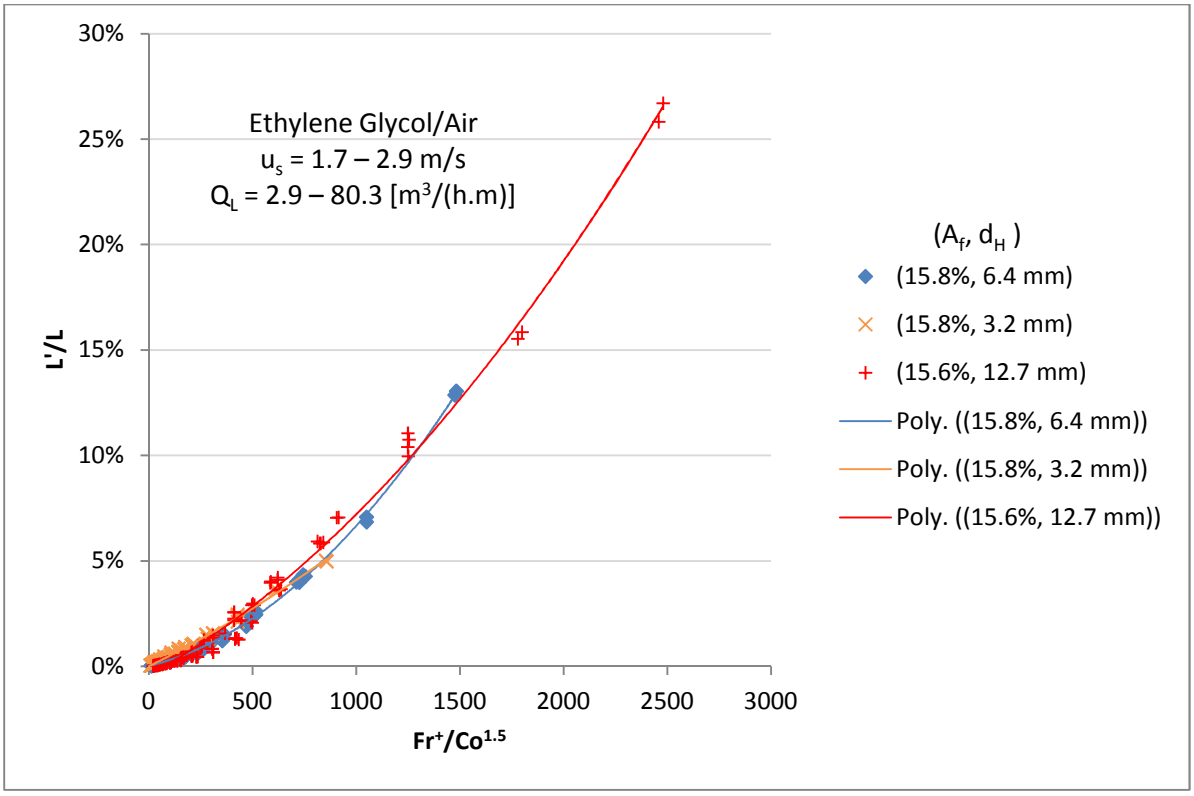

Figure 71 – Entrainment (L'/L) changing with the flow Froude number (Fr^+) to construction number (Co) ratio for ethylene-glycol/air at a fractional hole area of 15% and different hole diameters.

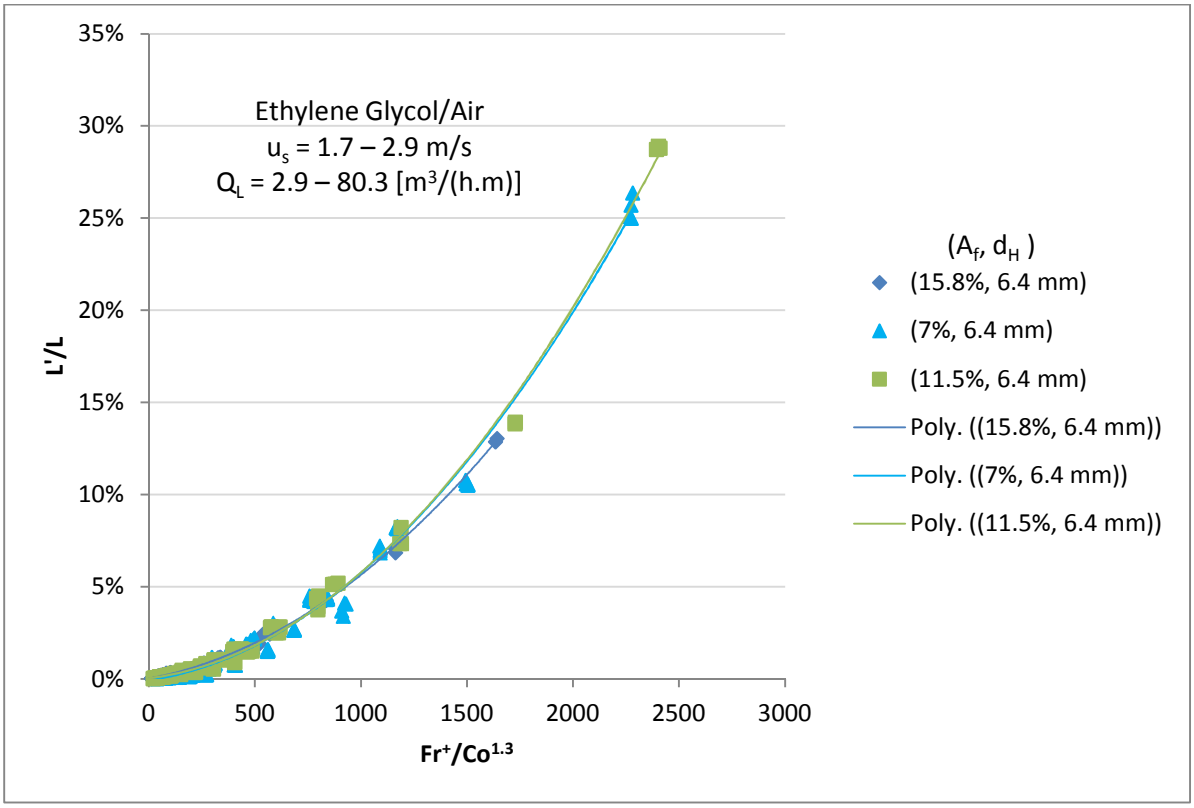

Figure 72 – Entrainment (L'/L) changing with the flow Froude number (Fr^+) to construction number (Co) ratio for ethylene-glycol/air at a hole diameter of 6.4 mm and different fractional hole areas.

The effect of gas physical properties is evaluated in Figure 73, where the entrainment rate (L'/L) is plotted against the flow Froude number (Fr^+) multiplied by the fluid density ratio. The fluid density ratio, developed by Colwell (1981), uses the gas density and divides it by the difference in density between the liquid and gas. The curves for the different gases fit closely to one another, when the flow Froude number is multiplied by the fluid density ratio to the power of 1.3 for a water system. The good agreement between the trends for the air and carbon dioxide (CO_2) systems show that the fluid density ratio can be used in the development of entrainment correlations.

Figures 165 and 166 in Appendix F shows the gas physical properties for silicone oil systems and ethylene glycol systems, respectively, where entrainment (L'/L) is plotted against the flow Froude number (Fr^+), multiplied by the fluid density. The curves for the different gases and liquid systems fit closely to one another, when the flow Froude number is multiplied by the fluid density ratio to the power of 0.8 for the silicone oil system and 1 for the ethylene glycol system. In the entrainment investigation by Uys (2012), the fluid density ratio is 1.15 for a water system and 0.95 for an ethylene glycol system which fits closely to the current entrainment experimental data.

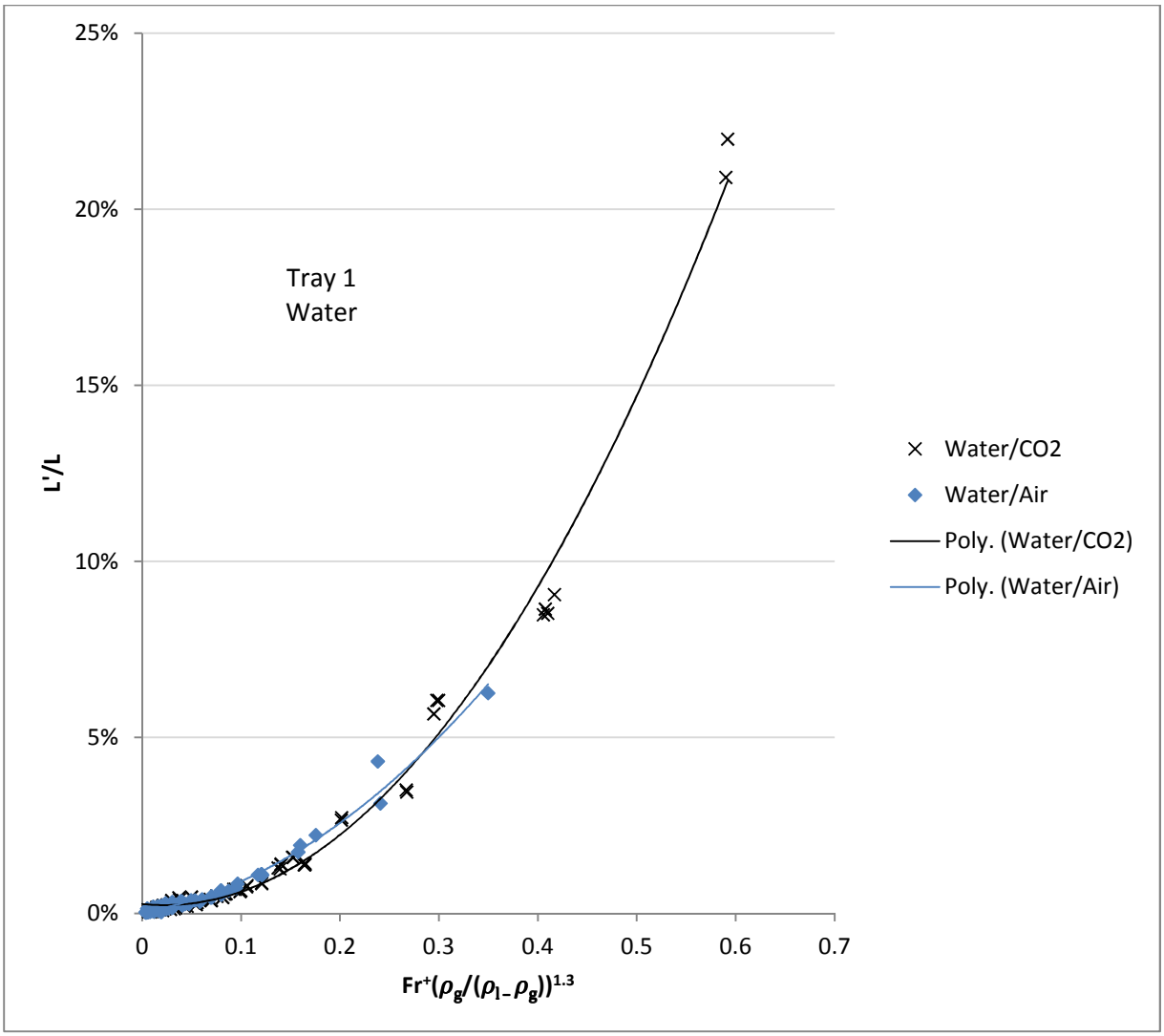

Figure 73 – Entrainment (L'/L) changing with the flow Froude number (Fr^+) to fluid density ratio for water with Tray 1 (15.8% fractional hole area, 6.4 mm hole diameter).

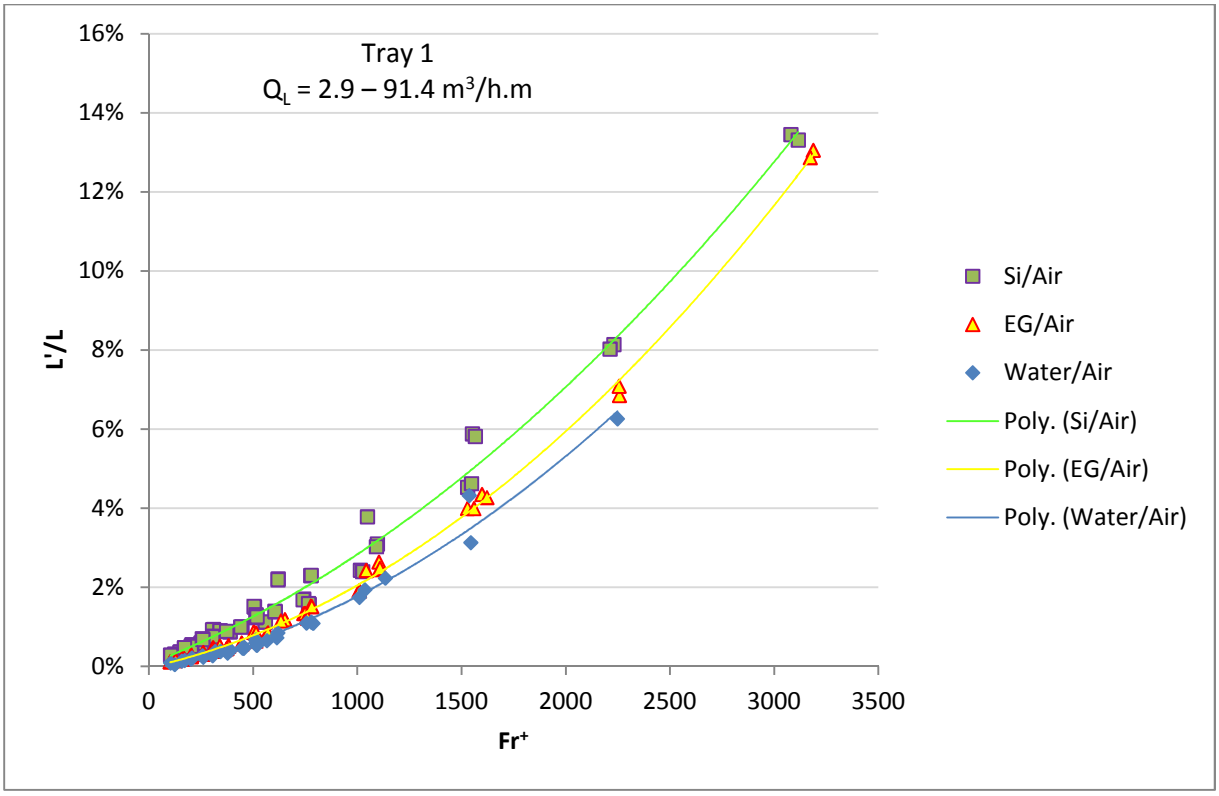

Figure 74 – Entrainment (L'/L) changing with the flow Froude number (Fr^+) for different liquids with air and Tray 1 (15.8% fractional hole area, 6.4 mm hole diameter).

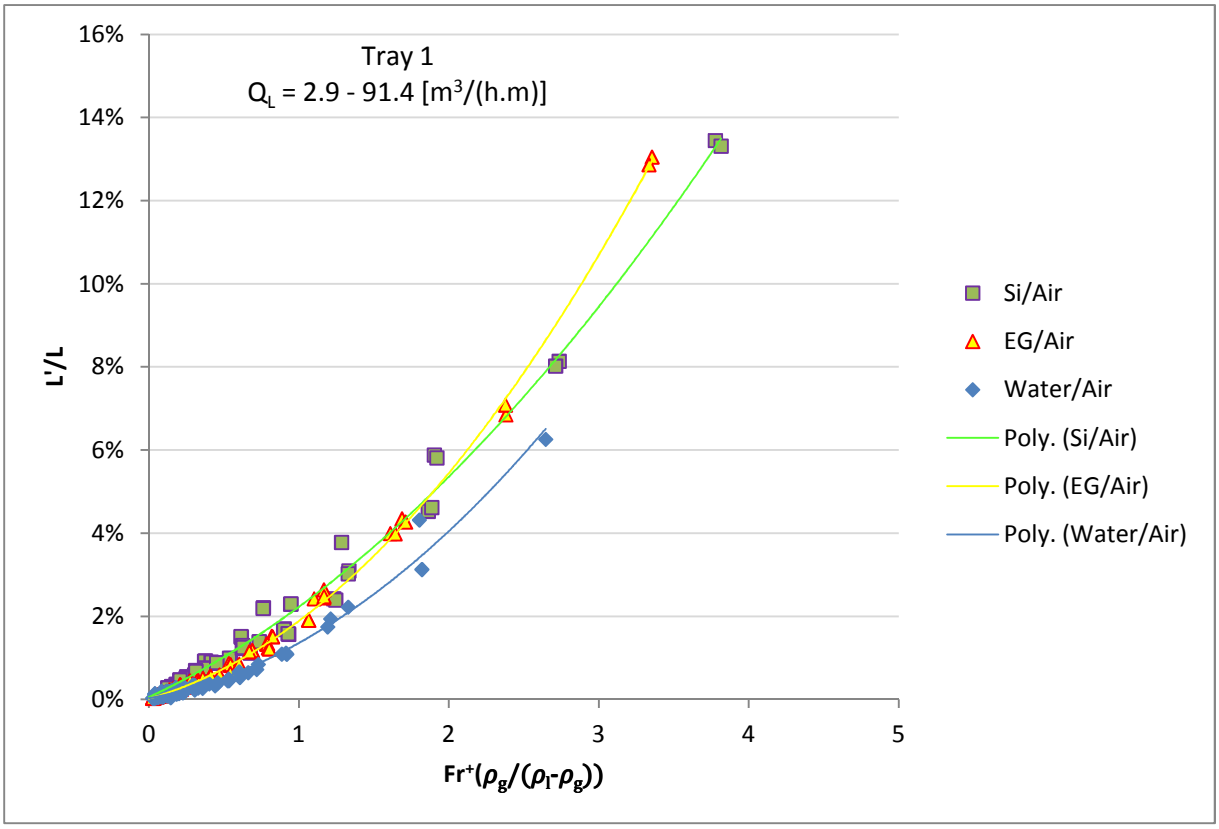

Figure 75 – Entrainment (L'/L) changing with the flow Froude number (Fr+) to fluid density ratio for different liquids with air and Tray 1 (15.8% fractional hole area, 6.4 mm hole diameter).

The effect of liquid physical properties is evaluated in Figure 74 for different liquids in air and Figure 167 in Appendix F for different liquids in carbon dioxide systems. The entrainment (L'/L) is plotted against the flow Froude number (Fr^+) for a liquid flow rate of 2.9 to 91.4 m^3/(h.m) and a superficial gas velocity of 1.7 to 2.9 m/s with Tray 1. The entrainment follows a similar trend with the flow Froude number for different liquids systems. The entrainment is plotted against the flow Froude number multiplied by the density ratio in Figure 75. The density ratio term shifts the silicone oil system closer to the water and ethylene glycol system, but does completely explain the effect of fluid properties. This shows that the entrainment is a strong function of the liquid surface tension and liquid viscosity.

5.4 Entrainment Results Summary

1) The effect of liquid and gas physical properties:
   i) A reduction in the surface tension, decrease in the liquid density and a decrease in the liquid viscosity leads to an increase in entrainment, where the dominating physical property mechanisms change with the gas and liquid flow rate.
   ii) Gases with a high density have a higher mass flow rate through the sieve tray at a constant superficial gas velocity, consequently leading to an increase in the interaction between the liquid and gas, thereby increasing entrainment.
2) The effect of tray fractional hole area and hole diameter:
   i) In the spray regime, entrainment increases with decreasing tray fractional hole area and increasing hole diameter.
   ii) At intermediate liquid flow rates [approximately 23 m^3/(h.m) to 60 m^3/(h.m)], tray fractional hole area and hole diameter have a minimal effect on entrainment (little to no change in entrainment magnitude), due to the dominance of the liquid cross flow.
   iii) At low to intermediate liquid flow rates, the liquid flow rate range of constant entrainment magnitude decreases as the hole diameter increases.
   iv) At high liquid flow rates, entrainment increases with decreasing fractional hole area and decreasing hole diameter.
   v) As the liquid density decreases and liquid viscosity increases, the influence that hole diameter and fractional hole area have on entrainment increases.
3) Literature model comparison:
   i) Literature models explain experimental data trends well, however deviate from the experimental results due to the mostly untested parameter range used in the current investigation
4) Dimensionless number analysis:
   i) By grouping dimensionless numbers like the liquid hold-up Froude number, Weber number, Reynolds number, flow Froude number, construction number and the fluid density ratio, a comprehensive entrainment model can be developed.
   ii) Based on the entrainment trends with the dimensionless numbers in the spray regime, entrainment increases with increasing hole diameter, gas density, gas viscosity, superficial gas velocity and decreasing liquid hold-up, liquid flow rate, liquid density, liquid viscosity and liquid surface tension.

Chapter 6 - Weeping Results and Discussion

This chapter highlights the results achieved during the sieve tray distillation hydrodynamic test for the weeping investigation and discusses the trends observed based on the knowledge gained by the literature investigation. The effects of the different parameters investigated and their impact on the amount of weeping are shown. The dimensionless numbers that help describe weeping trends are highlighted. The experimental investigation produced over 7 000 data points for weeping. The data points for tray 1 using silicone oil are shown as example in Appendix G, where the rest of the data points if required should be requested with permission from the University of Stellenbosch.

6.1 Effect of Fluid Physical Properties and Fluid Flow

This section highlights the effects of the liquid density, liquid surface tension, liquid viscosity, gas density and gas viscosity, where the effects of these parameters on weeping are explained as far as they can be separated from one another. The experimental limits of the different fluid systems are represented in Table 13. Systems with carbon dioxide (CO_2) are only measured up to a superficial gas velocity of 2.6 m/s as the de-entrainment section flooded at higher superficial gas velocities. The flooding process for butanol systems occurred at an even lower superficial gas velocity. The table shows both the capacity factor (C_s) and flow factor (F_s) limits of the different systems, where the effect of the fluid properties are shown with respect to these factors.

6.1.1 Effect of Liquid Properties and Flow on Weeping

The liquid densities change from a minimum of 835 kg/m^3 for butanol to as high as 1 100 kg/m^3 for ethylene glycol. The surface tension varies from as low as 20.9 mN/m for silicone oil to as high as 57.8 mN/m for water. The surface tensions for silicone oil (20.9 mN/m) and butanol (22.1 mN/m) are similar making it easier to separate the effects of the liquid surface tension from the liquid density and the liquid viscosity. The liquid viscosities of the different liquids changes from 0.9 mPa.s for water to as high as 51 mPa.s for silicone oil, where in industry liquid viscosities can exceed 50 000 mPa.s for polymer mixture distillation processes.

Weeping is represented as W'/L to signify the amount of weeping as a distillation column separation efficiency response, where high W'/L weeping values signify a low potential for fluid separation inside a distillation column as in Figure 76. Weeping is represented as W'/G to signify the magnitude of weeping magnitude as a distillation column capacity response, where high W'/G weeping values signify that a larger distillation column or equipment should be used. In the current weeping experimental investigation the gas superficial velocities and liquid flow rates at which the weeping magnitude is zero are not shown.

In literature it is noted that the spray regime is associated with low liquid flow rates and the froth regime with high liquid flow rates. A clear distinction between low liquid flow rates [typically below 23 m^3/(h.m)] and high liquid flow rates [typically above 23 m^3/(h.m)] dispersions are seen in the weeping investigation. At low liquid flow rates, the dispersion sloshes in different directions (highly unstable dispersion), but the jet associated with the spray regime cannot be clearly seen. At high liquid flow rates the dispersion appears to be more uniform and stable across the tray. In the

following weeping investigation the spray regime will be defined as a liquid flow rate typically below 23 $m^3/(h.m)$ [V_L = 4 m^3/h] and the froth regime as a liquid flow rate typically above 23 $m^3/(h.m)$.

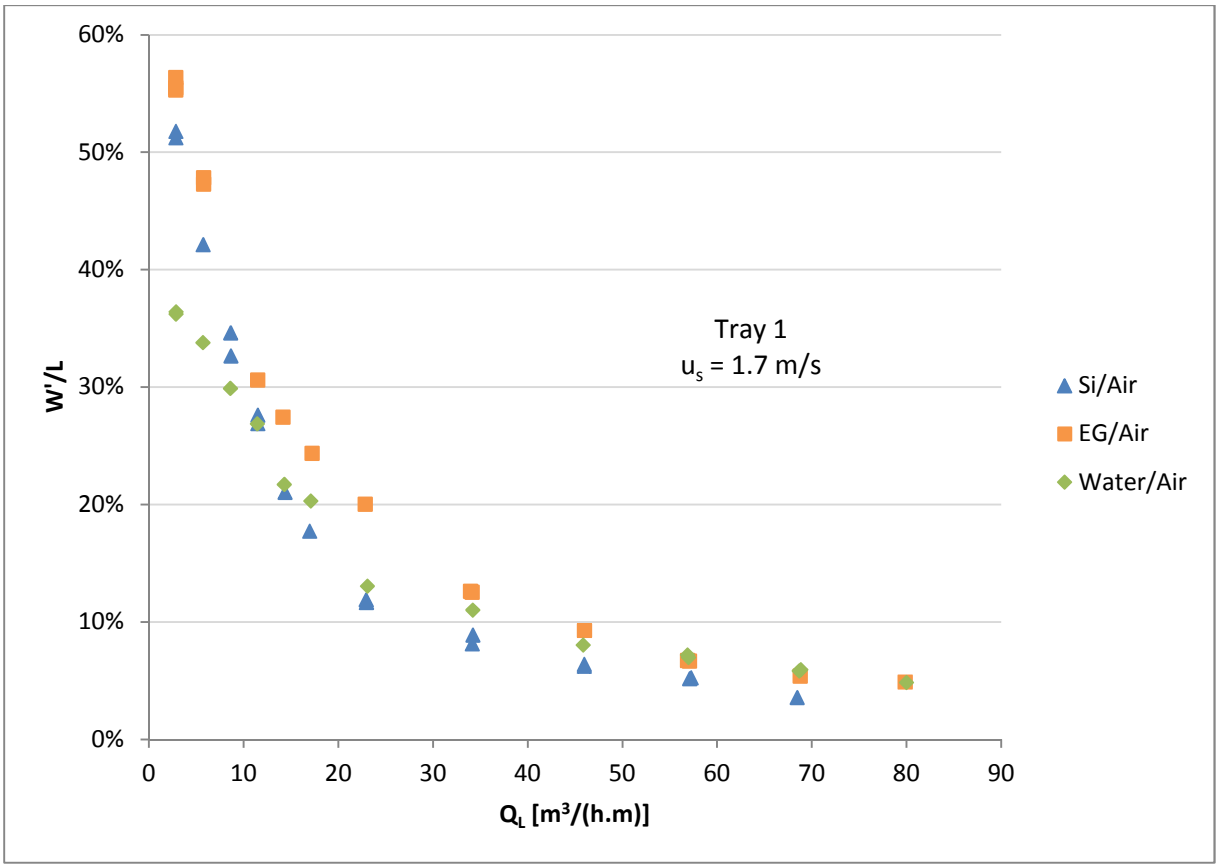

Figure 76 – Weeping (W'/L) of different liquids with air for Tray 1 (15.8% fractional hole area, 6.4 mm hole diameter) at a superficial gas velocity of 1.7 m/s.

Figure 76 shows the weeping (W'/L) for different liquids in air at a superficial gas velocity of 1.7 m/s. The current section identifies the effects of fluid physical properties, with only Tray 1 and Section 6.2 identifies the contributing effects of tray geometry and fluid physical properties. The weeping (W'/L) decreases with increasing liquid flow rate (Fig. 76). The effect of the liquid flow rate on weeping is more significant at low liquid rates [spray regime typically below 23 $m^3/(h.m)$] than at high liquid flow rates [froth regime typically above 23 $m^3/(h.m)$]. A clear distinction can be seen between the weeping (W'/L) in the spray regime and in the froth regime, where it is believed that weeping through the sieve tray holes is caused by two different mechanisms.

The percentage difference between the weeping (W'/L) for the different liquids is large at moderate liquid flow rates (point at which the weeping (W'/L) slope changes in Figure 76). There is a large difference in the weeping (W'/L) between the different liquids investigated in air, which shows that liquid physical properties have a large effect on the magnitude of weeping. The ethylene glycol exhibits higher weeping than water (intermediate weeping magnitude) and silicone oil (lowest weeping magnitude), since the spray layer for silicone oil is larger than the other liquids observed in air. Weeping depends highly on clear liquid dispersion (froth layer), where a larger clear liquid dispersion is produced at intermediate liquid flow rates. The butanol system is not tested with air because of it being highly flammable.

The froth dispersion layer for water systems was projected to a greater height than that of ethylene glycol (EG), where the droplets in the spray layer were projected to a lesser height and the droplets projected in this layer were larger than those in the ethylene glycol systems. The silicone oil (Si) fluid system was seen to produce a higher froth layer than the water system, where the liquid droplets in the spray regime were smaller and seen to be projected to even greater heights than that of ethylene glycol and water during the experimental testing. Ethylene glycol produced the lowest liquid dispersion above the tray (liquid layer closer to sieve tray holes), where water was shown to have the second lowest liquid dispersion. The butanol system has the highest froth layer in dispersion layer, which means that a higher liquid percentage is further away from the sieve tray holes.

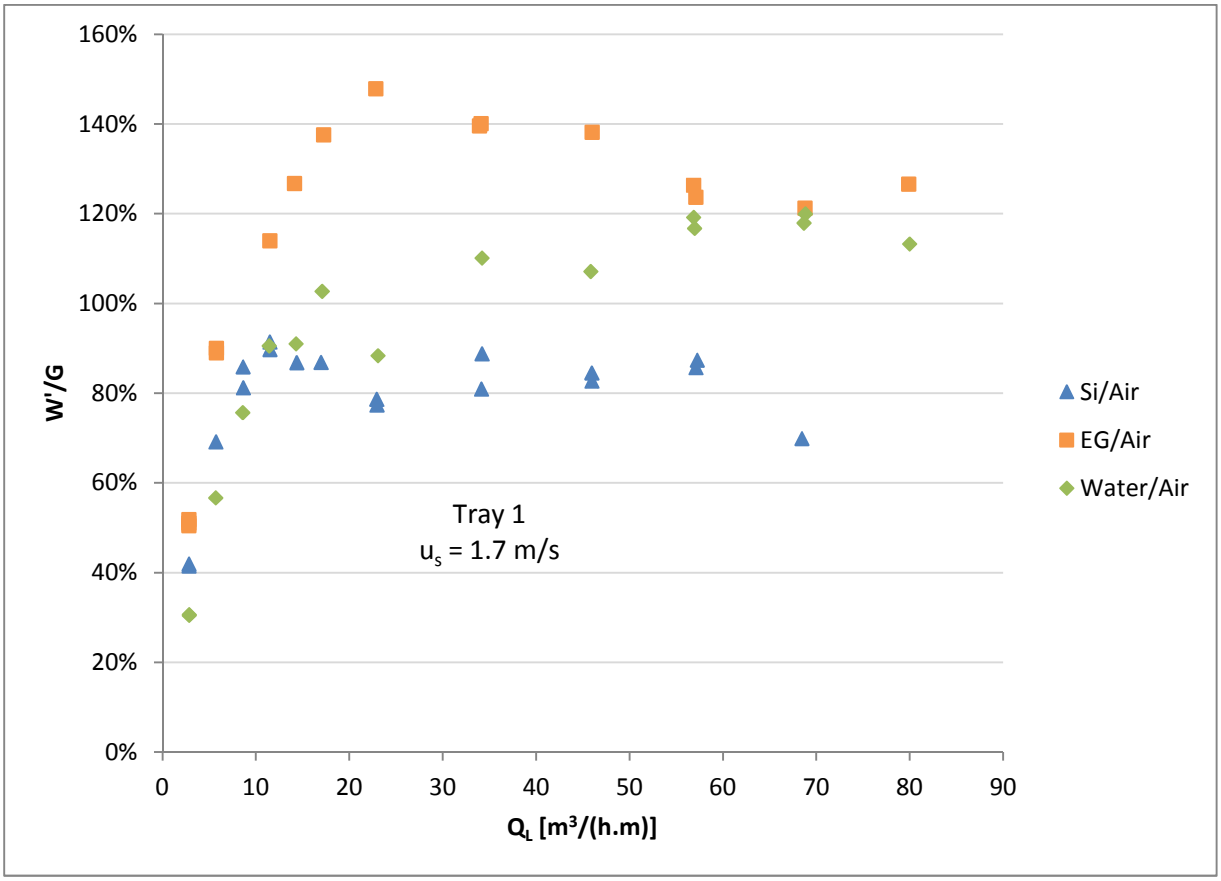

Figure 77 – Weeping (W'/G) of different liquids with air for Tray 1 (15.8% fractional hole area, 6.4 mm hole diameter) at a superficial gas velocity of 1.7 m/s.

Figure 77 shows the weeping (W'/G) for different liquids in air at a superficial gas velocity of 1.7 m/s for Tray 1. The weeping (W'/G) is represented as a distillation column capacity parameter. There is no distinctive trend between weeping and fluid dispersion layers of the different liquids, since the interaction of the gas and liquid in the dispersion layer is more complex and highly dependent on the different liquid physical properties. There is a clear difference in the weeping (W'/G) trend in the spray regime and froth regime. In the spray regime, weeping (W'/G) increases with increasing liquid flow rate to a maximum for all the liquid systems investigated in air. In the froth regime, weeping (W'/G) decreases with increasing liquid flow rate for the ethylene glycol/air and silicone oil/air system. The weeping (W'/G) of the water systems initially increases with increasing liquid flow rate

at moderate liquid flow rates in the froth regime, and then decreases at higher liquid flow rates [typically above 60 $m^3/(h.m)$].

The W'/G weeping and the W'/L weeping are shown in Figures 168 and 169 in Appendix F, respectively, for a superficial gas velocity of 2.3 m/s using different liquids in air. Weeping decreases with increasing superficial gas velocity which supports the trends observed in literature. The percentage difference between the magnitudes of weeping of the different liquids in air is shown to decrease with increasing superficial gas velocity.

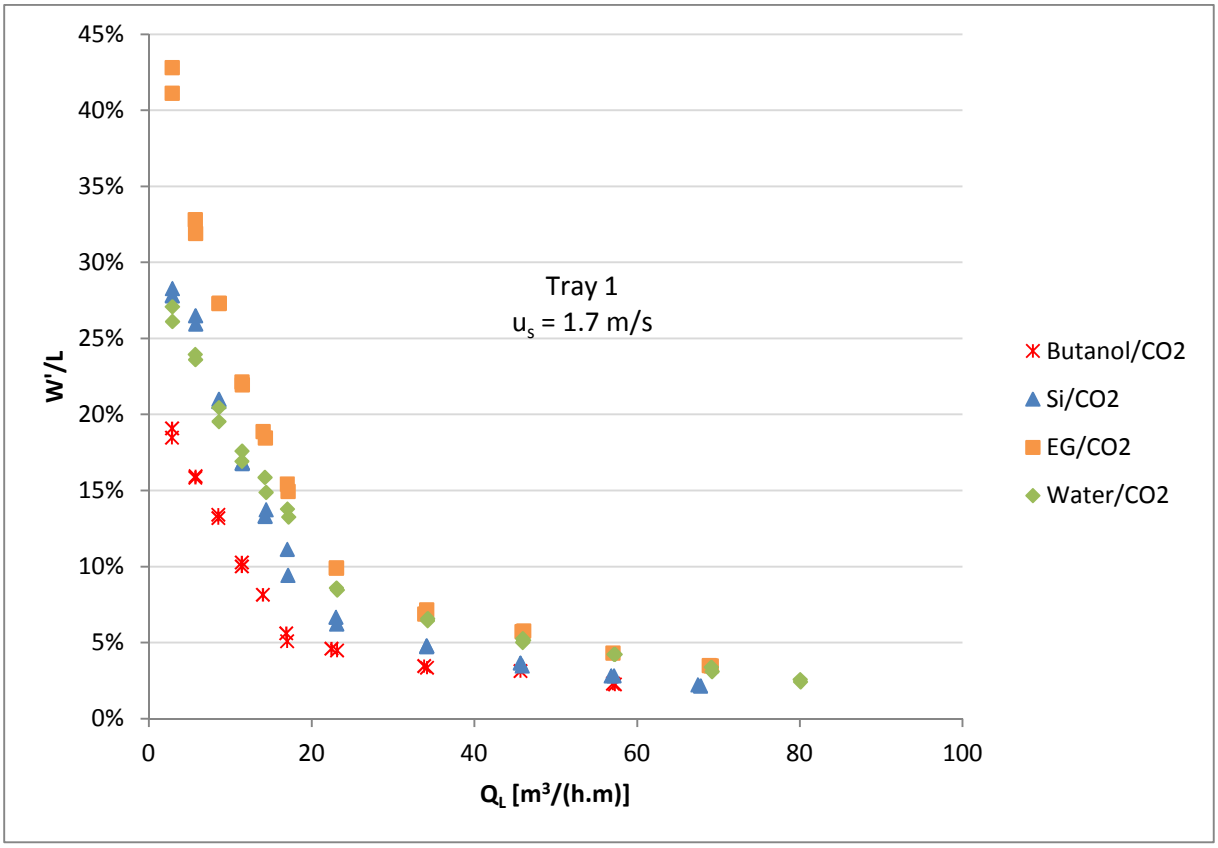

Figure 78 – Weeping (W'/L) of different liquids with CO_2 for Tray 1 (15.8% fractional hole area, 6.4 mm hole diameter) at a superficial gas velocity of 1.7 m/s.

Weeping for the different liquids investigated in carbon dioxide (CO_2) are shown in Figure 78 for W'/L and in Figure 79 for W'/G for a superficial gas velocity of 1.7 m/s. Butanol produces a much lower amount of weeping than that of silicone oil, where the weeping trend supports the visual observation that butanol produces the largest froth layer (clear liquid dispersion layer) leading to a lower magnitude of weeping. The liquid density is a highly important liquid physical property (especially in the froth regime), since weeping decreases with decreasing liquid density. In the spray regime at low liquid flow rates, the water and silicone oil systems have a similar weeping magnitude, thus it shows that weeping depends on a complex interaction between the liquid density, liquid surface tension and the liquid viscosity. The high viscosity of silicone oil in comparison to the other liquids leads to a higher amount of weeping in the spray regime

Mahiout and Vogelpohl (1984) showed that increasing the liquid viscosity leads to a decrease in the number of droplets formed, supporting the distinction in the weeping magnitudes between the

liquid systems. Decent *et al.* (2009) showed that viscosity plays a considerable role in the spray regime, which is supported by the weeping trends in Figures 78 and 79 (Higher viscosity = Higher weeping magnitude). Decent *et al.* (2009) shows that an increase in the liquid viscosity leads to an increase in dispersion layer's stability, producing a higher weeping magnitude in the spray regime (at low liquid rates). The liquid viscosity has a high significance in the spray regime, whereas the effect of viscosity in the froth regime cannot be distinguished from the effect of the other liquid physical properties, although its impact on weeping is still significant.

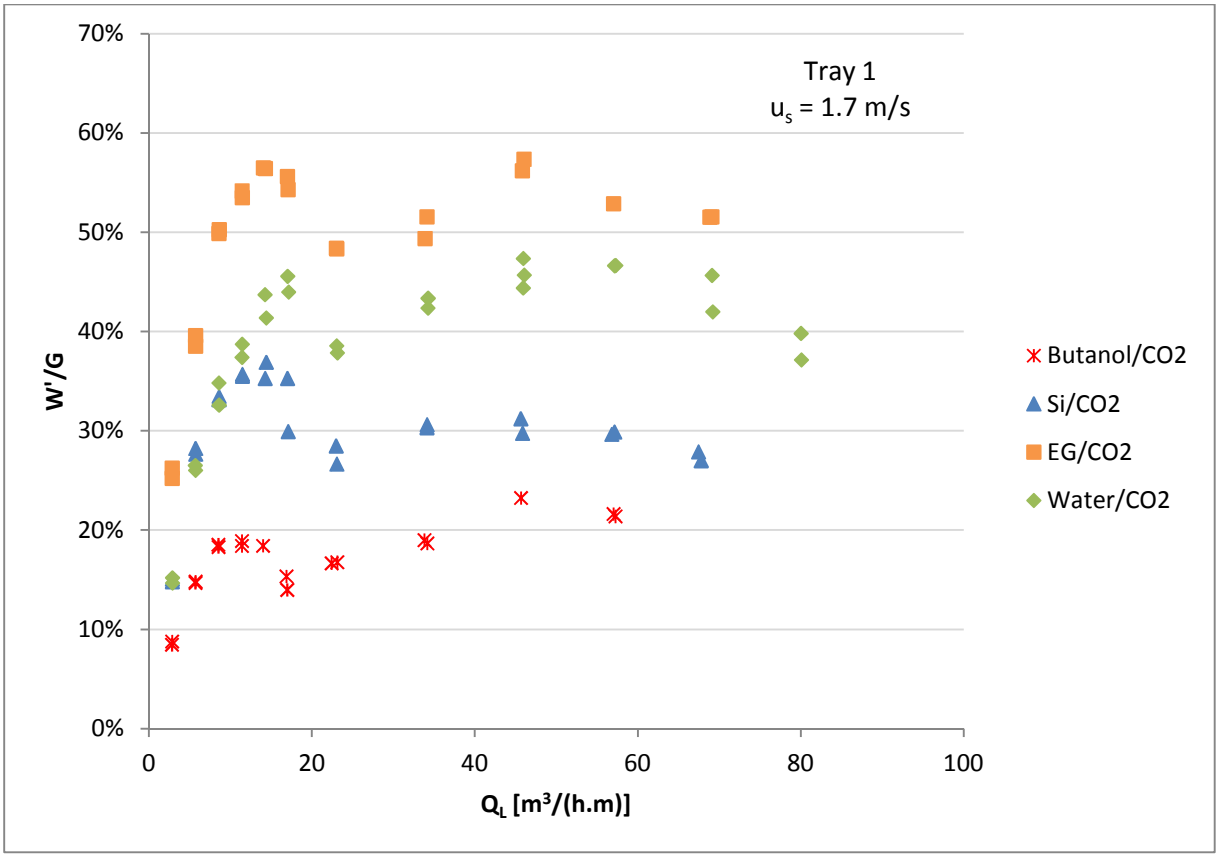

Figure 79 – Weeping (W'/G) of different liquids with CO_2 for Tray 1 (15.8% fractional hole area, 6.4 mm hole diameter) at a superficial gas velocity of 1.7 m/s.

The surface tension has a significant impact on weeping, not just in the spray regime as shown by Kister (1992) but also in the froth regime (Fig. 78 to 79). At high liquid flow rates, an increase in the liquid surface tension increases the stability of the gas bubbles formed in the froth regime increasing weeping, since the gas flowing through the liquid dispersion slows down when moving through a high surface tension liquid. All the fluid properties effects on the weeping magnitude cannot be truly separated from one another based on the scope of the liquid systems investigated. It is firmly believed that a complex interaction exists between the different liquid physical properties in each regime and that the dominating mechanisms changes with gas and liquid flow rates. It is believed that an increase in the liquid surface tension leads to an increase in the froth layer size in the dispersion, which in turn increases the magnitude of weeping.

The W'/L weeping and the W'/G weeping is shown in Figure 80 and 170 in Appendix F, respectively, for a superficial gas velocity of 2.3 m/s for different liquids in carbon dioxide. Weeping decreases

with increasing superficial gas velocity which supports the trends observed in literature. The percentage difference between the magnitudes of weeping of the different liquids in air is shown to decrease with increasing superficial gas velocity.

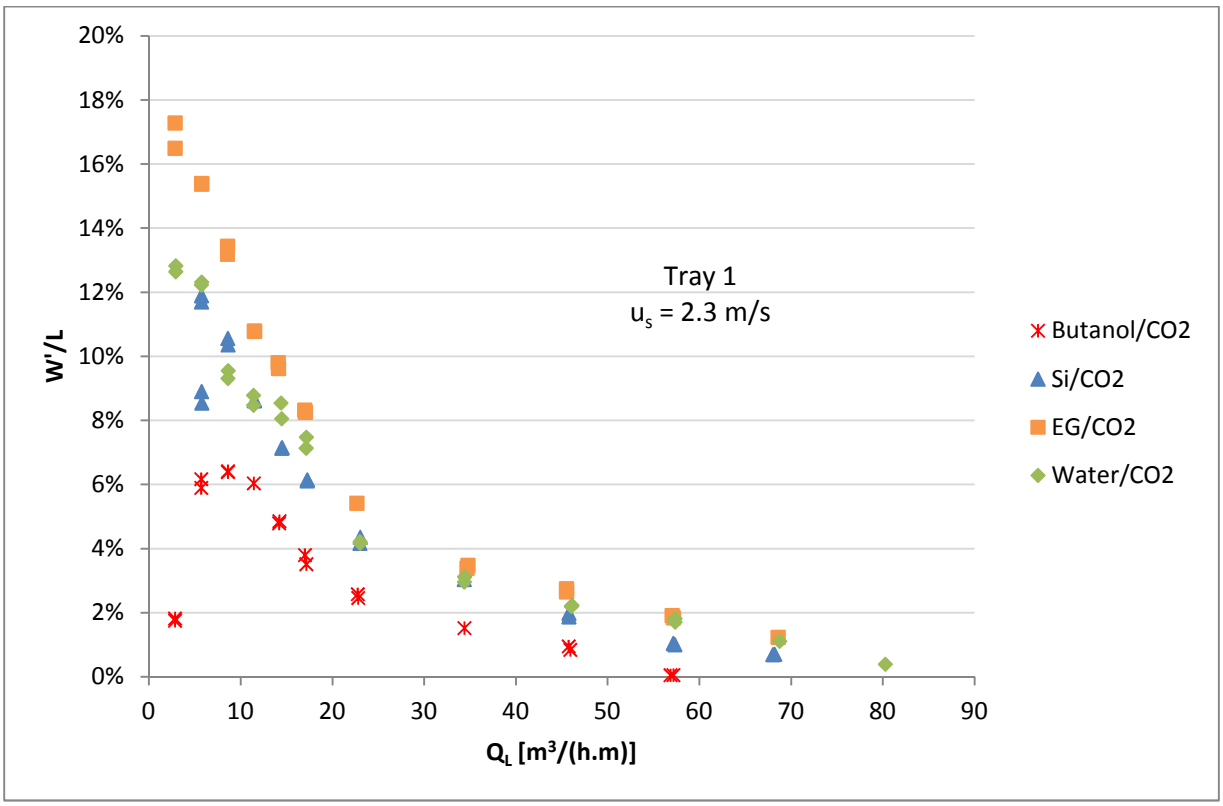

Figure 80 – Weeping (W'/L) of different liquids with CO_2 for Tray 1 (15.8% fractional hole area, 6.4 mm hole diameter) at a superficial gas velocity of 2.3 m/s.

6.1.2 Effect of Gas Properties and Flow on Weeping

This section shows the impact of the gas physical properties and the superficial gas velocity on weeping for Tray 1. The experimental investigation only investigates the impact of air and carbon dioxide (CO_2) on weeping. The gas density and gas viscosity for air are 1.18 kg/m^3 and 18.6x10^{-3} mPa.s, respectively, and the gas density and gas viscosity for carbon dioxide are 1.8 kg/m^3 and 14.9 x10^{-3} mPa.s, respectively.

The weeping (W'/L) for air and carbon dioxide in water is shown in Figure 81 and weeping (W'/G) is shown in Figure 82. The W'/L weeping trends are similar for air and for carbon dioxide, where air is observed to have a higher W'/L weeping than CO_2 over the entire range of liquid flow rates at a superficial gas velocity of 1.7 m/s in water (Fig. 81). The difference in weeping is supported by the fact that at constant gas superficial velocities, gases with a high density have a higher mass flow rate of gas through the sieve tray. The higher flow rate leads to an increase in the interaction between the liquid and the gas (more gas flows through the sieve tray hole) and decreases weeping. The increased interaction between the gas and liquid leads to a large dispersion layer moving the liquid away from the tray floor.

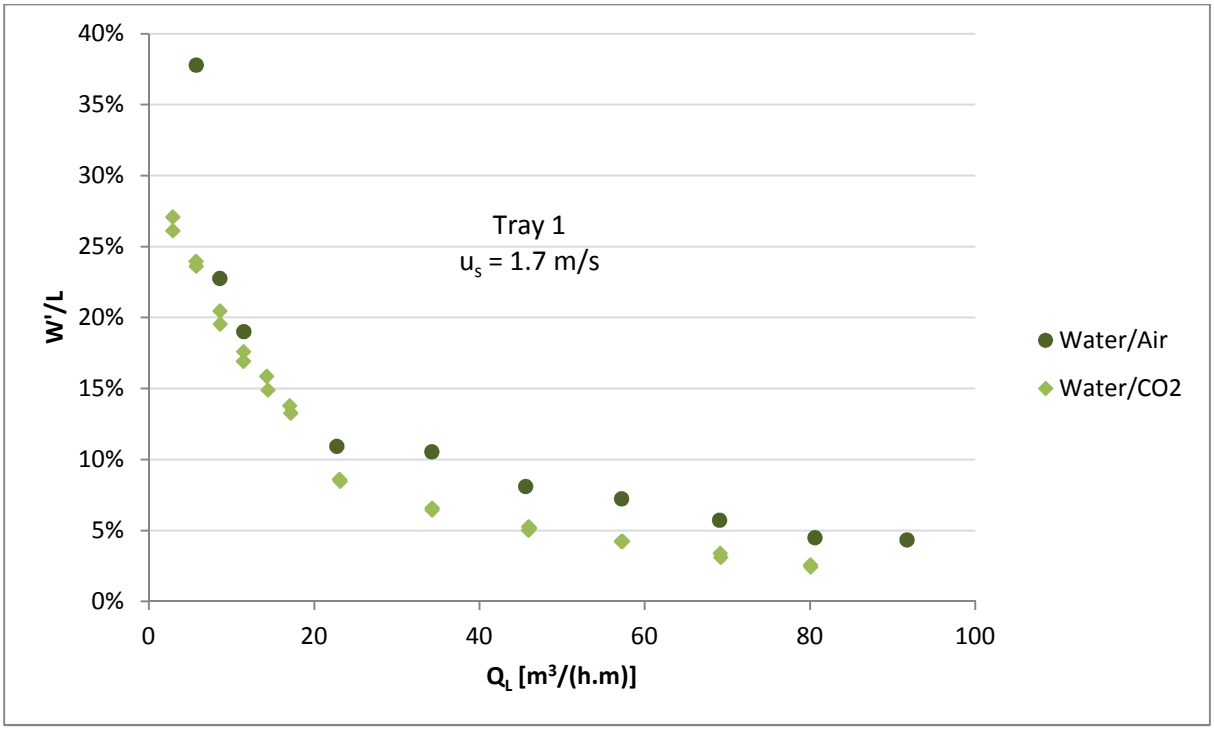

Figure 81 – Weeping of water (W'/L) with different gases for Tray 1 (15.8% fractional hole area, 6.4 mm hole diameter) at a superficial gas velocity of 1.7 m/s.

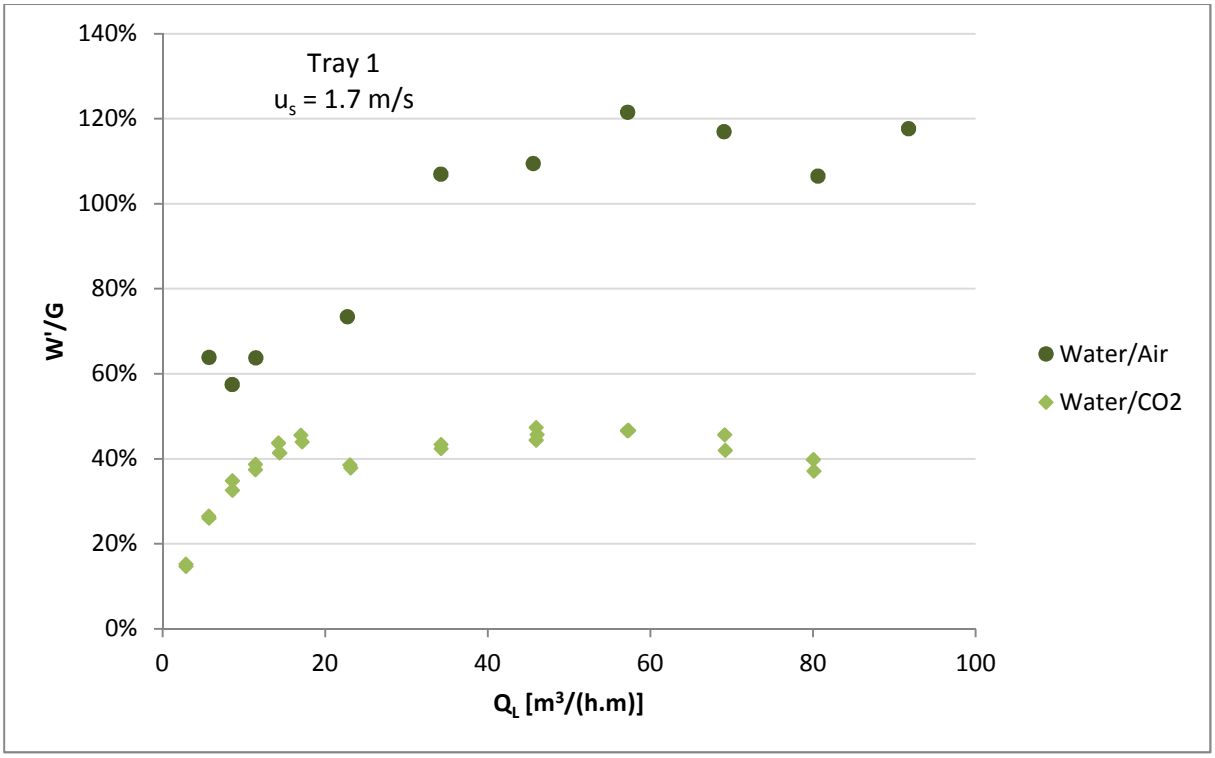

Figure 82 – Weeping of water (W'/G) with different gases for Tray 1 (15.8% fractional hole area, 6.4 mm hole diameter) at a superficial gas velocity of 1.7 m/s.

The weeping (W'/G) trends for air and carbon dioxide are not similar at a superficial gas velocity of 1.7 m/s (Fig. 82). At a superficial gas velocity of 1.7 m/s the capacity factor and flow factor for a

water/air system are 0.058 m/s and 1.85 [(m/s).(kg/m^3)$^{0.5}$], respectively, and the capacity factor and flow factor for a water/CO_2 system are 0.072 m/s and 2.28 [(m/s).(kg/m^3)$^{0.5}$], respectively. The air system has a lower gas capacity factor and flow factor than that of carbon dioxide at the same superficial gas velocity, where the difference in weeping (W'/G) is highly significant. In the distillation column for air and carbon dioxide to have the same capacity and flow factors, the air (lower gas density) system has to be operated at a greater superficial gas velocity than carbon dioxide (higher gas density) to decrease weeping.

Figure 83 shows the weeping (W'/L) and Figure 171 in Appendix F shows the weeping (W'/G) for air and carbon dioxide with water at a superficial gas velocity of 2.6 m/s. At a superficial gas velocity of 2.6 m/s, the capacity factor and flow factor for a water/air system are 0.089 m/s and 2.82 [(m/s).(kg/m^3)$^{0.5}$], respectively, and the capacity factor and flow factor for a water/CO_2 system are 0.098 m/s and 3.09 [(m/s).(kg/m^3)$^{0.5}$], respectively. The difference in the magnitude of weeping between air and carbon dioxide systems increases with increasing superficial gas velocity (Fig. 83 and 171). The differences in the amount of weeping at higher gas superficial velocities are larger in the spray regime than in the froth regime for the water systems, which could be attributed to an increased dependence on the liquid viscosity at high superficial gas velocities.

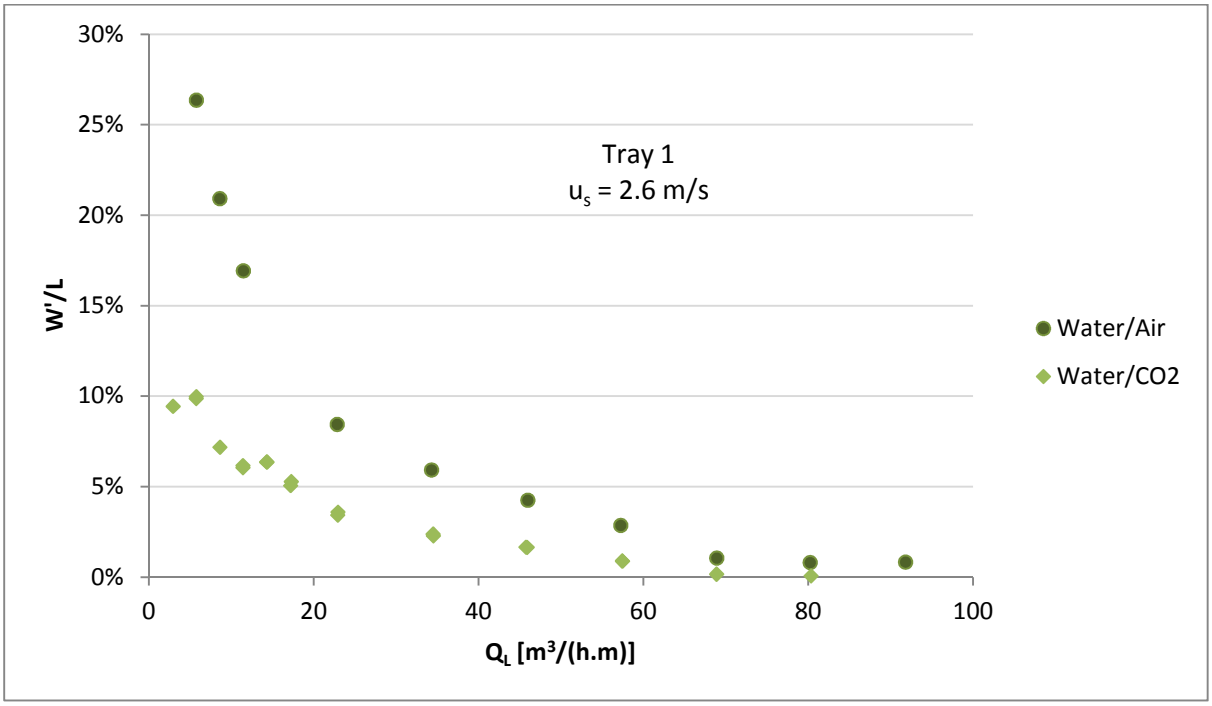

Figure 83 – Weeping of water (W'/L) with different gases for Tray 1 (15.8% fractional hole area, 6.4 mm hole diameter) at a superficial gas velocity of 2.6 m/s.

The weeping for silicone oil/air (Si/air) and silicone oil/carbon dioxide (Si/CO_2) are shown in Figure 84 for W'/L weeping and in Figure 85 for W'/G weeping at a superficial gas velocity of 1.7 m/s. At a superficial gas velocity of 1.7 m/s, the capacity factor and flow factor for a water/air system are 0.06 m/s and 1.85 [(m/s).(kg/m^3)$^{0.5}$], respectively, and the capacity factor and flow factor for a water/CO_2 system are 0.074 m/s and 2.28 [(m/s).(kg/m^3)$^{0.5}$], respectively. The interaction of silicone oil and the gases are different from that of the water systems. The differences between the CO_2 and air systems weeping (W'/L) increases when silicone oil is used as a liquid instead of water over the entire range

of liquid flow rates (Fig. 84). The weeping (W'/G) for the silicone oil/air is greater than that of silicone oil/CO_2, where the weeping differences are lower at very low liquid flow rates (Fig. 85).

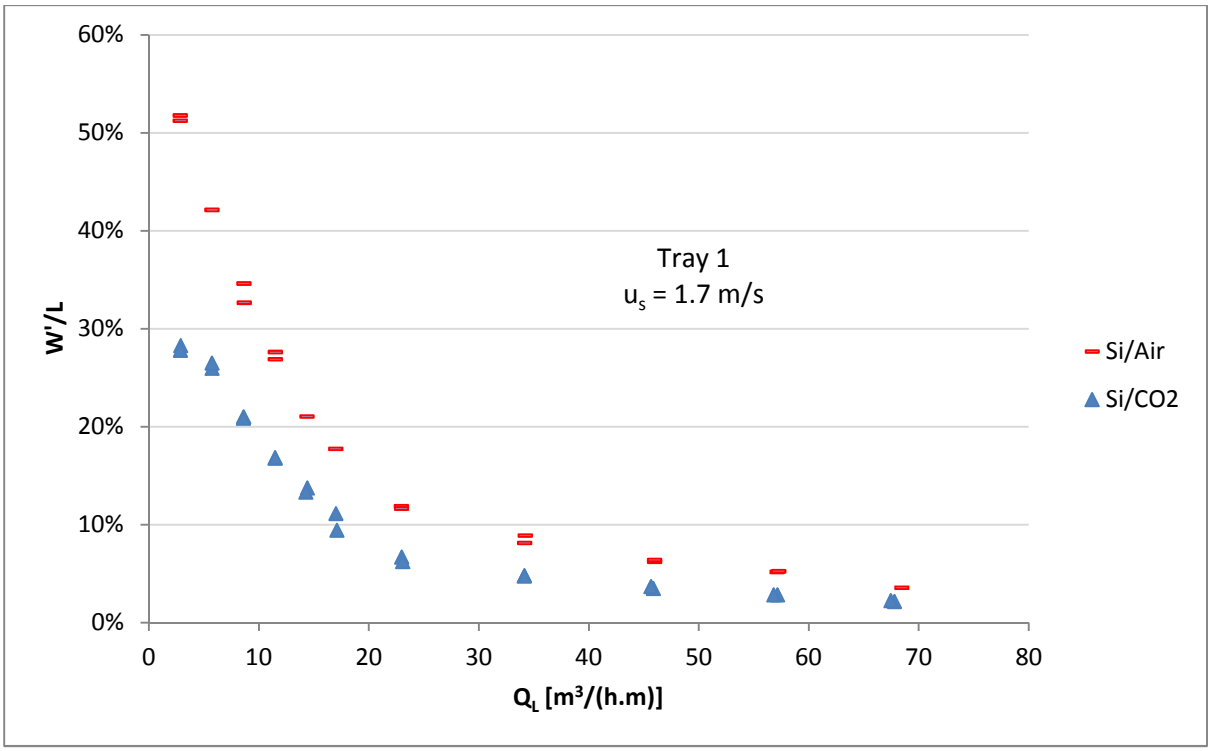

Figure 84 – Weeping of silicone oil (W'/L) with different gases for Tray 1 (15.8% fractional hole area, 6.4 mm hole diameter) at a superficial gas velocity of 1.7 m/s.

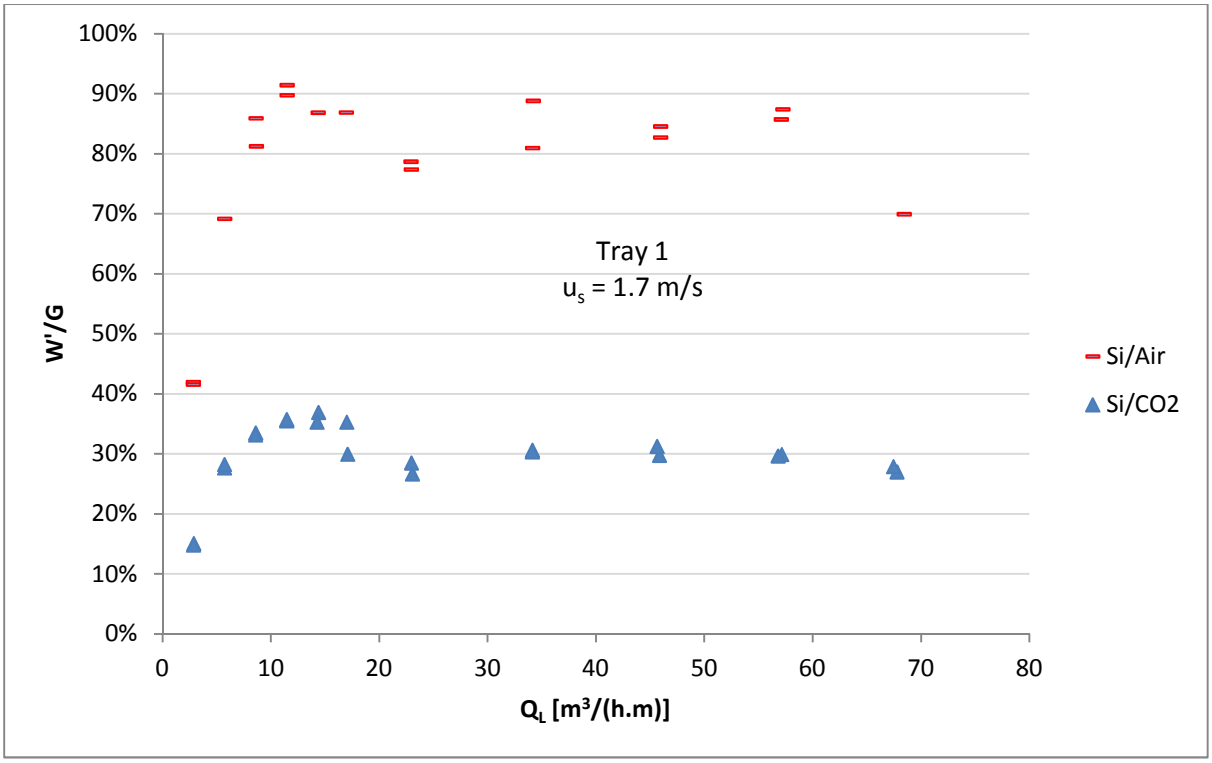

Figure 85 – Weeping of silicone oil (W'/G) with different gases for Tray 1 (15.8% fractional hole area, 6.4 mm hole diameter) at a superficial gas velocity of 1.7 m/s.

The weeping for (Si/air) and (Si/CO_2) systems are shown in Figure 172 for W'/L weeping and in Figure 173 in Appendix F for W'/G weeping at a superficial gas velocity of 2.6 m/s. The weeping (W'/L) for silicone oil systems follow a similar trend as the water system in Figure 83, where the Si/CO_2 system has a lower weeping rate than the Si/air system at higher gas superficial velocities. The weeping (W'/G) for Si/air has a higher magnitude than Si/CO_2 at a superficial gas velocity of 2.6 m/s, showing that the interaction between the gas and liquid flow properties are of a complex nature. This shows that weeping is a strong function of the gas density. The difference between the weeping (W'/G) for silicone oil systems is greater in the froth regime than in the spray regime (Fig. 173).

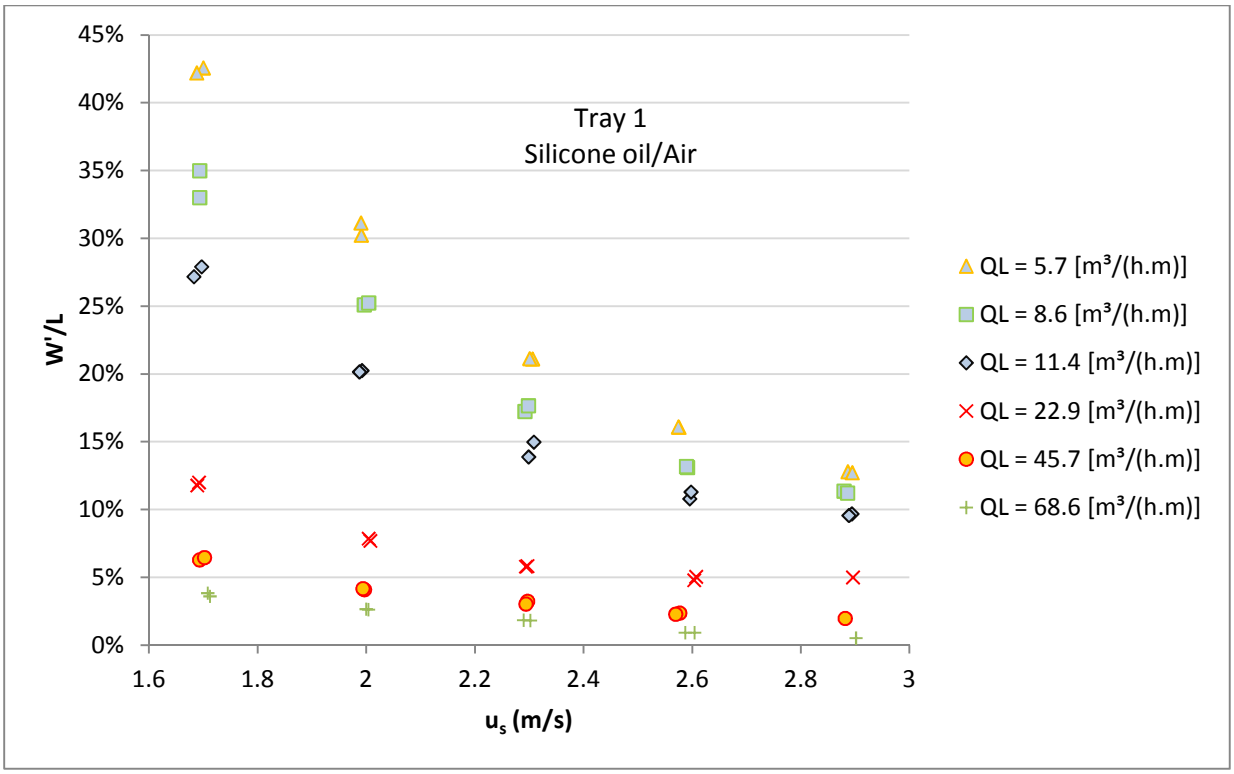

Figure 86 – Effect of superficial gas velocities on weeping (W'/L) at different liquid flow rates for Tray 1 (15.8% fractional hole area, 6.4 mm hole diameter) and silicone-oil/air.

The weeping (W'/L) for silicone oil/air at changing superficial gas velocities for different liquid flow rates is shown in Figure 86 for Tray 1. The weeping (W'/L) always decreases with increasing superficial gas velocity, to the point of zero distillation column weeping or distillation column flooding. As W'/L decreases with increasing superficial gas velocity and increasing liquid flow rate the separation efficiency increases inside the distillation column. The superficial gas velocity has a greater influence on weeping as the liquid flow rate decreases (Fig. 86).

6.2 Effect of Plate Characteristics

6.2.1 Effect of Fractional Hole Area on Weeping

The effect of sieve tray fractional hole area (A_f) on weeping is explained in the current section. Three different fractional hole areas were investigated, namely 7%, 11% and 15% at the three different hole diameters of 3.2 mm (⅛ in.), 6.4 mm (¼ in.) and 12.7 mm (½ in.). The pitch (P_t – distance between the sieve tray holes) to hole diameter (d_H) ratio was kept constant for a particular sieve tray

fractional hole area. The hole pitch to hole diameter ratio for 7% fractional hole area is 3.4, for 11% fractional hole area is 2.6 and for 15% fractional hole area is 2.28. At low fractional hole areas (7%) there was little to no weeping, especially for systems with a low liquid density, as identified previously.

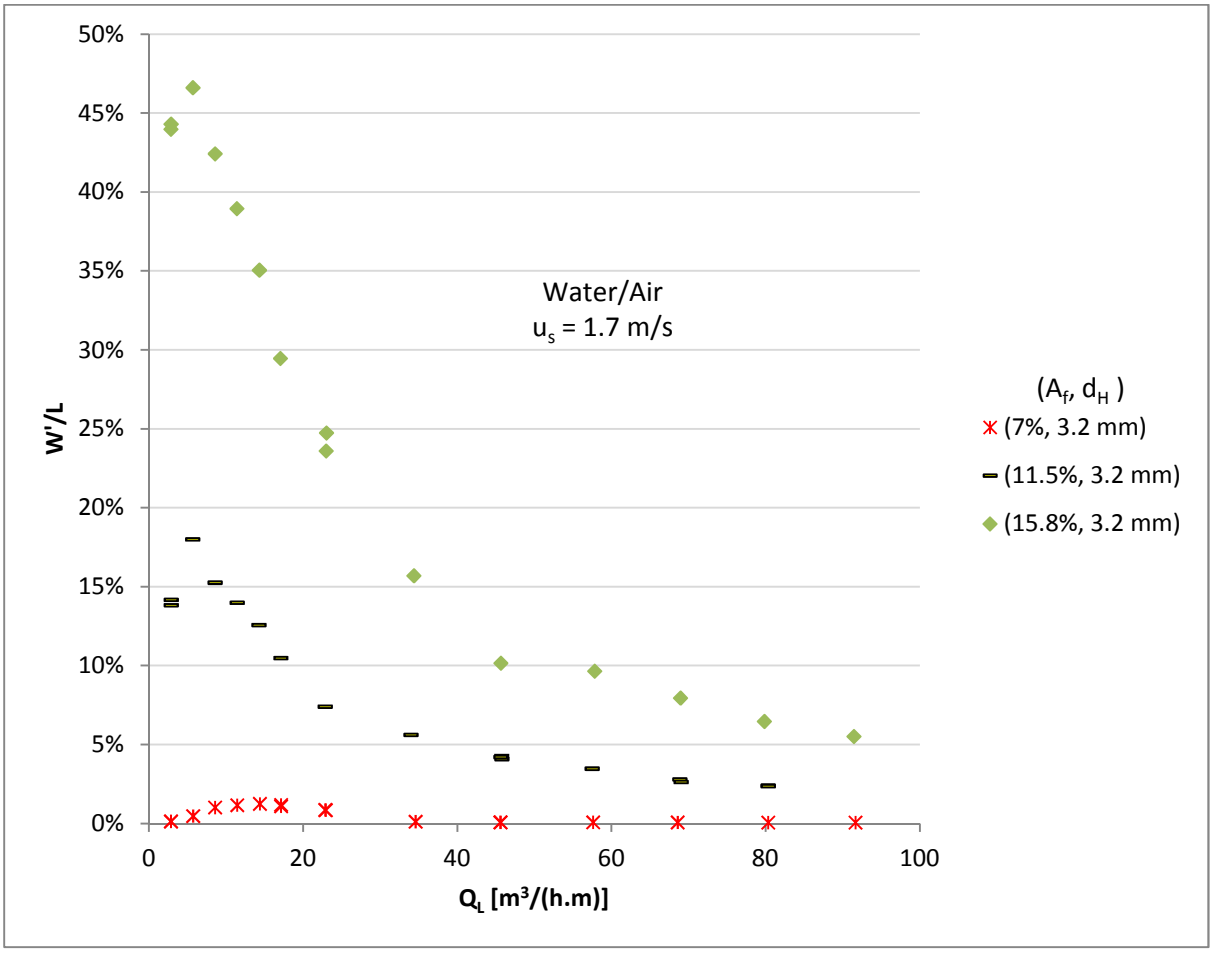

Figure 87 – Effect of fractional hole area on weeping (W'/L) for water/air with a 3.2 mm hole diameter and a superficial gas velocity of 1.7 m/s.

The weeping for different fractional hole areas at a hole diameter of 3.2 mm is shown in Figure 87 for W'/L weeping and in Figure 88 for W'/G weeping at a superficial gas velocity of 1.7 m/s. The influence of fractional hole area on weeping is considerably different for the spray regime [typically below 23 m^3/(h.m)] compared with the froth regime [typically above 23 m^3/(h.m)]. At a superficial gas velocity of 1.7 m/s the hole gas velocity is approximately 24 m/s for a 7% fractional hole area, 15 m/s for a fractional hole area of 11% and 11 m/s for a fractional hole area of 15 %. In the spray regime and the froth regime, weeping increases with increasing fractional hole area, where the difference between 7% and 11% fractional hole area weeping is considerably different from the 11% and the 15%. Thus the dependency of weeping on fractional hole area increases as the fractional hole area decreases in the spray regime.

Weeping reaches a maximum at a higher liquid flow rate as the fractional hole area increases, possibly due to the decrease in gas hole velocity (leading to a high weeping dominance or downward liquid hold-up force) (Fig. 87 and 88). The effect of the tray fractional areas on weeping becomes

more significant in the froth regime [typically above 23 m^3/(h.m)]. In the spray regime, gas jets through the sieve tray holes where weeping occurs throughout the flow path length of the sieve tray. In the spray regime some sieve tray holes jet and a small fraction of the sieve tray holes weep, where it is believed that the fraction of sieve tray holes that weep increases with increasing liquid flow rate, increasing weeping in the spray regime (Fig. 88). The weeping and gas jetting through the sieve tray holes makes the dispersion layer unstable and increases the amount of sloshing (instability) of the dispersion layer above the tray because of the pressure fluctuations below and above the sieve tray.

In the froth regime the dominance of the cross flowing liquid force is greater as the liquid flow rate increases. In this regime, weeping is impacted by the height of the dispersion layer, thus the magnitude of weeping is considerably impacted by the hole gas velocity or fractional hole area. The impact of liquid flow rate in the froth regime is different at high liquid flow rates [above 60 m^3/(h.m)] for high gas velocities (weeping decreases with increasing liquid flow rate) and low gas velocities [weeping (W'/G) increases or is relatively constant with increasing liquid flow rate].

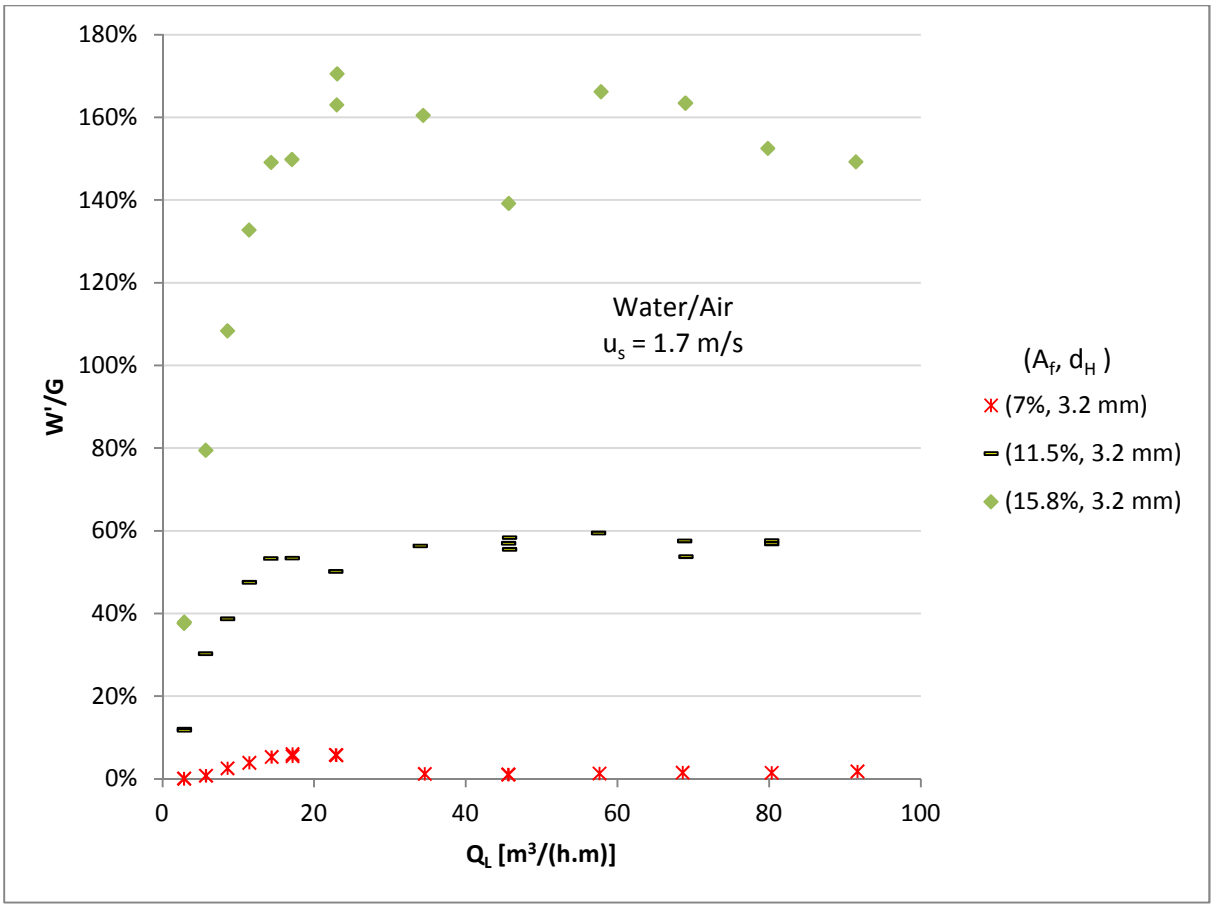

Figure 88 – Effect of fractional hole area on weeping (W'/G) for water/air with a 3.2 mm hole diameter and a superficial gas velocity of 1.7 m/s.

The weeping for different fractional hole areas in a water/air system at a hole diameter of 3.2 mm is shown in Figure 89 for W'/L weeping and in Figure 174 for W'/G weeping at a superficial gas velocity of 2.6 m/s. At a superficial gas velocity of 2.6 m/s the hole gas velocity is approximately 36 m/s for a 7% fractional hole area, 23 m/s for a fractional hole area of 11% and 16 m/s for a fractional hole area

of 15%. The percentage difference between the magnitudes of weeping for the different fractional hole area trays decreases with increasing liquid flow rate. Weeping decreases with increasing superficial gas velocity. At high liquid flow rates, the weeping magnitude tends to zero as the liquid flow rate increases at a higher superficial gas velocity. At both high liquid flow rates and high superficial gas velocities, the gas forces the dispersion layer liquid to jump over the sieve tray holes for the flow path length investigated.

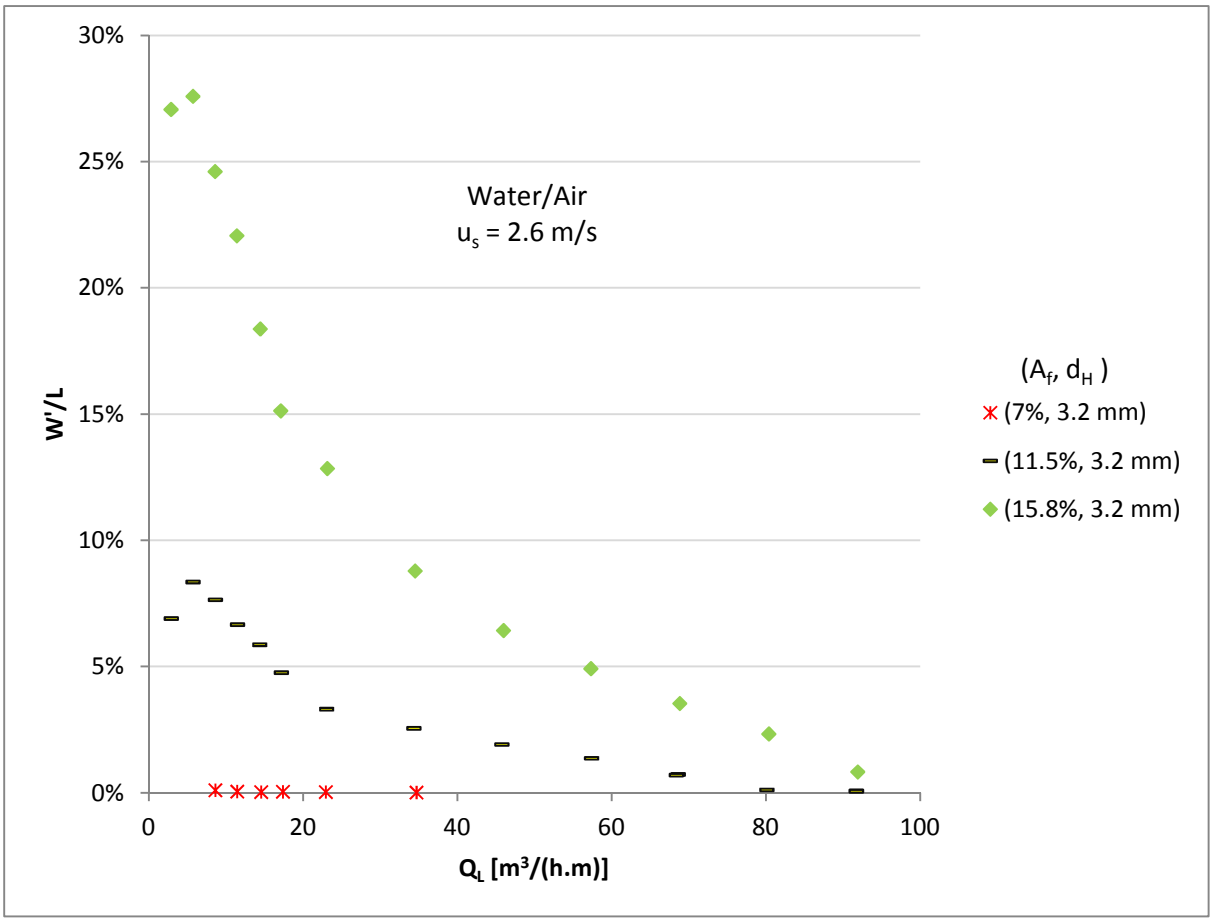

Figure 89 – Effect of fractional hole area on weeping (W'/L) for water/air with a 3.2 mm hole diameter and a superficial gas velocity of 2.6 m/s.

The weeping for silicone oil/carbon dioxide (Si/CO_2) at different fractional hole areas is shown in Figure 90 for W'/L weeping and in Figure 175 in Appendix F for W'/G weeping. The weeping follows a similar trend to that of water/air systems for a hole diameter of 3.2 mm (⅛ in.) and a superficial gas velocity of 1.7 m/s. The fractional hole area has a large influence on weeping in the spray regime at moderate liquid flow rates when the weeping magnitude reaches a maximum in the W'/G graph. The fluid physical properties have a significant influence on weeping. The 7% fractional hole area tray is not shown since it produces zero weeping for the Si/CO_2 system. Systems that produce a smaller froth layer in the dispersion layer produce a lower magnitude of weeping than systems that produce large froth layers in the dispersion layer. An increase in liquid density, increase in liquid surface tension and an increase in liquid viscosity increases the effect that fractional hole area has on weeping.

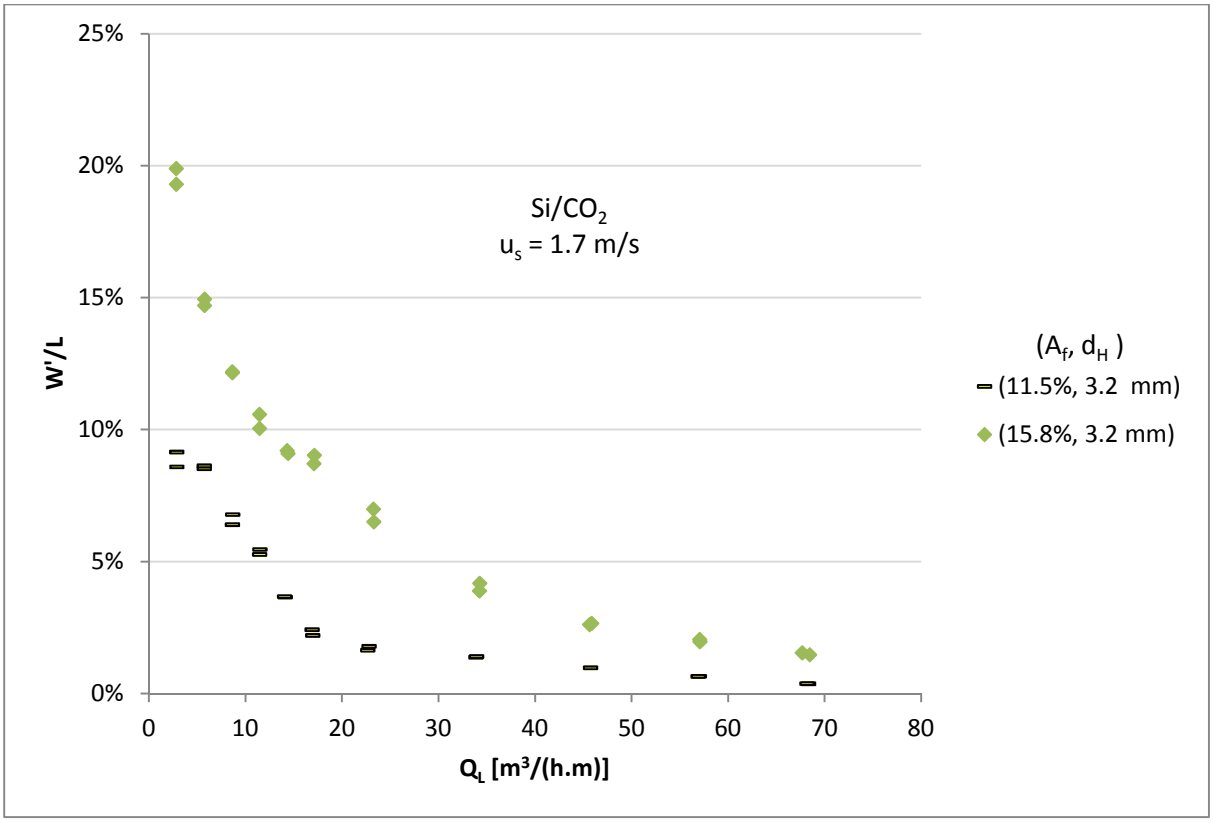

Figure 90 – Effect of fractional hole area on weeping (W'/L) for silicone-oil/CO_2 with a 3.2 mm hole diameter and a superficial gas velocity of 1.7 m/s.

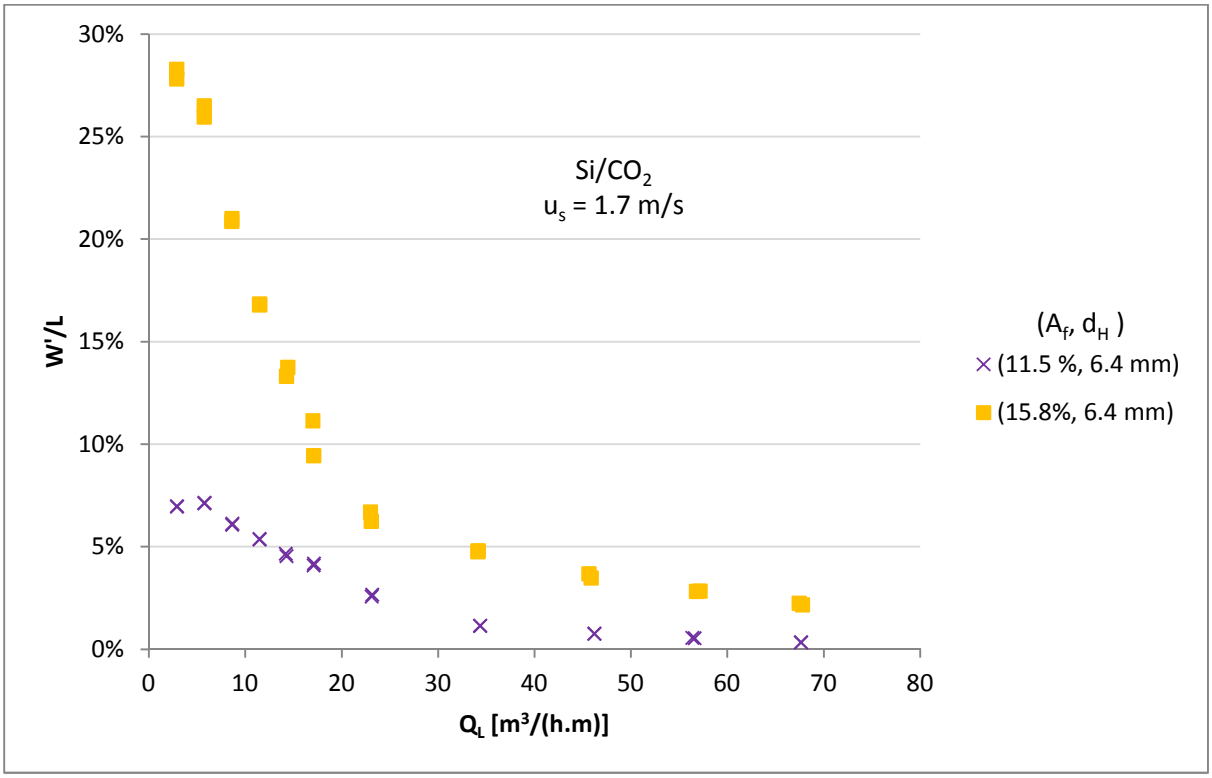

Figure 91 – Effect of fractional hole area on weeping (W'/L) for water/air with a 6.4 mm hole diameter and a superficial gas velocity of 1.7 m/s.

The weeping for silicone oil/carbon dioxide (Si/CO_2) at different fractional hole areas is shown in Figure 91 for W'/L weeping and in Figure 176 in Appendix F for W'/G weeping for a hole diameter of 6.4 mm (¼ in.) and a superficial gas velocity of 1.7 m/s. The weeping follows a significantly different trend compared to that of the 3.2 mm trays, where the fractional hole area has a large influence on weeping in the spray regime at low liquid flow rates. The weeping follows a similar trend as that described by Lockett and Banik (1986).

The trend of the weeping (W'/G) in the froth regime can be described by the observations of Lockett and Banik (1986). In the investigation it was found that weeping occurred mainly in the inlet half of the tray for a liquid flow rate of 30 $m^3/(h.m)$ and the exit half of the tray at a liquid flow rate of 60 $m^3/(h.m)$. It is described that the reason for the difference in weeping is that a hydraulic jump may be present at the inlet of the tray at high liquid loads. The trend of the experimental weeping can be described using the visual observations of the current experimental investigation and the dispersion layers description shown by Uys (2012) in Figure 5 (Section 5.2.1).

In Figure 5(a), Profiles 1 to 5 represent the systematic change in dispersion layer patterns observed above the sieve tray as the liquid flow rate is increased. Profile 1 represents moderate liquid flow rates where the peak of the dispersion layer occurs on the inlet half of the tray. As the height of dispersion layer drops from the peak with increasing flow path length, a high pressure zone is created causing weeping in the froth regime, where a jump in the fluid dispersion layer is observed at the peak of the dispersion layer. The liquid flow trajectory corresponds best with the upward gas flow trajectory. A high pressure zone is observed at the beginning of the dispersion layer as the liquid enters the tray and before a hydraulic jump occurs. Profile 2 in Figure 5(a) describes the froth regime dispersion layer at a higher liquid flow rate (higher than Profile 1), where the dispersion layer's peak is higher (longer hydraulic dispersion jump) and occurs at a higher flow path length. Thus the high pressure zone occurs at a higher flow path length similar to the trend of Lockett and Banik (1986). As the liquid flow rate increases to Profile 3, the gas velocity upward through the sieve tray holes and the high liquid cross flow causes the liquid to jump (hydraulic jump) over the entire flow path length, leading to a zero weeping magnitude.

6.2.2 Effect of Hole Diameter on Weeping

This section shows the impact of sieve tray hole diameter on weeping, where the sieve tray hole diameters are 3.2 mm (⅛ in.), 6.4 mm (¼ in.) and 12.7 mm (½ in.), which are multiples of one another. The effect of the sieve tray hole diameter is shown in Figure 92 for W'/L weeping and in Figure 93 for W'/G weeping. Weeping is represented with a silicone-oil/air (Si/air) system at a superficial gas velocity of 1.7 m/s. The subsequent figures in the current section are at a fractional hole area of 15%.

A clear difference is seen between the effect that hole diameter has on weeping in the spray regime [typically below 23 $m^3/(h.m)$] and froth regime [typically above 23 $m^3/(h.m)$] (Fig. 92 and 93). In the spray regime, weeping (W'/G) increases with decreasing sieve tray hole diameter. The impact that tray hole diameter has on weeping is less significant, where the magnitude of weeping reaches a maximum at a liquid flow rate of between 10 and 25 $m^3/(h.m)$. At a similar tray fractional hole area, the trays have a similar gas hole velocity through the sieve tray. It is believed that in the spray regime the stability of the gas jet through the sieve tray hole increases with increasing hole diameter, while in the froth regime the bubble diameter increases with increasing sieve tray hole diameter at

constant fractional hole area. The dispersion layer above the sieve tray becomes more unstable with increasing tray hole diameter.

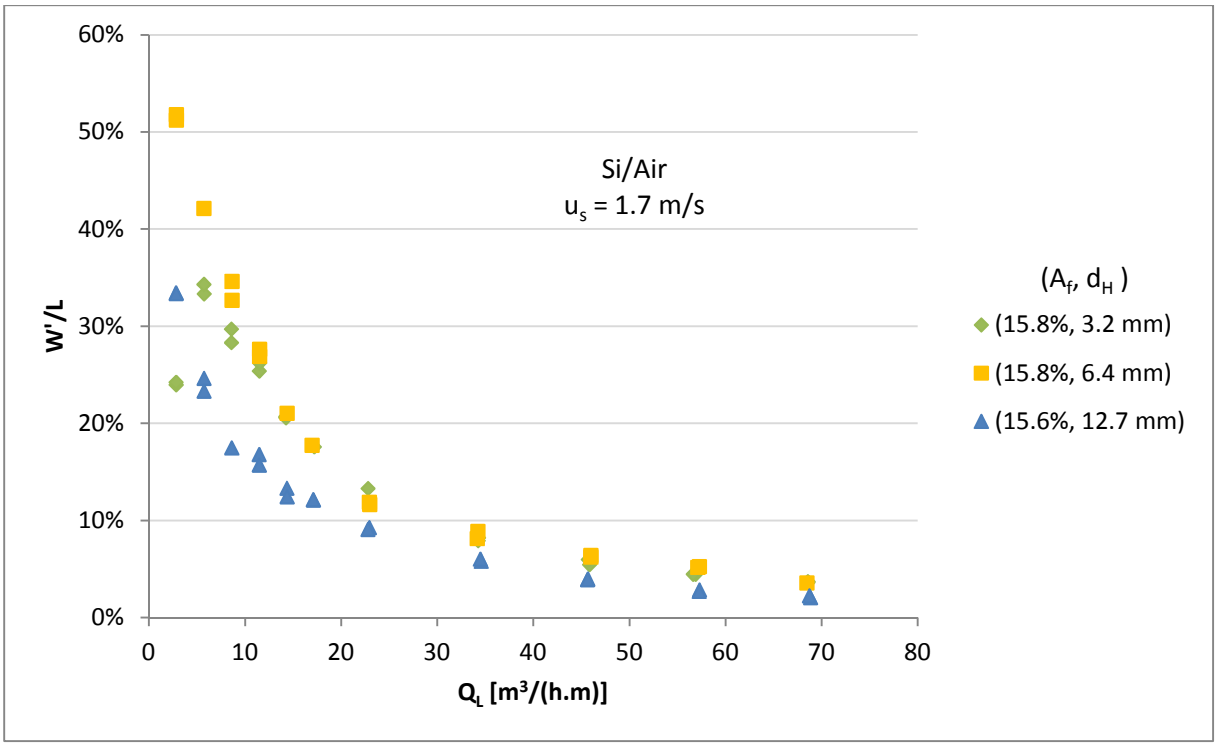

Figure 92 – Effect of hole diameter on weeping (W'/L) for silicone-oil/air with a 15% fractional hole area and a superficial gas velocity of 1.7 m/s.

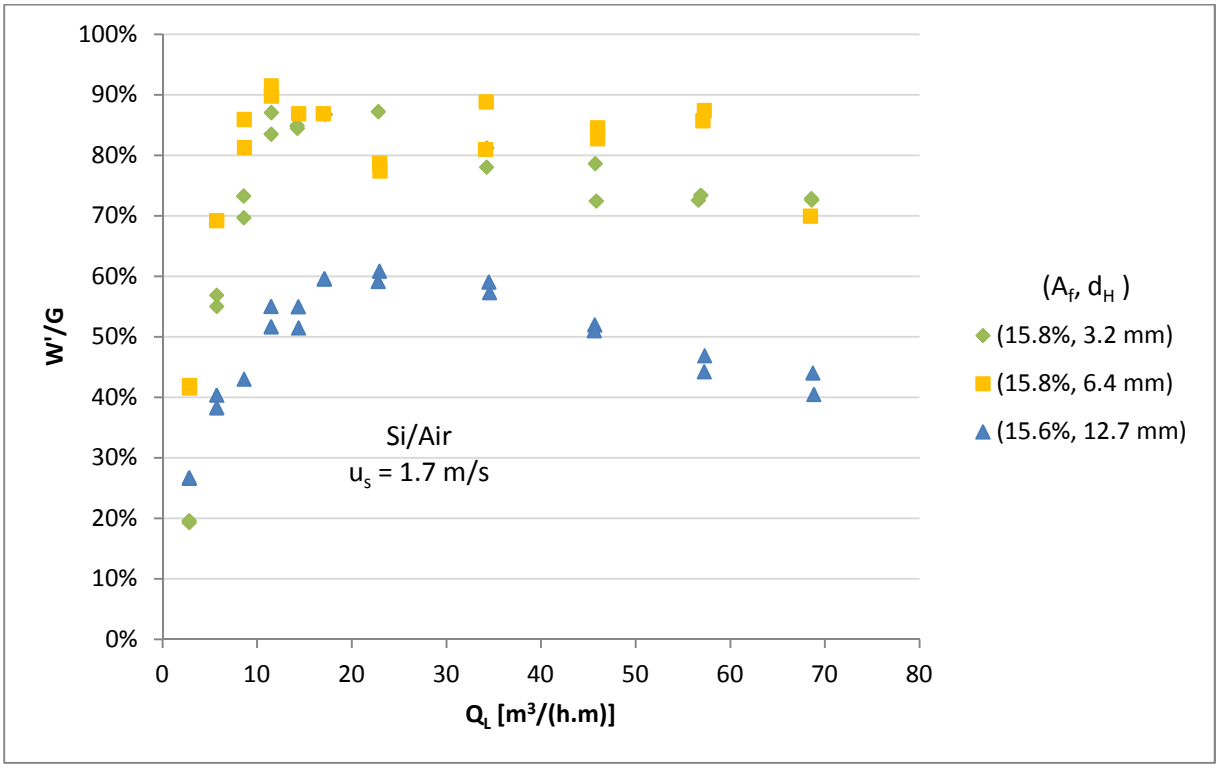

Figure 93 – Effect of hole diameter on weeping (W'/G) for silicone-oil/air with a 15% fractional hole area and a superficial gas velocity of 1.7 m/s.

Weeping does not have a clear distinctive trend (dependence) with changing hole diameter as the liquid flow rate increases (Fig. 92 and 93). The 6.4 mm tray has the highest weeping, the 3.2 mm tray has an intermediate weeping magnitude and the 12.7 mm tray has the lowest weeping magnitude for the silicone oil/air system. The trend observed for weeping is similar to the trend observed by Lockett and Banik (1986) for changing hole diameter. In the Lockett and Banik (1986) weeping experiments the differences in weeping with changing hole diameter was due to different weeping mechanisms through the sieve tray holes, as identified in Section 2.5.2. The difference in weeping mechanism through the sieve tray holes that is identified by Lockett and Banik (1986) cannot be visually distinguished for the different sieve tray hole sizes of the current experimental investigation. It is believed that the weeping mechanism through the sieve tray holes is due to a change in the liquid hold-up above the tray (changes in the high pressure zone locations as described by Figure 5).

The effect of the sieve tray hole diameter is shown in Figure 94 for W'/L weeping and in Figure 177 in Appendix F for W'/G weeping, where weeping is represented with a silicone-oil/air system at a superficial gas velocity of 2.6 m/s. The effect of tray hole diameter on weeping is clearly different as the superficial gas velocity increases for the Si/air system. In the spray regime [typically below 23 $m^3/(h.m)$], the 6.4 mm tray has the highest weeping, the 12.7 mm tray has an intermediate weeping magnitude and the 3.2 mm tray has the lowest weeping magnitude for the superficial gas velocity of 2.6 m/s. In the froth regime [typically above 23 $m^3/(h.m)$], the 6.4 mm tray has the highest weeping, the 3.2 mm tray has an intermediate weeping magnitude and the 12.7 mm tray has the lowest weeping magnitude for a superficial gas velocity of 2.6 m/s.

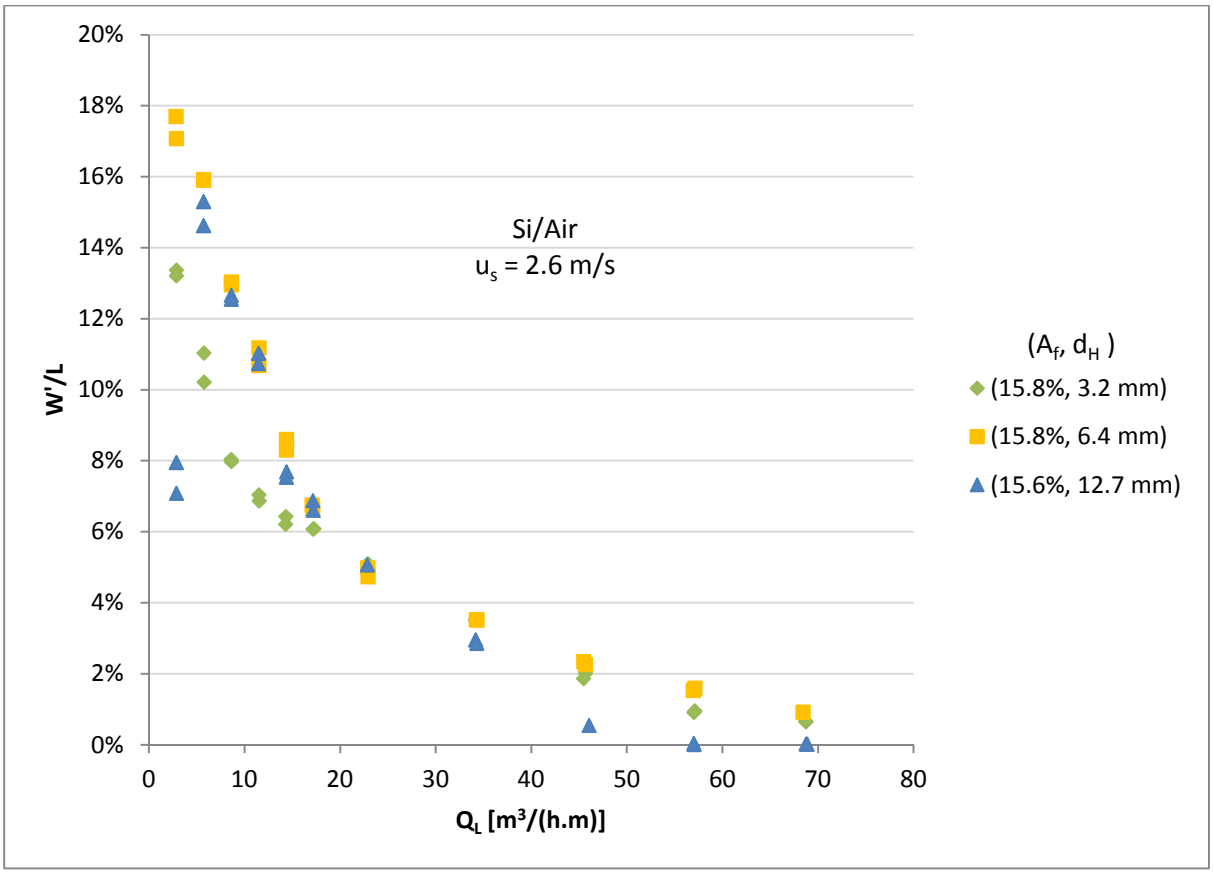

Figure 94 – Effect of hole diameter on weeping (W'/L) for silicone-oil/air with a 15% fractional hole area and a superficial gas velocity of 2.6 m/s.

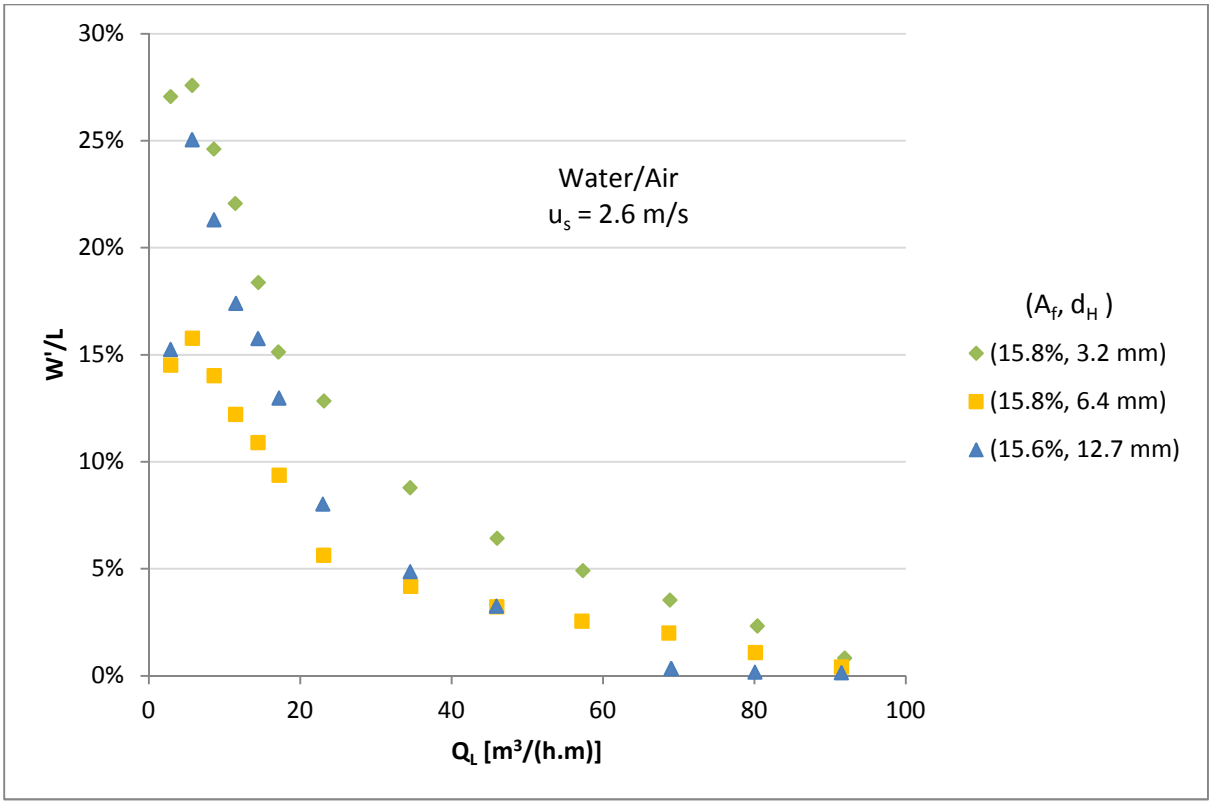

Figure 95 – Effect of hole diameter on weeping (W'/L) for water/air with a 15% fractional hole area and a superficial gas velocity of 2.6 m/s.

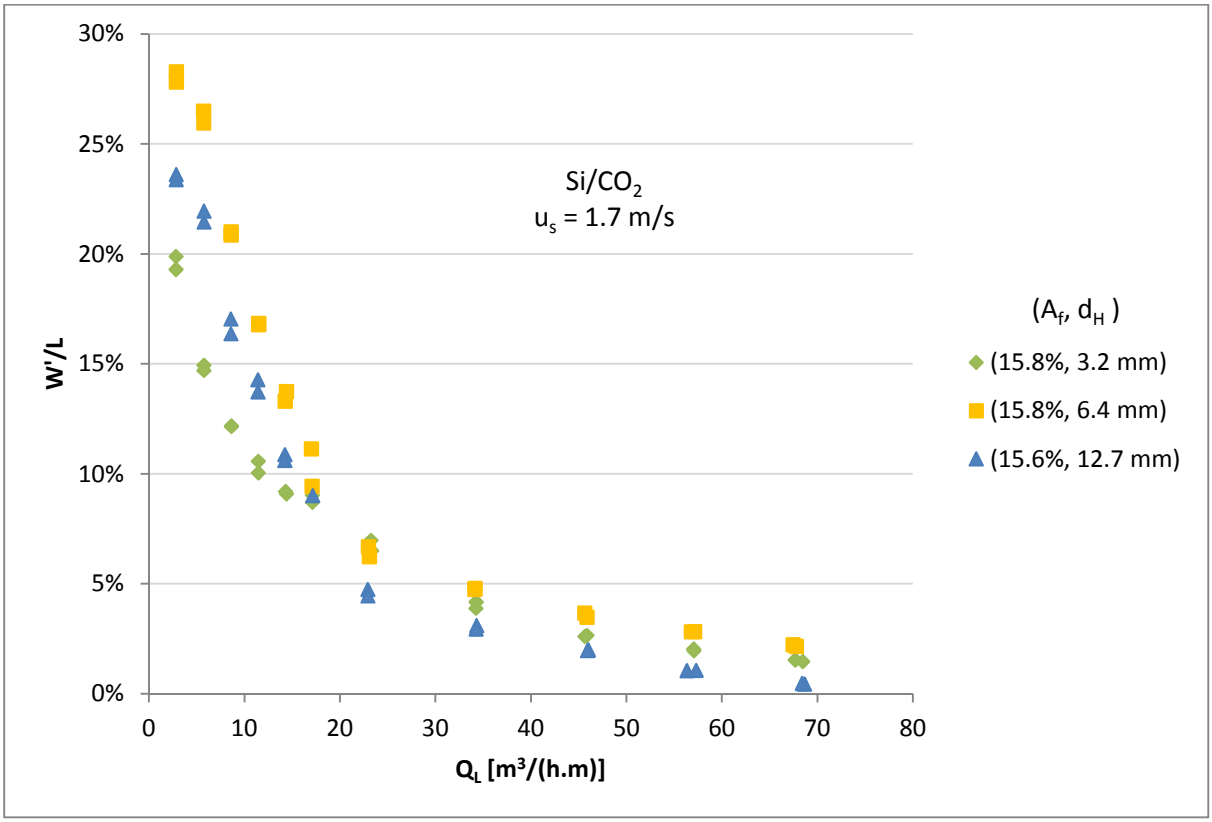

Figure 96 – Effect of hole diameter on weeping (W'/L) for silicone-oil/CO_2 with a 15% fractional hole area and a superficial gas velocity of 1.7 m/s.

Figure 95 shows the weeping (W'/L) and Figure 178 in Appendix F shows the weeping (W'/G) for different sieve tray hole diameters with a water/air system and a superficial gas velocity of 2.6 m/s. In the spray regime [typically below 23 m^3/(h.m)], the 3.2 mm tray has the highest weeping, the 12.7 mm tray has an intermediate weeping magnitude and the 6.4 mm tray has the lowest weeping magnitude for a superficial gas velocity of 2.6 m/s. In the froth regime [typically above 23 m^3/(h.m)], the 3.2 mm tray has the highest weeping, the 6.4 mm tray has an intermediate weeping magnitude and the 12.7 mm tray has the lowest weeping magnitude for the superficial gas velocity of 2.6 m/s. The trends observed with the water/air system shows that the effect of the sieve tray hole diameter on weeping is a function of the superficial gas velocity, liquid flow rate and fluid systems used inside the distillation column. The magnitude of weeping for the water/air system is different from that observed by Lockett and Banik (1986) when analysing the effect of the sieve tray hole diameter.

It is believed that weeping is a strong function of the liquid hold-up pressure drop across the sieve tray. The only clear trend for the effect hole diameter has on weeping is that the 12.7 mm hole diameter tray always produces the lowest weeping in the froth regime [typically above 23 m^3/(h.m)]. This could be because of the size (width) of the gas jetting through the hole which prevents the liquid from weeping through the tray holes, where hole diameters greater than 12.7 mm will produce an even lower weeping.

The effect of the sieve tray hole diameter is shown in Figure 96 for W'/L weeping and in Figure 179 in Appendix F for W'/G weeping, where weeping is represented with a Si/CO_2 system at a superficial gas velocity of 1.7 m/s. The Si/CO_2 system follows a similar trend to that of Si/air in Figure 94 (u_s = 2.6 m/s) but a different trend with Si/air in Figure 92 (u_s = 1.7 m/s), which shows that the gas physical properties have a strong influence on the amount of weeping. Carbon dioxide has a higher density than air, thus when used at the same superficial gas velocity the carbon dioxide has a larger mass flow rate and a similar influence on weeping as an air system which is operated at a higher superficial gas velocity.

Figure 97 shows the weeping (W'/L) and Figure 180 in Appendix F shows the weeping (W'/G) for different sieve tray hole diameters with a silicone oil/CO_2 system at superficial gas velocity of 2.6 m/s. The trend at 2.6 m/s is shown to be different from the trend of weeping at 1.7 m/s in Figure 96. In the spray regime [typically below 23 m^3/(h.m)], the 6.4 mm tray has the highest weeping, the 12.7 mm tray has an intermediate weeping magnitude and the 3.2 mm tray has the lowest weeping magnitude for the superficial gas velocity of 2.6 m/s. In the froth regime [typically above 23 m^3/(h.m)], the 6.4 mm tray has the highest weeping, the 3.2 mm tray has an intermediate weeping magnitude and the 12.7 mm tray has the lowest weeping magnitude for a superficial gas velocity of 2.6 m/s.

Weeping for six experimental sieve trays (fractional hole area of 11% and 15%, hole diameter of 3.2 mm, 6.4 mm and 12.7 mm) are shown in Figure 98 for W'/L weeping and Figure 181 in Appendix F for W'/G weeping. The figures are shown for an ethylene glycol/air (EG/air) system and a liquid flow rate 8.6 m^3/(h.m) (spray regime) at changing superficial gas velocity. The influence of the tray geometry on weeping increases with decreasing superficial gas velocity. The fractional hole areas effect is clearly distinguishable when analysing the effect of superficial gas velocity. The 7% tray produces no weeping for the EG/air fluid system, and is thus not shown in Figure 98.

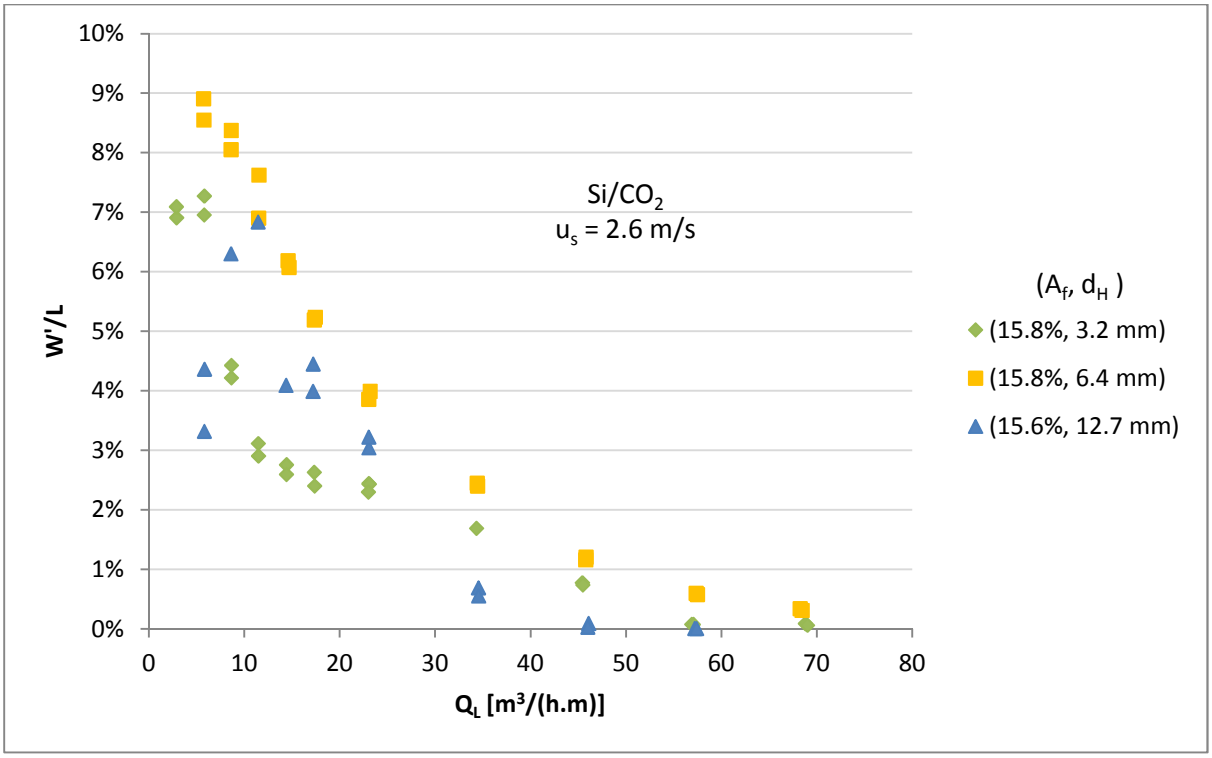

Figure 97 – Effect of hole diameter on weeping (W'/L) for silicone-oil/CO_2 with a 15% fractional hole area and a superficial gas velocity of 2.6 m/s.

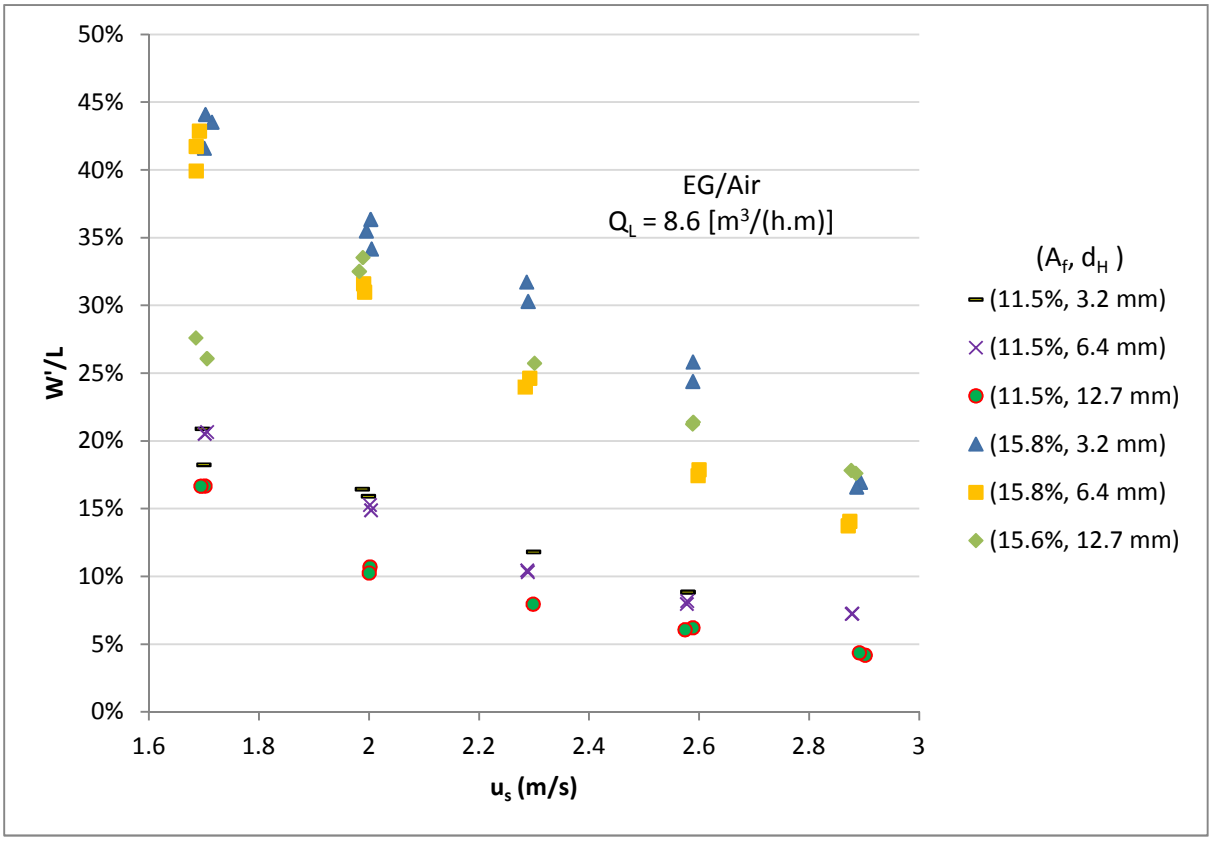

Figure 98 – Effect of tray geometry on weeping (W'/L) for ethylene-glycol/air with changing superficial gas velocity and a liquid flow rate of 8.6 m^3/(h.m).

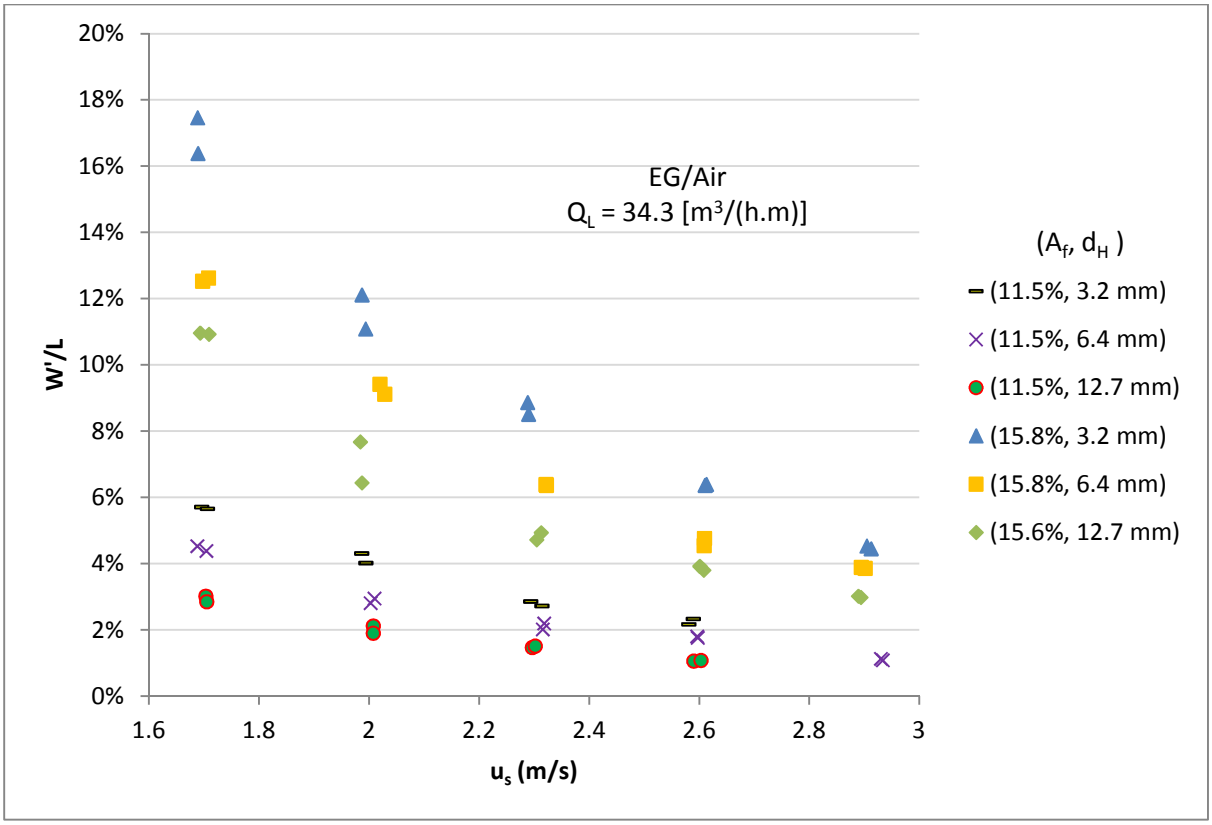

Figure 99 – Effect of tray geometry on weeping (W'/L) for ethylene-glycol/air with changing superficial gas velocity and a liquid flow rate of 34.3 m^3/(h.m).

The weeping for six of the experimental sieve trays are shown in Figure 99 for W'/L weeping and Figure 182 in Appendix F for W'/G weeping for an ethylene glycol/air (EG/air) system. The figures are plotted at liquid flow rate 34.3 m^3/(h.m) (froth regime with moderate liquid flow rates) at changing superficial gas velocity. At a moderate liquid flow rate the tray geometry has a high influence on weeping; by decreasing the superficial gas velocity the effect of tray geometry on weeping increases.

6.3 Evaluation of Dimensionless Number Trends for Weeping

In this section the weeping data (W'/L and W'/G) are compared to dimensionless fluid dynamic numbers in order to help explain the trends observed in the previous sections. The dimensionless numbers are taken from different literature sources and adjusted to fit the current sieve distillation column study. Weeping is mostly compared to dimensionless numbers with Tray 1, where the effects of fluid physical properties and tray geometry are addressed.

$$Fr_h^+ = u_h \left(\frac{\rho_g}{h_c \rho_l}\right)^{0.5} \quad \rightarrow \quad \text{Liquid Hold-up Froude Number} \quad [5.3.2.1]$$

The weeping (W'/L) experimental data are plotted against the inverse of the liquid hold-up Froude number (Fr_h^+) in Figure 100 in the spray regime, where the liquid hold-up Froude number is represented by Equation 5.3.2.1 (Lockett and Banik, 1986). The Froude number defines the ratio of the inertial forces to the gravitational forces acting on the fluid (speed over length ratio). Weeping changes with a similar trend at different liquid rates in the spray regime, where weeping is a strong function of the parameters used to define the liquid hold-up Froude number. Weeping (W'/L)

decreases with increasing liquid flow rate in the spray regime. Weeping (W'/L) decreases with increasing values for the inverse of the liquid hold-up Froude number. By analysing Equation 5.3.2.1, weeping (W'/L) increases with decreasing hole gas velocity (u_h), decreasing gas density (ρ_g), increasing clear liquid hold-up (h_c) and increasing liquid density (ρ_l) in the spray regime. The superficial gas velocity increases from 1.7 to 2.9 m/s at increments of 0.3 m/s, where the trend lines in Figure 98 represents a constant superficial gas velocity.

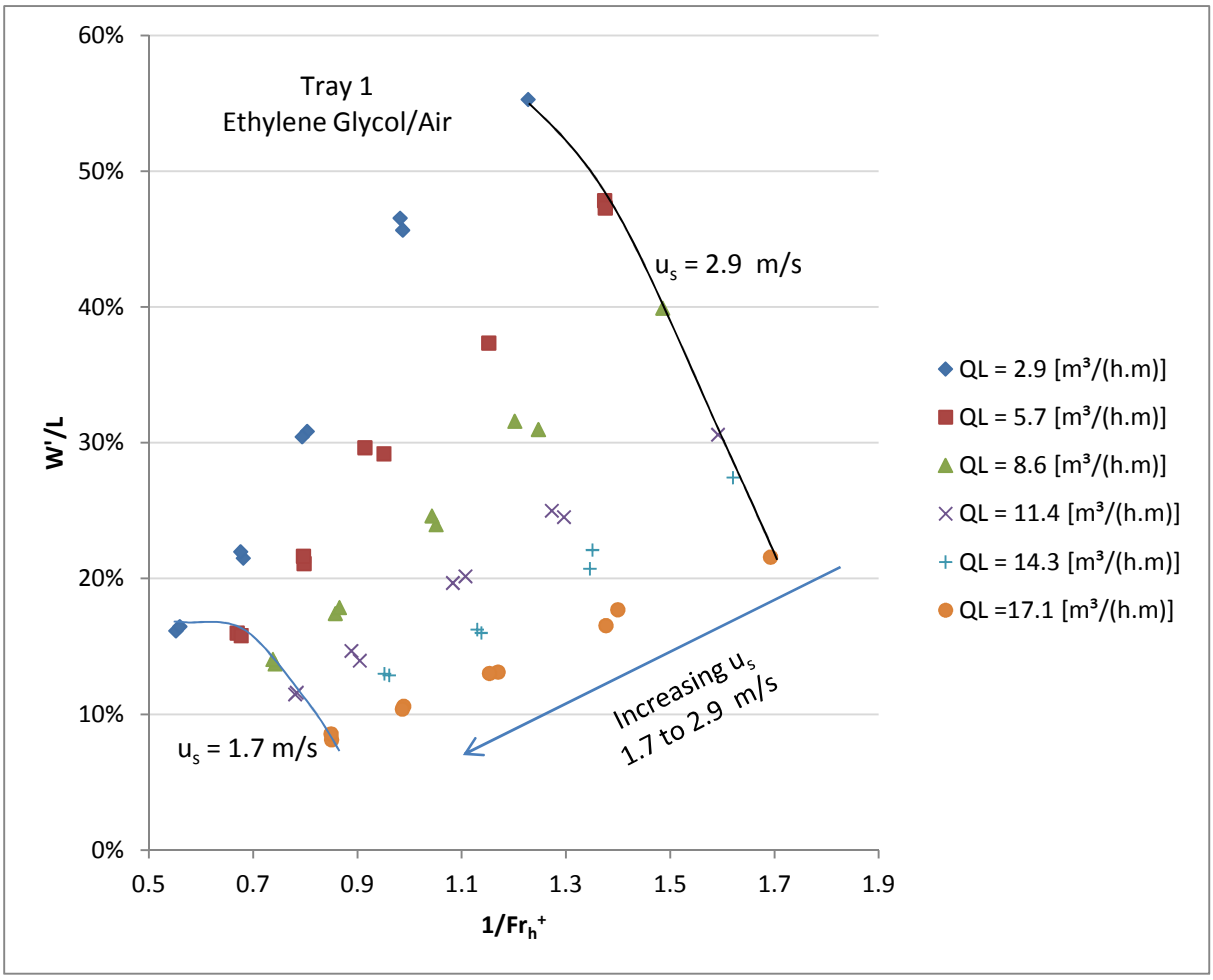

Figure 100 – Weeping (W'/L) changing with the inverse of the liquid hold-up Froude number (Fr_h^+) for ethylene-glycol/air with Tray 1 (15.8% fractional hole area, 6.4 mm hole diameter) in the spray regime.

Weeping (W'/L) has a different dependency on the liquid hold-up Froude number in the froth regime (Fig. 183 in Appendix F). The change in the inverse liquid hold-up Froude number in the froth regime with weeping (W'/L) follows the same liquid dispersion layer trend identified in Figure 100 at moderate liquid flow rates in the froth regime [approximately 23 to 46 m^3/(h.m)]. Weeping (W'/L) increases with a decreasing inverse liquid hold-up Froude number at low to moderate liquid Froude numbers in the froth regime (Fig. 183). Weeping (W'/L) increases with an increasing inverse liquid hold-up Froude number. Weeping increases with decreasing hole gas velocity (u_h), decreasing gas density (ρ_g), increasing clear liquid hold-up (h_c) and increasing liquid density (ρ_l) at high liquid flow rates [typically above 68.6 m^3/(h.m)].

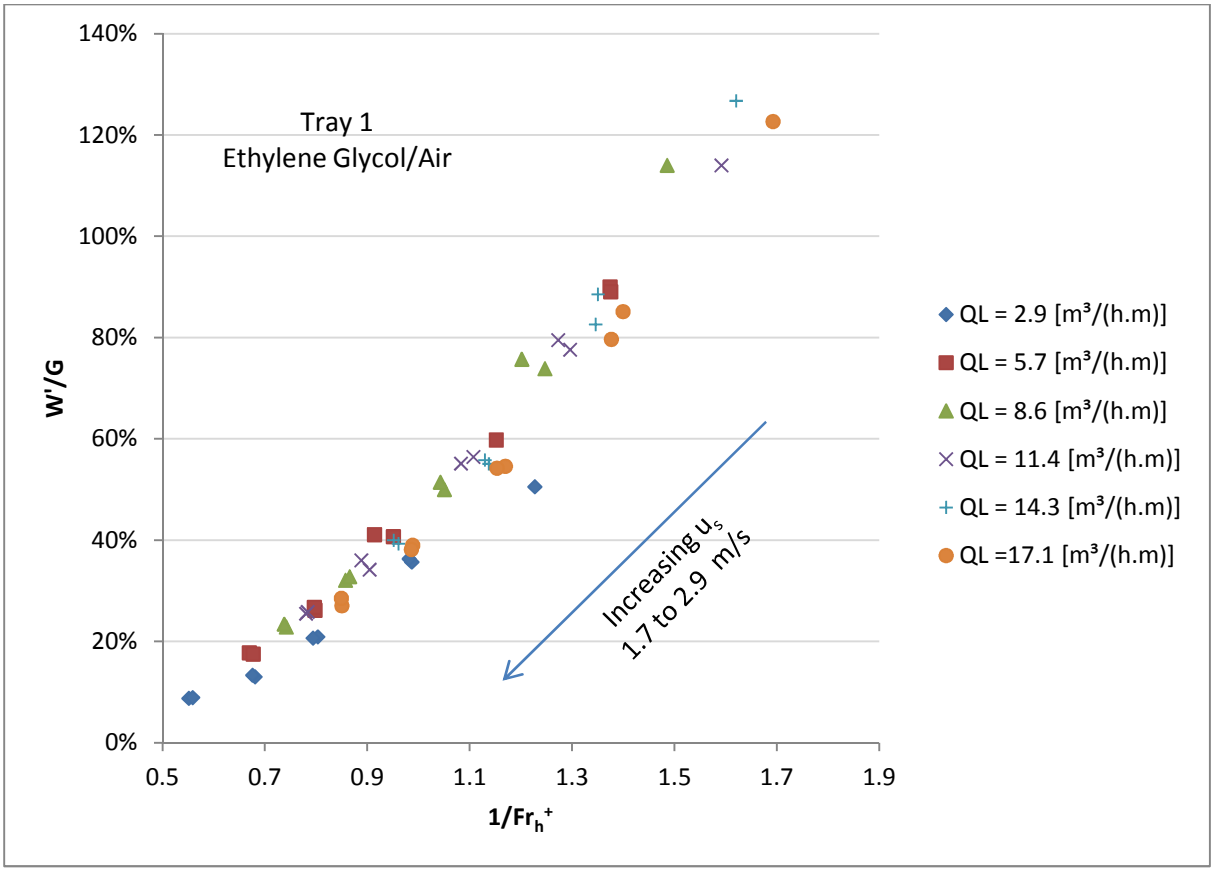

Figure 101 – Weeping (W'/G) changing with the inverse of the liquid hold-up Froude number (Fr_h^+) for ethylene-glycol/air with Tray 1 (15.8% fractional hole area, 6.4 mm hole diameter) in the spray regime.

The change in the weeping (W'/G) with inverse liquid hold-up Froude number at different liquid flow rates is shown in Figure 101 for the spray regime. The inverse liquid hold-up Froude number pulls the weeping (W'/G) data into an approximate straight line similar to the model used by Lockett and Banik (1986), although weeping cannot be fully described by the liquid hold-up Froude number alone. The outlying trend shown by the 2.9 m^3/(h.m) liquid flow rate can be explained by the low dispersion layer height at the liquid flow rate and low liquid velocity through the downcomer escape. The low liquid flow rate produces an unstable liquid dispersion layer above the sieve tray. The weeping is shown to be a strong function of the liquid hold-up.

The sieve tray weeping (W'/L) is plotted versus the Weber number (We) in Figure 102 for the spray regime. The Weber number is defined by Equation 2.2.4 (Uys, 2012), and defines the ratio between the inertial forces to surface tension forces of the fluid. The Weber number is used in multiphase flow to describe the behaviour of thin films and the tendency for the formation of bubbles and droplets.

$$We = \frac{\rho_g u_s Q_L}{3.6\sigma} \qquad \rightarrow \qquad \text{Weber Number} \qquad [2.2.4]$$

Weeping (W'/L) increases with a decreasing Weber number for a particular liquid flow rate for silicone oil/air (Fig. 102). Therefore weeping increases with decreasing gas density (ρ_g), decreasing superficial gas velocity (u_s) and increasing liquid surface tension (σ) in the spray regime. As the

superficial gas velocity increases, the dependency of weeping (W'/L) on the Weber number decreases, supporting the trend observed in earlier sections. Weeping (W'/L) is plotted versus the Weber number (We) in Figure 184 in Appendix F for the froth regime. The weeping (W'/L) follows a similar trend in the froth regime as it does in the spray regime, but has a stronger dependence on the Weber number in the froth regime. The Weber number affects weeping similarly over the entire liquid flow rate range since the liquid flow rate, gas velocity and gas density (Weber number parameters) terms affect weeping strongly. The gas velocity increases from 1.7 to 2.9 m/s at increments of 0.3 m/s, where the trend lines in Figure 102 represents a constant superficial gas velocity.

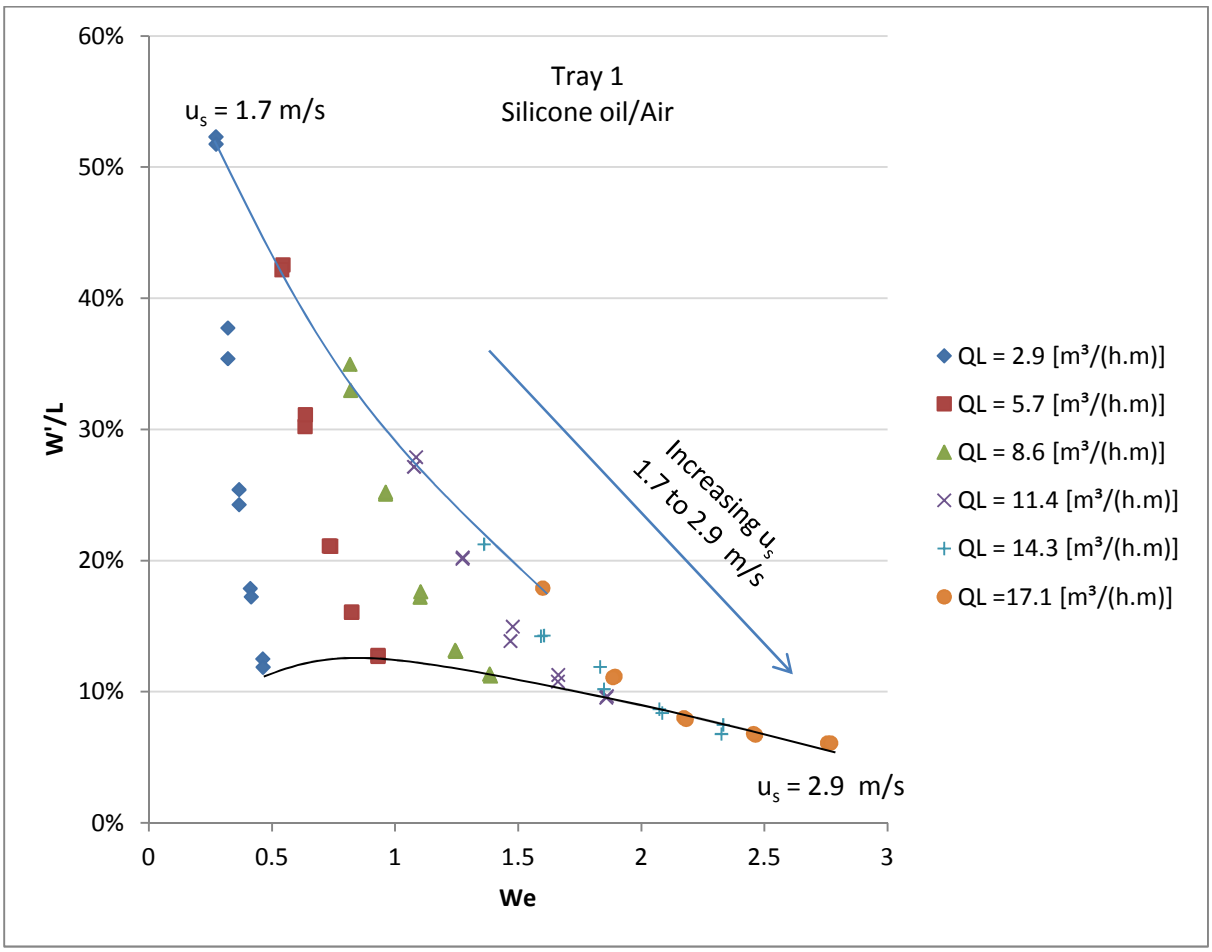

Figure 102 – Weeping (W'/L) changing with the Weber number (We) for silicone-oil/air with Tray 1 (15.8% fractional hole area, 6.4 mm hole diameter) in the spray regime.

The weeping (W'/G) is plotted against the Weber number in the spray regime in Figure 103 for silicone-oil/air. The sieve tray weeping (W'/G) follows a different trend with the Weber number to that of the W'/L weeping with increasing liquid flow rate. Weeping (W'/G) decreases with increasing Weber number in the spray regime, where weeping has a lower dependency on the Weber number in the higher liquid flow rates regime. Weeping (W'/G) is plotted versus the Weber number (We) in Figure 185 in Appendix F for the froth regime. The dependency of weeping (W'/G) on the liquid flow rate in the froth regime switches at high liquid flow rates, where weeping is shown to decrease with increasing liquid flow rate. At a constant superficial gas velocity, weeping (W'/G) follows a parabolic

trend with increasing Weber number. Weeping (W'/G) increases to a maximum and then decreases with increasing liquid flow rate.

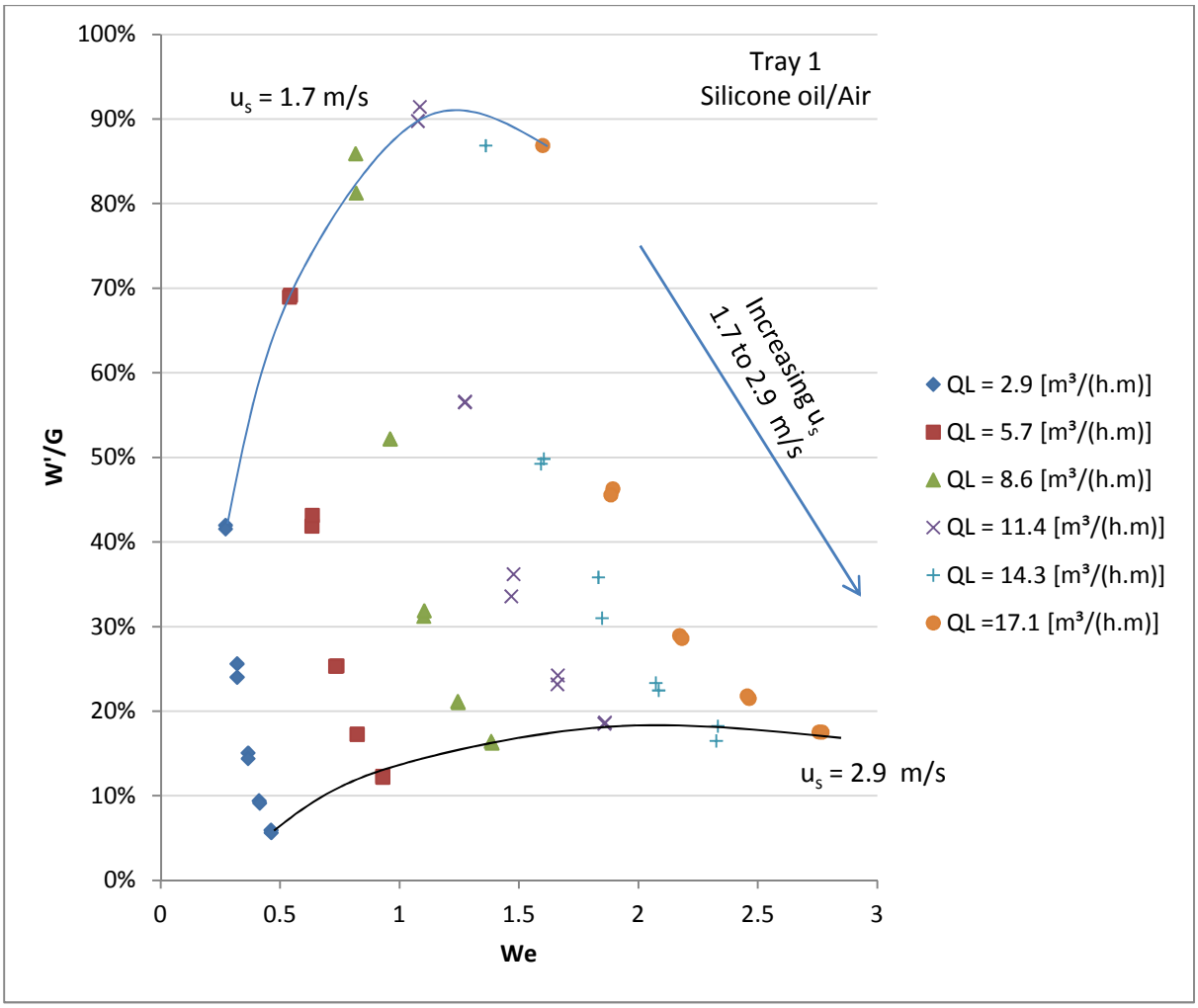

Figure 103 – Weeping (W'/G) changing with the Weber number (We) for silicone-oil/air with Tray 1 (15.8% fractional hole area, 6.4 mm hole diameter) in the spray regime.

Weeping (W'/L) is plotted versus the liquid Reynolds number (Re) in Figure 104 for the spray regime with ethylene-glycol/air. The liquid Reynolds number is defined by Equation 2.5.1.30 (Uys, 2012).

$$Re = \frac{\rho_g\left(\frac{Q_L}{3600}\right)}{\mu_g} \quad \rightarrow \quad \text{Liquid Reynolds number} \qquad [2.5.1.30]$$

The sieve tray weeping (W'/L) decreases with increasing liquid Reynolds numbers in the spray regime (Fig. 104). Based on the trends for the liquid Reynolds number, weeping (W'/L) increases with increasing gas viscosity (μ_g), decreasing gas density (ρ_g) and decreasing liquid flow rate, supporting the weeping trends observed in earlier sections. The weeping follows a similar trend in the froth regime as in the spray regime (Fig. 186 in Appendix F). The gas velocity increases from 1.7 to 2.9 m/s at increments of 0.3 m/s, where the trend lines in Figure 104 represent a constant superficial gas velocity.

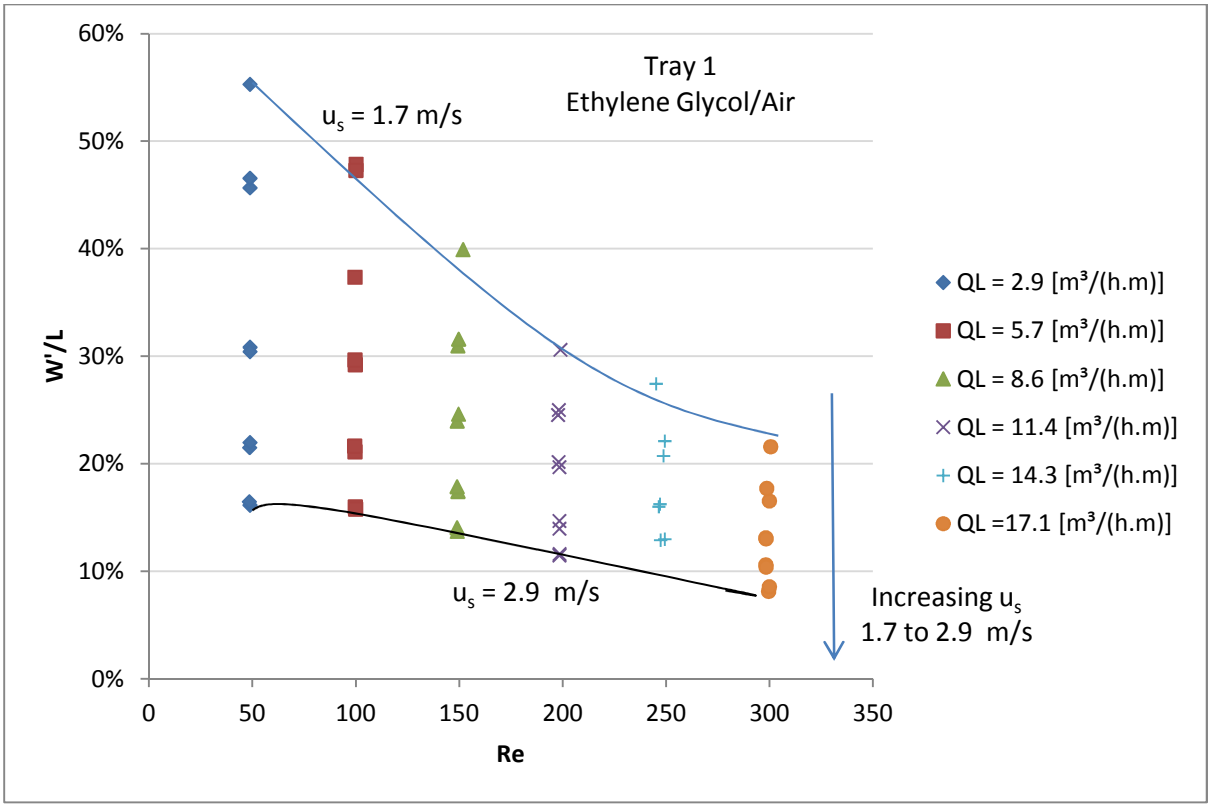

Figure 104 – Weeping (W'/L) changing with the liquid Reynolds number (Re) for ethylene-glycol/air with Tray 1 (15.8% fractional hole area, 6.4 mm hole diameter) in the spray regime.

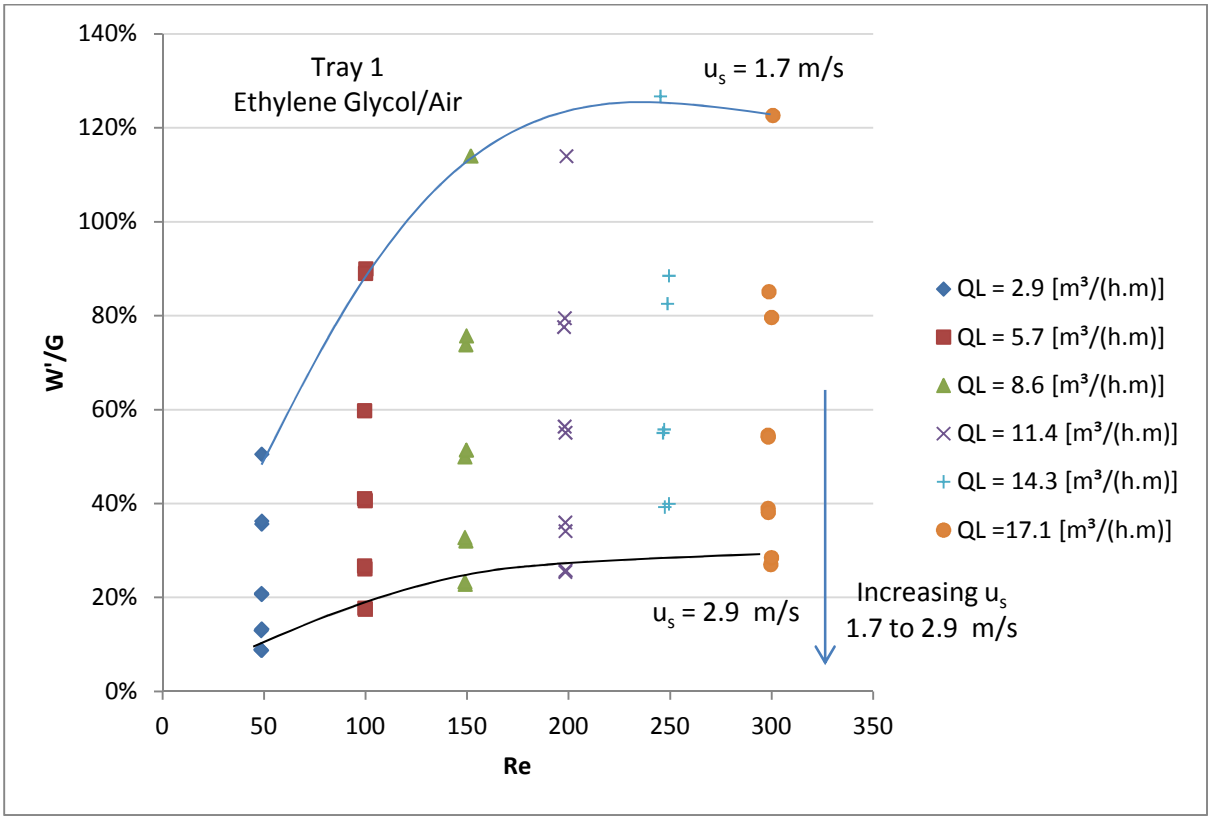

Figure 105 – Weeping (W'/G) changing with the liquid Reynolds number (Re) for ethylene-glycol/air with Tray 1 (15.8% fractional hole area, 6.4 mm hole diameter) in the spray regime.

Weeping (W'/G) increases with increasing liquid Reynolds number at low liquid flow rates in the spray regime (Fig. 105 for spray regime and Fig. 187 for froth regime). At moderate to high liquid flow rates, weeping (W'/G) decreases with increasing liquid Reynolds number, but becomes more dependent on superficial gas velocity at the highest liquid flow rate (it is possible that this is close to the point of weeping flooding). In the spray regime, the dispersion layer height increases with increasing liquid flow rate and, as a result weeping increases. In the froth regime the cross flowing liquid flow rate over powers the downward weeping effect consequently decreasing weeping with increasing liquid flow rate.

The weeping (W'/L) is plotted against the gas Reynolds number (Re_g) in Figure 106 for a water/air system and Tray 1 (15.8% fractional hole area with a hole diameter of 6.4 mm). The gas Reynolds number is shown by Equation 5.3.2.2.

$$Re_g = \frac{\rho_g u_h D_H}{\mu_g} \quad \rightarrow \quad \text{Gas Reynolds number} \qquad [5.3.2.2]$$

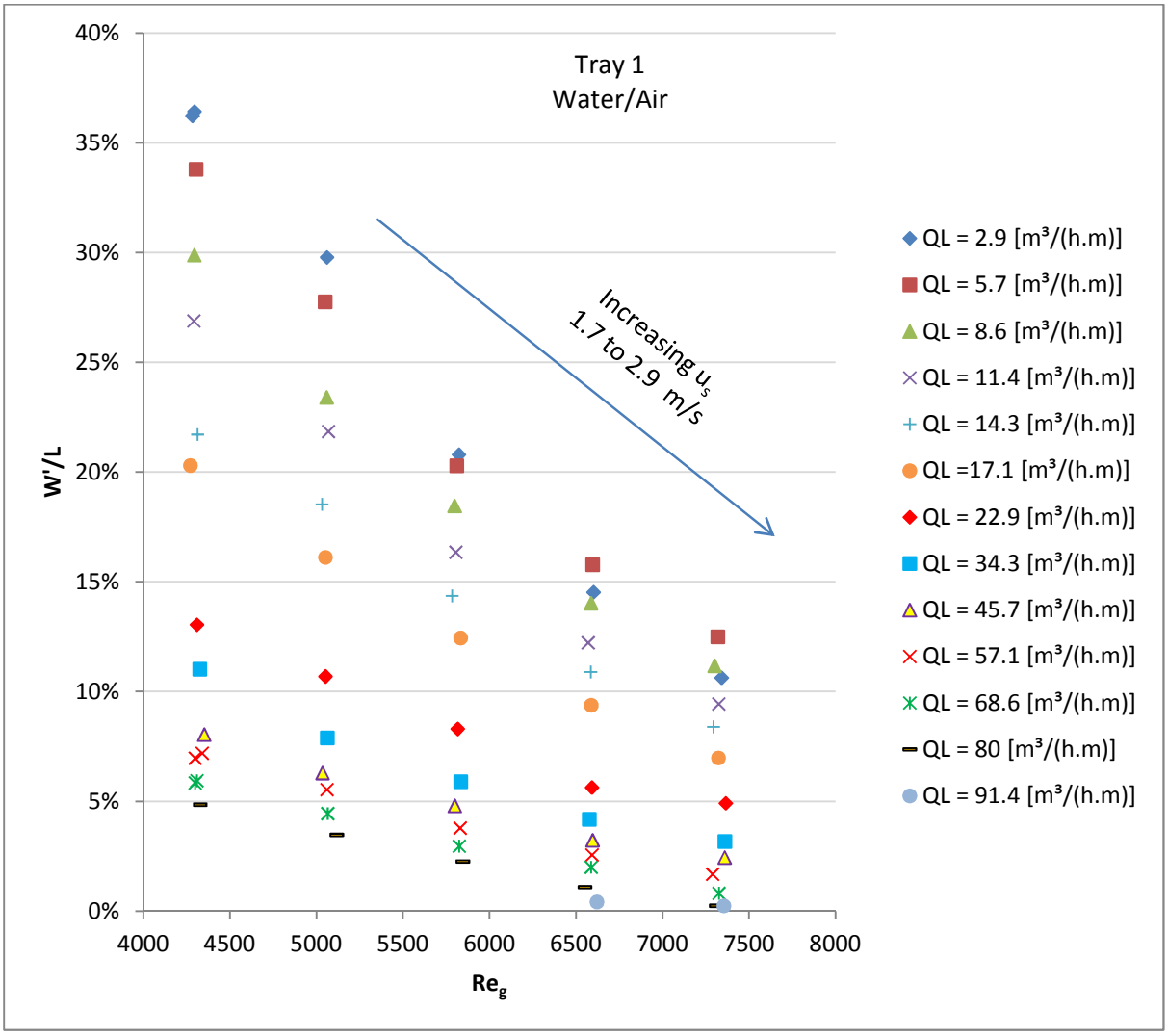

Figure 106 – Weeping (W'/L) changing with the gas Reynolds number (Re_g) for water/air with Tray 1 (15.8% fractional hole area, 6.4 mm hole diameter) at different liquid rates.

There is clearly a difference in the dependence of weeping (W'/L) in the spray regime and froth regime, where there is a clear decrease in the weeping from 17.1 m^3/(h.m) to 34.3 m^3/(h.m) (Fig. 106). The dependence of weeping on the gas Reynolds number shows that weeping decreases with increasing hole velocity.

The weeping (W'/L) is plotted against the flow Froude number (Fr^+) in Figure 107 with Tray 1 for a water/air system. The flow Froude number is represented by Equation 2.5.1.31 (Uys, 2012), where the flow Froude number includes only fluid flow terms, unlike the liquid hold-up Froude number (Fr_h^+) in Equation 5.3.2.1.

$$Fr^+ = \frac{3600 u_s^3}{g Q_L} \qquad \rightarrow \qquad \text{Flow Froude number} \qquad [2.5.1.31]$$

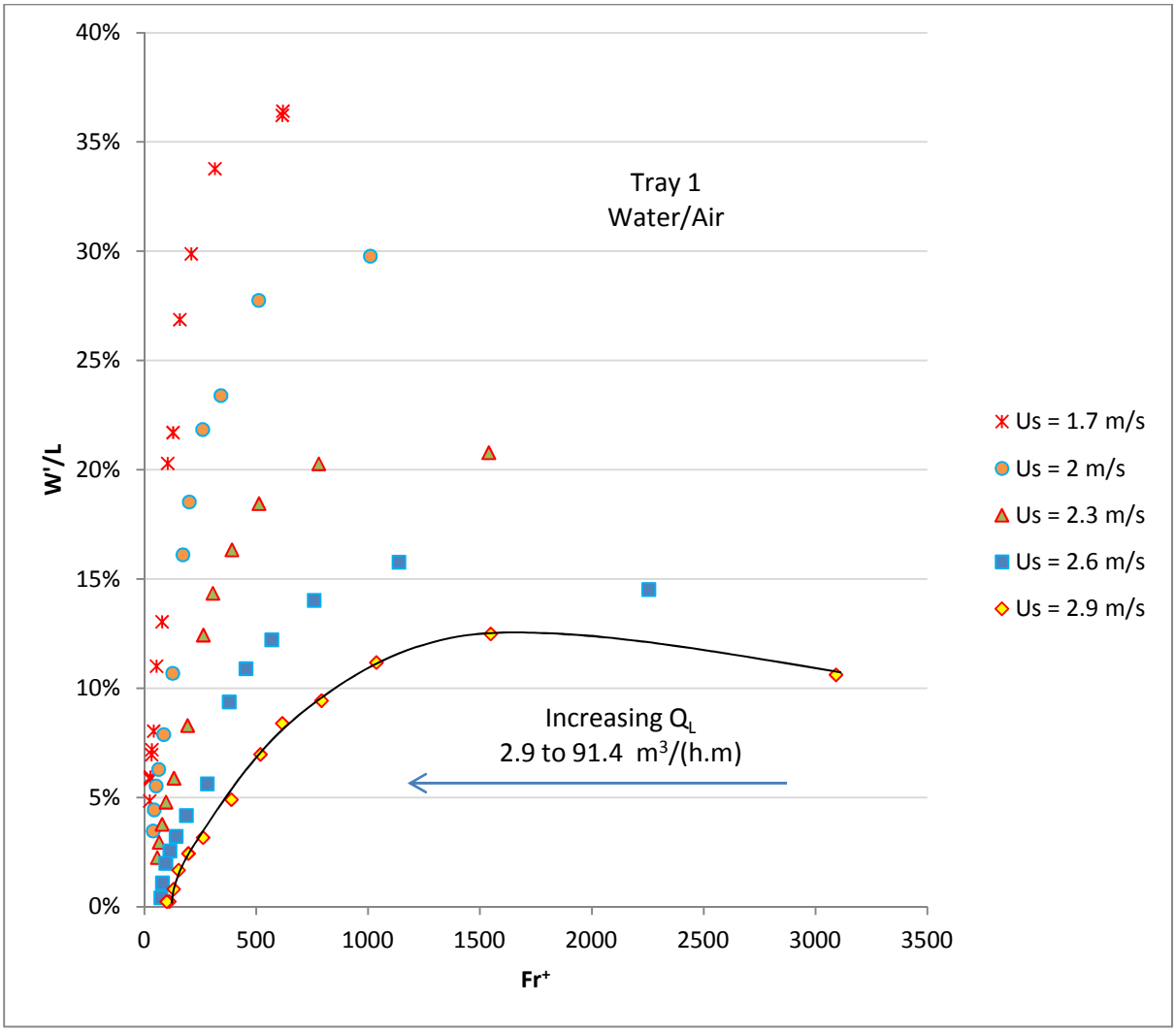

Figure 107 – Weeping (W'/L) changing with the flow Froude number (Fr) for water/air with Tray 1 (15.8% fractional hole area, 6.4 mm hole diameter) at different gas superficial velocities.

Weeping (W'/L) increases with increasing flow Froude number to a maximum as shown by the high gas superficial velocities and then decreases with increasing flow Froude number (Fig. 107). Over the entire range of the weeping investigation, weeping increases with decreasing superficial gas velocity.

Figure 107 shows that weeping (W'/L) decreases with increasing liquid flow rate as shown by the trend of the flow Froude number.

The effect of sieve tray geometry is evaluated in Figure 108, where weeping (W'/L) is plotted against the total lip length to weir height (h_{wo}) ratio for a water/air system. The total lip length is defined as the number of holes on a sieve tray multiplied by the circumference of the sieve tray holes (Equation 5.3.2.3). The aim of Figure 108 is to evaluate the impact of the total lip length in the spray regime during gas jetting through the sieve tray holes, where the weir height is kept constant for the current experimental investigation. Weeping (W'/L) has no distinctive dependence on the total lip length to weir height (h_{wo}) ratio, although it is shown that weeping is a stronger function of the fractional hole area than the hole diameter (Fig. 108).

$$Total\ lip\ length = (\pi d_H N_T) \qquad [5.3.2.3]$$

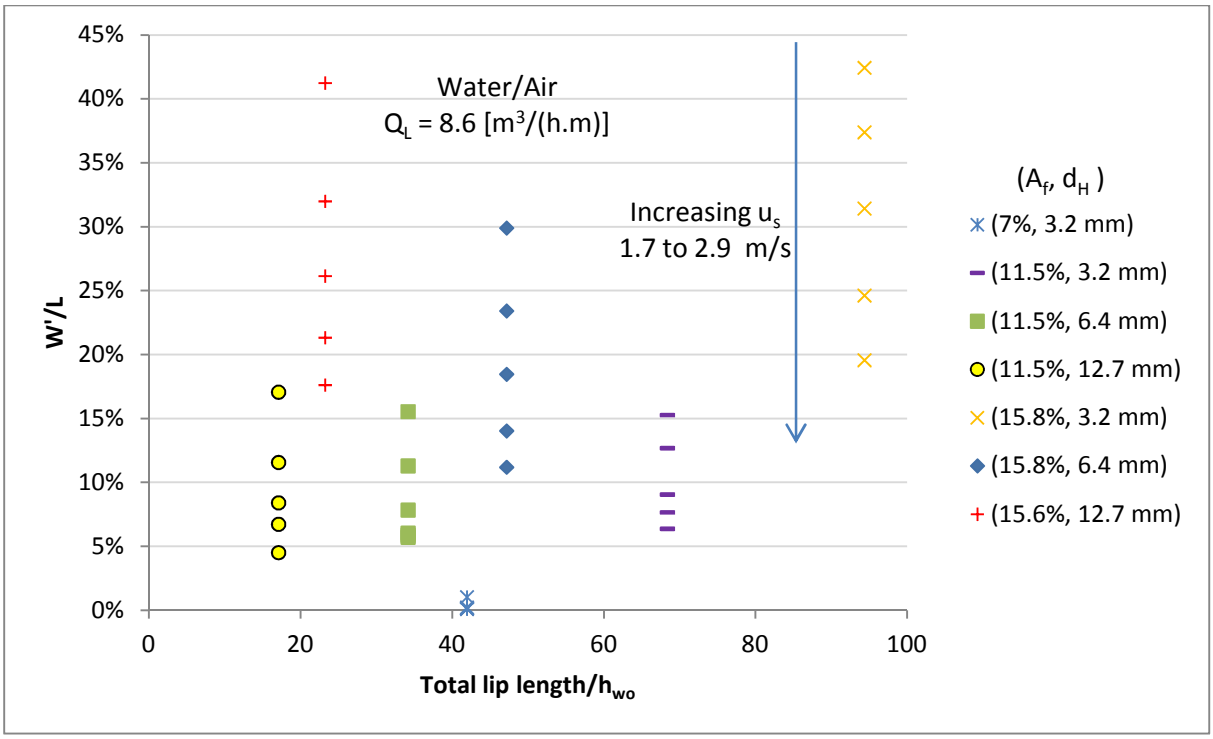

Figure 108 – Weeping (W'/L), changing with the tray hole total lip length divided by the weir height (h_{wo}) for water/air with different sieve trays at a liquid flow rate of 8.6 m^3/(h.m).

$$Co = \left(\frac{A_f S}{(D_c D_H)^{\frac{1}{2}}}\right) \qquad \rightarrow \qquad \text{Construction number} \qquad [2.5.1.20]$$

The effect of tray geometry on the weeping (W'/L) is evaluated using the construction number (Co) in Figure 109 (Kozoil and Mackowaik, 1990). The construction number relates the fractional hole area (A_f), tray spacing (S), column diameter (D_c) and hole diameter (D_h) to one another (Equation 2.5.1.20). The tray spacing is kept constant at 515 mm and the column diameter for the current rectangular column is determined making the area of the rectangular column equal to that of a round column. Weeping (W'/L) has no distinctive trend with the construction number (Fig. 109). The study with the dimensionless numbers showed that the grouping of dimensionless numbers investigated can possibly be used to develop a weeping model.

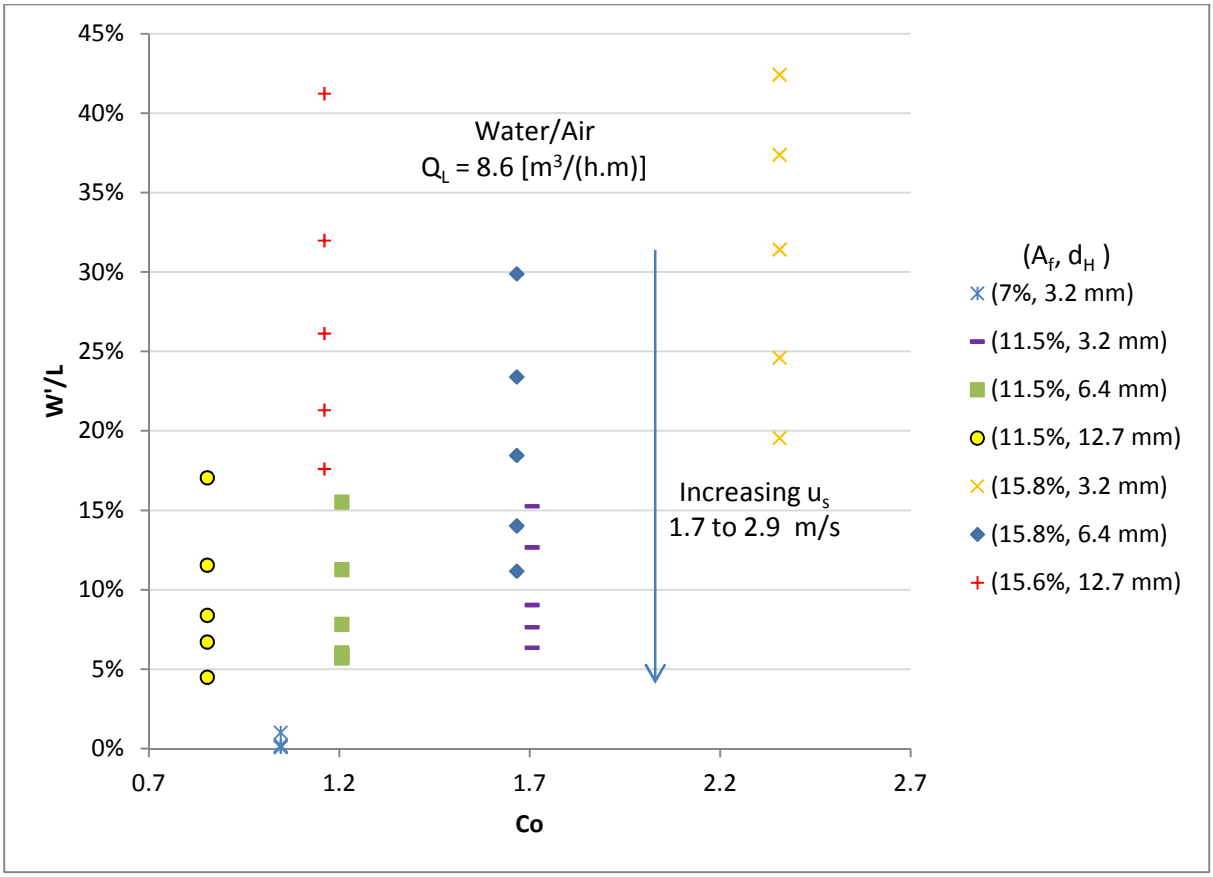

Figure 109 – Weeping (W'/L), changing with the construction number (Co) for water/air with different sieve trays at a liquid flow rate of 8.6 m^3/(h.m).

6.4 Hydrodynamic Hold-Up Result Evaluation

This section discusses the results for the liquid hold-up pressure findings and compares the trends observed to that of entrainment and weeping. The liquid hold-up graphs were determined by subtracting the dry tray pressure drop from the total pressure drop observed across the sieve tray when fluids are flowing through the distillation column.

The effect of the different liquids investigated in carbon dioxide systems on the liquid hold-up is shown in Figure 110 for Tray 1 at a superficial gas velocity of 1.7 m/s. The water has the highest liquid hold-up followed by ethylene glycol, silicone oil and butanol. The liquid hold-up follows a trend that is in direct contrast to that of entrainment when liquid properties are evaluated. Thus liquids that produce larger liquid hold-ups produce lower magnitudes of entrainment.

The magnitude of the liquid hold-up is directly related to the size of the froth layer in the dispersion layer above the tray as defined by Section 5.1.1, where a larger froth layer leads to a higher liquid hold-up. The difference in the liquid hold-up between the different liquids is larger in the froth regime [typically above 23 m^3/(h.m)] than in the spray regime [typically below 23 m^3/(h.m)], since a larger froth layer is observed in the former. The liquid hold-up can be used to model weeping, but it is highly dependent on the liquid physical properties. There is no clear trend for on a particular liquid physical property (Fig. 110). It is believed that the liquid hold-up has an opposite relationship with the liquid physical properties to that of entrainment.

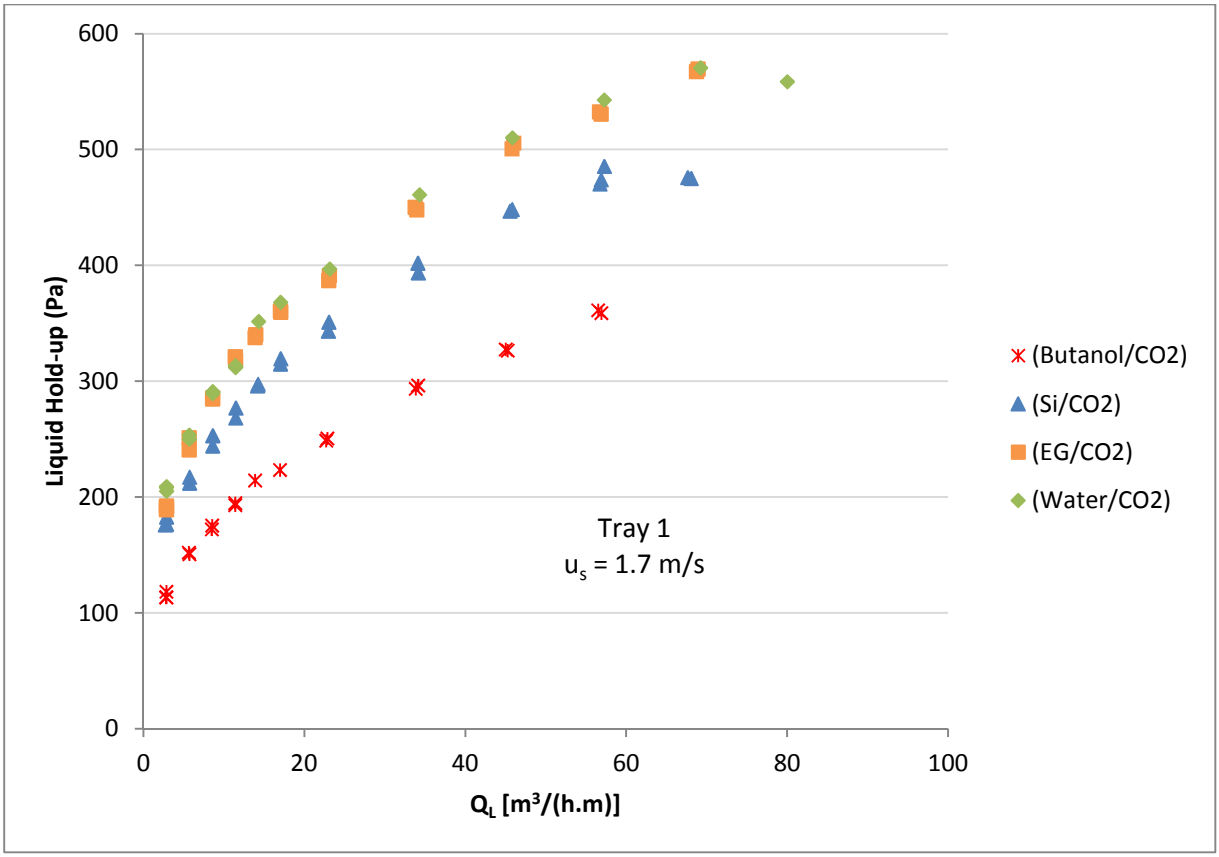

Figure 110 – Liquid hold-up of different liquids with CO_2 for Tray 1 (15.8% fractional hole area, 6.4 mm hole diameter) at a superficial gas velocity of 1.7 m/s.

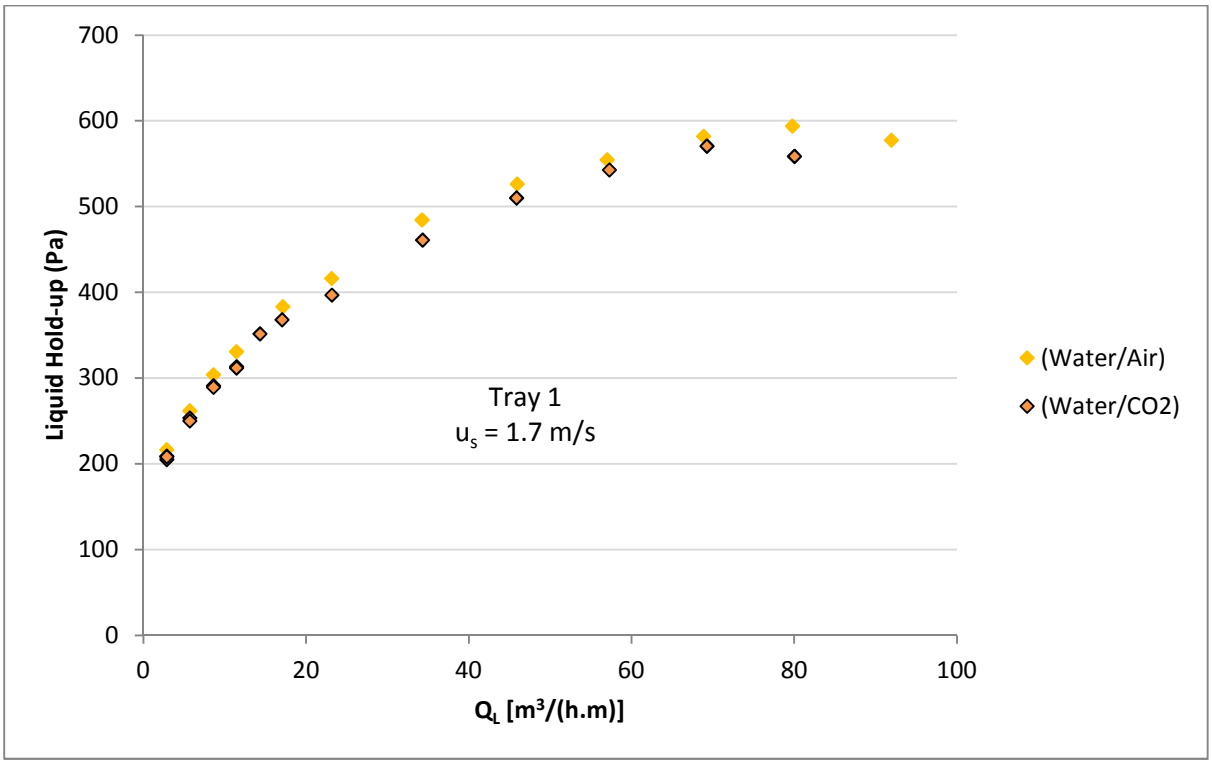

Figure 111 – Effect of gases in water systems on the liquid hold-up for Tray 1 (15.8% fractional hole area, 6.4 mm hole diameter) at a superficial gas velocity of 1.7 m/s.

The effect of different gases in water systems on the liquid hold-up is shown in Figure 111 for a superficial gas velocity of 1.7 m/s with Tray 1. The air system produces a marginally higher liquid hold-up than carbon dioxide, since air systems produce a smaller dispersion layer (liquid volume closer to tray floor). The dependency of the magnitude of the liquid hold-up on the gas physical properties is similar to that of weeping, although the dependency is opposite to that of entrainment observed (entrainment increases with increasing gas physical density).

Figure 112 shows the effect of the sieve tray hole diameter on the liquid hold-up for a fractional hole area of 15% with a water/air system. The liquid hold-up increases with decreasing tray hole diameter over the entire range of liquid flow rates, which is expected as it was earlier identified that the froth layer in the dispersion layer increases with decreasing tray hole diameter increasing the liquid hold-up. At intermediate liquid flow rates, the liquid hold-ups are at a similar value, which is a similar trend to that of the weeping and entrainment. The liquid hold-up is not the overall defining factor used to describe the entrainment and weeping since the dependencies on the hole diameter over the entire range of liquid flow rates are different.

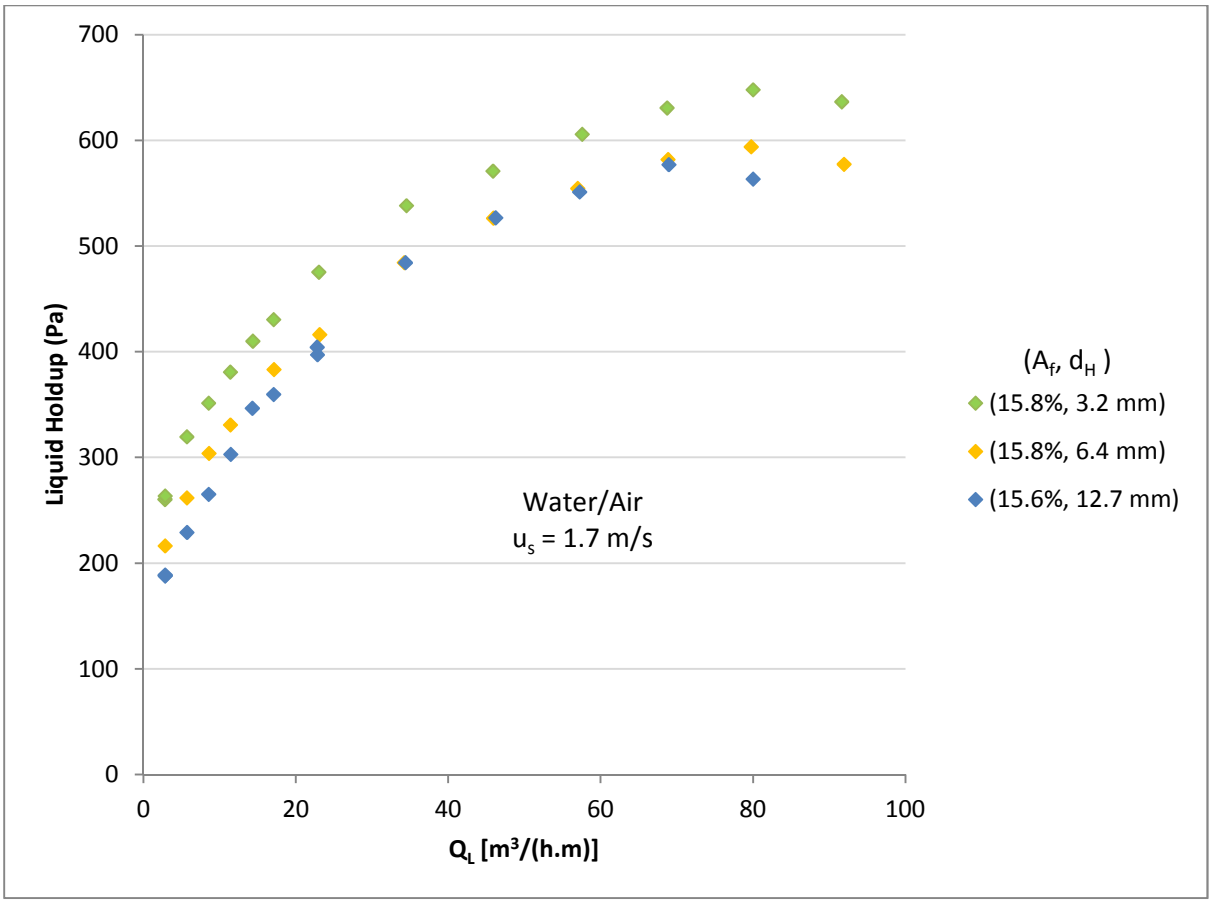

Figure 112 – Effect of hole diameter on the liquid hold-up for 15.8% fractional hole area trays in water/air at a superficial gas velocity of 1.7 m/s.

The effect of the fractional hole area on the liquid hold-up is shown in Figure 113 for a hole diameter of 6.4 mm. The liquid hold-up increases with increasing fractional hole area over the entire range of liquid flow rates investigated, which is expected since the froth layer increases in size with increasing

fractional hole area. The effect of the trend observed for the liquid hold-up for the fractional hole areas is similar to that of the weeping but not to the entrainment.

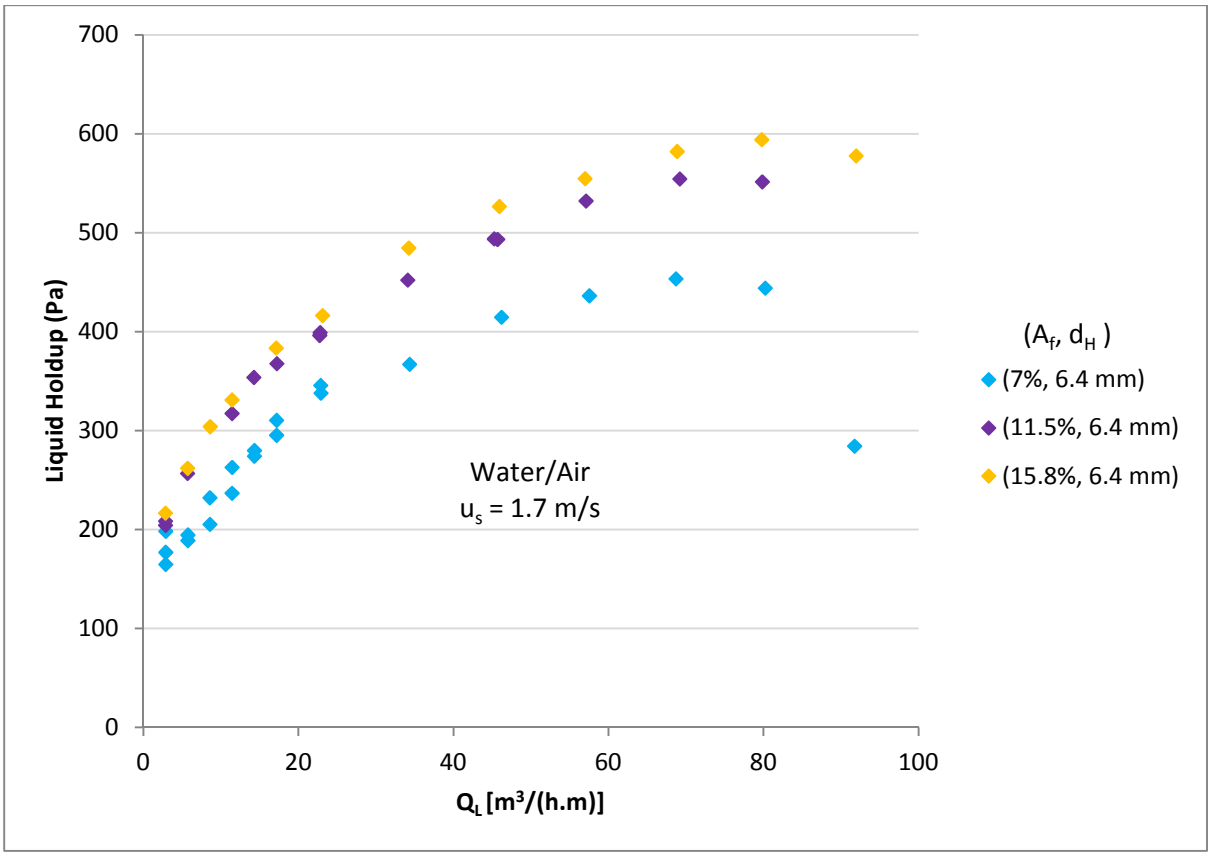

Figure 113 – Effect of fractional hole area on the liquid hold-up for 6.4 mm hole diameter trays in water/air at a superficial gas velocity of 1.7 m/s.

The liquid dispersion layer trends observed in the experimental investigation can be explained with Figure 5, where Profiles 1 to 5 represent the systematic change in dispersion layer patterns observed above the sieve tray as the liquid flow rate is increased. Profile 1 represents the dispersion layer in the spray regime, where the dispersion peak occurs at a low flow path length which allows two peaks to form in the dispersion layer, making the dispersion layer unstable. This increases the dependence of entrainment on the tray geometry (fractional hole area and hole diameter). Profile 1 represents low to moderate liquid flow rates where the peak of the dispersion layer occurs on the inlet half of the tray (Fig. 5). As the height of the dispersion layer drops from the peak (liquid falls to the tray floor) with increasing flow path length a high pressure zone is created, causing weeping in the froth regime. A low liquid fraction is believed to be present at the tray floor in zones with high dispersion peaks. The liquid flow trajectory corresponds best with the upward gas flow trajectory where a liquid jump is observed at the peak of the dispersion layer (gas flow through the sieve tray holes causes no weeping at the low pressure zones).

A high pressure zone is observed at the beginning of the dispersion layer as the liquid enters the tray and before a hydraulic jump. As the liquid flow rate increases, the dispersion layer shape changes from Profiles 1 to 2 and then to 3, where Profiles 2 and 3 show typical dispersion layer trends for intermediate liquid flow rates. At intermediate liquid flow rates [around 25 to 50 m^3/(h.m)], the

dispersion layer becomes stable and less dependent on the upward gas force and more dependent on the horizontal liquid force. Profile 2 describes froth regime dispersion at higher liquid flow rates (higher than Profile 1), where the dispersion layer peak is higher (longer hydraulic dispersion jump) and occurs at a higher flow path length, thus the higher pressure zone occurs at a higher flow path length (see Fig. 5).

As the liquid flow rate increases, the dispersion layer shape changes from Profiles 3 to 4, which causes the liquid dispersion layer to change the force dependency from horizontal liquid flow rate force to upward gas force (at high liquid rates in the froth regime). As the liquid flow rate increases to Profile 4, the gas velocity upward through the sieve tray holes and the high liquid cross flow causes the liquid to jump (hydraulic jump) over the entire flow path length leading to a zero weeping magnitude. At high liquid flow rates, entrainment increases as the dispersion layer height increases (Profiles 4 to 5), because of the increase in the hole gas velocity as the tray fraction hole area decreases. At this point, the dispersion layer becomes highly dependent on the gas velocity, where high gas velocities lead to entrainment flooding.

6.5 Weeping Results Summary

1) The effect of liquid and gas physical properties:
   i) An increase in the surface tension, liquid density and liquid viscosity leads to an increase in weeping, where liquid density has a strong effect on weeping.
   ii) Gases with a high density have a higher mass flow rate through the sieve tray at a constant superficial gas velocity, consequently increasing the interaction between the gas and liquid. Such increased interaction produces a larger dispersion layer by lifting a larger portion of the liquid away from the tray floor, thereby decreasing the magnitude of weeping.
2) The effect of tray fractional hole area and hole diameter:
   i) The amount of weeping increases with increasing tray fractional hole area, due to a decrease in the dispersion layer's height at a constant superficial gas velocity.
   ii) There is no clear trend between the tray hole diameter and the magnitude of weeping
   iii) The 12.7 mm hole size caused notably less weeping than the 3.2 mm and 6.4 mm trays at higher liquid flow rates.
3) Dimensionless number analysis:
   i) By grouping dimensionless numbers like the liquid hold-up Froude number, Weber number, Reynolds number, flow Froude number, construction number and the fluid density ratio, a comprehensive weeping model can be developed.
   ii) Based on the weeping (W'/G) trends with the dimensionless numbers in the spray regime, weeping (W'/G) increases with decreasing hole diameter, gas density, gas viscosity, superficial gas velocity and increasing liquid hold-up, liquid flow rate, liquid density, liquid viscosity and liquid surface tension (opposite to the entrainment).

Chapter 7 - Conclusions

Multiple flow regimes were recognised in the literature review, whereas in the experimental investigation the dispersion layer was only categorised into the spray regime [typically below a liquid flow rate of 23 m^3/(h.m)] and froth regime [typically above a liquid flow rate of 23 m^3/h.m]. Contrary to literature, a minima in entrainment on the L'/G graph is not necessarily representative of the transition from the froth to the spray regime. Rather, it is believed that the regime transition happens across a liquid flow range, around 23 m^3/(h.m), depending on the experimental variables. The dispersion layer above the sieve tray consisted of two layers namely, the froth layer (bottom liquid layer) and the spray layer (top droplet layer). At low liquid flow rates, the oscillatory behaviour of the dispersion layer in different directions increased, whereas at high liquid flow rates the dispersion layer appeared to be more uniform and stable across the tray. The gas jet associated with the spray regime could be identified visually at low liquid flow rates.

The experimental results for the entrainment (L'/L) and weeping (W'/L) were found to be repeatable. The experimental data had a standard deviation of 0.21% and a percentage deviation as high as 9.93% at high entrainment ratios (L'/L) and a standard deviation of 0.9% and a percentage deviation as high as 7.6% at high weeping ratios (W'/L). The experimental entrainment data followed the same trend as that of Uys (2012), where the differences in entrainment magnitude were attributed to equipment and experimental error, typical of these hydrodynamic studies. The experimental L'/L entrainment compared reasonably well with the data produced by Nutter (1971). Differences between Nutter (1971) and this work are attributed to the differences in column geometry and slight difference in the fluid physical properties and tray geometry.

As an initial objective, the effect of liquid physical properties on entrainment and weeping was investigated. The differences between entrainment for the different liquids investigated were found to be more significant in the spray regime than in the froth regime. A higher entrainment magnitude was found due to larger spray layer dispersion above the sieve tray in the spray regime. Butanol was entrained more easily than silicone oil, ethylene glycol and water, where fluids with larger spray layers in the dispersion layer produced a larger entrainment magnitude (L'/L as high as 35% for butanol).

The liquid viscosity has a high influence on entrainment in the spray regime, after which its significance decreases as the dispersion tends to the froth regime. Entrainment increased with decreasing liquid density, decreasing liquid surface tension and decreasing liquid viscosity, where the more unstable the dispersion, the higher the entrainment. Ethylene glycol had the highest weeping followed by water, silicone oil and butanol with the lowest (W'/L as high as 45% for ethylene glycol). Fluids with larger froth layer dispersions produced a higher amount of weeping; on the other hand fluids that produced a larger spray layer produced the lowest amount of weeping (lower liquid fraction closer at tray floor). The trends observed by the liquid systems showed that the liquid density was a strong defining parameter used to describe weeping, where weeping increases with increasing liquid density.

Carbon dioxide was observed to have a higher entrainment at a constant superficial gas velocity, where entrainment trends were similar for air and carbon dioxide. The differences between the

entrainment of carbon dioxide and air systems increased with increasing superficial gas velocity. The weeping trends are similar for air and carbon dioxide systems, although air was observed to have a higher weeping magnitude than carbon dioxide at constant gas superficial velocities. Gases with a high density have a higher mass flow rate, increasing the interaction between the liquid and the gas, which in turn results in an increase in entrainment and decreasing weeping.

In the spray regime, entrainment increased with decreasing tray fractional hole area. The dependence of entrainment on tray fractional hole area increased as the fractional hole area decreased in the spray regime (over 100% higher between 7% and 11% fractional hole area). Weeping increased with increasing tray fractional hole area. The change in weeping magnitude between the 7% and 11% fractional hole areas was considerably less than the difference between the 11% and 15% fractional hole areas. In the spray regime the dependence of weeping on the fractional hole area increased as the fractional hole area decreased.

In the spray regime, entrainment increased with increasing sieve tray hole diameter, where the impact that tray hole diameter size has on entrainment increased with increasing hole diameter (over 100% higher between. 6.4 mm and 12.7 mm hole). The sieve tray hole diameter was shown to have a small effect on entrainment at moderate to high liquid flow rates [approximately between 23 and 60 $m^3/(h.m)$]. At high liquid flow rates [typically above 60 $m^3/(h.m)$], the influence of the tray hole diameter on entrainment increased. Entrainment was shown to increase with decreasing hole diameter at high liquid rates in the froth regime. In the evaluation of the effect of the sieve tray hole diameter on weeping, the trends differed notably with changing fluid combinations. Furthermore, the 12.7 mm hole size caused notably less weeping than the 3.2 mm and 6.4 mm trays at higher liquid flow rates.

At low liquid flow rates the fluid dispersion layer peak occurred at a low flow path length. Consequently, more than one fluid dispersion layer peak and localised pressure zone could develop before the liquid reached the overflow weir. This amplified the dependence of entrainment on the fractional hole area in the specific test rig. It was concluded that weeping occurred preferentially at so-called localised high pressure zones on the sieve tray at the beginning of the fluid dispersion layer as the liquid enters the tray before the dispersion layer peak. A low liquid fraction was thought to be present at the tray floor in zones with high dispersion peaks. In these zones, the liquid flow trajectory corresponds best with the upward gas flow trajectory (i.e. the liquid ‘jumps’ over tray holes). At higher liquid flow rates, dispersion peaks were higher (longer hydraulic dispersion jump) and occurred at a higher flow path length, thus the higher pressure zone occurs at a higher flow path length. At high gas and liquid flow rates, the extended dispersion layer allowed minimal intimate contact between the plate and the liquid (minimising such localized high-pressure zones). In effect, the liquid ‘jumped’ over the entire flow path length in the test rig, thus resulting in low amounts of weeping at high gas and liquid flow rates.

The Kister (1992) and Bennett and Ludwig (1994) models were shown to explain water/air systems trends with a minimal deviation, but deviated significantly when other combinations of fluid system were used. A fundamental dimensionless number analysis confirmed that well-known dimensionless numbers could be used to develop entrainment and weeping correlations. The flow Froude number was shown to be the most useful dimensionless number since it had a monotonic relationship with entrainment for a particular system and tray configuration. The construction number was shown to

be a useful dimensionless number that could be used to describe the effect of tray geometry on entrainment. The flow Froude number and construction number ratio (Fr^{+}/Co^{n}) with the construction number to the power of 1.5 for ethylene glycol/air, 1.65 for water/air and 1.2 for a silicone-oil/air system explained the effect sieve tray hole diameter has on the entrainment well. In the same way the flow Froude number (Fr^{+}) and construction number (Co) ratio with the construction number to the power of 1.3 for ethylene glycol/air, 1.6 for water/air and 1.15 for a silicone-oil/air system explained the effect fractional hole area on entrainment well.

The fluid density ratio was shown to be a useful dimensionless number that could be used to describe the effect of gas properties on entrainment. The effect of the gas physical properties are explained well when the flow Froude number is multiplied by the fluid density ratio to the power of 0.8 for the silicone oil, 1 for the ethylene glycol and 1.3 for water systems. The liquid hold-up Froude number explained the trend of weeping well, where it was shown that weeping is not linearly dependent on the liquid hold-up Froude number. Ultimately the entrainment and weeping hydrodynamic study showed a wide experimental database is essential to completely characterise the flow of fluid inside a sieve tray distillation column and that all the distillation parameter hydrodynamic effects need to be understood.

Chapter 8 - Recommendations

This section highlights the steps to be taken in order to broaden the understanding of sieve tray distillation processes. In the current experimental investigation the effect of fluid properties on the entrainment and weeping could not be fully separated from one another. The effect of the tray geometry could not be fully described, especially the effect that hole diameters has on weeping because of the small number of tray geometry parameters investigated. The steps that need to be followed in order to better understand and describe sieve tray distillation hydrodynamics are as follows:

1. A principal component analysis should be performed in order to better understand which parameters affect entrainment and weeping the most and which parameters should be further investigated.
2. Use sieve trays where the weir height can be altered. By altering the weir heights of the sieve trays a better understanding of the shape of the liquid dispersion layers will be produced, where the effect of the spray layer and the froth layer will be improved. The weir height experiments will produce a more comprehensive entrainment and weeping model.
3. Perform experimental investigations into the effect of the flow path length and tray hole pitch length of a sieve tray distillation column. By performing flow path length experiments, a better understanding of the effect of dispersion layer peak development can be produced. A better understanding of flow dispersion layer stability can be produced for the spray and the froth regime.
4. Increase the amount of liquids and gases in the experimental database for the entrainment and weeping experiments. By broadening the amount of gases and liquids investigated, a larger range of fluid properties can be produced, thus increasing the understanding of the effect of the each fluid physical property. The larger experimental database will allow the separation of the effects of the different gas and fluid physical property trends. The combined effects of the interactions of the different fluid physical properties will be evaluated.
5. Investigate the effect of round distillation columns with a similar perforated area to that of a rectangular distillation column. If experiments are performed on a round distillation column, a better understanding of the significance of the expansion effects at the downcomer tray entrance and contraction of the fluid at the outlet weir will be produced. Thus a correction term can be produced for entrainment and weeping in round and rectangular columns.
6. Increase the amount of different sieve trays investigated by altering the hole diameter and fractional hole area of the tray. This will aid in the understanding of the effect of tray geometry on entrainment and weeping especially since the effect of hole diameter could be described from system to system for weeping magnitude experiments.
7. Evaluate the effect of punch sieve tray holes and laser cut sieve tray holes on entrainment and weeping. The effect of punching tray holes and laser cut sieve trays have to be determined, where most industrial sieve trays are punched, since it is a cheaper process. By performing tray hole machining methods experiments, the effect on the liquid hold-up, entrainment and weeping can be better understood by understanding what effect it has on the dispersion layer characteristics.

8. Perform experimental investigations into the dispersion layer density or droplet size of different fluids at different locations above the sieve tray. By understanding the dispersion layers density and droplet diameter and velocity at different flow settings, a complete description of the dispersion layer can be given at every flow setting.
9. Develop an entrainment model and weeping model based on the composite database of the current experimental results and the recommended distillation experiments. Models need to be developed to better describe entrainment and weeping since literature models do not fully explain the trends well and the literature models do not have a large experimental database and are not comprehensive.
10. Develop a CFD (Computational Fluid Dynamics) model for entrainment and weeping. By understanding the dispersion layer trends and producing a large experimental database, a CFD model could perhaps be produced that will aid understanding of the effect of different parameters without the need for pilot plant experimentation.

Chapter 9 – References

1. Bain, J.L. and Van Winkle, M. (1961) 'A Study of Entrainment, Perforated Plate Column – Air-Water System', *AIChE Journal*, vol. 7, no. 3, September, p. 363.

2. Bennett, D.L., Agawal, R. and Cook, P.J. (1983) 'New pressure drop correlation for sieve tray distillation columns', *AIChE Journal*, vol. 29, no. 3, pp. 434-436.

3. Bennett, D.L., Kao, A.S. and Wong, L.W. (1995) 'A Mechanistic Analysis of Seive Tray Froth Height and Entrainment', *AIChE Journal*, vol. 41, no. 9, September, pp. 2067-2081.

4. Bennett, D.L. and Ludwig, K.A. (1994) 'Understand the Limitations of Air/Water Testing of Distillation Equipment', *Chemical Engineering Progress*, vol. 90, no. 113, April, pp. 72-79.

5. Bennett, D.L., Watson, D.N. and Wiescinski, M.A. (1997) 'New Correlation for Sieve-Tray Point Efficiency, Entrainment, and Section Efficiency', *AIChE Journal*, vol. 43, no. 6, June, pp. 1611-1624.

6. Calcaterra, R.J., Nicholls, C.W. and Weber, J.H. (1968) 'Free and Capture entrainment and plate spacing in a perforated tray column', *British Chemical Engineering*, vol. 13, no. 9, September, pp. 1294-1297.

7. Chen, G.X., Chuang, K.T., Chien, C. and Ye, Y. (1992) 'Mass Transfer and Hydraulics of Packed Sieve Trays', *Gas Separation and Purification*, vol. 6, no. 4, pp. 207-213.

8. Colwell, C.J. (1981) 'Clear Liquid Height and Froth Density on Sieve Trays', *Industrial Engineering Chemical Process Design*, vol. 20, no. 2, pp. 298-307.

9. De Goederen, C.W.J. (1965) 'Distillation tray efficiency and interfacial area', *Chemical Engineering Science*, vol. 20, May, pp. 1115-1124.

10. Decent, S.P., King, A.C., Simmons, M.J.H., Parau, E.I., Wallwork, I.M., Gurney, C.J. and Uddin, J. (2009) 'The Trajectory and Stability of a Spiralling Liquid Jet: Viscous Theory', *Applied Mathematical Modelling*, vol. 33, pp. 4283-4302.

11. Fakhari, A. and Rahimian, M.H. (2010) 'Investigation of Deformed and Breakup of a Falling Droplet Using a Multiple-Relaxation-Time Lattice Boltzmann Method', *Computers and Fluids*, vol. 40, August, pp. 156-171.

12. Faesan, S.O. (1987) 'Hydraulic Characteristics of Sieve and Valve Trays', *Industrial Engineering Chemical Research*, vol. 26, no. 10, May, pp. 2114-2121.

13. Fractional Research, Inc. (2009) 'On Distillation Tray Weir Loadings', Distillation Symposium, 1-13.

14. Fractionation Research, Inc. (2011) 'Modeling Fraction Jetting on Distillation Trays', The Dr. James Fair Heritage Distillation Symposium, Chicago, 1-9.

15. Hofhuis, P.A.M. and Zuiderweg, F.J. (1979), IChemE Symposium series No. 56, 2.2/1.

16. Hunt, C.D., Hanson, D.N. and Wilke, C.R. (1955) 'Capacity Factor in the Performance of Perforated-plate Columns', *AIChE Journal*, vol. 1, no. 4, December, pp. 441-451.

17. Hu, B., Yang, H.-m. and Hewitt, G.F. (2007) 'Measurement of Bubble Size Distribution Using A Flying Optical Probe Technique: Application in the Highly Turbulent Region Above a Distillation Plate', *Chemical Engineering Science*, vol. 62, January, pp. 2652-2662.

18. Jacimovic, B.M. and Genic, S.B. (2000) 'Froth Porosity and Clear Liquid Height in Trayed Columns', *Chemical Engineering and Technology*, vol. 23, no. 2, pp. 171-176.

19. Jeronimo, M.A.d.S. and Sawistowski, H. (1973) 'Phase Inversion Correlation for Sieve Trays', *Trans. Institution of Chemical Engineers*, vol. 51, pp. 265-.

20. Keskinen, K.I., Ahlfors, H.-M. and Aittamaa, J. (2006) 'Hydraulic Measurements of Sieve Plate', *IChemE*, no. 152, July, pp. 920-925.

21. Kister, H.Z. (1992) *Distillation Design*, McGraw-Hill.

22. Kister, H.Z. and Haas, J.R. (1988) 'Entrainment from Sieve Trays in the Froth Regime', *Industrial Engineering Chemistry*, vol. 27, no. 12, July, pp. 2331-2341.

23. Kister, H.Z. and Haas, J.R.H. (1990) 'Predict Entrainment Flooding on Sieve and Valve Trays', *Chemical Engineering Progress*, vol. 89, no. 9, September, pp. 62-69.

24. Kister, H.Z., Pinczewski, W.V. and Fell, C.J.D. (1981) 'Entrainment from Sieve Trays Operating in the Spray Regime', *Industrial Engineering Chemical Process Design*, vol. 20, no. 3, April, p. 528.

25. Kozoil, A. and Mackowaik, J. (1990) 'Liquid Entrainment in Tray Columns with Downcomers', *Chemical Engineering and Processing: Process Intensification*, vol. 27, October, pp. 145-153.

26. Lamprecht, S.M., Knoetze, J.H., and Burger, A.J. (2010) 'Establishing the Faculty to Measure Packed Column Hydrodynamics'. Stellebosch: Stellenbosch University.

27. Lemieux, E.J. and Scotti, L.J. (1969) 'Perforated Tray Performance', *Chemical Engineering Progress*, vol. 65, no. 3, March, pp. 52-58.

28. Lockett, M.J. (1981) 'The Froth to Spray Transition on Sieve Trays', *Institution of Chemical Engineers*, vol. 59, pp. 26-34.

29. Lockett, M.J. (1986) *Distillation tray fundamentals*, New York: Cambridge University Press.

30. Lockett, M.J. and Banik, S. (1986) 'Weeping in Sieve Trays', *Industrial Engineering Chemical Process Design and Development*, vol. 25, no. 2, pp. 561-569.

31. Lockett, M.J., Spiller, G.T. and Porter, K.E. (1976) 'The Effect of the Operating Regime on entrainment from Sieve Plates', *Trans. Institution of Chemical Engineer*, vol. 54, March, pp. 202-204.

32. Loon, R.E., Pincewski, W.V. and Fell, C.J.D. (1973) 'Dependence of the Froth-to-Spray Transition on Sieve Tray Design Parameters', *Trans. Institution of Chemical Engineers*, vol. 51, April, pp. 374-376.

33. Mahiout, S. and Vogelpohl, A. (1984) 'Mass Transfer in High Viscosity Media', *Chemical Engineering Processes*, vol. 18, pp. 225-232.

34. Mayfield, F.D., Church, W.L., Green, A.C., Lee, D.C. and Rasmussen, R.W. (1952) 'Perforated-Plate Distillation Columns', *Engineering and Process Development*, vol. 44, no. 9, September, pp. 2238-2249.

35. Mohan, T., Rao, K.K. and Rao, D.P. (1983) 'Effect of Vapor Maldistribution and Entrainment on Tray Efficiency', *Industrial Engineering Chemical Process Design*, vol. 22, no. 3, pp. 380-385.

36. Nutter, D.E. (1971) 'Ammonia Stripping Efficiency Studies', *American Institute of Chemical Engineering Symposium Series*, vol. 68, no. 124, pp. 73-83.

37. Ohe, S. and Yanagi, T. (2001) 'Entrainment Characteristics on Distillation Trays', AiChE Annual Meeting, Nevada, 70-76.

38. Olujic, Z., Jodecke, M., Skilkin, A., Schuch, G., Kaibel, B., (2009) 'Equipment improvement trends in distillation', Chem. Eng. Process., 48, 1089-1104.

39. Pan, K.L. and Hung, C.Y. (2010) 'Droplet Impact Upon a Wet Surface with Varied Fluid and Surface Properties', *Journal of Colloid and Interface Science*, vol. 352, no. 1, pp. 186-193.

40. Payne, G.J. and Prince, R.G.H. (1975) 'The Transition from Jetting to Bubbling at a Submerged Orifice', *Trans. Institution of Chemical Engineers*, vol. 53, March, pp. 209-223.

41. Payne, G.J. and Prince, R.G.H. (1977) 'The Relationship between the Froth and Spray Regimes, and the Orifice Processes Ocurring on Perforated Distillation Plates', *IChemE*, vol. 55, March, pp. 266-273.

42. Pinczewski, W.V., Benke, N.D. and Fell, C.J.D. (1975) 'Phase Inversion on Sieve Trays', *AIChE Journal*, vol. 21, no. 6, November, pp. 1210-1212.

43. Pinczewski, B.E. and Fell, C.J.D. (1972) 'The Transition from Froth-to-Spray Regime on Commercially Loaded Sieve Trays', *Trans. Institution of Chemical Engineers*, vol. 50, pp. 102-.

44. Pinczewski, W.V. and Fell, C.J.D. (1974) 'Nature of the Two-Phase Dispersion on Sieve Plates Operating in the Spray Regime', *Trans. Institution of Chemical Engineers*, vol. 52, April, pp. 294-299.

45. Pinczewski, W.V. and Fell, C.J.D. (1975) 'Oscillations on Sieve Trays', *AIChE Journal*, vol. 21, no. 5, September, pp. 1019-1021.

46. Pinczewski, W.V. and Fell, C.J.D. (1977) 'Droplet Sizes on Sieve Plates Operating in the Spray Regime', *Trans. Institution of Chemical Engineers*, vol. 55, May, pp. 46-52.

47. Pinczewski, W.V. and Fell, C.J.D. (1982) 'Froth to Spray Transition on Sieve Trays', *Industrial Engineering Chemical Process Design*, vol. 21, no. 4, May, pp. 774-776.

48. Porter, K.E. and Jenkins, J.D. (1979) 'Distillation 1979', IChemE no. 56, 5.1/1.

49. Porter, K.E. and Wong, P.F.Y. (1969) 'Transition from Spray to Bubbling on Sieve Plates', Institution of Chemical Engineers, London, 222-233.

50. Puppich, P. and Geodecke, R. (1987) 'Investigation of Entrainment in Tray Columns', *Chemical Engineering Technology*, vol. 10, pp. 224-230.

51. Rahimi, R., Sotoodeh, M.M. and Bahramifar, E. (2012) 'The Effect of Tray Geometry on the Sieve Tray Efficiency', *Chemical Engineering Science*, vol. 76, January, pp. 90-98.

52. Raper, J.A., Kearney, M.S., Burgess, J.M. and Fell, C.J.D. (1981) 'The Structure of Industrial Sieve Tray Froths', *Chemical Engineering Science*, vol. 37, no. 4, pp. 501-506.

53. Resetarits, M.R. and Ogundeji, A.Y. (2009) 'On Distillation Tray weir Loadings', AIChE Spring Meeting, Tampa, 1-13.

54. Seader, J.D. and Henley, E.J., (1998) Separation Process Principles, John Wiley & Sons, Inc.

55. Seader, J.D. and Henley, E.J. (2006) *Separation Process Principles*, 2nd edition, Hoboken: John Wiley and Sons, Inc.

56. Shen Li, Q., Song, C.Y., Wu, H.L., Liu, H. and Qian, Y.Q. (2008) 'Performance and application of flow-guided sieve trays for distillation of highly viscous mixtures', *Chemical Engineering*, vol. 25, May, pp. 1509-1513.

57. Souders, M. and Brown, G.G. (1934) 'Design of Fractionating Columns (Entrainment and Capacity)', *Industrial and Engineering Chemistry*, vol. 25, no. 1, January, pp. 98-103.

58. Stichlmair, J. (1978) *Grundlagen der Dimensionierung a Gas/Fluessig keit – kontakt apparatus Bodenkolonne*, John Wiley, TU Munchen.

59. Thomas, W.J. and Ogboja, O. (1978) 'Hydraulic Studies in Sieve Tray Columns', *Industrial Engineering Chemical Process Design*, vol. 17, no. 4, April, pp. 429-443.

60. Uys, E.C. (2012). 'The influence of gas and liquid physical properties on entrainment inside a sieve tray column'. Stellenbosch.

61. Uys, E.C., Knoetze, J. H., and Burger, A.J. (2009) 'Entrainment in Air/Water System Inside a Sieve Tray Column'. Stellenbosch: Stellenbosch University.

62. Uys, E.C., Schwarz, C.E., Burger, A.J. and Knoetze, J.H. (2012) 'New Froth Behaviour Observation and Comparison of Experimental Sieve Tray Entrainment Data with Existing Correlations', *Chemical Engineering Research and Design*, vol. 90, no. 12, May, pp. 2072-2085.

63. Van Sinderen, A.H., Wijn, E.F. and Zanting, R.W.J. (2003) 'Entrainment and Maximum Vapour Flow Rate of Trays', *IChemE*, vol. 81, January, pp. 94-107.

64. Wijn, E.F. (1999) 'Weir flow and liquid height on sieve and valve trays', *Chemical Engineering Journal*, vol. 73, August, pp. 191-204.

65. Yanagi, T. and Sakata, M. (1982) 'Performance of a Commercial Scale 14% Hole Area Sieve Tray', *Industrial Engineering Chemical Process Design*, vol. 21, no. 4, May, pp. 712-717.

66. Zuiderweg, F.J. (1982) 'Sieve Trays – A View on the state of the art', *Chemical Engineering Science*, vol. 37, no. 10, April, pp. 1441-1464.

67. Zuiderweg, F.J., Hofhuis, P.A.M. and Kuzniar, J. (1984) 'Flow Regimes on Sieve Trays: The Significance of the Emulsion Flow Regime', *Institution of Chemical Engineers*, vol. 62, January, pp. 39-47.

Appendix A – Extended Literature Analysis

A.1 Dispersion Liquid and Clear Liquid

In equation 2.2.5, 'C_d' represents the weir coefficient which is determined by equations A.1.1 and A.1.2 (Colwell, 1981), where 'H_{ow}' and 'H_{wo}' represents the height of the froth flowing over the weir and the height of the weir, respectively.

$$C_d = 0.61 + 0.08\frac{H_{ow}}{H_{wo}}; \qquad \frac{H_{ow}}{H_{wo}} \leq 8.135 \qquad \text{[A.1.1]}$$

$$C_d = 1.06\left(1 + \frac{H_{wo}}{H_{ow}}\right)^{1.5}; \qquad \frac{H_{ow}}{H_{wo}} \geq 8.135 \qquad \text{[A.1.2]}$$

$$H_{ow} = H_F - H_{wo} \qquad \text{[A.1.3]}$$

In equation A.1.4 'H_F' is the height of the froth on the tray.

$$u_b = 1.55\left(\frac{\sigma(\rho_l - \rho_g)g}{\rho_l^2}\right)^{\frac{1}{4}}\left(\frac{\rho_g}{\rho_l}\right)^{\frac{1}{24}} \qquad \text{[A.1.4]}$$

$$\varepsilon_w = 1 - \alpha \qquad \text{[A.1.5]}$$

(Hofhuis and Zuiderweg, 1979) has developed three different models based on the Froude number (Fr) for sieve trays, which expresses the ratio of the kinetic energy of vapour to the potential energy of the liquid. The models shown by equations A.1.6 to A.1.8 shows that fluid physical properties has a large effect on the dispersion characteristics within the distillation column (Hofhuis and Zuiderweg, 1979).

$$\eta = 3.4Fr^{*0.75} \qquad Fr < 1 \text{ All systems} \qquad \text{[A.1.6]}$$

$$\eta = 3.4Fr^{*0.3} \qquad 1 < Fr < 15.3 \text{ Air/water} \qquad \text{[A.1.7]}$$

$$1 < Fr < 4 \text{ Hydrocarbons}$$

$$\eta = 420Fr^*\left(\frac{\rho_g}{\rho_l}\right) \qquad Fr > 15.3 \text{ Air/water} \qquad \text{[A.1.8]}$$

$$Fr > 4 \text{ Hydrocarbons}$$

Lockett, 1986) has identified that the determination of the dispersion layer height (H_F) has the general form represented by equation A.1.9. In the equation A, B, C and D are constants to be defined experimentally and 'F_s' is the superficial F-factor. (Zuiderweg, 1982) shows that the dispersion layer height in the spray regime increases more rapidly with increasing gas velocity than in the other flow regimes.

$$H_F = AH_{wo} + BF_S + C\frac{Q_L}{l} + D \qquad \text{[A.1.9]}$$

The froth dispersion height determined by (Thomas and Ogboja, 1978) is defined by equation A.1.10 and A.1.11.

$$H_F = 0.08L'' + 1.56Fr^* + 3.52$$ for rectangular columns (D_h =1 in.) [A.1.10]

$$H_F = 0.055L'' - 2.16Fr^* + 4.83$$ for round columns (D_h =1 in.) [A.1.11]

The froth dispersion layer height model is shown by equations A.1.12 to A.1.16 as a function of the weir height (Bain and Van Winkle, 1961).

$$H_F = \left(\frac{(0.094+0.014H_{wo}^2)L}{100}\right) + I$$ [A.1.12]

$$I = 3.2 - \frac{3.23G'}{1000} + 2.13\left(\frac{G'}{1000}\right)^2$$ for no weir [A.1.13]

$$I = 2.22 - \frac{1.16G'}{1000} + 1.35\left(\frac{G'}{1000}\right)^2$$ for ½ in. weir [A.1.14]

$$I = 2{,}22 - \frac{0.029G'}{1000} + 0.74\left(\frac{G'}{1000}\right)^2$$ for 1 in. weir [A.1.15]

$$I = 3.57 - \frac{1.23G'}{1000} + 0.996\left(\frac{G'}{1000}\right)^2$$ for 2 in. weir [A.1.16]

A.2 Pressure Drop

The orifice coefficient is dependent on the tray thickness (t) to hole diameter (D_h) ratio as suggested by (Stichlmair, 1978), which leads to the orifice equations A.2.1 and A.2.2 which accounts for the effect of fractional hole area (A_F). In equation A.2.1 and A.2.2, ξ_0 represent the orifice coefficient as the fractional hole area approaches zero ($A_f \rightarrow 0$).

$$\xi = \xi_0 + A_F^2 - 2A_F\xi_0^{0.5}$$ For $\frac{t}{D_h} < 2$ [A.2.1]

$$\xi = \xi_0 + A_F^2 - 2A_F$$ For $\frac{t}{D_h} > 2$ [A.2.2]

A.3 Flow Regime Transition

A investigation is done into the froth-to-spray transition, where it is shown that the spray regime is considered to consist of continuous jets of gas through the liquid, and the transition occurs when the liquid bridges the jet and becomes stable (Lockett, 1981). The clear liquid height is defined by the general model in equation A.3.1 (Lockett, 1981), where n = 1,2 or 4 in published literature and 'a' is experimentally determined constant.

$$\frac{H_L}{D_H} = \frac{\left[\frac{4+n}{n}\right]}{\left[\frac{4}{n}\right]^{\frac{4}{4+n}}}\left(\frac{\rho_g}{\rho_l}\right)^{\frac{4}{4+n}}\frac{u_h^{\frac{2n}{4+n}}}{a^{\frac{4}{4+n}}}\frac{(1-\varepsilon)^{\frac{4}{4+n}}}{(gD_H)^{\frac{n}{4+n}}} - \frac{1-\varepsilon}{\alpha}$$ [A.3.1]

In an investigation done by (Barber and Wijn, 1979) the clear liquid height at the transition from froth-to-spray regime is determined using equation A.3.2 taking fractional hole area into account, where n = 1. In the equation the gas inertia is neglected, changing the exponent on $\left(\frac{\rho_g}{\rho_l}\right)$.

$$\frac{H_L}{D_H} = 1.65\left(\frac{\rho_g}{\rho_l}\right)^{0.25}\frac{u_h^{0.4}}{(gD_H)^{0.2}}\left(\frac{p_t}{D_H}\right)^{0.33} - 0.59\left(\frac{p_t}{D_H}\right)$$ [A.3.2]

The equation for clear liquid height at the transition for (Hofhuis and Zuiderweg, 1979) is presented by equation A.3.3, where n = 2.

$$\frac{H_L}{D_H} = 1.07\left(\frac{\rho_g}{\rho_l}\right)^{0.33}\left(\frac{u_h(1-\varepsilon)^{0.5}}{(gD_H)^{0.5}}\right) \quad [A.3.3]$$

The equation for clear liquid height at the transition used by (Payne and Prince, 1977) is shown by equation A.3.4, where n = 4.

$$\frac{H_L}{D_H} = 1.5\left(\frac{\rho_g}{\rho_l}\right)^{0.5}\left(\frac{u_h(1-\varepsilon)^{05}}{(gD_H)^{0.5}}\right) \quad [A.3.4]$$

A.4 Additional Entrainment Literature

The two phase dispersion height ($H_{2\phi}$) is calculated using equation A.4.1 (Bennett *et al.*, 1995), where the two phase dispersion height is the maximum height the droplet are project above the froth layer.

$$\frac{H_{2\Phi}}{H_F} = 1 + \frac{Fr}{2} \quad [A.4.1]$$

The froth height (H_F) in equation A.4.1 is determined using equations A.4.2 and A.4.3 (Bennett *et al.*, 1995).

$$H_F = H_{wo} + C\left(\frac{Q_L}{\eta}\right)^{\frac{2}{3}} \quad [A.4.2]$$

$$C = 0.501 + 0.439\exp(-137.8H_{wo}) \quad [A.4.3]$$

The froth regime entrainment model for air/water systems using froth-to-spray transition data from (Pinczewski and Fell, 1982) is shown by equation A.4.4 (Bennett *et al.*, 1995).

$$\left(\frac{L'}{G}\right)_{AW,f} = 0.125\left(\frac{S}{h_{2\Phi}}\right)^{-1.95} \quad [A.4.4]$$

The froth regime entrainment model for air/water systems using data from (Hofhuis and Zuiderweg, 1979) is shown by equation A.4.5 (Bennett *et al.*, 1995).

$$\left(\frac{L'}{G}\right)_{AW,f} = 0.0469\left(\frac{S}{h_{2\Phi}}\right)^{-1.86} \quad [A.4.5]$$

The froth regime entrainment model for non-air/water system using data from (Hofhuis and Zuiderweg, 1979) is shown by equation A.4.5 (Bennett *et al.*, 1995).

$$\left(\frac{L'}{G}\right)_{NAW,f} = 0.00164\left(\frac{S}{h_{2\Phi}}\right)^{-1.86}\left(\frac{\rho_l}{\rho_g}\right)^{0.5} \quad [A.4.5]$$

Equations A.4.6 to A.4.13 are used to calculate the entrainment magnitudes for (Bennett *et al.*, 1995) correlations. It should be noted that the Froude number is determined in terms of effective froth height (H_{Fe}) and not in terms of froth height as defined by equation 1.2.2.3.

$$H_L = \eta_e H_{Fe} \quad [A.4.6]$$

$$H_{Fe} = H_{wo} + C\left(\frac{Q_L}{3600\eta}\right)^{\frac{2}{3}} \quad [A.4.7]$$

$$\eta_e = \exp(-12.55K_s^{0.91}) \quad [A.4.8]$$

$$H_F = 1 + \left(1 + c\left(\frac{H_L}{D_H}\right)^d\right)\left(\frac{Fr}{2}\right) \quad [A.4.9]$$

c = 6.9 for froth and 4.77 for spray

D =-1.85 for froth and -3.29 for spray

$$Fr = \left(\frac{u_{D0}^2}{gH_{Fe}}\right) \quad [A.4.10]$$

$$u_{D0} = 3K_s\sqrt{\frac{\sqrt{3}}{A_f\eta_e}} \quad [A.4.11]$$

$$\beta = 0.5\left(1 - \tanh\left[1.3\ln\left(\frac{H_L}{D_H}\right) - 0.15\right]\right) \quad [A.4.12]$$

$$C = 0.501 + 0.439\exp[-137.8H_{wo}] \quad [A.4.13]$$

A model for the overall entrainment for air/water and non-air/water systems has been developed by (Bennett *et al.*, 1995), represented by equation A.4.14 and A.4.15, respectively, where the constants are determined experimentally. The observed entrainment for the (Bennett *et al.*, 1995) experimental data is predicted with equation A.4.16.

$$E\sqrt{\frac{\rho_g}{\rho_l}} = 0.00164\left(\frac{S}{h_{2\Phi}}\right)^{-186-0.26(H_L D_H)^d}\alpha^\beta \quad [A.4.14]$$

$$E\sqrt{\frac{\rho_g}{\rho_l}} = 0.04\left(\frac{S}{h_{2\Phi}}\right)^{-1.04}\alpha^\beta\left(\frac{\rho_l}{\rho_g}\right)^{0.5} \quad [A.4.15]$$

$$E = 0.04\left(\frac{S}{h_{2\Phi}}\right)^{-1.04}\alpha^\beta\left(\frac{\rho_l}{\rho_g}\right)^{0.5} \quad [A.4.16]$$

In the sieve tray distillation investigation performed by (Uys, 2012) a correlation is developed to help define the entrainment process inside a distillation column when the tray spacing, gas flow rate, liquid flow rate, gas and liquid physical properties are varied. Equation A.4.17 shows all the parameters that influence the entrainment magnitude based on the scope of the investigation.

$$\frac{L'}{G} = f\left(u_s^a, \rho_g^b, Q_L^c, \rho_l^d, \sigma^e, \mu_l^f, g^g, \mu_g^h, s^i\right) \quad [A.4.17]$$

In order to develop the entrainment correlation, (Uys, 2012) used well known hydrodynamic dimensionless numbers, the Weber Number, Reynolds number and the Froude number.

$$\left(\frac{\sigma}{\rho_g u_s Q_L}\right) \rightarrow \frac{1}{We}; \left(\frac{\mu_L}{\rho_g Q_L}\right) \rightarrow \frac{1}{Re_{e_L}}; \left(\frac{\mu_g}{\rho_g Q_L}\right) \rightarrow \frac{1}{Fr}; \left(\frac{\mu_g}{\rho_g Q_L}\right) \rightarrow \frac{1}{Re_{eg}}$$

In the correlation development the Buckingham π-theorem is used to produce equations A.4.18 and A.4.19. In the equations the symbols $a_{1\ to\ 6}$, $b_{1\ to\ 6}$, $N_{1\ to\ 6}$ and $k_{0\ to\ 6}$ are constants, where $N_{1\ to\ 6}$ are used to normalize the dimensionless numbers so that the dimensionless numbers are unaffected by scale.

$$\frac{L'}{G} = f\left(\left(\frac{\rho_l}{\rho_g}\right)^{a_1}, \left(\frac{\sigma}{\rho_g u_s Q_L}\right)^{a_2}, \left(\frac{\mu_L}{\rho_g Q_L}\right)^{a_3}, \left(\frac{g Q_L}{u_s^3}\right)^{a4}, \left(\frac{\mu_g}{\rho_g Q_L}\right)^{a5}, \left(\frac{u_s s}{Q_L}\right)^{a6}\right) \quad [A.4.18]$$

$$= k\left(\frac{\rho_l}{\rho_g}\right)^{a_1}\left(\frac{\sigma}{\rho_g u_s Q_L}\right)^{a_2}\left(\frac{\mu_L}{\rho_g Q_L}\right)^{a_3}\left(\frac{g Q_L}{u_s^3}\right)^{a4}\left(\frac{\mu_g}{\rho_g Q_L}\right)^{a5}\left(\frac{u_s s}{Q_L}\right)^{a6}$$

$$\frac{L'}{G} = k_0\left(\left(\frac{\rho_l}{N_1\rho_g}\right)^{b_1} + k_1\right)^{a_1}\left(\left(\frac{\sigma}{N_2\rho_g u_s Q_L}\right)^{b_2} + k_2\right)^{a_2}\left(\left(\frac{\mu_L}{N_3\rho_g Q_L}\right)^{b_3} + k_3\right)^{a_3}\left(\left(\frac{g Q_L}{N_4 u_s^3}\right)^{b_4} + k_4\right)^{a_4}\left(\left(\frac{\mu_g}{N_5\rho_g Q_L}\right)^{b_5} + k_5\right)^{a_5}\left(\left(\frac{u_s s}{N_6 Q_L}\right)^{b_6} + k_6\right)^{a_6} \quad [A.4.19]$$

A.5 Additional Weeping Literature

Colwell and O'Bara weeping correlation as defined by (Kister, 1992) is shown equation A.5.1.

$$\frac{W^*}{A_h^*} = \frac{1.841}{Fr_h^{1.533}} \qquad \text{for } Fr_h > 0.2 \quad [A.5.1]$$

Hsieh and Mcnulty weeping correlation as defined by (Kister, 1992) is shown equations A.5.2 to A.5.5 correlation (m = 1.94 and C_w = 0.79 for sieve trays)

$$\sqrt{J_G^*} + m\sqrt{J_L^*} = C_w \quad [A.5.2]$$

$$\sqrt{J_G^*} = u_h^*\left[\frac{\rho_g^*}{g^* Z(\rho_l^* - \rho_g^*)}\right]^{0.5} \quad [A.5.3]$$

$$\sqrt{J_L^*} = \frac{W^*}{448{,}83 A_h^*}\left[\frac{\rho_l^*}{g^* Z(\rho_l^* - \rho_g^*)}\right]^{0.5} \quad [A.5.4]$$

$$Z = \frac{h_L^{*1.5}}{12\left(d_H^*\right)^{0.5}} \quad [A.5.5]$$

A.6 Distillation Capacity

The maximum capacity factor ($C_{b(max)}$) is determined by equation A.6.1. (Lemieux and Scotti, 1969) states that the maximum capacity of a distillation column is a function of the vapour and the liquid flow rate.

$$C_{\mathrm{b(max)}} = u_b\left(\frac{\rho_g}{\rho_l}\right)^{0.5} = 0.037 g^{0.5}\left(\frac{(S - H_L)^{0.59}}{H_L^{0.09}}\right) \quad [A.6.1]$$

(Zuiderweg, 1982) shows that the capacity of the distillation column decreases with decreasing liquid surface tension and decreasing difference between the liquid and vapour density. A model developed by (Zuiderweg, 1982) is presented by equations A.6.2 to A.6.4, when flooding in the column is due to the choking in the downcomer in the emulsion regime, where (c'') is a constant determined experimentally. The emulsion regime should be avoided because of foaming.

$$\frac{C_{\mathrm{b(max)}}}{A_f{}^{0.2}}\left(\frac{\rho_l - \rho_g}{\rho_l}\right)^{\frac{1}{6}}\left(\frac{\mu_l}{\sigma}\right)^{\frac{1}{3}} = c'\left(\frac{FP}{l H_L}\right)^{-\frac{2}{3}} \quad [A.6.2]$$

$$FP = \frac{u_l}{u_g}\sqrt{\frac{\rho_g}{\rho_l}} \quad [A.6.3]$$

$$c' = \frac{c''\left(g^{\frac{1}{3}}\left(\frac{A_d}{A_b}\right)^{\frac{1}{3}}\right)}{l^{\frac{7}{12}}H_{wo}^{\frac{1}{6}}p_t^{\frac{1}{2}}} \quad [A.6.4]$$

(Zuiderweg, 1982) shows that weeping produces a loss in pressure and tray efficiency, where the capacity limit for weeping is shown by equations A.6.5 and A.6.6.

$$CF_w = A_F(gH_L)^{\frac{1}{2}}\left[1 - \frac{0.15FP}{lH_L}\right] \quad \text{for mixed free bubbling regime} \quad [A.6.5]$$

$$CF_w = 0.45A_F(gH_L)^{\frac{1}{2}} \quad \text{for emulsion regime} \quad [A.6.6]$$

In the emulsion regime liquid containing vapour flows into the downcomer where if the phases are insufficiently separated the downcomer capacity will increase and be exceeded leading to flooding in the distillation column (Zuiderweg *et al.*, 1984). The point at incipient flooding occurs when the downcomer is just filled with foam. The capacity factor ($C_{b(inc)}$) at incipient flooding is shown by equation A.6.7.

$$C_{b(inc)} = 0.9C_{b(\max)} \quad [A.6.7]$$

The capacity factor at incipient flooding is shown by equation A.6.8 (Zuiderweg *et al.*, 1984). In the investigation it is shown that the capacity factor is independent of tray spacing and downcomer length, but this is not true (Zuiderweg *et al.*, 1984). In equation A.6.8, 'FP' represents the flow parameter. (Lemieux and Scotti, 1969) shows that by decreasing the fractional hole area the pressure drop across the tray is increased, allowing flooding to occur at lower gas flow rates. (Zuiderweg, 1982) defines flooding to occur when the downcomer is filled up to the weir with a vapour/liquid mixture.

$$C_{b(inc)} = 0.035\left[g^{\frac{1}{3}}\left(\frac{A_d}{A_b}\right)^{\frac{1}{3}}A_f^{\frac{1}{5}}\right]\left[\frac{H_L}{(FP)^{\frac{7}{12}}}\right]\left(\frac{\rho_l}{\rho_l - \rho_g}\right)^{\frac{1}{6}}\left(\frac{\rho}{\mu}\right)^{\frac{1}{3}} \quad [A.6.8]$$

In an investigation done by (Thomas and Ogboja, 1978) the flooding limits are investigated. The Souders and Brown capacity parameter is shown by equation A.6.9 (Thomas and Ogboja, 1978), where it is coupled with the F-factor. The superficial velocity of the gas at the flooding point is shown by equation A.6.10, where the equation applies only for liquid with a surface tension of 20 dynes/cm and has to be corrected for other surface tensions.

$$C_f = K_s = C_s = u_s\sqrt{\frac{\rho_g}{\rho_l - \rho_g}} \quad [A.6.9]$$

$$u_{s(flooding)} = (C_f)_{\sigma=20}\left(\frac{\sigma}{20}\right)^{0.2}\left(\frac{\rho_l - \rho_g}{\rho_g}\right)^{\frac{1}{2}} \quad [A.6.10]$$

Appendix B – Correlation Graphs

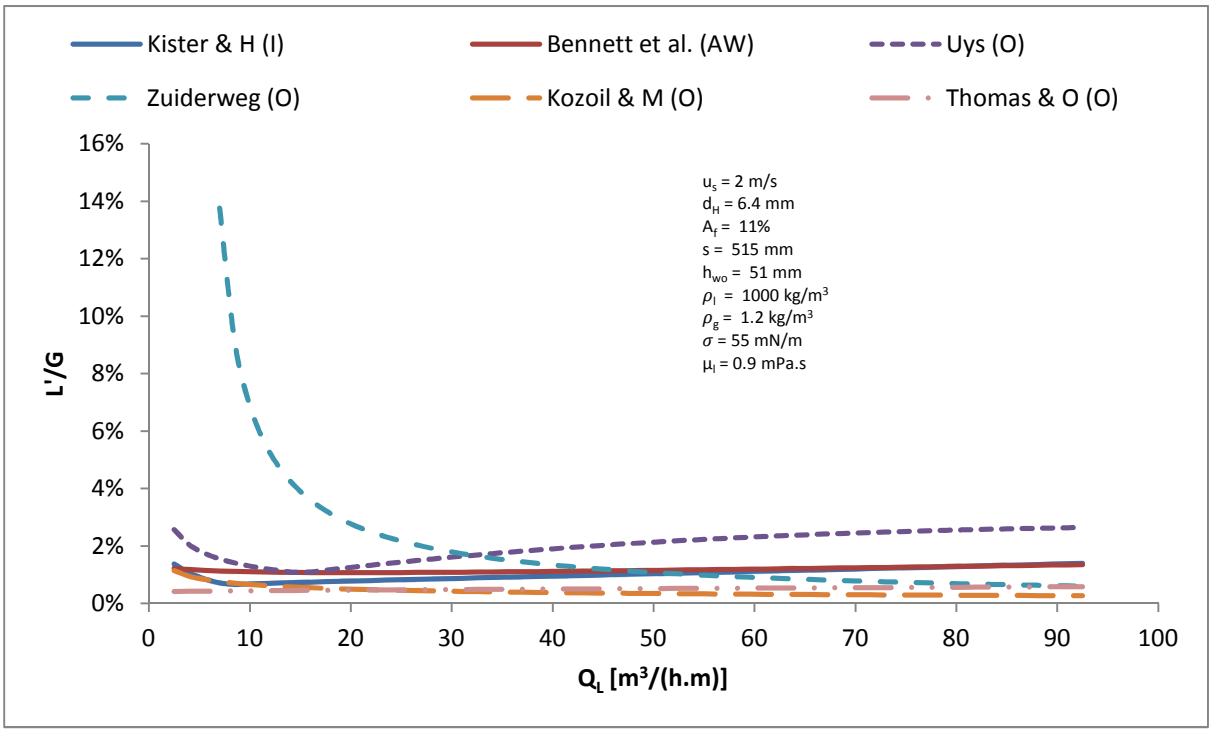

Figure 114 – Modelling the effect of liquid flow rate on entrainment for u_s = 2 m/s

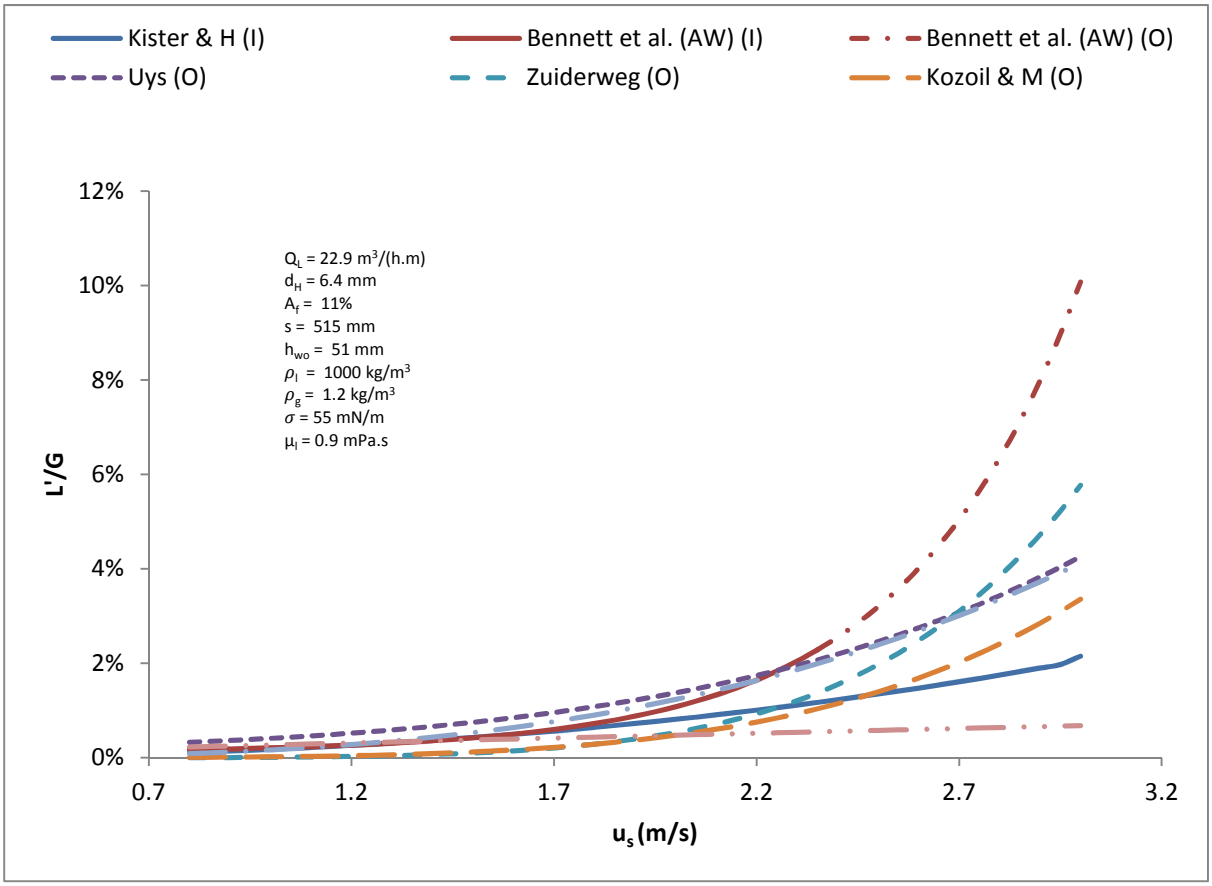

Figure 115 – Modelling the effect of gas superficial velocity on entrainment for Q_L = 23 [m³/(h.m)]

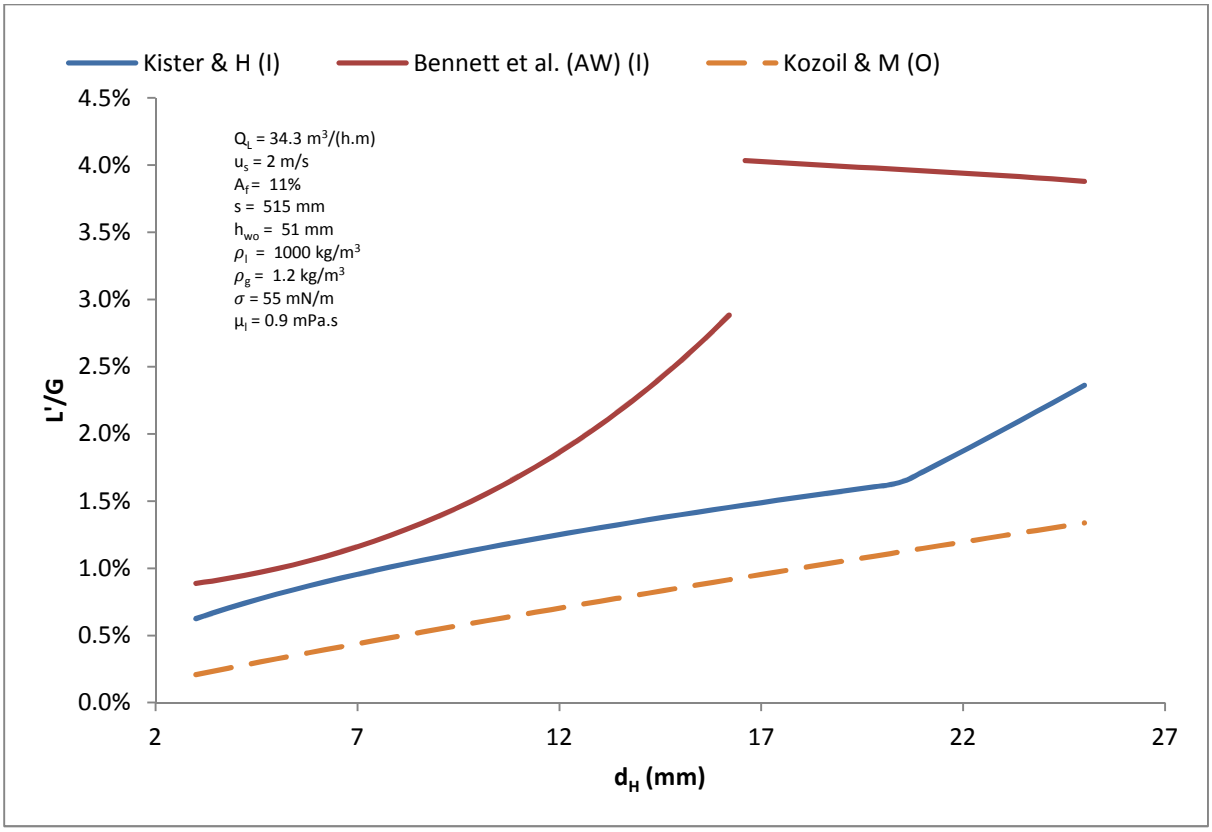

Figure 116 – Modelling the effect of hole diameter on entrainment for Q_L = 34.3 [m³/(h.m)] and u_s = 2 m/s

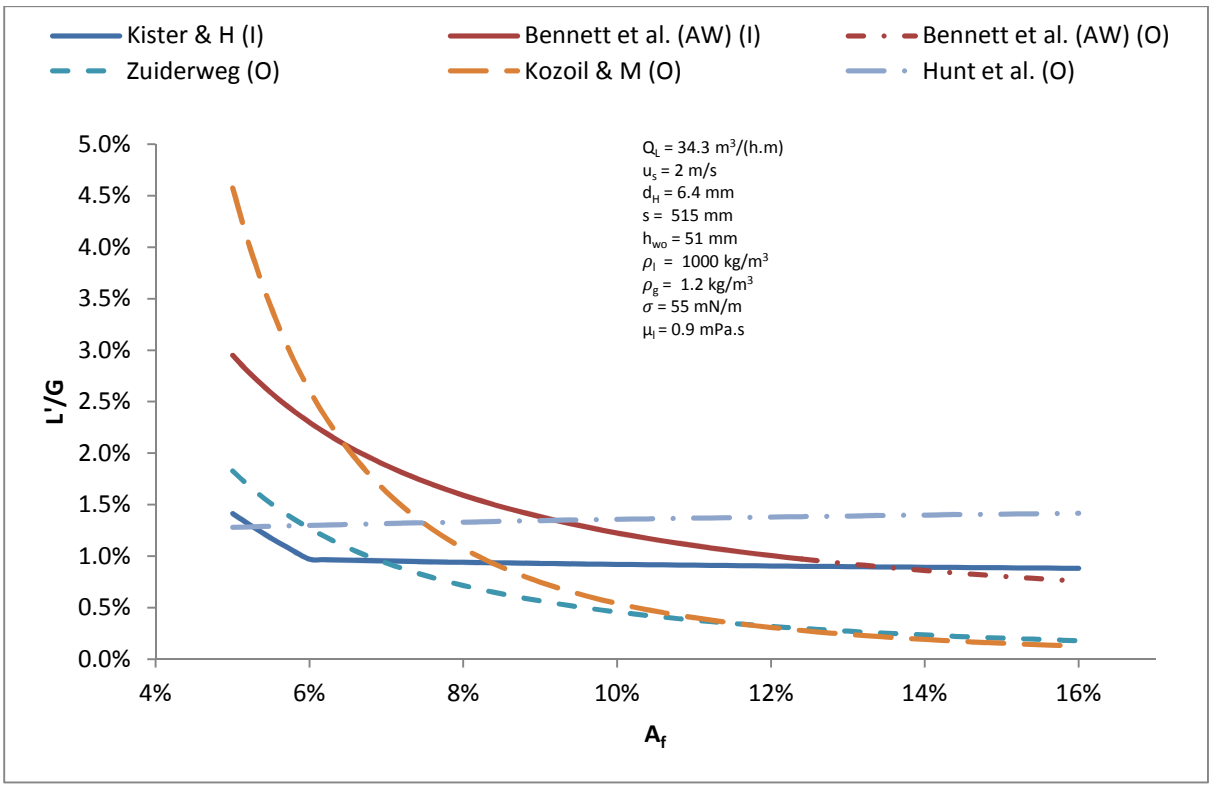

Figure 117 – Modelling the effect of fractional hole area on entrainment for QL = 34.3 [m³/(h.m)] and us = 2 m/s

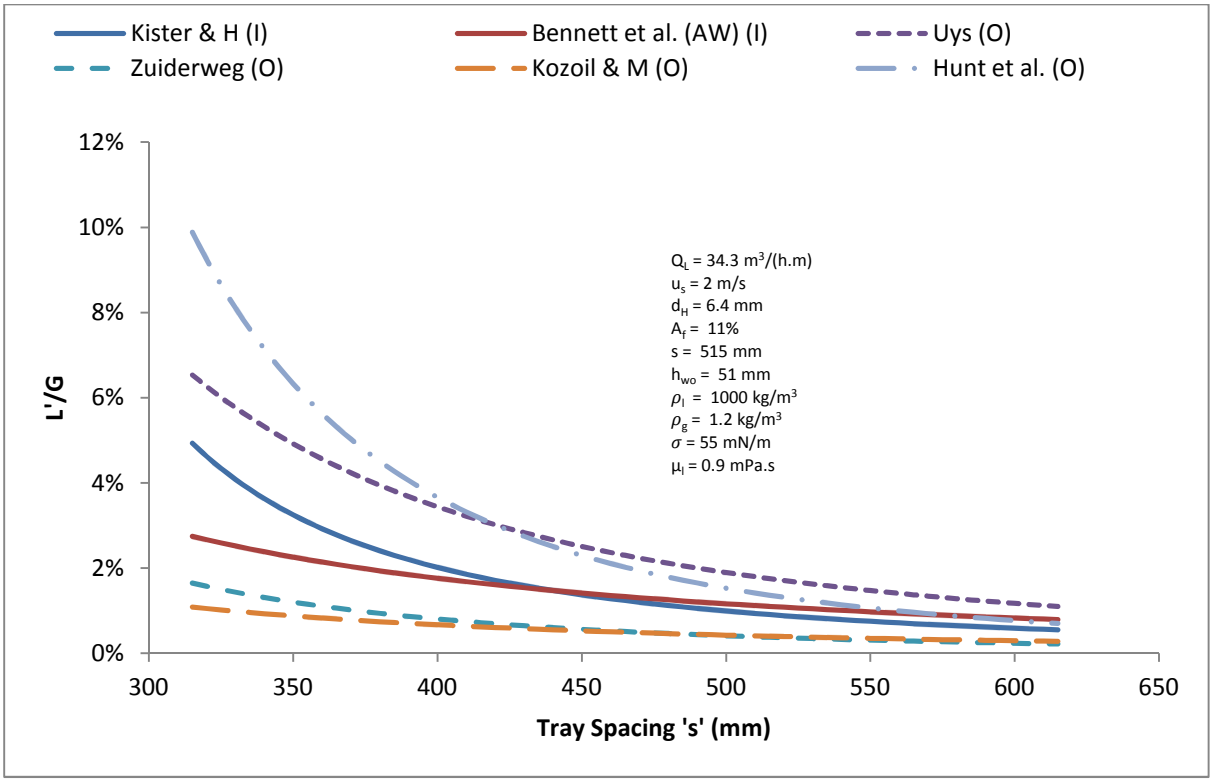

Figure 118 – Modelling the effect of tray spacing on entrainment for Q_L = 34.3 [m³/(h.m)] and u_s = 2 m/s

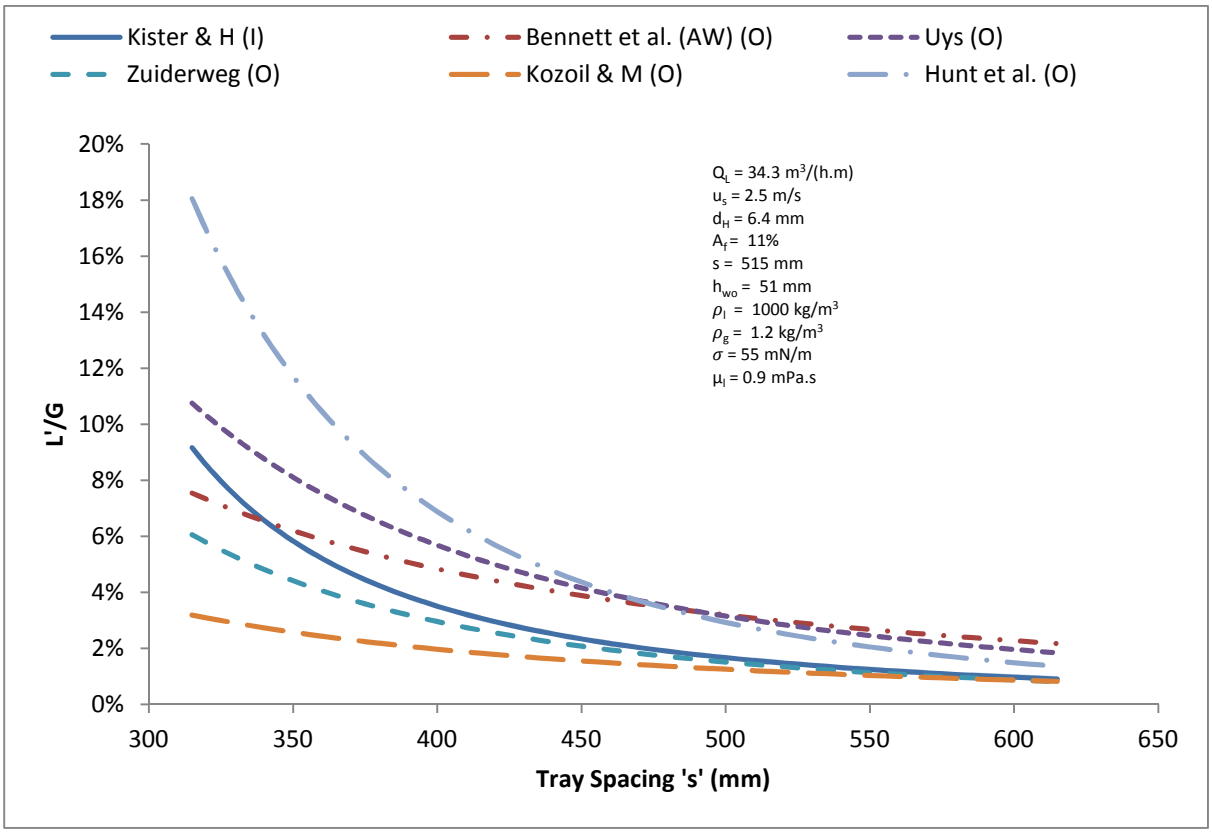

Figure 119 – Modelling the effect of tray spacing on entrainment for Q_L = 34.3 [m³/(h.m)] and u_s = 2.5 m/s

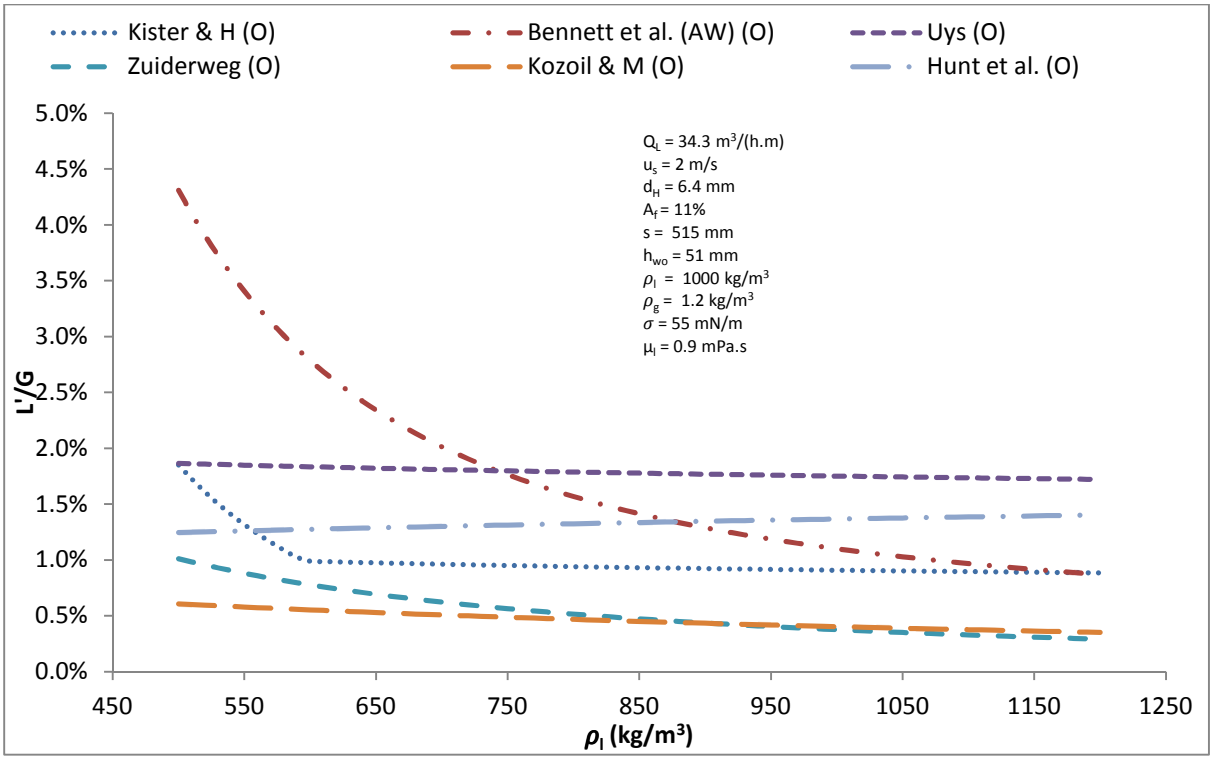

Figure 120 – Modelling the effect of liquid density on entrainment for Q_L = 34.3 [m³/(h.m)] and u_s = 2 m/s

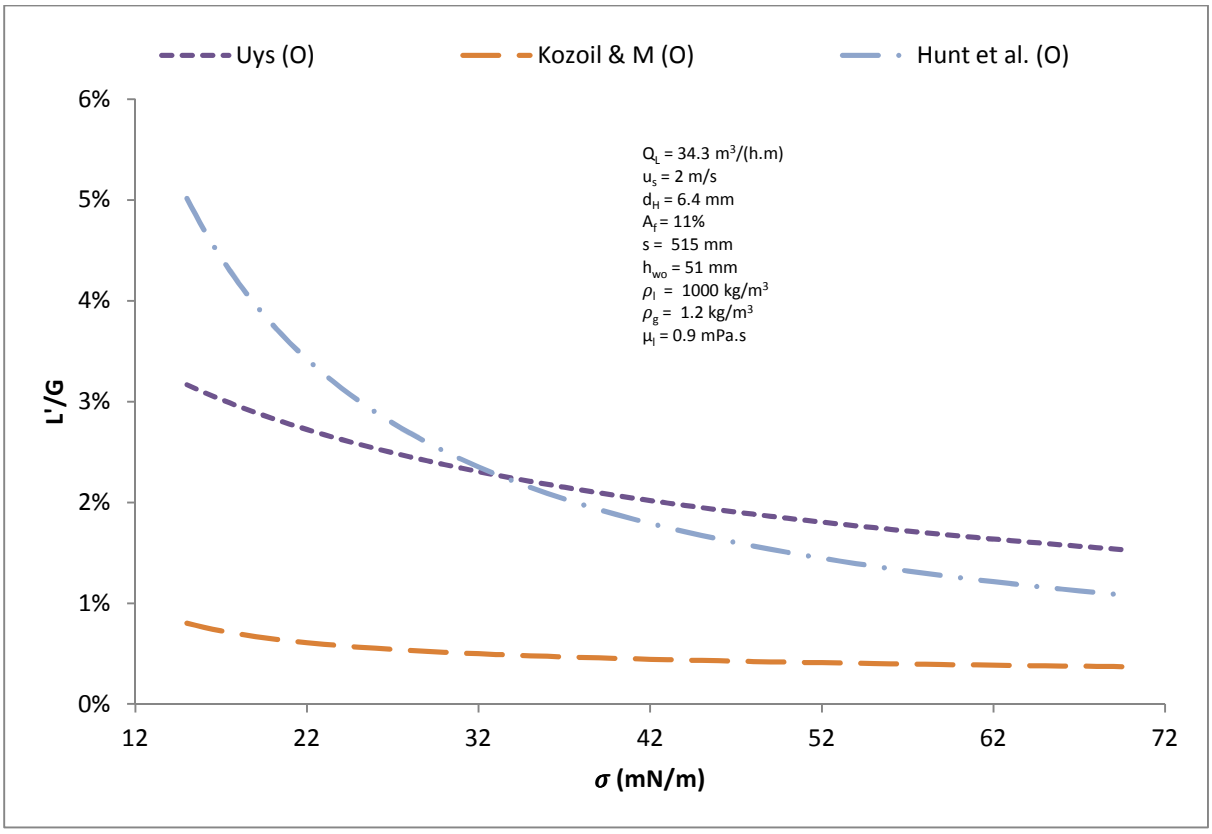

Figure 121 – Modelling the effect of surface tension on entrainment for Q_L = 34.3 [m³/(h.m)] and u_s = 2 m/s

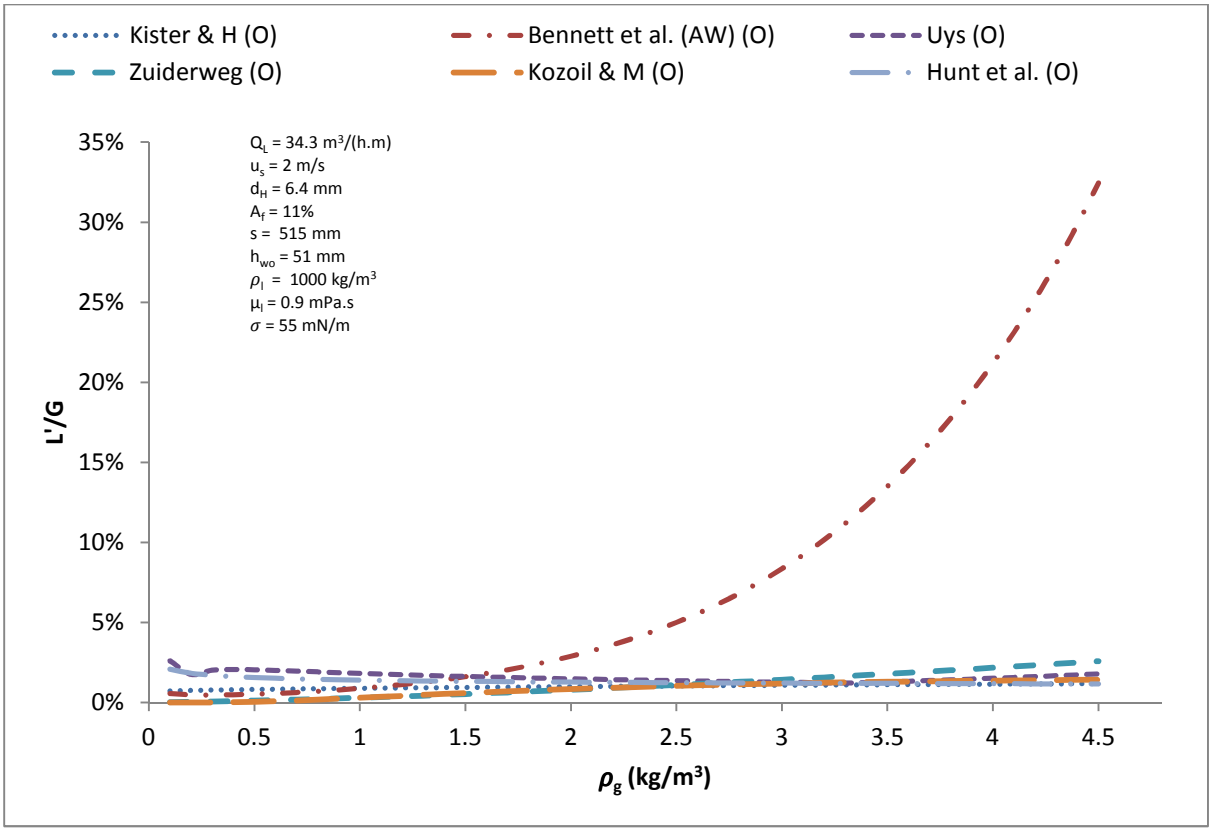

Figure 122 – Modelling the effect of gas density on entrainment for Q_L = 34.3 [m^3/(h.m)] and u_s = 2 m/s

Appendix C – Experimental Sieve Tray Designs

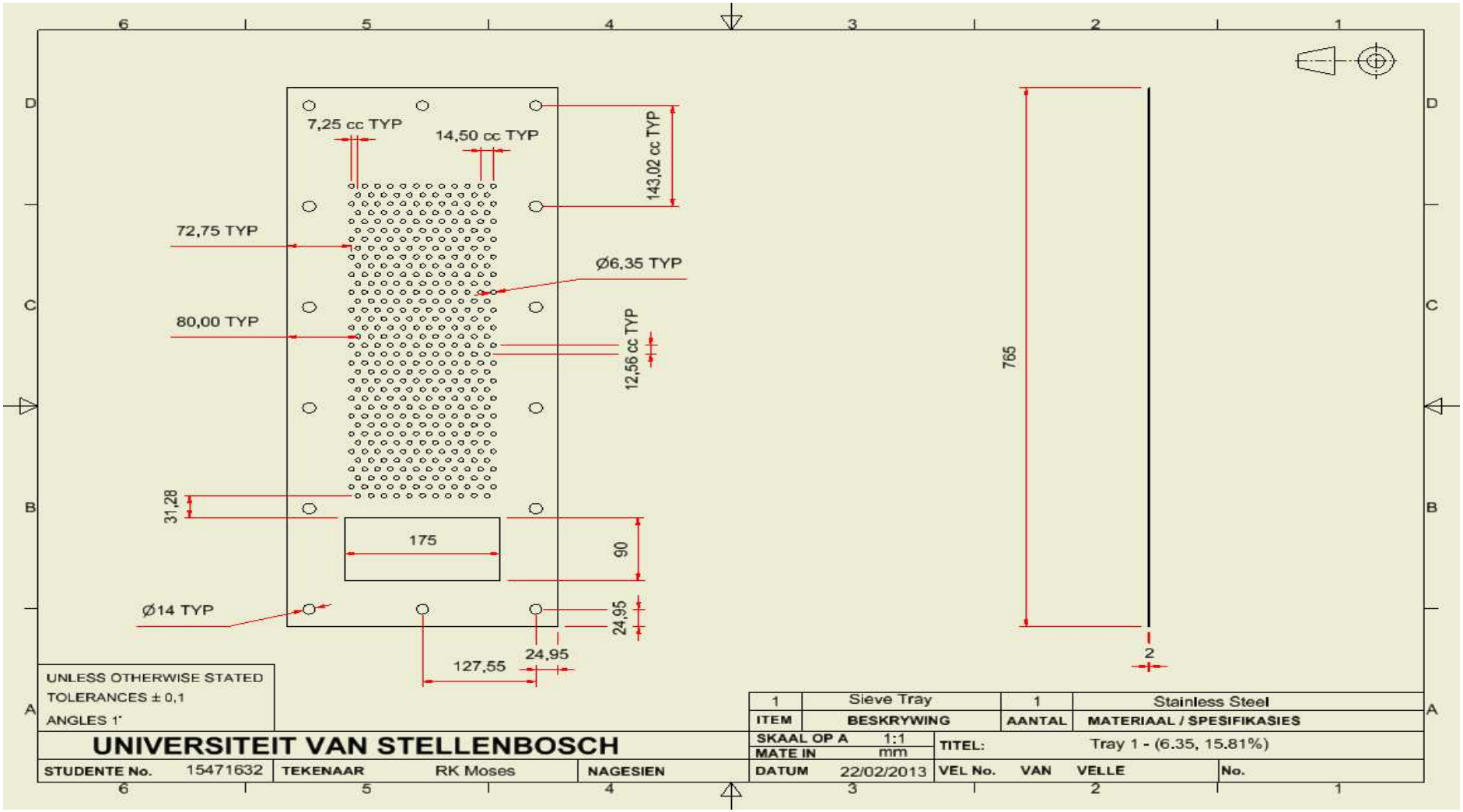

Figure 123 – Tray 1 with ¼ in. (6.4 mm) hole diameter and a fractional hole area of 15.8%

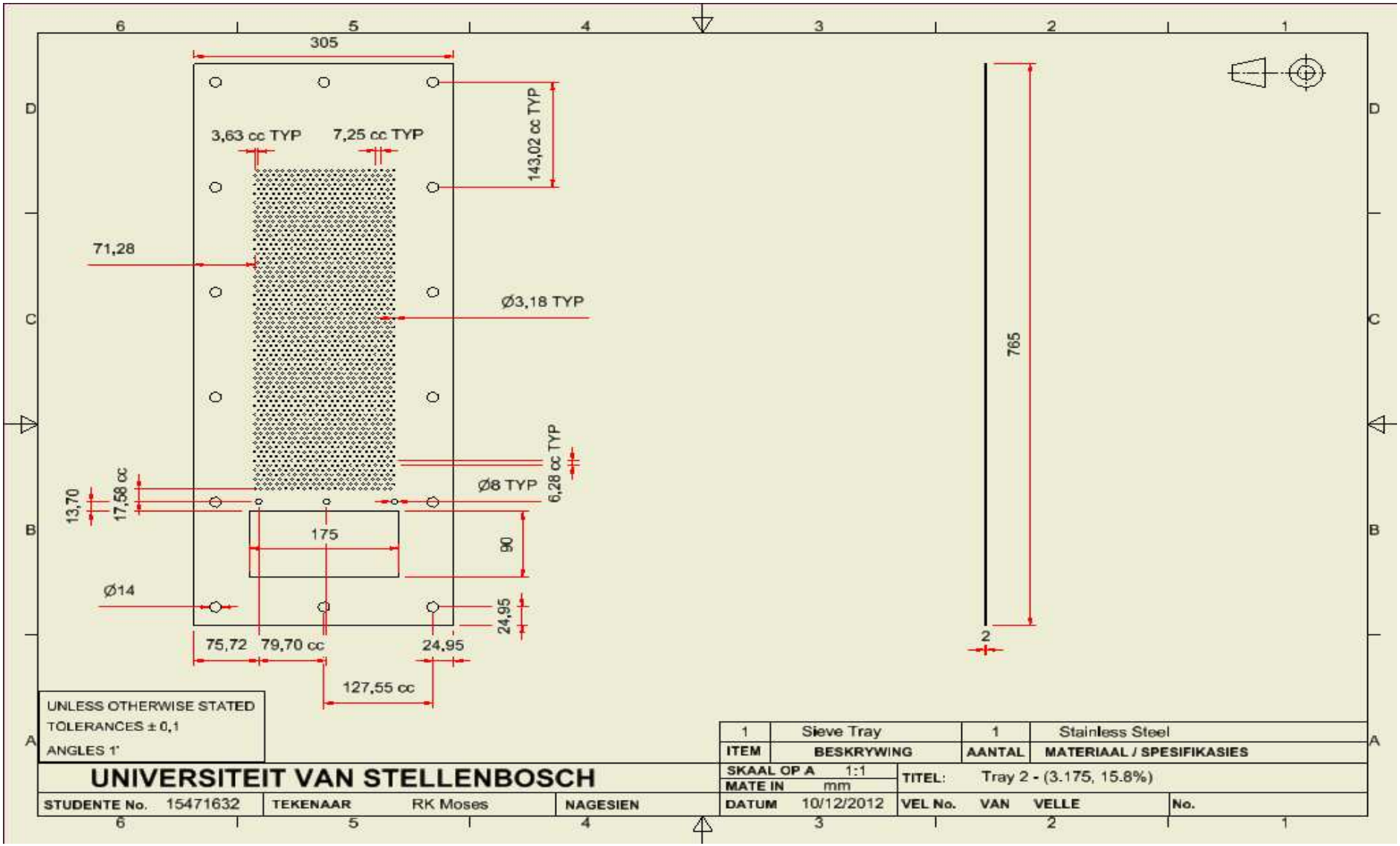

Figure 124 – Tray 2 with ⅛ in. (3.2 mm) hole diameter and a fractional hole area of 15.8%

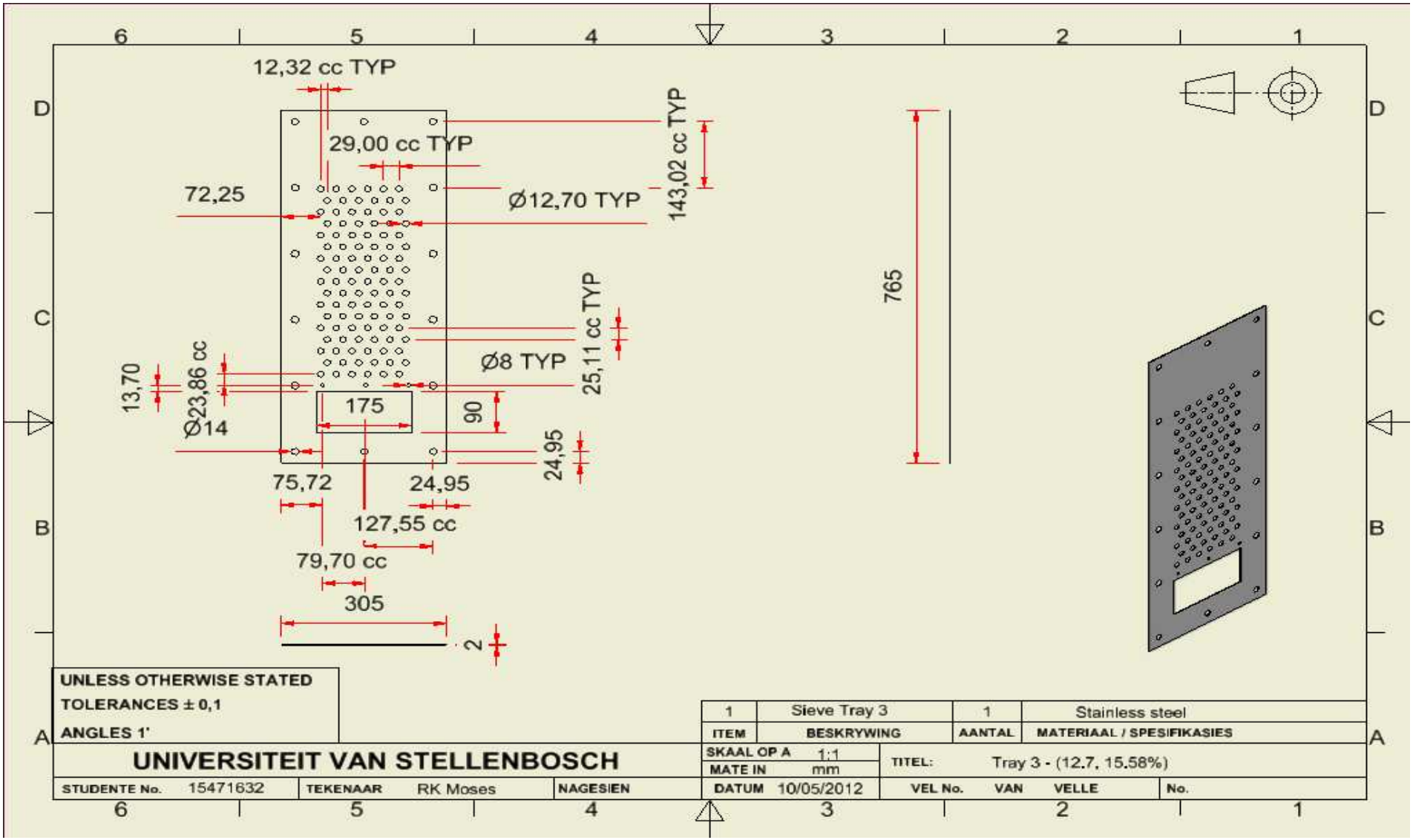

Figure 125 – Tray 3 with ½ in. (12.7 mm) hole diameter and a fractional hole area of 15.6%

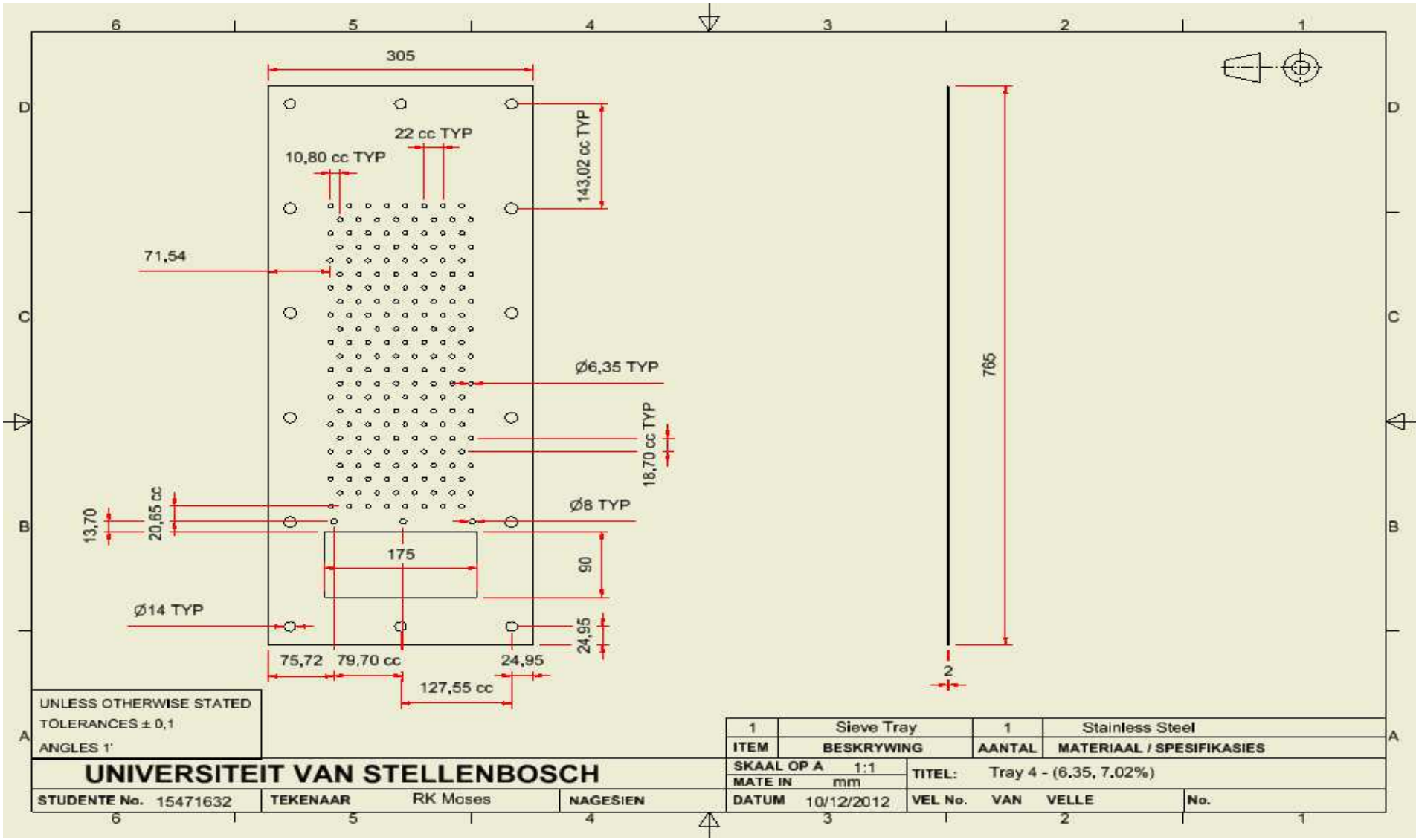

Figure 126 – Tray 4 with ¼ in. (6.4 mm) hole diameter and a fractional hole area of 7%

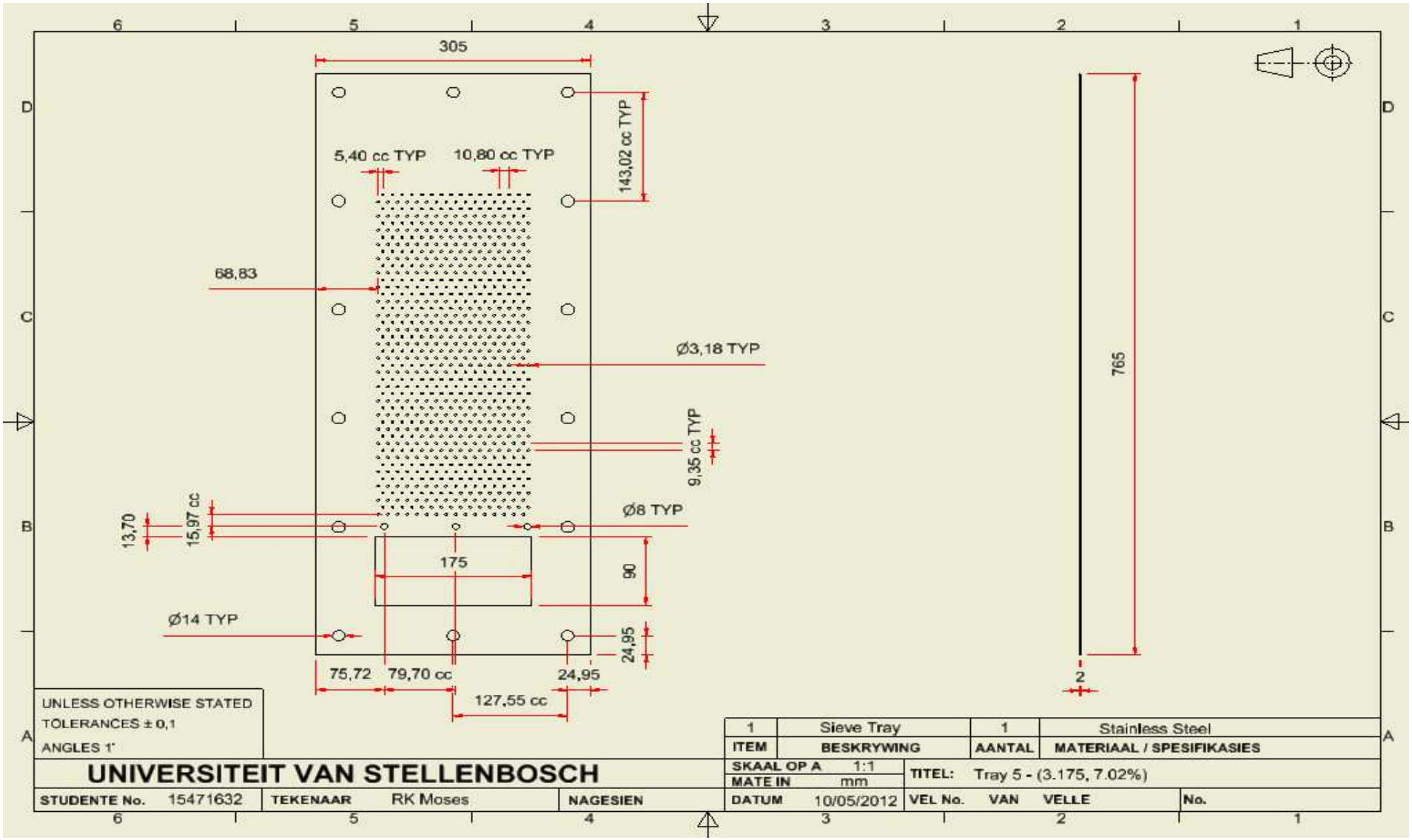

Figure 127 – Tray 5 with ⅛ in. (3.2 mm) hole diameter and a fractional hole area of 7%

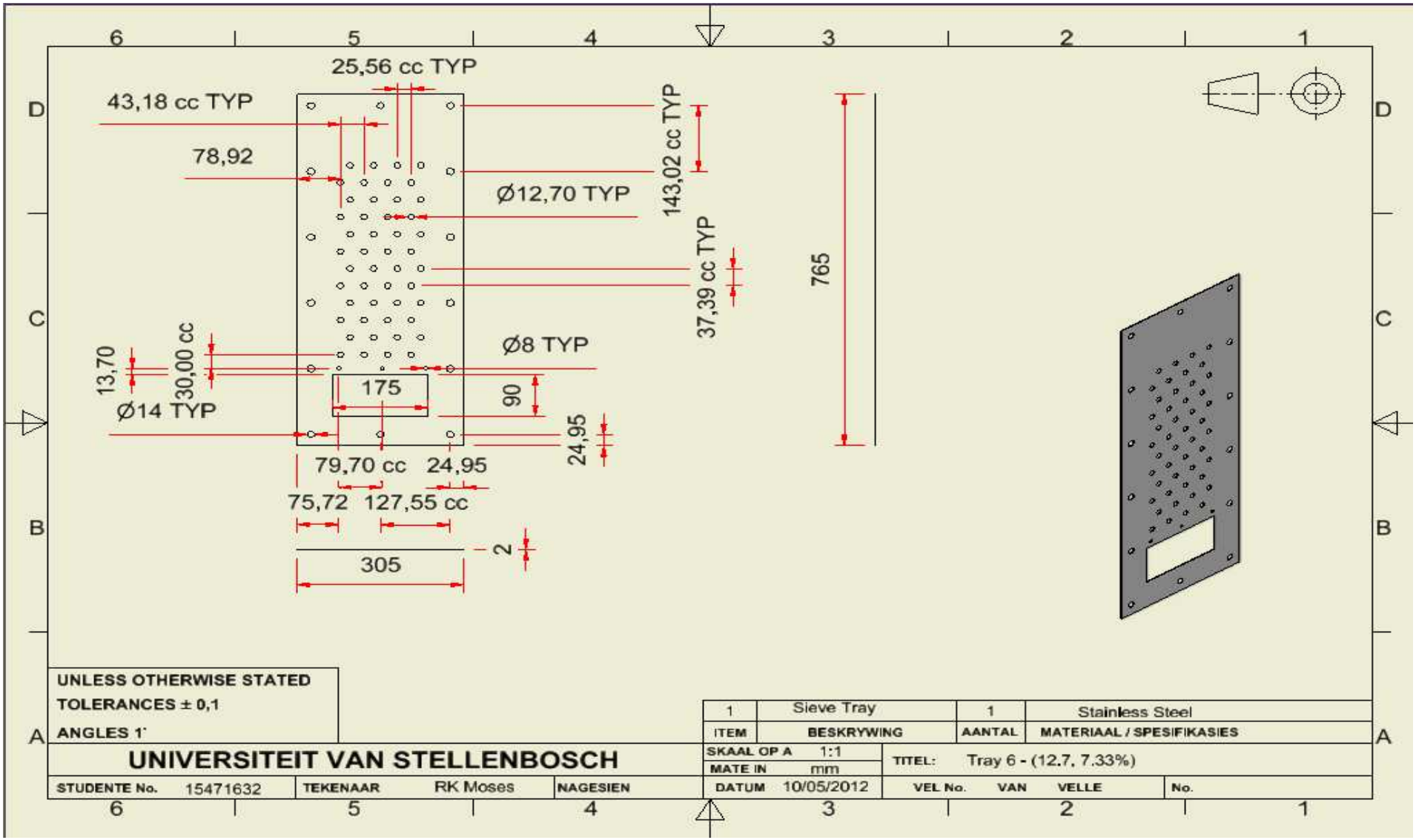

Figure 128 – Tray 6 with ½ in. (12.7 mm) hole diameter and a fractional hole area of 7.3%

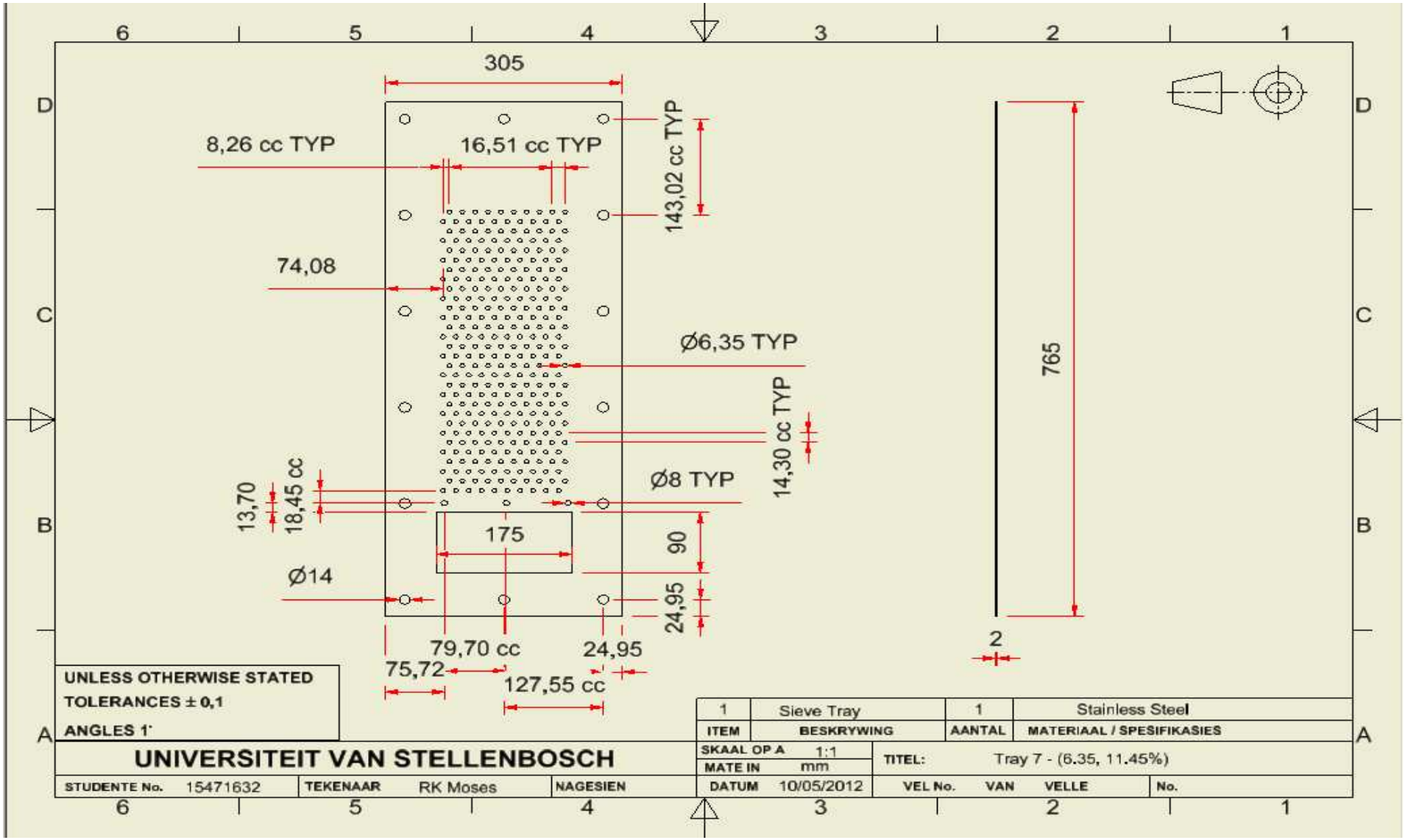

Figure 129 – Tray 7 with ¼ in. (6.4 mm) hole diameter and a fractional hole area of 11. 5%

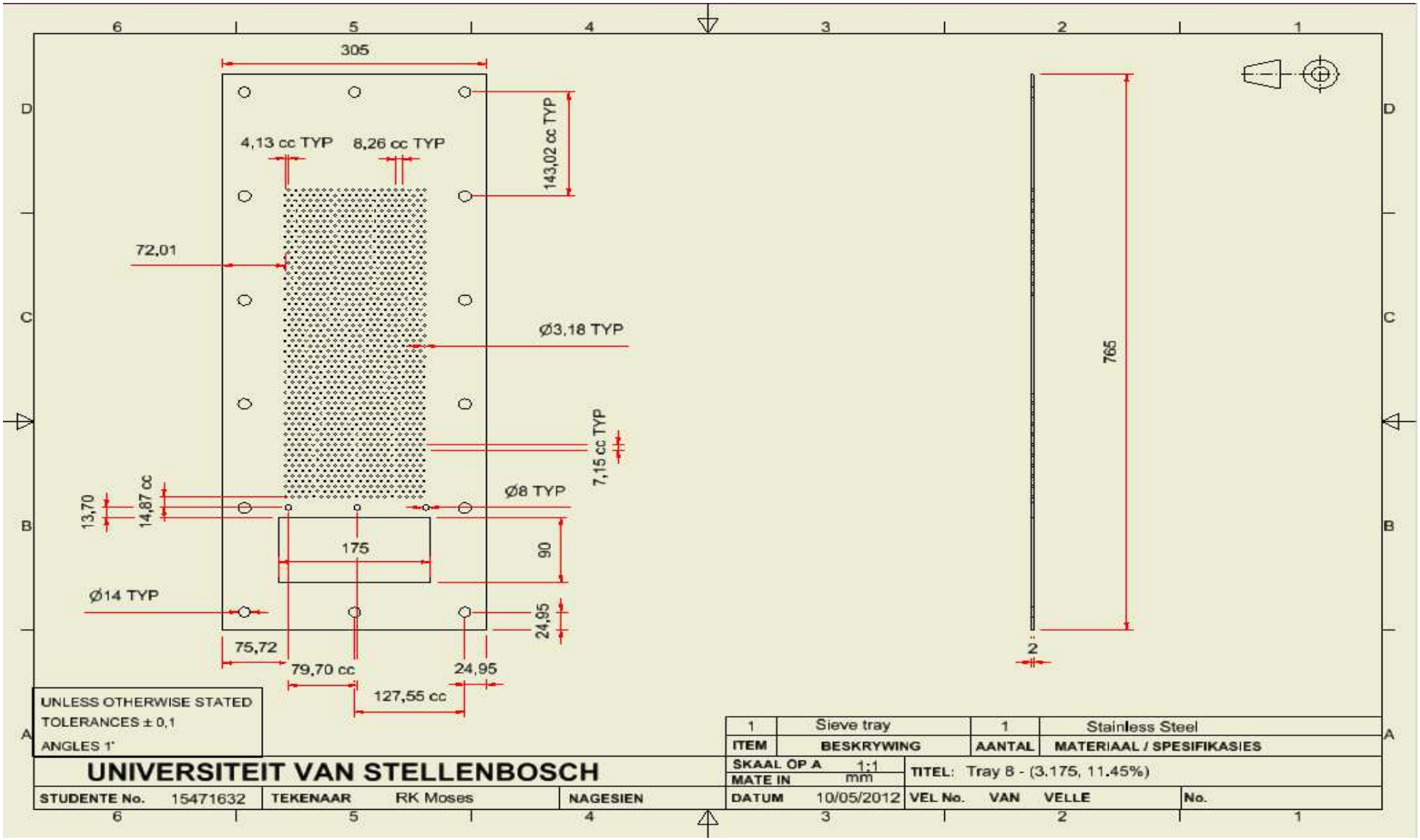

Figure 130 – Tray 8 with ⅛ in. (3.2 mm) hole diameter and a fractional hole area of 11.5%

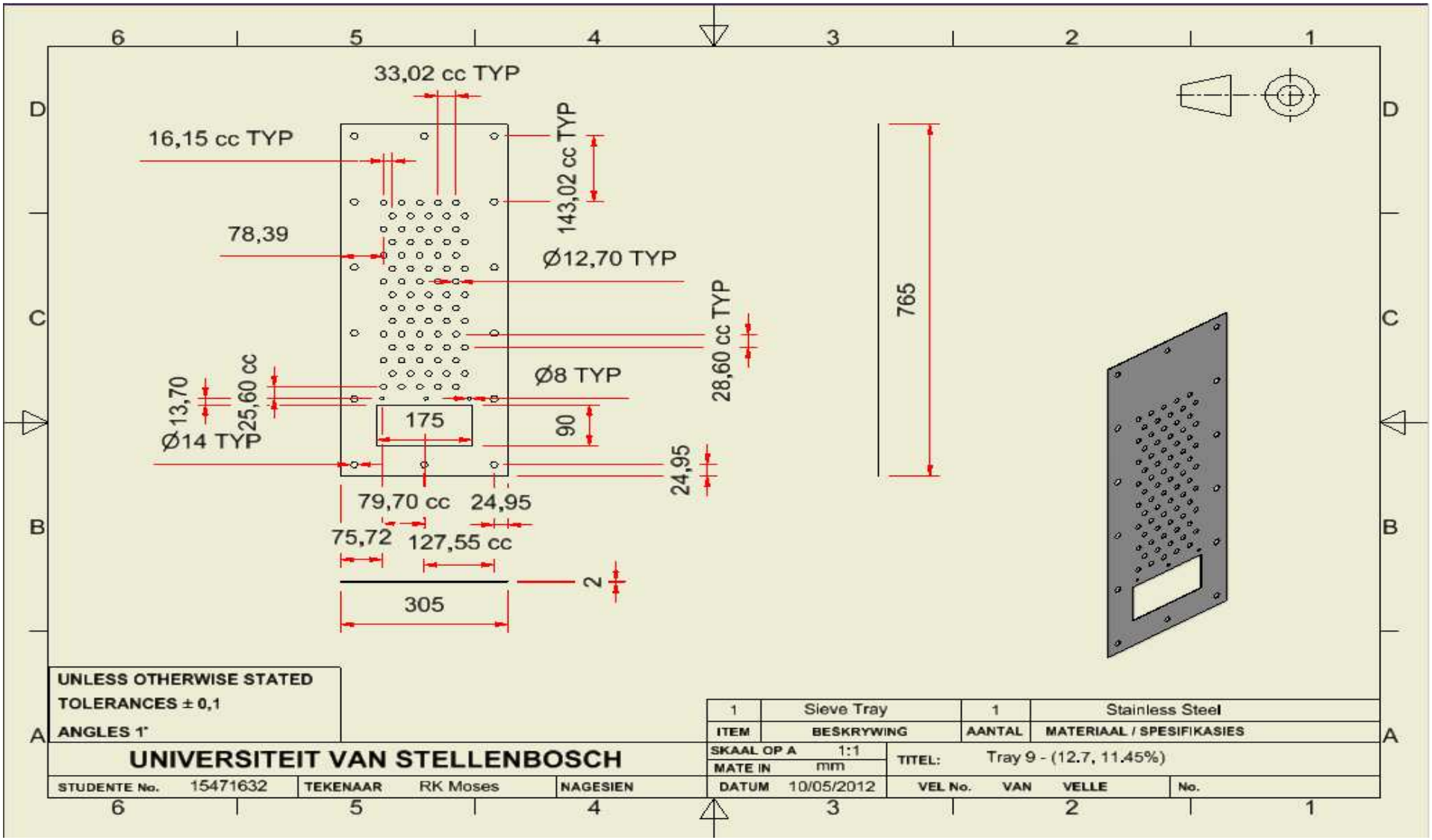

Figure 131 – Tray 9 with ½ in. (12.7 mm) hole diameter and a fractional hole area of 11.5%

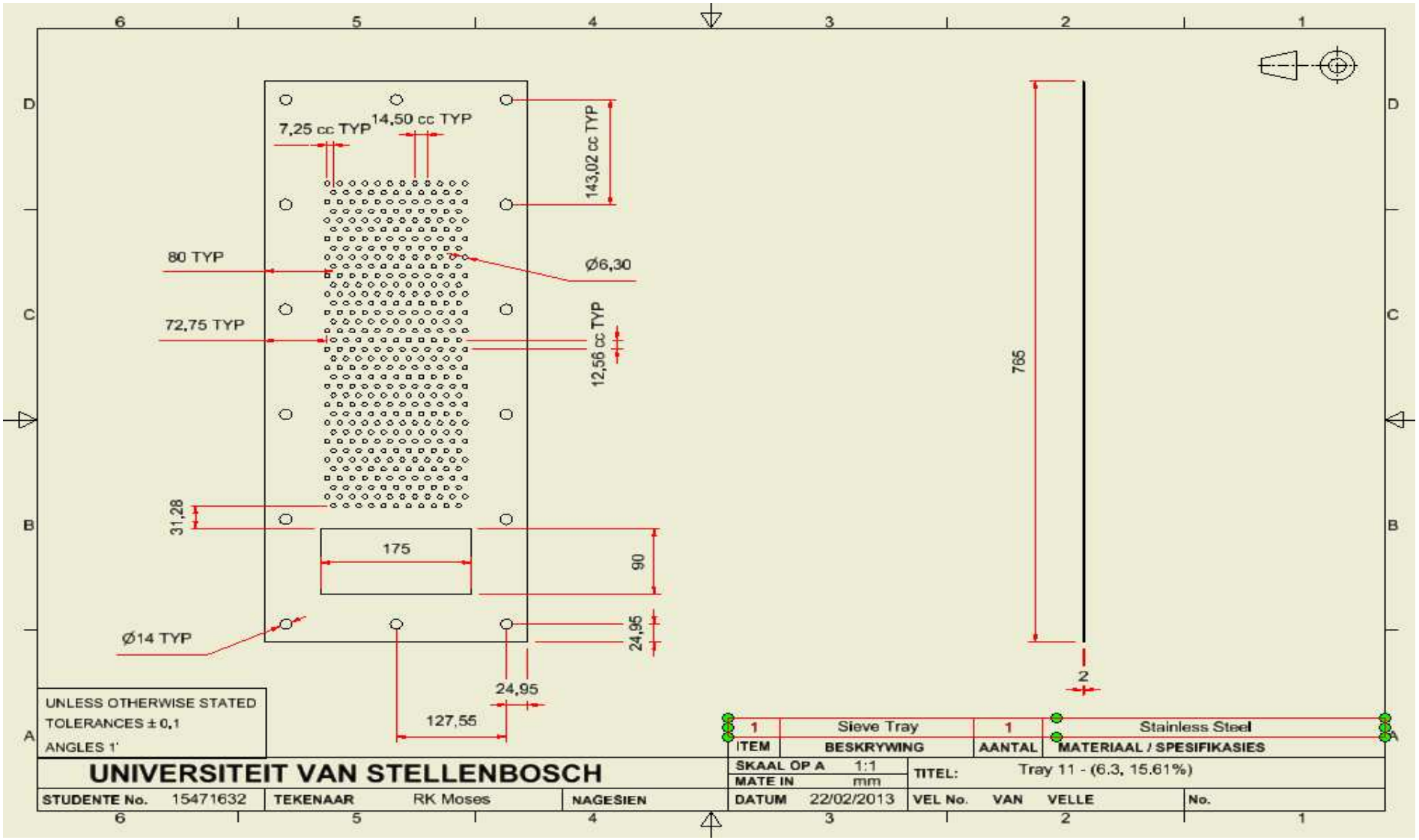

Figure 132 – Tray 11 with 6.3 mm holes and a fractional hole area of 15.6%

Appendix D – Equipment Design Specification

The following section address the design specifications of the equipment in the sieve tray distillation pilot plant as obtained from (Uys *et al.*, 2009).

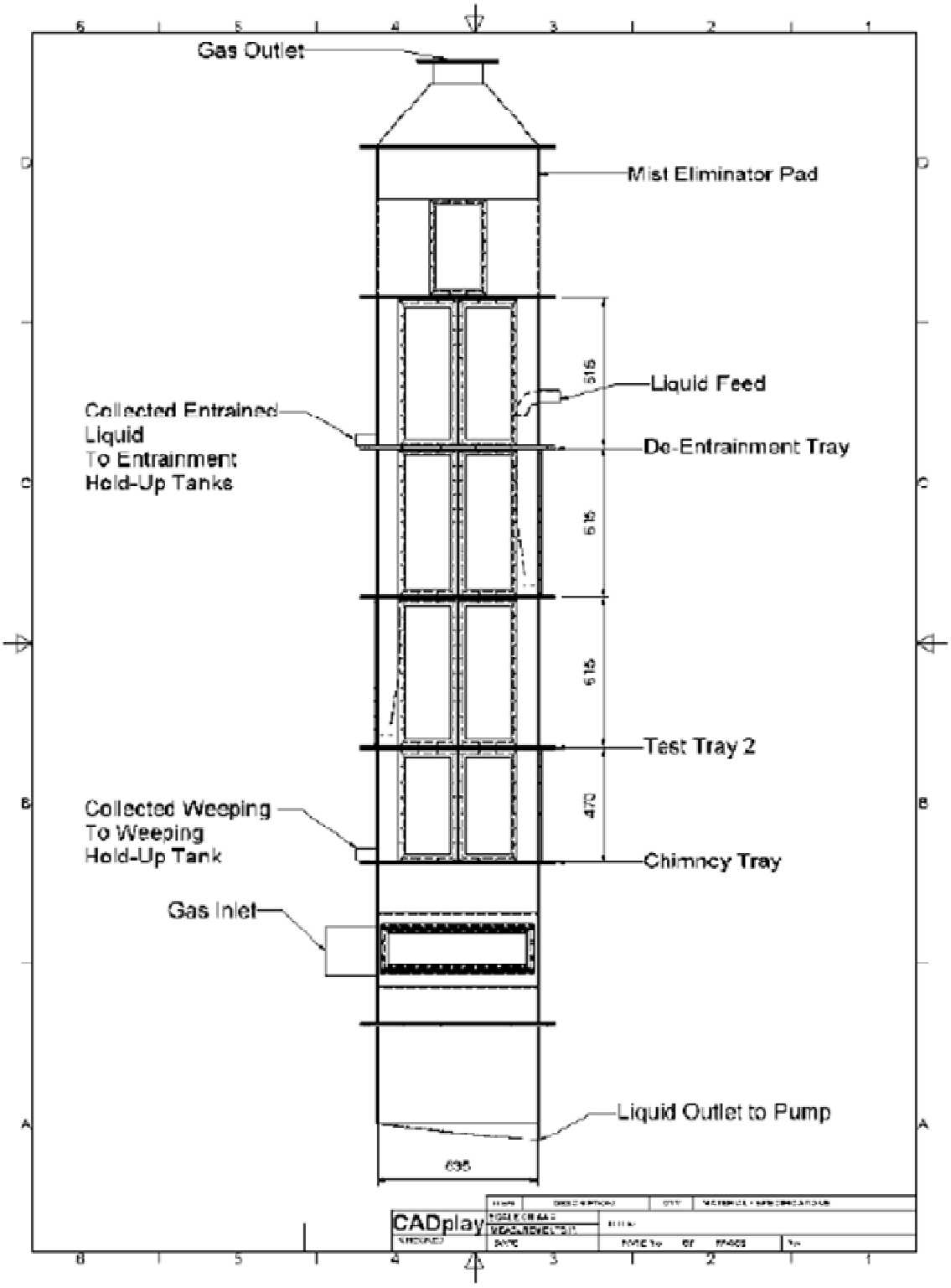

Figure 133 – Front view of distillation column [obtained with permission from (Uys *et al.*, 2009)]

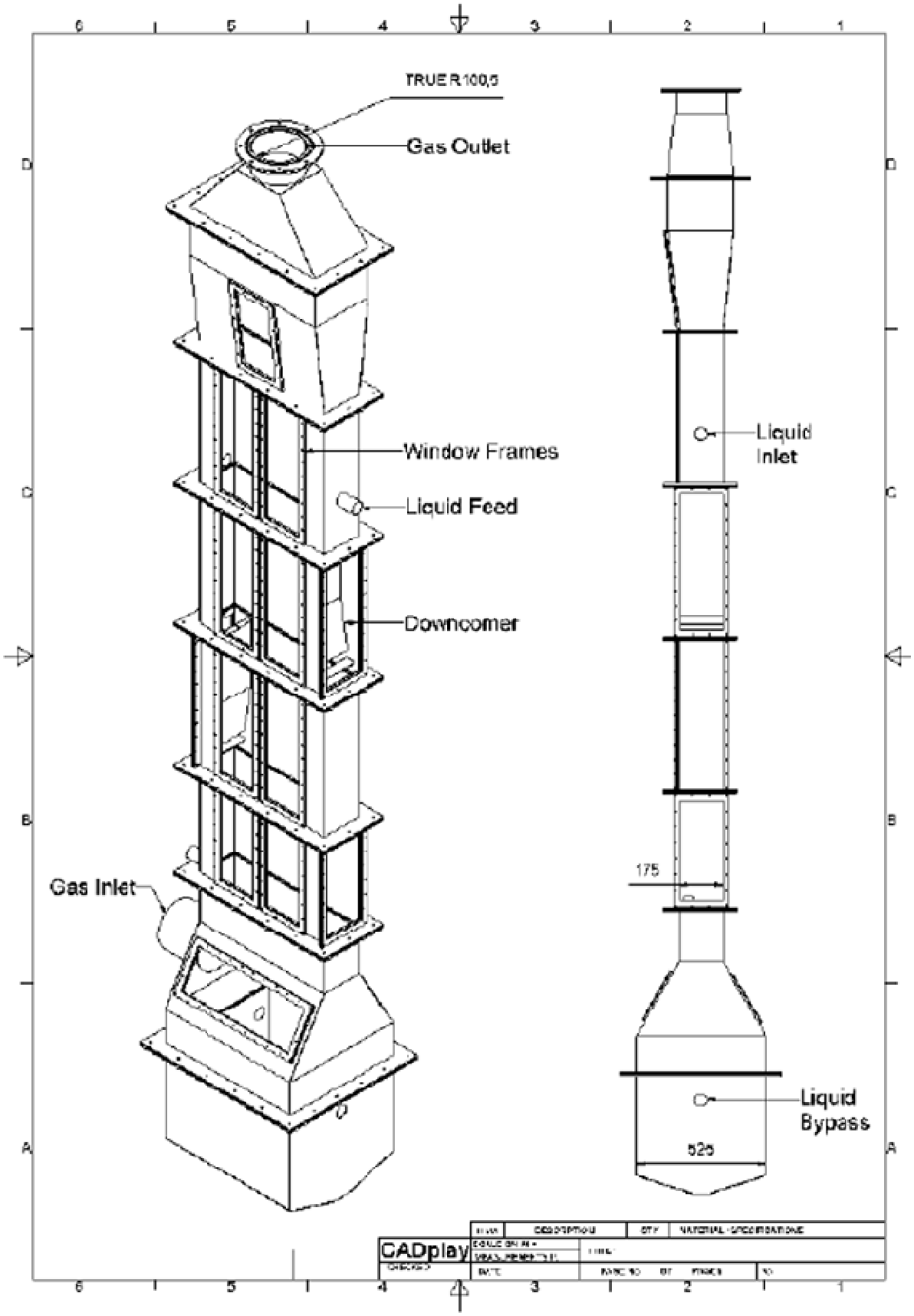

Figure 134 – Side view of distillation column [obtain with permission from (Uys *et al.*, 2009)]

Table 15 shows the specifications of the gasses to be used in the blower (E-102).

Table 15 – Blower gas specification [obtained with permission from (Uys *et al.*, 2009)]

Gasses to be used	Flow rate (m^3/h)	Delivery Pressure (kPa)
Air	5600	12
CO_2	2100	16

Figures 135 and 137 show the specification for the small and large de-entrainment vessels that are attached to the distillation pilot plant, respectively.

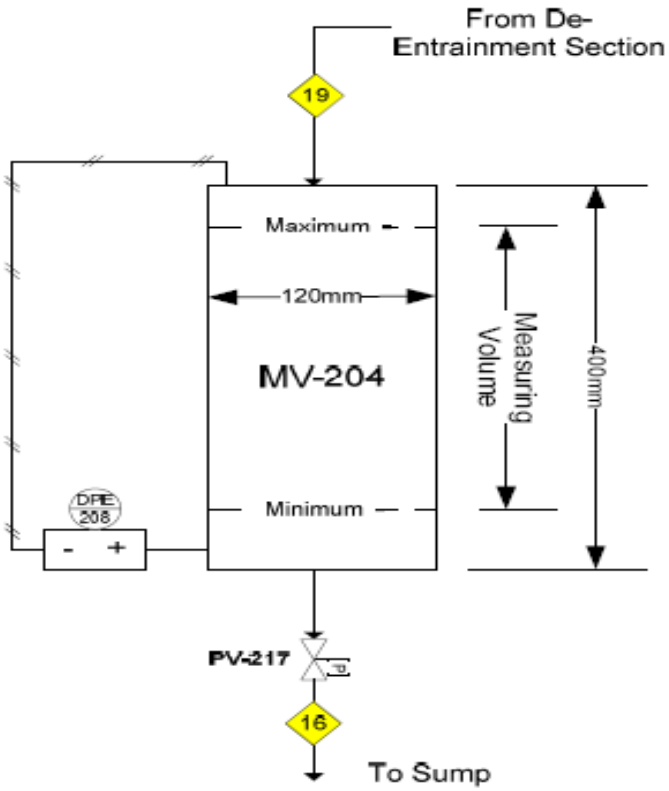

Figure 135 – Small entrainment measuring tank [obtained from (Uys *et al.*, 2009)]

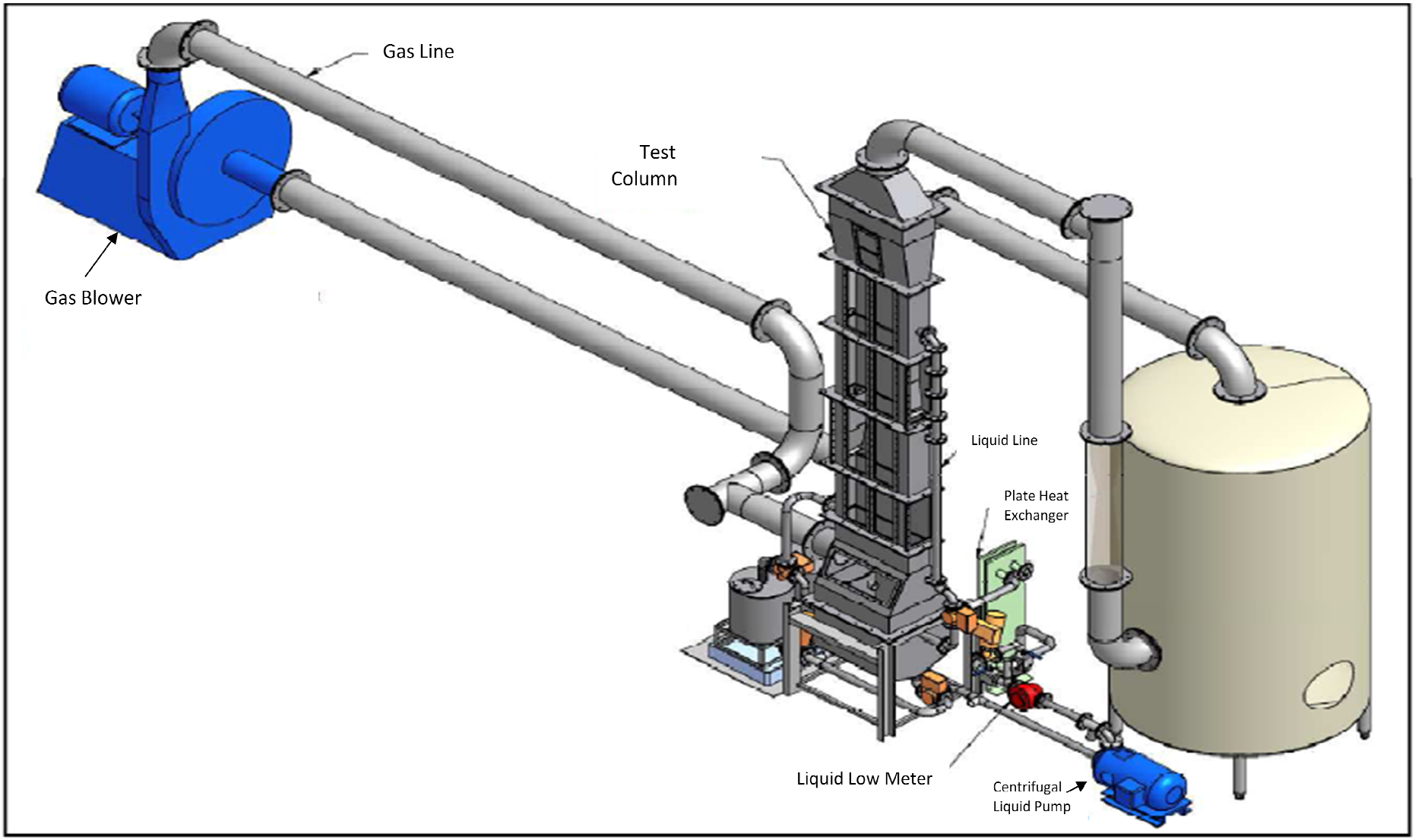

Figure 136 – Distillation pilot plant [Adapted with permission from (Uys *et al.*, 2009)]

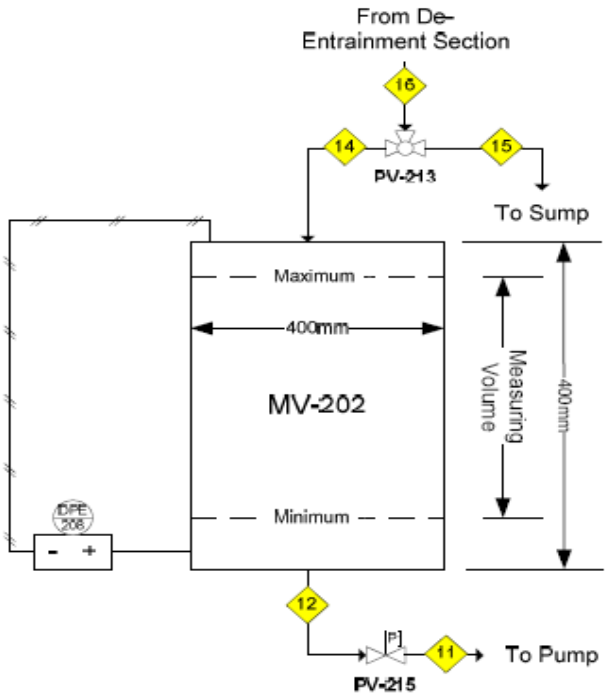

Figure 137 – Large entrainment measuring tank [obtained from (Uys *et al.*, 2009)]

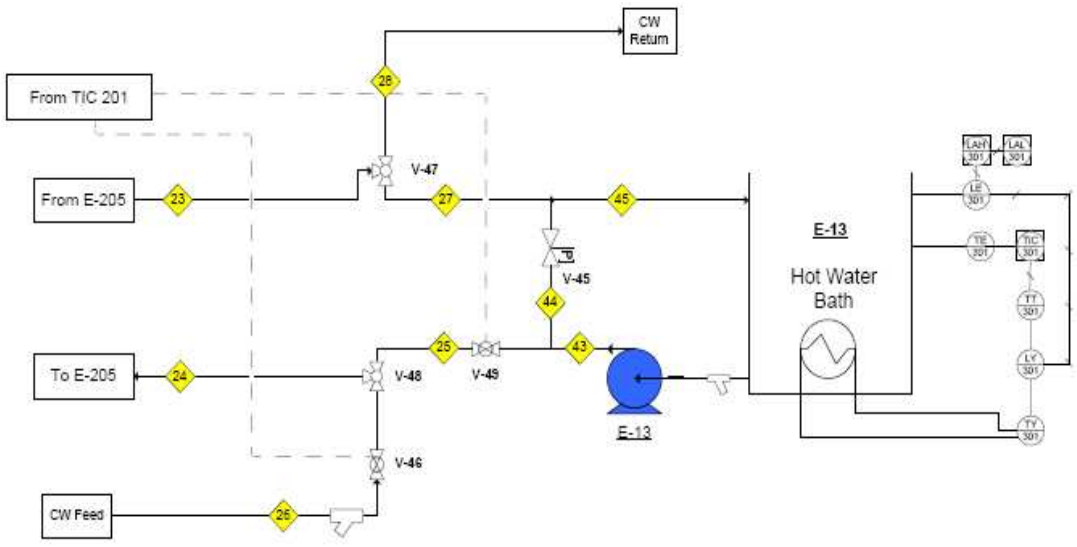

Figure 138 – Temperature control system [obtained with permission from (Uys *et al.*, 2009)]

Table 16 shows the design specifications of the blower (E-102). In the design of the gas blower by (Uys *et al.*, 2009) it is shown that the gas blower is gas tight, motor should be spark proof, a radial vane control valve is placed at the inlet of the blower to control the gas flow rate and safety sensors are attached to the blower to measure vibration and bearing temperature.

Table 16 – Blower (E-102) design specifications [obtained with permission from (Uys *et al.*, 2009)]

Details	Magnitude
Operating temp. range	5 - 80 C
Inlet and exit pipe diameter	203 mm

Table 17 – Pump liquid specification [obtained with permission from (Uys *et al.*, 2009)]

Liquids to be used	Flow rate (m^3/h)	Delivery pressure
Water	20	300
Silicone oil	20	300
Ethylene glycol	20	300
n-Butanol	20	300
n-propanol	20	300

Table 17 shows the specifications of the liquids to be used in the pump (E-204). The specifications of the pump (E-204) are shown by table 16, where the pump is spark proof.

Table 18 – Pump (E-204) design specifications [obtained with permission from (Uys *et al.*, 2009)]

Details	Magnitude
Operating temp. range	5 - 80 ℃
Inlet and exit pipe diameter	2''

The geometrical specifications of the surge tank (E-101) used to regulate pressure fluctuation in the pilot plant and store process gas is shown table 19.

Table 19 – Surge tank (E-101) geometrical specification [obtained with permission from (Uys *et al.*, 2009)]

Description	Magnitude	Units
Vessel Diameter (D_v)	1.6	m
Height	2.8	m
Volume	5	m^3
Inlet Height ($D_v/2$)	0.8	m

The specifications of fluids in heat exchanger (E-205) are shown by Table 20.

Table 20 – Heat exchanger (E-205) fluid specification [obtained with permission of (Uys *et al.*, 2009)]

Description	Inlet Temp. (℃)	Outlet Temp. (℃)	Mass Flow (kg/s)	Volumetric Flow (m^3/h)
Liquid section (water)	25.7	25	5.5	20
Cooling water section	20	22	2.1	8

The heat exchanger (E-205) design conditions are shown by Table 21.

Table 21 – Heat exchanger (E-205) design conditions [obtained with permission from (Uys *et al.*, 2009)]

Specification	Magnitude	Units
Heat exchanger type	Plate	
Operating temperature range	20 - 85	℃
Inlet and outlet pipe diameters	2	in.
Maximum pressure drop	2	bar (gauge)
Maximum pressure	6 - 7.5	bar (gauge)
Material of construction	Stainless steel 316	

The design specifications of the digital pressure transmitter used to measure the differential pressure drop across section of the distillation pilot plant are shown by Table 22.

Table 22 – Differential pressure transmitter specifications [obtained with permission from (Uys *et al.*, 2009)]

Specification	Magnitude and Type
Type	Endress + Hauser
Measuring range	0 - 10 kPa
Turn down ratio	15:1
Measuring accuracy	±0.05%
Maximum linearity error	±0.075%
Special classification	ATEX II 2G EEx d IIC T6
Membrane material	316L
Seal	Viton
output	0 - 20mA

The specifications of the digital absolute pressure transmitter used to measure the absolute pressure in the distillation column and the absolute pressure in the venture pipe are shown by Table 23.

Table 23 – Absolute pressure transmitter specifications [obtained with permission from (Uys *et al.*, 2009)]

Specification	Magnitude and Type
Type	Endress + Hauser
Measuring range	0 - 200 kPa
Turn down ratio	15:1
Measuring accuracy	±0.05%
Maximum linearity error	±0.075%
Special classification	ATEX II 2G EEx d IIC T6
Membrane material	316L
Fill fluid	Silicon Oil
output	0 - 20mA

The specifications of the liquid flow meter used to measure the liquid flow rate to the top sieve tray in the distillation column are shown by Table 24.

Table 24 – Liquid flow meter specifications [obtained with permission by (Uys *et al.*, 2009)]

Specification	Magnitude and Type
Make	Flomec
Measuring range	1.8 - 27 m^3/h
Zero and span	Adjustable
Analogue output	4 - 20 mA
Analogue output accuracy	±0.25% Full Scale
Special Classification	IECEX and ATEX approved, intrinsically safe RT 12

The specification of the gas flow meter is shown by table 25.

Table 25 – Gas flow meter specifications [obtained with permission of (Uys *et al.*, 2009)]

Specification	Magnitude and Type
Make	Sierra
Type	Hot wire anemometer
Measuring range	200 - 2100 kg/h
Analogue output	4 - 20mA
Repeatability	±0.2% Full Scale

Appendix E – Experimental Methodology

E.1 Start up Procedure

1. Switch on the pilot plant control panel and switch to the tray distillation pilot plant.
2. Start the data logging program on the attach PC.
3. Insert the liquid physical properties and the universal gas constant (based on the gas concentration) into the control panel.
4. Open gas inlet valve (V-102), open gas outlet valve (V-104) and close purge valve (V-103) to allow gas flow though distillation pilot plant
5. Start the blower (E-202) at a output frequency of about 15 Hz
6. Adjust the radial control valve to 30% open when the blower finishes its start-up cycle. (At 30% valve opening small fluctuations in the valves position will not affect the gas flow rate as when the valve opening is 25% and the lower).
7. Set the downcomer opening height on the pilot plant to 20 mm to allow sufficient liquid flow to the sieve tray
8. Adjust the liquid flow rate on the touch control panel to a flow rate of 10 – 20 m^3/h, at high flow setting.
9. After about 30 seconds the liquid flow rate control valve (PCV – 205) will open, at which time the liquid pump (E-204) should be switched on at an output frequency of 15 Hz.
10. Switch the three-way valve (PV-212) so that the liquid flows through the column (line 9) and not through the bypass line (line 8), after the start-up cycle of the pump is complete.
11. Switch on the cooling water system or the column heating system and pump (depending on the fluids temperature) and adjust the liquid temperature set point to 25℃, which will control the column temperature to an average temperature of 25℃.
12. Monitor the level of liquid in de-entrainment section and ensure that the liquid level does not exceed 70 mm. (When the liquid exceeds 70 mm, the liquid starts exiting through the gas/liquid separating device (de-entrainment tray cylinder openings)).
13. If flooding occurs, the output frequency of the blower (E-102) should be reduced.
14. The liquid captured by the de-entrainment section is the entrained liquid and is measured by the hold-up tank (MV-204) for low liquid rates or by hold up tank (MV-202) for large liquid flow rates (close to flooding point).
15. The liquid captured by the chimney tray is the weeping liquid and is measured with hold-up tank (MV-203)
16. To obtain steady state in the column values (PV-214) and (PV-215) should be arranged so that the liquid flows to the sump instead of the hold-up tanks.
17. The weeping and the entrainment hold-up tanks should be flushes with liquid before commencing with the experiment, as to ensure that the hold-up tanks and the column area at similar temperatures.

E.2 Experimental Operating Procedure

1. Set the specific gas constant to the concentration of the gas in the column (readjust gas constant every 2 hours when running the pilot plant).

2. Set the absolute pressure of the column so that it maintained at 101.15 kPa (+-1 kPa).
3. Set the downcomer escape height to the height of the liquid flow rate as specified by table 7.
4. Set the required control valve position to 20 on the control panel. (The control valve will be fully open at which point the set value of liquid volumetric flow rate will be 20 m^3/h, to ensure that the liquid flow rate is constant and uninfluenced by the valve)
5. For a low liquid flow rate (below 2 m^3/h):
    a. Set the control panel for low liquid flow
    b. Adjust the pump frequency between 15 – 50 Hz for the desired liquid flow rate

6. For a high liquid flow rate (above 2 m^3/h):
    a. Set the control panel for high flow.
    b. The pump output frequency should then be adjusted so that it is about 15 – 50 Hz, until the liquid volumetric flow rate is approximately 0.5 m^3/h above the set flow rate.
    c. Set the liquid flow rate on the control panel, so that the control valve (PCV-205) can continuously control the liquid flow rate.
7. Adjust the gas flow rate by changing the rotational speed of the blower, so that the limit of 10mm and 70mm visible liquid height on the de-entrainment section is obtained.
8. A sample set should be taken 15 minutes after the column temperature, differential pressure of each section, gas flow rate and the liquid flow rate has stabilized. (Graphs are plotted on the HMI to determine if the system is stable).
9. 5 minutes after all the HMI graphs show no change the system is considered stable
10. Set the entrainment tank hold-up mass, amount of sample points and initiate the entrainment sampling procedure:
    a. Closing the valve (PV-217) will fill the hold-up tank (MV-204) with liquid exiting from the de-entrainment section.
    b. The mass flow rate of the entrainment liquid is measured by logging the mass of the liquid in the hold-up tank (MV-204) with time.
    c. When the sample volume is reached, the valve (PV-217) should be opened to drain the liquid into the sump.
11. The entrainment sampling procedure should be repeated 3 – 4 times to ensure that the results are accurate for each liquid and gas flow rate and determine if the system was stable.
12. Set the weeping tank hold-up mass and initiate the weeping sampling procedure:
    a. Opening the valve (PV-214) will fill the hold-up tank (MV-203) with liquid exiting from the chimney tray section.
    b. The mass flow rate of the entrainment liquid is measured by logging the mass of the liquid in the hold-up tank (MV-203) with time.
    c. When the sample volume is reached, the valve (PV-216) and valve (PV-201) is switch to drain the liquid into the column with the centrifugal pump.
13. The weeping sampling procedure should be repeated 3 – 4 times to ensure that the results are accurate for each liquid and gas flow rate and determine if the system was stable.
14. Measure at least five gas flow rates per liquid flow rate

15. To test repeatability the conditions at which the experiment is run should be repeated on different dates.

E.3 Shutdown Procedure

1. Switch off the column heating system and pump
2. Switch the three-way valve (PV-212) so that the liquid flows through the bypass line (line 8), and not through the column (line 9), after the start-up cycle of the pump is complete.
3. Switch off the centrifugal pump (E-204) to stop the flow of the liquid.
4. Switch off the blower (E-202) to stop the flow of gas through the distillation column.
5. Close gas inlet valve (V-102) and close gas outlet valve (V-104) to minimize the loss off gas from the system.
6. Stop the data logging program on the attach PC.
7. Switch off the pilot plant control panel.

E.4 Gas Loading Procedure

The following procedure demonstrates the method used to purge the distillation column with a particular gas before the experimental investigation commences.

1. Close gas inlet valve (V-102), open gas outlet valve (V-104) and open purge valve (V-103) to allow gas pressure to be realised from the surge tank(E-101) of distillation pilot plant.
2. Ensure that the manhole opening in the surge tank (E-101) is completely closed.
3. Connect the absolute pressure meter (PE -206) to the gas inlet line (line 34).
4. Replace the differential pressure ports across the gas venturi (E103) in line 38 with plugs.
5. Attach the water line connection (water hose) to the top of the surge tank (E-101).
6. Allow water to enter the surge tank by opening the water line into the surge tank (E-101) for about 6 hours maximum (Once done switch off water line and close the valve on top of the surge tank (E-101)).
7. Close gas outlet valve (V-104) and close purge valve (V-103) to allow gas pressure to be realised from the surge tank (E-101) of distillation pilot plant.
8. Set the column pressure to 103 kPa on the control panel, which will control the gas inlet control valve (PCV-107) into the surge tank (E-101).
9. Open the gas line valve at the gas cylinder to allow the gas of choice to enter the surge tank (E-101) and partially open the drain valve (V-108) at the bottom of the surge tank (E-101) to displace the water in the surge tank (E-101) with gas (which is about 2.5 hours, once done close the drain valve (V-108) below the surge tank (E-101)).
10. To purge the distillation column:
    - 10.1. Connect the absolute pressure meter (PE -206) distillation column.
    - 10.2. Replace the differential pressure ports that have plugs across the gas venturi (E-103) in line 38 the differential pressure meter lines.
    - 10.3. Set the column pressure to 103 kPa on the control panel, which will control the gas inlet control valve (PCV-107) into the surge tank (E-101).
    - 10.4. Open gas inlet valve (V-102), close gas outlet valve (V-104) and close purge valve (V-103) to allow gas pressure to be realised from the surge tank (E-101) of distillation pilot plant.

10.5. Allow about 1 hour to purge the column and close the purge valve (V-103).

10.6. Take a sample of the gas in the sample port in line 36 and analyze (once the gas concentration is about 97 %, the ideal gas concentration is reached).

E.5 Sampling Techniques

This section identifies the techniques used to analyze the gas and liquid physical properties. During the operation of the distillation pilot the liquid is heated to about 28 ℃ and a long glass cylinder is filled with the liquid. The liquid density measured using a hydrometer (resolution of 0.5 kg/m^3). The hydrometer is placed into the cylinder to measure the liquid density. A portion of the liquid sample is used to measure the liquid surface tension using a Sigma 702 surface tensionometer (resolution of 0.01 mN/m).

A liquid sample is taken in order to measure its viscosity using an Anton Paar Physica MCR501 2007 rotaviscometer (resolution of 0.01 mPa.s). In order to measure the composition in the distillation column a sample of the gas is taken from the sample port in line 36 into a gas sampling cylinder. The composition of the sample is measured using a HP 5890 GC (gas chromatograph).

Appendix F – Experimental Result Graphs

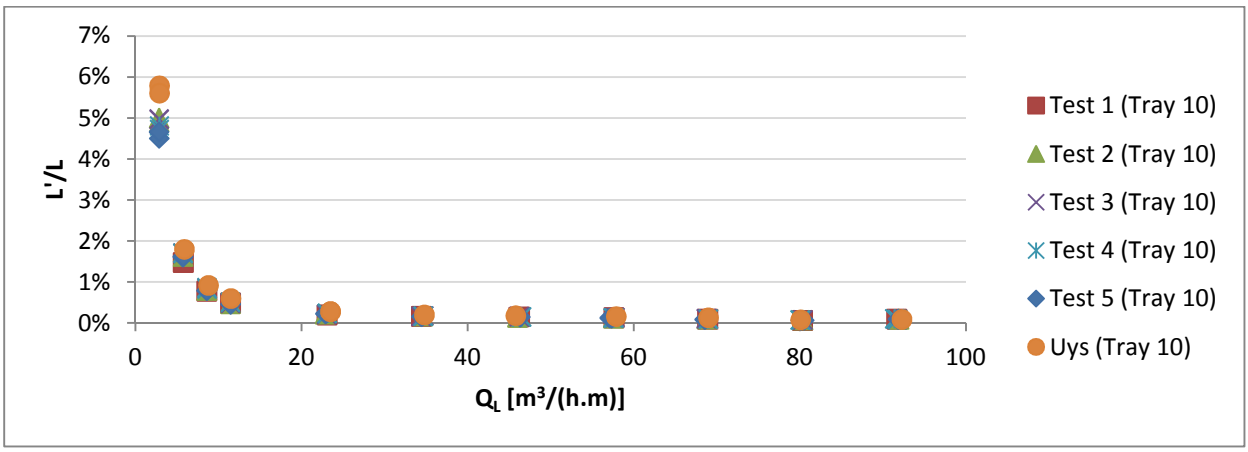

Figure 139 – L'/L entrainment repeatability and 'Uys' data comparison for Tray 10 (15.6%, 6.3 mm) and u_s = 2.6 m/s

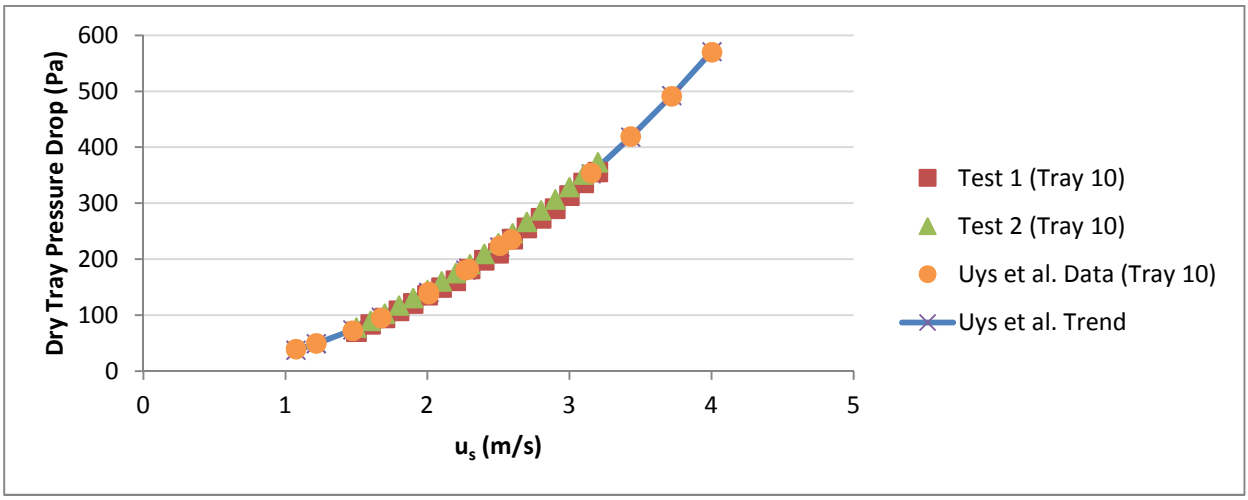

Figure 140 – Dry tray pressure drop repeatability and 'Uys' data comparison for Tray 10 (15.6%, 6.3 mm)

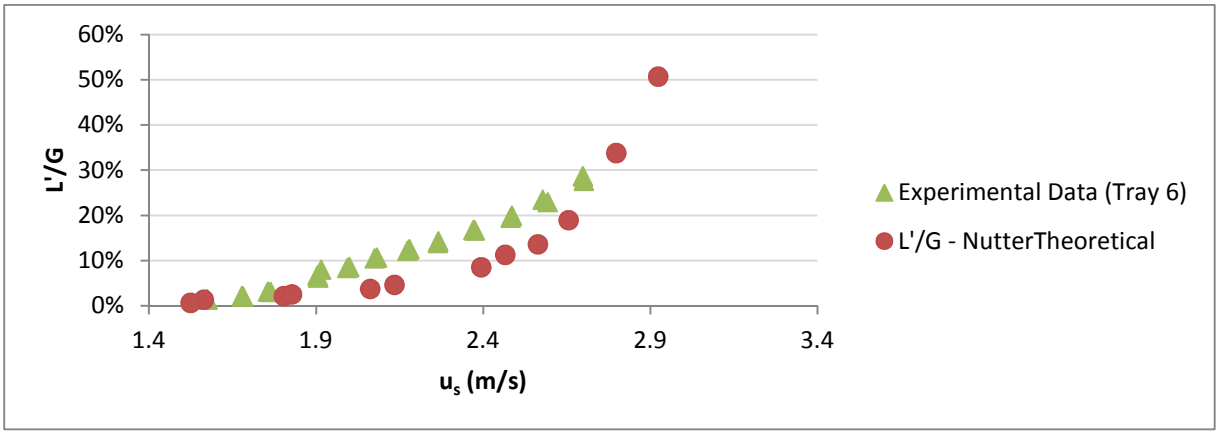

Figure 141 – L'/G experimental data comparison (Nutter, 1971) for Tray 6 (7%, 12.7 mm) and Q_L = 13.1 m³/(h.m)

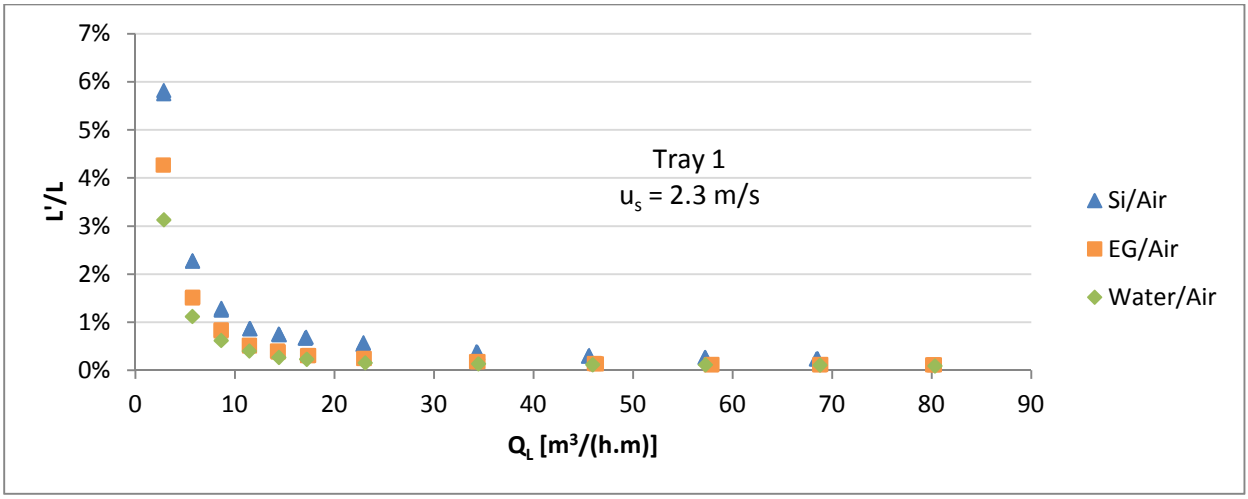

Figure 142 – Entrainment (L'/L) of different liquids with air for tray 1 (15.8% fractional hole area, 6.4 mm hole diameter) at a superficial gas velocity of 2.3 m/s.

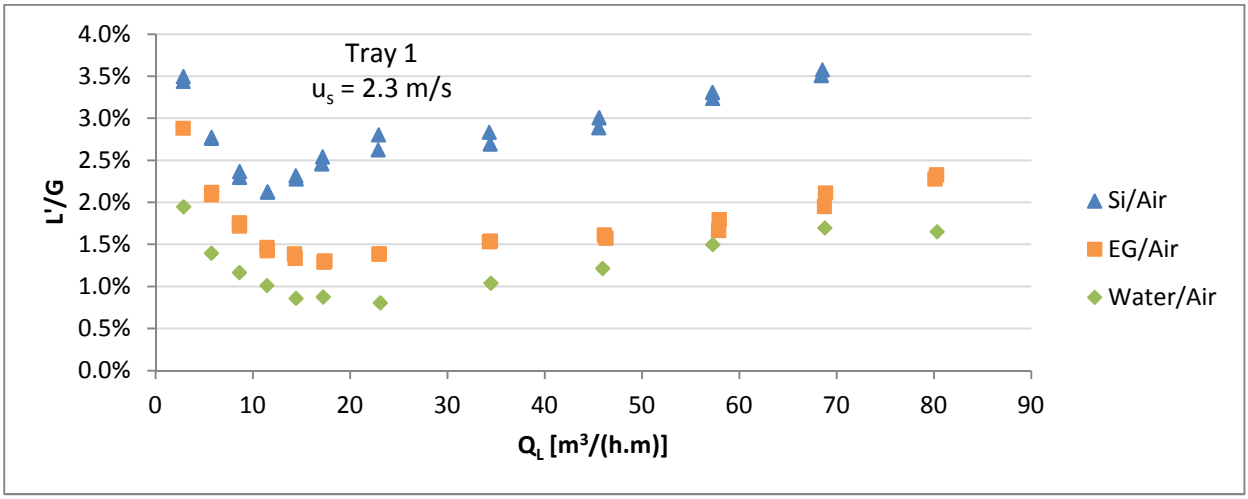

Figure 143 – Entrainment (L'/G) of different liquids with air for tray 1 (15.8% fractional hole area, 6.4 mm hole diameter) at a superficial gas velocity of 2.3 m/s.

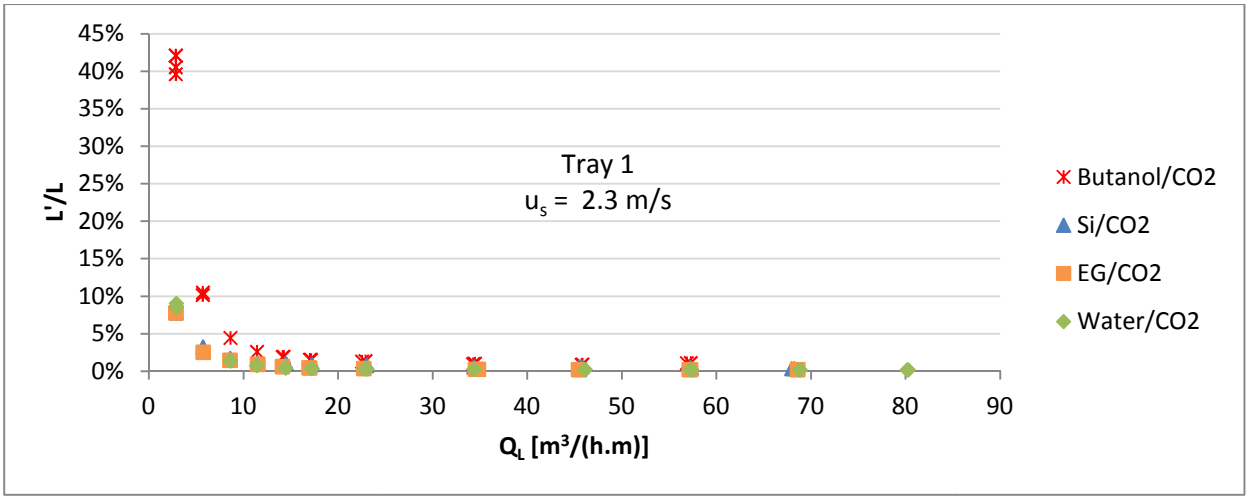

Figure 144 – Entrainment (L'/L) of different liquids with CO_2 for tray 1 (15.8% fractional hole area, 6.4 mm hole diameter) at a superficial gas velocity of 2.3 m/s.

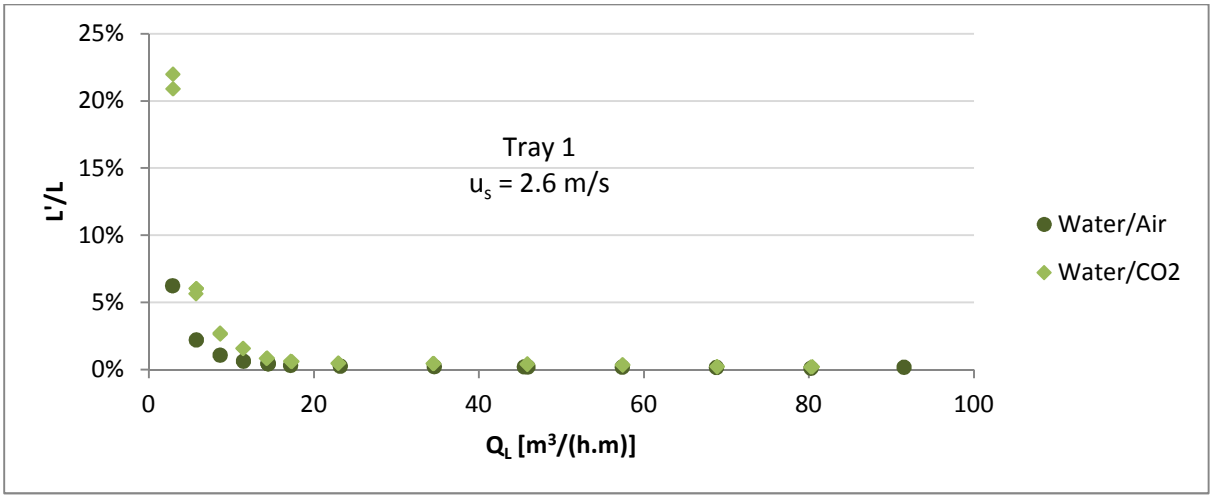

Figure 145 – Entrainment of water (L'/L) with different gasses for tray 1 (15.8% fractional hole area, 6.4 mm hole diameter) at a superficial gas velocity of 2.6 m/s.

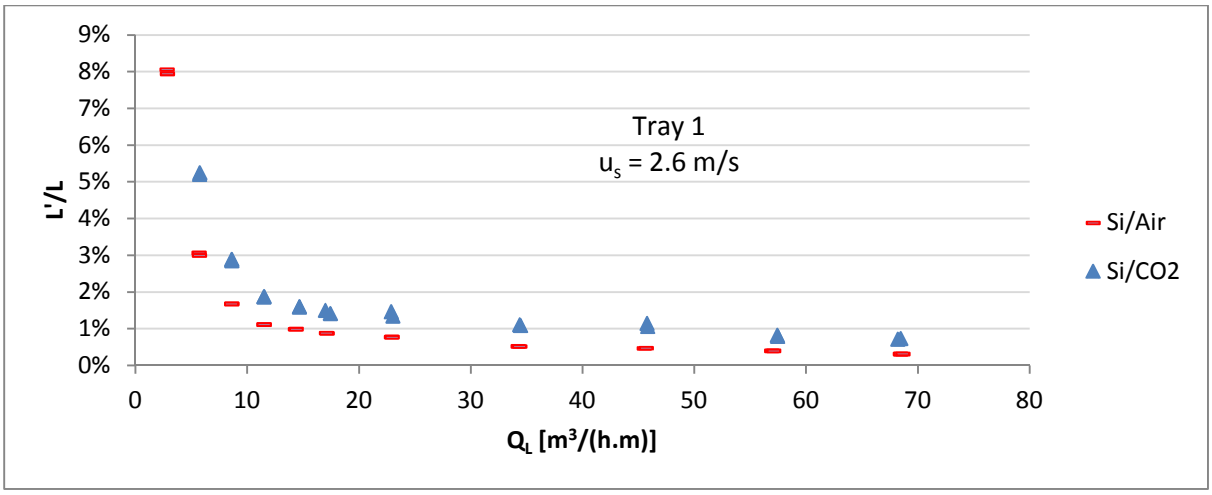

Figure 146 – Entrainment of silicone oil (L'/L) with different gasses for tray 1 (15.8% fractional hole area, 6.4 mm hole diameter) at a superficial gas velocity of 2.6 m/s.

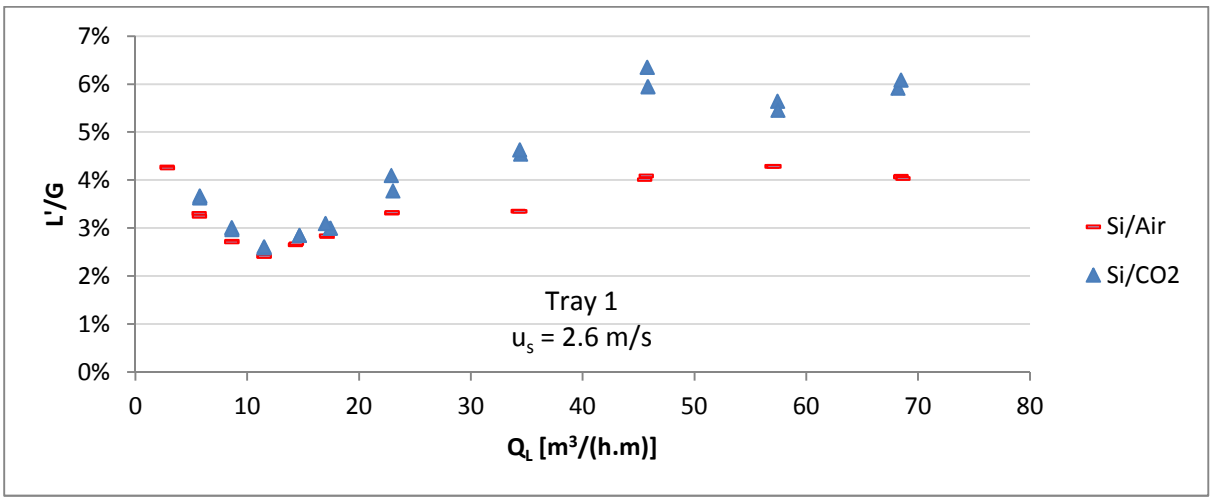

Figure 147 – Entrainment of silicone oil (L'/G) with different gasses for tray 1 (15.8% fractional hole area, 6.4 mm hole diameter) at a superficial gas velocity of 2.6 m/s.

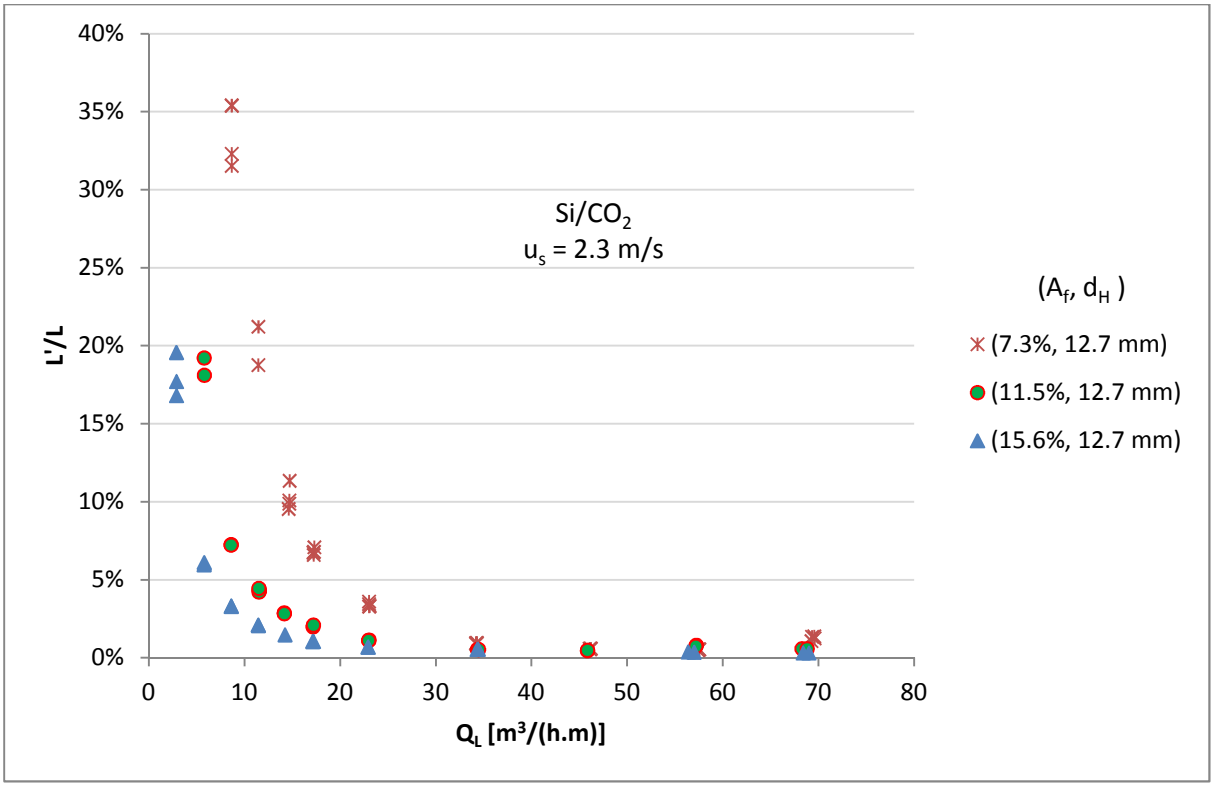

Figure 148 – Effect of fractional hole area on entrainment (L'/L) for silicone-oil/CO_2 with a 12.7 mm hole diameter and a superficial gas velocity of 2.3 m/s.

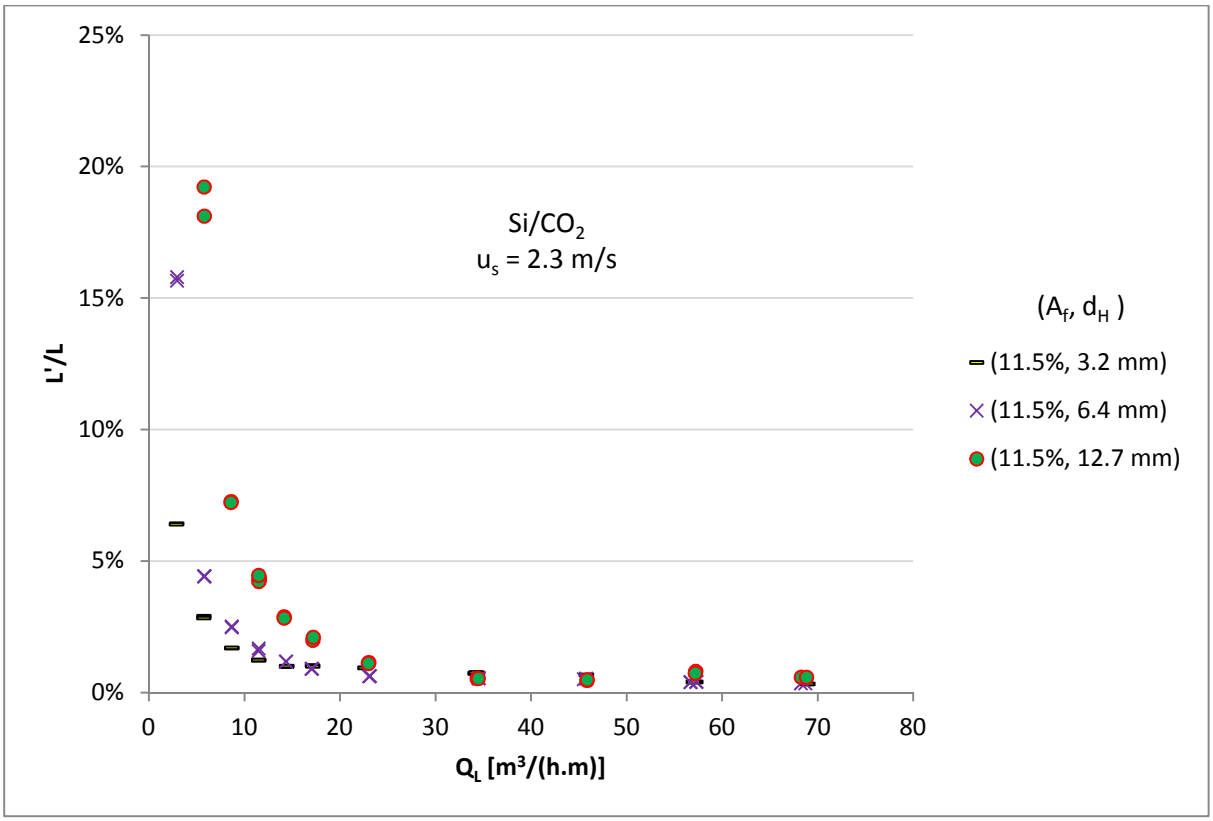

Figure 149 – Effect of hole diameter on entrainment (L'/L) for silicone-oil/CO_2 with a 11% fractional hole area and a superficial gas velocity of 2.3 m/s.

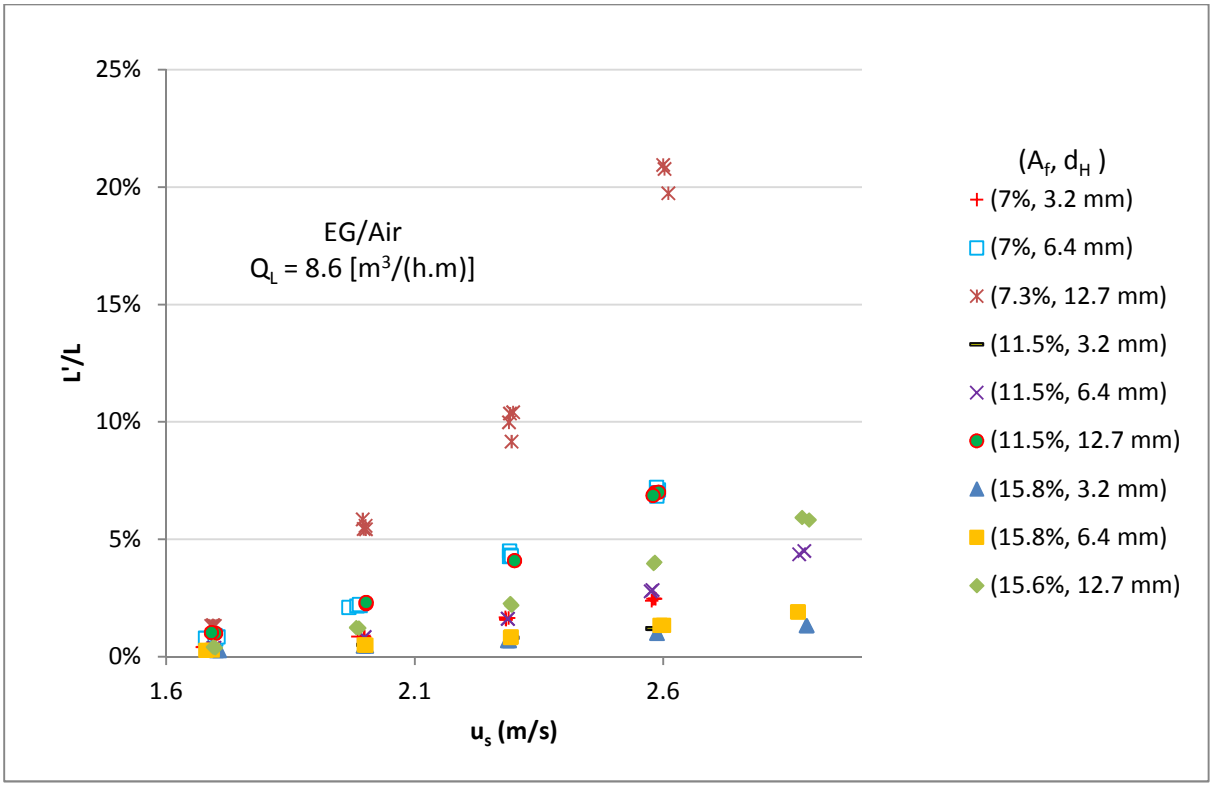

Figure 150 – Effect of tray geometry on entrainment (L'/L) for ethylene-glycol/air with changing superficial gas velocity and a liquid flow rate of 8.6 [m^3/(h.m)].

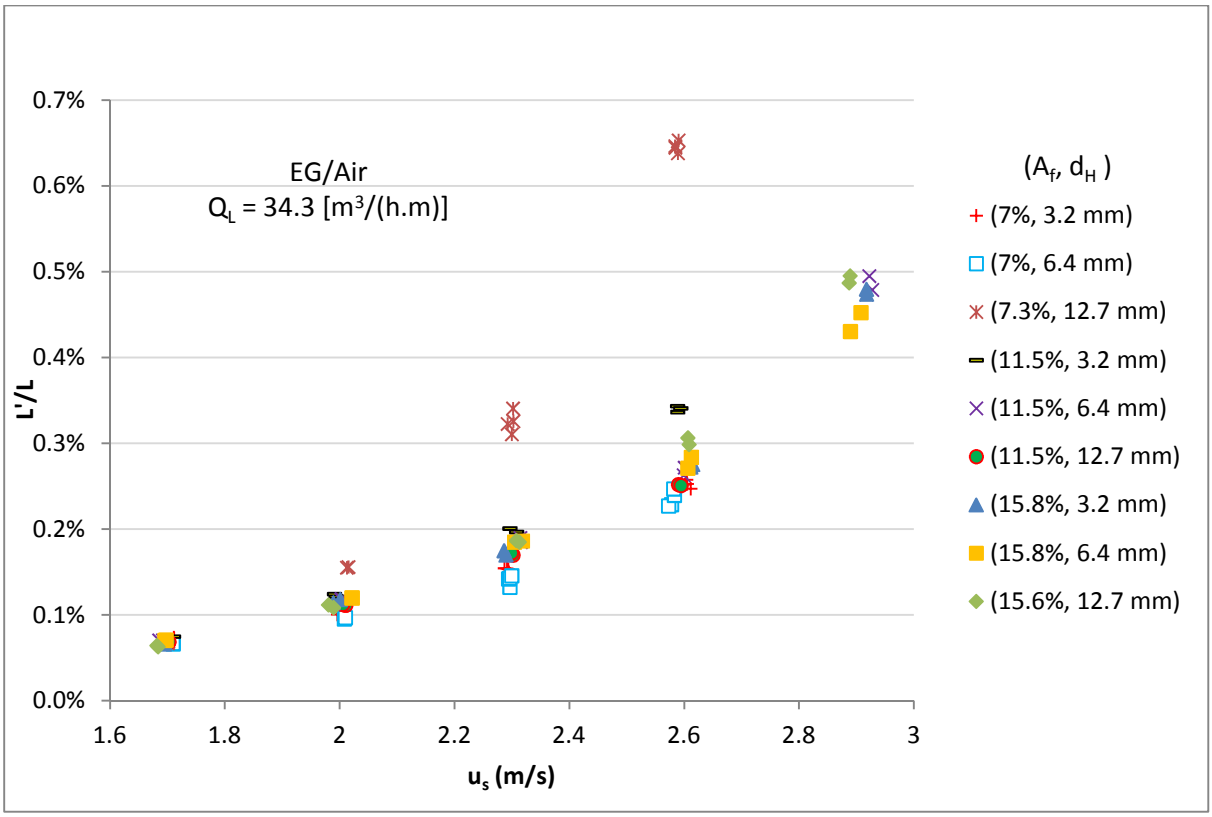

Figure 151 – Effect of tray geometry on weeping (L'/L) for ethylene-glycol/air with changing superficial gas velocity and a liquid flow rate of 34.3 [m^3/(h.m)].

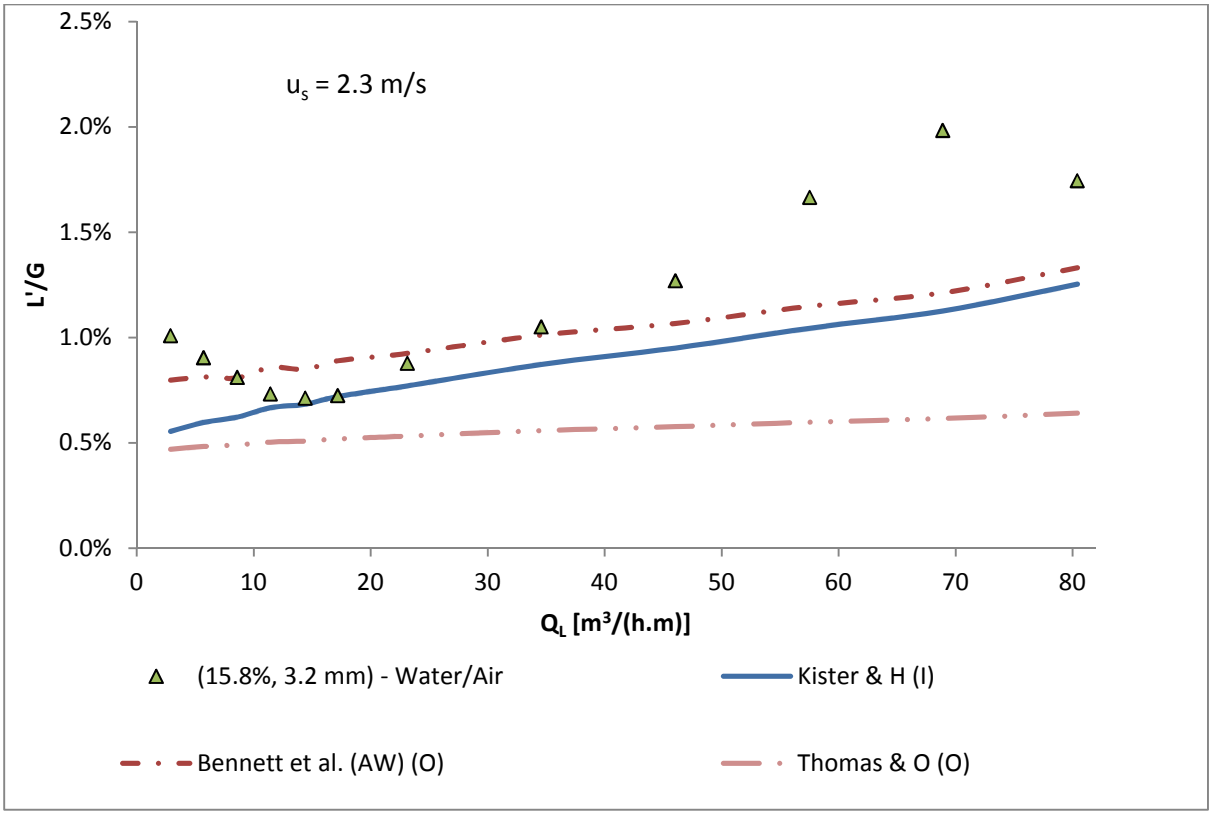

Figure 152 – Experimental entrainment comparison to entrainment models for tray 2 (15.8% fractional hole area, 3.2 mm hole diameter) with water/air at a superficial gas velocity of 2.3 m/s.

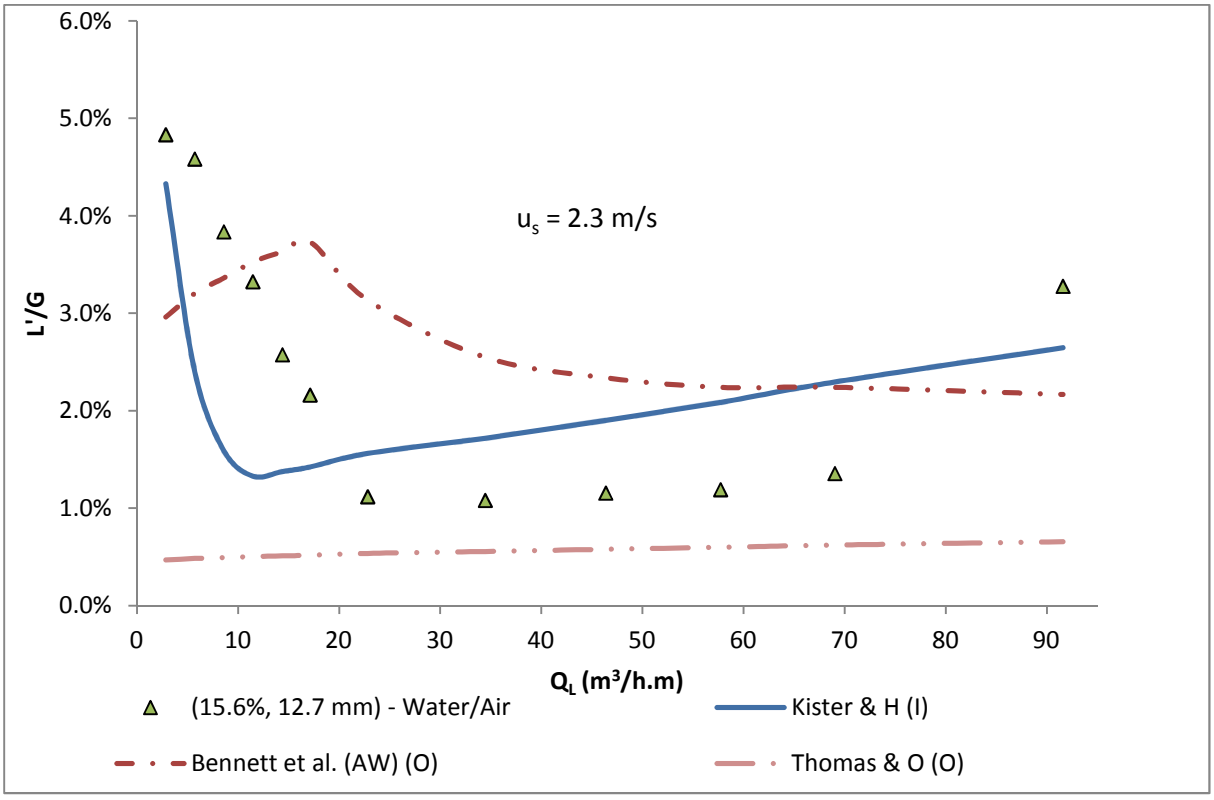

Figure 153 – Experimental entrainment comparison to entrainment models for tray 3 (15.6% fractional hole area, 12.7 mm hole diameter) with water/air at a superficial gas velocity of 2.3 m/s.

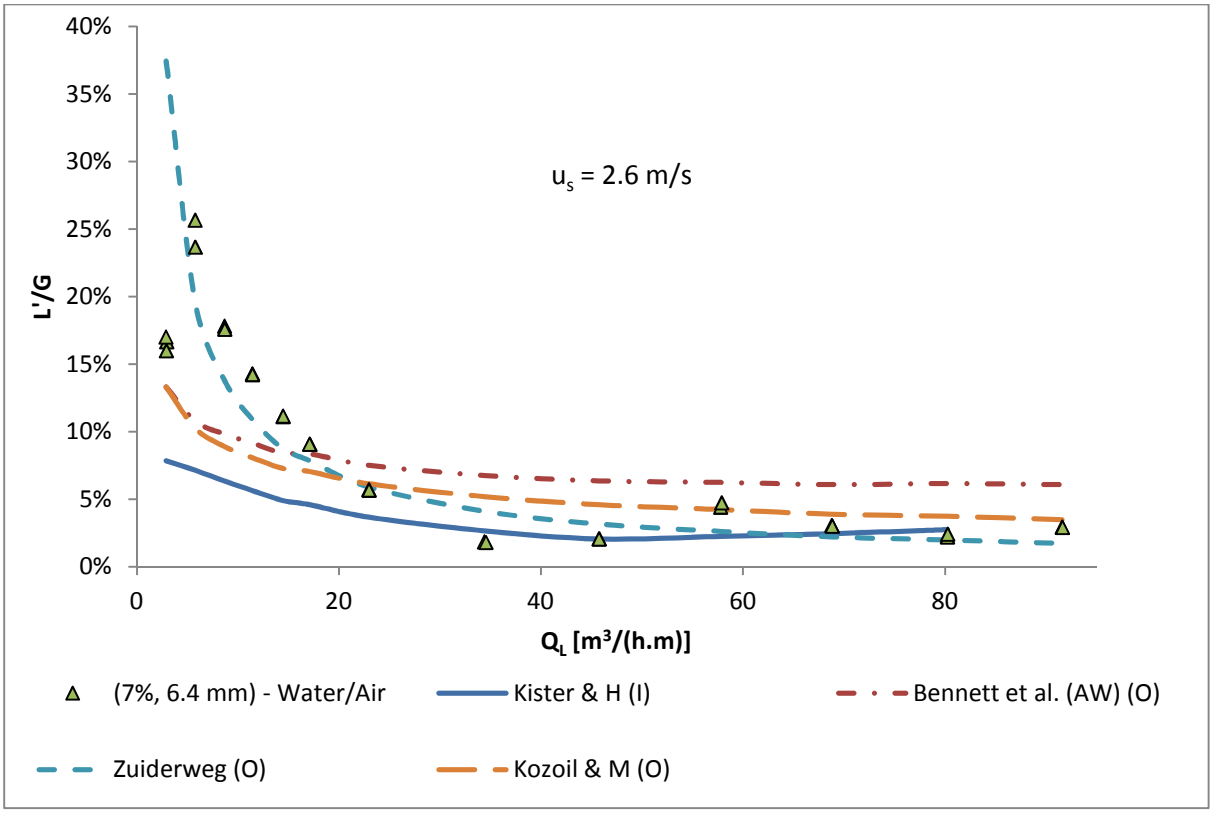

Figure 154 – Experimental entrainment comparison to entrainment models for tray 4 (7% fractional hole area, 6.4 mm hole diameter) with water/air at a superficial gas velocity of 2.6 m/s.

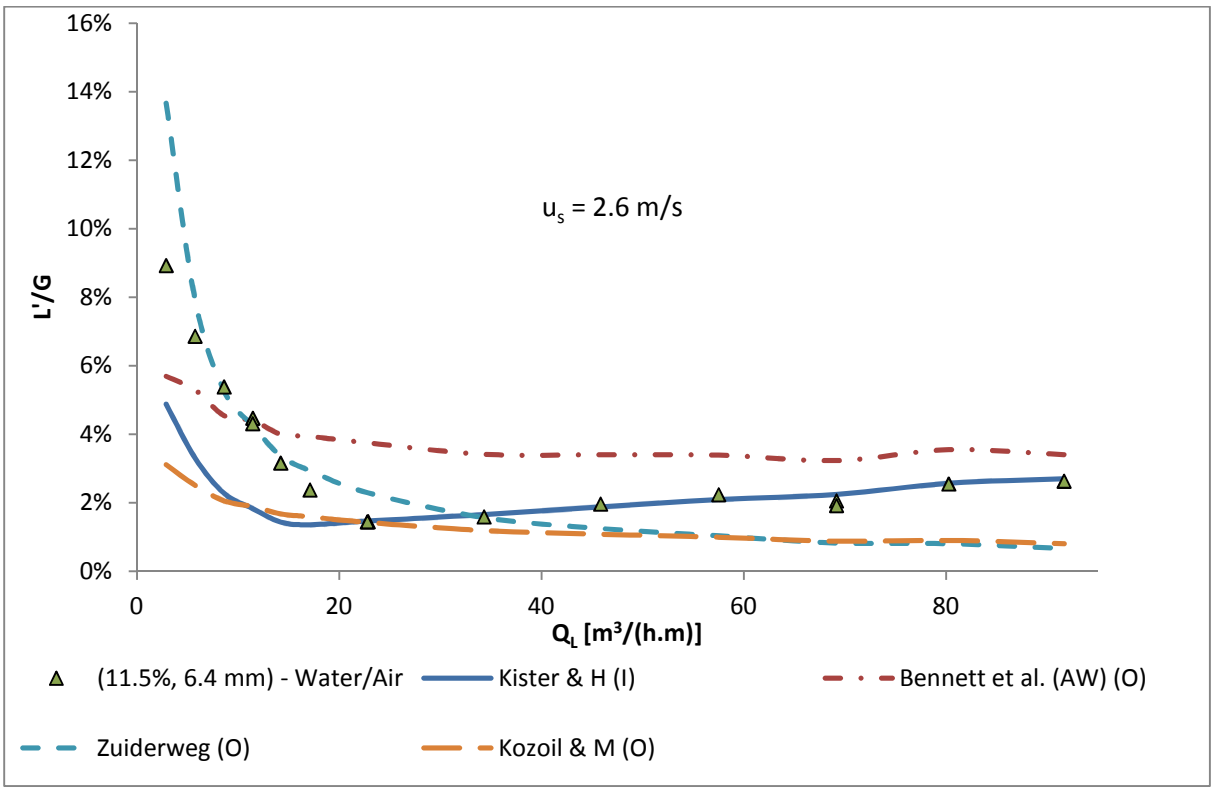

Figure 155 – Experimental entrainment comparison to entrainment models for tray 7 (11.5% fractional hole area, 6.4 mm hole diameter) with water/air at a superficial gas velocity of 2.6 m/s.

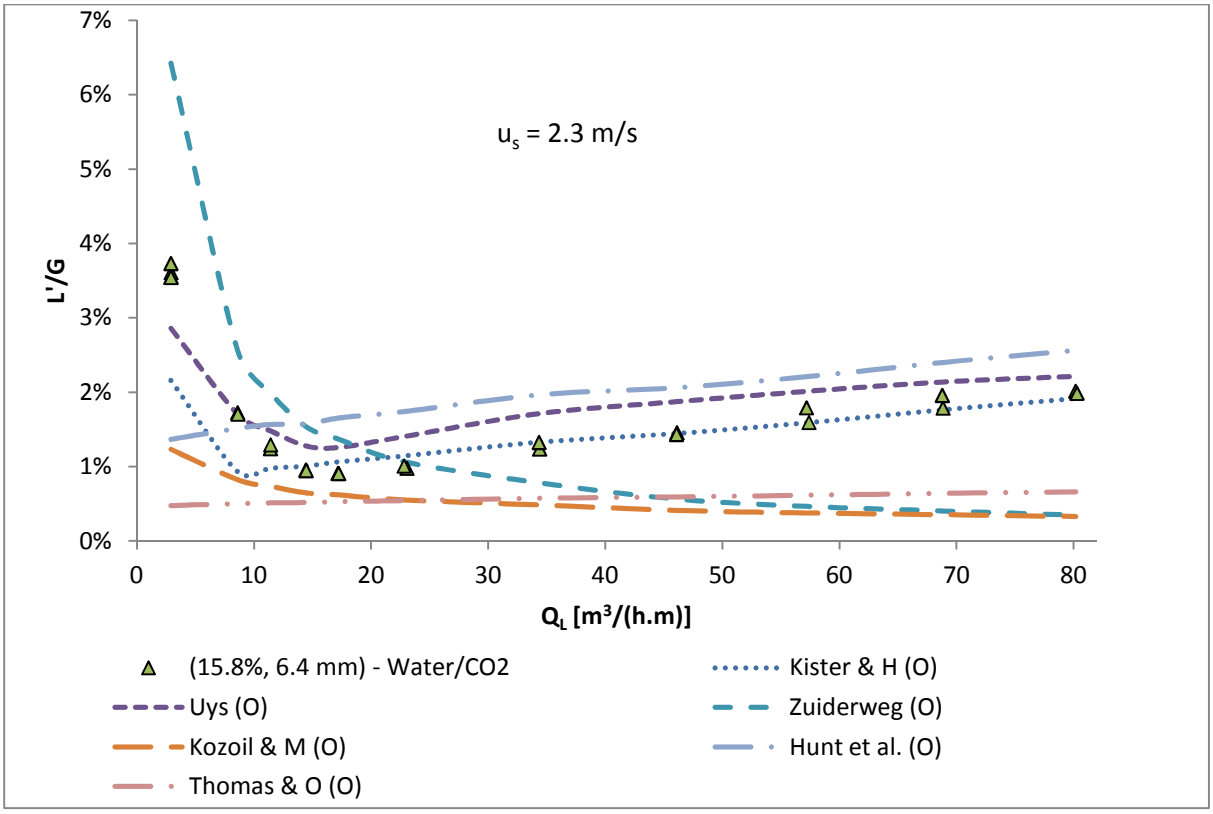

Figure 156 – Experimental entrainment comparison to entrainment models for tray 1 (15.8% fractional hole area, 6.4 mm hole diameter) with water/CO_2 at a superficial gas velocity of 2.3 m/s.

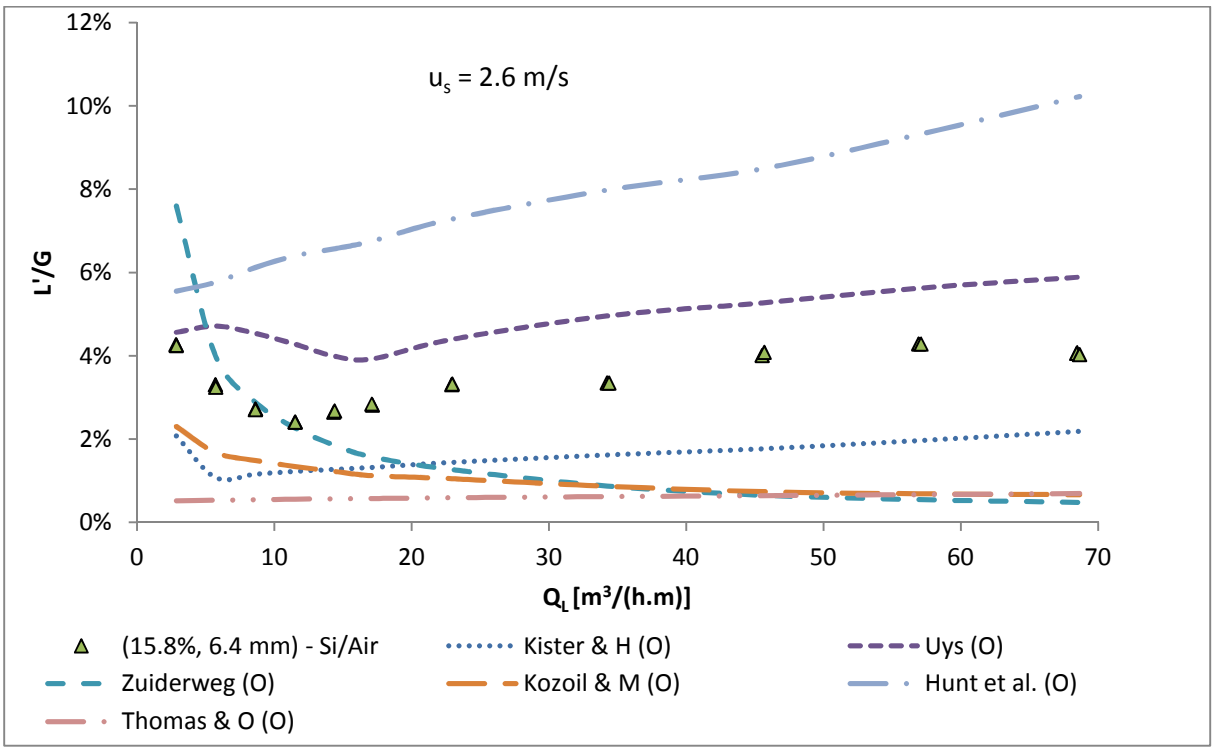

Figure 157 – Experimental entrainment comparison to entrainment models for tray 1 (15.8% fractional hole area, 6.4 mm hole diameter) with silicone-oil/air at a superficial gas velocity of 2.6 m/s.

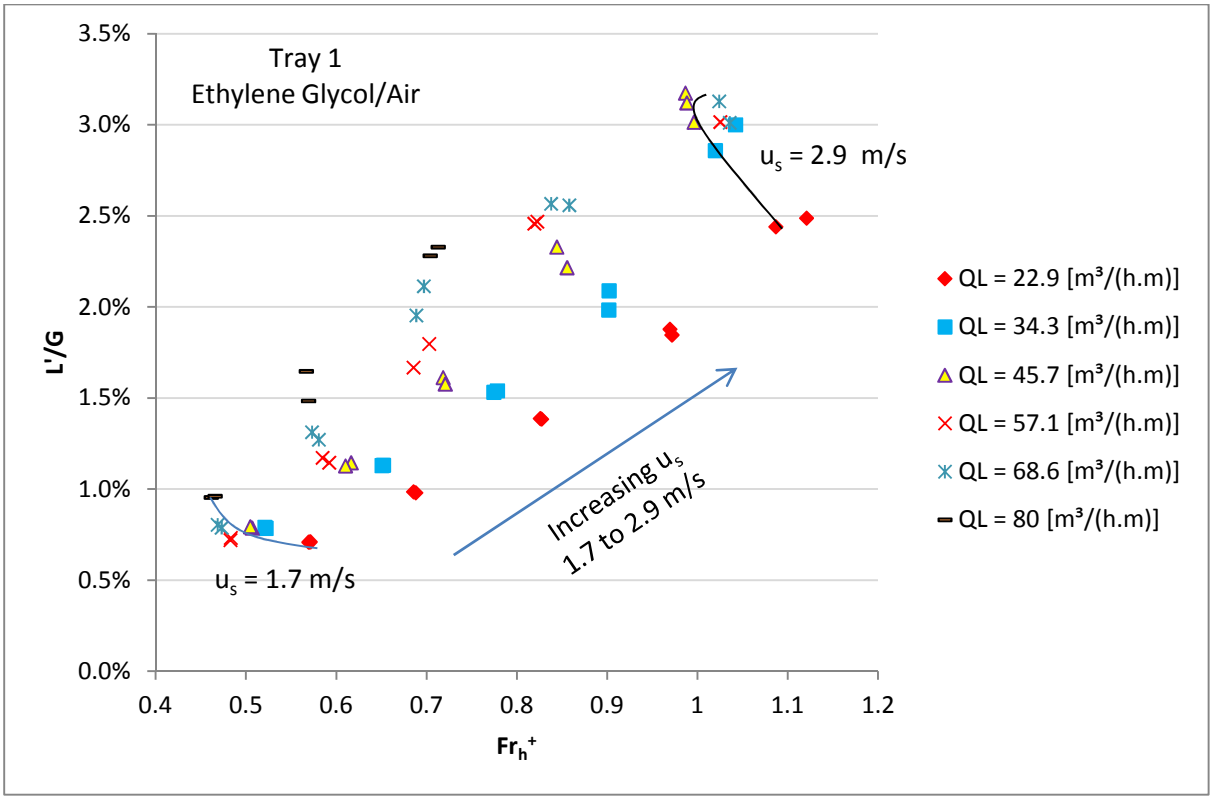

Figure 158 – Entrainment (L'/G) changing with the liquid holdup Froude number (Fr_h^+) for ethylene-glycol/air with tray 1 (15.8% fractional hole area, 6.4 mm hole diameter) in the froth regime.

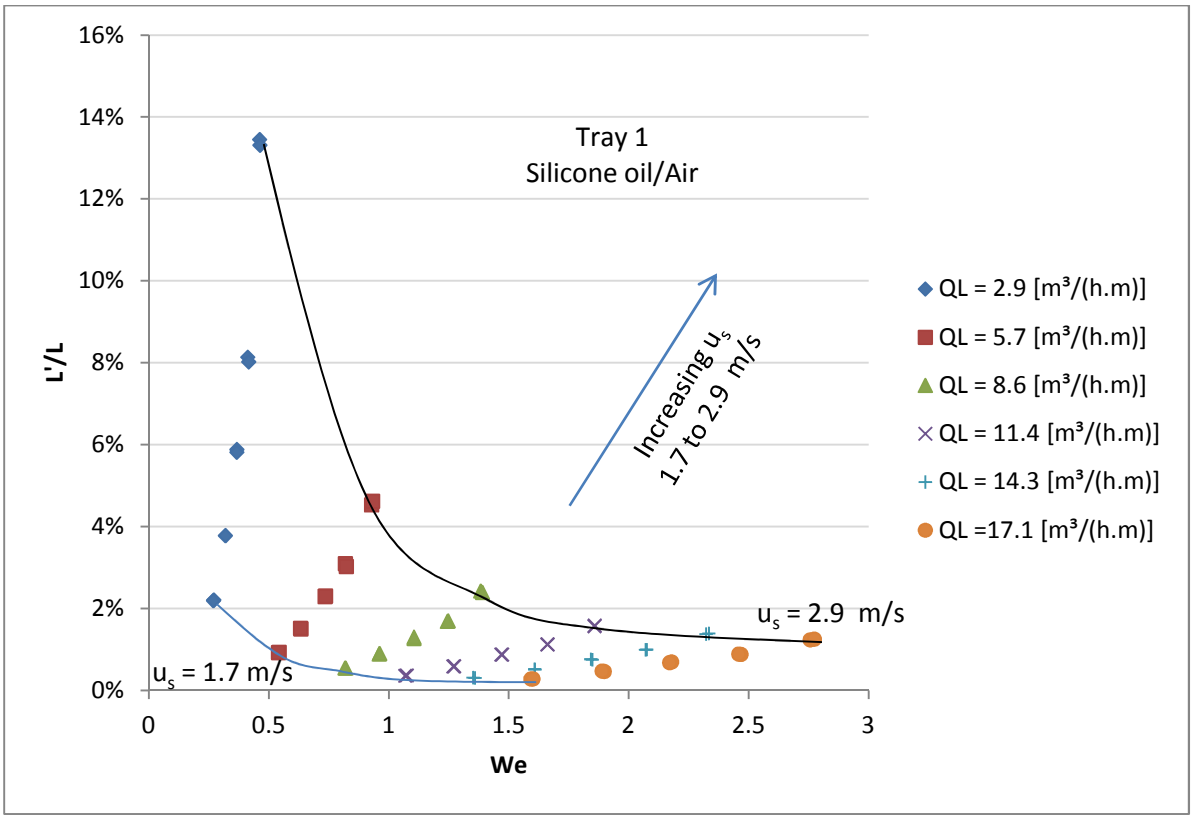

Figure 159 – Entrainment (L'/L) changing with the Weber number (We) for silicone-oil/air with tray 1 (15.8% fractional hole area, 6.4 mm hole diameter) in the spray regime.

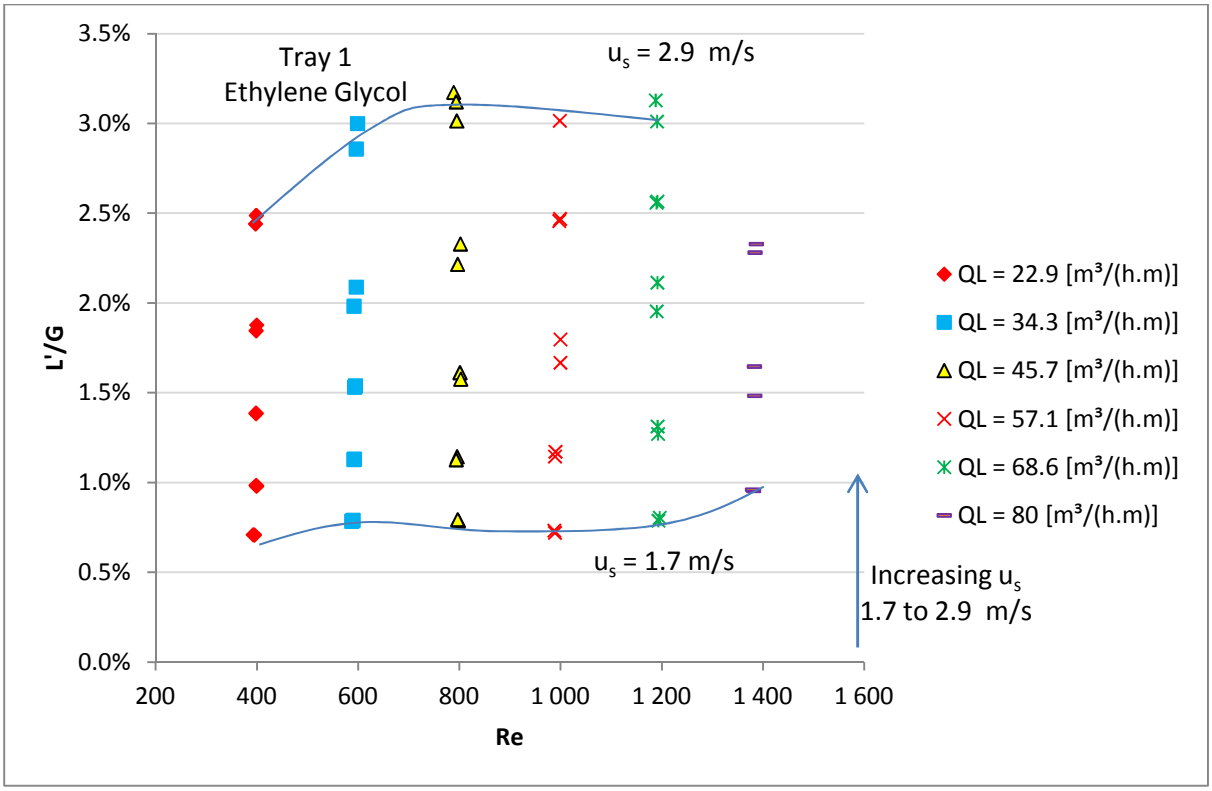

Figure 160 – Entrainment (L'/G) changing with the Reynolds number (Re) for ethylene-glycol/air with tray 1 (15.8% fractional hole area, 6.4 mm hole diameter) in the froth regime.

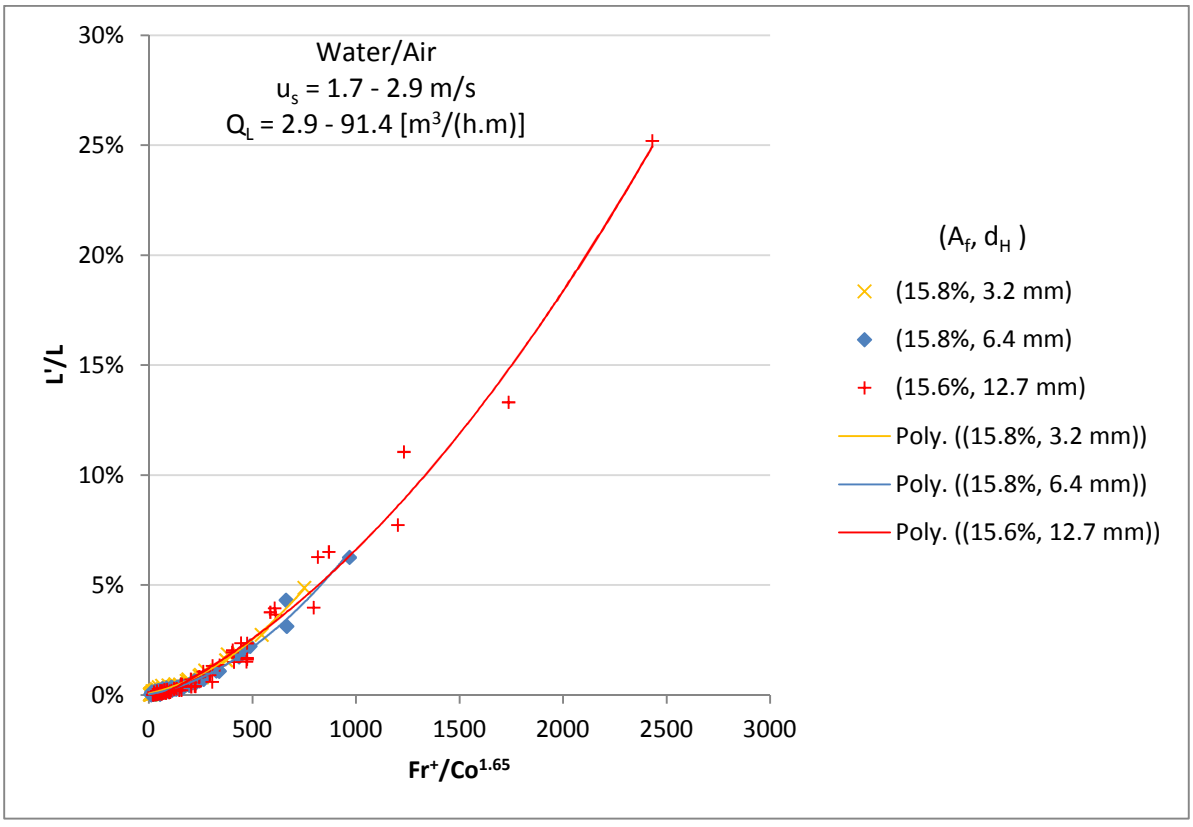

Figure 161 – Entrainment (L'/L) changing with the flow Froude number (Fr^+) to construction number (Co) ratio for water/air at a fractional hole area of 15% and different hole diameters.

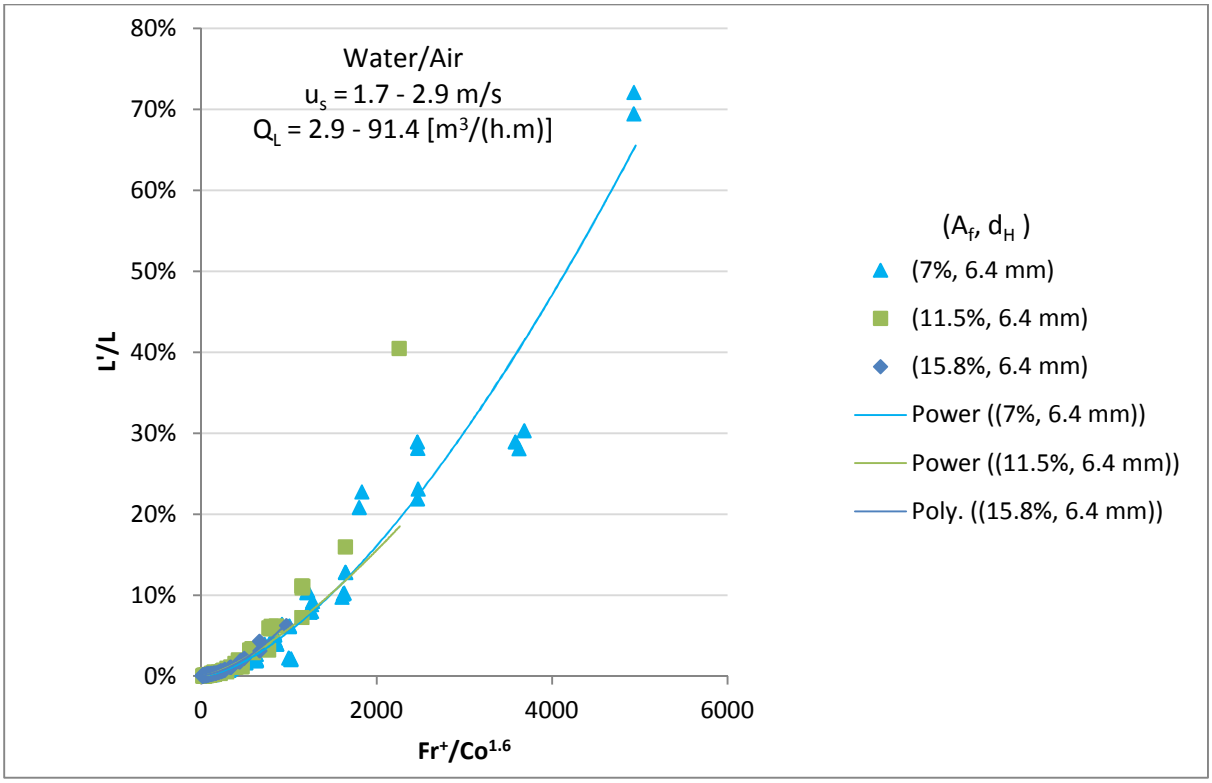

Figure 162 – Entrainment (L'/L) changing with the flow Froude number (Fr^+) to construction number (Co) ratio for water/air at a hole diameter of 6.4 mm and different fractional hole areas.

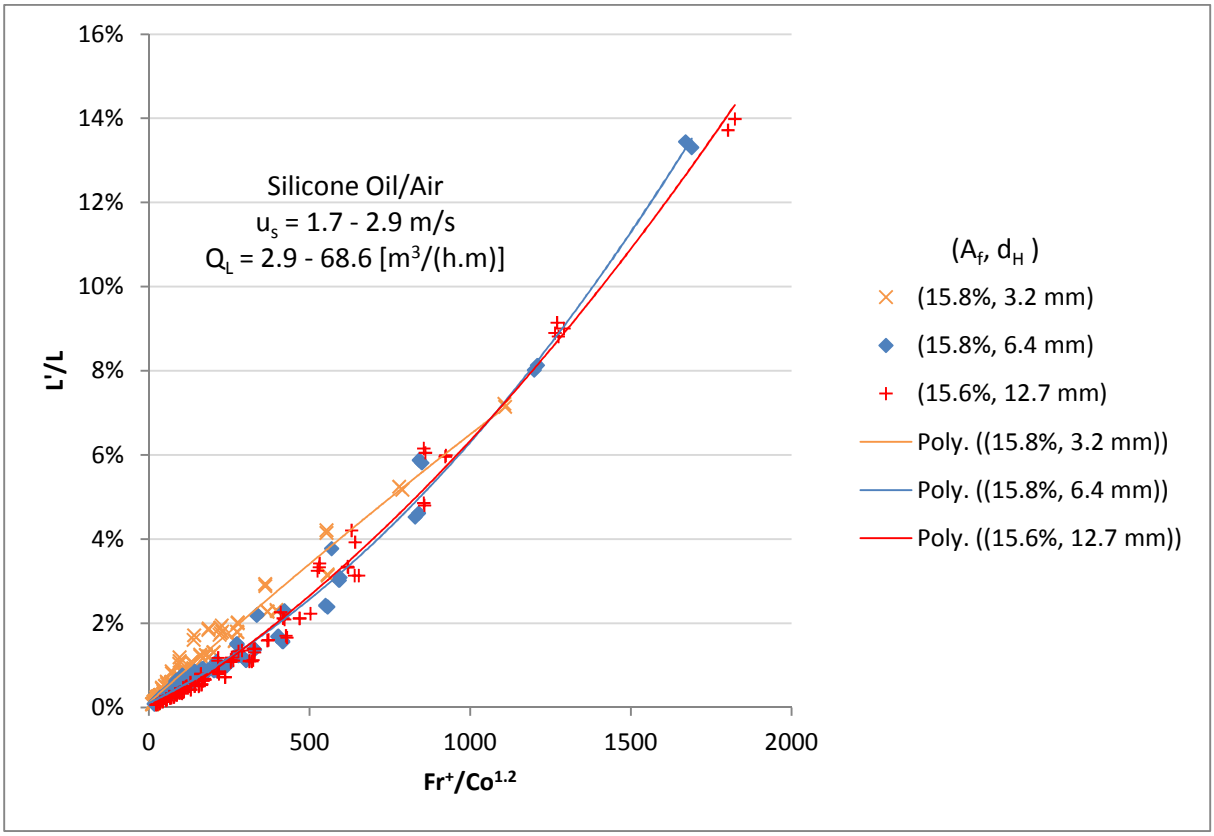

Figure 163 – Entrainment (L'/L) changing with the flow Froude number (Fr^+) to construction number (Co) ratio for silicone-oil/air at a fractional hole area of 15% and different hole diameters.

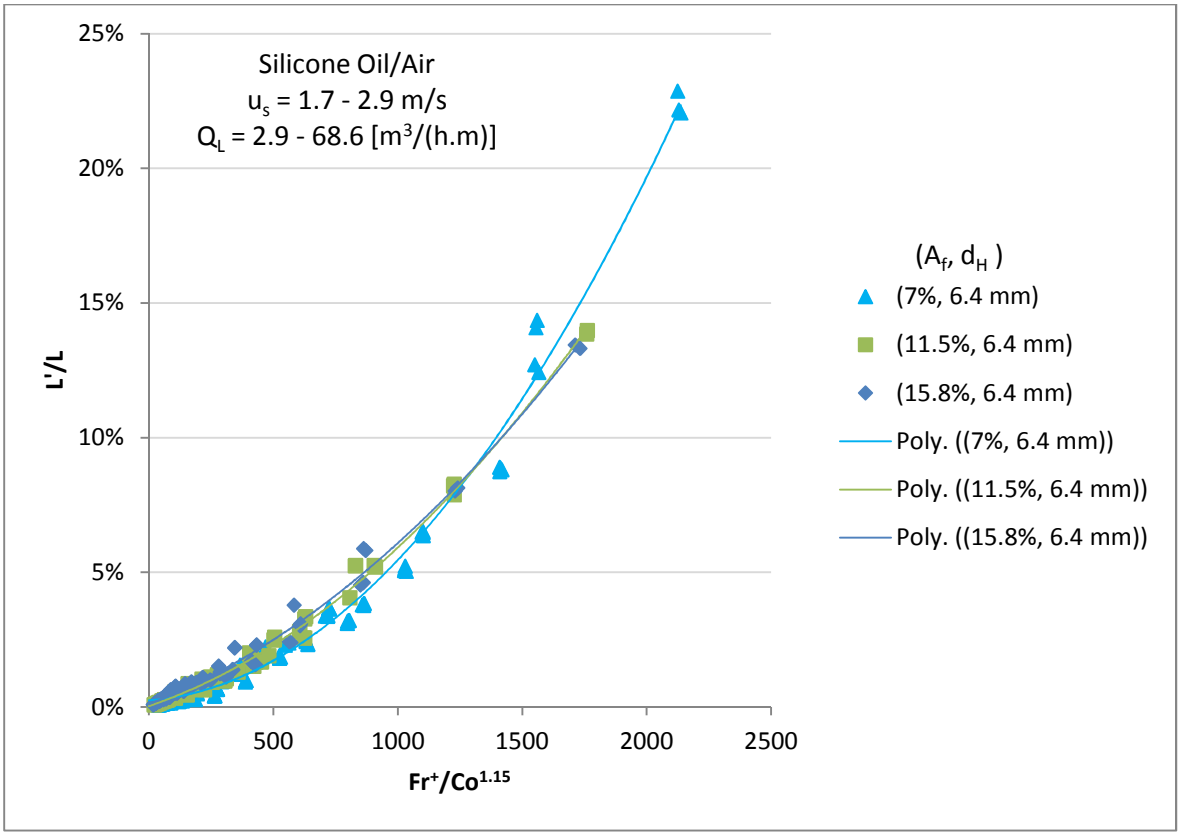

Figure 164 – Entrainment (L'/L) changing with the flow Froude number (Fr^+) to construction number (Co) ratio for silicone-oil/air at a hole diameter of 6.4 mm and different fractional hole areas.

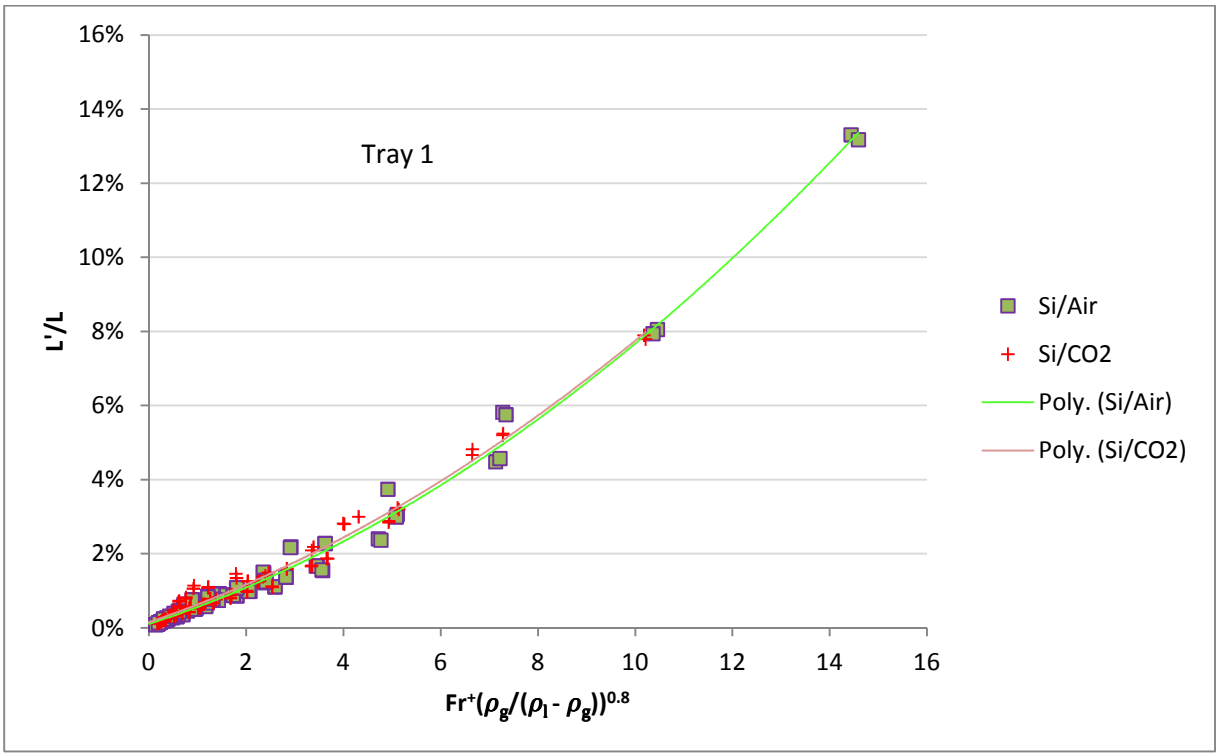

Figure 165 – Entrainment (L'/L) changing with the flow Froude number (Fr^+) and fluid density ratio for different gasses in silicone oil with tray 1 (15.8% fractional hole area, 6.4 mm hole diameter).

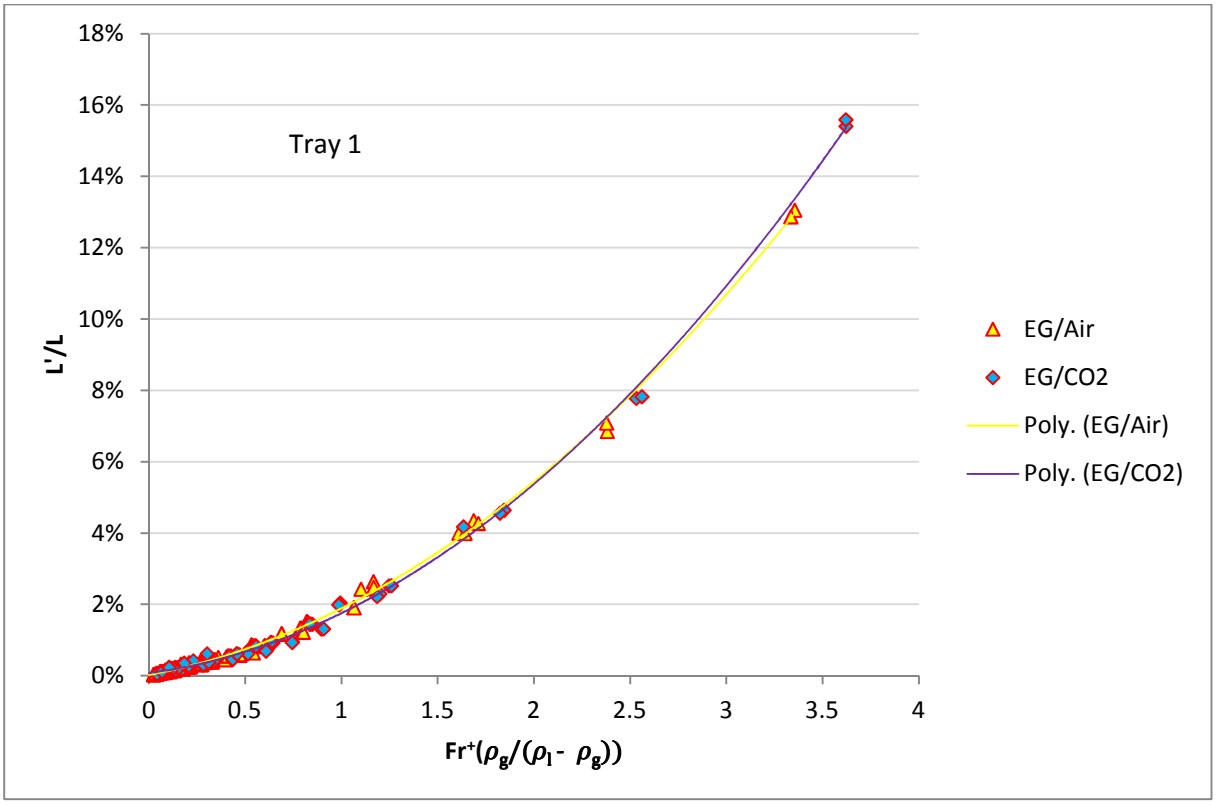

Figure 166 – Entrainment (L'/L) changing with the flow Froude number (Fr^+) and fluid density ratio for different gasses in ethylene glycol with tray 1 (15.8% fractional hole area, 6.4 mm hole diameter).

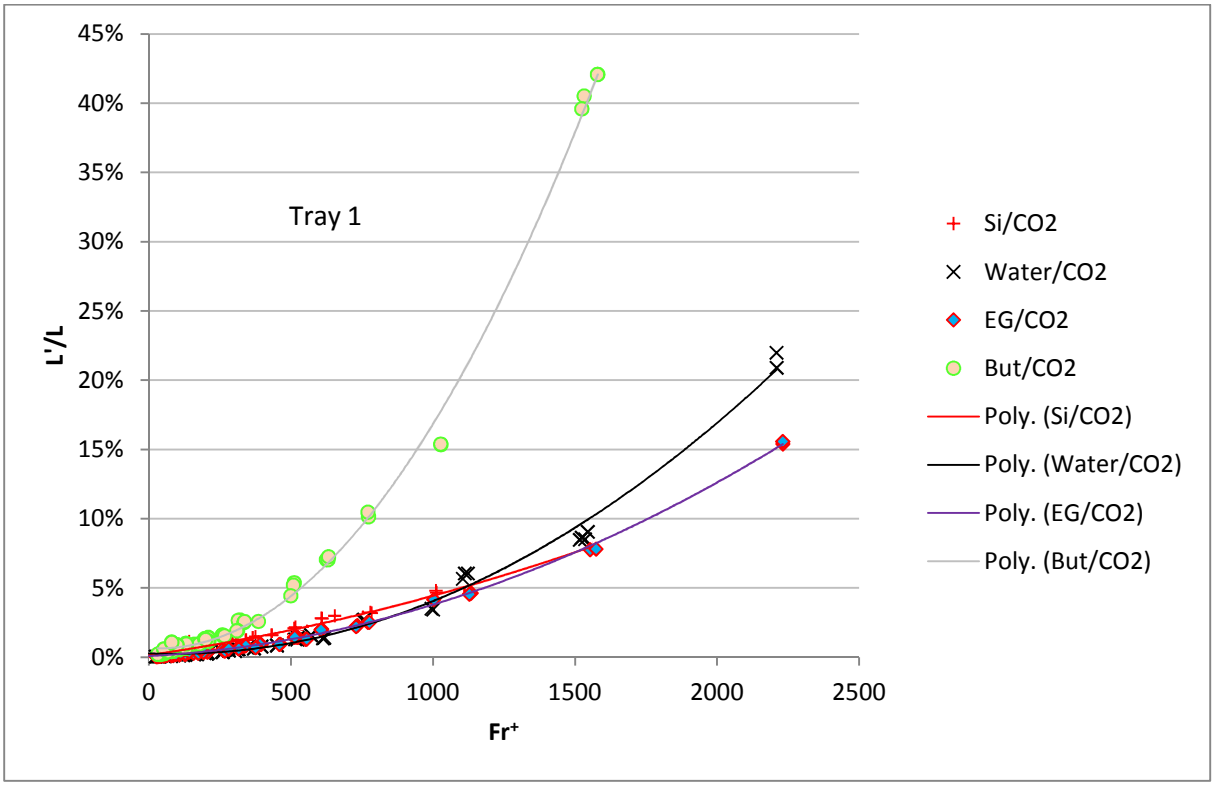

Figure 167 – Entrainment (L'/L) changing with the flow Froude number (Fr^+) for different liquid in CO_2 with tray 1 (15.8% fractional hole area, 6.4 mm hole diameter) in the spray regime.

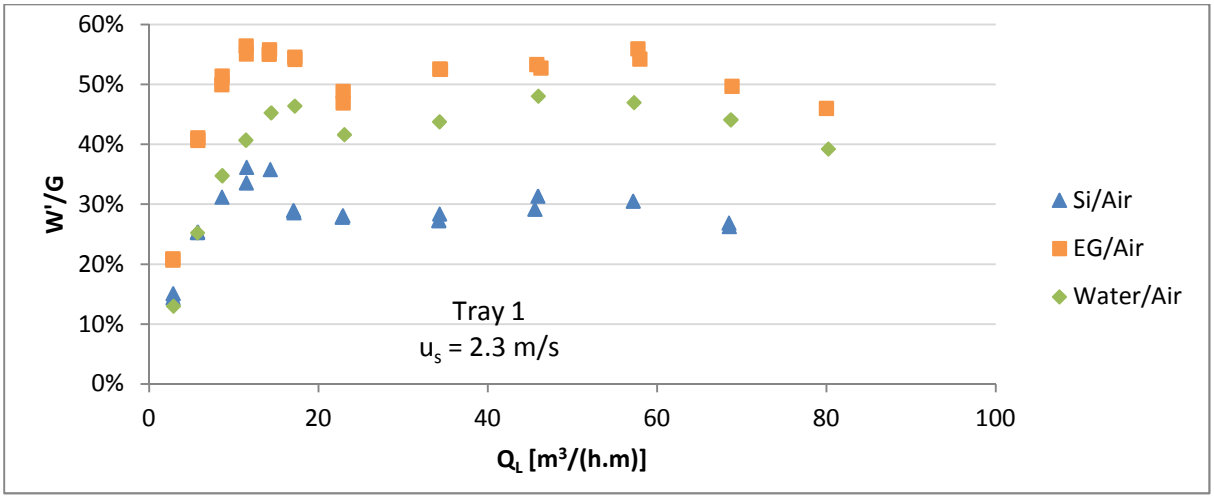

Figure 168 – Weeping (W'/G) of different liquids with air for tray 1 (15.8% fractional hole area, 6.4 mm hole diameter) at a superficial gas velocity of 2.3 m/s.

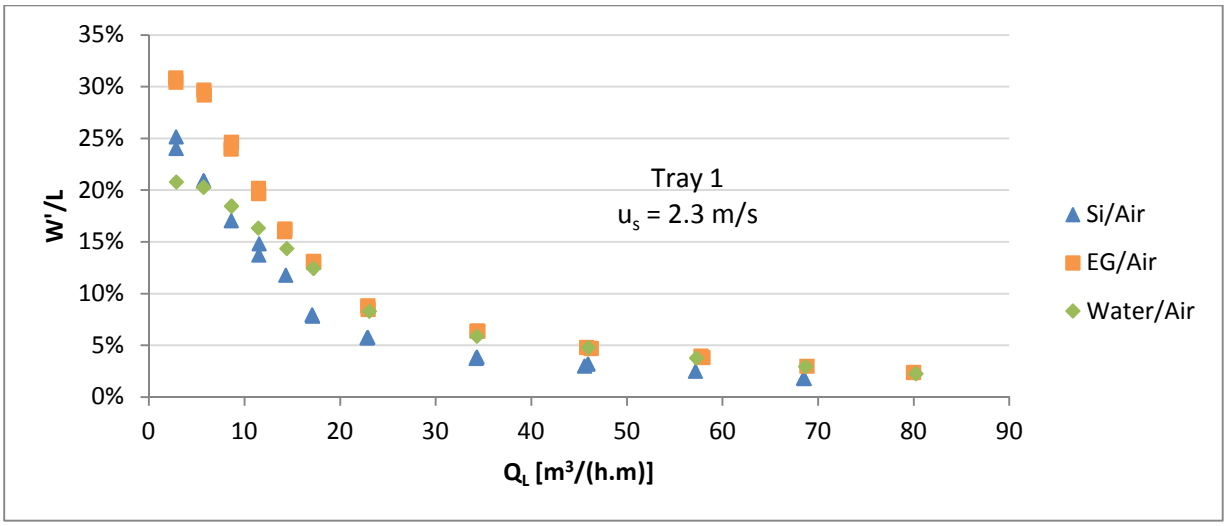

Figure 169 – Weeping (W'/L) of different liquids with air for tray 1 (15.8% fractional hole area, 6.4 mm hole diameter) at a superficial gas velocity of 2.3 m/s.

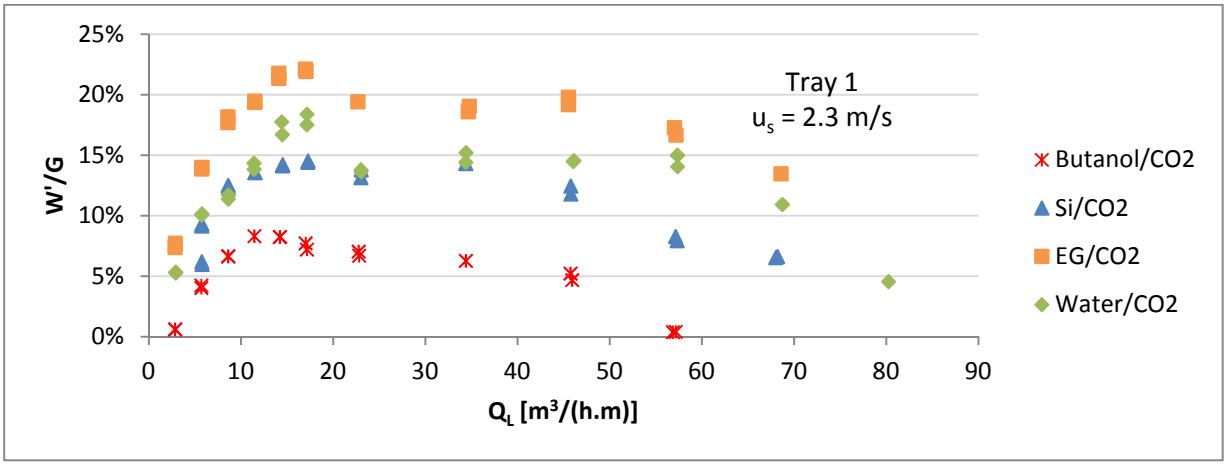

Figure 170 – Weeping (W'/G) of different liquids with CO_2 for tray 1 (15.8% fractional hole area, 6.4 mm hole diameter) at a superficial gas velocity of 2.3 m/s.

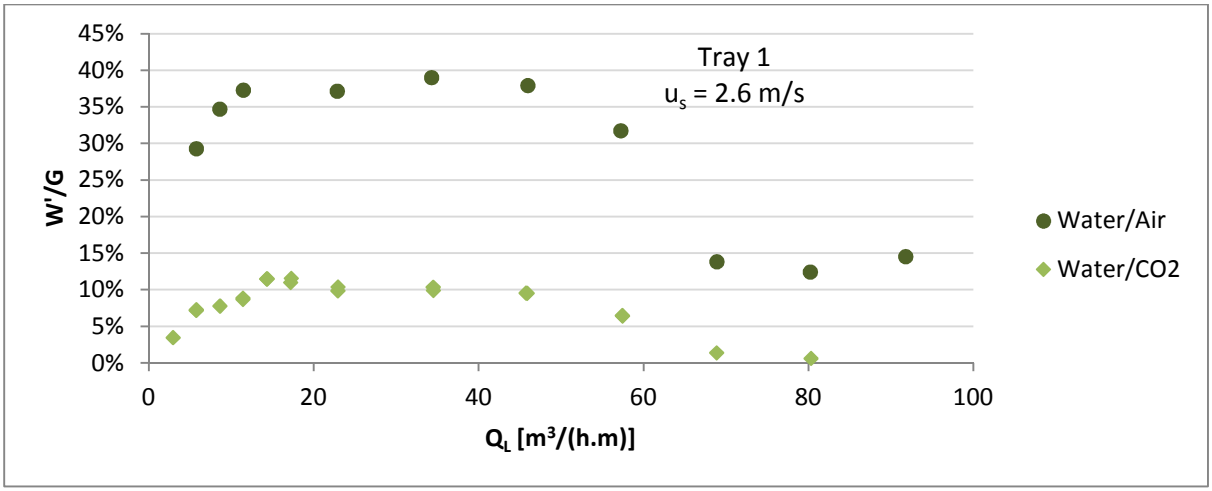

Figure 171 – Weeping of water (W'/G) with different gasses for tray 1 (15.8% fractional hole area, 6.4 mm hole diameter) at a superficial gas velocity of 2.6 m/s.

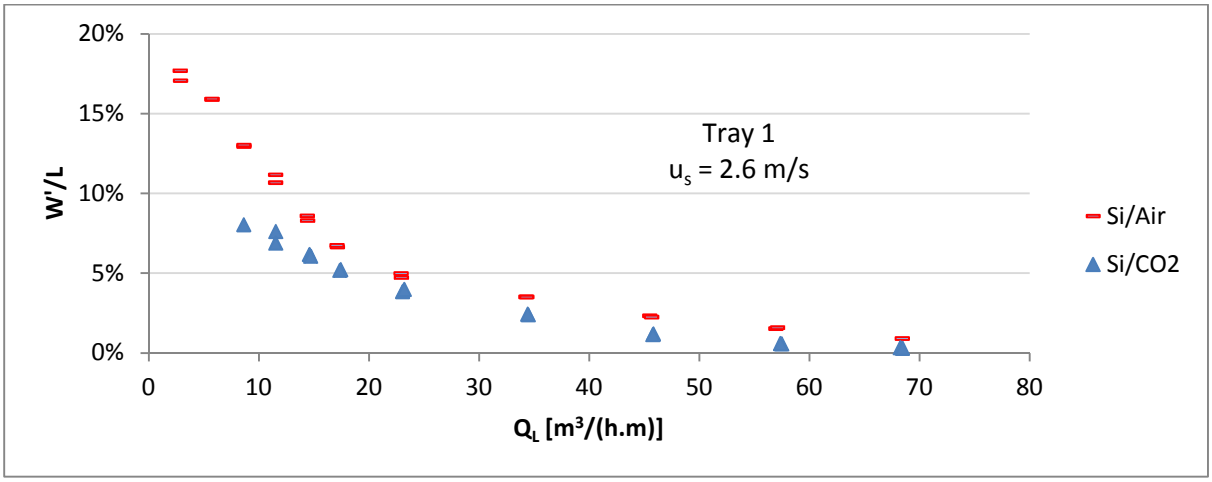

Figure 172 – Weeping of silicone oil (W'/L) with different gasses for tray 1 (15.8% fractional hole area, 6.4 mm hole diameter) at a superficial gas velocity of 2.6 m/s.

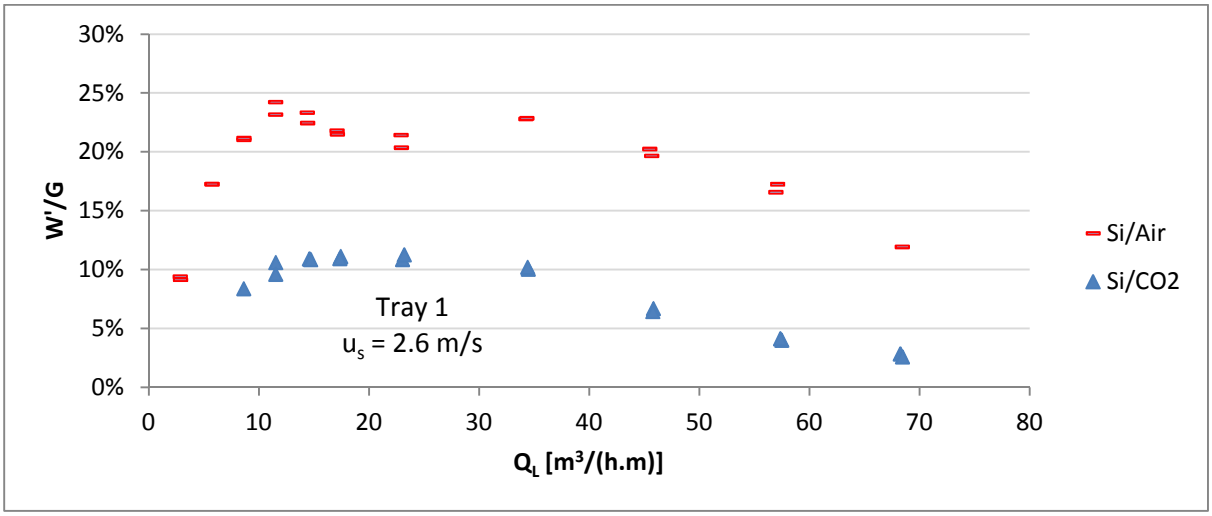

Figure 173 – Weeping of silicone oil (L'/G) with different gasses for tray 1 (15.8% fractional hole area, 6.4 mm hole diameter) at a superficial gas velocity of 2.6 m/s.

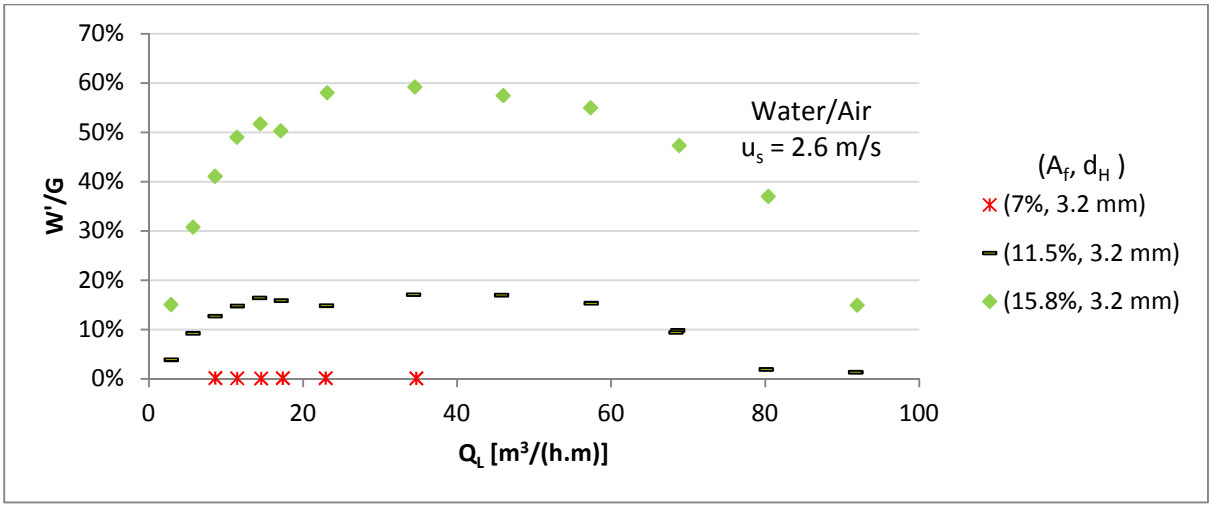

Figure 174 – Effect of fractional hole area on weeping (W'/G) for water/air with a 3.2 mm hole diameter and a superficial gas velocity of 2.6 m/s.

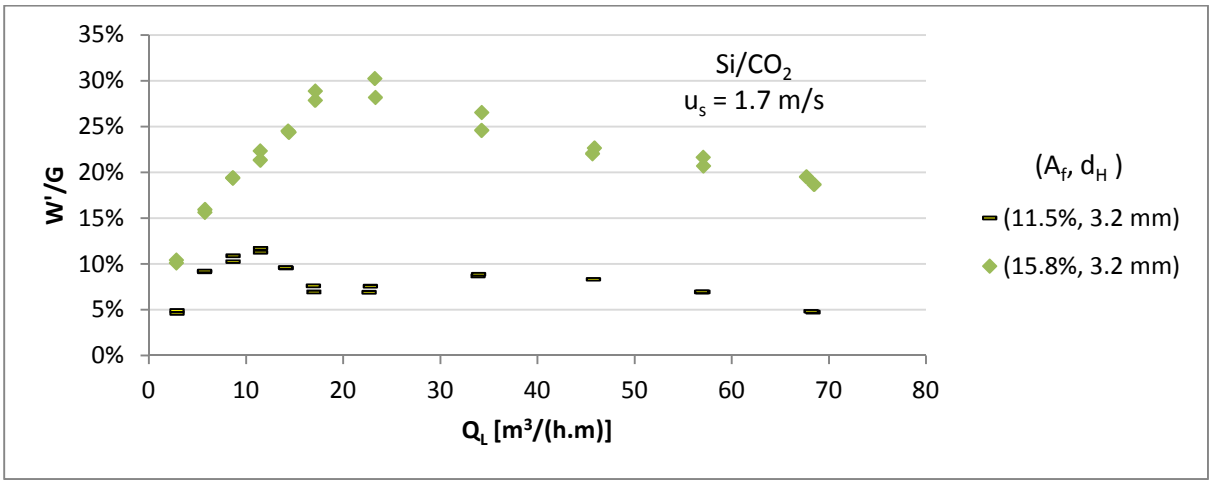

Figure 175 – Effect of fractional hole area on weeping (W'/G) for silicone-oil/CO_2 with a 3.2 mm hole diameter and a superficial gas velocity of 1.7 m/s.

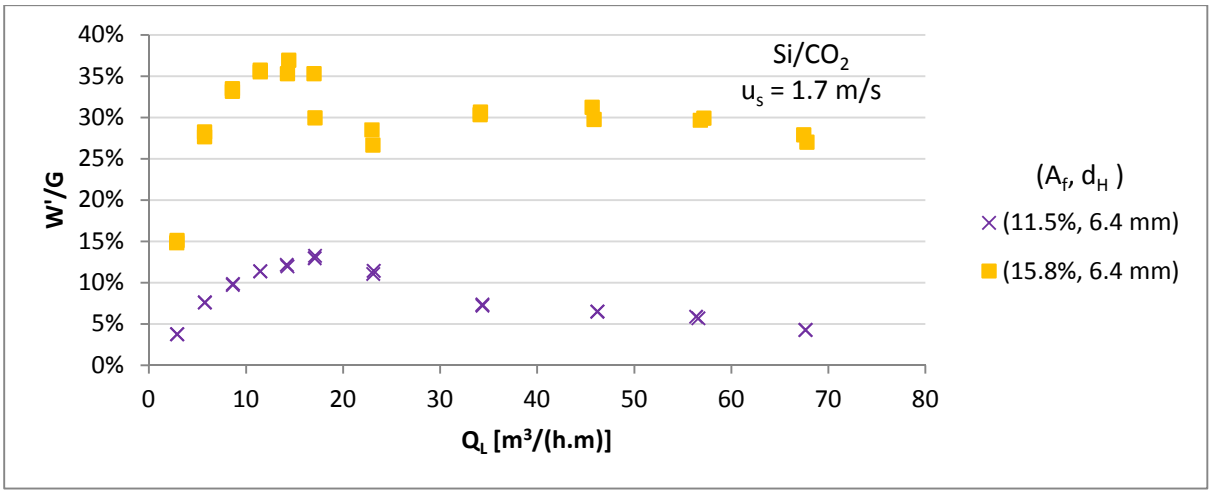

Figure 176 – Effect of fractional hole area on weeping (W'/G) for silicone-oil/CO_2 with a 6.4 mm hole diameter and a superficial gas velocity of 1.7 m/s.

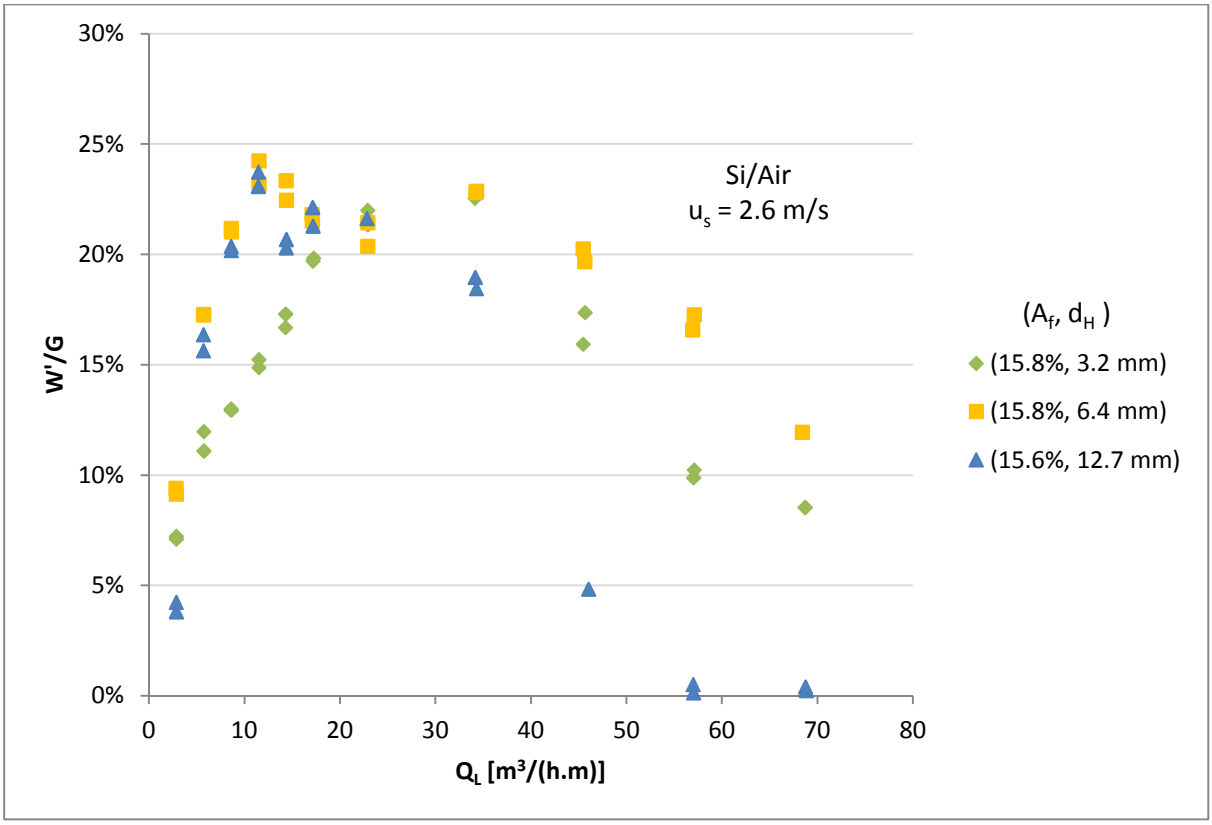

Figure 177 – Effect of hole diameter on weeping (W'/G) for silicone-oil/air with a 15% fractional hole area and a superficial gas velocity of 2.6 m/s.

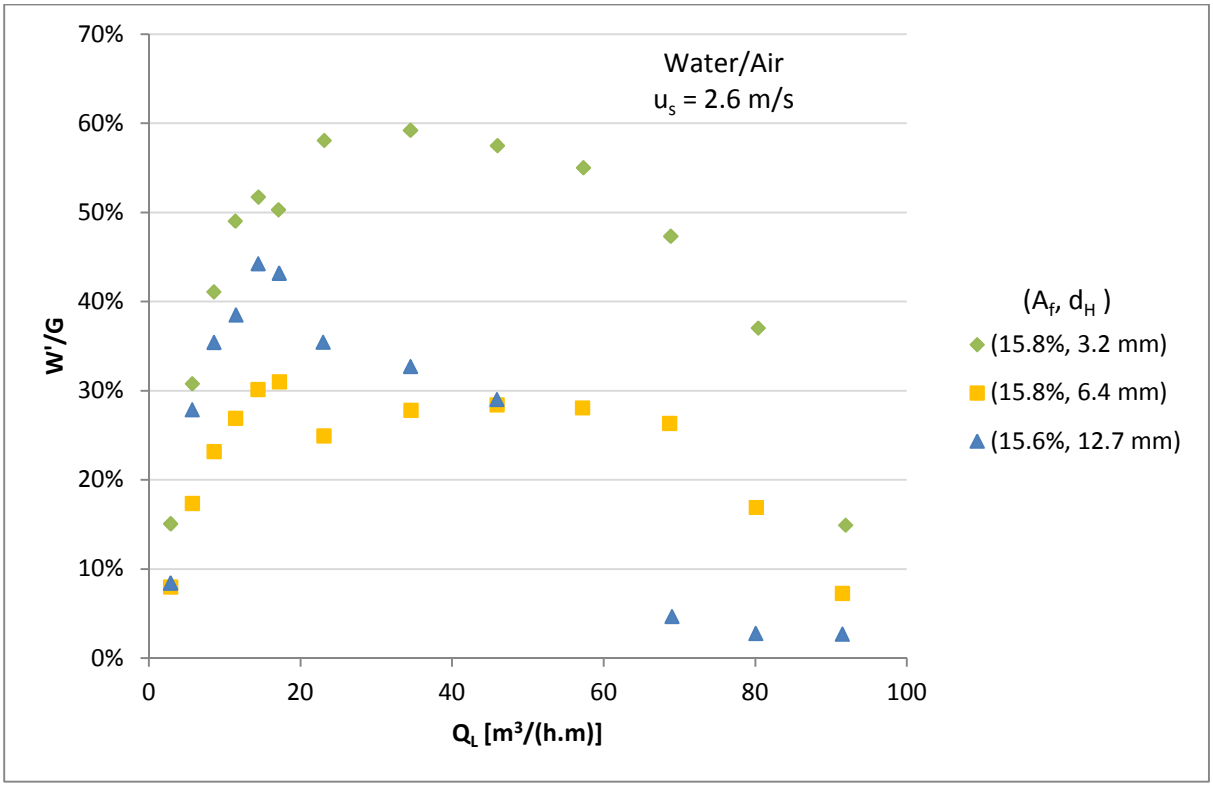

Figure 178 – Effect of hole diameter on weeping (W'/G) for water/air with a 15% fractional hole area and a superficial gas velocity of 2.6 m/s.

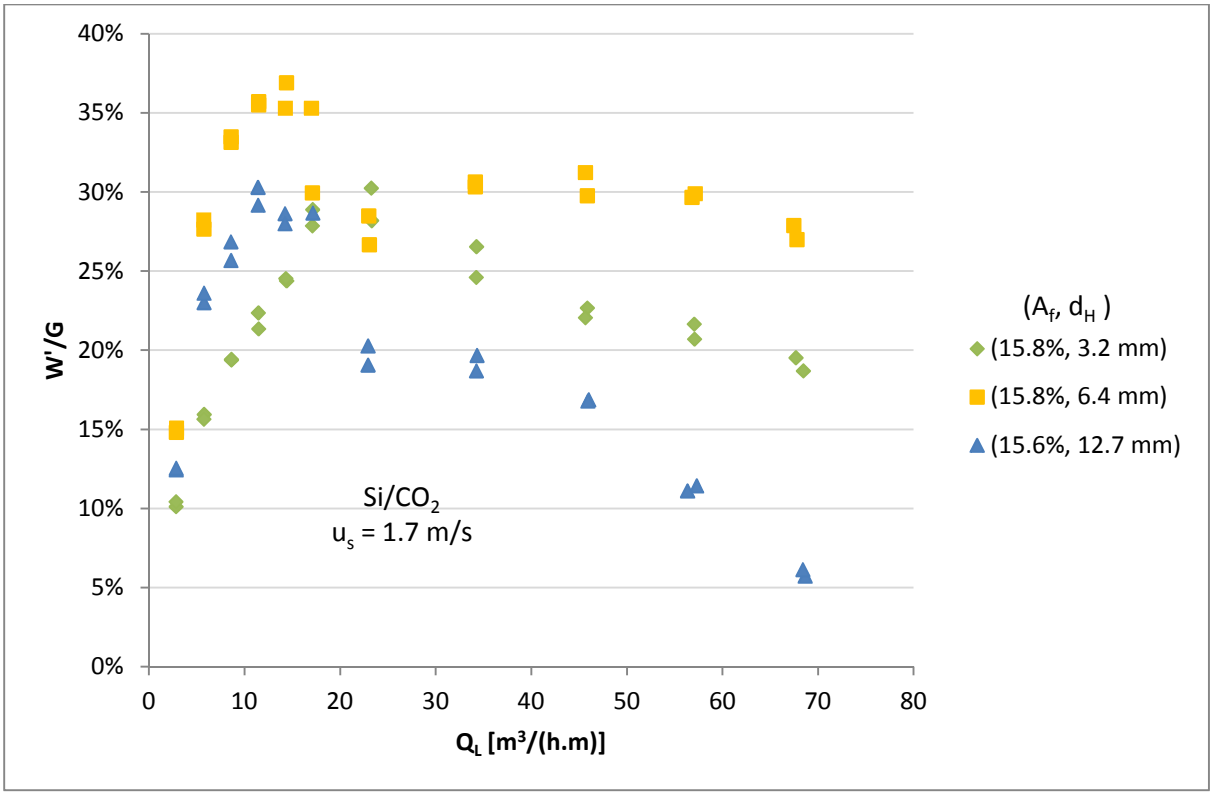

Figure 179 – Effect of hole diameter on weeping (W'/G) for silicone-oil/CO_2 with a 15% fractional hole area and a superficial gas velocity of 1.7 m/s.

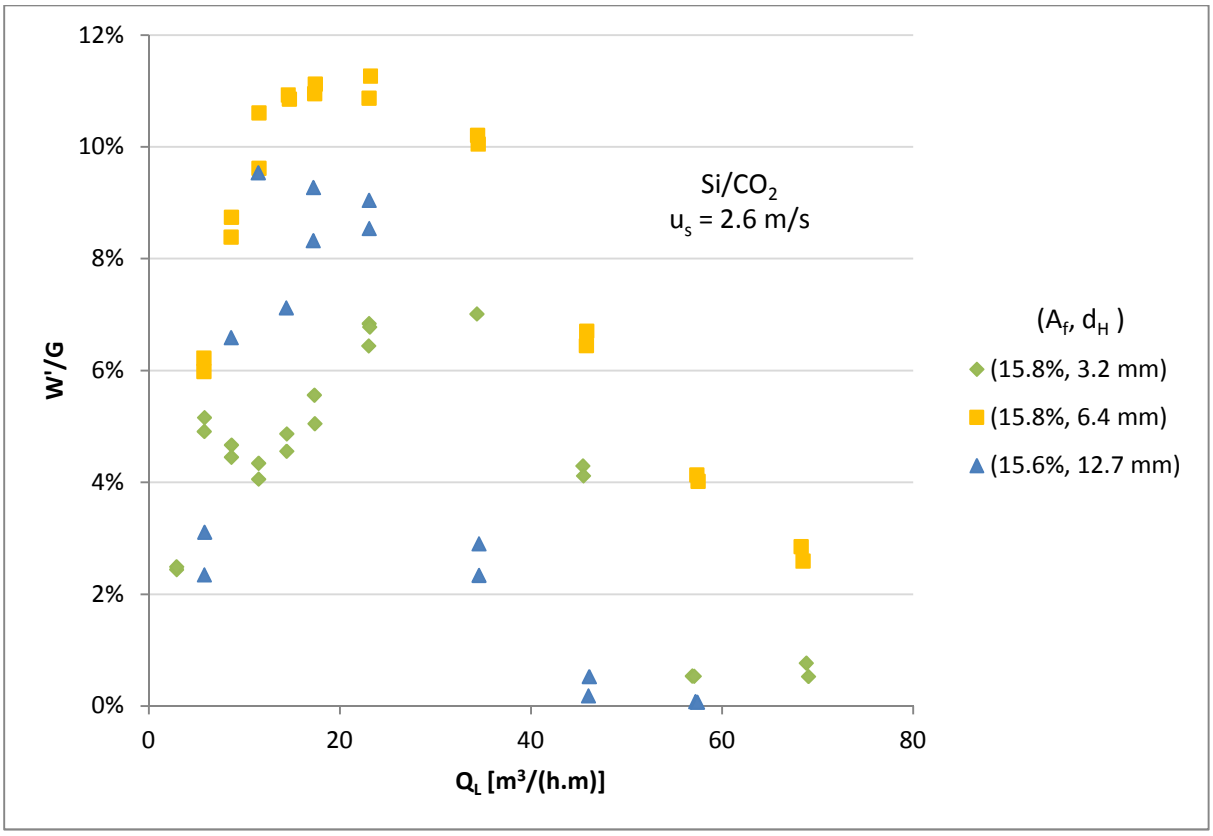

Figure 180 – Effect of hole diameter on weeping (W'/G) for silicone-oil/CO_2 with a 15% fractional hole area and a superficial gas velocity of 2.6 m/s.

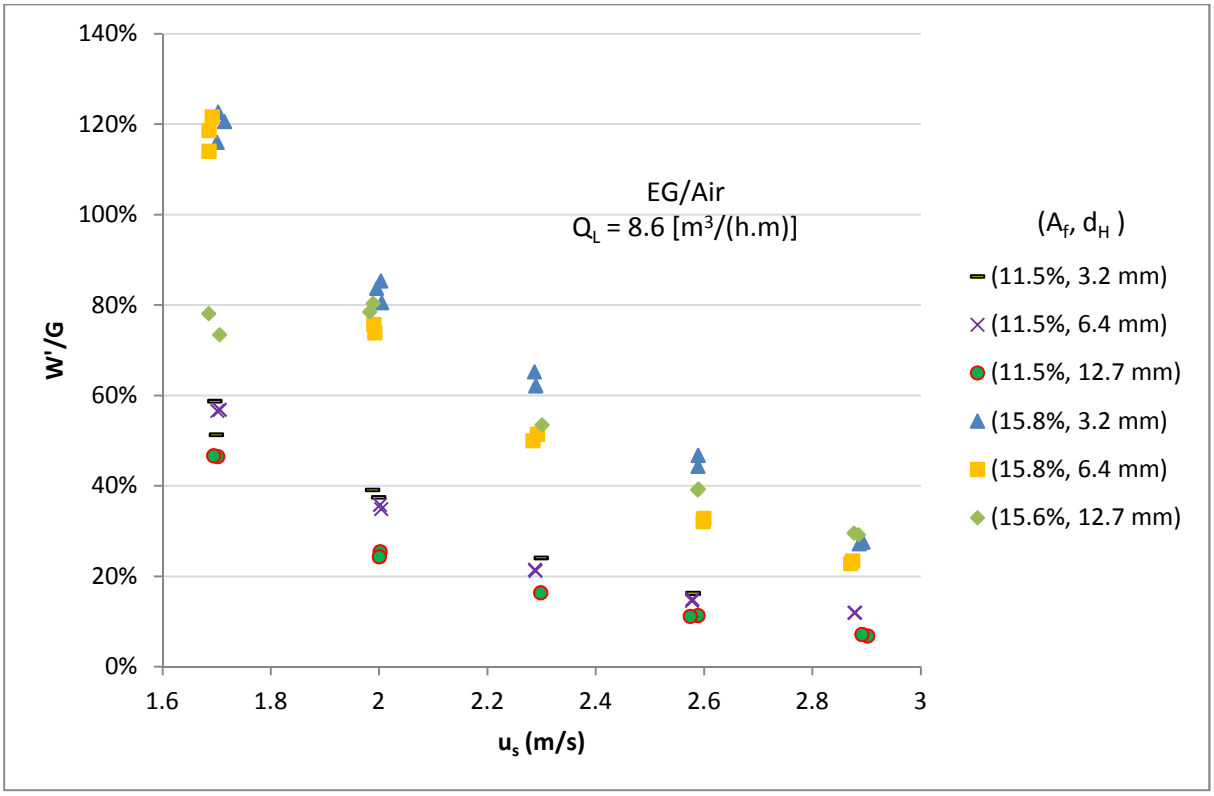

Figure 181 – Effect of tray geometry on weeping (W'/G) for ethylene-glycol/air with changing superficial gas velocity and a liquid flow rate of 8.6 m^3/(h.m).

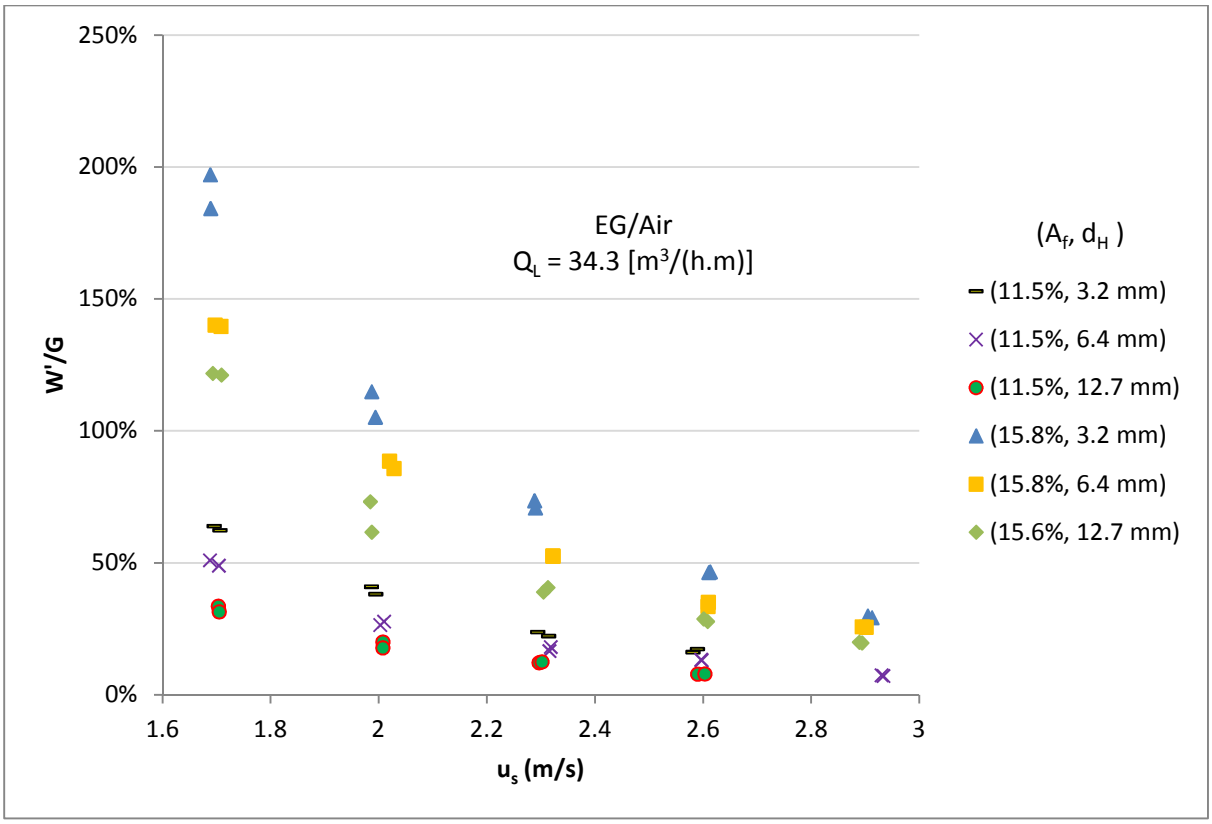

Figure 182 – Effect of tray geometry on weeping (W'/G) for ethylene-glycol/air with changing superficial gas velocity and a liquid flow rate of 34.3 m^3/(h.m).

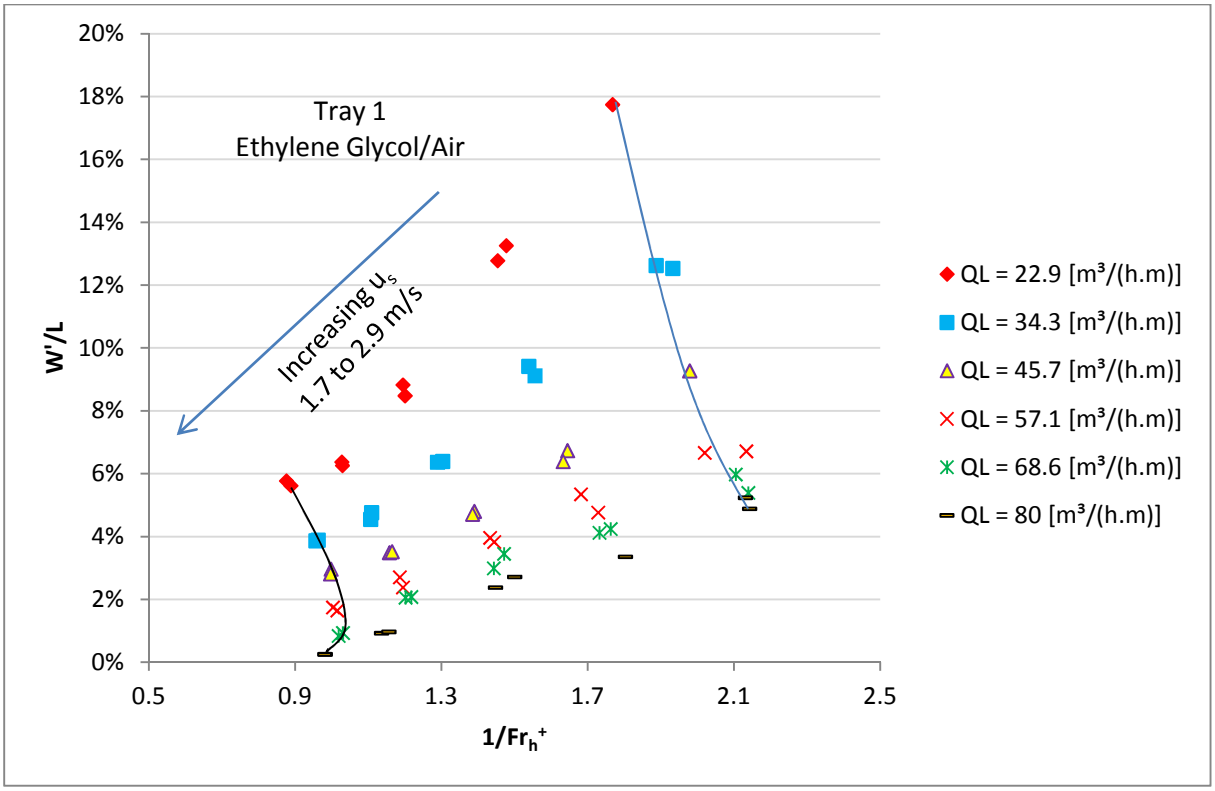

Figure 183 – Weeping (W'/L) changing with the inverse liquid holdup Froude number (Fr_h^+) for ethylene-glycol/air with tray 1 (15.8% fractional hole area, 6.4 mm hole diameter) in the froth regime.

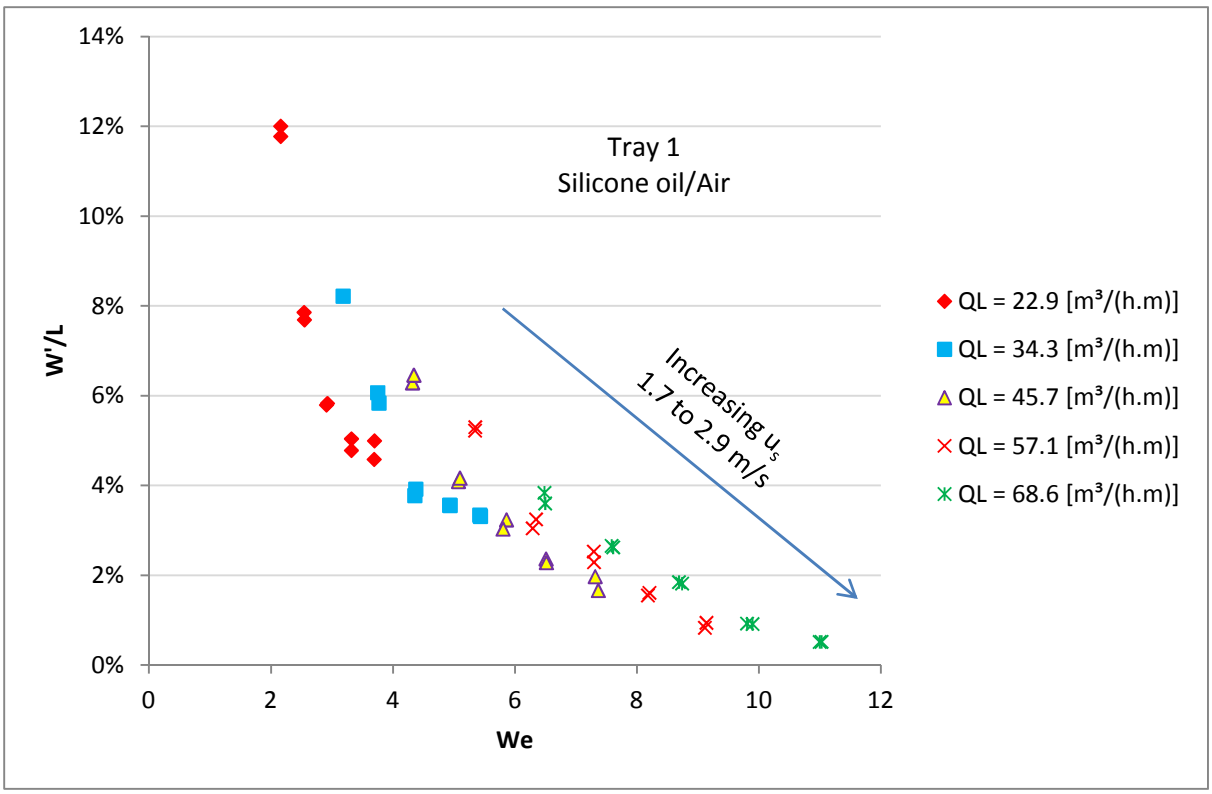

Figure 184 – Weeping (W'/L) changing with the Weber number (We) for silicone-oil/air with tray 1 (15.8% fractional hole area, 6.4 mm hole diameter) in the froth regime.

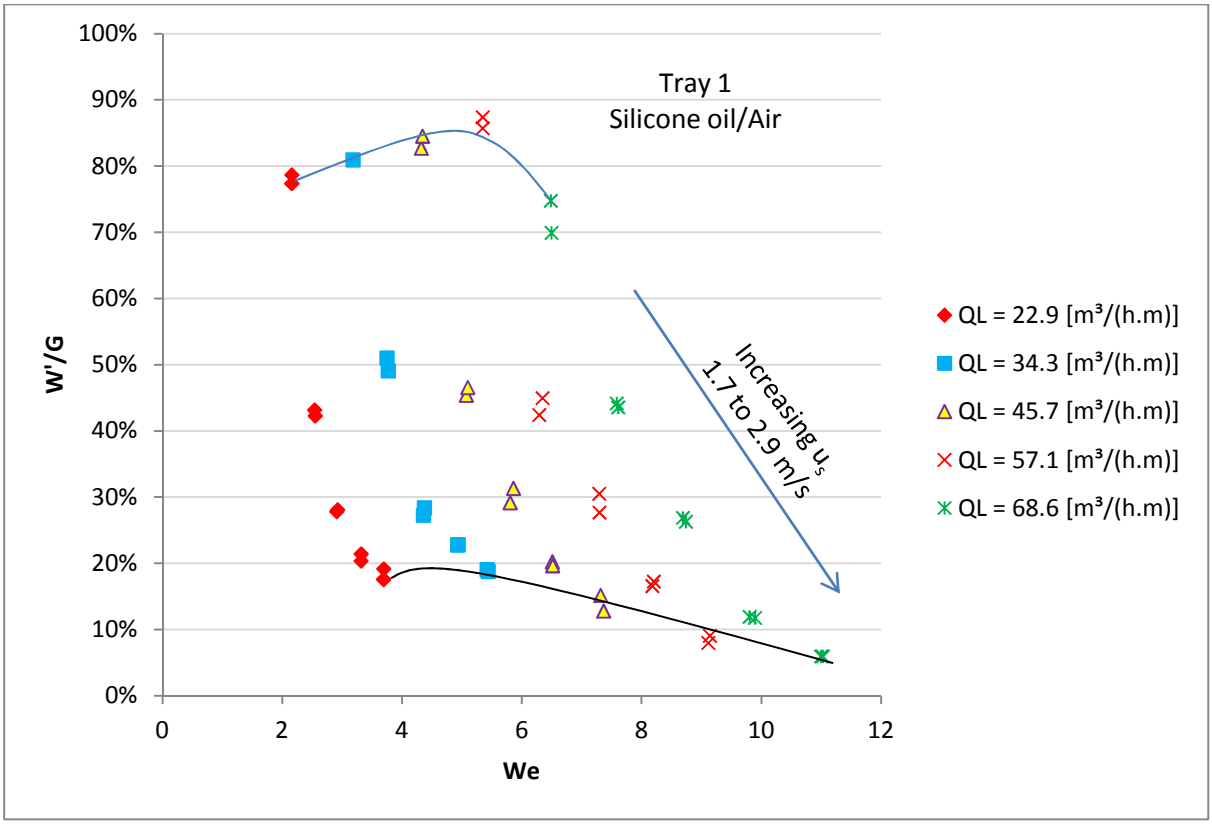

Figure 185 – Weeping (W'/G) changing with the Weber number (We) for silicone-oil/air with tray 1 (15.8% fractional hole area, 6.4 mm hole diameter) in the froth regime.

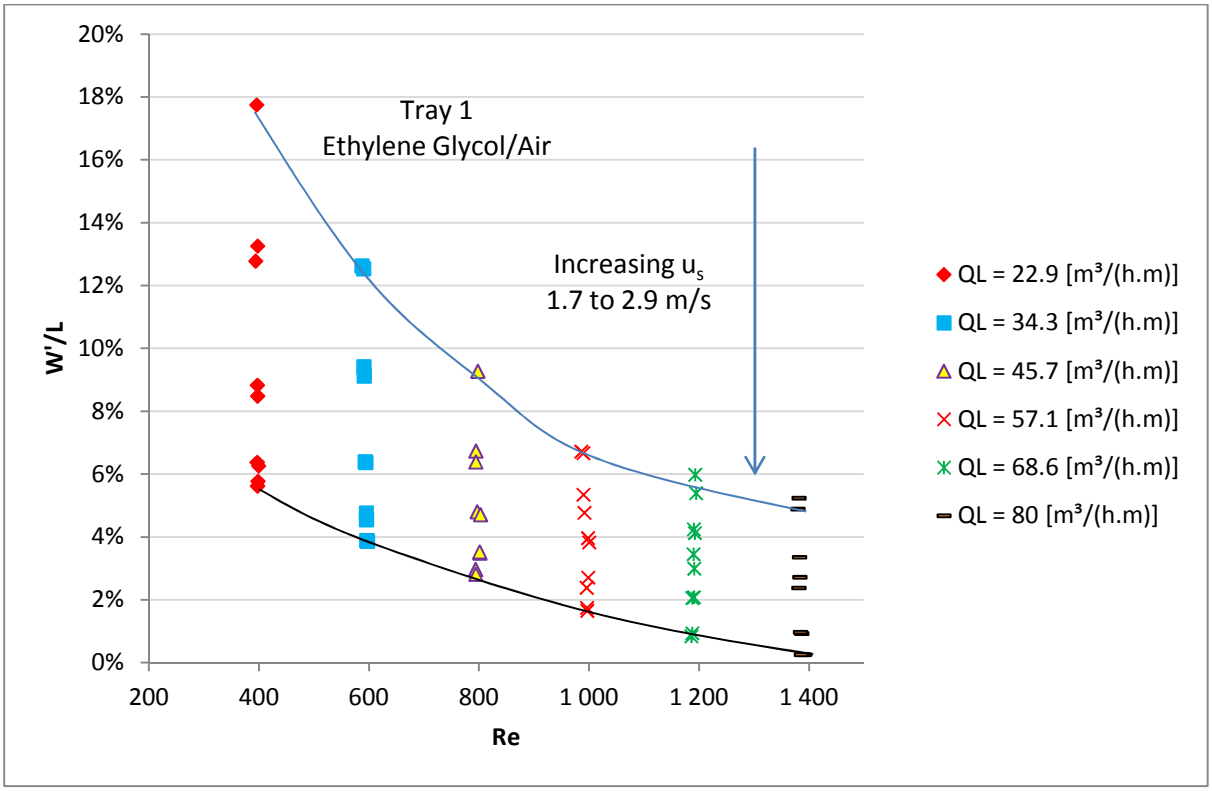

Figure 186 – Weeping (W'/L) changing with the liquid Reynolds number (Re) for ethylene-glycol/air with tray 1 (15.8% fractional hole area, 6.4 mm hole diameter) in the froth regime.

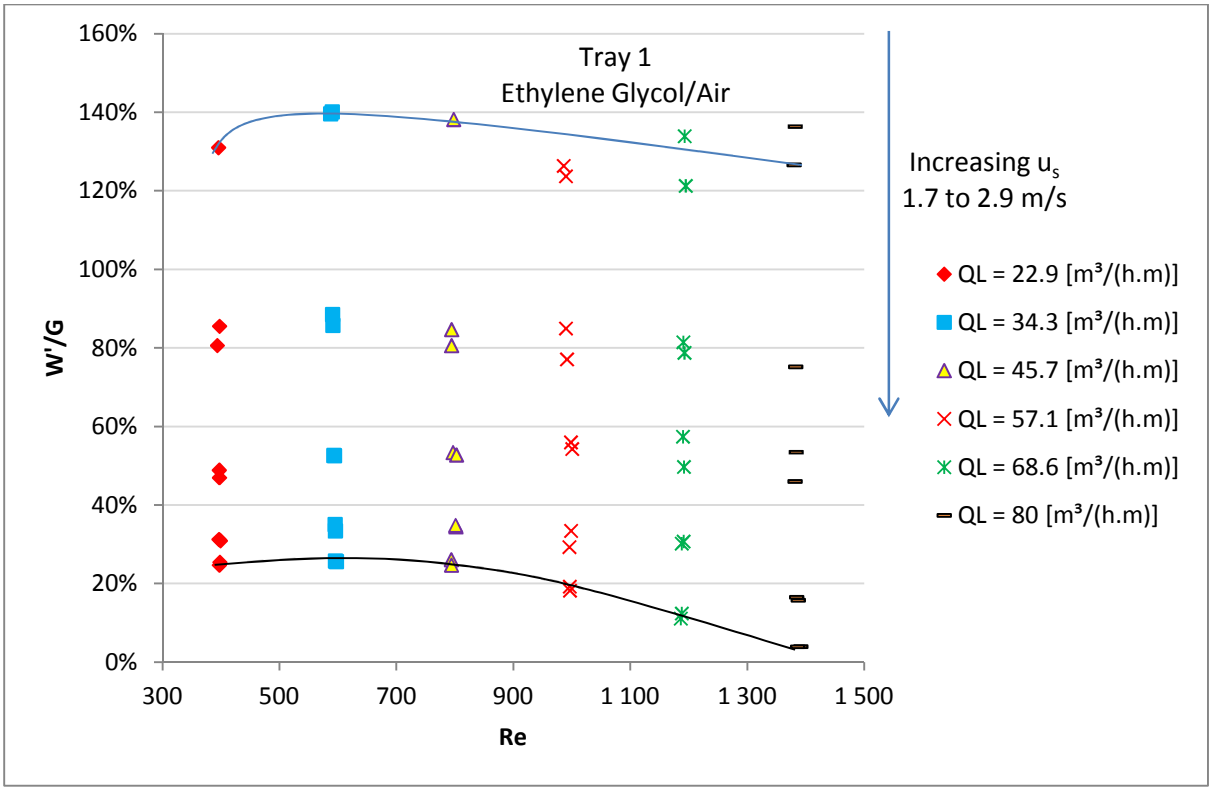

Figure 187 – Weeping (W'/G) changing with the liquid Reynolds number (Re) for ethylene-glycol/air with tray 1 (15.8% fractional hole area, 6.4 mm hole diameter) in the froth regime.

Appendix G - Raw Experimental Results

Table 26 – Silicone oil/air tray 1 (15.8%, 6.4 mm) entrainment

A_p (m^2)	s (mm)	ρ_l (kg/m^3)	σ (mN/m)	μ_l (mPa.s)	ρ_g (kg/m^3)	μ_g (Pa.s)	u_s (m/s)	Q_L [m^3/(h.m)]	L'/L	L'/G	Holdup (Pa)	Holdup (mm liq)
0.08295	515	959	20.9	51	1.18	1.86E-02	1.69	2.8	2.19%	1.78%	161.2	17.1
0.08295	515	959	20.9	51	1.18	1.86E-02	1.68	2.8	2.17%	1.76%	159.5	17.0
0.08295	515	959	20.9	51	1.17	1.86E-02	1.69	5.7	0.93%	1.53%	196.9	20.9
0.08295	515	959	20.9	51	1.17	1.86E-02	1.68	5.7	0.92%	1.52%	200.6	21.3
0.08295	515	959	20.9	51	1.17	1.86E-02	1.70	8.6	0.54%	1.34%	236.0	25.1
0.08295	515	959	20.9	51	1.17	1.86E-02	1.69	8.6	0.54%	1.35%	237.6	25.3
0.08295	515	959	20.9	51	1.16	1.86E-02	1.68	11.5	0.36%	1.22%	265.6	28.2
0.08295	515	959	20.9	51	1.16	1.86E-02	1.67	11.5	0.36%	1.20%	267.1	28.4
0.08295	515	959	20.9	51	1.17	1.86E-02	1.69	14.4	0.30%	1.26%	285.2	30.3
0.08295	515	959	20.9	51	1.17	1.86E-02	1.69	14.3	0.31%	1.29%	288.0	30.6
0.08295	515	959	20.9	51	1.16	1.86E-02	1.69	17.0	0.28%	1.38%	301.0	32.0
0.08295	515	959	20.9	51	1.16	1.86E-02	1.69	17.0	0.28%	1.38%	304.8	32.4
0.08295	515	959	20.9	51	1.16	1.86E-02	1.69	22.9	0.22%	1.48%	336.5	35.8
0.08295	515	959	20.9	51	1.16	1.86E-02	1.69	22.9	0.22%	1.48%	340.8	36.2
0.08295	515	959	20.9	51	1.16	1.86E-02	1.69	34.3	0.15%	1.51%	401.7	42.7
0.08295	515	959	20.9	51	1.16	1.86E-02	1.68	34.2	0.15%	1.48%	394.8	42.0
0.08295	515	959	20.9	51	1.16	1.86E-02	1.70	45.9	0.11%	1.48%	429.2	45.6
0.08295	515	959	20.9	51	1.16	1.86E-02	1.70	45.8	0.11%	1.45%	439.0	46.7
0.08295	515	959	20.9	51	1.16	1.86E-02	1.69	57.2	0.09%	1.51%	469.2	49.9
0.08295	515	959	20.9	51	1.16	1.86E-02	1.69	57.2	0.09%	1.48%	459.6	48.9
0.08295	515	959	20.9	51	1.17	1.86E-02	2.01	2.8	3.74%	2.55%	138.2	14.7
0.08295	515	959	20.9	51	1.17	1.86E-02	1.99	5.7	1.49%	2.08%	168.6	17.9
0.08295	515	959	20.9	51	1.17	1.86E-02	1.99	5.7	1.51%	2.11%	177.7	18.9
0.08295	515	959	20.9	51	1.17	1.86E-02	2.00	8.6	0.88%	1.85%	213.8	22.7
0.08295	515	959	20.9	51	1.17	1.86E-02	2.00	8.6	0.90%	1.88%	214.6	22.8
0.08295	515	959	20.9	51	1.16	1.86E-02	1.99	11.5	0.59%	1.66%	243.4	25.9
0.08295	515	959	20.9	51	1.16	1.86E-02	1.99	11.5	0.58%	1.64%	242.0	25.7
0.08295	515	959	20.9	51	1.17	1.86E-02	2.00	14.4	0.52%	1.81%	263.6	28.0
0.08295	515	959	20.9	51	1.17	1.86E-02	2.00	14.4	0.51%	1.78%	265.1	28.2
0.08295	515	959	20.9	51	1.16	1.86E-02	2.00	17.1	0.46%	1.93%	275.2	29.3
0.08295	515	959	20.9	51	1.16	1.86E-02	1.99	17.0	0.47%	1.97%	275.1	29.2
0.08295	515	959	20.9	51	1.16	1.86E-02	2.01	22.9	0.38%	2.09%	310.8	33.0
0.08295	515	959	20.9	51	1.16	1.86E-02	2.01	22.8	0.38%	2.12%	306.3	32.6
0.08295	515	959	20.9	51	1.16	1.86E-02	1.98	34.3	0.24%	2.06%	354.7	37.7

A_p (m^2)	s (mm)	ρ_l (kg/m^3)	σ (mN/m)	μ_l (mPa.s)	ρ_g (kg/m^3)	μ_g (Pa.s)	u_s (m/s)	Q_L [$m^3/(h.m)$]	L'/L	L'/G	Holdup (Pa)	Holdup (mm liq)
0.08295	515	959	20.9	51	1.16	1.86E-02	1.99	34.4	0.24%	2.04%	357.7	38.0
0.08295	515	959	20.9	51	1.16	1.86E-02	1.99	46.3	0.19%	2.20%	415.8	44.2
0.08295	515	959	20.9	51	1.16	1.86E-02	2.00	46.1	0.19%	2.16%	404.6	43.0
0.08295	515	959	20.9	51	1.16	1.86E-02	1.99	57.2	0.16%	2.24%	433.5	46.1
0.08295	515	959	20.9	51	1.16	1.86E-02	2.00	57.1	0.17%	2.33%	427.0	45.4
0.08295	515	959	20.9	51	1.16	1.86E-02	2.01	68.5	0.14%	2.37%	453.3	48.2
0.08295	515	959	20.9	51	1.16	1.86E-02	1.99	68.4	0.14%	2.42%	460.5	48.9
0.08295	515	959	20.9	51	1.17	1.86E-02	2.29	2.8	5.82%	3.50%	124.6	13.2
0.08295	515	959	20.9	51	1.17	1.86E-02	2.30	2.8	5.76%	3.44%	114.5	12.2
0.08295	515	959	20.9	51	1.16	1.86E-02	2.30	5.7	2.27%	2.76%	171.2	18.2
0.08295	515	959	20.9	51	1.16	1.86E-02	2.30	5.7	2.28%	2.77%	160.8	17.1
0.08295	515	959	20.9	51	1.17	1.86E-02	2.30	8.6	1.26%	2.30%	198.2	21.1
0.08295	515	959	20.9	51	1.17	1.86E-02	2.30	8.6	1.29%	2.37%	194.1	20.6
0.08295	515	959	20.9	51	1.16	1.86E-02	2.30	11.5	0.87%	2.13%	213.2	22.7
0.08295	515	959	20.9	51	1.16	1.86E-02	2.30	11.5	0.87%	2.12%	214.0	22.7
0.08295	515	959	20.9	51	1.17	1.86E-02	2.29	14.4	0.76%	2.32%	236.3	25.1
0.08295	515	959	20.9	51	1.17	1.86E-02	2.29	14.4	0.74%	2.28%	245.6	26.1
0.08295	515	959	20.9	51	1.16	1.86E-02	2.29	17.2	0.69%	2.54%	243.8	25.9
0.08295	515	959	20.9	51	1.16	1.86E-02	2.29	17.1	0.67%	2.46%	241.6	25.7
0.08295	515	959	20.9	51	1.16	1.86E-02	2.30	22.9	0.54%	2.63%	268.9	28.6
0.08295	515	959	20.9	51	1.16	1.86E-02	2.30	22.9	0.58%	2.80%	284.9	30.3
0.08295	515	959	20.9	51	1.16	1.86E-02	2.30	34.3	0.39%	2.84%	330.9	35.2
0.08295	515	959	20.9	51	1.16	1.86E-02	2.31	34.4	0.37%	2.69%	315.8	33.6
0.08295	515	959	20.9	51	1.16	1.86E-02	2.30	45.5	0.30%	2.89%	375.4	39.9
0.08295	515	959	20.9	51	1.16	1.86E-02	2.30	45.6	0.31%	3.01%	377.8	40.2
0.08295	515	959	20.9	51	1.16	1.86E-02	2.31	57.2	0.27%	3.31%	400.4	42.6
0.08295	515	959	20.9	51	1.16	1.86E-02	2.30	57.3	0.27%	3.24%	400.3	42.5
0.08295	515	959	20.9	51	1.16	1.86E-02	2.30	68.4	0.24%	3.51%	407.5	43.3
0.08295	515	959	20.9	51	1.16	1.86E-02	2.30	68.5	0.24%	3.58%	418.7	44.5
0.08295	515	959	20.9	51	1.17	1.86E-02	2.58	2.8	8.06%	4.28%	105.6	11.2
0.08295	515	959	20.9	51	1.17	1.86E-02	2.58	2.9	7.94%	4.25%	109.6	11.6
0.08295	515	959	20.9	51	1.17	1.86E-02	2.57	5.7	3.06%	3.31%	139.8	14.9
0.08295	515	959	20.9	51	1.17	1.86E-02	2.57	5.7	3.00%	3.25%	142.5	15.1
0.08295	515	959	20.9	51	1.16	1.86E-02	2.59	8.6	1.68%	2.73%	174.6	18.6
0.08295	515	959	20.9	51	1.16	1.86E-02	2.59	8.6	1.67%	2.71%	176.6	18.8
0.08295	515	959	20.9	51	1.16	1.86E-02	2.60	11.5	1.11%	2.42%	208.0	22.1
0.08295	515	959	20.9	51	1.16	1.86E-02	2.60	11.5	1.11%	2.41%	202.5	21.5
0.08295	515	959	20.9	51	1.17	1.86E-02	2.59	14.3	0.99%	2.66%	210.8	22.4
0.08295	515	959	20.9	51	1.17	1.86E-02	2.59	14.4	0.99%	2.68%	208.4	22.1

A_p (m^2)	s (mm)	ρ_l (kg/m^3)	σ (mN/m)	μ_l (mPa.s)	ρ_g (kg/m^3)	μ_g (Pa.s)	u_s (m/s)	Q_L [$m^3/(h.m)$]	L'/L	L'/G	Holdup (Pa)	Holdup (mm liq)
0.08295	515	959	20.9	51	1.16	1.86E-02	2.59	17.1	0.87%	2.83%	223.9	23.8
0.08295	515	959	20.9	51	1.16	1.86E-02	2.59	17.1	0.88%	2.85%	219.8	23.4
0.08295	515	959	20.9	51	1.16	1.86E-02	2.61	22.9	0.77%	3.31%	258.7	27.5
0.08295	515	959	20.9	51	1.16	1.86E-02	2.60	23.0	0.77%	3.33%	258.3	27.5
0.08295	515	959	20.9	51	1.16	1.86E-02	2.60	34.2	0.52%	3.36%	312.4	33.2
0.08295	515	959	20.9	51	1.16	1.86E-02	2.60	34.4	0.52%	3.35%	304.8	32.4
0.08295	515	959	20.9	51	1.16	1.86E-02	2.58	45.5	0.46%	4.01%	357.8	38.0
0.08295	515	959	20.9	51	1.16	1.86E-02	2.57	45.7	0.47%	4.09%	358.7	38.1
0.08295	515	959	20.9	51	1.16	1.86E-02	2.59	56.9	0.40%	4.29%	367.7	39.1
0.08295	515	959	20.9	51	1.16	1.86E-02	2.59	57.1	0.40%	4.29%	353.6	37.6
0.08295	515	959	20.9	51	1.16	1.86E-02	2.58	68.5	0.31%	4.08%	338.1	35.9
0.08295	515	959	20.9	51	1.16	1.86E-02	2.58	68.4	0.31%	4.07%	336.3	35.7
0.08295	515	959	20.9	51	1.16	1.86E-02	2.60	68.7	0.31%	4.04%	322.3	34.3
0.08295	515	959	20.9	51	1.17	1.86E-02	2.88	2.9	13.31%	6.37%	94.2	10.0
0.08295	515	959	20.9	51	1.17	1.86E-02	2.89	2.9	13.18%	6.29%	94.5	10.0
0.08295	515	959	20.9	51	1.17	1.86E-02	2.88	5.8	4.48%	4.36%	126.9	13.5
0.08295	515	959	20.9	51	1.17	1.86E-02	2.90	5.8	4.57%	4.43%	143.5	15.3
0.08295	515	959	20.9	51	1.16	1.86E-02	2.88	8.6	2.40%	3.52%	145.5	15.5
0.08295	515	959	20.9	51	1.16	1.86E-02	2.89	8.6	2.37%	3.46%	140.4	14.9
0.08295	515	959	20.9	51	1.16	1.86E-02	2.89	11.5	1.55%	3.03%	167.9	17.9
0.08295	515	959	20.9	51	1.16	1.86E-02	2.89	11.6	1.57%	3.07%	176.7	18.8
0.08295	515	959	20.9	51	1.17	1.86E-02	2.88	14.5	1.37%	3.34%	204.5	21.7
0.08295	515	959	20.9	51	1.16	1.86E-02	2.88	14.5	1.38%	3.39%	194.6	20.7
0.08295	515	959	20.9	51	1.16	1.86E-02	2.89	17.2	1.22%	3.56%	213.5	22.7
0.08295	515	959	20.9	51	1.16	1.86E-02	2.90	17.2	1.24%	3.61%	212.8	22.6
0.08295	515	959	20.9	51	1.16	1.86E-02	2.90	23.0	1.08%	4.20%	245.6	26.1
0.08295	515	959	20.9	51	1.16	1.86E-02	2.90	23.0	1.08%	4.20%	241.2	25.6
0.08295	515	959	20.9	51	1.16	1.86E-02	2.88	33.8	0.87%	4.98%	280.6	29.8
0.08295	515	959	20.9	51	1.16	1.86E-02	2.89	34.0	0.84%	4.81%	280.6	29.8
0.08295	515	959	20.9	51	1.16	1.86E-02	2.88	45.5	0.76%	5.91%	311.3	33.1
0.08295	515	959	20.9	51	1.16	1.86E-02	2.88	45.7	0.76%	5.90%	315.3	33.5
0.08295	515	959	20.9	51	1.16	1.86E-02	2.89	57.2	0.60%	5.86%	297.8	31.7
0.08295	515	959	20.9	51	1.16	1.86E-02	2.89	56.9	0.64%	6.18%	294.2	31.3
0.08295	515	959	20.9	51	1.16	1.86E-02	2.90	68.4	0.45%	5.26%	259.3	27.6
0.08295	515	959	20.9	51	1.16	1.86E-02	2.92	68.4	0.44%	5.01%	249.7	26.5

Table 27 – Silicone oil/CO_2 tray 1 (15.8%, 6.4 mm) entrainment

A_p (m^2)	s (mm)	ρ_l (kg/m^3)	σ (mN/m)	μ_l (mPa.s)	ρ_g (kg/m^3)	μ_g (mPa.s)	u_s (m/s)	Q_L [$m^3/(h.m)$]	L'/L	L'/G	Holdup (Pa)	Holdup (mm liq)
0.08295	515	959	20.5	51	1.80	1.49E-02	1.69	2.7	3.00%	1.51%	176.0	18.7
0.08295	515	959	20.5	51	1.80	1.49E-02	1.68	2.9	2.80%	1.50%	182.8	19.4
0.08295	515	959	20.5	51	1.79	1.49E-02	1.68	2.9	2.82%	1.51%	176.5	18.8
0.08295	515	959	20.5	51	1.79	1.49E-02	1.69	5.7	1.26%	1.34%	217.2	23.1
0.08295	515	959	20.5	51	1.79	1.49E-02	1.69	5.7	1.27%	1.35%	212.1	22.5
0.08295	515	959	20.5	51	1.79	1.49E-02	1.70	8.6	0.77%	1.23%	253.1	26.9
0.08295	515	959	20.5	51	1.79	1.49E-02	1.70	8.6	0.77%	1.23%	244.1	25.9
0.08295	515	959	20.5	51	1.78	1.49E-02	1.70	11.5	0.55%	1.16%	268.3	28.5
0.08295	515	959	20.5	51	1.78	1.49E-02	1.72	11.5	0.55%	1.17%	276.9	29.4
0.08295	515	959	20.5	51	1.79	1.49E-02	1.70	14.3	0.43%	1.13%	297.5	31.6
0.08295	515	959	20.5	51	1.78	1.49E-02	1.69	14.2	0.43%	1.14%	296.0	31.5
0.08295	515	959	20.5	51	1.78	1.49E-02	1.70	17.0	0.40%	1.26%	315.0	33.5
0.08295	515	959	20.5	51	1.79	1.49E-02	1.70	17.1	0.40%	1.25%	319.5	34.0
0.08295	515	959	20.5	51	1.79	1.49E-02	1.70	23.0	0.32%	1.34%	343.2	36.5
0.08295	515	959	20.5	51	1.79	1.49E-02	1.70	23.1	0.31%	1.33%	351.0	37.3
0.08295	515	959	20.5	51	1.79	1.49E-02	1.69	34.1	0.21%	1.35%	402.0	42.7
0.08295	515	959	20.5	51	1.79	1.49E-02	1.69	34.2	0.21%	1.35%	393.6	41.8
0.08295	515	959	20.5	51	1.78	1.49E-02	1.69	45.8	0.17%	1.42%	448.2	47.6
0.08295	515	959	20.5	51	1.78	1.49E-02	1.69	45.6	0.17%	1.45%	446.9	47.5
0.08295	515	959	20.5	51	1.78	1.49E-02	1.71	56.9	0.15%	1.54%	473.9	50.4
0.08295	515	959	20.5	51	1.78	1.49E-02	1.71	56.8	0.15%	1.52%	470.3	50.0
0.08295	515	959	20.5	51	1.79	1.49E-02	1.70	57.3	0.15%	1.55%	485.5	51.6
0.08295	515	959	20.5	51	1.78	1.49E-02	1.71	68.1	0.12%	1.51%	475.0	50.5
0.08295	515	959	20.5	51	1.78	1.49E-02	1.71	67.7	0.12%	1.52%	475.8	50.6
0.08295	515	959	20.5	51	1.79	1.49E-02	1.99	2.9	4.67%	2.11%	152.3	16.2
0.08295	515	959	20.5	51	1.79	1.49E-02	1.99	2.9	4.82%	2.18%	153.2	16.3
0.08295	515	959	20.5	51	1.79	1.49E-02	2.01	5.8	2.19%	1.97%	187.6	19.9
0.08295	515	959	20.5	51	1.78	1.49E-02	2.00	5.8	2.10%	1.90%	185.0	19.7
0.08295	515	959	20.5	51	1.79	1.49E-02	2.00	8.6	1.26%	1.70%	224.3	23.8
0.08295	515	959	20.5	51	1.79	1.49E-02	2.00	8.6	1.24%	1.68%	230.5	24.5
0.08295	515	959	20.5	51	1.79	1.49E-02	2.00	11.5	0.80%	1.45%	250.2	26.6
0.08295	515	959	20.5	51	1.80	1.49E-02	1.99	11.5	0.83%	1.49%	254.0	27.0
0.08295	515	959	20.5	51	1.79	1.49E-02	2.00	16.9	0.64%	1.71%	270.9	28.8
0.08295	515	959	20.5	51	1.78	1.49E-02	2.00	17.2	0.64%	1.73%	275.1	29.2
0.08295	515	959	20.5	51	1.79	1.49E-02	2.00	22.8	0.53%	1.90%	307.8	32.7
0.08295	515	959	20.5	51	1.78	1.49E-02	1.99	22.9	0.54%	1.98%	317.0	33.7
0.08295	515	959	20.5	51	1.78	1.49E-02	2.00	34.0	0.36%	1.93%	370.7	39.4

A_p (m^2)	s (mm)	ρ_l (kg/m^3)	σ (mN/m)	μ_l (mPa.s)	ρ_g (kg/m^3)	μ_g (mPa.s)	u_s (m/s)	Q_L [$m^3/(h.m)$]	L'/L	L'/G	Holdup (Pa)	Holdup (mm liq)
0.08295	515	959	20.5	51	1.79	1.49E-02	2.00	34.2	0.36%	1.93%	360.7	38.3
0.08295	515	959	20.5	51	1.79	1.49E-02	2.01	45.8	0.32%	2.27%	417.9	44.4
0.08295	515	959	20.5	51	1.78	1.49E-02	2.01	45.6	0.31%	2.22%	410.8	43.7
0.08295	515	959	20.5	51	1.78	1.49E-02	2.00	57.1	0.25%	2.24%	439.5	46.7
0.08295	515	959	20.5	51	1.78	1.49E-02	2.01	56.8	0.26%	2.34%	426.9	45.4
0.08295	515	959	20.5	51	1.78	1.49E-02	1.98	65.0	0.22%	2.24%	419.3	44.6
0.08295	515	959	20.5	51	1.79	1.49E-02	1.99	68.7	0.20%	2.21%	423.6	45.0
0.08295	515	959	20.5	51	1.79	1.49E-02	2.30	2.9	7.79%	3.07%	127.0	13.5
0.08295	515	959	20.5	51	1.78	1.49E-02	2.30	2.9	7.90%	3.12%	117.9	12.5
0.08295	515	959	20.5	51	1.79	1.49E-02	2.30	5.7	3.25%	2.54%	172.9	18.4
0.08295	515	959	20.5	51	1.79	1.49E-02	2.30	5.7	3.20%	2.50%	172.7	18.4
0.08295	515	959	20.5	51	1.78	1.49E-02	2.29	8.6	1.67%	1.98%	198.7	21.1
0.08295	515	959	20.5	51	1.79	1.49E-02	2.29	8.6	1.69%	2.00%	201.5	21.4
0.08295	515	959	20.5	51	1.79	1.49E-02	2.29	11.5	1.13%	1.77%	216.1	23.0
0.08295	515	959	20.5	51	1.79	1.49E-02	2.30	11.5	1.10%	1.74%	214.2	22.8
0.08295	515	959	20.5	51	1.79	1.49E-02	2.30	14.4	0.97%	1.92%	243.6	25.9
0.08295	515	959	20.5	51	1.79	1.49E-02	2.30	14.5	1.00%	1.99%	247.6	26.3
0.08295	515	959	20.5	51	1.79	1.49E-02	2.30	17.2	0.90%	2.12%	253.1	26.9
0.08295	515	959	20.5	51	1.79	1.49E-02	2.30	17.3	0.91%	2.13%	266.8	28.4
0.08295	515	959	20.5	51	1.79	1.49E-02	2.29	23.0	0.78%	2.47%	293.0	31.1
0.08295	515	959	20.5	51	1.78	1.49E-02	2.29	23.0	0.79%	2.50%	292.5	31.1
0.08295	515	959	20.5	51	1.79	1.49E-02	2.30	34.4	0.58%	2.72%	333.6	35.5
0.08295	515	959	20.5	51	1.78	1.49E-02	2.29	34.4	0.52%	2.46%	342.2	36.4
0.08295	515	959	20.5	51	1.78	1.49E-02	2.31	45.7	0.55%	3.44%	370.5	39.4
0.08295	515	959	20.5	51	1.78	1.49E-02	2.31	45.5	0.59%	3.65%	369.2	39.2
0.08295	515	959	20.5	51	1.79	1.49E-02	2.30	57.3	0.46%	3.63%	374.4	39.8
0.08295	515	959	20.5	51	1.78	1.49E-02	2.31	57.3	0.45%	3.54%	362.4	38.5
0.08295	515	959	20.5	51	1.79	1.49E-02	2.30	57.3	0.44%	3.41%	367.6	39.1
0.08295	515	959	20.5	51	1.78	1.49E-02	2.29	57.2	0.45%	3.57%	367.7	39.1
0.08295	515	959	20.5	51	1.79	1.49E-02	2.30	68.3	0.34%	3.21%	339.6	36.1
0.08295	515	959	20.5	51	1.78	1.49E-02	2.30	68.0	0.35%	3.24%	350.9	37.3
0.08295	515	959	20.5	51	1.78	1.49E-02	2.59	5.8	5.25%	3.67%	152.9	16.3
0.08295	515	959	20.5	51	1.79	1.49E-02	2.59	5.8	5.21%	3.64%	154.5	16.4
0.08295	515	959	20.5	51	1.78	1.49E-02	2.61	8.6	2.89%	3.01%	176.2	18.7
0.08295	515	959	20.5	51	1.78	1.49E-02	2.61	8.6	2.85%	2.97%	177.8	18.9
0.08295	515	959	20.5	51	1.79	1.49E-02	2.60	11.5	1.87%	2.59%	210.5	22.4
0.08295	515	959	20.5	51	1.79	1.49E-02	2.59	11.5	1.88%	2.61%	209.2	22.2
0.08295	515	959	20.5	51	1.79	1.49E-02	2.58	14.7	1.60%	2.85%	236.4	25.1
0.08295	515	959	20.5	51	1.79	1.49E-02	2.59	14.7	1.60%	2.85%	223.5	23.8

A_p (m^2)	s (mm)	ρ_l (kg/m^3)	σ (mN/m)	μ_l (mPa.s)	ρ_g (kg/m^3)	μ_g (mPa.s)	u_s (m/s)	Q_L [m^3/(h.m)]	L'/L	L'/G	Holdup (Pa)	Holdup (mm liq)
0.08295	515	959	20.5	51	1.78	1.49E-02	2.59	17.4	1.42%	3.00%	239.6	25.5
0.08295	515	959	20.5	51	1.79	1.49E-02	2.59	17.0	1.50%	3.10%	227.3	24.2
0.08295	515	959	20.5	51	1.79	1.49E-02	2.58	23.0	1.35%	3.78%	273.5	29.1
0.08295	515	959	20.5	51	1.78	1.49E-02	2.57	22.9	1.46%	4.10%	254.5	27.1
0.08295	515	959	20.5	51	1.79	1.49E-02	2.59	34.4	1.09%	4.54%	302.5	32.2
0.08295	515	959	20.5	51	1.78	1.49E-02	2.59	34.4	1.11%	4.63%	292.7	31.1
0.08295	515	959	20.5	51	1.77	1.49E-02	2.60	45.8	1.06%	5.95%	313.8	33.4
0.08295	515	959	20.5	51	1.78	1.49E-02	2.60	45.8	1.15%	6.35%	316.9	33.7
0.08295	515	959	20.5	51	1.79	1.49E-02	2.63	57.4	0.82%	5.65%	295.9	31.5
0.08295	515	959	20.5	51	1.79	1.49E-02	2.63	57.5	0.79%	5.46%	292.7	31.1
0.08295	515	959	20.5	51	1.78	1.49E-02	2.59	68.2	0.71%	5.92%	319.8	34.0
0.08295	515	959	20.5	51	1.78	1.49E-02	2.61	68.5	0.73%	6.09%	316.3	33.6

Table 28 – Silicone oil/air tray 1 (15.8%, 6.4 mm) weeping

A_p (m^2)	s (mm)	ρ_l (kg/m^3)	σ (mN/m)	μ_l (mPa.s)	ρ_g (kg/m^3)	μ_g (Pa.s)	u_s (m/s)	Q_L [m^3/(h.m)]	W'/L	W'/G	Holdup (Pa)	Holdup (mm liq)
0.08295	515	959	20.9	51	1.18	1.86E-02	1.69	2.8	51.78%	41.97%	163.9	17.4
0.08295	515	959	20.9	51	1.18	1.86E-02	1.69	2.9	51.24%	41.55%	164.7	17.5
0.08295	515	959	20.9	51	1.17	1.86E-02	1.70	5.7	42.13%	69.17%	193.5	20.6
0.08295	515	959	20.9	51	1.17	1.86E-02	1.69	8.6	34.62%	85.91%	244.4	26.0
0.08295	515	959	20.9	51	1.17	1.86E-02	1.69	8.7	32.66%	81.25%	240.1	25.5
0.08295	515	959	20.9	51	1.16	1.86E-02	1.70	11.5	27.62%	91.44%	266.3	28.3
0.08295	515	959	20.9	51	1.16	1.86E-02	1.68	11.5	26.89%	89.76%	262.9	27.9
0.08295	515	959	20.9	51	1.17	1.86E-02	1.70	14.4	21.05%	86.85%	286.9	30.5
0.08295	515	959	20.9	51	1.16	1.86E-02	1.69	17.0	17.74%	86.87%	301.7	32.1
0.08295	515	959	20.9	51	1.16	1.86E-02	1.69	22.9	11.88%	78.68%	338.7	36.0
0.08295	515	959	20.9	51	1.16	1.86E-02	1.69	23.0	11.65%	77.39%	346.0	36.8
0.08295	515	959	20.9	51	1.16	1.86E-02	1.69	34.1	8.14%	80.96%	397.6	42.3
0.08295	515	959	20.9	51	1.16	1.86E-02	1.68	34.2	8.89%	88.81%	406.5	43.2
0.08295	515	959	20.9	51	1.16	1.86E-02	1.69	46.0	6.23%	82.72%	435.8	46.3
0.08295	515	959	20.9	51	1.16	1.86E-02	1.70	46.0	6.40%	84.54%	442.2	47.0
0.08295	515	959	20.9	51	1.16	1.86E-02	1.69	57.1	5.17%	85.72%	459.7	48.9
0.08295	515	959	20.9	51	1.16	1.86E-02	1.69	57.3	5.25%	87.40%	460.5	48.9
0.08295	515	959	20.9	51	1.16	1.86E-02	1.71	68.5	3.57%	69.93%	483.8	51.4
0.08295	515	959	20.9	51	1.16	1.86E-02	1.71	68.5	3.80%	74.78%	480.0	51.0
0.08295	515	959	20.9	51	1.18	1.86E-02	2.00	2.8	37.37%	25.60%	147.4	15.7

A_p (m^2)	s (mm)	ρ_l (kg/m^3)	σ (mN/m)	μ_l (mPa.s)	ρ_g (kg/m^3)	μ_g (Pa.s)	u_s (m/s)	Q_L [m^3/(h.m)]	W'/L	W'/G	Holdup (Pa)	Holdup (mm liq)
0.08295	515	959	20.9	51	1.18	1.86E-02	2.00	2.8	35.05%	24.02%	141.4	15.0
0.08295	515	959	20.9	51	1.16	1.86E-02	1.99	5.7	29.92%	41.87%	179.6	19.1
0.08295	515	959	20.9	51	1.17	1.86E-02	1.99	5.7	30.82%	43.15%	169.9	18.1
0.08295	515	959	20.9	51	1.17	1.86E-02	2.00	8.6	24.84%	52.19%	216.3	23.0
0.08295	515	959	20.9	51	1.17	1.86E-02	2.00	8.6	24.98%	52.17%	218.4	23.2
0.08295	515	959	20.9	51	1.16	1.86E-02	1.99	11.5	20.04%	56.61%	245.3	26.1
0.08295	515	959	20.9	51	1.16	1.86E-02	1.99	11.5	19.94%	56.50%	237.8	25.3
0.08295	515	959	20.9	51	1.17	1.86E-02	1.99	14.4	14.16%	49.83%	263.3	28.0
0.08295	515	959	20.9	51	1.17	1.86E-02	1.99	14.3	14.10%	49.25%	265.1	28.2
0.08295	515	959	20.9	51	1.16	1.86E-02	2.00	17.1	11.08%	46.29%	284.6	30.3
0.08295	515	959	20.9	51	1.16	1.86E-02	2.00	17.0	10.99%	45.57%	270.9	28.8
0.08295	515	959	20.9	51	1.16	1.86E-02	2.00	22.8	7.78%	43.18%	311.1	33.1
0.08295	515	959	20.9	51	1.16	1.86E-02	2.01	22.8	7.62%	42.29%	306.7	32.6
0.08295	515	959	20.9	51	1.16	1.86E-02	1.99	34.3	5.78%	49.09%	346.8	36.9
0.08295	515	959	20.9	51	1.16	1.86E-02	1.98	34.2	6.01%	51.05%	355.5	37.8
0.08295	515	959	20.9	51	1.16	1.86E-02	2.00	45.8	4.05%	45.41%	391.1	41.6
0.08295	515	959	20.9	51	1.16	1.86E-02	1.99	46.0	4.13%	46.59%	406.0	43.2
0.08295	515	959	20.9	51	1.16	1.86E-02	1.99	57.0	3.02%	42.42%	441.9	47.0
0.08295	515	959	20.9	51	1.16	1.86E-02	2.00	57.2	3.22%	44.96%	429.4	45.6
0.08295	515	959	20.9	51	1.16	1.86E-02	2.00	68.5	2.60%	43.57%	456.1	48.5
0.08295	515	959	20.9	51	1.16	1.86E-02	2.00	68.4	2.63%	44.18%	460.6	49.0
0.08295	515	959	20.9	51	1.17	1.86E-02	2.29	2.8	25.16%	15.08%	124.6	13.2
0.08295	515	959	20.9	51	1.17	1.86E-02	2.29	2.8	24.03%	14.39%	125.9	13.4
0.08295	515	959	20.9	51	1.17	1.86E-02	2.31	5.7	20.89%	25.37%	147.9	15.7
0.08295	515	959	20.9	51	1.17	1.86E-02	2.30	5.7	20.92%	25.31%	155.4	16.5
0.08295	515	959	20.9	51	1.17	1.86E-02	2.29	8.6	17.06%	31.21%	190.5	20.2
0.08295	515	959	20.9	51	1.16	1.86E-02	2.31	11.5	14.83%	36.20%	222.3	23.6
0.08295	515	959	20.9	51	1.16	1.86E-02	2.30	11.5	13.74%	33.58%	211.2	22.4
0.08295	515	959	20.9	51	1.17	1.86E-02	2.29	14.3	11.79%	35.81%	242.6	25.8
0.08295	515	959	20.9	51	1.16	1.86E-02	2.30	17.1	7.95%	28.95%	256.8	27.3
0.08295	515	959	20.9	51	1.16	1.86E-02	2.30	17.1	7.83%	28.61%	243.3	25.9
0.08295	515	959	20.9	51	1.16	1.86E-02	2.30	22.9	5.77%	28.10%	290.0	30.8
0.08295	515	959	20.9	51	1.16	1.86E-02	2.29	22.8	5.74%	27.85%	278.0	29.6
0.08295	515	959	20.9	51	1.16	1.86E-02	2.30	34.2	3.74%	27.29%	330.9	35.2
0.08295	515	959	20.9	51	1.16	1.86E-02	2.30	34.3	3.88%	28.40%	323.3	34.4
0.08295	515	959	20.9	51	1.16	1.86E-02	2.30	45.9	3.21%	31.36%	370.2	39.4
0.08295	515	959	20.9	51	1.16	1.86E-02	2.29	45.6	3.00%	29.19%	385.6	41.0
0.08295	515	959	20.9	51	1.16	1.86E-02	2.31	57.2	2.51%	30.53%	404.9	43.0
0.08295	515	959	20.9	51	1.16	1.86E-02	2.29	68.5	1.83%	26.89%	404.0	42.9
0.08295	515	959	20.9	51	1.16	1.86E-02	2.30	68.5	1.80%	26.30%	408.1	43.4

A_p (m^2)	s (mm)	ρ_l (kg/m^3)	σ (mN/m)	μ_l (mPa.s)	ρ_g (kg/m^3)	μ_g (Pa.s)	u_s (m/s)	Q_L [m^3/(h.m)]	W'/L	W'/G	Holdup (Pa)	Holdup (mm liq)
0.08295	515	959	20.9	51	1.17	1.86E-02	2.58	2.8	17.70%	9.41%	108.1	11.5
0.08295	515	959	20.9	51	1.17	1.86E-02	2.58	2.9	17.08%	9.14%	107.1	11.4
0.08295	515	959	20.9	51	1.17	1.86E-02	2.58	5.7	15.91%	17.26%	143.7	15.3
0.08295	515	959	20.9	51	1.17	1.86E-02	2.57	5.7	15.93%	17.28%	144.2	15.3
0.08295	515	959	20.9	51	1.17	1.86E-02	2.59	8.6	12.96%	21.03%	176.1	18.7
0.08295	515	959	20.9	51	1.16	1.86E-02	2.59	8.6	13.04%	21.18%	175.3	18.6
0.08295	515	959	20.9	51	1.16	1.86E-02	2.60	11.5	10.69%	23.18%	197.1	20.9
0.08295	515	959	20.9	51	1.16	1.86E-02	2.60	11.5	11.18%	24.24%	207.3	22.0
0.08295	515	959	20.9	51	1.17	1.86E-02	2.59	14.4	8.31%	22.46%	216.9	23.1
0.08295	515	959	20.9	51	1.17	1.86E-02	2.58	14.4	8.61%	23.34%	209.3	22.2
0.08295	515	959	20.9	51	1.16	1.86E-02	2.59	17.1	6.65%	21.51%	226.9	24.1
0.08295	515	959	20.9	51	1.16	1.86E-02	2.59	17.1	6.76%	21.81%	222.2	23.6
0.08295	515	959	20.9	51	1.16	1.86E-02	2.60	22.9	4.74%	20.37%	263.4	28.0
0.08295	515	959	20.9	51	1.16	1.86E-02	2.61	22.9	4.99%	21.44%	258.2	27.4
0.08295	515	959	20.9	51	1.16	1.86E-02	2.60	34.2	3.53%	22.80%	312.8	33.3
0.08295	515	959	20.9	51	1.16	1.86E-02	2.60	34.3	3.52%	22.86%	308.9	32.8
0.08295	515	959	20.9	51	1.16	1.86E-02	2.58	45.5	2.35%	20.25%	357.1	38.0
0.08295	515	959	20.9	51	1.16	1.86E-02	2.57	45.7	2.26%	19.67%	355.7	37.8
0.08295	515	959	20.9	51	1.16	1.86E-02	2.60	56.9	1.54%	16.58%	362.1	38.5
0.08295	515	959	20.9	51	1.16	1.86E-02	2.60	57.1	1.60%	17.26%	361.0	38.4
0.08295	515	959	20.9	51	1.16	1.86E-02	2.59	68.4	0.92%	11.94%	332.8	35.4
0.08295	515	959	20.9	51	1.16	1.86E-02	2.60	68.7	0.91%	11.77%	324.2	34.5
0.08295	515	959	20.9	51	1.17	1.86E-02	2.88	2.9	12.39%	5.93%	96.0	10.2
0.08295	515	959	20.9	51	1.17	1.86E-02	2.89	2.9	11.77%	5.64%	96.5	10.3
0.08295	515	959	20.9	51	1.17	1.86E-02	2.89	5.8	12.67%	12.32%	130.7	13.9
0.08295	515	959	20.9	51	1.17	1.86E-02	2.89	5.8	12.59%	12.18%	132.0	14.0
0.08295	515	959	20.9	51	1.16	1.86E-02	2.88	8.6	11.25%	16.45%	150.2	16.0
0.08295	515	959	20.9	51	1.16	1.86E-02	2.89	8.6	11.10%	16.23%	144.9	15.4
0.08295	515	959	20.9	51	1.16	1.86E-02	2.89	11.5	9.58%	18.66%	169.5	18.0
0.08295	515	959	20.9	51	1.16	1.86E-02	2.89	11.6	9.46%	18.52%	175.3	18.6
0.08295	515	959	20.9	51	1.16	1.86E-02	2.88	14.5	7.41%	18.23%	190.5	20.2
0.08295	515	959	20.9	51	1.16	1.86E-02	2.89	17.2	6.05%	17.54%	215.4	22.9
0.08295	515	959	20.9	51	1.16	1.86E-02	2.90	17.2	6.05%	17.53%	210.9	22.4
0.08295	515	959	20.9	51	1.16	1.86E-02	2.90	23.0	4.95%	19.19%	241.6	25.7
0.08295	515	959	20.9	51	1.16	1.86E-02	2.90	23.0	4.54%	17.60%	248.7	26.4
0.08295	515	959	20.9	51	1.16	1.86E-02	2.89	33.9	3.31%	19.08%	280.1	29.8
0.08295	515	959	20.9	51	1.16	1.86E-02	2.90	33.9	3.28%	18.79%	279.1	29.7
0.08295	515	959	20.9	51	1.16	1.86E-02	2.88	45.7	1.96%	15.19%	318.6	33.9
0.08295	515	959	20.9	51	1.16	1.86E-02	2.89	57.1	0.94%	9.08%	303.0	32.2

A_p (m^2)	s (mm)	ρ_l (kg/m^3)	σ (mN/m)	μ_l (mPa.s)	ρ_g (kg/m^3)	μ_g (Pa.s)	u_s (m/s)	Q_L [m^3/(h.m)]	W'/L	W'/G	Holdup (Pa)	Holdup (mm liq)
0.08295	515	959	20.9	51	1.16	1.86E-02	2.89	57.0	0.83%	8.00%	299.1	31.8
0.08295	515	959	20.9	51	1.16	1.86E-02	2.90	68.5	0.51%	5.96%	258.0	27.4
0.08295	515	959	20.9	51	1.16	1.86E-02	2.92	68.4	0.52%	5.96%	253.8	27.0

Table 29 – Silicone oil/CO_2 tray 1 (15.8%, 6.4 mm) weeping

A_p (m^2)	s (mm)	ρ_l (kg/m^3)	σ (mN/m)	μ_l (mPa.s)	ρ_g (kg/m^3)	μ_g (mPa.s)	u_s (m/s)	Q_L [m^3/(h.m)]	W'/L	W'/G	Holdup (Pa)	Holdup (mm liq)
0.08295	515	959	20.5	51	1.80	1.49E-02	1.69	2.9	28.29%	15.09%	186.1	19.8
0.08295	515	959	20.5	51	1.80	1.49E-02	1.68	2.9	27.82%	14.81%	180.3	19.2
0.08295	515	959	20.5	51	1.78	1.49E-02	1.70	5.7	25.96%	27.66%	211.9	22.5
0.08295	515	959	20.5	51	1.78	1.49E-02	1.70	5.7	26.50%	28.24%	215.7	22.9
0.08295	515	959	20.5	51	1.78	1.49E-02	1.70	8.6	21.01%	33.49%	241.8	25.7
0.08295	515	959	20.5	51	1.78	1.49E-02	1.71	8.6	20.87%	33.15%	245.2	26.1
0.08295	515	959	20.5	51	1.79	1.49E-02	1.71	11.5	16.79%	35.51%	280.7	29.8
0.08295	515	959	20.5	51	1.78	1.49E-02	1.71	11.5	16.85%	35.71%	271.7	28.9
0.08295	515	959	20.5	51	1.78	1.49E-02	1.69	14.4	13.75%	36.91%	293.5	31.2
0.08295	515	959	20.5	51	1.78	1.49E-02	1.70	14.3	13.32%	35.30%	294.2	31.3
0.08295	515	959	20.5	51	1.79	1.49E-02	1.69	17.0	11.15%	35.30%	314.1	33.4
0.08295	515	959	20.5	51	1.78	1.49E-02	1.70	17.1	9.44%	29.95%	310.4	33.0
0.08295	515	959	20.5	51	1.78	1.49E-02	1.70	23.0	6.69%	28.49%	332.4	35.3
0.08295	515	959	20.5	51	1.79	1.49E-02	1.70	23.1	6.24%	26.66%	343.4	36.5
0.08295	515	959	20.5	51	1.78	1.49E-02	1.69	34.1	4.81%	30.64%	398.4	42.4
0.08295	515	959	20.5	51	1.78	1.49E-02	1.69	34.1	4.76%	30.33%	389.7	41.4
0.08295	515	959	20.5	51	1.79	1.49E-02	1.69	45.9	3.49%	29.76%	437.2	46.5
0.08295	515	959	20.5	51	1.79	1.49E-02	1.69	45.7	3.68%	31.23%	434.3	46.2
0.08295	515	959	20.5	51	1.79	1.49E-02	1.70	57.2	2.84%	29.90%	472.5	50.2
0.08295	515	959	20.5	51	1.78	1.49E-02	1.71	56.8	2.83%	29.66%	483.2	51.4
0.08295	515	959	20.5	51	1.78	1.49E-02	1.72	67.8	2.17%	27.00%	478.2	50.8
0.08295	515	959	20.5	51	1.78	1.49E-02	1.72	67.5	2.24%	27.89%	476.9	50.7
0.08295	515	959	20.5	51	1.79	1.49E-02	1.99	2.9	18.14%	8.23%	154.6	16.4
0.08295	515	959	20.5	51	1.79	1.49E-02	1.99	2.9	18.04%	8.14%	152.4	16.2
0.08295	515	959	20.5	51	1.79	1.49E-02	2.01	5.8	16.85%	15.22%	190.8	20.3
0.08295	515	959	20.5	51	1.78	1.49E-02	2.00	5.8	16.88%	15.30%	186.9	19.9
0.08295	515	959	20.5	51	1.79	1.49E-02	2.00	8.6	14.02%	18.98%	221.6	23.6
0.08295	515	959	20.5	51	1.78	1.49E-02	2.00	8.6	14.38%	19.59%	217.1	23.1
0.08295	515	959	20.5	51	1.80	1.49E-02	1.99	11.5	11.77%	21.20%	249.7	26.5

A_p (m^2)	s (mm)	ρ_l (kg/m^3)	σ (mN/m)	μ_l (mPa.s)	ρ_g (kg/m^3)	μ_g (mPa.s)	u_s (m/s)	Q_L [$m^3/(h.m)$]	W'/L	W'/G	Holdup (Pa)	Holdup (mm liq)
0.08295	515	959	20.5	51	1.80	1.49E-02	1.99	11.5	11.87%	21.37%	251.4	26.7
0.08295	515	959	20.5	51	1.79	1.49E-02	2.00	14.5	8.76%	20.00%	262.9	27.9
0.08295	515	959	20.5	51	1.80	1.49E-02	2.00	14.5	9.18%	20.84%	258.9	27.5
0.08295	515	959	20.5	51	1.78	1.49E-02	2.00	17.1	6.98%	18.84%	277.7	29.5
0.08295	515	959	20.5	51	1.79	1.49E-02	1.99	17.1	7.35%	19.74%	282.6	30.0
0.08295	515	959	20.5	51	1.79	1.49E-02	2.00	23.0	4.65%	16.77%	306.8	32.6
0.08295	515	959	20.5	51	1.79	1.49E-02	2.00	23.0	4.69%	16.94%	315.4	33.5
0.08295	515	959	20.5	51	1.79	1.49E-02	2.01	34.2	3.21%	17.19%	360.5	38.3
0.08295	515	959	20.5	51	1.79	1.49E-02	2.01	45.7	2.48%	17.75%	408.7	43.4
0.08295	515	959	20.5	51	1.78	1.49E-02	2.01	45.7	2.48%	17.75%	411.9	43.8
0.08295	515	959	20.5	51	1.78	1.49E-02	2.01	57.2	1.79%	16.09%	436.0	46.3
0.08295	515	959	20.5	51	1.79	1.49E-02	2.01	56.8	1.78%	15.76%	443.0	47.1
0.08295	515	959	20.5	51	1.78	1.49E-02	1.99	67.7	1.34%	14.37%	421.1	44.8
0.08295	515	959	20.5	51	1.79	1.49E-02	2.30	2.9	10.32%	4.06%	126.3	13.4
0.08295	515	959	20.5	51	1.78	1.49E-02	2.30	2.9	10.93%	4.32%	118.8	12.6
0.08295	515	959	20.5	51	1.79	1.49E-02	2.30	5.7	11.90%	9.32%	184.6	19.6
0.08295	515	959	20.5	51	1.79	1.49E-02	2.30	5.7	11.70%	9.15%	172.1	18.3
0.08295	515	959	20.5	51	1.79	1.49E-02	2.29	8.6	10.36%	12.28%	201.2	21.4
0.08295	515	959	20.5	51	1.79	1.49E-02	2.29	8.6	10.56%	12.50%	197.0	20.9
0.08295	515	959	20.5	51	1.79	1.49E-02	2.29	11.5	8.62%	13.56%	213.1	22.7
0.08295	515	959	20.5	51	1.79	1.49E-02	2.30	11.5	8.64%	13.56%	205.0	21.8
0.08295	515	959	20.5	51	1.79	1.49E-02	2.30	14.5	7.14%	14.14%	240.7	25.6
0.08295	515	959	20.5	51	1.79	1.49E-02	2.30	14.5	7.16%	14.23%	248.4	26.4
0.08295	515	959	20.5	51	1.79	1.49E-02	2.30	17.2	6.12%	14.43%	262.2	27.9
0.08295	515	959	20.5	51	1.79	1.49E-02	2.30	17.3	6.15%	14.53%	259.4	27.6
0.08295	515	959	20.5	51	1.79	1.49E-02	2.29	23.0	4.17%	13.16%	291.4	31.0
0.08295	515	959	20.5	51	1.78	1.49E-02	2.29	23.0	4.36%	13.79%	289.8	30.8
0.08295	515	959	20.5	51	1.79	1.49E-02	2.30	34.4	3.04%	14.31%	333.9	35.5
0.08295	515	959	20.5	51	1.78	1.49E-02	2.31	45.8	1.99%	12.45%	367.6	39.1
0.08295	515	959	20.5	51	1.78	1.49E-02	2.30	45.8	1.88%	11.79%	370.3	39.4
0.08295	515	959	20.5	51	1.78	1.49E-02	2.31	57.3	1.01%	7.95%	362.9	38.6
0.08295	515	959	20.5	51	1.78	1.49E-02	2.30	57.2	1.05%	8.29%	370.1	39.3
0.08295	515	959	20.5	51	1.79	1.49E-02	2.30	68.2	0.71%	6.63%	343.1	36.5
0.08295	515	959	20.5	51	1.78	1.49E-02	2.30	68.0	0.70%	6.54%	348.9	37.1
0	0	0	0	0	0.00	1.49E-02	0.00	0.0	0.00%	0.00%	0.0	0.0
0.08295	515	959	20.5	51	1.78	1.49E-02	2.59	5.8	8.55%	5.98%	153.8	16.3
0.08295	515	959	20.5	51	1.78	1.49E-02	2.59	5.7	8.91%	6.22%	147.4	15.7
0.08295	515	959	20.5	51	1.78	1.49E-02	2.61	8.6	8.37%	8.74%	175.2	18.6
0.08295	515	959	20.5	51	1.78	1.49E-02	2.61	8.6	8.05%	8.39%	184.1	19.6
0.08295	515	959	20.5	51	1.79	1.49E-02	2.60	11.5	7.63%	10.61%	206.8	22.0

A_p (m^2)	s (mm)	ρ_l (kg/m^3)	σ (mN/m)	μ_l (mPa.s)	ρ_g (kg/m^3)	μ_g (mPa.s)	u_s (m/s)	Q_L [$m^3/(h.m)$]	W'/L	W'/G	Holdup (Pa)	Holdup (mm liq)
0.08295	515	959	20.5	51	1.79	1.49E-02	2.59	11.5	6.90%	9.62%	207.6	22.1
0.08295	515	959	20.5	51	1.79	1.49E-02	2.59	14.6	6.19%	10.93%	225.1	23.9
0.08295	515	959	20.5	51	1.79	1.49E-02	2.59	14.7	6.07%	10.85%	222.6	23.7
0.08295	515	959	20.5	51	1.78	1.49E-02	2.59	17.4	5.24%	11.12%	237.0	25.2
0.08295	515	959	20.5	51	1.79	1.49E-02	2.59	17.3	5.19%	10.95%	244.2	26.0
0.08295	515	959	20.5	51	1.78	1.49E-02	2.58	23.0	3.86%	10.87%	271.5	28.9
0.08295	515	959	20.5	51	1.79	1.49E-02	2.58	23.2	4.00%	11.26%	270.5	28.7
0.08295	515	959	20.5	51	1.79	1.49E-02	2.59	34.5	2.40%	10.05%	298.7	31.8
0.08295	515	959	20.5	51	1.79	1.49E-02	2.59	34.4	2.45%	10.21%	294.1	31.3
0.08295	515	959	20.5	51	1.78	1.49E-02	2.60	45.8	1.21%	6.71%	318.4	33.8
0.08295	515	959	20.5	51	1.78	1.49E-02	2.60	45.8	1.16%	6.44%	311.3	33.1
0.08295	515	959	20.5	51	1.78	1.49E-02	2.62	57.5	0.58%	4.02%	293.5	31.2
0.08295	515	959	20.5	51	1.78	1.49E-02	2.62	57.4	0.60%	4.13%	294.2	31.3
0.08295	515	959	20.5	51	1.78	1.49E-02	2.59	68.3	0.34%	2.85%	320.9	34.1
0.08295	515	959	20.5	51	1.78	1.49E-02	2.61	68.5	0.31%	2.59%	318.8	33.9